MINERALOGICAL ASSOCIATION OF CANADA

SHORT COURSE HANDBOOK
ON
ENVIRONMENTAL
GEOCHEMISTRY
OF SULFIDE MINE-WASTES

WATERLOO
ONTARIO
MAY, 1994

Editors: J.L. Jambor & D. W. Blowes

Mineralogical Association of Canada

THE ENVIRONMENTAL GEOCHEMISTRY OF SULFIDE MINE-WASTES

SHORT COURSE HANDBOOK
Volume 22, May 1994
Waterloo, Ontario
Editors: D. W. Blowes & J. L. Jambor

Charles N. Alpers
U.S. Geological Survey
Federal Building, 2800 Cottage Way
Sacramento, California 95825

Geneviève Béchard
Environmental Laboratory, CANMET
555 Booth Street
Ottawa, Ontario K1A 0G1

Jerry M. Bigham
Department of Agronomy
The Ohio State University
Columbus, Ohio 43210-1086

David W. Blowes
Waterloo Centre for Goundwater
University of Waterloo
Waterloo, Ontario N2L 3G1

Emil O. Frind
Waterloo Centre for Groundwater
Research
University of Waterloo
Waterloo, Ontario N2L 3G1

W. Douglas Gould
Environmental Laboratory, CANMET
555 Booth Street
Ottawa, Ontario K1A 0G1

John L. Jambor
Waterloo Centre for Groundwater
Research
University of Waterloo
Waterloo, Ontario N2L 3G1

Lyne Lortie
Environmental Laboratory, CANMET
555 Booth Street
Ottawa, Ontario K1A 0G1

John W. Molson
Waterloo Centre for Groundwater
Research
University of Waterloo
Waterloo, Ontario N2L 3G1

Ronald V. Nicholson
Waterloo Centre for Groundwater
Research University of Waterloo
Waterloo, Ontario N2L 3G1

D. Kirk Nordstrom
U.S. Geological Survey
Box 25046
Lakewood, Colorado 80225

Carol J. Ptacek
Canada Centre for Inland Waters
867 Lakeshore Road, P.O. Box 5050
Burlington, Ontario L7R 4A6

A. Ian M. Ritchie
Environmental Physics
Australian Nuclear Science and
Technology Organization, Private Mailbag
Menai NSW, Australia 2234

William D. Robertson
Waterloo Centre for Groundwater
Research
University of Waterloo
Waterloo, Ontario N2L 3G1

Adrian Smith
Kea Pacific Holdings
2555 Edgemont Blvd
North Vancouver, B.C. V7R 2M9

Distribution

Copies of the Short Course Handbook Volume 22 can be obtained by writing to:

The Business Manager
Mineralogical Association of Canada
Cityview 78087
Nepean, Ontario
Canada
K2G 5W2

PREFACE

Environmental geochemistry has long been a subject of serious scientific pursuit, but only in the last decade or so have the environment and its preservation become everyday topics among the general public. In the exploitation of new mineral deposits, the mining industry of today has formidable obstacles to overcome, in part because of the legacy of scarred landscapes and polluted drainage that were at one time simply accepted as a natural consequence of the extraction of metals, upon which civilisation has depended for centuries of progress. Despite the monumental efforts that have been expended recently in attempts to rectify past errors and develop new mine-waste technologies, it can still be argued with much validity that our understanding of acid mine drainage and ways to ameliorate it effectively and economically is in a foetal stage of development. It is only in recent years, for example, that it has been recognized that vegetative covers, although aesthetically pleasing and successful in reducing or eliminating eolian dispersion of tailings, are not effective in reducing acid drainage from decommissioned tailings impoundments. Proposals for mitigating acid drainage are manifold, but to date only underwater disposal, with its attendant restriction of oxidation, has been demonstrated to be effective on a long-term, cost-effective basis. The search for equally effective and economic solutions continues because, obviously, underwater disposal is not always a viable option. Thus, it is necessary to obtain a better understanding of the chemical and biological reactions that occur in mine wastes. We need to know more about the factors that govern the rates of these reactions, and the effects that reaction rates have on influencing the strength and other characteristics of the resulting acid drainage. Only with such knowledge can meaningful and economically practical steps be taken to minimize or eliminate acid drainage from existing sources, as well as from future minesites. Thus, this Short Course on the geochemistry of sulfide-bearing mine wastes is timely and relevant, and the collection of papers within this Volume provides examples of current progress and of how science can be applied in a practical way to environmental objectives.

The organizers thank the Mineralogical Association of Canada for its encouragement and financial support in bringing this Short Course to fruition. We also thank the panel of Short-course contributors for their generosity in donating their time, and for the willingness to share their expertise.

J.L. Jambor, D.W. Blowes
May 15, 1994

Chapter 1

The Physical Hydrology of Mill-tailings Impoundments

W.D. Robertson

Chapter 2

Modelling of Mill-tailings Impoundments

E.O. Frind & J.W. Molson

Chapter 3

Mineralogy of Sulfide-rich Tailings and Their Oxidation Products

J.L. Jambor

Chapter 4

Mineralogy of Ochre Deposits Formed by Sulfide Oxidation

J.M. Bigham

Chapter 5

The Waste-rock Environment

A.I.M. Ritchie

Chapter 6

Iron-sulfide Oxidation Mechanisms: Laboratory Studies

R.V. Nicholson

Chapter 7

The Nature and Role of Microorganisms in the Tailings Environment

W.D. Gould, G. Béchard & L. Lortie

Chapter 8

Sulfide Oxidation Mechanisms: Controls and Rates of Oxygen Transport

A.I.M. Ritchie

Chapter 10

Acid-neutralization Mechanisms in Inactive Mine Tailings

D.W. Blowes, C.J. Ptacek

Chapter 11

The Geochemistry of Cyanide in Mill Tailings

Adrian Smith

Chapter 12

A Geochemical Study of the Main Tailings Impoundment at the Falconbridge Limited, Kidd Creek Division Metallurgical Site, Timmins, Ontario

T.A. Al, D.W. Blowes, J.L. Jambor

Chapter 13

Remediation and Prevention of Low-quality Drainage from Tailings Impoundments

D.W. Blowes

Chapter 1

The Physical Hydrogeology of Mill-tailings Impoundments

W.D. Robertson
Waterloo Centre for Groundwater Research
University of Waterloo
Waterloo, Ontario
N2L 3G1

1.1. INTRODUCTION

Mill-tailings comprise the non-economic mineral fraction that is separated during ore processing. As non-economic minerals commonly represent more than 90% of the constituents in base-metal and precious-metal ores, large volumes of tailings are generated and these require disposal at nearby locations. Effective separation during ore processing usually requires that the ore be ground to sand- and silt-size particles, after which mineral separation can be effected by processes such as gravitational settling, surfactant-enhanced flotation, chemical leaching, *etc.*

Because of the large volumes of sand- and silt-size tailings waste that are generated, disposal usually occurs by pumping as a sediment—water slurry to an impoundment constructed close to the mill. Tailings disposal may occur initially by infilling of nearby topographic depressions, lakes, or drainage basins. As mining activity progresses or expands, however, areas available for disposal become limited; consequently, tailings impoundments commonly are increased in height by the construction of retaining dams, thus becoming elevated above the surrounding topography. Retaining dams vary widely in construction. In the past, many were constructed with the coarser grained tailings material and were thus quite permeable. The present trend is to construct impermeable dams that not only minimize the amount of subsurface seepage, but also assist in maintaining high water-table levels within the tailings. Dams with low permeability can be constructed with clay cores or with impermeable synthetic liners. In environmentally sensitive areas the entire impoundment may be lined with a low-permeability clay or synthetic membrane to minimize seepage.

1.2. TAILINGS SEDIMENTOLOGY

Although tailings may vary over a wide range of grain sizes and be deposited using a variety of methods, tailings from base-metal mines are commonly pumped to the impoundment as a slurry containing 20—40 wt% solids, and are discharged via one or several spigotting points that are periodically moved. Solid particles are allowed to settle out of the slurry, and the water accumulates in a tailings pond which is usually decanted from the tailings basin. Figure 1.1 shows representative grain-size curves for tailings from four large base-metal mines in Ontario. The tailings material is predominantly silt and fine to medium sand with low (<10%) clay content.

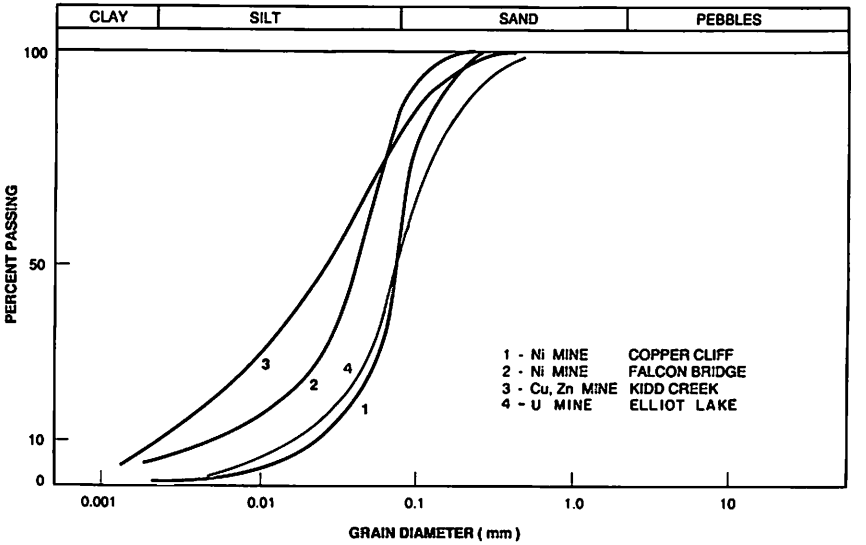

Figure 1.1. Representative grain-size curves for mill-tailings at four sites in Ontario. Curves represent average composition of cored samples (N = 4—25).

The most important process affecting the stratigraphy of a tailings impoundment is the hydraulic sorting of grain size that occurs after tailings discharge. Most impoundments possess two distinct depositional environments: a subaerial beach zone that may extend tens of meters to several hundred meters outward from the spigotting point, and a lacustrine zone that occurs where ponded water is present in the impoundment. Sedimentary processes are distinctly different in the two zones (Figure 1.2). The subaerial beach zone is characterized by high-energy fluvial sediments that are deposited as the discharge stream meanders across the beach area. Deposition of the coarser sand fraction occurs along the bed and banks of the stream, gradually increasing the elevation of the stream bed until breaching occurs and a new stream-course develops. This depositional environment is analogous to that of a braided stream. Sedimentary structures are lenticular or sinuous and may exhibit cross-bedding,

but areally extensive layering is uncommon. Because the finer grained silt-size tailings, commonly referred to as "slimes", are not retained in this higher energy zone, the sediment type is usually fine to medium, silt-deficient sand.

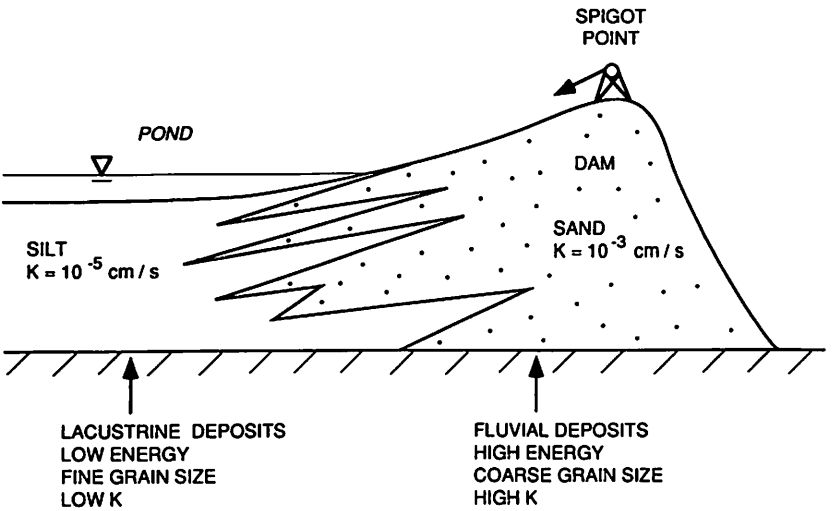

Figure 1.2. Depositional environments of an impoundment receiving slurried tailings.

Where the subaerial tailings stream discharges into ponded water, the lower energy environment allows deposition of the silt and the fine sand-size particles. Sediments deposited are similar to those of a lacustrine environment. In the near-shore zone, deltaic structures exhibiting cross-bedding on a larger scale may occur, and wave action along the shoreline may further enhance size sorting, producing beach sands that are virtually free of the finer fractions. In the zone farther offshore, where energy levels are lowest, the silt and clay fractions are deposited; here, areally extensive layering may develop and varve-like structures may occur.

During infilling of a tailings impoundment the position of the spigotting point is usually changed many times with the result that the position of the beach and pond perimeter also changes. Thus, at most locations, changing depositional environments occur over the life of the impoundment, resulting in sedimentary heterogeneity.

At mining operations using the thickened-tailings disposal technique, the viscosity of the tailings slurry has been increased by lowering water content. At these locations hydraulic sorting of the tailings particles is minimized after discharge. Deposition occurs via a sheet-like action that allows much less grain-size sorting, and the result is a steeper-sloped, cone-shaped tailings deposit (Robinsky *et al.*, 1991).

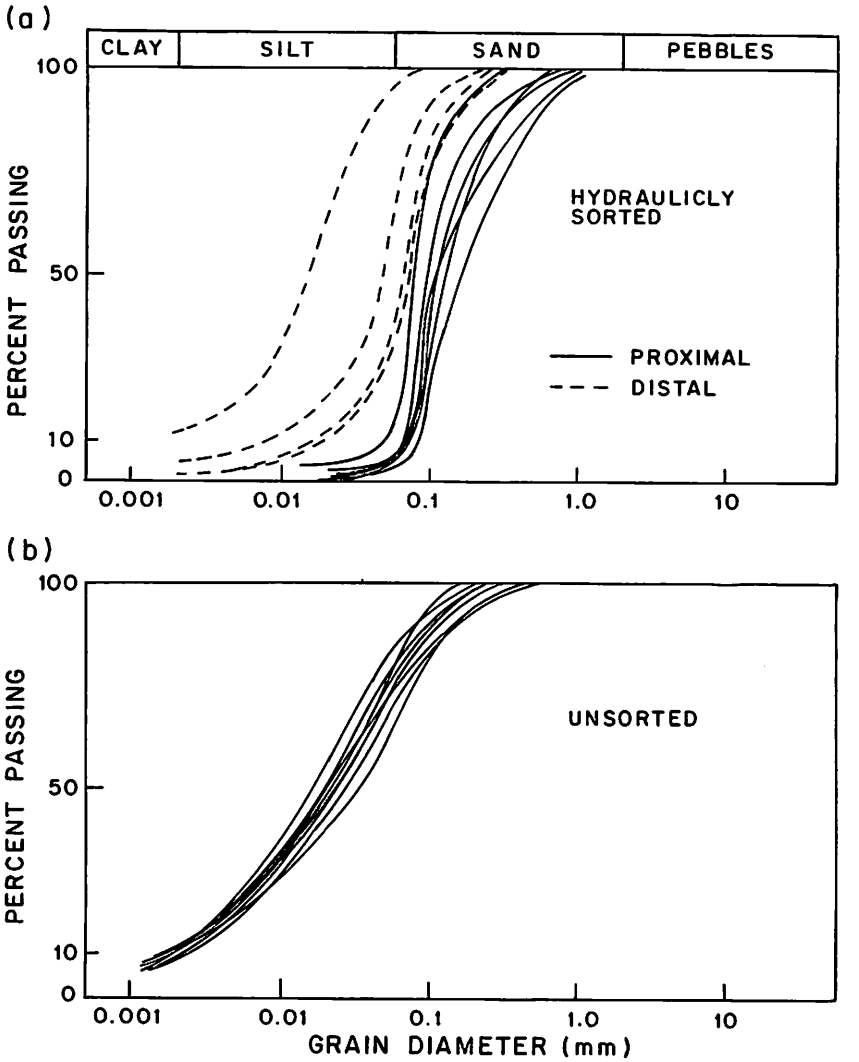

Figure 1.3. Comparison of grain-size variability in impoundments receiving hydraulically sorted and unsorted tailings; (a) slurried tailings from the Copper Cliff Ni mine, Ontario, at locations both proximal and distal from the spigot point; (b) thickened tailings from the Kidd Creek, Zn-Cu mine, Ontario (0.45 m to 12.5 m depth; from Robinsky *et al.*, 1991).

Figure 1.3 compares grain-size distribution in two large base-metal-mine tailings impoundments in Ontario, one at which the tailings have been hydraulically sorted (Copper Cliff), and the other at which the tailings are unsorted (Kidd Creek). At the Copper Cliff site, a wide variation of grain-size distributions occurs. The tailings near the spigotting point are silt-free, well-sorted, fine to medium sand, whereas silt-rich sediments are present at locations distal from the spigotting point. At the Kidd Creek site, a thickened tailings slurry is discharged, and a much more homogeneous deposit results. In general, because of variations in slurry viscosity, loading rates, and spigotting practices, each tailings pile is expected to be stratigraphically unique.

1.3. HYDRAULIC CONDUCTIVITY

The hydraulic conductivity *(K)* of tailings is a function of grain size. For sandy tailings an approximate estimate of K can be obtained from grain-size data using the simple empirical equation of Hazen (Freeze and Cherry, 1979):

$$K = Ad_{10}^2 \qquad (1)$$

where d_{10} is the grain-size diameter at which 10% of the material is finer, and A is a proportionality factor equal to 1 when d_{10} is in units of mm and K is in units of cm/s. Although the Hazen relationship was originally formulated for use in sands, experience has shown that it can also be used to obtain an approximate estimate of K in silty sand material such as tailings. Other more rigorous relationships that relate grain-size distribution to K are available (*e.g.*, Masch and Denny, 1966). For the grain-size curves shown in Figure 1.3a, d_{10} ranges from about 0.002 mm to 0.08 mm, indicating a K range of from 4×10^{-6} cm/s to 6×10^{-3} cm/s, a variation of more than three orders of magnitude for tailings from a single impoundment. Similar large K ranges are reported in other tailings studies (*e.g.*, Blair, 1981; Dave *et al.*, 1986; Blowes, 1990; Coggans, 1992) and are the result of the spatial and temporal variations in the impoundment depositional environments.

In horizontally stratified formations such as tailings, the bulk horizontal hydraulic conductivity (K_x) and vertical hydraulic conductivity (K_z) are determined by the relationships shown in Figure 1.4. Inspection shows that K_x is primarily influenced by the more permeable layers, and K_z is most strongly influenced by the less permeable layers. For example, consider an impoundment site at which sedimentary deposition is primarily in the sandy subaerial zone, but at which less permeable silt-rich sediments are occasionally deposited when the area is periodicly engulfed by the tailings pond. If the silt layers comprise 10% of the tailings thickness, and have K of 10^{-5} cm/s, typical of silt, whereas the remaining sand zones have K of 10^{-3} cm/s, the relationships given in

Figure 1.4 indicate that bulk K_x = 9.01 x 10^{-4} cm/s, and K_z = 9.2 x 10^{-5} cm/s. Thus, low-K layers of minor thickness can have a major influence on vertical permeability, but have little effect on horizontal permeability. Conversely, a high-K layer of minor thickness can have a major impact on bulk K_x, but will have little effect on K_z. K anisotropy in layered systems can have an important impact on groundwater flowpaths, and generally results in preferential migration along high-K layers.

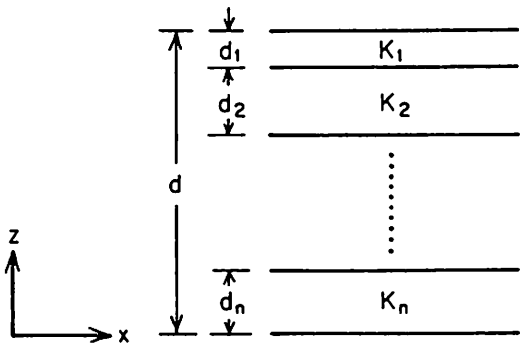

$$K_x = \sum_{i=1}^{n} \frac{K_i d_i}{d}$$

$$K_z = \frac{d}{\sum_{i=1}^{n} d_i / K_i}$$

Figure 1.4. Determination of bulk horizontal (K_x) and vertical (K_z) hydraulic conductivity in horizontally layered systems (from Freeze and Cherry, 1979).

1.3.1. Hydraulic Conductivity Measurement

In heterogeneous materials such as tailings, in which K contrast can be several orders of magnitude over distances of a few meters, determination of representative bulk K values can be problematic. As discussed above, K can be inferred from grain-size analyses if sufficient samples are available from a sufficient number of locations to give a statistically valid representation of K. For grain-size analyses, which individually represent only a small volume of material, numerous analyses are usually required, from locations throughout the tailings pile, to yield a representative value of K. To obtain samples for grain-size analyses, coring of the tailings material must be undertaken.

If tailings cores are available, a more direct method of K estimation can be obtained from permeameter testing. In this test, tailings sediment is placed in a permeameter device, an excess head of water is applied, and the flow rate through the tailings is measured to establish K. Permeameter testing procedure and the apparatus used for sandy sediments are described in detail by Sudicky (1986).

Direct *in-situ* measurement of tailings K can be obtained by water-level-response testing of piezometers, or by conducting well-pumping tests. Piezometer response-tests

are conducted by abruptly adding or removing water or a solid slug device from a piezometer, then monitoring the time required for the static water level to re-equilibrate. For homogeneous, isotropic porous media the following relationship can be used to estimate K from a piezometer response-test (Freeze and Cherry, 1979):

$$K = \frac{r^2 \ln(L/R)}{2LT_o} \qquad (2)$$

where r = radius of piezometer pipe, L = screened length of piezometer tip, R = radius of piezometer tip, and T_0 = Hvorslev's basic time-lag, *i.e.*, the time required for 63% of water-level recovery after disturbance of the static water level. Although Hvorslev's relationship was developed for use in confined aquifers, it usually provides an adequate approximation of K in tailings, provided that the piezometer tip is not positioned close to the water table. Other more rigorous solutions are available for analysis of response-tests in unconfined aquifers (*e.g.*, Chapius, 1988).

Most response-tests involve removal or addition of a quantity of water of only several liters or less; thus, a relatively small area around the piezometer tip is hydraulically stressed during the test. In heterogeneous tailings this again requires that a large number of tests be conducted to obtain a statistically valid representation of K. A more reliable estimate of bulk-tailings K can be obtained by conducting pumping tests in which usually hundreds or thousands of liters of water are pumped over a period of hours to days from a specifically constructed pumping well. The test is performed by measuring the pumping rate and observing the distribution and rate of water-level drawdown in the pumping well and in nearby monitoring wells. Numerous methods of analysis are available for pumping tests. A convenient compilation of these is provided by Kruseman and de Ridder (1970).

In horizontally stratified material such as tailings, vertical permeability may be an order of magnitude (or more) lower than horizontal permeability. K_z is difficult to measure because it frequently is controlled by the finer grained clay and silt layers; these may be several orders of magnitude less permeable than the bulk tailings, but may comprise only a few percent of the total tailings thickness. Piezometer response-tests and pumping tests are influenced predominantly by the more permeable layers, thus providing K values representative of K_x. The presence of low-K layers or lamellae would not generally be indicated during response-testing or during conventional pumping tests. K_z, however, can be estimated from specifically designed pumping tests in which monitoring wells are placed in the stratigraphic layers located above or below the pumped layer (*e.g.*, Neuman and Witherspoon, 1972). The time lag between arrival of the depressurized zone at a location in the pumped layer to that at a location in the overlying or underlying layers can be used to estimate K_z.

A second, more direct, method for estimation of K_z is the use of the Darcy equation in conjunction with knowledge of the vertical flow rate obtained from the use of conservative tracers (see Section 1.8), and measured vertical gradients:

$$V_z = \frac{K_z i_z}{n} \qquad (3)$$

where V_z is vertical flow velocity, i_z is the vertical hydraulic gradient, and n is porosity. In tailings impoundments, V_z can sometimes be established using tracers such as tritium or sulfate, and i_z can be measured directly by installation of multiple-piezometer nests, thus allowing K_z to be estimated.

1.4. GROUNDWATER FLOW IN TAILINGS

Because of hydraulic loading that occurs during the deposition of slurried tailings, and because of water-table mounding that usually persists after decommissioning in elevated impoundments located in humid climatic regions, tailings impoundments are often areas of groundwater recharge. In these areas, downward hydraulic gradients are present, and process water or precipitation that infiltrates the tailings migrates downward from the tailings surface into the underlying groundwater flow system. Figure 1.5 shows an example of the groundwater flow system associated with a very large (1100 ha) tailings impoundment from a base-metal mine near Copper Cliff, Ontario. This impoundment consists of a number of sub-impoundments that were decommissioned between 1940 and 1988. The flow system shown is based on water-table levels measured in 1989, and is substantially the result of natural recharge from precipitation, and through the storage of water on the tailings surface. The tailings pile is 20 to 30 m thick, and is significantly elevated. Substantial water-table mounding in the impoundment has resulted in the highest water levels in the area: up to 30 m higher than in the surrounding terrain. Consequently, the tailings impoundment is a regional groundwater-recharge area from which groundwater migrates radially outward. Figure 1.6 shows the groundwater flowpaths inferred along section A—A', which is a flow transect passing through the older impoundment areas decommissioned between 1940 and 1960. Flowpaths originating at the water table migrate downward into the tailings pile and then discharge southward to surface-water and overburden groundwater flow systems adjacent to the impoundment.

At locations where the water-table elevation in the tailings is lower than in the surrounding terrain, such as occurs when tailings are deposited in lake basins, groundwater may migrate into the tailings from the surrounding terrain. In such cases the tailings area may be one of groundwater discharge at sites where vertically upward groundwater flowpaths are present.

1.5. WATER-TABLE DEPTH

The water-table depth in a decommissioned tailings impoundment is a function of several site-specific factors such as the impoundment geometry, tailings permeability, dam permeability, and rate of water-table recharge. In inpoundments in which sulfide

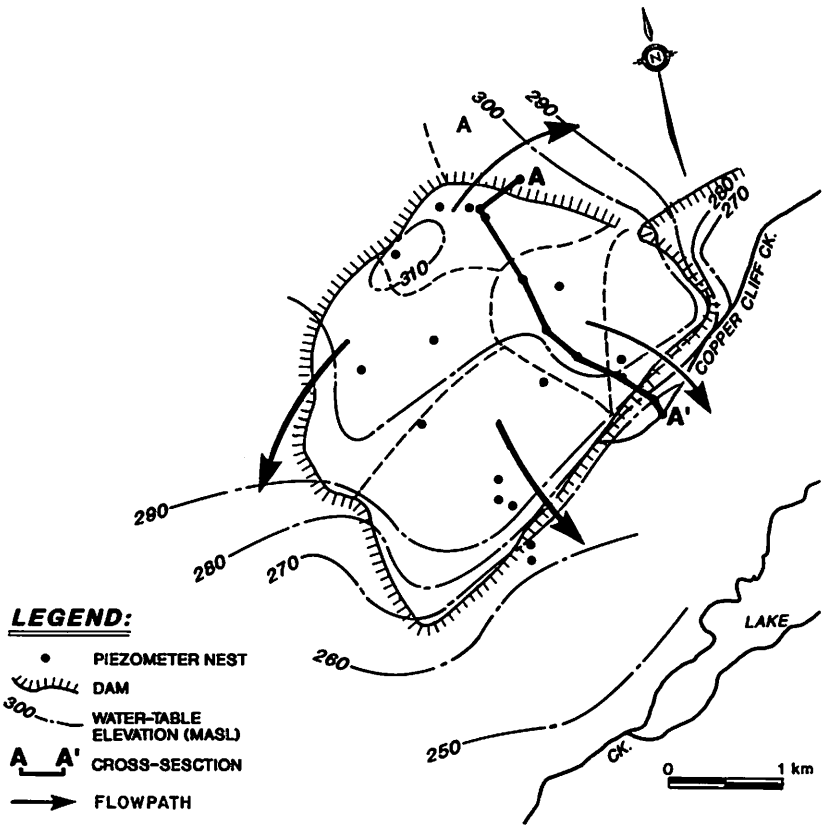

Figure 1.5. Water-table contours and groundwater flowpaths associated with a very large decommissioned tailings impoundment from a base-metal mine near Copper Cliff, Ontario (adapted from Coggans, 1992).

minerals are present, water-table depth is often of concern because sulfide-oxidation reactions that occur in the vadose zone can potentially cause acid generation and mobilization of metals. Because the rate of diffusion of atmospheric oxygen through porous media can decrease by more than three orders of magnitude as degreesaturation increases (Reardon and Moddle, 1985), mimimizing oxidation of tailings by keeping tailings saturated is a desirable goal in some impoundment designs. Recent effort in impoundment design has sought to minimize the thickness of the unsaturated zone by

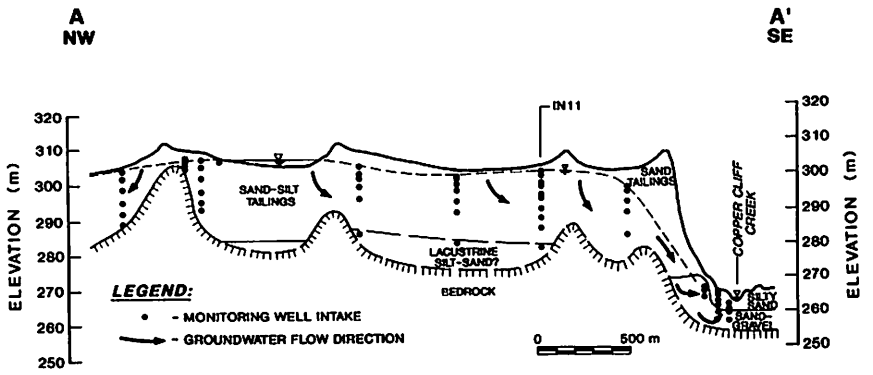

f

Figure 1.6. Groundwater flowpaths along section A—A' through the Copper Cliff tailings (adapted from Coggans, 1992).

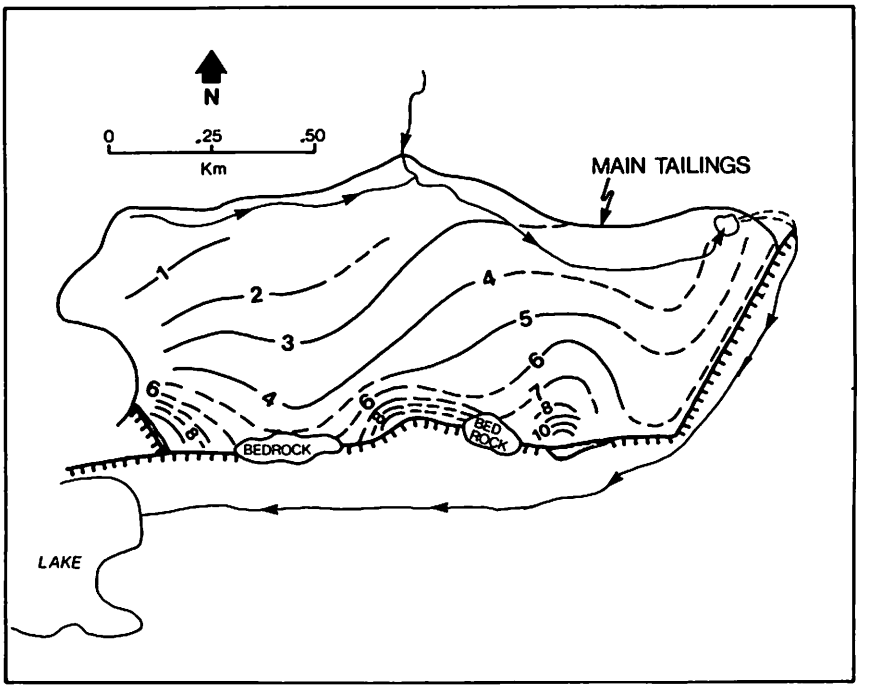

Figure 1.7. Depth to water-table in a decommissioned uranium-mine tailings impoundment, Elliot Lake, Ontario, where tailings spigotting occurred from the south perimeter dams (adapted from Cherry *et al.*, 1980).

decreasing seepage loss using techniques such as construction of impermeable dams, use of impermeable liners, and selection of disposal sites where shallow water-table depths are easily maintained, such as in lake basins. Past disposal practices, however, were commonly conducive to maintaining low water levels. Spigotting the tailings slurry from positions on the perimeter dams, as depicted in Figure 1.2, resulted in deposition of the more permeable coarser grained sediments in the upgradient near-dam area. As a

result, the dams were relatively leaky and low water-table levels resulted, particularly in the areas near the perimeter dams. Figure 1.7 shows depth-to-water in a decommissioned impoundment near Elliot Lake, Ontario, at which spigotting occurred from the south perimeter dams. The water-table depth is relatively shallow (<2 m) in the north-central area of the impoundment where finer grained tailings are present, but depth increases rapidly to up to 10 m as the more permeable near-dam area is approached.

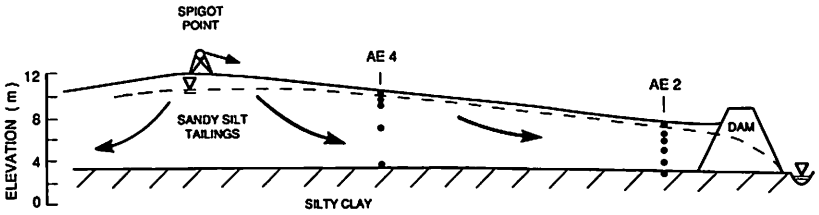

Figure 1.8. Water-table profile through a decommissioned gold-mine tailings impoundment, Joutel, Québec, where spigotting occurred from the impoundment center.

A method that can be used to maintain high water-table levels is the practice of spigotting from the center of an impoundment rather than from the periphery. In this way the more permeable deposits are restricted to the center of the impoundment whereas the less permeable fines are deposited around the periphery, thus helping to minimize leakage through the dams. Figure 1.8 shows the water-table profile through a decommissioned tailings impoundment of a gold mine near Joutel, Québec, where spigotting occurred from the impoundment center. Shallow water-table levels (<2 m depth) are shown to persist to within 50 m of the perimeter dam, largely as a result of the low-K tailings present in that area.

1.6. MONITORING NETWORKS

The primary monitoring device used to collect hydrogeologic information from tailings impoundments is the narrow-diameter monitoring well (piezometer) which has a screened tip that is usually short in length. The localized zone of intake allows measurement of hydraulic head, pore-water chemistry, and response testing for hydraulic conductivity at discrete depths within a tailings impoundment. Most impoundments exhibit distinct vertical gradation in chemistry, hydraulic head, and K; therefore, monitoring wells are usually arranged in nested configurations in which several wells are installed to various depths at a single location.

Well construction and installation techniques vary widely. Where drill-rig access is available, piezometers can be installed using a hollow-stem auger. The piezometer,

commonly constructed of PVC pipe, is installed into the tailings to the desired depth by insertion through the auger annulus, which acts as a removable casing. When drilling in tailings, care is usually exercised to minimize or eliminate the use of drilling fluids because considerable piezometer flushing may be required to remove these fluids after their introduction into the tailings formation.

Tailings sediments are generally loosely consolidated, and will usually slough into, and fill, an open borehole when drill casing is removed. In such circumstances it is commonly advantageous to use multiple-piezometer bundles, as these can provide multiple-depth, discrete-point sampling capability in a single borehole. The bundles consist of sampling tubes that are attached at various depth intervals to a rigid center stalk, usually of PVC pipe. Bundle-piezometer construction and installation techniques are described in detail by Cherry *et al.* (1983).

Where drill-rig access is limited, drive-point-type piezometers are commonly used. These are constructed of rigid pipe with a tapered drive-point, and they can usually be advanced with relative ease into sandy tailings using hand-portable percussion equipment. Figure 1.9 shows a piezometer nest where drive-point piezometers have been installed into the tailings to various depths; monitoring of an aquifer present below the tailings has been accomplished using a multiple-piezometer bundle installed using an auger drill-rig.

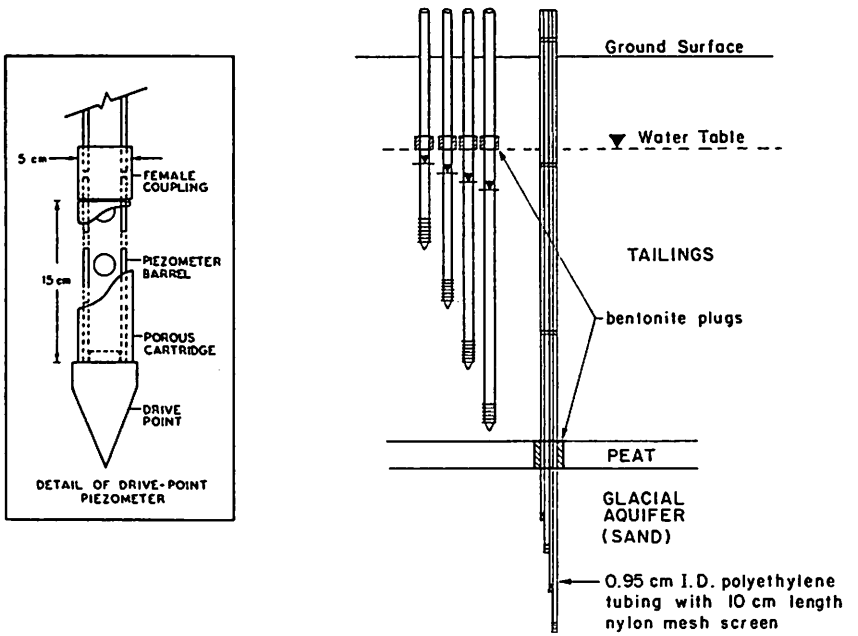

Figure 1.9. Schematic diagram of a piezometer nest consisting of drive-point-type piezometers in the tailings, and a bundle-type piezometer nest in the aquifer below the tailings (from Dubrovsky *et al.*, 1984).

In addition to not requiring drill-rig use, drive-points do not require introduction of drilling fluids, and they cause minimal disturbance of the tailings during installation. Auger drilling, on the other hand, may cause vertical mixing of pore water. This mixing can be a considerable disadvantage during tailings studies because vertically abrupt chemical trends are commonly present within sluggish flow systems in which disturbed pore water does not quickly migrate away from the monitoring zone. Figure 1.10 shows a comparison of chemical profiles provided by a drive-point piezometer nest and an adjacent auger drill-rig-installed piezometer bundle at a groundwater recharge area located on thick silty sand deposits similar in texture to tailings. Whereas abrupt vertical trends, in this case of tritium content, were established in the drive-point nest shortly after installation, the auger-drilled bundle provided erroneous tritium values for a period of more than two months after installation, reflecting the lingering effects of drilling-induced vertical mixing.

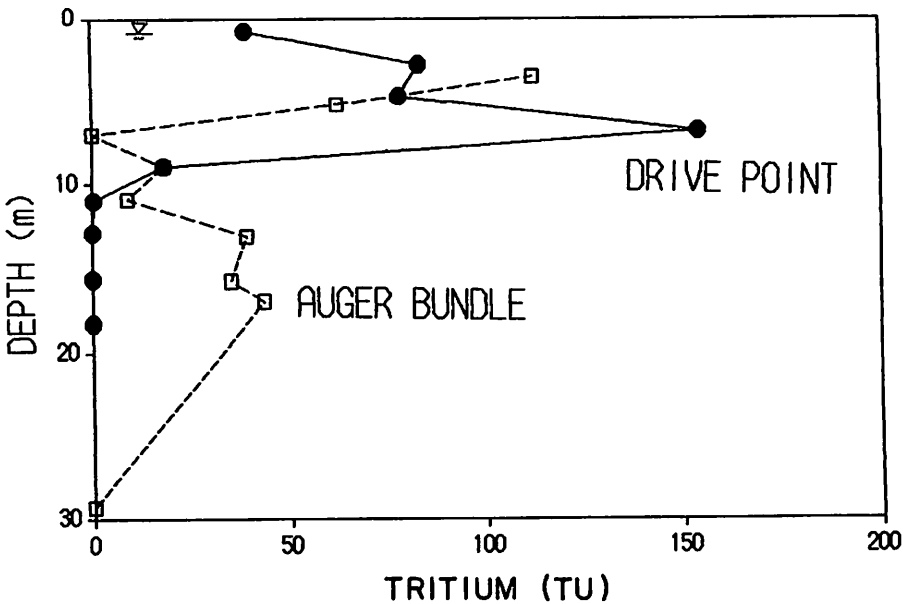

Figure 1.10. Comparison of tritium profiles at a silty sand recharge area obtained from a drive-point piezometer nest and from an adjacent auger drill-rig-installed multiple-piezometer bundle sampled two months after drilling (adapted from Robertson, 1992).

1.7. VADOSE-ZONE SAMPLING TECHNIQUES

Due to the fine-grained texture of tailings, the water content of the tailings material in the vadose zone may also be relatively high. In silt-rich sediments the zone

of tension saturation (capillary fringe) may extend several meters above the water table (Gillham, 1984). In the tension-saturated zone, suction lysimeters can be used to obtain pore-water samples. These devices consist of a porous ceramic cup, to which suction is applied using a vacuum pump to overcome the negative pressure head in the porous media, causing pore water to flow into the lysimeter. A second method of vadose-zone pore-water extraction is the core-squeezing technique described by Patterson *et al.* (1978). In this method an undisturbed core is retrieved in an aluminum tube, and pore water is extracted using machined end-pistons and a hydraulic jack (Figure 1.11). This method can be augmented with immiscible-displacement techniques that allow pore water to be extracted from cores that have even very low (5—10 vol. %) water contents.

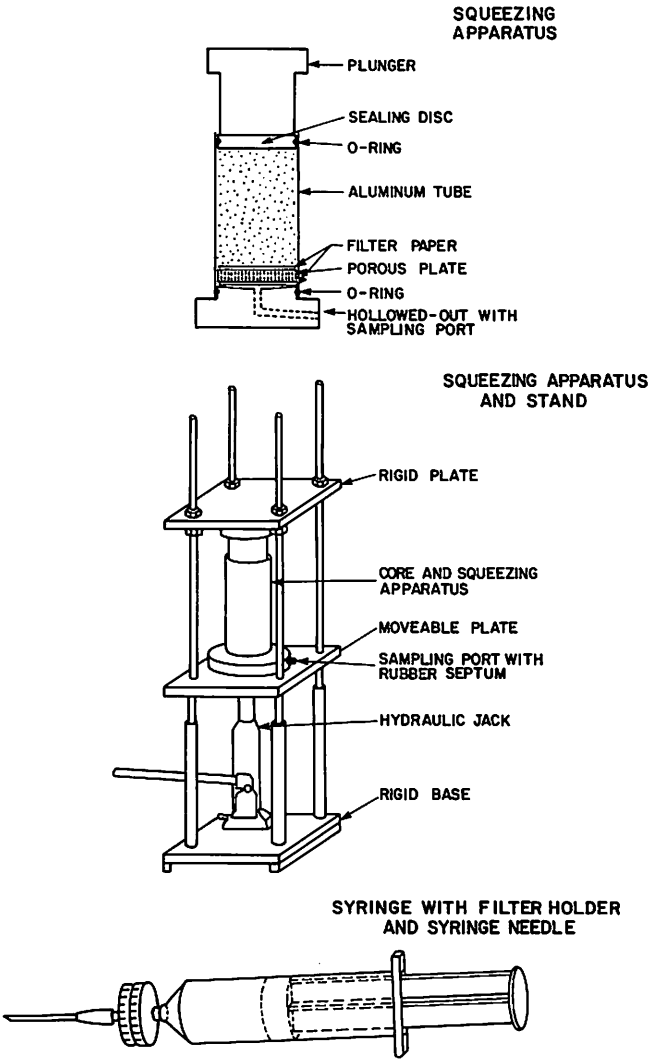

1.8. GROUNDWATER TRACERS AND RECHARGE ESTIMATION

After decommissioning, the tailings flow-system and the quantity of acid mine drainage that is generated is ultimately controlled by the rate of water-table recharge on the tailings surface. This rate may be difficult to estimate because of the complexity of the process and the seasonal variability that exists. Most tailings pore-waters, however, contain one or several mobile dissolved constituents that can serve as tracers to establish the downward rate of groundwater flow, thus allowing the rate of recharge to be estimated. One such tracer is tritium (^3H), a radioactive isotope of hydrogen (half life = 12.4 a) that is incorporated into the water molecule. Figure 1.12 shows 1989 ^3H distribution along section A—A' (Figure 1.5) through the Copper Cliff tailings area decommissioned in 1960. Groundwater with elevated tritium values (>100 TU) represents precipitation that recharged the water table in the mid-1960s, shortly after decommissioning, when atmospheric ^3H levels reached a peak due to atmospheric testing of hydrogen bombs. The position of the mid-1960s water, at about 12 m depth in 1989, indicates an average downward flow rate of about 0.5 m/a, which equates to a recharge rate of 0.25 m/a assuming a porosity of 0.5. This recharge rate is in the same range as other ^3H-indicated recharge rates on similar flat-lying, silty sand, non-tailings terrain in this region (Robertson and Cherry, 1989), and the rate represents about 30% of annual precipitation.

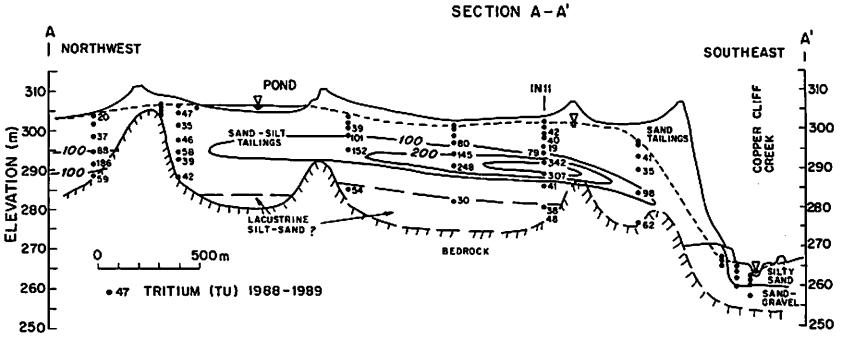

Figure 1.12. Tritium distribution in 1989 along section A-A_, Copper Cliff tailings (adapted from Coggans, 1992).

Figure 1.11. (facing page) Core-squeezing apparatus for obtaining pore-water samples from above the water table (from Smyth, 1981).

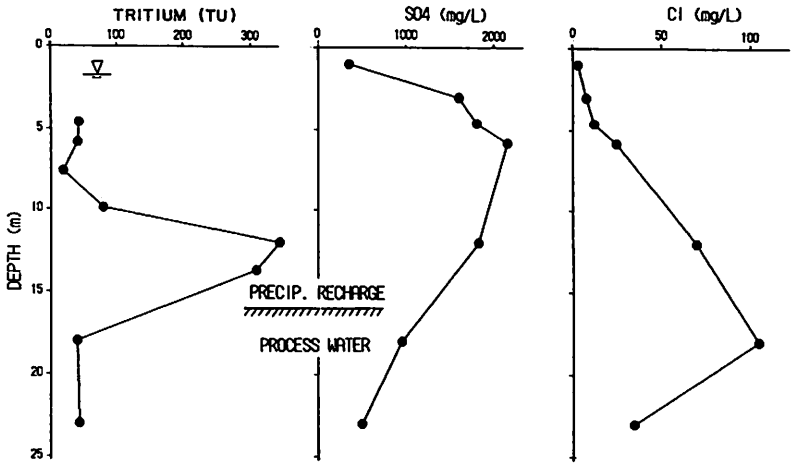

Figure 1.13. Comparison of ^3H, SO_4^{2-}, and Cl^- levels in process-water and precipitation recharge-water at nest IN11, Copper Cliff tailings (adapted from Coggans, 1992).

At the Copper Cliff site, the tritium plume marks the approximate boundary between the underlying pre-1960 process-water and the overlying precipitation recharge-water. Groundwater origin can also be distinguished by other mobile constituents that are in contrast in the two zones (*e.g.*, Dubrovsky *et al.*, 1984a; Coggans, 1992). Figure 1.13 compares the ^3H profile at nest IN11 in the Copper Cliff tailings to the profiles of SO_4^{2-} and Cl^- at the same location. Precipitation-derived pore water is shown to have much lower Cl^- levels (<50 mg/L) but substantially higher SO_4^{2-} levels (>1400 mg/L) than the process-water; thus, both of these parameters can be used as tracers to establish the rate of water-table recharge. In this case, the results from all three tracers (^3H, Cl^-, and SO_4^{2-}) give similar vertical flow velocities (0.3—0.5 m/a). Increased SO_4^{2-} levels are the result of vadose-zone sulfide-oxidation processes that have become more active after decommissioning.

Other groundwater age-dating techniques that have been investigated recently and offer promise as tracers in tailings studies are the use of ^3He, which is the daughter product of ^3H radioactive decay (*e.g.*, Solomon *et al.*, 1992), and the use of chlorofluorocarbons (*e.g.*, Busenberg and Plummer, 1992). These two methods offer the potential of providing very precise age estimates in recently-recharged groundwater.

1.9. CONCLUSIONS

Groundwater flow conditions in tailings impoundments are site specific and can vary widely depending on a number of factors such as impoundment geometry and thickness, depositional mode, grain size, dam permeability, permeability of surrounding formation material, water-table elevation, and climatic conditions. In addition, the hydraulic sorting that occurs during the deposition of most slurried tailings results in the development of sedimentary anisotropy and heterogeneity over the impoundment area. In many cases, flow conditions can be established only after very detailed and time-consuming site investigations have been conducted.

A method that can aid in providing additional insight into site-specific tailings flow systems is the use of computer flow models. Models allow flow systems to be simulated numerically if values are available for the important parameters that govern flow, or the models can provide, through calibration procedures and sensitivity analyses, estimates for those parameters.

Chapter 2

Modelling of Mill-Tailings Impoundments

E.O. Frind, J.W. Molson
Waterloo Centre for Groundwater Research
Department of Earth Sciences
University of Waterloo, Waterloo, Ontario N2L 3G1

2.1. INTRODUCTION

Mathematical models are tools that help us to understand the physical, chemical and biochemical processes taking place in groundwater systems. The models also help us to understand the complex interactions between these processes, and they provide the information we need in order to help manage our groundwater resources and reduce environmental contamination (see, for example, Schwartz, 1990). Groundwater modelling is therefore of particular use in the study of the potentially serious threat to groundwater resources posed by mill-tailings impoundments.

In this Chapter, we present an overview of the most common modelling approaches used to simulate hydrogeological systems, in particular, the impact of mill-tailings impoundments. The focus is on simulating groundwater flow and contaminant mass transport within saturated porous aquifers. The relevant flow and transport processes are illustrated through analytical and numerical simulations of generic mill-tailings sites, as well as specific case studies. Emphasis is placed on developing conceptual models, use of correct model-boundary conditions, and understanding the limitations of model predictions. Included are recent state-of-the-art simulations of multicomponent reactive transport of mill-tailings contaminants.

2.1.1. Hydrogeologic Processes

The behavior of contaminants in the subsurface is affected by a variety of physical, chemical, and biological processes. When a dilute chemical contaminant enters a typical porous medium, it is transported by the background flow-field (advection); the contaminant will disperse because of microscopic variations in the velocity field (mechanical dispersion) and because of random motion (molecular diffusion). A contaminant may also be retarded by adsorption, or it may decay due to radioactive processes (see, for example, Domenico and Schwartz, 1990).

Let us start with one of the most basic solute-transport processes: advective transport of a non-reacting substance (such as chloride). Let us assume that the solute is dissolved at a low concentration within a saturated porous groundwater system under isothermal conditions. (Saturated flow conditions exist beneath the water table where the pores are completely filled with water). In advective transport, particles of the dissolved contaminant are simply carried along with the flowing groundwater at a velocity u [L/T]. In a porous medium with hydraulic conductivity K [L/T], porosity θ, and hydraulic gradient ∇h, the contaminant velocity is given by $v = -(K/\theta)\nabla h$ (Freeze and Cherry, 1979). To describe this advective process, we must be able to simulate the flow system with reasonable accuracy. We will therefore devote the first section of this Chapter to modelling groundwater flow systems.

The second basic transport process is dispersion. On a small scale, this process describes the spreading of the dissolved contaminant due to the tortuous flow paths in the pore space of the aquifer material. On a larger scale, the process also describes the spreading due to geologic lenses, stratification, and other irregularities in the material. The dispersion process, therefore, depends on the spatial scale of the problem. Incorporating the different dispersion scales into a model is not straightforward. Usually the problem is circumvented by assuming the largest dispersion scale to be the dominant one. Unfortunately, dispersive parameters cannot be measured directly, except by highly sophisticated and expensive techniques. In routine investigations, the dispersion parameters are usually estimated, requiring some experience and judgment.

Beyond these basic processes, however, a host of other processes may occur in a groundwater system. As a rule, at least some of these are dependent upon other processes. Systems in which such inter-dependence occurs are known as nonlinear systems.

One example of a highly nonlinear system is the transport of chemically reacting contaminants which can occur within and downstream of mill-tailings impoundments. In such systems, the various chemical components of the groundwater are continually exposed to new chemical environments while being transported. This causes a continual re-equilibration and redistribution of mass among the various constituents. Thus, the fate of every component of the system depends on the behavior of every other component, as well as on the driving forces acting on the flow system and the boundary conditions.

Another example of nonlinearity occurs when a contaminant concentration is high enough that the fluid density is noticeably greater than the density of the resident groundwater. The denser fluid will sink and the lighter fluid will rise in the aquifer, with the degree of motion dependent on the relative concentration contrast. Density effects also exist when water in some part of the system is at a different temperature than in other areas. In a mill-tailings impoundment, for example, sulfide-oxidation

reactions generate heat which can be transferred to an underlying, cooler aquifer. Reactive mass-transport and density coupling are just two examples within a common group of coupled processes that are the rule rather than the exception in natural systems.

Despite these complex processes, one common modelling approach is to simulate first the transport of a conservative species (chloride, for example) which will represent a worst-case scenario in terms of travel distance. More complex reactions can then be added, depending on the scope of the investigation and on the availability of field data.

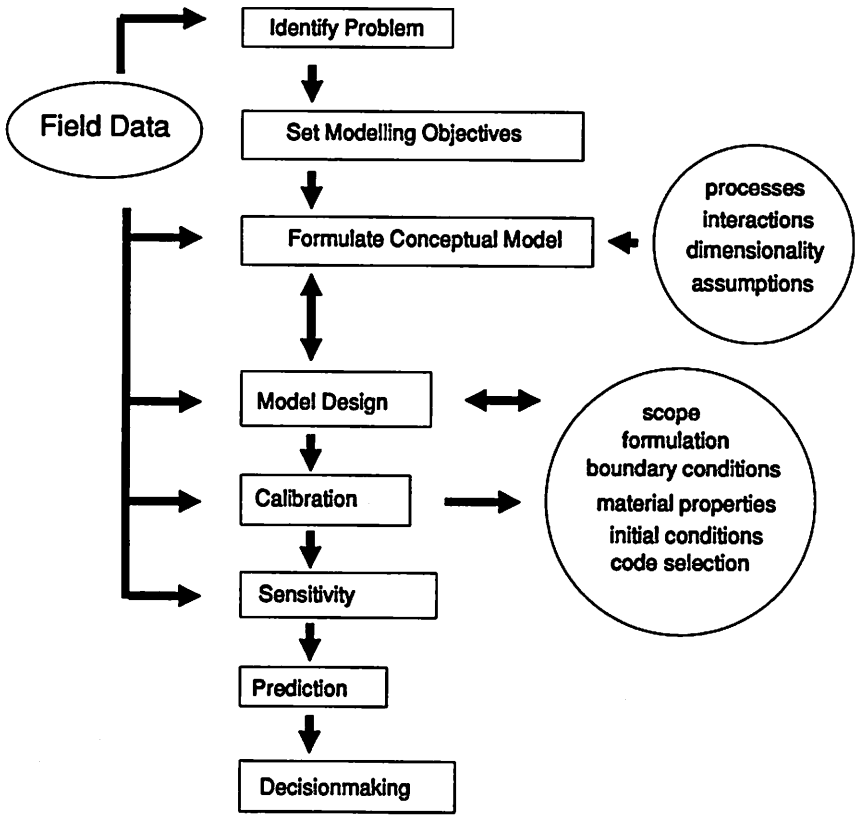

Figure 2.1. A simplified flowchart of the modelling process.

2.1.2. *The Modelling Process*

The modelling process begins with identifying and defining the problem, and setting the modelling objectives (Figure 2.1). The objectives in modelling a mill-tailings impoundment, for example, commonly focus on a determination of the chances of a

contaminant reaching a critical point at concentrations beyond drinking-water objectives, or on a comparative evaluation of various remediation strategies. Tsang (1991) reviewed some important issues related to groundwater modelling.

Typical questions to be addressed by a hydrogeological model can include:

- what are the possible migration paths and travel times of contaminants?
- what is the relative importance of the various processes and parameters on the system?
- what is the possible worst-case scenario?
- how effective might natural or artificial remediation processes be in removing contaminants?
- are there limitations to the existing field data, and if so, what additional data are required, and from where should they be obtained?

The key step is to formulate a conceptual model of the tailings site. As the real hydrogeological system is invariably complex, we create an idealization of this system which, in essence, incorporates whatever we know about it. The information consists of the extent, configuration, and properties of the hydrogeological units, as well as the processes relevant to our objectives. The coupling and interactions among these processes is particularly important, as are the assumptions that justify excluding certain processes or interactions. In selecting dimensionality, for example, we must consider what spatial dimensions are necessary to properly represent the selected processes in the given system. As a rule, we choose the simplest dimensionality that will satisfy the objectives.

In most porous media, advective—dispersive transport is usually dominant. In low-permeability material, however, diffusion may become the primary mode of transport, whereas in fractured or heterogeneous porous media, both advection and diffusion may be significant. The characterization of these different processes is important because this will form the basis of the conceptual model, and will dictate the transport modelling approach or solution technique required.

On the basis of the conceptual model, we can design the physically-based mathematical model. This step involves identifying the governing physical principles and the corresponding equations that express these principles, the definition of boundary and initial conditions and material properties, and the selection and implementation of the solution method. Solution methods can be broadly divided into analytical and numerical methods. Table 2.1 summarizes the advantages and disadvantages of each. Several texts are available which introduce the use of analytical and numerical solutions to hydrogeological problems (*e.g.*, Pinder and Gray, 1977; Huyakorn and Pinder, 1983; de Marsily, 1986; Kinzelbach, 1986; Luckner and Schestakow, 1991; Anderson and Woessner, 1992).

Once the conceptual model is developed, the solution domain must be defined, boundary conditions chosen, and depending on the chosen solution method, discretized in some way. Discretization methods vary considerably, depending on the type of model and solution method. Finite-element methods tend to favor triangles, or tetrahedra and triangular prisms in three dimensions (3D), because of their simplicity and versatility in defining irregular geometry. Deformed quadrilaterals or deformed-brick elements are also common in finite-element models (Figure 2.2). Finite-difference methods most commonly use rectangular-based cells, either node- or block-centered.

Table 2.1. Comparison of common solution methods

Solution Method	Advantages	Disadvantages
Analytical	• provides an exact solution • computationally less demanding	• less realistic • less versatile • restricted to linear systems • properties must be uniform
Particle Tracking	• commonly low computational demands • no numerical dispersion • well-suited for advective problems, pathlines, capture zones • no matrix solution required	• sophisticated velocity interpolation required • local concentrations are difficult to define • complex processes difficult to include
Numerical Finite-difference Method (FDM)	• relatively simple compared to FEM • may require less memory than FEM • versatile • coupled systems can be solved	• computationally demanding • geometry must be simple • grid layout less flexible • susceptible to numerical dispersion
Numerical Finite-element Method (FEM)	• geometry can be complex • realistic and versatile • coupled systems allowed • grid layouts very flexible	• computationally demanding • susceptible to numerical dispersion

Finally, the hydrogeologic information has to be processed in some way compatible with the chosen computer code and method of discretization.

Often, the first application of a model is calibration. In cases where one of the model parameters, for example dispersivity, is unknown, calibration can be used to estimate this parameter from the model by fitting a simulation to an observed response under controlled conditions. Commonly, only one such parameter can be determined uniquely by calibration. If more than one parameter is unknown, fits may be obtained

with different combinations of parameters; however, the parameter selection will then be non-unique.

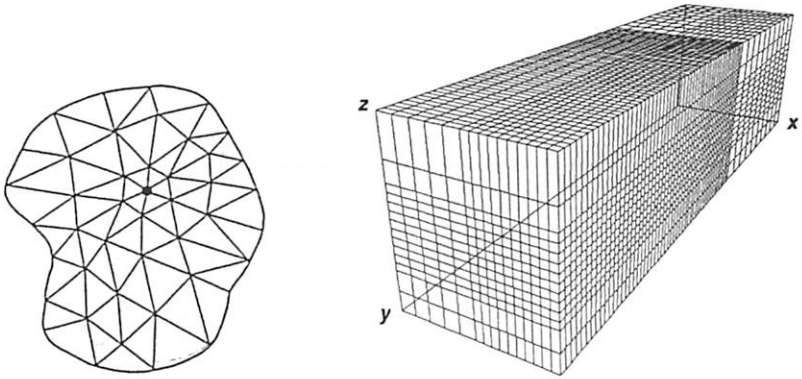

Figure 2.2. Sample 2D triangular and 3D block prismatic finite-element grids.

One of the most important uses of models is in determining the sensitivity of the system with respect to the various parameters. A sensitivity analysis is usually done by defining a base case, and then varying the parameters, one at a time, within their respective ranges. These ranges are generally known to an experienced hydrogeologist and are fairly well-defined, although the actual parameter values may not be accurately known. Sensitivity analyses provide the hydrogeologist with insight about the behavior of the system under various conditions, and about the importance of the individual parameters and processes.

Throughout conceptualization, design, validation, and calibration, gaps in the available data can be identified and remedied, and new data can be incorporated. This process also gives insight into the value of new data in relation to the corresponding improvement in the simulation results.

2.1.3. Errors and Misconceptions in Modelling

A model can provide valuable insight and understanding in site investigations but, if used incorrectly, model results can be misleading. Interpretive errors and misconceptions can result from losing sight of the underlying assumptions, from using a model in situations for which it is unsuited, from using inappropriate or grossly incomplete data, and from placing undue faith in the computational precision of the model. Some key limitations are:

Structural Limitations

The model can only handle processes for which it has been designed. The user should remain alert for the possibility that a process which is significant in a particular application is not accounted for in the model. This possibility exists if the model response differs significantly from the response observed in the field. Standard assumptions such as steady-state flow, isothermal conditions, and negligible fluid and aquifer compressibility must be recognized.

Dimensionality

Is the dimensionality of the chosen model compatible with the real problem? For example, the likely presence of density effects or chemical processes indicates that the vertical dimension is essential. If, in addition, the source is of small extent and the flow field is complex, a 3D model may be needed.

Data Limitations

Have all significant hydrogeologic characteristics been identified? For example, a window in an aquitard could mean that the contaminant enters a different aquifer than expected. Low-permeability lenses can retain contaminant mass which can substantially increase cleanup times in remediation schemes.

Non-uniqueness

This problem can arise when more than one parameter is unknown. In a flow model, for example, if the hydraulic conductivity and recharge are not known accurately, vastly different flow velocities can result even though the hydraulic-head solution matches the observed data. This case of non-uniqueness occurs because the hydraulic head is only dependent on the ratio of recharge to conductivity. Similar examples occur in contaminant transport.

Undue Faith in Numerical Precision

Numerical results can be highly impressive when printed out to many significant figures, or plotted in the form of smooth curves and contours. The modeller must keep in mind, however, that the accuracy of the results is no better than the accuracy of the data that went into the model.

Above all, however, one must realize that a mathematical model is merely a conceptual model, never the real world itself. Any prediction, therefore, is valid only under the condition that the conceptual model is a reasonable and valid representation of the real system.

2.2. MODELLING GROUNDWATER FLOW

2.2.1. 2D Steady-state Groundwater Flow

Many groundwater-flow processes relevant to the study of mill-tailings impoundments can be illustrated through the simplified two-dimensional flow system of Figure 2.3. This conceptual model consists of an unconfined aquifer with an impermeable base, a no-flow (symmetry) boundary at the left, recharge across the upper water table, and discharge to a down-gradient stream. The unsaturated zone above the water table can be neglected if its thickness is small relative to the horizontal-flow distances within the aquifer. In considering the aquifer in the vertical plane, we are neglecting transverse horizontal-flow gradients.

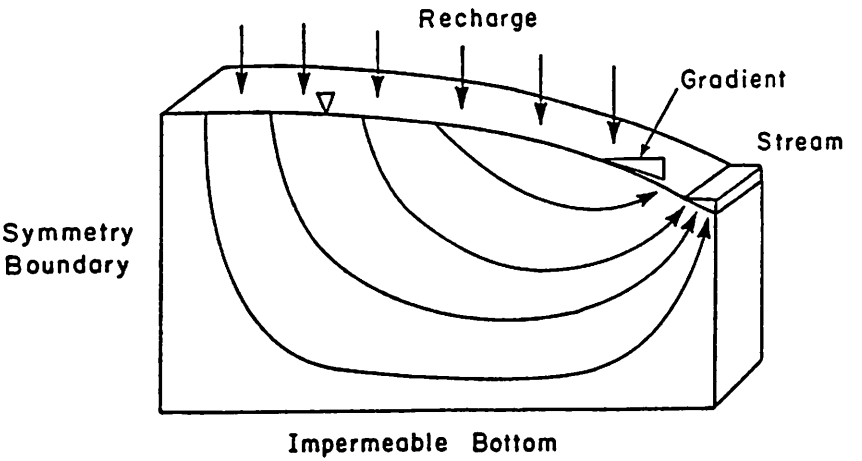

Figure 2.3. A conceptual model of an unconfined aquifer.

From a flow-modelling perspective, the relevant aquifer properties are its geometry (length, thickness, and base elevations), the hydraulic conductivity distribution (Kx, Ky), porosity (θ), the elevation of the water table, and estimated recharge to the aquifer. As we cannot know these properties exactly, we make simplifying assumptions and calibrate those that are unknown. Often, as a first approach, we can assume that the flow system is at steady state and that the flow model is calibrated to match the long-term average water-table elevations.

Real aquifers or aquifer—aquitard systems are generally either of sedimentary origin or contain some degree of fracturing. In either case, the hydraulic conductivity can in most cases be expected to differ in the horizontal and the vertical directions. Sandy aquifers, for example, are rarely homogeneous but contain many different thin layers or lenses. In such a case, the horizontal conductivity will be dominated by the more permeable layers, whereas the vertical conductivity will be dominated by the less

permeable layers, with the result that the horizontal component is, as a rule, greater. The detailed hydraulic conductivity structure can be an important component of a successful flow model.

At most mill-tailings sites, flow in the vertical dimension will be of prime concern because of active depth-dependent processes, complex aquifer stratification, or the potential for vertical contaminant migration to underlying aquifers. A powerful method of solving steady-state, saturated-groundwater flow problems involves the use of both hydraulic head (h) and streamfunctions (ψ), in what is known as the "dual formulation" (Frind and Matanga, 1985). The technique is useful because it defines groundwater travel paths directly. Groundwater flow velocities are also more accurate when determined using streamfunctions, whereas velocities defined by hydraulic head gradients are highly susceptible to roundoff error within long and thin domains (*i.e.*, where the length to thickness ratio is 100:1 or greater).

Flownet models assume steady-state, isothermal conditions, and aquifer deformation due to dewatering is neglected. If the streamlines are used to interpret advective contaminant transport, the dispersion process is assumed not to be significant.

In two dimensions, the corresponding equations for hydraulic potential (h) [L] and streamfunctions (ψ) [L^2/T] are given by

$$\frac{\partial}{\partial x}\left(K_{xx}\frac{\partial h}{\partial x}\right) + \frac{\partial}{\partial y}\left(K_{yy}\frac{\partial h}{\partial y}\right) = 0 \qquad (1)$$

$$\frac{\partial}{\partial x}\left(\frac{1}{K_{yy}}\frac{\partial \psi}{\partial x}\right) + \frac{\partial}{\partial y}\left(\frac{1}{K_{xx}}\frac{\partial \psi}{\partial y}\right) = 0 \qquad (2)$$

where K_{xx} and K_{yy} are the principal components of the hydraulic conductivity tensor. Matanga (1993) has recently extended the theory to handle 3D geometries.

The dual formulation generates a quantitatively accurate flownet which can be used to evaluate groundwater flux rates and to determine the advective travel paths of a groundwater contaminant. A full theoretical development using finite elements is given by Frind and Matanga (1985), and a field-scale application is provided in Frind *et al.* (1985).

Constraints for model calibration are provided by observed hydraulic head data in the vertical section, including the position of the water table. In a flownet model, the hydraulic conductivity and surface recharge are common calibration parameters because the estimated or observed range of these variables can be quite large.

The boundary conditions for the potential formulation can be either first type (fixed head) or second type (specified flux) (Figure 2.4). Symmetry, or flow-divide boundaries, and impermeable boundaries are both represented using a zero-gradient boundary condition (Frind and Matanga, 1985). At inflow or outflow boundaries, either boundary condition is acceptable; where natural outflow boundaries do not exist, however, they should be placed at a distance where they will not interfere with the solution in the area of interest. To obtain a unique solution, at least one boundary portion must be a fixed head. As the streamfunction boundary conditions can be derived from those of the potential equation, models of this type usually require only the potential boundary conditions to be specified by the user.

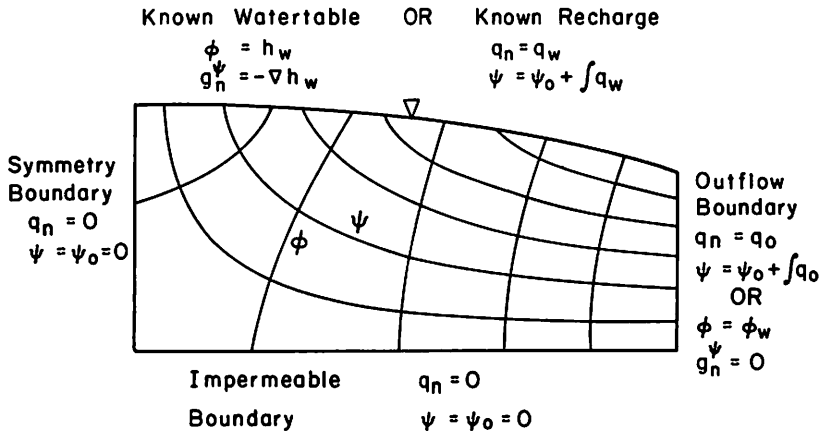

Figure 2.4. Typical boundary conditions for use in a flownet model.

Equations (1) and (2) must be solved numerically in order to handle arbitrary geometry or heterogeneous properties. The flow domain must therefore be discretized, and, to reduce numerical error, the aspect-ratio criteria, which are given by

$$\frac{K_{xx}}{\Delta x^2} \approx \frac{K_{yy}}{\Delta y^2} \qquad (3)$$

must be satisfied where Δx and Δy are the grid spacings in the x and y directions, respectively.

Flownet Model Applications

A flownet modelling approach can be applied to either the mill-tailings deposit itself, or to a connected aquifer, provided that the medium is assumed porous, saturated, and at steady state. We present here one example of each case. The first illustrates a flownet model of the Nickel Rim tailings impoundment at Sudbury,

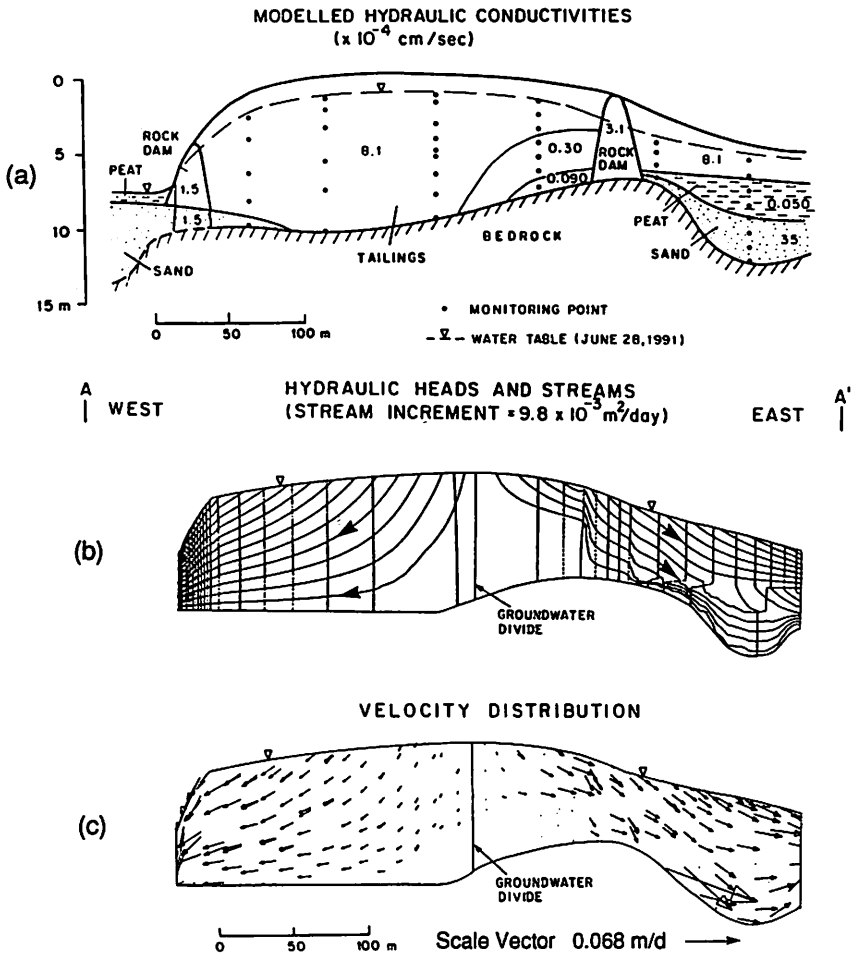

Figure 2.5. A flownet model of the Nickel Rim tailings impoundment, Sudbury, Ontario: (a) model domain and calibrated hydraulic conductivity distribution; (b) groundwater flownet; (c) velocity field. (After Johnson, 1993; vertical exaggeration = 10x).

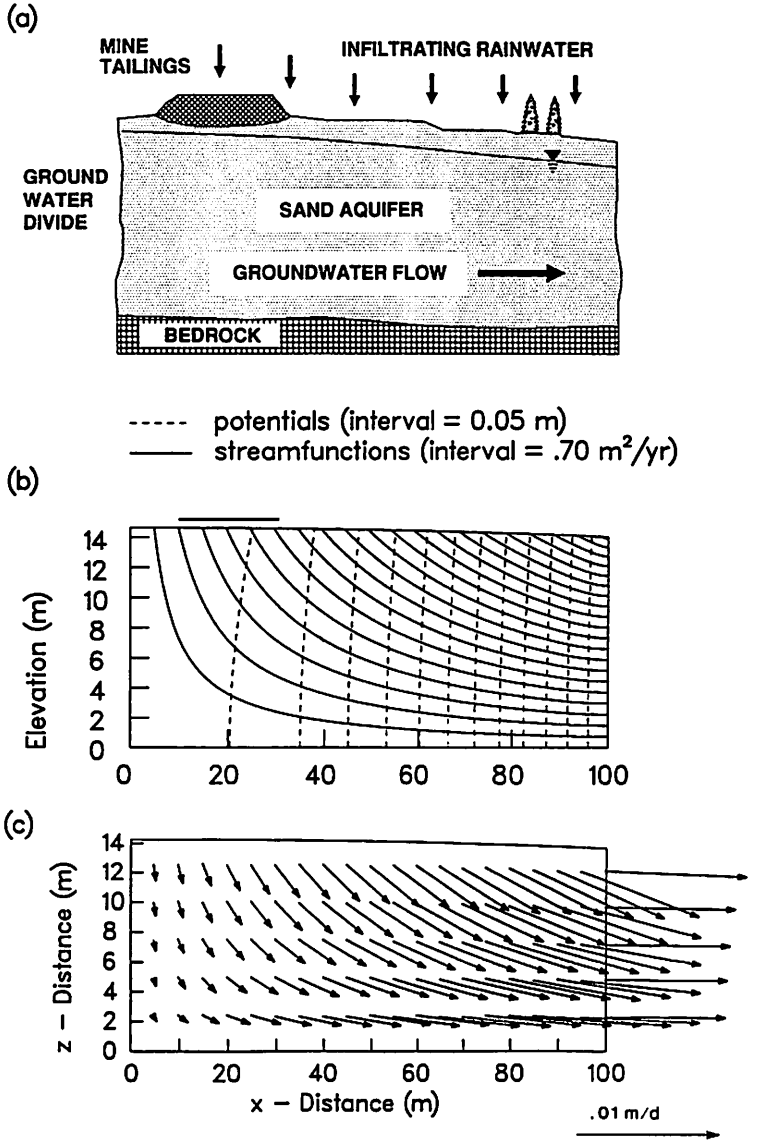

Figure 2.6. A flownet model of a saturated aquifer below a mill-tailings site: (a) conceptual model and flow boundary conditions; (b) simulated groundwater flownet; (c) velocity vector field.

Ontario, and the second is a flownet model of an aquifer below a hypothetical tailings deposit. The second example provides the flow field for the 2D contaminant-transport simulations presented in later sections of this Chapter.

In his study of the Nickel Rim mill-tailings impoundment, Johnson (1993) applied the interactive finite-element FLONET model (Guiguer *et al.*, 1994) to simulate hydraulic potentials and groundwater flowpaths within the porous tailings. In the chosen vertical cross-section, the tailings deposit is approximately 250 m long by 10 m high, and is situated above impermeable bedrock. The tailings deposit is bounded on each side by permeable rock dams. The flow system was simulated by applying constant-head conditions along the left and right boundaries just beyond the dams, a no-flow condition along the bottom, and a recharge of 24 cm/yr across the water table. Hydraulic conductivities varied from 0.05×10^{-6} to 35×10^{-6} m/s (Figure 2.5a). The flownet solution and corresponding velocity vectors are provided in Figure 2.5b and 5c, respectively. The model reproduced the observed flow divide within the center of the tailings, and the simulated travel paths correlated well with the observed contaminant distribution. Using the streamtubes from the flownet solution, Johnson (1993) then applied a 1D transport model to predict contaminant migration and impact to the adjoining aquifers.

We now consider a hypothetical mill-tailings impoundment where a tailings site overlies an unconfined aquifer similar to our conceptual model of Figure 2.3. The aquifer is bounded by an impermeable bedrock base, a no-flow (symmetry boundary) upgradient from the tailings, and the right discharge boundary is assumed at a uniform hydraulic head of 14 m (Figure 2.6a). A recharge of 14.2 cm/yr is applied as the boundary condition along the water table.

The cross-sectional domain measures 100 x 14 m and is discretized into 200 x 56 elements of size 0.5 m horizontally x 0.25 m vertically. The aquifer is assumed isotropic and homogeneous with a hydraulic conductivity of 2.5×10^{-6} m/s, and the porosity is 0.3.

We apply the FLONET model (Guiguer *et al.*, 1994) to simulate the hydraulic head and streamfunction distribution for this problem. Figure 2.6b provides the steady-state hydraulic head and streamfunction flow solution, and the velocity vector field is provided in Figure 2.6c. As the top boundary in this simulation is not constrained, we allow the water table to reach its natural equilibrium position. This is the most realistic approach where, at a real field site, the aquifer recharge and hydraulic conductivity can be varied until the simulated water table matches that observed. This same flow system will be used in Section 2.3.4 and 2.4.3 to illustrate the advective—dispersive transport of mill-tailings contaminants.

2.2.2. *Unsaturated Flow*

In a large-scale groundwater model, it is common practice to neglect the unsaturated zone if its depth is not significant relative to the aquifer thickness, and if the areal extent of the site is large. From a mill-tailings perspective, however, the unsaturated zone may be important because the availability of oxygen can have important consequences on oxidation rates, and hence can significantly affect the source concentrations and contaminant-plume evolution.

The distinction between the saturated and unsaturated zones is critical from a flow-modelling perspective because in the unsaturated zone the hydraulic conductivity becomes a nonlinear function of the moisture content, which can vary in depth over a range as small as a few centimeters. This variation must be well-resolved by the model, which then requires much finer grids and a higher computational effort compared with that required for the saturated zone alone. A model of variably saturated flow must be run in either the 2D vertical section, or in a fully 3D domain.

In addition to the data required to run a model of saturated flow, to run a model of variably saturated flow it is necessary to obtain detailed vertical profiles of pressure head, and field or lab data defining the variation of hydraulic conductivity with moisture content. A fully three-dimensional model for simulating variably saturated flow is described by Huyakorn *et al.* (1986), and Therrien (1992) presents a 3D variable-saturation model for fractured media.

2.2.3. *Three-dimensional Groundwater Flow*

Many field-scale flow systems are inherently complex because of a heterogeneous conductivity distribution and irregular geometry. These conditions commonly demand a three-dimensional simulation. Furthermore, if the effects of remediation wells are to be simulated, or if the problem is non-linear, a fully transient approach is usually required.

In a 3D approach, the steps involved in developing the model and defining boundary conditions are identical to those of a 2D model, only now there are two additional boundary surfaces to consider. Although the larger grid of a 3D domain increases the computational effort by about an order of magnitude over a 2D simulation, today's efficient algorithms and high-speed computers make 3D simulations a viable option.

Under transient conditions in a 3D homogeneous, isotropic groundwater system, saturated groundwater flow is represented by the equation:

$$\frac{\partial}{\partial x}\left(K_{xx}\frac{\partial h}{\partial x}\right) + \frac{\partial}{\partial y}\left(K_{yy}\frac{\partial h}{\partial y}\right) + \frac{\partial}{\partial z}\left(K_{zz}\frac{\partial h}{\partial z}\right) - Q = S_s\frac{\partial h}{\partial t} \quad (4)$$

where x, y, and z are the spatial dimensions, K_{xx}, K_{yy}, and K_{zz} are the respective hydraulic conductivities, S_s is the storage coefficient, h is the hydraulic head, Q is a source or sink, and t is time. The form of (4) assumes x, y, and z follow the principle directions of K_{ij}. Equation (4) is the mathematical statement of the Law of Conservation of fluid mass. It considers the water balance in a control volume, and equates the change in the water flowing through the volume (left-hand-side) to the change in the water stored in the volume during a unit of time, t (right-hand side).

The parameter S_s is the specific storage, which represents the volume of water that is stored (mainly due to elastic compression of the soil skeleton and expansion of water) under a unit increase in head. The equation is based on the assumption that the stratification in the aquifer coincides with the coordinate directions. A more general form valid for arbitrary directions can be found in Bear (1972).

In a study of contaminant migration from a surface waste disposal site, Frind and Molson (1989) used the steady-state form of (4), obtained by setting the right-hand-side to zero, to simulate the 3D field of groundwater flow within a shallow, unconfined aquifer. Although the contaminant source in this example is a landfill and not a tailings deposit, this case study provides a good example of a 3D modelling approach suitable for mill-tailings sites because, assuming a non-reactive contaminant, the basic flow and contaminant-transport processes are identical.

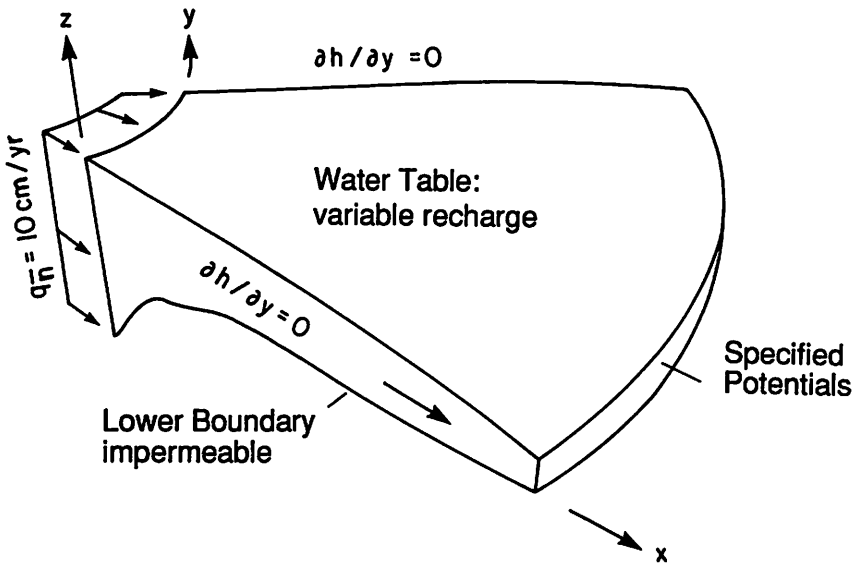

Figure 2.7. Boundary conditions in the 3D flow model (after Frind and Molson, 1989).

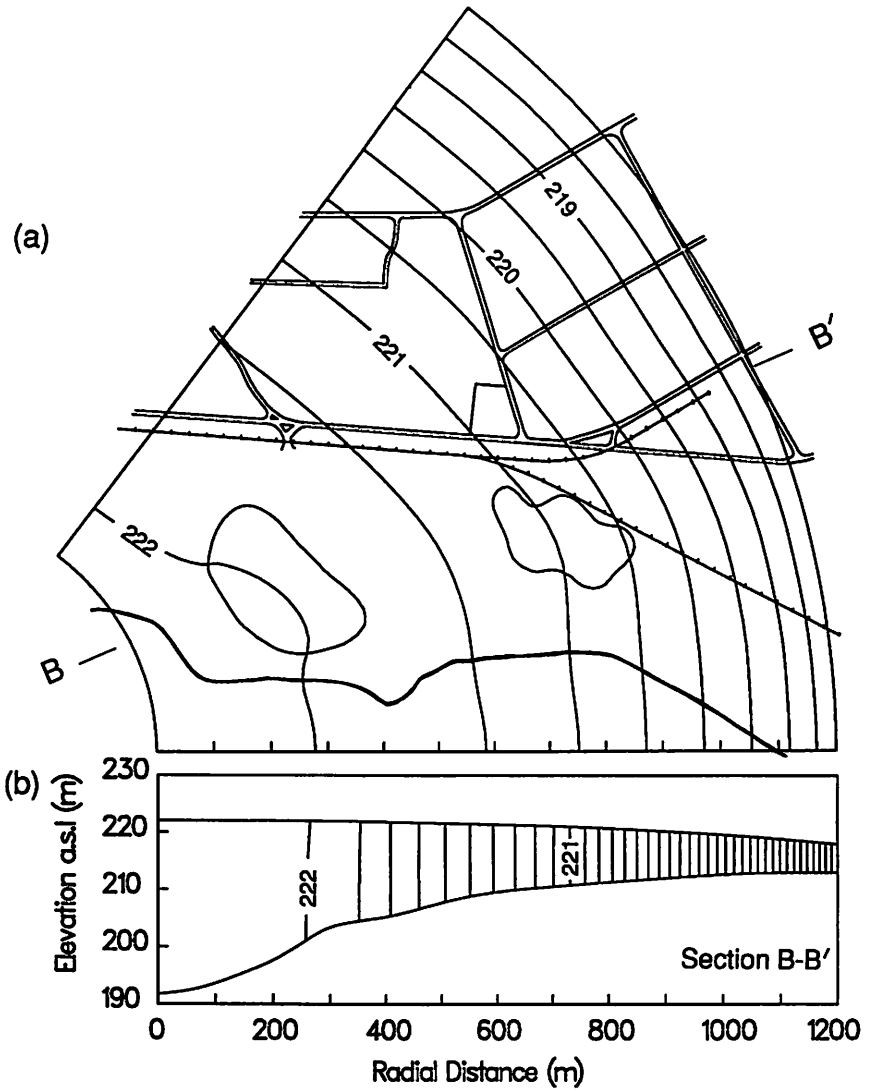

Figure 2.8. Simulation of 3D hydraulic head flow: (a) plan view of water-table elevations (contour interval is 0.5m); (b) longitudinal cross-section (contour interval is 0.1 m).

Boundary conditions for the 3D flow domain are shown in Figure 2.7. Lacking nearby natural flow boundaries, a wedge-shaped domain was designed to accommodate the observed diverging flow field and the anticipated future extent of the contaminant plume. A groundwater influx was assigned at the upgradient boundary, constant heads along the downgradient boundary, and a recharge flux assigned across the upper water-table boundary. The two vertical transverse boundaries were assumed symmetry boundaries and were therefore represented with a zero head-gradient. The region was resolved with 27,000 elements, and the flow model required approximately 20 Mbytes of memory to run.

The flow system is simulated here using an approach similar to that used by Frind and Molson (1989) but we use instead a more robust finite-element flow model (FLOW3D; WCGR, 1994). The model was calibrated by adjusting the hydraulic conductivity and recharge until the simulated heads matched those observed. From the hydraulic-head solution (Figure 2.8), it is clear that the water-table gradient dominates the 3D flow field. Subtle vertical gradients below the source, although not visible in Figure 2.8b , did have a significant influence on the simulated behavior of leachate contaminants (see Section 2.4), justifying the use of a fully 3D approach.

2.3. MODELLING CONTAMINANT TRANSPORT

2.3.1. Theory

Techniques for modelling advective—dispersive transport have been studied intensively over the last fifteen years. Assuming isothermal conditions, insignificant density differences, and a non-deforming porous medium, the governing differential equation is given by

$$\frac{\partial}{\partial x_i}\left(\frac{D_{ij}}{R}\frac{\partial c}{\partial x_j}\right) - \frac{v_i}{R}\frac{\partial c}{\partial x_i} - \lambda c = \frac{\partial c}{\partial t} \qquad (5)$$

where x_i are the spatial coordinates [L], t is time [T], $c = c(x_i, t)$ is the concentration [M/L^3], vi is the average linear pore-water velocity [L/T], D_{ij} is the hydrodynamic dispersion tensor [L^2/T], and where the decay constant, λ [T^{-1}], is given by

$$\lambda = \ln(2) / t_{1/2} \qquad (6)$$

with t1/2 being the half-life [T]. The form of (5) assumes the adsorbed phase also decays, and at the same rate as that of the solution phase. Adsorption is represented here as a linear equilibrium-partitioning process between the dissolved and adsorbed phases where R is the retardation coefficient (Freeze and Cherry, 1979), given by

$$R = \left(1 + \frac{\rho_b K_d}{\theta}\right) \tag{7}$$

where ρ_b is the bulk density of the saturated porous medium, θ is the effective porosity, and K_d is the distribution coefficient [L^3/M] that governs the partitioning of the solute into dissolved and adsorbed phases.

The boundary conditions for equation (5) can be either first-type (specified concentration), second-type (specified concentration gradient), or third-type (concentration-dependent mass flux) conditions (Figure 2.9). At a source boundary, the third-type condition is most realistic, although a first-type is also commonly used. At an impermeable flow boundary, a second-type transport boundary is used with the concentration gradient fixed to zero. The concentration gradient can also be fixed to zero at an outflow boundary allowing the mass to leave the domain.

The hydrodynamic dispersion tensor D_{ij} in equation (5) is defined by Bear (1972), and is a function dependent on the groundwater velocity, aquifer dispersivities, and the effective molecular diffusion coefficient (D^*). In one dimension, the dispersion term reduces to

$$D_x = \alpha_L v + D^* \tag{8}$$

where α_L is the longitudinal dispersivity [L]. In three dimensions, besides the longitudinal dispersivity, transverse horizontal (α_{TH}) and transverse vertical (α_{TV}) dispersivities are also required. The dispersive parameters, which are related to the spatial variability of the porous material, are commonly obtained by calibrating an advection—dispersion model against an observed plume. Values of α_L = 1—10 m, α_{TH} = .1—1 m, and α_{TV} = .01—.001 m are typical values for a sandy aquifer.

2.3.2. *Diffusive Transport*

The transport equation given by (5) can be applied to 1D, 2D, or 3D systems, and can be solved using the standard analytical or numerical methods identified in Section 2.1.2. One of the simplest transport problems occurs when the groundwater velocity is negligible and equation (5) reduces to the diffusion equation for a conservative contaminant (Crank, 1975):

$$D^* \frac{\partial^2 c}{\partial x_i^2} = \frac{\partial c}{\partial t} \tag{9}$$

Assuming an initial concentration of zero, and a source concentration at the inflow acting continuously for all time >0, an exact analytical solution to the one-

dimensional form of (5) is given by (Carslaw and Jaeger, 1959):

$$\frac{c(x,t)}{Co} = \left(1 - \frac{x}{L}\right) - \frac{2}{\pi}\sum_{n=1}^{n=\infty}\frac{1}{n}\sin\left(\frac{n\pi x}{L}\right)\exp\left(\frac{-n^2\pi^2 D^* t}{L^2}\right) \qquad (10)$$

where L is the domain length, and Co is the source concentration. Consider, for example, a tailings deposit situated on a low-permeability clay which is 5 m thick and underlain by a permeable sand aquifer. The diffusion coefficient is 0.018 m^2/yr, and we will assume that the tailings source began instantaneously and will persist indefinitely at a concentration of 500 mg/L. If we further assume that advection is negligible within the clay, and that the flow within the underlying aquifer is sufficient to maintain a concentration of zero just below the clay, then equation (9) is a reasonable model for this problem.

Vertical profiles of contaminant concentration at selected times using equation (10) are provided in Figure 2.10. We observe that the diffusion profiles are steep at early time near the source, and that they gradually reach the steady-state linear profile. Through such an analysis, one could determine the ability of the clay to protect the underlying aquifer.

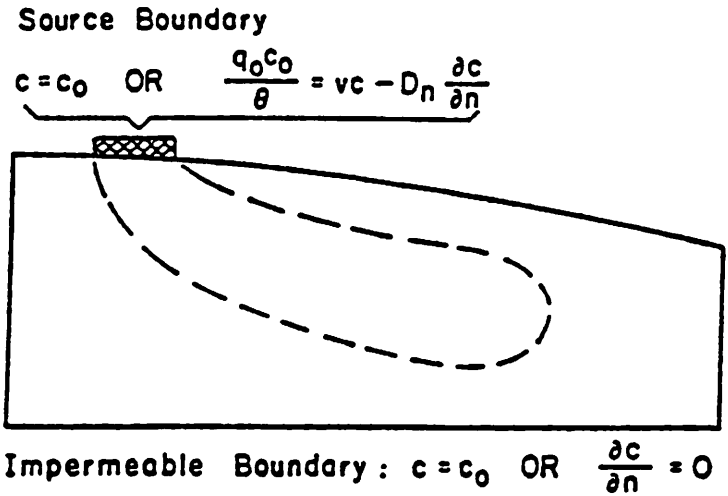

Figure 2.9. (Facing page) Typical contaminant-transport boundary conditions.

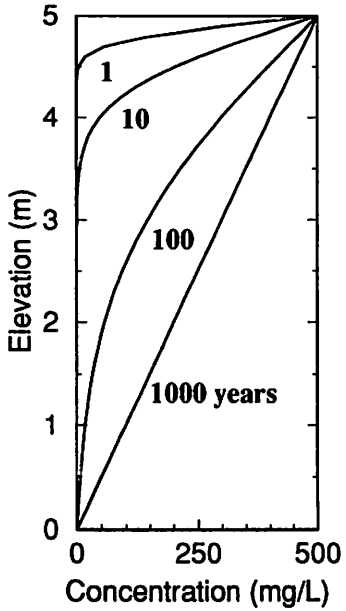

Figure 2.10. One-dimensional analytical solution for chloride diffusion through clay.

2.3.3. Advective—Dispersive Transport: 2D Analytical Solution

The sensitivity of the advective—dispersive process to longitudinal and transverse dispersion is illustrated by employing an analytical solution of equation (5) (LINE2D, WCGR 1994) to a mill-tailings contamination problem. The 2D conceptual model represents a plan view of a confined aquifer down-gradient from a mill-tailings impoundment. A contaminant source, emanating from a tailings dam for example, is assumed to be restricted to a 5 m length which extends vertically throughout the aquifer.

The base case parameters are: V_x = 0.1 m/day, α_L = 1 m, α_T = 0.1 m, R = 1.0 (no adsorption), λ = 0 (no decay). A fixed concentration is assigned at the left-source boundary, and the concentration gradient is fixed at zero along the remaining boundaries. Concentration contours at t = 1000 days are shown in Figure 2.11a, and longitudinal profiles along the center-line of the plume are shown in Figure 2.11b.

In Figure 2.12, comparisons are made which illustrate the effects of changing the dispersive transport parameters from the base case conditions. We see that increasing α_L (Figure 2.12a) produces a typical stretching of the profile, whereas increasing α_T by the same proportion (Figure 2.12b) gives a much different response because of the increased transverse spreading which depresses the profile. Allowing the source

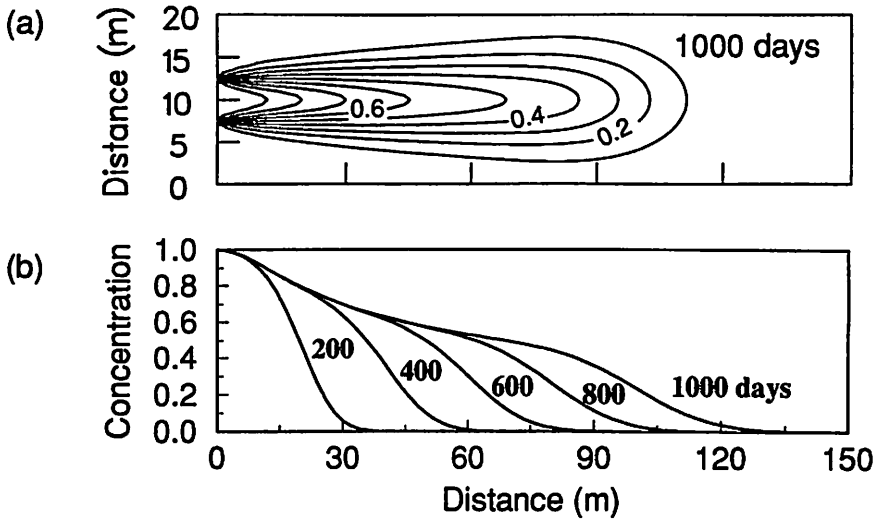

Figure 2.11. An advective—dispersive transport simulation: (a) concentration contours at 1000 days; (b) longitudinal profiles through the plume center-line.

concenltration to decay asymptotically ($t_{1/2}$ = 500 days) produces the effects shown in Figure 2.12c, wherein a pulse of contaminants is seen transported through the aquifer. The source concentrations could decay, for example, because of flooding of the mill-tailings impoundment.

2.3.4. *Advective—Dispersive Transport: 2D Numerical Solution*

The degree of complexity in the preceding examples is limited because of our choice of an analytical solution. Identical results to those of Figures 2.10, 2.11, and 2.12 could be obtained using a numerical transport model which would also allow a greater flexibility of boundary geometry and material properties. With a finite-element model, for example, the geometry of the aquifer base could closely follow that observed, aquifer heterogeneities could be introduced, and complex chemical reactions could be simulated.

Using our previous 2D flownet simulation (Figure 2.6) to provide the velocity field, we can illustrate a somewhat more realistic contaminant plume using a 2D finite-element transport model (PLUME2D, WCGR 1994). We assume that a conservative contaminant is originating from a mill-tailings source located 10 m from the left boundary along the upper water table. A third-type-transport boundary condition is used to represent the source, which we will assume is continuous in time. The longitudinal and transverse dispersivities are assumed to be 3.0 m and 0.03 m, respectively, and the diffusion coefficient is 5 x 10^{-3} m^2/yr.

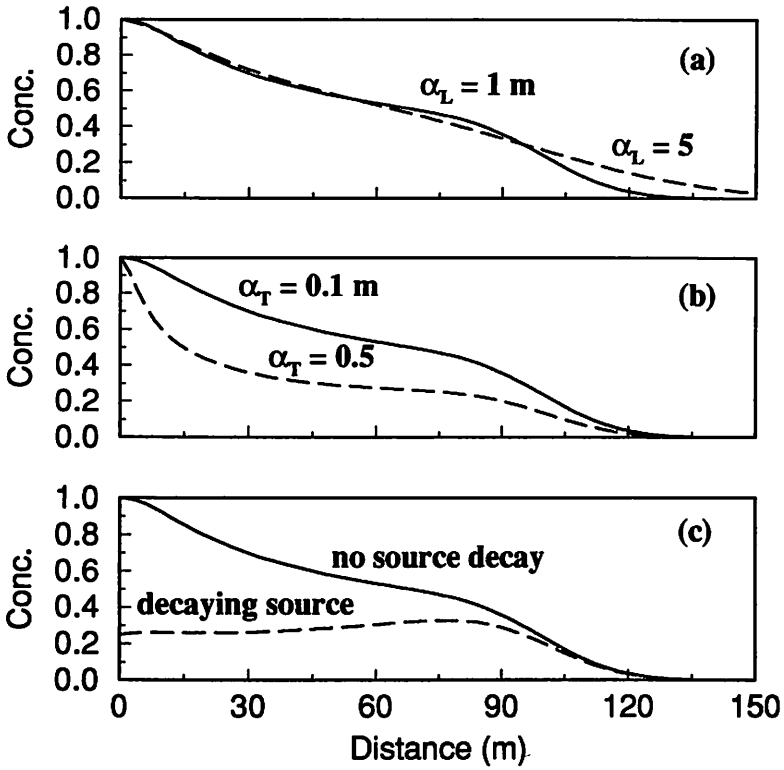

Figure 2.12. The sensitivity of advective—dispersive contaminant transport to (a) longitudinal dispersivity, (b) transverse dispersivity, (c) source concentration function (continuous source *versus* decaying source with $t_{1/2}$ = 500 days). Base case is shown as solid line in each plot; solutions represent t = 1000 days.

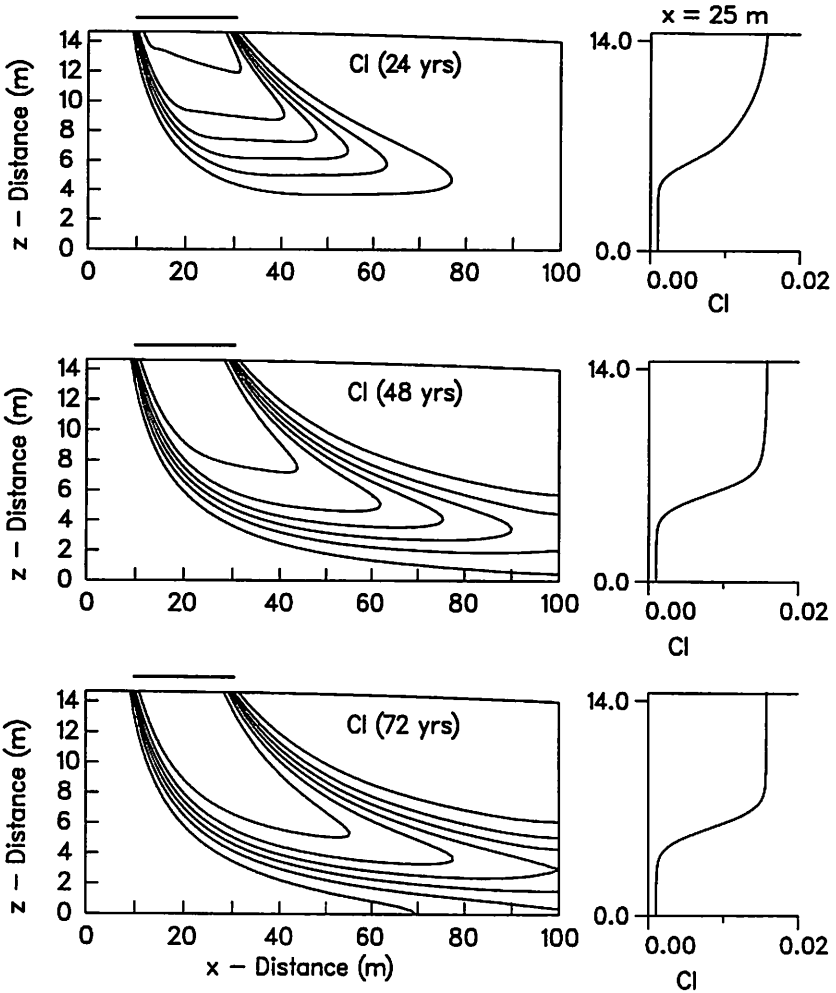

Figure 2.13. Numerical simulation of chloride transport in the 2D vertical section at 24, 48, and 72 years (contour interval is 0.0025 mol.).

Figure 2.13 illustrates the simulated chloride plume after 24, 48, and 72 years. The plume disperses, both in the longitudinal and transverse dimensions, producing high vertical concentration gradients typical of many observed plumes within long and thin aquifers. The concentration contours also closely follow the streamtubes simulated

in Figure 2.6b. The behavior of this conservative contaminant can be compared with that of several reactive contaminants presented in Section 2.4.3.

2.3.5. A 3D Numerical Transport Model

To realistically account for the effects of complex groundwater flow fields on the behavior of a contaminant plume, a fully three-dimensional numerical transport simulation is required. To illustrate the 3D behavior of a contaminant plume, we will apply the fully 3D Galerkin finite element transport model PLUME3D (WCGR, 1994) to simulate the observed contaminant plume within the flow domain presented in Section 2.2.3. The approach is similar to that used by Frind and Molson (1989), but instead of using the Alternating Direction Galerkin (ADG) model, we will use the more robust PLUME3D model.

The entire water table, including the contaminant source, was represented as a third type boundary condition as shown in Figure 2.14. The source concentrations were varied in time to provide an accurate match with the observed plume. The remaining boundary surfaces were represented with a zero concentration gradient condition. The aquifer dispersivities were α_L = 1 m, α_{TH} = 2.0, and α_{TV} = 0.008 m. Further details are provided by Molson (1988).

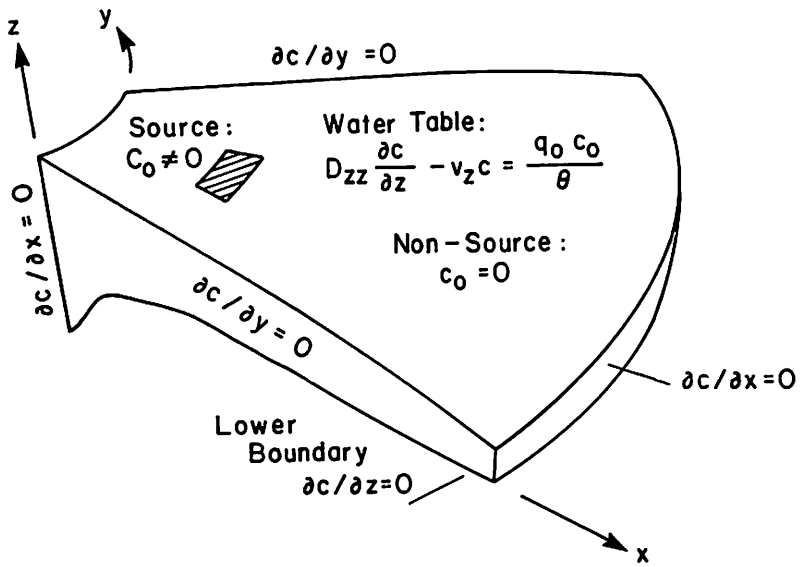

Figure 2.14. Boundary conditions for the 3D transport model.

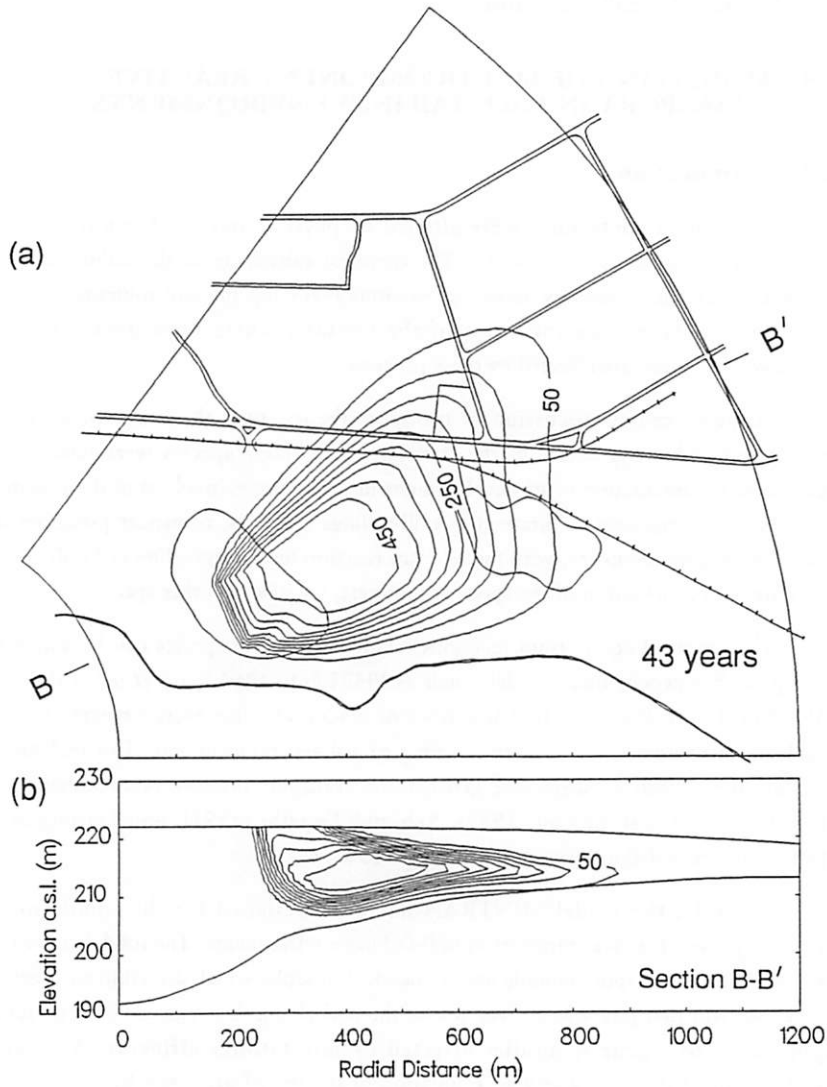

Figure 2.15. Simulated 3D non-reactive contaminant plume: (a) peak concentrations; (b) longitudinal cross-section (contour interval is 50 mg/L).

The simulated contaminant plume at 43 years (1983 A.D.) is shown as peak concentrations in the horizontal plane, together with a vertical profile along section B-B' (Figure 2.15). The simulated plume shows a very good correlation with the observed distribution in both the plan view and vertical cross-section (see Molson, 1988). The

choice of the fully 3D approach in this example is justified from the sloping aquifer base, the high vertical concentration gradients, and the marked divergence of the plume from the relatively small source area.

2.4. MODELLING OF MULTICOMPONENT REACTIVE TRANSPORT IN MILL-TAILINGS ENVIRONMENTS

2.4.1. Introduction

Mill-tailings contaminants are affected by physical and geochemical processes taking place in groundwater systems. The chemical substances in the tailings effluent will participate in a complex series of reactions involving the soil minerals, altering both the concentration and form of the contaminants. Transport rates and groundwater quality are affected by these processes.

In the preceding discussion of transport theory, only the linear processes of retardation and decay active in the transport of a single species were considered. Because of the interaction of physical and chemical processes involved in the transport of the many components contained in mill-tailings effluents, transport processes are commonly highly nonlinear, with the relevant reaction terms depending not only on the concentration distribution of the species of interest, but also on other species.

The chemical equilibrium reactions involving multiple species can be simulated with powerful geochemical models such as PHREEQE (Parkhurst *et al.*, 1985) and MINTEQ (Felmy *et al.*, 1983). These types of models are, however, restricted to local geochemical processes and require coupling to a mass-transport model to realistically simulate the advective—dispersive geochemical transport process. Narasimhan *et al.* (1986), Liu and Narasimhan (1989), Yeh and Tripathi (1991), and Lensing *et al.* (1994) have provided important advances in this area.

Recently, the model MINTRAN has been designed for the simulation of multicomponent reactive transport in mill-tailings environments. The model consists of two modules, a transport module and a chemical module, which are coupled together. Below, we will first give a brief overview of the underlying theory, and then provide an application to a generic aquifer affected by mill-tailings effluents. A detailed development of the theory and an evaluation of the model are given by Walter *et al.* (1994a).

Because of the complexity of models of this type, and the extensive field-characterization data that are required to uniquely define the relevant physical and chemical processes in real situations, absolute predictions made on the basis of model simulations carry a large degree of uncertainty. Models of this type are, therefore, best used to determine parameter sensitivity, to make relative comparisons of different scenarios, or to investigate worst case situations. In this way, a model can provide

valuable insights that are not otherwise obtainable.

2.4.2. *Theory Overview*

To model the reactive transport of the chemical contaminants that emanate from a mill-tailings site, we need to define one transport equation of the form of (5) for each of the chemicals involved. We have the choice of either writing the equations in terms of the chemical components (for example lead (Pb), and carbonate (CO_3)), or in terms of chemical species (for example lead carbonate $PbCO_3^\circ$). Because the individual components can react to form a number of different species, there are generally more species than components in the system. It is therefore wise to choose the chemical components as a basis to write the transport equations. The relevant processes are the advection and dispersion of each of the components in aqueous form, and the reactions of these components with each other and with the soil minerals. In mill-tailings environments, the reactions have been found to follow the equilibrium laws of thermodynamics (Morin and Cherry, 1988). Each component can exist in either the aqueous or the solid phase.

Assuming there are N_c components, we define the total component concentration T_k (M/M) of component k as the sum of the aqueous-phase part C_k and the solid-phase part S_k of the concentration of component k:

$$T_k = C_k + S_k \qquad k = 1, \ldots N_c \qquad (11)$$

For brevity, we will refer to C_k as the aqueous concentration (moles/1000g H_2O) and to S_k as the solid concentration (moles/1000 g H_2O) of component k. In our case, assuming dilute solutions, we can take 1000 g to equal 1 L of water. In the case of the aqueous components, the unit of concentration is molality, and in the case of the solid component, it represents moles of solid per liter of water.

The aqueous and solid phases of component k are related to the corresponding n_a aqueous and n_s solid-phase species through the stoichiometric mass-balance equations:

$$C_k = \sum_{l=1}^{n_a} a_{lk}\, c_l \qquad k = 1, \ldots N_c \qquad (12)$$

$$S_k = \sum_{l=1}^{n_s} b_{lk}\, s_l \qquad k = 1, \ldots N_c \qquad (13)$$

where c_l is the concentration of species l in the aqueous phase, s_l is the concentration of

species l in the solid phase, a_{lk} is the stoichiometric coefficient of component k in aqueous species l, and b_{lk} is the stoichiometric coefficient of component k in solid species l.

The geochemical equilibrium model MINTEQA2 (Allison *et al.*, 1990) includes a comprehensive set of chemical reactions that includeg chemical speciation, acid—base reactions, mineral precipitation—dissolution, oxidation—reduction, and adsorption reactions. The ion-association equilibrium-constant approach, which is valid for ionic strengths of 0—0.5, is used to represent the geochemical reactions. The ion-association model involves the masses of aqueous species and complexes, the equilibrium constants relating these complexes in solution, and the individual ion-activity coefficients for each species. These quantities are linked through nonlinear algebraic equations that can be solved for the individual ion activities, which are in turn used to calculate the component concentrations at equilibrium. Activity coefficients are calculated using the WATEQ, extended Debeye-Hückel, or Davies equations. The Newton-Raphson iterative technique is used for the numerical solution. The chemistry of acidic mine waters is discussed in more detail in later chapters of this volume.

Each of the N_c aqueous components is transported through the porous medium by advection, dispersion, and molecular diffusion. The transport equations for the aqueous part of component k is:

$$\frac{\partial C_k}{\partial t} - \frac{\partial}{\partial x_i}\left(D_{ij}\frac{\partial C_k}{\partial x_j}\right) + \frac{\partial}{\partial x_i}\left(v_i C_k\right) - R_k = 0 \qquad k = 1, \ldots, N_c \tag{14}$$

where x_i are the cartesian coordinates (L), t is time (T), v_i are the vector components of the average fluid velocity (L/T), D_{ij} represents the hydrodynamic dispersion tensor (L^2/T), which in turn depends on the longitudinal and transverse dispersivities α_L and α_T (L), and the molecular diffusion coefficient D_d (L/T), (for definition see Bear, 1972); R_k is the chemical source/sink term ($M/M/T$) representing the changes in aqueous-component concentrations.

The solid-phase part of component k, which remains stationary, is governed by the mass-conservation equation:

$$\frac{\partial S_k}{\partial t} - R_k^S = 0 \qquad k = 1, \ldots, N_c \tag{15}$$

where R_k^S represents the change in solid component concentration ($M/M/T$) due to precipitation/dissolution and adsorption/desorption reactions. The boundary conditions for each aqueous component k are either of the Dirichlet type, with specified concentrations along the boundary, or the Cauchy type, with specified mass flux across the boundary. A complete set of boundary conditions and an initial condition are required for each aqueous component, and an initial condition is required for each

solid-phase component. The equations are solved using the finite-element method. To apply this method, we discretize the domain into a number of elements (usually triangles or rectangles). At the vertices of these elements, the nodes, we write algebraic approximations of the governing transport equations. The resulting set of equations is then solved for the unknown concentrations. The reader interested in the details of the numerical formulation and solution is referred to Huyakorn and Pinder (1983), or Frind (1993).

Some care must be used in planning the solution strategy for equation (14). The equation shows that the concentration of component k at a point (x,y) is linked to the corresponding concentration at a neighboring point through the advection and dispersion terms, and to the concentrations of the other components through the reaction term. One approach would be to solve for the concentrations of all components at all nodal points simultaneously (the one-step approach); this approach would be very costly. For example, a modestly-sized 3D system containing 200,000 spatial nodes and 30 chemical components would generate 6 million highly nonlinear equations in 6 million unknowns, which must be solved for at least several hundreds of time steps. This task would challenge the capabilities of a supercomputer. Therefore, to make the problem tractable, we first decouple the physical and chemical computations.

We realize that when the chemical components react according to equilibrium laws, the reaction at a point depends only on the concentrations at the point itself, but not on the concentrations at the neighboring points. This fact provides for a natural decoupling between the physical and chemical processes. Conceptually, we can visualize the reactive transport process taking place in two steps: a physical step, in which the aqueous components are advected and dispersed through space and time without reacting, and a chemical step, in which the components react instantaneously without being transported. A similar concept is used in mixing-cell models (Schulz and Reardon, 1983; Appelo and Willemsen, 1987). Through the equilibrium reactions, the chemical step restores the chemical equilibrium that has been perturbed through the transport step, but does not affect the transport step itself. The physical-chemical coupling is therefore linear, although the chemical reactions themselves remain nonlinear. We can develop a conceptually simple two-step time-marching solution procedure by writing (14) in time-discretized form as:

$$\frac{C_k^{n+1} - C_k^{n}}{\Delta t} = L\left(C_k\right)^{n+1/2} + R_k^{equil}\,\delta\left(t + t^{equil}\right) \qquad k = 1, \ldots, N_c \tag{16}$$

where n, $n+1$ represent the old and new time levels, respectively, Δt is the time step, and L represents the spatial terms which are centrally weighted in time for optimum accuracy. The reaction term R_k^{equil} represents the relative mass (M/M) generated or consumed instantaneously in equilibrating the system at time $t+t^{equil}$ during the

physical transport step, and $\delta(t+t^{equil})$ is the Dirac delta function ($1/T$), which satisfies:

$$\int_{t}^{t+\Delta t} \delta\left(t + t^{equil}\right) dt = 1 \qquad (17)$$

The chemical equilibration is allowed to take place at the end of the time step, at time $(t + \Delta t)$. We can split equation (16) into two steps:

- Step 1 (physical):

$$\frac{C_k^{phys} - C_k^n}{\Delta t} = L\left(C_k\right)^{n+1/2} \qquad k = 1, \ldots, N_c \qquad (18)$$

- Step 2 (chemical):

$$\left(C_k^{n+1} - C_k^{phys}\right) \delta\left(t+\Delta t\right) = R_k^{equil}\, \delta\left(t+\Delta t\right) \qquad k = 1, \ldots, N_c \qquad (19)$$

where C_k^{phys} is the concentration at the end of the physical step. Adding (18) and (19) and integrating over the time interval $[t + \Delta t]$ results in:

$$\left(C_k^{n+1} - C_k^n\right) = \left(L\left(C_k\right)^{n+1/2}\right) \Delta t + R_k^{equil} \qquad k = 1, \ldots, N_c \qquad (20)$$

which is identical to the similarly integrated form of (16). Solving (18) and (19) is therefore equivalent to solving (16). For each time step, we first solve for the unequilibrated set of concentrations C_k^{phys} for each component and nodal point using (18), then supply these concentrations, one nodal component set at a time, to the chemical routine, where they are equilibrated. The values returned by the chemical routine are the concentrations for the end of the time step, C_k^{n+1}.

To avoid numerical dispersion, the finite-element discretization and the time-stepping scheme must be designed to satisfy the grid Peclet and Courant criteria (Daus *et al.*, 1985). These criteria are:

$$P_e = \frac{v\,\Delta L}{D} \leq 2 \qquad (21)$$

$$C_o = \frac{v\,\Delta t}{\Delta L} \leq \frac{P_e}{2} \qquad (22)$$

where v and D are the velocity and dispersion coefficient in the principal (flow) direction, respectively, ΔL is the effective element length in the flow direction, and Δt is the time step. Equation (21) is used to constrain the spatial discretization ΔL, and equation (22) is used to constrain the time step.

In nonreactive transport, small oscillations can be tolerated and the Peclet and Courant constraints are commonly exceeded by a factor of 2 to 4. In reactive transport, on the other hand, numerical oscillations can cause negative concentrations that may be fatal for the chemical equilibrium calculations. Therefore criteria (21) and (22) should be strictly satisfied everywhere. In addition, the numerical equations should be centrally time-weighted.

In practice, the above constraints can be relaxed as time increases and concentration gradients diminish. As a general rule, a higher grid resolution is required to define irregular changes in material properties and where gradients are high, as for example, near pumping wells and near contaminant sources or sinks.

Because the chemical perturbation that must be equilibrated at each time step increases with the time-step length, the time step Δt is also constrained by the chemistry, although a quantitative relationship has not yet been established. The simplest approach is to constrain Δt on the basis of the number of Newton-Raphson iterations performed by the chemical equilibration routine, keeping the iterations at a reasonable number (say, no more than 20). The chemical iteration constraint will normally override the Courant number constraint.

2.4.3. Application to a Generic Site

This example gives a limited illustration of the controlling geochemical transport processes occurring in a carbonate aquifer under the impact of acidic mine tailings effluent. We consider the water-table aquifer shown in Figure 2.6a, which has a mill-tailings site situated at its upstream end. The aquifer system and the site chemistry resemble conditions at the Nordic site near Elliot Lake in northern Ontario. The groundwater flownet and the velocity field in the vertical cross-section are shown in Figure 2.6b and 2.6c, respectively. In order to be able to use a cross-sectional analysis, we assume that the tailings impoundment extends a large distance in the transverse horizontal direction. We also assume a set of aqueous components and initial mineral reserves that are similar to those observed by Morin *et al.* (1988a) at the Nordic site, and that include the dissolved metals ferrous iron Fe(II), ferric iron Fe(III), Al, Cr, Pb, and Mn, as well as the minerals calcite $CaCO_3$, siderite $FeCO_3$, gibbsite $Al(OH)_3$, gypsum $CaSO_4 \cdot 2H_2O$, amorphous silica SiO_2, and "ferrihydrite" $Fe(OH)_3$. In addition, we allow the mineral phases anglesite $PbSO_4$, cerussite $PbCO_3$, rhodochrosite $MnCO_3$, and amorphous chromium hydroxide $Cr(OH)_3$, which are not present in the aquifer initially, to precipitate under supersaturated conditions.

The physical boundary condition for transport at the water table is of the Cauchy type, with the mass flux specified for each aqueous component. The tailings-effluent source covers the area 10 m $< x <$ 30 m. The dispersivities in the transport model are 3.00 m and 0.03 m in the longitudinal and transverse directions,

respectively, and the effective molecular diffusion coefficient is 5.0×10^{-3} m²/yr. The aquifer temperature is assumed constant at 25 °C. Plume contours of nonreactive chloride at 24, 48, and 72 years are shown in Section 2.3.4 (see Figure 2.13). These contours can be used as a basis of comparison for the reactive plumes given below.

The primary factor controlling the chemistry of the mill-tailings effluent water is the pH. Figure 2.16 shows the evolution of the low-pH plume in the aquifer, migrating downstream in the direction of groundwater flow. The plume, which is distinctly different from the Cl plume (Figure 2.13) has three plateaus (see vertical profile at x = 25 m) where the pH is constant, separated by two fairly sharp fronts. The total decrease in pH over the two fronts is about three pH-units. The fronts arise because of the acid-buffering reactions in the aquifer. As the acidic tailings water infiltrates into the column, calcite is progressively dissolved, buffering the pH. As long as calcite is present, even in small quantities, the pH remains relatively constant. As calcite dissolves, the water becomes supersaturated with respect to siderite, which precipitates. After calcite is completely dissolved at a point, the pH decreases, almost instantaneously, to a lower value maintained by equilibrium with respect to the second pH-buffering mineral, siderite. As siderite dissolves, the pH again remains relatively constant. After siderite has been depleted, the pH decreases once again to a new level which is controlled by equilibrium with respect to gibbsite. The precipitation and dissolution of these three mineral phases, and the resulting changes in pH, control changes in the concentrations of the other chemical components.

As an illustrative example of dissolved-metal transport and mobility, Figure 2.17 shows concentrations of Al, Cr, and Pb at 48 years, and Figure 2.18 shows the corresponding results for the associated minerals gibbsite $Al(OH)_3$, amorphous chromium hydroxide $Cr(OH)_3$, and cerussite $PbCO_3$. The contours of the aqueous components are in terms of moles/L (mol.), and those of the mineral components are in terms of moles of solid per L (M). In comparing the plumes of the various aqueous components, the differing concentration scales (logarithmic *versus* linear) should be kept in mind. The vertical cross-sections at x = 25 m show the sharp concentration changes. Recommended drinking-water levels (D.L.) for the dissolved metals (Ontario Ministry of the Environment, 1983) are also shown in the cross-sections.

Dissolved Al enters the aquifer at high concentrations, but drops off sharply over almost five orders of magnitude at the calcite- and siderite-dissolution fronts. Due to the precipitation of gibbsite, Al concentrations drop substantially below the recommended drinking-water level. Chromium similarly attains the drinking-water level as the concentration drops sharply at the calcite- and siderite-dissolution fronts and $Cr(OH)_3$) precipitates. Lead also enters the aquifer at a high concentration, and drops about one order of magnitude at the calcite-dissolution front, precipitating as cerussite. Lead concentrations downstream of the front, however, remain above the drinking-water level.

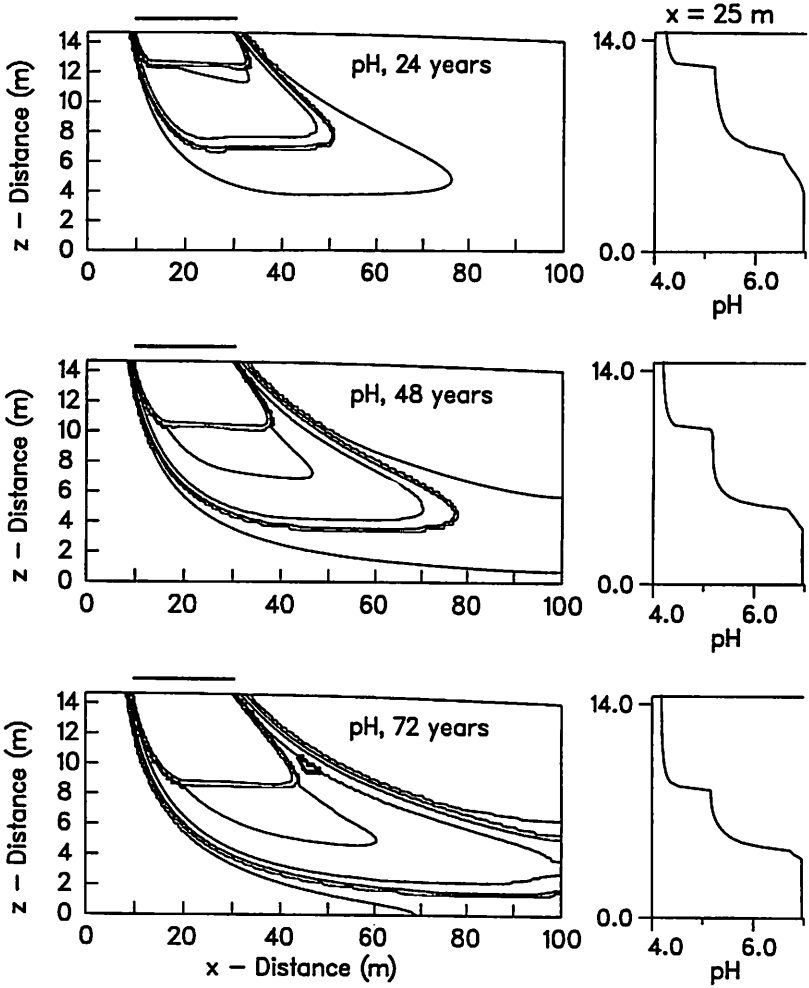

Figure 2.16. Evolution of a low-pH plume at 24, 48, and 72 years, continuous source (contour interval is 0.4 pH units).

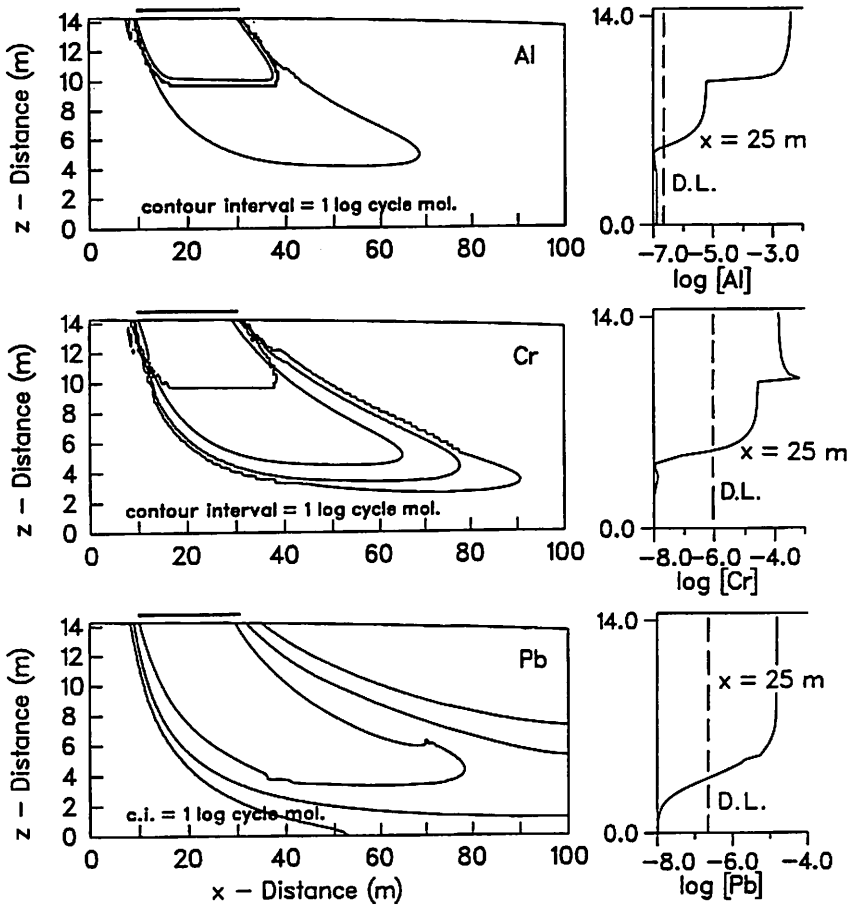

Figure 2.17. Concentration distribution of aqueous Al, Cr, and Pb at 48 years. Acceptable concentration limits for aqueous components are shown as dashed lines in the vertical profiles at $x = 25$ m.

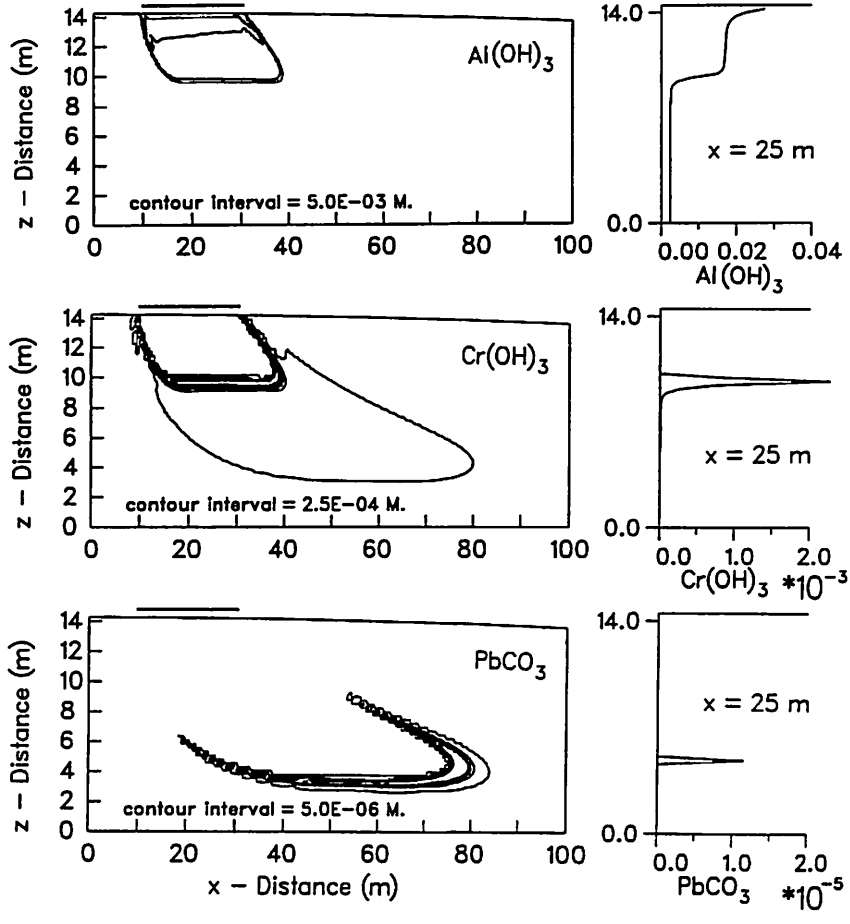

Figure 2.18. Concentration distribution at 48 years for solid-phase gibbsite $Al(OH)_3$, amorphous chromium hydroxide $Cr(OH)_3$, and cerussite $PbCO_3$.

As the zones of calcite and siderite dissolution move down gradient with time, the heavy-metal precipitates are redissolved by the advancing low-pH water, and reprecipitated farther downstream. The rate of advance of the precipitates is, however, generally less than the migration velocity of the dissolved contaminants.

The process of metal precipitation suggests that if the source input were terminated after some finite period of time, the metals would remain immobilized. This process is illustrated in Figure 2.19, which shows the mass fate of Cr in the aqueous and solid phases, under a continuous-source scenario and a scenario in which the source is terminated after 12 years. The figure shows that the greater part of the mass of Cr will always be in the solid phase, and that under the finite-source scenario, the

aqueous-phase concentration will eventually decline to a very low value. Thus the risk of chromium contamination of water resources is diminished. Similar sensitivity analyses can be conducted for the other harmful contaminants.

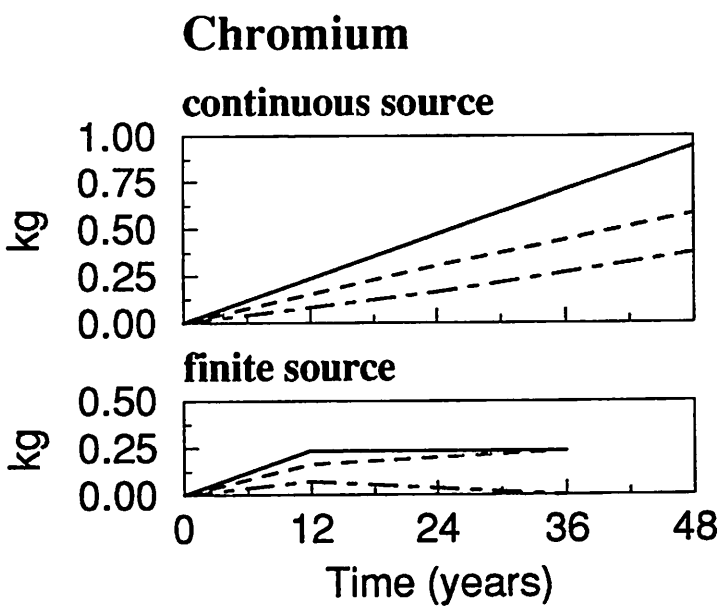

Figure 2.19. Mass fate of Cr over time, comparing the continuous and finite-source scenarios.

The simulations show that under certain conditions, toxic heavy metals originating at mine tailings sources can be effectively immobilized by buffering in an aquifer downstream of the source. As a result, the groundwater may meet drinking water standards with respect to those metals without costly remediation measures. Complete chemical data for the aqueous and mineral components participating in this example, as well as comprehensive discussions of the migration of the most important of these components, are given by Walter *et al.* (1994b).

2.5. DIMENSIONALITY

Within natural hydrogeologic systems, groundwater flow and contaminant transport are inherently three-dimensional processes. Contaminants advect through complex 3D groundwater flow systems, and disperse and diffuse in three dimensions. When considering a site to be modelled, however, the real system can commonly be simplified to one or two dimensions, or it may include the complete 3D domain. Table 2.2 presents an overview of the choices of dimensionality and relevant assumptions and limitations of each. The choice of dimensionality will significantly affect the computational effort required and the realism of the results obtained.

Table 2.2. Applications and limitations of various degrees of dimensionality in groundwater modelling

	Typical Applications:	Assumptions/Limitations:
1D	• preliminary concept evaluation • vertical migration from a large source • Darcy's Law applications • migration through liners, tailings dams • local-scale processes, sensitivity analyses • unsaturated-zone modelling	• transverse flow neglected • transverse dispersion neglected • no geometry • highly simplified
2D areal	• areal extensive, vertically thin aquifers • capture zones, purge-well networks • multi-aquifer models, leaky aquifers • for aquifers where $Kz/Kx >> 1/100$ • transport from a laterally wide source	• vertical flow neglected or simplified • vertical dispersion neglected • fully screened wells • no depth-dependent processes
2D vertical	• flownet simulations • depth-dependent processes • vertically heterogeneous aquifers • laterally extensive sources	• horizontal dispersion neglected • horizontal flow neglected • lateral continuity assumed
2D radial	• radially symmetric problems • single-source well or purge well	• restrictive geometry • radially symmetric
3D	• depth-dependent processes within 3D heterogeneous systems • complex aquifer geometry and structure • multiple, partly screened wells • long-term transport from small source	• high computational demands (memory/execution time) • large effort: data collection, model development, and calibration

The effect of dimensionality on advective—dispersive transport is illustrated in Figure 2.20, in which we compare the longitudinal concentration profiles from the previous 2D base case (Figure 2.11) with those from otherwise equivalent 1D and 3D simulations. In the 1D simulation, the profiles are symmetrical about the 0.5 concentration level, which will always appear at a distance equivalent to (vt). The concentrations in the 2D simulation are lower than those in the 1D simulation because of the added transverse dispersion in the former. The 2D and 3D profiles are both distinctly asymmetrical because of the effects of transverse dispersion. Because of the increased dispersion in the third dimension, the concentrations from the 3D simulation are lower than those from the 2D simulation.

Burnett and Frind (1987) used numerical transport simulations to illustrate dimensionality effects on the evolution of contaminant plumes. Differences in plume behavior due to dimensionality can have important consequences in terms of meeting acceptable drinking-water limits for mill-tailings contaminants.

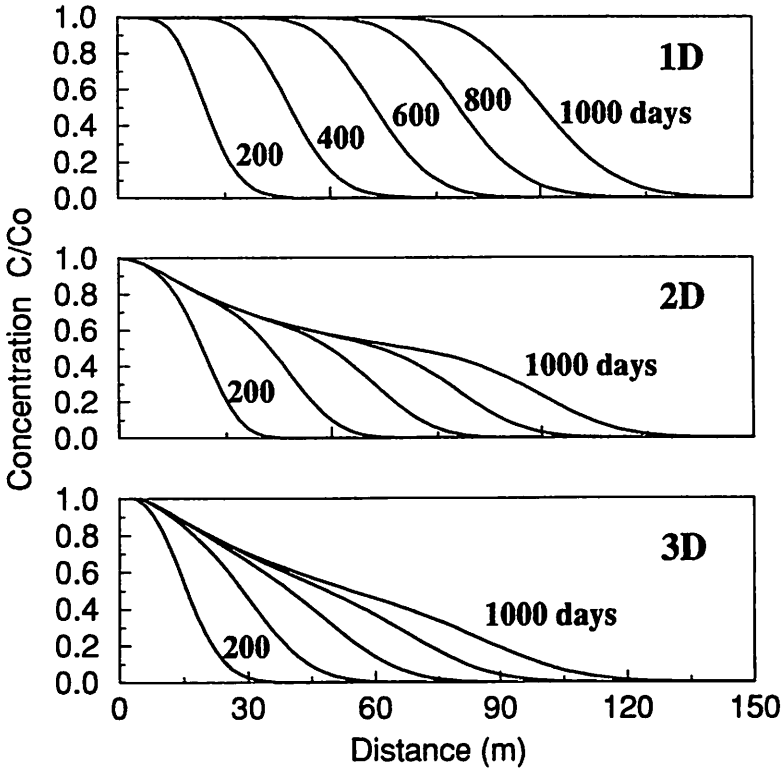

Figure 2.20. Longitudinal profiles through plume center-line, showing dimensionality effect in advective—dispersive mass transport.

2.6. UNCERTAINTY AND NON-UNIQUENESS

At all natural field sites, there will always be some degree of hydrogeological uncertainty because of natural variation in material properties and processes, and a finite quantity of observed data. Furthermore, even if the existing conditions are fairly well-known, there is future uncertainty in additional model parameters, including source functions, river levels, and long-term recharge and water-use changes, all of which will affect predictions of contaminant transport.

One of the most common sources of uncertainty in the problems of groundwater flow and contaminant transport is the natural spatial variability in material properties, most importantly the hydraulic conductivity. Sudicky and Huyakorn (1991) provide a thorough review of methodologies to describe contaminant migration in complex heterogeneous systems. Methods to handle uncertainty include Monte-Carlo analyses,

stochastic approaches, probabilistic models, and risk-analysis models. However, these techniques are usually restricted to larger-scale problems such as vault design for disposal of radioactive wastes, or to the management of highly toxic industrial wastes where long-term predictions under future uncertainties are required.

Uncertainty in the model input parameters can produce uncertainty in the output in the form of non-uniqueness, *i.e.*, where more than one set of input parameters will produce, in essence, the same result. To reduce uncertainty and to avoid the non-uniqueness problem, independently derived original field data should be used whenever possible in the calibration process. Without independent data, however, models too commonly are calibrated using a trial-and-error approach whereby one or more parameters are varied until a reasonable match with the observed data is obtained. Inverse and optimization methods have been developed to improve the calibration process, but because of their complexity, they are not regularly used in practice.

A calibrated model does not imply that it is valid for a given site: calibration is usually only a curve-fitting exercise, and many models, some based on non-valid assumptions, could be calibrated to the same data. Furthermore, if the model is not sensitive to the calibrated parameter, then an apparently good calibration may be misleading. Konikow and Bredehoeft (1992) discuss some of these and additional problems associated with the calibration process.

If the model input parameters are not well-defined, a parameter sensitivity analysis may help identify which parameters require more accurate definition. By using the extremes of the parameter ranges, worst-case or conservative scenarios can be investigated.

Finally, the model can be used to predict contaminant migration or estimate the effectiveness of proposed remediation measures. Predictions are usually made using the calibration simulation as the initial condition and extending the model in time. It is in this predictive mode that models are most useful, but also most susceptible to misuse. All assumptions and uncertainties in the modelling process must be recognized. Konikow (1986) and Freyberg (1988) for example, document examples in which model predictions have been seriously flawed, in part due to improper calibration.

Non-uniqueness is not a fault of the model itself, but reflects instead the quality and quantity of the observed data. If non-uniqueness is present, perhaps the chosen model and/or scope of the study may be too complex and unrealistic for the limited field data.

2.7. SUMMARY

We have presented only a brief outline of a very complex subject. Before engaging in a modelling project, we recommend further background reading.

Modelling too often becomes a "black-box" exercise if either the physical system or chosen model is not adequately understood.

In summary, we offer the following guidelines:

- Always acknowledge the inherent assumptions and limitations of the chosen modelling approach, and include them in your interpretation of the results.
- Hydrogeological models are best suited to assess the validity of conceptual models, assess parameter sensitivity, or to make comparative predictions. They should not be used to make absolute predictions.
- Keep the modelling in perspective. The model parameters, boundary conditions, and material properties should all be realistic and be kept as simple as possible. Before attempting a complex numerical model of your site, perhaps an analytical solution will be useful in your preliminary conceptual analysis.
- Respect the model accuracy criteria, stability criteria, and mass-balance requirements.

Chapter 3

Mineralogy of Sulfide-rich Tailings and Their Oxidation Products

J.L. Jambor
Department of Earth Sciences
University of Waterloo
Waterloo, Ontario N2L 3G1

3.1. INTRODUCTION

3.1.1. General Aspects

The generation of acidic waters from mine wastes is inextricably linked not only with mine closure, but also with the potential development of new mines. In mine development it always has been necessary to plan for the disposal of waste-rock and tailings, and these aspects enter into the spatial arrangement of the minesite and the capital costs of the operation. In the past the costs associated with waste disposal were minimal because there was little concern for site rehabilitation and the potential release of hazardous effluents over the long term. Such environmental concerns are taken for granted today, but it is only since the 1970s that abandonment without rehabilitation measures has been prohibited in all jurisdictions in North America.

North American mines today operate under stringent environmental controls, commonly as a consequence of the combination of legislated regulation and the participation of special-interest groups, and environmental aspects may dominate both the economic viability and public acceptance of mining an orebody. It is not enough to have a good orebody and assured markets for the minerals or metals to be produced; the environmental concerns may be the dominating factor that could prohibit mining of the orebody, or the costs related to environmental requirements could increase the cut-off grade so that a significant proportion of "ore" becomes waste. As noted by Vallée *et al.* (1992), the environmental perspective "...is now more important than estimating the grade of the reserves accurately, than mining efficiently, or maintaining a profitable operation."

3.1.2. Acid Mine Drainage

Acid mine drainage (or more appropriately, mine acidic drainage, with the unfortunate acronym MAD) originates from the oxidation of sulfide minerals that at most mining sites are gradually accumulated and exposed in waste-rock piles and tailings impoundments. For example, a mine that mills at 3000 tpd will produce roughly 1,000,000 tonnes of tailings annually. The porphyry copper deposit of Valley Copper Mines in British Columbia produces at 135,000 tpd, and as the ore grades only about 0.5% Cu, nearly all of the milled material (about 99%) is discharged as tailings that are accumulating at approximately 45 million tonnes per year. Thus the storage requirements for tailings alone may be exceedingly large, as at Sudbury, Ontario, where the main tailings site for INCO Limited's production covers an area of 2,024 ha (Hunt, 1991). Tailings are, however, not necessarily acid generators: the net amount of acid produced depends largely on the mineral composition of the tailings. In all waste-rock and tailings accumulations there are some minerals that oxidize to produce acid and release potentially deleterious elements, and there are other minerals that react with the acids to neutralize them. Accompanying the neutralization there may be the formation of stable precipitates and the incorporation of harmful elements into them. Geochemical studies of the gases, pore fluids, and aqueous effluents are invaluable in providing information about reactions that occur within an impoundment, but that information can be enhanced considerably by acquiring mineralogical knowledge about what solid phases are reacting, how they are reacting (both the degree and course of reaction), and what secondary precipitates are formed.

Murray (1977) determined the average S content of tailings from 43 minesites to be 4.02 wt%, with the range 0.01 to 38.87 wt%. The upper part of this range is typical for volcanogenic massive sulfide deposits which, because of their high sulfide content, are among the principal contributors to acid mine drainage in Canada and in many other parts of the world.

Although much has been written about acid mine drainage (AMD), relatively little has been published about the mineralogy of sulfide-rich tailings and their ensuing oxidation products. Such studies have a major role to play in the investigation of AMD as they should be the foundation of models that seek to predict effluent qualities, quantities, and the lifespan of acid generation from mine wastes. As was noted by Blowes and Jambor (1990), the integration of the results of simultaneous mineralogical and hydrogeochemical investigations of a tailings impoundment can lead to conclusions whose sum is greater than that derivable if the two studies were conducted independently. The bonus arises because the hydrogeochemical results can focus the mineralogical search for specific secondary solid phases that may not have been observed initially; on the other hand, the mineralogical results can expand, confirm, or possibly reconcile results predicted solely from geochemical parameters.

The use of geochemical parameters unsupported by mineralogical data is particularly disturbing when one considers the validity of models whose objective is to predict the future course of AMD for a specific impoundment. In Canada, to date, much more effort and funding have been dedicated to the development of predictive models than to determining the mineralogical data that are fundamental parameters in such models. The current program under the auspices of the Northern Ontario Development Agreements, in which several tailings impoundments are undergoing simultaneous mineralogical and hydrogeochemical investigations, represents a step in the right direction in terms of accumulating data for expanding the applicability and validity of predictive models.

This Chapter deals specifically with the mineralogy of sulfide-rich tailings impoundments. In terms of scientific progress the studies are still in their infancy, and even less has been unequivocally demonstrated for the mineralogical reactions that occur in mine waste-rock piles. A comprehensive study of a large, oxidized impoundment involves a time-consuming examination of a large number of samples, and difficulties may arise because of the fine grain size of the tailings, the fine-scale intergrowth or heterogeneity of the oxidation products, and in some cases, the paucity of the secondary phases. The last makes Debye-Scherrer-type X-ray methods an essential tool in studying tailings. X-ray diffractometry of bulk samples has an important role to play, but only rarely is diffractometry capable of detecting the oxidized products in bulk samples. The principal purpose of this Chapter is to summarize the methodology that has evolved from the mineralogical investigations of several sulfide-bearing impoundments that have oxidized in the cool, temperate climate that prevails in Canada.

3.2. CLASSIFICATION OF TAILINGS PRODUCTS

3.2.1. Tailings Minerals

Tailings represent the ground, mill-processed gangue in which the ore minerals occurred, and because recoveries of the valuable minerals are never 100%, the tailings always contain small amounts of ore minerals. Grain sizes of tailings are governed by the fineness of grind that is used to liberate the ore minerals from their host rocks; thus, most tailings fall within particle sizes used geologically for sand (1/16— 2 mm; 63—2000 μm) or silt (1/16—1/256 mm; 63—4 μm). Somewhat different, but similar, particle sizes are commonly used in the mineral industry (Down and Stocks, 1977): 20—200 μm for sand, 5—20 μm for silt, and 2—5 μm for slimes.

Much like find-grained sediments, tailings are typically transported and deposited in an aqueous milieu. Sedimentary structures such as stratification, graded bedding, and cross-bedding are commonplace features, and pronounced grain-size

sorting and redeposition of fines can occur over wide areas, particularly if the terrain or developing impoundment surface has a distinct slope. All of these sedimentary features, and the particles that form them, are considered to be primary in that only physical, as distinct from chemical, processes are involved.

Few mineral-processing plants employ reagents that chemically attack the bulk mill-feed, and the discharged tailings at most sites thus contain the minerals in their chemically unaltered, pristine state. To distinguish these minerals from subsequent chemically-derived precipitates, the following classification of tailings minerals has been proposed (Jambor and Owens, 1993):

i) primary minerals: those that constitute the ore and gangue assemblages, and which were processed through the mill and subsequently were deposited in the impoundment without having undergone change other than comminution;

ii) secondary minerals: those that form within the impoundments, typically by the precipitation of constituents derived from oxidation reactions at and near the tailings-impoundment surface. Gypsum ($CaSO_4.2H_2O$) can be one of the rare exceptions to oxidation-derivation in that it may crystallize *in situ* from constituents that were in the mill's process-waters. Secondary minerals are not confined to the near-surface zone, and may occur prominently in buried former oxidation sites (see paleosurfaces, below). Typical secondary minerals are the iron oxyhydroxides such as goethite FeO(OH), and sulfates such as jarosite $KFe_3(SO_4)2(OH)_6$;

iii) tertiary minerals: those that crystallize after the tailings samples have been removed from the environment of the impoundment. A typical example is fine-grained gypsum that crystallizes during drying of the tailings. The constituents of the tertiary products originate in the tailings pore-waters, and gypsum and ferrous sulfates thus are characteristic tertiary products whose crystallization may provide cohesion to tailings samples, rigidly cementing some. Tertiary precipitates also commonly form white surface blooms of gypsum and Fe—Mg sulfates. Covellite (CuS) has been observed both as a secondary and a tertiary product in tailings from Heath Steele, New Brunswick (Jambor *et al.*, 1992), and covellite, lepidocrocite [γ-FeO(OH)], and ferrihydrite ($5Fe_2O_3.9H_2O$) occur as tertiary precipitates on tailings from the Nickel Rim impoundment at Sudbury, Ontario (Jambor and Owens, 1993);

iv) quaternary minerals: those that form by surficial oxidation during storage of the dried samples. Quaternary products known to date are exclusively

the hydrous, water-soluble, simple sulfate hydrates of the type $FeSO_4.nH_2O$. Time of crystallization of the surface blooms is a distinguishing criterion; although the distinction between tertiary and quaternary efflorescences may be difficult in some cases, in others the time gap between drying and the appearance of quaternary blooms is substantial. Thus, recognition of the development of quaternary minerals can be clear-cut, especially where tailings are relatively coarse so that prolonged pore-water retention is not a factor. Quaternary minerals, which usually form only on massive-sulfide samples, are typically rozenite ($FeSO_4.4H_2O$) and siderotil ($FeSO_4.5H_2O$).

In summary, the minerals deposited in a pristine condition in the impoundment are classified as primary, those that crystallize by chemical reactions (mainly oxidation) within the impoundment are secondary, and phases that form during drying of tailings samples which have been removed from the impoundment are tertiary. Minerals that form during storage, after the samples have dried, are classified as quaternary. The qualifier concerning removal from the impoundment is important in that white sulfate-bearing blooms commonly occur on impoundment surfaces; the blooms may appear and disappear daily, with the frequency dependent on dry (hot) or damp (cool) cycles. The conditions that govern the precipitation or dissolution of these sulfates are part of the overall tailings environment rather than divorced from it as in the case of the formation of tertiary and quaternary minerals; thus, the surface blooms are considered to be secondary phases

3.2.2. Paleosurfaces

At most processing plants the tailings are transported from the mill or concentrator via a fixed or movable pipeline, and are deposited onto the impoundment from a temporarily stationary discharge point or discharge line. Fluctuations in the discharge rate, whether by plan or otherwise, and other factors such as a change in discharge point or the almost inevitable erosional channelling at the impoundment surface, commonly isolate areas from continuous tailings accumulation (Robertson, this Volume). Oxidation of the isolated, exposed tailings may begin immediately, and an appreciable depositional hiatus may produce secondary minerals and ochreous discoloration. Such layers are also commonly marked by minor accumulations of vegetal matter such as leaves and small twigs. Upon renewed tailings deposition, the partly oxidized assemblage is buried, sometimes to considerable depths in the impoundment. These "ancient", buried oxidized layers are referred to as *paleosurfaces.* Their existence is a vivid demonstration that sulfide oxidation, and possible acid generation, may begin long before an impoundment is decommissioned.

3.3. SAMPLE COLLECTION

Methods for the collection of tailings solids are outlined by Ritcey (1989), MEND (1989), Blowes (1990), Palmer (1992), and others (this Volume). The methods used specifically for the collection and mineralogical study of cores from the Waite Amulet impoundment, Quebec, are given in Blowes and Jambor (1990). Near-surface oxidation zones can be studied and sampled by digging pits in an impoundment, and deeper samples can be obtained with an auger, but various coring techniques, some of which are quite elegant, are the only practical method of obtaining samples that are intact and from several sites in a thick tailings pile.

The simplest, cheapest, most universally accessible, least time-consuming coring method is to physically drive a small-diameter (5—7.5 cm) pipe vertically through the tailings. Core barrels are typically of PVC or thin-walled aluminium, and core retention can be accomplished by insertion of an iris-diaphragm-type cup at the entry point. PVC pipe has the advantage of being chemically inert, but suffers in having a relatively low strength; the attendant lack of rigidity may also lead to difficulties in maintaining downhole alignment in deep holes and through naturally cemented tailings. Aluminium pipes have the advantages of being relatively strong and light-weight, but have the disadvantage of being chemically reactive. To minimize oxidation and other chemical reactions, and to prevent the loss of pore waters, cores should be end-sealed and frozen at the minesite. Freezing is also essential if the tailings are to be extricated intact, preferably by subsequent cutting of the barrel, and its contained core, along length with a band saw. Although freezing may affect some physical aspects, such as porosity and shear strength, these properties are not routinely measured on cores taken mainly for mineralogical purposes. Moreover, as a drill-bit is not used in the standard coring procedure, a more profound effect is that of compression, and the bedding may severely distorted, smeared, or completely destroyed in fine-grained silty tailings.

3.4. SAMPLE SELECTION AND PREPARATION

As the number of samples taken for mineralogical studies cannot be infinitely large, a judicious selection must be made from the tens, and possibly hundreds, of meters of core that may be available. For practical reasons of storage, transportation, and handling, the core barrel and its contents are cut in the field into lengths of 20 cm to 30 cm on which the down-hole or up-hole orientation and depth are marked.

In the laboratory, logging of the cores can be general or in exhaustive detail in accordance with the particular mineralogical objectives and time constraints. Only a few points that are possibly helpful will be mentioned here.

Logging will be facilitated by extruding the frozen cores, preferably in downhole sequence, onto plastic-lined trays on which the information on the core barrel (depth

and orientation) has been transferred. Use of a tray-shaped receptacle is important at this stage because cores are commonly saturated with pore waters from which the tertiary precipitates will crystallize as drying proceeds. Because smearing commonly will have occurred at the interface of the cores and barrel, lengthwise shaving or minor cuts along the core length should be done while the core is still wet and uncemented by tertiary precipitates. Logging should proceed as this is the stage at which color variations, and physical features such as mineral variations and sedimentary structures and textures, are most evident. This is also the only opportunity to identify unequivocally the intervals where secondary (*i.e.*, *in situ*) cementation has occurred. The logs should be supplemented during drying, and after drying of the cores has been completed, which at room temperature requires about a week, so that the distribution and type of tertiary precipitates can be recorded. Forced drying, such as low-temperature heating of the cores, is not recommended because the mineralogy of the secondary and tertiary precipitates can be severely affected by the changed stability relations and especially by dehydration reactions.

The saturated zone is defined geologically as that in which the functional permeable rocks are saturated with water under pressure equal to or greater than atmospheric (American Geological Institute, 1957). This definition also applies to a tailings impoundment. Above the saturated zone is the unsaturated (or vadose) zone, in which most of the oxidation reactions occur. Mineralogical examination of the saturated zone is important because the samples from this zone are generally the best representation of the primary mineralogy of the tailings in a decommissioned impoundment. To avoid contamination from tailings that are usually smeared along the contact between the core and its casing, and to obtain a representative bulk composition, channel sampling along the interior and length of the core sample, or a portion of it, is recommended.

The unsaturated-tailings zone typically encompasses the oxidized layers at the surface of the impoundment, and may extend to the underlying hardpan layer and part of the reduction zone (*e.g.*, Boorman and Watson, 1976; Blowes *et al.*, 1992). The unsaturated zone thus will have the largest variations in mineralogy and hydrogeochemistry, and commensurate with these variations the sampling should be much more detailed than for the saturated zone. Channel sampling, if done, should be for only narrow core intervals so that alteration zoning with depth is not obscured. Ideally, a series of samples is removed intact for microscopic examination, and companion pieces or the surrounding material are utilized for related studies such as X-ray diffractometry and chemical analyses. The advantages of using intact specimens of the tailings are the minimization of losses of secondary minerals that occur as fines, and better preservation of the textural relationships of the primary and secondary minerals.

Dried tailings solids, even from the oxidized zone, are commonly poorly cemented and difficult to handle without disintegration. To facilitate mineralogical

studies of intact specimens, a procedure devised principally by J. M Greer of CANMET, Ottawa, is to impregnate the specimen with low-viscosity cyanoacrylic adhesive ("crazy glue"). To prevent dissolution of minerals, especially the water-soluble secondary and tertiary precipitates, polished and thin sections are prepared dry or without the use of aqueous lubricants. Detailed descriptions of the preparation of polished sections and thin sections are given by Laflamme (1990) and Fitzpatrick (1984).

3.5. MINERALOGICAL TECHNIQUES

3.5.1. Determinative Methods

Numerous sophisticated microbeam and spectroscopic techniques are available to investigate minerals and near-minerals, and their surfaces and associated ions (*e.g.*, McIntyre, 1984; Hawthorne, 1993; Eberhart, 1991; Hochella and White, 1990; Busek, 1992; Bigham, this Volume). These various techniques have an important place in the study of mine wastes, but as yet no application to a systematic investigation of the mineralogy of a tailings impoundment has been completed. The primary reason is that, worldwide, only a few comprehensive studies of impoundments have been completed to date; secondary reasons are the limited availability or accessibility to the required instrumentation or laboratory facilities, the relatively lengthy time required for some of the specialized investigations, and the typically more focused approach (to answer a specific question or solve a particular problem). As an example of the last, SIMS (secondary-ion mass spectrometry) analyses may prove to be useful in deciphering the chemistry or mineralogical character of the complex alteration layers that surround some sulfide cores. X-ray photoelectron spectroscopy has recently provided exciting new information on the structural and chemical changes that occur at the surface and near-surface of pyrrhotite and arsenopyrite as these minerals oxidize (Muir *et al.*, 1993; Pratt *et al.*, 1993a,b). Such studies, although extremely valuable in their own right, would achieve maximum usefulness if they were included as a part of the larger context of a chemically reacting impoundment.

Integrated hydrogeochemical-mineralogical studies that have been completed for sulfide-rich tailings impoundments have involved mainly optical microscopy, standard X-ray diffraction methods (both film and diffractometry), and scanning electron microscopy and electron-microprobe analyses. X-ray diffractometry is generally the most useful tool to determine the primary mineralogy because the method can efficiently determine the mineralogical constituents in bulk samples. Because bulk samples are used, however, diffractometry is less useful for identifying secondary minerals, which may form only a minute percentage of the sample mass. Inadequate visual observation and the absence of independent confirmation of the minerals identified are the two major pitfalls in the study of tailings mineralogy, as discussed

below.

3.5.2. *Observation and Confirmation*

As tailings are the comminuted wallrocks and gangue minerals from an ore deposit, an approach that incorporates petrologically compatible mineral associations can be highly advantageous in interpreting X-ray diffractograms. One would not expect, as an extreme example, to find olivine $(Mg,Fe)_2SiO_4$ or anorthite $CaAl_2Si_2O_8$ in sialic igneous rock, mature sandstone, or shale, but experience has demonstrated that automated X-ray diffractometry programs may lead to such misidentifications in bulk samples. The problem arises because X-ray diffraction-line overlap and multiplicity can be extreme for bulk samples, and because the identification of a specific species of feldspar within the Na-Ca and the K series is difficult without specialized routines. In the example cited, identification of the presence of olivine or anorthite would be suspect because these minerals are petrologically incompatible with the remainder of the assemblage; verification by an independent method would be essential. As a general rule, the presence of all minerals identified by X-ray diffractometry should be confirmed by other means, such as optical microscopy, microprobe analyses, or Debye-Scherrer X-ray patterns.

The preceding caveat concerning X-ray diffractometry also applies to other instrumental methods. For example, even though an electron microprobe can be operated at a beam diameter of 1 μm, the volume influenced by the beam is considerably larger. Thus, unusual compositions may result from the analysis of fine-grained precipitates and alteration rims on sulfides. These results should not be taken at face value and calculated as mineral formulas; rather than indicating the presence of peculiar or heretofore undescribed new minerals, the first assumption should always be that anomalous results signify the probable presence of mixtures. This assumption should apply not only to the studies in progress, but also to published analyses that lack indisputable identification of the analyzed material.

Although it is tempting in the examination of tailings to rely on instrumental methods as a way of processing large numbers of samples with rapidity, much information can be gleaned from careful microscopic examination combined with Deby-Scherrer X-ray films prepared from mounts of individual grains or portions thereof. Observation of oxidized tailings under a good binocular microscope generally will reveal products or features that are not apparent under a petrographic or ore microscope, and vice versa. As unequivocal identification of most secondary sulfates and iron oxyhydroxides is not possible by SEM or electron-microprobe analyses, numerous Deby-Scherrer mounts should be prepared both from the loose tailings material under observation with a binocular microscope, and from particles in thin sections or polished sections under observation with a transmitted-light or reflected-light microscope. As well, the tertiary and quaternary precipitates are best identified by

Debye-Scherrer patterns, generally with supplementary microbeam analyses to confirm cation predominance and minor-element substitutions.

3.6. TAILINGS-MINERAL IDENTIFICATION

3.6.1. Primary Minerals

The primary minerals in an impoundment are as diverse as those in the ore deposit from which the tailings were derived. Most ore deposits, however, belong to a particular geological class, each of which has its characteristic mineral assemblage or mineral associations. Thus, a literature review of the geological data for on ore-deposit type, even if not site-specific, can provide substantial pertinent information about the potential for AMD (Plumlee, 1993, 1994) and about the kinds of minerals expected to occur in the tailings.

Figure 3.1 shows some typical X-ray diffractograms of tailings derived from various deposits. The initial identification of the component minerals is easier for minerals that have characteristic, relatively strong diffraction lines at high *d* values; again it is cautioned that independent verification should be the rule, particularly as it may be necessary to give diffraction-line assignments to a mineral on the basis of only one or two peaks on a diffractogram. Although gypsum and other soluble sulfates are not normally primary, their identification can be confirmed by subsequent water-washing of a portion of the sample, whereupon the diffraction peaks for these phases should disappear, thus facilitating identification of the primary phases.

The majority of tailings derived from sulfide-bearing ore deposits will consist of quartz, various silicates, carbonates, and iron sulfides. There are a few exceptions, but it can be generalized that AMD is principally caused by the oxidation of pyrite (cubic FeS_2) and pyrrhotite $Fe_{1-x}S$. Marcasite (orthorhombic FeS_2) can be an additional important contributor to AMD from coal wastes and some sulfide-rich deposits (*e.g.*, the volcanogenic massive-sulfide ores at Faro, Yukon Territory), but in general this mineral is sparser and less widely distributed than pyrite and pyrrhotite. Arsenopyrite FeAsS, which is of particular environmental concern because of its arsenic content, is commonly present in vein-type gold deposits and volcanogenic massive-sulfide deposits, but it is rarely detectable in X-ray diffractograms because its relatively low abundance. Other sulfides and sulfosalts such as chalcopyrite $CuFeS_2$, galena PbS, sphalerite (Zn,Fe)S, and tetrahedrite-tennantite $(Cu,Fe)_{12}Sb_4S_{13}$ — $(Cu,Fe)_{12}As_4S_{13}$, are typically undetected by diffractograms. Low abundance of a mineral, however, does not mean that its dissolution products are environmentally benign; on the contrary, most of the deleterious elements in mine-waste effluents are derived from the accessory, non-valuable sulfides and unrecovered ore minerals. Optical microscopy, which is also the only method for readily distinguishing between the FeS_2 polymorphs, is the most rapid

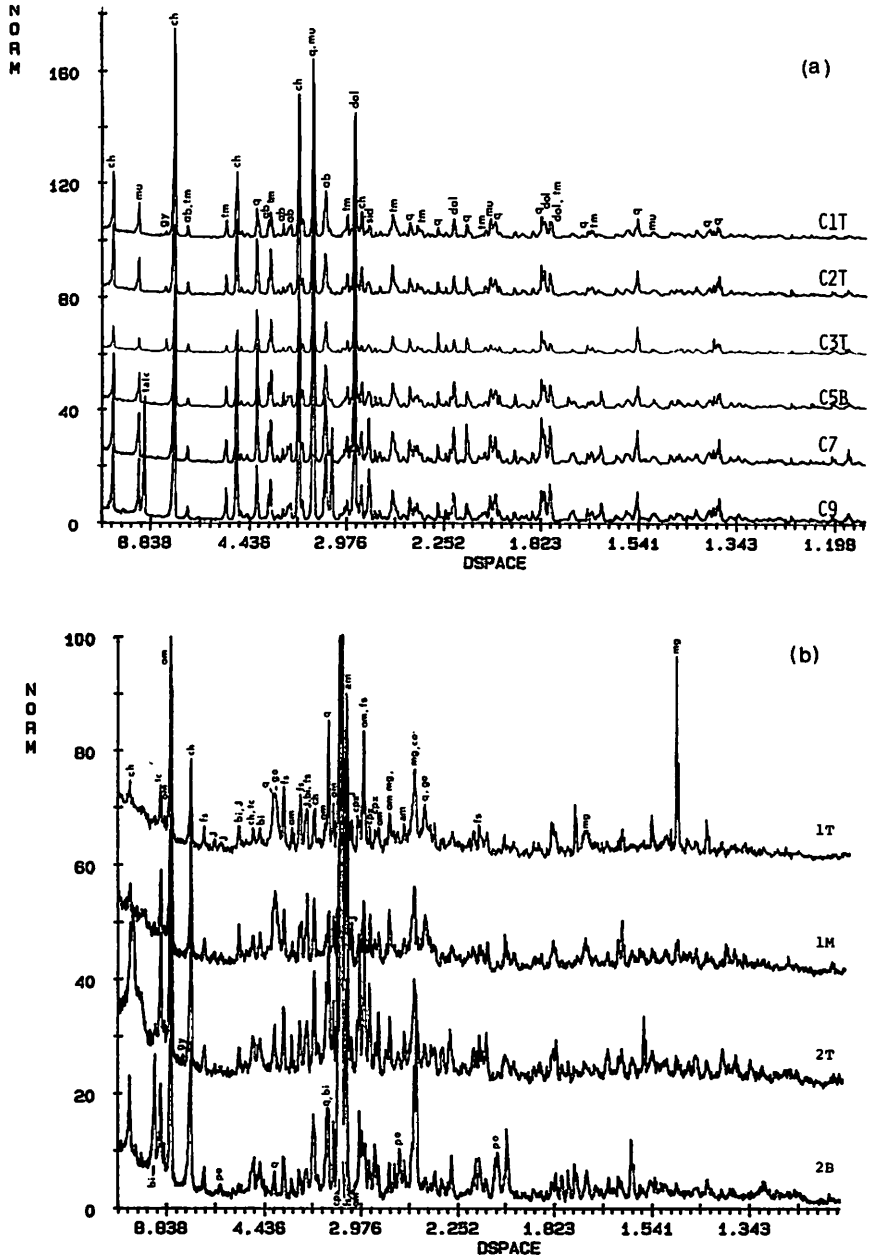

Figure 3.1. X-ray diffractograms of tailings samples. Each C number indicates core from a 20-cm interval; thus, C1 is from the interval 0—20 cm, and C2 is from 20—40, *etc.* (a) Core sequence from the Delnite tailings, Timmins area, Ontario. Abbreviations are ch chlorite, mu muscovite, gy gypsum, tm tourmaline, q quartz, ab albite, dol dolomite-ankerite, sid siderite (after Jambor and Blowes, 1991); (b) more complex assemblage from the Nickel Rim tailings, Sudbury, showing the downward disappearance of jarosite (J) and goethite (go), and the coincident appearance of pyrrhotite (po). Other abbreviations are tc talc, am amphibole, fs plagioclase, bi biotite, cpx clinopyroxene, mg magnetite (after Jambor and Owens, 1993).

and useful method of detecting the sulfides and determining their distributions. Subsequent SEM examination, combined with qualitative energy-dispersion analyses (EDX) and supplemented by quantitative microprobe analyses, will provide essential information on the mineral sources of various trace elements. For example, although the formula for tetrahedrite is written ideally as $(Cu,Fe)_{12}Sb_4S_{13}$ (Fleischer and Mandarino, 1991), the metal position is commonly partly occupied by Zn, Ag, Cd, and Hg, and the semi-metal position has substitutions of As, Bi, and Te (Johnson *et al.*, 1986; Johnson, 1994). Similarly, sphalerite (Zn,Fe,Cu,Cd,Mn)S, is typically the principal source of Cd in deposits, pyrite and pyrrhotite are generally the sources of Ni and Co in non-nickeliferous ores, and Cr is most commonly derived from magnetite $Fe^{2+}(Fe^{3+},Al^{3+},Cr^{3+})O_4$.

The recognition of carbonate minerals in the primary assemblage is geochemically important because these minerals are generally the principal acid neutralizers in oxidizing tailings. The most commonly occurring carbonate minerals in ore deposits are one or more of calcite $CaCO_3$, dolomite $CaMg(CO_3)_2$, ankerite $Ca(Fe^{2+},Mg,Mn)(CO_3)_2$, and siderite $Fe^{2+}CO_3$. Partial cation substitutions such as Fe and Mn for Mg in dolomite, and Mg and Mn for Fe in siderite are the norm; less common, but also of potential significance locally, are Zn and Sr substitutions. Because the carbonates are the first to be attacked following acid generation, they are commonly the principal sources of Mg and Mn, as well as adding Ca, Fe, and other elements to the hydrogeochemical system. The carbonate minerals, however, have different buffering capacities (*e.g.*, MEND 1991), and for the purposes of predictive models (*e.g.*, Scharer *et al.*, 1994) it should be noted that siderite and dolomite-ankerite are among the principal species occurring in most tailings accumulations from massive-sulfide and vein-type gold deposits, both types of which account for the bulk of Canadian acid-generating impoundments.

The presence of carbonate minerals in tailings is generally readily detected using transmitted-light microscopy, or by exposing a portion of the tailings sample to a mild acid (such as dilute HCl) and checking for effervescence, which signifies carbonate-mineral digestion. The distribution and associations of calcite in thin sections of some tailings can be determined using Alizarin red A (Friedman, 1959), which imparts a bright red stain to calcite grains; although it is also useful for the detection of dolomite-ankerite in rock specimens, the stain is ineffective for these minerals in tailings because of the fine particle sizes.

Acidification of portions of tailings samples may divulge useful qualitative information about the nature of the carbonates. For example, a 10% solution of acetic acid will generally attack only calcite, so that this phase can be selectively removed from X-ray diffractograms. In some instances it has been found useful to obtain successive diffractograms of a sample portion after water-washing to remove gypsum, after acetic-acid treatment to remove calcite, after acidification with a 5—10% HCl

solution to remove dolomite, and after treatment with stronger acid to remove siderite. The diffractogram of the residue thus not only provides an indication of the simpler, carbonate-free assemblage, but may also reveal previously hidden diffraction lines that contributed to the apparent peak heights intitially assignable to carbonates alone.

The quantitative determination of the various carbonate minerals that may be present in a tailings sample is not easy because the positions of the X-ray diffraction lines and their peak heights will shift according to the cation substitutions that have occurred. Further complications are that the minerals do not diffract with equal intensity, and that compositions of each mineral are generally highly variable not only within a deposit, but also within a single tailings sample. As these variations can have a profound effect in interpreting analytical CO_2 contents (Table 3.1), determinations of the carbonate-mineral compositions and mineral proportions are highly desirable. Depending on the complexity of the carbonate-mineral assemblage, at least semi-quantitative apportionment of the various carbonate minerals may be achievable by microprobe analyses of numerous grains to obtain composition ranges and means, and by combining these results with data obtained by an image-analysis technique or the use of calibrated X-ray curves constructed from mixtures of the relevant minerals.

Table 3.1. Theoretical compositions of some relevant carbonate minerals

		Composition (wt%)				
Mineral	**Formula**	**CO_2**	**CaO**	**MgO**	**FeO**	**MnO**
calcite	$CaCO_3$	43.97	56.03			
magnesite	$MgCO_3$	52.19		47.81		
siderite	$FeCO_3$	37.99			62.01	
rhodochrosite	$MnCO_3$	38.29				61.71
dolomite	$CaMg(CO_3)_2$	47.73	30.41	21.86		
ankerite	$CaFe(CO_3)_2$	40.76	25.97		33.27	
1:1	$Ca(Mg,Fe)(CO_3)_2$	43.97	28.01	10.07	17.95	
kutnohorite	$CaMn(CO_3)_2$	40.93	26.08			32.99

As a final comment about the primary mineralogy, it should be noted that the absence of a specific mineral or minerals in the oxidized zone of an impoundment does not necessarily mean that dissolution has occurred. On the contrary, mineralogical variations with respect to abundance and species are the norm in an impoundment because the source (the ore deposit) is rarely uniform and, on a smaller scale, because substantial mechanical sorting can occur during tailings accumulation. The sorting may arise from natural causes, but could also be the result of mine procedures designed to impart stability to the impoundment, or could be related to the retention of cycloned

coarse fractions for use as backfill. In some instances the feed to an impoundment of a single deposit may be sufficiently diverse that large-scale mineralogical zoning ensues (Jambor *et al.*, 1993b).

3.6.2. Secondary Minerals

The dearth of mineralogical information about the mineralogy of oxidized sulfide-rich tailings impoundments is truly remarkable, especially when compared to the voluminous literature on hydrogeochemical aspects of AMD, and to the laboratory and computer simulations of AMD generation. Perhaps because of the health implications of radioactivity, in the past more studies have been done for uranium-bearing tailings than for sulfide-rich ores. A recent comprehensive study of element migration from the Poços de Caldos U-Th-REE deposit in Brazil (Chapman *et al.*, 1992a,b) perhaps provides a model of the integration of mineralogical investigations and geochemistry even though processed wastes were not dealt with. In terms of mineralogical investigations related to AMD, for historical reasons pyritiferous coal wastes have received the most attention; coal mining and the attendant accumulation of wastes has taken place for centuries, commonly in populated areas where the environmentally detrimental aspects are most evident, whereas the differential flotation of massive sulfides only came into being with the exploitation of the Zn-Pb deposits at Buchans, Newfoundland, in the 1920s (Swanson *et al.*, 1981).

a. Coal Deposits

Many coal deposits contain small amounts of pyrite, pyrrhotite, and marcasite, and these are usually responsible for the environmentally negative sulfur-emission aspects that are associated with the burning of massive amounts of coal for heat or power generation. The investigation of secondary minerals developed through the oxidation of iron sulfides in coal has usually been in relation to spoils (waste heaps) rather than tailings, but the secondary products that have evolved are germane to sufide-bearing wastes in general.

Table 3.2 lists the minerals that have been identified as secondary products in coal spoils. The predominance of iron sulfates is apparent; these are derived from oxidation of the iron sulfides, whereas the aluminum-rich sulfates are generally derived from the oxidized shaly host rocks. The list of spoil-associated secondary minerals is relatively small in comparison to the large number of iron sulfates that have been identified within coal workings. The paucity may be related to the lesser amount of mineralogical studies of spoils, but more likely reflects the different conditions prevailing at surface.

Table 3.2. Secondary minerals formed from the oxidation of coal wastes.*

Mineral	Formula	Mineral	Formula
gypsum**	$CaSO_4.2H_2O$	coquimbite	$Fe_23+(SO_4)3.9H_2O$
bassanite	$2CaSO_4.H_2O$	alunogen	$Al_2(SO_4)_3.18H_2O$
melanterite	$FeSO_4.7H_2O$	halotrichite	$FeAl_2(SO_4)_4.22H_2O$
rozenite	$FeSO_4.4H_2O$	thenardite	Na_2SO_4
szomolnokite	$FeSO_4.H_2O$	jarosite	$KFe_3(SO_4)_2(OH)_6$
römerite	$Fe^{2+}Fe_2^{3+}(SO_4).14H^2O$	goethite	FeO(OH)
copiapite	$Fe^{2+}Fe_4^{3+}(SO_4)_6(OH)_2.20H_2O$	lepidocrocite	FeO(OH)
illite-smectite	mica-clay minerals	hematite***	Fe_2O_3
kaolinite***	$Al_2Si_2O_5(OH)_4$	sulfur	S

*Data from Palache *et al.* (1951), Taylor (1973), Taylor and Hardy (1974), Zodrow and McCandlish (1978), Wagner *et al.* (1982), Kerth and Wiggering (1990), Davidson (1990), Wiggering (1987), and Cravotta (1994). Oxidation of iron sulfides is an exothermic reaction which in coal wastes commonly leads to high tempertures and may progress to spontaneous ignition. Many of the higher temperature products, which are not included as secondary minerals, have been characterized and accepted as legitimate minerals by the Commission on New Minerals and Mineral Names, International Mineralogical Association. The CNMMN recently suspended the policy of accepting that the high-temperature products are minerals.

** Dehydrates to bassanite, then to anhydrite (CaSO4) at progressively higher temperatures.

*** Identification as secondary minerals uncertain.

b. Gossans

Gossans are the yellowish to reddish deposits of iron oxides and oxyhydroxides that are produced near surface as a consequence of the natural oxidation and leaching of sulfide minerals (Bates and Jackson, 1980). The formation and mineral character of gossans are discussed at length by Blain and Andrew (1977) and Nickel and Daniels (1985).

The number of secondary minerals identified to date in tailings is minute in comparison to that found in gossans. Gossans and sulfide-rich mine tailings have similarities in that, with maturity, both generally yield a leached, sulfide-depleted and silica-enriched surface zone which is succeeded downward by a zone enriched in iron oxides and oxyhydroxides, and then by a zone of precipitation of secondary sulfides. An important distinction between the two initial entities, however, is that gossans represent the weathered surface residue of the combined ore and gangue minerals in a deposit, whereas in tailings nearly all of the valuable minerals have been extracted. Ore processing modifies the physical character of the original minerals by comminution, disturbs the original mineral associations, and changes the mineral proportions and therefore the bulk chemistry of the original assemblage (usually decreasing the total sulfide content, sometimes drastically). Thus, although analogies between an oxidizing tailings impoundment and an assumed precursor gossan can be drawn (Blowes *et al.*, 1992; Boyle, 1994), it also can be argued that the two have little more than superficial similarities.

The mechanisms and pathways that lead to the generation of secondary minerals from primary assemblages are broadly similar for gossan development, weathering and soil formation (*e.g.*, Pickering, 1989; Thorez, 1989), and for the development of AMD. In tailings oxidation the prior removal of the ore metals during beneficiation lessens the potential for development of exotic mineral species, but the increased accessibility to oxidation and acid generation in most tailings enhances the possibility that elements present in only trace amounts can occur in significant concentrations in the hydrogeochemical system. Tailings differ from gossans and most soils in that chemical reactions in sulfide-rich tailings are geologically extremely rapid, thus leading to the potential selective dissolution and "dumping" of trace metals rather than their slow dispersion and dissipation into the aqueous environment.

c. Sulfide-rich Tailings

One of the primary purposes, as envisaged here, of determining the mineralogy of a tailings impoundment is to distinguish between geochemically inferred secondary minerals and those which have actually been observed. For example, many geochemical models adopt $Al(OH)_3$ as the solid-phase precipitate that decreases pore-water Al concentrations, but the reality is that this phase has never been identified either as a secondary mineral in tailings or as an AMD precipitate. The implication is not that the

geochemical attribution is incorrect, but that mineralogists should be alerted to this and other related correlations which remain to be documented; awareness of what to search for might bridge the current gap between theory and observation, ultimately leading to revised and improved parameters for geochemical and predictive models.

Table 3.3. Secondary minerals identified in sulfide-rich tailings

	Iron oxyhydroxides	**Sulfates (cont'd)**	
goethite	α-FeO(OH)	anglesite	$PbSO_4$
lepidocrocite	γ-FeO(OHO)	alunogen	$Al_2(SO_4)_3.17H_2O$
akaganéite	β-FeO(OH,Cl)	unidentified	$(Cu,Fe)(SO_4,AsO_4,PO_4)$
maghemite	γ-Fe_2O_3	copiapite	$Fe^{2+}Fe_4^{3+}(SO_4)_6(OH)_2.20H_2O$
ferrihydrite	nominally $5Fe_2O_3.9H_2O$ or $Fe_5HO_8.4H_2O$		
	Sulfates	**Other minerals**	
gypsum	$CaSO_4.2H_2O$	marcasite	FeS_2
bassanite	$2CaSO_4.H_2O$	covellite	CuS
jarosite	$KFe_3(SO_4)_2(OH)_6$	sulfur	S
hydronium jarosite	$(H_3O)Fe_3(SO_4)_2(OH)_6$	cristobalite	SiO_2
melanterite	$FeSO_4.7H_2O$	vermiculite	$(Mg,Fe,Al)_3(Si,Al)_4(OH)_2.4H_2O$
goslarite	$ZnSO_4.7H_2O$	mixed-layer mica-vermiculite	—
ferrohexahydrite	$FeSO_4.6H_2O$	smectite	$X_{0.3}Y_{2.3}(Si,Al)_4O_{10}(OH)_2.nH_2O$
epsomite	$MgSO_4.7H_2O$	kaolinite	$Al_2Si_2O_5(OH)_4$
hexahydrite	$MgSO_4.6H_2O$		
siderotil	$FeSO_4.5H_2O$		
rozenite	$FeSO_4.4H_2O$		

Table 3.3 lists the secondary minerals that have been identified in sulfide-rich tailings. The tabulation is rigidly restricted to confirmed "*in situ*" impoundment occurrences because the present objective is correlation with impoundment hydrogeochemistry. Other secondary salts have been observed in laboratory experiments and lysimeter studies simulating tailings oxidation (*e.g.*, Ritcey, 1989), and the list could be expanded considerably by including secondary minerals that have formed on mine rock-wastes and stockpiles (*e.g.*, Jambor and Boyle, 1965; Jambor, 1987; Graeme, 1981; Kwong, 1991; Williams, 1990). Several secondary minerals also have been found on weathered slags (McSweeny and Madison, 1988), and the ancient slags at Laurium, Greece, are a famous site for minerals of this type (Palache *et al.*, 1951). The recent recognition of a sulfite and thiosulfates as the products of the weathering of slags is of particular interest because these phases represent intermediate products between the oxidation of sulfides to sulfates (Braithwaite *et al.*, 1993).

In sulfide-rich tailings impoundments, the most abundant secondary minerals have been found to be gypsum $CaSO_4.2H_2O$, and goethite $\alpha FeO(OH)$, which occur universally; jarosite $KFe_3(SO_4)2(OH)_6$ is also common, but may be sparse in some

deposits, and is generally more restricted in distribution in the vertical oxidation profile. Goethite, which is formed principally from the oxidation of pyrite and pyrrhotite, typically occurs throughout the unsaturated zone. In a mature oxidation profile, however, there may be relative decrease in goethite abundance in the at-surface leached zone, and intermediate to mature profiles both show maximum accumulations at depth, commonly forming a hardpan layer that marks the zone of increased pH in the profile. Jarosite distribution roughly follows that of goethite, but seems to be slightly more sensitive to maturity. In a mature profile, jarosite may be absent or scarce in the at-surface leached zone, but increases in depth to, and including, the hardpan layer. This type of profile seems to mimic that of pH, which in strongly oxidized tailings will be slightly higher near surface because of exhaustion of the acid-generating sulfides.

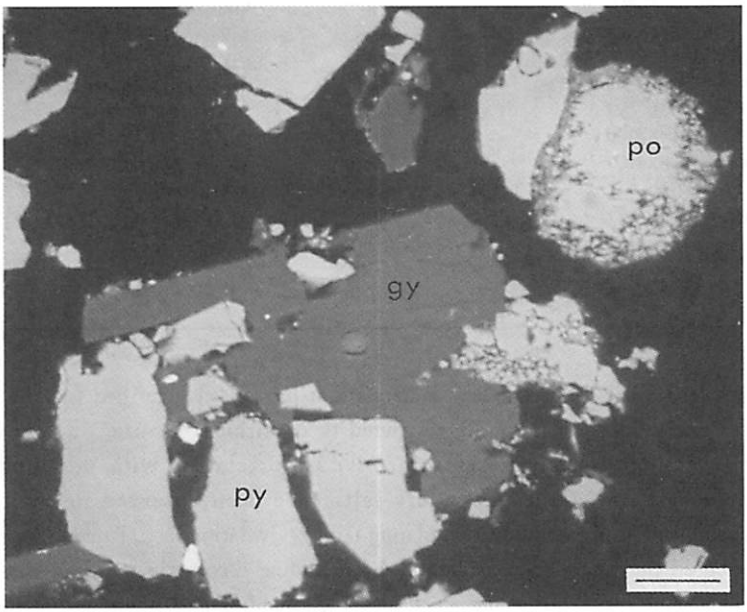

Figure 3.2. Crystal of secondary gypsum (dark grey, gy) cementing several grains of pyrite (py) in a polished section of tailings from the Heath Steele, N.B., impoundment. Pyrrhotite grain at top right (po) is rimmed by iron sulfate and extensively penetrated by covellite. Backscattered-electron image; bar scale represents 20 μm (after Jambor and Blowes, 1989).

Secondary gypsum is characterized by its relatively coarse grain size, with individual crystals commonly a millimeter or more in length (Figure 3.2). Secondary gypsum is typically most abundant in the oxidized zone, but the mineral may also be plentiful throughout the saturated zone. In the oxidized zone the main sources of Ca

and SO_4^{2-} are carbonate-mineral dissolution and sulfide-mineral oxidation, respectively. In the saturated zone the SO_4^{2-} is probably derived from the milling reagents. Lime is commonly added to the mill process-water to elevate its pH prior to discharge with the tailings solids, thus providing a ready source of the Ca for gypsum crystallization.

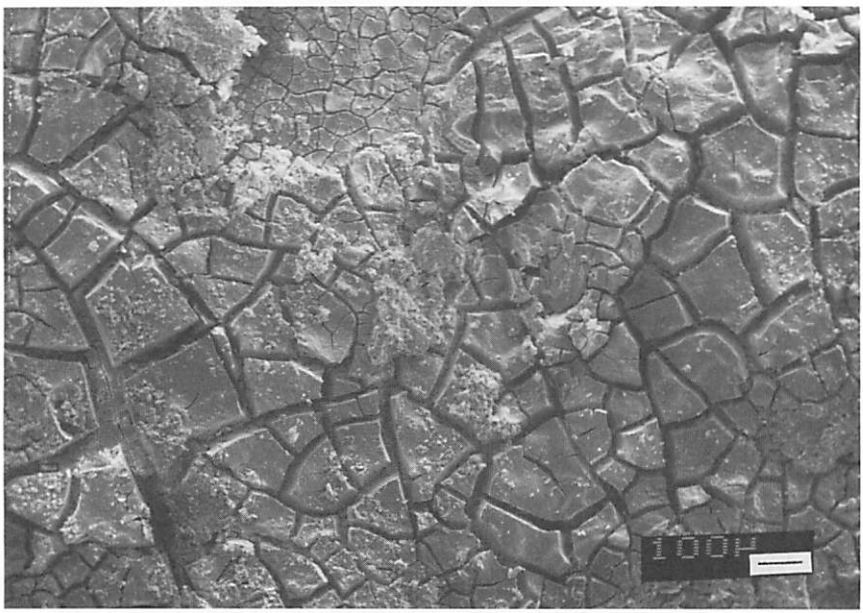

Figure 3.3. Backscattered-electron image of ferrihydrite, showing the typical mudcrack-type texture that develops from dehydration. Sample from Waite Amulet, Quebec. Bar scale represents 100 µm (after Jambor, 1987).

The remaining iron oxyhydroxides observed in tailings (lepidocrocite, akaganéite, and ferrihydrite; Table 3.3) are rare in comparison to the abundance of goethite. The absence of hematite from the secondary minerals is notable, but is in accord with observation by Schwertmann and Murad (1983) that conditions favoring the formation of goethite are generally unfavorable for the formation of hematite, and vice versa. The properties and occurrence of the oxyhydroxide minerals have been discussed in several reviews (*e.g.*, Schwertmann and Taylor, 1977; Murray, 1979; Brown, 1980; Waychunas, 1991; Schwertmann and Cornell, 1991; Bigham, this Volume). The structure of lepidocrocite is well-known, and that of akaganéite has recently been refined by Post and Buchwald (1991), who concluded that Cl- is probably an essential structural constituent. The properties of ferrihydrite and metal-substituted ferrihydrite are reviewed by Childs (1992) and Giovanoli and Cornell (1992), and the

most recent of numerous structural proposals for this mineral are given by Parfitt *et al.* (1992), Manceau and Drits (1993), and Drits *et al.* (1993); although the formula for ferrihydrite remains nominal rather than specific (Table 3.3; see also Bigham, this Volume), it should be noted that the formula $Fe(OH)_3$ corresponds to the mineral bernalite (Birch *et al.*, 1993).

As mentioned, lepidocrocite, akaganéite, and ferrihydrite in sulfide-rich tailings are rare relative to goethite. Akaganéite has been identified only in the oxidized tailings at Heath Steele, New Brunswick, and at Joutel, northern Quebec. At Joutel, the mineral occurs with goethite in spontaneously disintegrating core. At Heath Steele the occurence is as orangy, flaky aggregates that apparently replaced an iron sulfide, probably pyrrhotite. Ferrihydrite has been detected in several tailings sites, occurring as dark reddish brown, thin rinds on various tailings minerals, and as an interstitial cement. The best examples found to date are from the Waite Amulet Zn-Cu mine, Quebec (Figure 3.3).

Lepidocrocite is relatively common in that it has been identified in tailings from numerous sites, though always in only small amounts. The mineral is usually admixed with goethite, and at Waite Amulet both minerals occur as well-defined, complete pseudomorphs after pyrrhotite (Jambor, 1986, 1987). At a former Cu producer in the Joutel area of northern Quebec, pulverulent reddish brown lepidocrocite underlies surface encrustations of melanterite.

Maghemite is rare, but has been identified in the oxidized tailings of the Agnico-Eagle Au mine at Joutel, Quebec. Although the mineral can be derived from the oxidation of magnetite or the transformation of iron oxyhydroxides (Schwertmann and Taylor, 1977), in this particular instance the mineral seems to have been derived from the alteration of pyrrhotite or its oxyhydroxide alteration products.

Most of the $FeSO_4.nH_2O$ sulfates occur as evanescent blooms on impoundment surfaces, but melanterite (together with gypsum) is the principal binder that forms the hardpan layer at Heath Steele, N.B. (Blowes *et al.*, 1991). Epsomite and hexahydrite have been identified as surface blooms at three sulfide-rich impoundments containing abundant dolomite. The origin is attributable to dissolution of dolomite, with subsequent precipitation of Mg as hexahydrite and epsomite, and Ca as gypsum. The presence of goslarite efflorescences on tailings in the Netherlands was reported by Schuiling (1992).

Anglesite is the principal alteration product of galena, typically occurring as rims on it. Occurrences of bassanite are rare and would normally be suspect because of the possibility that it had formed by the dehydration of gypsum. In one of the boreholes from the periphery of the Waite Amulet impoundment, however, bassanite occurs in the loose tailings as snow-white partial coatings on silicates, and as an interstitial

binder among grain aggregates.

Copiapite has been found only in an area of seepage over tailings adjacent to the impoundment at Waite Amulet. The mineral occurred as a bright yellow coating on a portion of a twig that was elevated above ground level. Samples taken at ground level contained jarosite, but no copiapite.

At Heath Steele, some alteration rims on pyrrhotite consist, in part, of Cu-Fe sulfate containing several percent arsenate. The rims are too narrow to obtain an X-ray identification of the phase. In tailings from the impoundment at Delnite Mines Ltd., a former gold producer near Timmins, Ontario, alteration rims on sulfides have been found to contain up to 18.7 wt% As_2O_5, but no arsenate phase could be identified (Jambor and Blowes, 1991). A small amount of arsenopyrite-rich tailings stored near the Delnite impoundment has surface coatings of scorodite $FeAsO_4.2H_2O$, as well as other unidentified phases.

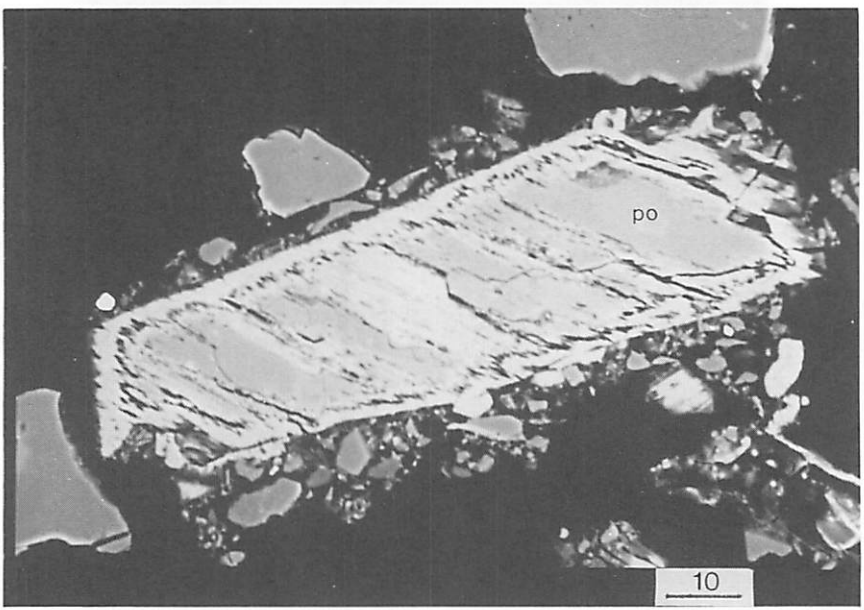

Figure 3.4. Backscattered-electron image of pyrrhotite grain (po) in a polished section of the Heath Steele tailings, showing a rim and extensive replacement by covellite (white). Adjacent large, unaltered grains are pyrite. Bar scale represents 10 μm (after Jambor *et al.*, 1992).

Among the "other minerals" in Table 3.3, covellite, marcasite, and native sulfur are the most common. Covellite has been found at several impoundments, occurring typically at the bottom of the oxidized zone as disseminated grains, rims, and partial

replacements of sulfides, especially pyrrhotite and chalcopyrite (Figure 3.4). Thus, covellite deposition in impoundments emulates supergene enrichment, and deposition of covellite seems to be a principal control on pore-water Cu concentrations.

Marcasite and sulfur are generally closely associated, occurring as the initial alteration products of pyrrhotite (Figures 3.5, 3.6). Alteration commonly progresses in a zonal pattern, ultimately ending in zoned pseudomorphs of iron oxyhydroxides, or iron oxyhydroxides plus sulfur, after pyrrhotite (Figures 3.7, 3.8). Secondary marcasite to date has been found only within the outlines of pyrrhotite grains; sulfur, however, also occurs as an interstitial binder and as minute, dispersed spheres.

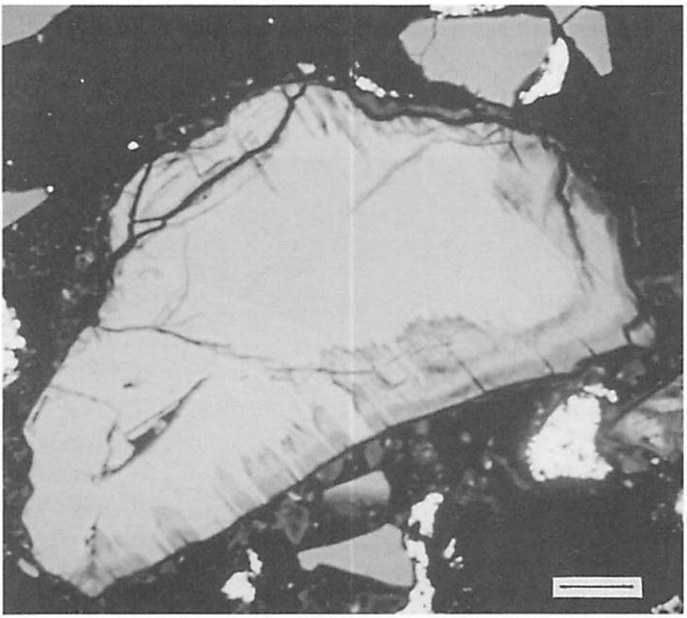

Figure 3.5. Backscattered-electron image of a pyrrhotite grain, rimmed and partly replaced by marcasite, in tailings from a former Cu mine at Joutel, Quebec. Bar scale represents 20 μm.

Cristobalite and mixed-layer mica-vermiculite have been observed only in tailings from the Sudbury area. Biotite-phlogopite in the oxidized zone of these tailings shows a pronounced decrease in color and pleochroic effects as alteration intensity increases. These changes are marked initially by a decrease in potassium, and ultimately by the elimination of potassium and a decrease in iron content (Jambor and Owens, 1993). The non-pleochroic residuals are commonly silica-rich and give poor X-ray patterns in which cristobalite has been detected.

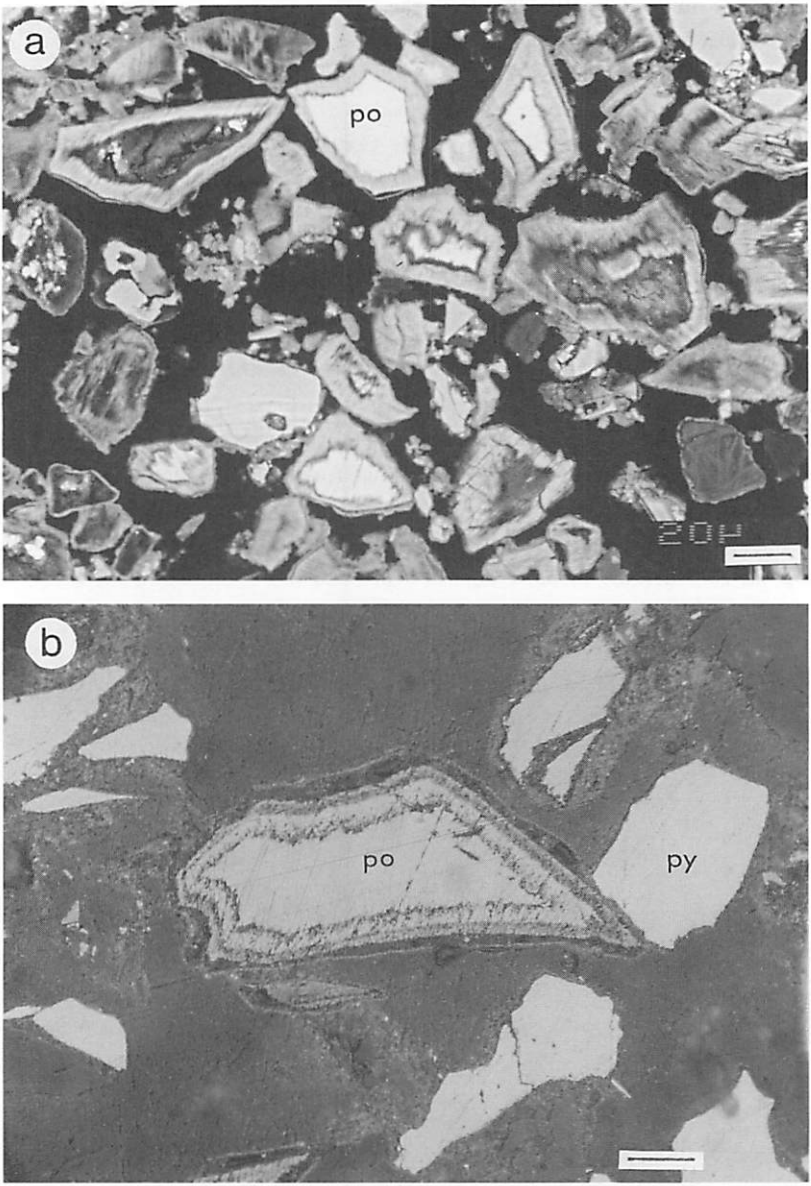

Figure 3.6. Alteration of pyrrhotite to marcasite as seen in polished sections of tailings grains. (a) Backscattered-electron image, showing a few residual cores of pyrrhotite (po) enclosed in rims of marcasite. Some of the cores have been replaced completely and are occupied by iron sulfate (± sulfur). Waite Amulet tailings; bar scale represents 20 µm. (b) Large pyrrhotite grain (po) accompanied by several smaller grains of pyrite (py). The pyrrhotite is surrounded by a rim of marcasite (similar shade of grey), with a thin rim of iron sulfate (dark grey) separating the pyrrhotite-marcasite boundary. Tailings are from an impoundment area near Joutel, Quebec. Reflected light; bar scale represents 20 µm.

The clay mineralogy of tailings from the Copper Cliff Cu-Ni mine at Sudbury, and the Geneva Lake Pb-Zn mine to the northwest of Sudbury, were determined by Rutherford *et al.* (1982). The Geneva Lake mine had ceased production in 1944, and its tailings and those from Copper Cliff both showed well-developed oxidation zones. The clay fraction of some samples from the Copper Cliff oxidized tailings were reported to contain frequent to common (>20% of clay fraction) smectite, kaolinite, and vermiculite. Smectite was absent in the oxidized tailings from Geneva Lake, which in general contained a higher proportion of kaolinite and less vermiculite than the Copper Cliff tailings.

The above brief summary of the occurrence of secondary minerals in sulfide-rich tailings indicates that relatively few minerals have been identified to date. The reasons for the low number are probably related mainly to the scarcity of mineralogical investigations that have been done in the past, and to the restricted climatic conditions (temperate) and deposit types (mainly volcanogenic, Au-vein, and Sudbury-type Cu-Ni) that have been examined recently. Even though tailings are ore-depleted wastes, it is readily predictable that the variety of sulfate minerals occurring in sulfide-rich tailings will expand considerably as more deposit types and more impoundment sites are examined.

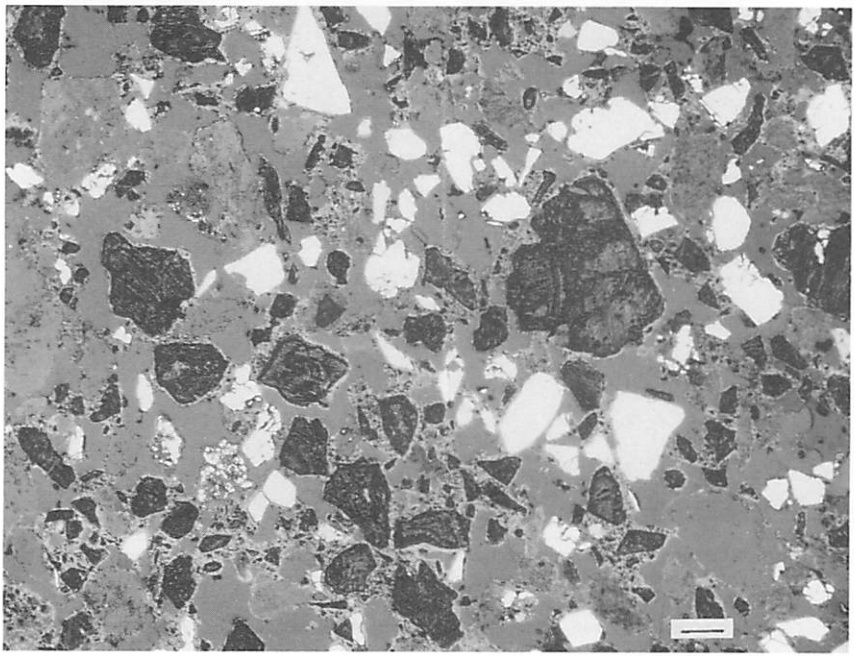

Figure 3.7. Reflected-light photograph of a polished section of tailings from a former Cu mine at Joutel, Quebec, showing numerous grains of pyrite (white), and mottled black grains of native sulfur that are pseudomorphs after pyrrhotite. Bar scale represents 20 μm.

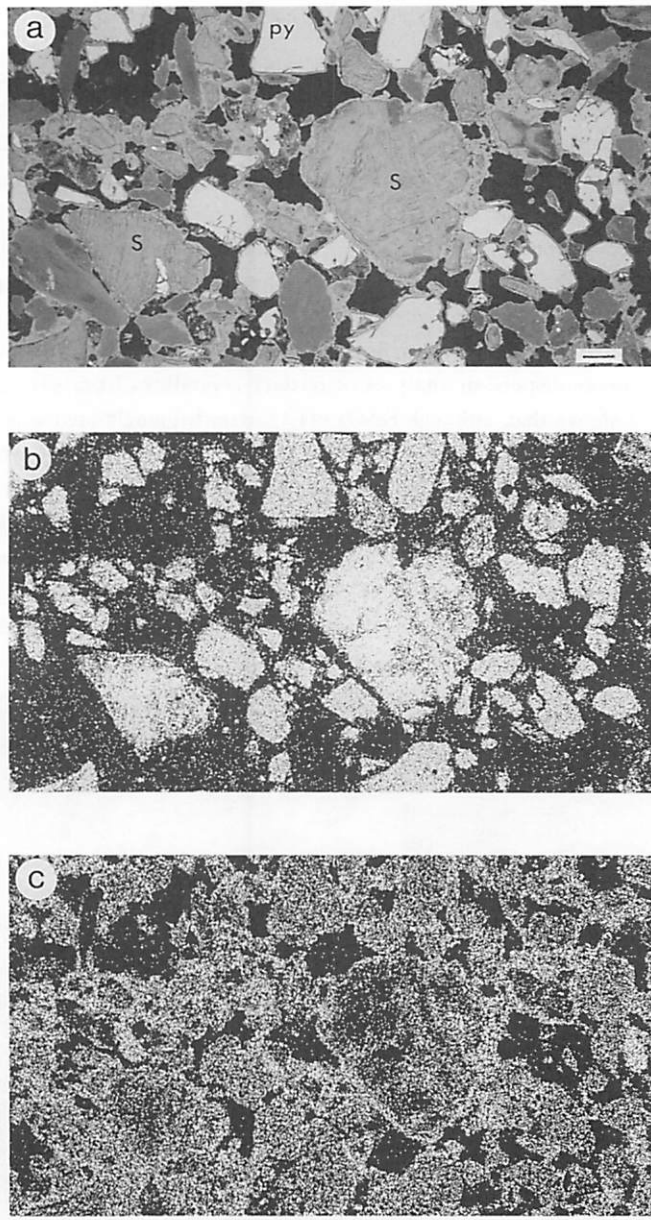

Figure 3.8. Polished section of tailings from Joutel, Quebec (as in Figure 3.7). (a) Backscattered-electron image, showing white grains of pyrite (py) accompanied by numerous large grains of native sulfur (S), cemented by iron oxyhydroxides; (b) X-ray map, corresponding to the BSE image, showing the distribution of S and the concentrations of this element in pyrite and native sulfur; (c) equivalent X-ray map for the distribution of Fe shows iron-rich rims and cementing material, known to be mainly goethite. Bar scale represents 100 μm.

3.6.3. Tertiary Minerals

Tertiary minerals were defined in Section 3.2 as those that crystallize after the tailings samples have been removed from the environment of the impoundment. Tertiary minerals thus represent the precipitates that form from the metal-laden pore waters. As would be expected in pyrite- and pyrrhotite-rich oxidized tailings, most of the tertiary minerals identified to date have been simple iron-rich sulfates in various hydration states: melanterite $FeSO_4.7H_2O$, ferrohexahydrite $FeSO_4.6H_2O$, siderotil $FeSO_4.5H_2O$, and rozenite $FeSO_4.4H_2O$. The trihydrate and dihydrate compounds of this series do not exist; the monohydrate (szomolnokite) is a well-known secondary mineral of relatively common occurrence, but its existence has not yet been confirmed in tailings. Energy-dispersion analyses of tertiary crystallites from various tailings localities have shown that, although $FeSO_4.nH_2O$ overwhelmingly predominates, there are local occurrences in which Zn is dominant (Figure 3.9), and others in which Mg is dominant. Thus, the expected mineral series would be goslarite $ZnSO_4.7H_2O$, bianchite $ZnSO_4.6H_2O$, boyleite $ZnSO_4.4H_2O$, and gunningite $ZnSO_4.H_2O$. The corresponding Mg series would be epsomite $MgSO_4.7H_2O$, hexahydrite $MgSO_4.6H_2O$, pentahydrite $MgSO_4.5H_2O$, starkeyite $MgSO_4.4H_2O$, and kieserite $MgSO_4.H_2O$. Manganese commonly substitutes in all of the above minerals, but the amount of substitution detected in tailings precipitates has been low.

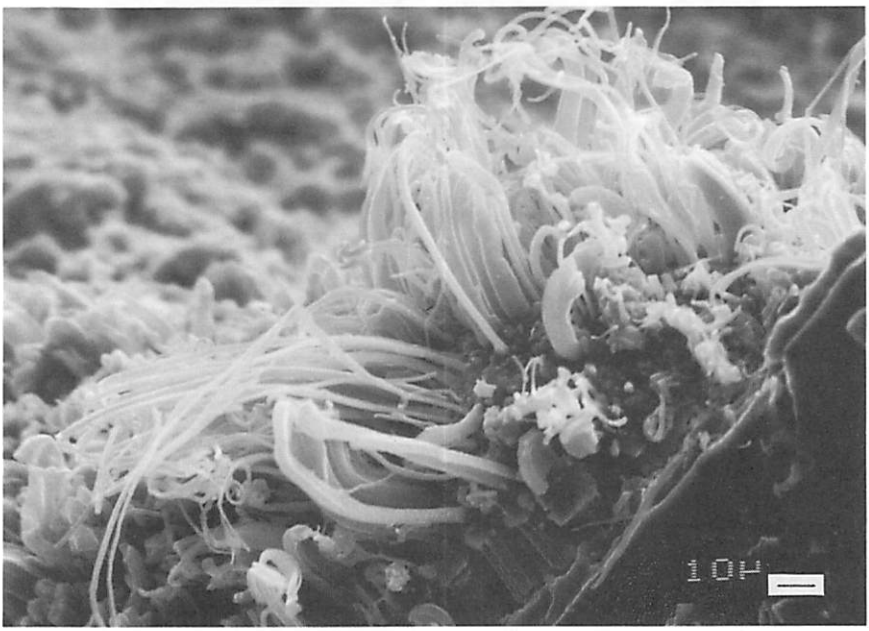

Figure 3.9. Typical filiform habit of tertiary sulfates of the type $XSO_4.nH_2O$, where X is usually Fe and n is 4-7. This particular sample, on tailings from Heath Steele, contains Zn-Fe-Mn-Mg, with Zn dominant. Backscattered-electron image; bar scale represents 10 μm.

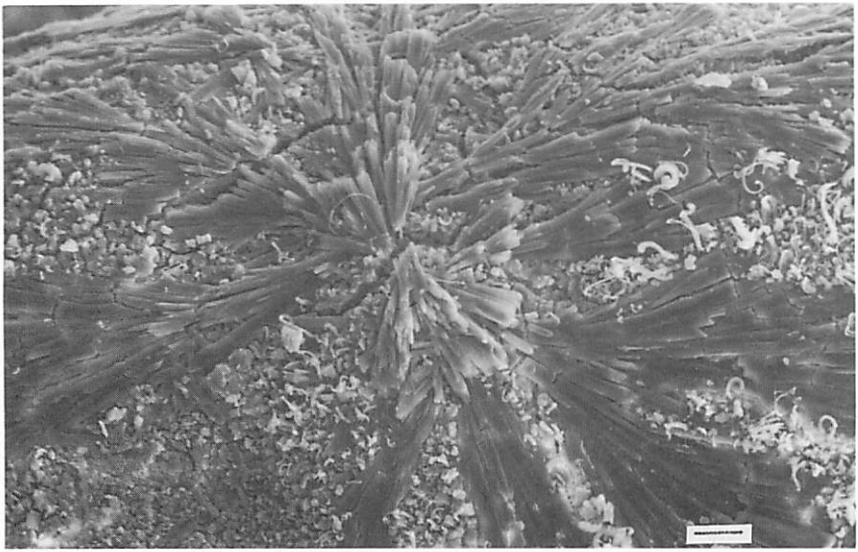

Figure 3.10. Fine-grained sprays of tertiary gypsum on core from Heath Steele tailings. Backscattered-electron image; bar scale represents 40 μm.

Although iron sulfates are common tertiary precipitates, they are generally superseded in abundance and frequency of occurrences by gypsum, which has been observed on cores from almost all tailings-impoundment boreholes. The mineral typically occurs as water-stain-pattern white efflorescences that reflect the gradual saturation in pore-water calcium sulfate as evaporation progresses. Also typical are white to grey, pinhead-size, vitreous dots on core surfaces. The grey color is derived from the core surface, and the gypsum itself consists of transparent, microscopically radial aggregates (Figure 3.10).

At Heath Steele, tailings from the unsaturated zone, as well as a core from the saturated zone, contain white to pale yellowish globules of Al sulfates, one of which has been identified as alunogen (Jambor and Blowes, 1989). These sulfates also occur in the matrix, thereby suggesting the possibility that they may be secondary as well as tertiary precipitates. Aluminum sulfates also occur in cores from the unsaturated zones of the Nickel Rim and Copper Cliff impoundments at Sudbury. In both cases the sulfates are concentrated at the periphery of the cores, suggesting that the tailings pore water may have reacted with the aluminum core barrels.

Covellite has been observed on core surfaces as macroscopic black dots which, in detail, are arborescent-like aggregates. The mineral occurs in this tertiary form at Heath Steele, N.B., and at Nickel Rim, Sudbury, at their hardpan layers and immediately below the unsaturated zone; at these positions the pore-water Cu values are high and

there is active supergene enrichment in (secondary) covellite.

At Waite Amulet, ferrihydrite is present as a secondary precipitate, but the mineral also occurs as razor-thin, brownish, translucent, tertiary coatings on tension cracks that formed during drying of the cores. Ferrihydrite was also detected in cracks in the Nickel Rim cores, and one surface contained a reddish brown, pulverulent coating of lepidocrocite.

Cores from the Kidd Creek tailings impoundment at Timmins, Ontario, contain thenardite (Na_2SO_4) as tertiary efflorescences (Jambor *et al.* 1993a). As the tailings are from the processing of a volcanogenic Cu-Zn deposit, the presence of thenardite is unexpected. The occurrence is thought to result, in part, from the dissolution of natrojarosite-rich residues that are produced in the refining of zinc concentrates and which, since 1985, have been combined with the tailings prior to deposition (Al *et al.*, 1994b).

3.6.4. Quaternary Minerals

Quaternary minerals are those that form on the tailings surfaces after the pore waters have evaporated and the cores have stabilized at room temperature. Quaternary minerals identified to date are siderotil $FeSO_4.5H_2O$, and rozenite $FeSO_4.4H_2O$. These form as efflorescences on core surfaces as a result of the reaction of fine-grained iron sulfides and atmospheric humidity. Tarnishing of mineral specimens in museums is an analogous phenomenon, as is the instability of some pyrrhotite concentrates when stored unprotected under normal laboratory conditions.

3.7. REACTIVITY OF MINERALS

3.7.1. Sulfides

Field observations of mineral deposits, laboratory tests using the mineralogist's standard reagents, the instability of some pyrrhotite-rich concentrates (and even some mine workings), and similar observations leave no doubt that the susceptibility to breakdown is much greater for pyrrhotite than for pyrite, both under natural conditions and those prevailing in tailings impoundments (see also Nicholson, this Volume). An extension of this relative reactivity to other sulfide minerals would be highly desirable in that it would establish an alteration sequence pertinent to geochemical modelling. As can be seen in Table 3.4, however, sulfide reactivities can differ immensely; marcasite, for example, is listed as highly reactive in one sequence, but relatively unreactive in another.

The differences in the proposed or observed reactivities of the sulfides in part reflect the different conditions under which oxidation occurs (*e.g.*, gossans, waste-rock

Table 3.4. Relative reactivity of sulfide minerals

Increasing order of resistance	Condition	Ref.
sphalerite > galena > chalcopyrite > pyrite	abiotic, calculated	1
marcasite > pyrrhotite > chalcopyrite > pyrite = arsenopyrite	waste rock	2
pyrrhotite > chalcopyrite > fine pyrite > sphalerite > galena > coarse pyrite	gossan	3
pyrrhotite > arsenopyrite > pyrite > chalcopyrite > sphalerite > galena	laboratory, pH 2-6	4
pyrrhotite > pyrrhotite-pyrite > pyrrhotite-arsenopyrite > arsenopyrite > pyrite > chalocpyrite > sphalerite > galena > chalcocite	___	5
pyrrhotite > chalcocite > tetrahedrite > galena > arsenopyrite > sphalerite > pyrite > marcasite > chalcopyrite	___	6
sphalerite > tetrahedrite group > chalcopyrite > Bi-Sb sulfosalts > galena > arsenopyrite > pyrite	gossan	7
pyrite > chalcopyrite > galena > sphalerite	air oxidation	8

1. Sarveswara Rao et al. (1991)
2. Kwong & Ferguson (1990)
3. Andrew (1984)
4. Kakovsky & Kosikov (1975)
5. Flann & Lucaszewski (1970)
6. Brock et al. (1984), abridged
7. Boyle (1994)
8. Brion (1980), by X-ray photoelectron spectroscopy

piles, abiotic *versus* biotic, *etc.*). It is noteworthy that in Table 3.4 there is also apparently some importance given to grain sizes and mineral associations. About the only trends common to the various sequences are that pyrite is generally stable whereas pyrrhotite is highly reactive, with galena and sphalerite lying somewhere between these two "end members". Having the sulfide minerals as tailings serves only to diminish the range in particle sizes, but it does not eliminate the problem; depositional sorting can be pronounced, and tailings particle sizes may differ significantly from the sizes of the grains that make up the particles. Thus, a particle of pyrite may consist of a single homogeneous grain, or the particle may consist of hundreds of grains, as in framboidal aggregates.

Another important feature that impedes the development of a simplified, all-encompassing reactivity sequence is that the stabilities of the minerals are strongly affected by element substitutions that can either promote or detract from stabilization. For example, sphalerite can accommodate more than 20 wt% Fe, as well as significant amounts of other elements, most commonly Cu, Mn, Cd, and In; such substitutions introduce structural distortions that make the mineral less stable, and therefore more amenable to dissolution. Similarly, Ag-Bi-Sb substitutions in galena are limited, but their effect is also to make the galena less stable because atoms of different ionic radii and valences are incorporated into the structure. Thus, it can be visualized that a particular mineral deposit will yield sphalerite that is more reactive than galena, whereas for another deposit the opposite might be true.

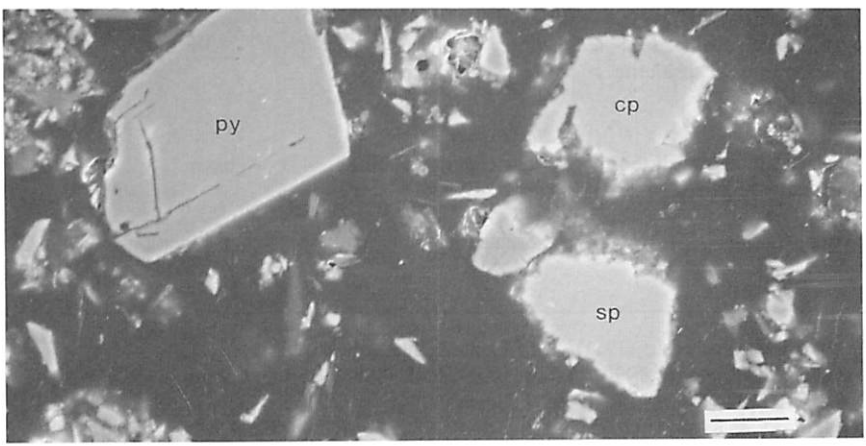

Figure 3.11. Backscattered-electron image of tailings from the unsaturated zone of the Heath Steele impoundment, showing corroded margins resulting from partial dissolution of chalcopyrite (cp) and sphalerite (sp), but with pyrite (py) relatively unaffected. Bar scale represents 10 μm.

Solid-solution substitutions are not necessarily destabilizing, however, and an example of the extreme opposite effect can be seen with ankerite $Ca(Fe,Mg)(CO_3)_2$. The end-member $CaFe(CO_3)_2$ is not known in nature or synthetically (Reeder, 1983;

Woods and Garrels, 1992), thus indicating that partial Mg substitution is necessary to stabilize the structure.

The reactivities of sulfides contained in tailings may eventually be found to differ as widely as the sequences shown in Table 3.4. In most, but not all, impoundments examined to date, however, the general sequence from readily attacked to increasingly resistant seems to be:

pyrrhotite > galena-sphalerite > pyrite-arsenopyrite > chalcopyrite > magnetite

The progression contains some surprises, such as the lack of distinction between pyrite and arsenopyrite breakdown. In this writer's experience, arsenopyrite decomposition in surface deposits generally precedes that of associated pyrite, but in tailings impoundments this distinction, if valid, has not yet been evident. The apparent resistance of chalcopyrite is also surprising, and it should be noted that most chalcopyrite grains observed to date in sulfide-depleted oxidized tailings are encapsulated in silicates, thereby accounting for their escape from the beneficiation process. Survival of liberated chalcopyrite grains is the basis of the relative rating, and in some strongly oxidized zones this mineral has been found to be the only surviving sulfide. At Heath Steele, however, dissolution of chalcopyrite precedes that of pyrite (Figure 3.11).

3.7.2. Other Minerals

Oxide minerals, such as quartz, magnetite, and ilmenite in sulfide-rich tailings impoundments have been observed to be resistant to alteration in comparison with the associated sulfides. The weathering of silicates is well-known to follow the trend of Bowen's reaction series: olivine > augite > hornblende > biotite > K-feldspar > muscovite > quartz, that is, olivine is less stable than augite, augite is less stable than hornblende, etc. in the weathering cycle. A comparable series applies to the plagioclase feldspars, with calcic varieties being the most susceptible to destruction in the series $CaAl_2Si_2O_8$ (anorthite) — $NaAlSi_3O_8$ (albite). Bowen's reaction series for the primary rock-forming minerals is emulated in Goldich's (1938) weathering series which, according to Velbel (1984), is generally confirmed by laboratory studies.

A review of the weathering mechanisms of several rock-forming silicates, including feldspars, micas, pyroxenes, and amphiboles, is given by Velbel (1984), and a succinct summary of modern ideas on the weathering of silicate rocks is given in the introductory section of the paper by Drever and Zobrist (1992). Reactions in a decommissioned tailings impoundment involve minimal mechanical transportation, so analogies with soil formation should focus on the chemical rather than the physical aspects. Recent investigations and discussions of silicate-mineral dissolution are numerous (*e.g.*, Anbeek 1992a,b; Knauss and Wolery, 1989; Knauss *et al.*, 1993; Muir and Nesbitt, 1992; Schott and Berner, 1983; Schott *et al.*, 1981; Velbel, 1993); as

noted by Velbel (1984), however, mineral stability depends in large part on the chemistry of the reactant solutions, which in sulfide-rich impoundments are the tailings pore-waters rather than laboratory milieu. Little is known about the details of silicate-mineral dissolution in tailings, and this aspect remains as fertile ground for future mineralogical investigations.

The widespread formation of jarosite in oxidized impoundments is indicative of silicate-mineral dissolution as a source of K for the jarosite. In most cases the dissolution sources preferred for K release have been biotite $K(Mg,Fe)_3(Al,Fe)Si_3O_{10}(OH,F)_2$ and stilpnomelane $K(Fe^{2+},Mg,Fe^{3+})_8(Si,Al)_{12}(O,OH)_{27}$, with the more stable minerals K-feldspar $KAlSi_3O_8$ and muscovite $KAl_2(Si_3Al)O_{10}(OH,F)_2$ available as supplementary sources.

The apparent dissolution of chlorite in the oxidized zone of the Heath Steele tailings was noted by Jambor and Blowes (1989), and Jambor *et al.* (1992). In Sudbury-area tailings the alteration of biotite-phlogopite to vermiculite and mixed-layer mica-vermiculite was mentioned previously (Table 3.3). On the basis of laboratory studies, Acker and Bricker (1992) reported that both the rate of biotite dissolution and the mechanism of dissolution are pH-dependent; a vermiculite-type product was formed at pH 4 and above, and it was suggested that cation release rates from biotite would be rapid and highly variable in the unsaturated zone.

Almost all of the carbonate minerals listed in Table 3.1 have been noted to occur as primary minerals in tailings impoundments. The extent of solid solution of Fe-Mg-Mn is extensive, but is extremely limited for Ca. Thus, calcite typically contains no more than a few wt% of substitution elements. In dolomite-ankerite and siderite, substitution of Mn is generally minor relative to Fe-Mg interchange. The carbonate minerals are the first non-sulfide minerals to be affected by acid generation in an impoundment, and the relative dissolution rates of calcite, dolomite-ankerite, and siderite seem to follow that of straight-forward acid digestion; *i.e.*, calcite is readily attacked and disappears first, and siderite is the most resistant.

3.8. ALTERATION INDEX

In their study of the Waite Amulet tailings, Blowes and Jambor (1990) found that pyrrhotite and pyrite had been totally oxidized in the near-surface zone of the impoundment, but altered remnants of these minerals reappeared beneath this zone, and the degree of alteration decreased with depth. This replacement of sulfides was numerically classified into an alteration index as shown in Table 3.5. Vertical plots representing core depth showed that the alteration index correlated well with several other mineralogical and geochemical parameters (Figure 3.12), including pore-gas O_2 and CO_2 concentrations (Figure 3 in Blowes and Jambor, 1990).

The sulfide alteration index is nothing more than a scale to indicate the relative degree of alteration of the sulfides. Consequently, such a scale can be constructed for any impoundment in which significant oxidation has occurred. Although any mineral or group of minerals can be used as the key indicators of alteration intensity, the sulfides are obvious choices because these minerals are the first to be oxidized, and the amount of replacement is visually evident by optical microscopy. As pyrrhotite is generally the most susceptible to alteration (*cf.* Section 3.7), the extent of its replacement is a good basis for construction of an alteration index.

Table 3.5. Sulfide altertion index for the Waite Amulet tailings, Quebec (after Blowes and Jambor, 1990)

Numerical scale	Degree of alteration of sulfides
10	Pyrrotite and pyrite obliterated; only traces of sulfide, typically chalcopyrite, are present.
9	Similar to 10, but with a few scattered remnant grains of pyrite.
8-7	First appearance of trace amounts of pyrrhotite (at scale 8); at scale 7 the vestiges of strongly altered pyrrhotite increase in abundance or degree of preservation.
6-2	At scale 6 the pyrrhotite grains have broad alteration rims, but the cores of numerous grains are preserved; gradation to scale 2 is marked by the appearance of narrower alteration rims and a predominance of unaltered grains.
1-0	Only a few grains of pyrrhotite are weakly altered along rims and fractures; >95% of the grains have sharp, fresh margins.

3.9. ADSORPTION BY SECONDARY MINERALS

Secondary minerals act as solid-phase controls on the pore-water concentrations of various elements. This aspect of the geochemistry of sulfide-rich tailings impoundments is discussed by Blowes *et al.* and Alpers *et al.* (this Volume). In addition to the major elements evident from the compositions listed in Tables 3.2 and 3.3, there are numerous trace elements, such as Ni, Co, and Cr, that occur in pore waters, but which are unaccounted for (*e.g.*, no specific mineral of Ni appears in Tables 3.2 or 3.3). Although a detailed discussion of trace-element distributions will not be given here, a few general comments are warranted on the basis of what has been observed in impoundment secondary mineralization as distinct from AMD precipitates in general.

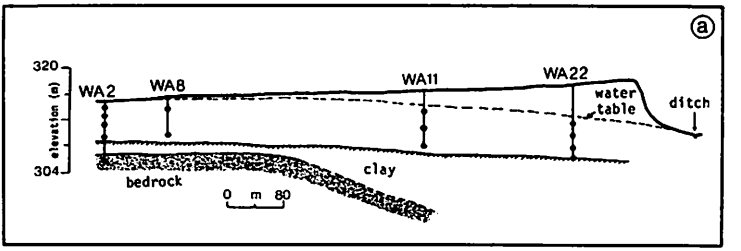
a
320
304
elevation (m)
WA2
WA8
WA11
WA22
water table
ditch
bedrock
clay
0 m 80

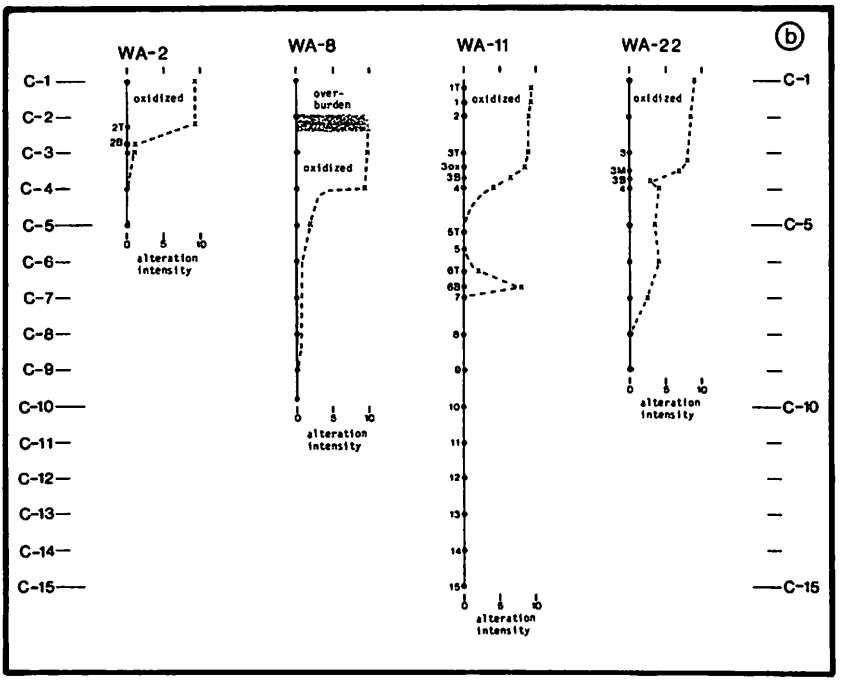
b
WA-2
WA-8
WA-11
WA-22
C-1
C-2
C-3
C-4
C-5
C-6
C-7
C-8
C-9
C-10
C-11
C-12
C-13
C-14
C-15
oxidized
over-burden
alteration intensity

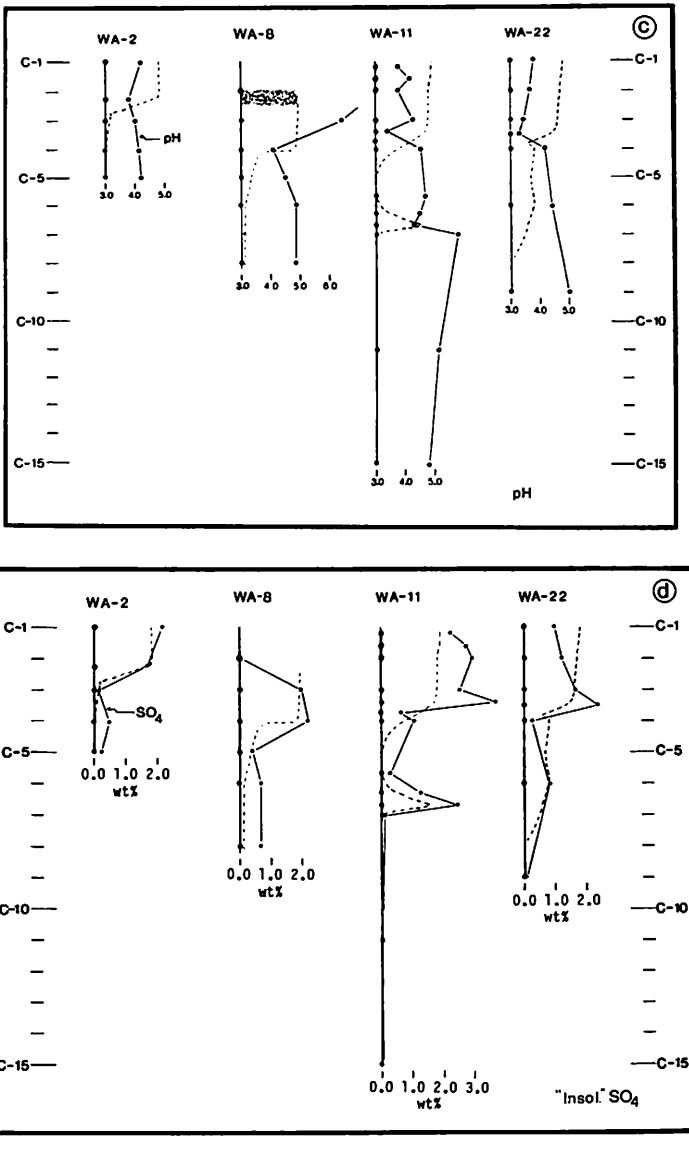

Figure 3.12. (a) Longitudinal section of the Waite Amulet tailings impoundment (Blowes, 1990), showing locations of cored holes and piezometers (dots); (b) alteration index for sulfides (Table 3.5) versus depth. C-1 to C-15 represent vertical core intervals (each 20 cm, total 3 m), dots along the boreholes are positions of mineralogical samples, and each x indicates the intensity of alteration as determined microscopically; (c) alteration index (dashed line) versus pH for the water-soluble fraction of the mineralogical samples (after Jambor, 1987); (d) alteration index versus water-insoluble sulfate, which is a measure of jarosite abundance, showing sympathetic decreases with depth; anomalously strong alteration and high SO_4 at about the C-7 position in hole WA-11 correlate well with a strongly oxidized paleosurface zone (after Jambor and Blowes, 1990).

The strong adsorptive property of clay minerals and zeolites is well-known (*e.g.*, Farrah *et al.*, 1980; Goodman, 1986; Leppert, 1990), and much has been written about the adsorptive affinity of iron oxyhydroxides for various elements (*e.g.*, Manceau *et al.*, 1992). Zeolites are foreign to sulfide-rich deposits, and the clay-mineral contents of most sulfide-rich tailings are low. Natural weathering processes characteristically lead to the development of clay-rich soils, but this seems not to be the case for sulfide-rich tailings impoundments. Whether this relative scarcity of clays is a reflection of the special environment that prevails in impoundments, or a lack of maturity, remains to be seen. The presence of vermiculite and mixed-layer mica-vermiculite alteration products of biotite-phlogopite is generally regarded as a young stage in clay-mineral evolution. The predominance of these vermiculite-type minerals in Sudbury-area tailings, which at roughly forty years are the oldest decommissioned tailings mineralogically examined to date, suggests that immaturity may be an important factor in limiting clay development. Bulk composition of the tailings, which in some cases consist overwhelmingly of sulfides and quartz, clearly would also be an impediment to clay development.

Vermiculite containing up to 13 wt% CuO was reported by Ildefonse *et al.* (1986), who noted that the precursor biotite was Cu-free. The parent biotite in the Sudbury-area tailings is Ni-free, but small amounts of Ni have been detected in the resultant vermiculite-type minerals. Generally, however, the sheer volumes of the secondary minerals in oxidized tailings dictate that, because the incorporation of trace elements in gypsum is negligible, jarosite and goethite must be the principal solid-phase repositories for most trace elements. Although jarosite is capable of incorporating numerous solid-solution elements, such as Pb, Ag, Cu, Al, As, and P, the very few electron microprobe analyses done to date on tailings jarosite have indicated mainly K-Na-H_3O substitutions, without appreciable uptake of other anions or heavy metals.

Substantial solid-solution substitution in synthetic goethite has been demonstrated for Al (Schulze and Schwertmann, 1984; Wolska and Schwertmann, 1993), for Cr (Schwertmann *et al.*, 1989; Manceau *et al.* 1992) for Mn, Ni, and Co (Stiers and Schwertmann, 1985; Cornell, 1991), and for several other cations such as Cu^{2+}, Zn^{2+}, Cd^{2+}, Pb^{4+}, *etc.* (Gerth 1990). Various anions such as carbonate (Russell *et al.*, 1975), phosphate (Parfitt *et al.*, 1975), and sulfate (Turner and Kramer, 1991), are also known to adsorb on goethite. The presence of carbonate in solution has been demonstrated to favor the precipitation of goethite (Ross and Wang, 1982; Carlson and Schwertmann, 1990). Where there is solid solution, the unit-cell dimensions of the goethite structural cell are affected because of the substitution by ions of different sizes. In goethite occurring in oxidized tailings, SEM X-ray images almost always show an intimate association of various trace elements with the goethite, but it has not yet been demonstrated by cell-dimension variations that these elements have been structurally incorporated in the goethite. On the contrary, where the potential substituting elements

occur in appreciable amounts (percentage quantities), Debye-Scherrer X-ray diffraction patterns to date have indicated that the affinity with goethite is spatial rather than structural, *i.e.*, there has been no change in the cell dimensions of the goethite even though no other crystalline phases are detectable on the X-ray patterns.

The affinity of silicon for goethite in tailings is a good example of the spatial *versus* structural relationship. Electron-microprobe compositions of tailings goethite invariably contain silicon (see also Deer *et al.*, 1962) and, although concentrations are highly variable in X-ray maps of Si, in some areas the Si appears to be homogeneously distributed within the goethite. An apparently uniform distribution of an element is commonly interpreted by mineralogists to be a sign of solid-solution substitution, but detailed studies of silica-associated goethite have indicated that structural incorporation of Si does not occur in any quantitatively significant amount (Quin *et al.*, 1988; Smith and Eggleton, 1983; Torrent *et al.*, 1992). Arsenic, which is of particular environmental concern because of its toxicity, also has been shown to have a strong affinity for goethite in tailings (Jambor and Blowes, 1991; Jambor *et al.*, 1992). As with silicon, the concentrations of arsenic are locally high and are too great to be accommodated within the goethite structure; furthermore, as the cell dimensions of goethite are unchanged, solid solution is an unacceptable mechanism to account for the arsenic presence. The general rule for minor-element associations in tailings goethite is that adsorption is prevalent unless proved otherwise.

3.10. ALTERATION AT SULFIDE SURFACES

It is evident from the foregoing text that the complex reactions that ultimately lead to AMD are initially triggered by the oxidation that occurs at the surfaces of the sulfide grains near the subaerial interface of an impoundment. Recent studies of sulfide minerals by using surface-sensitive spectroscopic techniques has provided intriguing information not only on the transformations that occur during the alteration of sulfide minerals, but also on the profound effects that different media and various compositions of aqueous media have in governing what products are formed.

3.10.1. Iron Sulfides

a. Pyrrhotite

Study of the surface oxidation of pyrrhotite ($Fe_{0.89}S$) by X-ray photoelectron spectroscopy (XPS) showed that the initial reaction in air was to have an outward diffusion of iron, thus leaving behind an iron-deficient (or sulfide-enriched) phase of composition $Fe_{0.8}S$ (Buckley and Woods, 1985a). The diffused iron formed a Fe(II) oxide in the transition to a Fe(III) oxide or oxyhydroxide. After further exposure to air only a small amount of sulfate was formed. Treatment of fresh fracture surfaces in aqueous solutions (Buckley and Woods, 1985b) containing hydrogen peroxide led to

the formation of sulfate and elemental sulfur, whereas treatment with acetic acid solution (pH = ~3) did not produce sulfate. Exposure to an ammonia solution (pH = ~11) showed a surface reaction to sulfate and oxidized iron, but no formation of elemental sulfur. After immersion in ammonia solution, however, the sulfate was not detectable, thus indicating dissolution and the formation of an iron oxide layer that inhibited further oxidation.

XPS and Auger electron spectroscopic studies (AES) by Pratt *et al.* (1993a,b) showed that the sulfur at freshly fractured pyrrhotite surfaces exposed to air for a few hours varied in oxidation state from S^{2-} (monosulfide) to S^{6+} (sulfide), and up to 52% of the iron occurred as Fe(III), most likely as hematite. Fresh surfaces leached by de-ionized water and by H_2SO_4 (pH = 3) showed a depletion of sulfur, an enhancement in oxygen, and a predominance of Fe(III) bonded to oxygen. Oxygen and sulfur varied antipathetically, and at a depth of about 100 Å the sulfur attained abundances appropriate for pyrrhotite. Although leaching rates were faster with H_2SO_4 than H_2O, the leaching mechanism seemed to be similar. Upon exposure to HCl (pH = 3), however, the surfaces became enriched in sulfur, predominantly as polysulfide; iron at the surfaces was decreased, and occurred nearly equally as Fe(III) and Fe(II). As well, a monolayer of oxygen was present at the surface.

b. Pyrite

XPS study of pyrite (Buckley and Woods, 1987) revealed that, within minutes of exposure, iron sulfate formed on fresh fracture surfaces, whereas iron oxide formed on abraided surfaces. With prolonged exposure of fracture surfaces the amount of iron sulfate increased, and an iron oxide but no sulfur appeared.

Fracture surfaces exposed to water led to the formation of iron oxide, but no sulfate was detected. Alteration proceeded stoichiometrically, with iron-rich and sulfur-rich regions formed. In contrast, a thick sulfur-rich layer with properties between those of iron sulfide and elemental sulfur appeared after prolonged exposure to acid solution (mixed HCl and HNO_3). Exposure to air-saturated acetic acid resulted in the development of a thin layer of metal-deficient (sulfur-enriched) iron sulfide; because the mineral was not attacked further, it was inferred that this sulfide product must have a protective, outermost layer of sulfur atoms. Exposure of pyrite to air-saturated alkaline solutions led to the formation of iron sulfate and elemental sulfur.

3.10.2. Other Sulfides

a. Arsenopyrite

XPS and AES were used by Richardson and Vaughan (1989a) to examine arsenopyrite surfaces that had been treated with a variety of inorganic oxidants. These authors concluded that arsenopyrite will oxidize rapidly in the low-pH conditions that

prevail in parts of some tailings impoundments, and that the concentrations of sulfur on the surface layer of the mineral can be influenced by the associated chemical conditions.

Muir *et al.* (1993) determined by XPS and AES that a one-day exposure of fresh arsenopyrite in air increased the concentrations of arsenic and oxygen at the surface. At the upper 20-30Å, about 35% of the arsenic appeared as As(III) and As (V) oxides, and only a minor amount of Fe(II) was oxidized to Fe(III). Sulfur remained unoxidized and buried beneath the surface oxides, to a depth of about 100 Å. In water, however, the mineral underwent oxidative dissolution; a large amount of Fe(III) was detected, presumably from iron oxyhydroxides, and sulfur occurred as sulfide, polysulfide, and minor sulfate.

b. Chalcopyrite

XPS study of chalcopyrite ($CuFeS_2$) fracture surfaces exposed to air showed that, initially, an iron (III) oxyhydroxide and a sulfur-rich sulfide (CuS_2) formed at the surface (Buckley and Woods, 1984a). Subsequently, sulfate appeared, probably as copper (II) sulfate, and the Cu:S ratio of the CuS_2 phase changed to 1:>2.

Oxidation in dilute ammonia solution gave results similar to those for air: copper remained bonded to sulfur, and an iron oxyhydroxide appeared. In contrast, no oxyhydroxide appeared after immersion of fresh fracture surfaces in acetic acid solution, but iron and sulfur values increased, suggesting the presence of a 1-nm layer of $Cu_{0.8}S_2$. Reaction of an acid-treated surface and hydrogen peroxide produced a thicker oxidized layer of metal-deficient copper sulfide, as well as elemental sulfur.

c. Bornite

Bornite (Cu_5FeS_4), although much less widespread and less abundant than chalcopyrite, can be an important ore mineral in some deposits, such as those of porphyry copper. Bornite is also of interest because it quickly takes on a purplisn iridescent tarnish and is less stable than chalcopyrite when exposed to weathering.

XPS study by Buckley and Woods (1983) showed that freshly cleaved surfaces of bornite tarnish rapidly in air, producing a purplish tarnish that is close to its limiting thickness after about two days. Initially, iron migrates to the surface to form an Fe(III) oxide, leaving behind a copper sulfide of possible composition Cu_5S_4; with time the iron oxide segregates to the surface as an overlayer of variable thickness on the copper sulfide. Bluish patches may also form after as little as one or two days exposure, and these patches have been found to contain Cu(II). The Cu(II) may be present as a Cu(II) hydroxide which forms by oxidation of the Cu_5S_4 layer.

d. Galena

The oxidation of galena has been studied by numerous authors (Buckley and

Woods, 1984b; Eggleston and Hochella, 1994, and references therein). Buckley and Woods (1984b) determined by XPS that, upon exposure to air, the initial products of oxidation were lead hydroxide, oxide, and carbonate, thus leaving behind a metal-deficient sulfide. Extended exposures to air resulted in the formation of a sulfate, which was preceded by the appearance of a basic sulfate. Treatment with hydrogen peroxide solution resulted in the formation of elemental sulfur and lead sulfate.

e. Sphalerite

XPS study of pyrite, chalcopyrite, galena, and sphalerite showed that sphalerite was the most resistant to oxidation in air (Brion, 1980; Table 3.4). Surface oxidation of sphalerite was reported to lead directly to the formation of zinc sulfate (Brion, 1980).

f. Pentlandite

Pentlandite $(Fe,Ni)_9S_8$ is of interest because it is the principal source of nickel in the ores at Sudbury, Ontario. Synthetic pentlandite with the composition $Fe_{4.5}Ni_{4.5}S_8$ was examined by Richardson and Vaughan (1989b) after treatment with a variety of inorganic oxidants. It was found that various iron compounds formed more rapidly on the surface than did nickel compounds. After initial oxidation and development of an iron-rich oxidized layer, further oxidation was impeded; oxidation occurred by diffusion through the oxidized layer, resulting in further preferential iron loss and the consequent formation of violarite ($FeNi_2S_4$). The composition of the oxidized layer varied with the oxidant used, and depletion of nickel compounds occurred where dissolution was a factor.

g. Comparisons with Tailings Sulfides

The generation of AMD is related not only to the products that form from the oxidation of sulfides, but also to the rate at which oxidation occurs (*cf.* Nicholson, this Volume). The above spectroscopic studies demonstrate that the products derived from the alteration of a mineral of fixed composition will depend on the composition of the fluid or medium that induces the alteration. Similarly, the rate of oxidation strongly influences the nature of the products and their spatial arrangement, which in turn influences reactions that occur at the solid — liquid interface.

Optical microscopy and SEM studies provide, in a sense, a macroscopic view relative to XPS—AES. Nevertheless, a reiteration of what has been observed in the unsaturated zone of sulfide-rich tailings is informative. For example, no alteration rims have been detected on iron-poor sphalerite, and this is in accord with the experimental results indicating that the oxidation product is a highly soluble zinc sulfate. The typical reaction for galena, both experimentally and in tailings, is to form $PbSO_4$ as an end-product. Chalcopyrite in tailings, however, seems to be subject to dissolution without the formation of the alteration rims detected in the XPS studies. This difference possibly is related to the experimental formation of Cu(II) sulfate, which in a tailings environment would be highly soluble and readily dissipated.

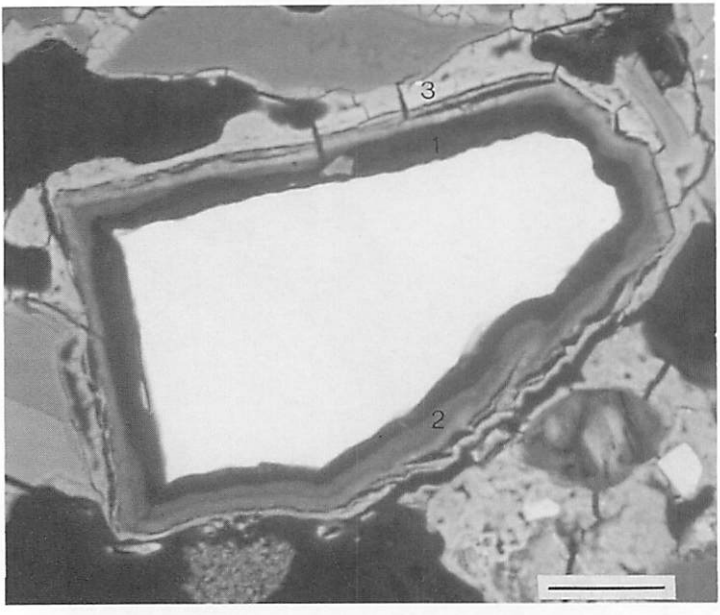

Figure 3.13. Backscattered-electron image of a pyrrhotite grain in sharp contact with an alteration layer of native sulfur (zone 1, black), which is succeeded outward by a slightly zoned layer iron oxyhydroxide, probably goethite (zone 2). The outermost zone (3) is also iron oxyhydroxide, probably goethite, but is sulfate-bearing. The pyrrhotite grain contains trace amounts of Ni, but Ni was not detected in the alteration rim. Tailings sample is from Copper Cliff, Sudbury, Ontario. Bar scale represents 33 μm.

Pyrite and arsenopyrite in tailings commonly develop alteration rims. These rims, which are characteristically narrower than those on associated pyrrhotite, typically consist of goethite. Some rims contain high percentages of sulfate-type sulfur, suggesting that there may be simultaneous formation of iron oxyhydroxide and iron sulfate; arsenic-rich rims on arsenopyrite similarly suggest the presence of iron oxyhydroxide and iron arsenate phases. In some cases, sulfide-type sulfur is present in the rims; although its source is not known, interference from the associated precursor sulfide does not seem to be a good explanation in some instances. Elemental sulfur has not yet been detected in X-ray diffraction patterns of any rim surrounding tailings pyrite or arsenopyrite.

The relationship between the results from XPS—AES experiments and the observed alteration rims on pyrite and arsenopyrite in tailings is difficult to interpret. Possibly the predominant reactions are the initial precipation of ferric hydroxide and dissolution of iron sulfate to form a partly protective layer within which additional dissolution is retarded. Where alteration is more mature and has progressed to the

stage of complete pseudomorphism, compositions of the iron oxyhydroxide are simpler and do not contain the S and As excesses detected in some rims.

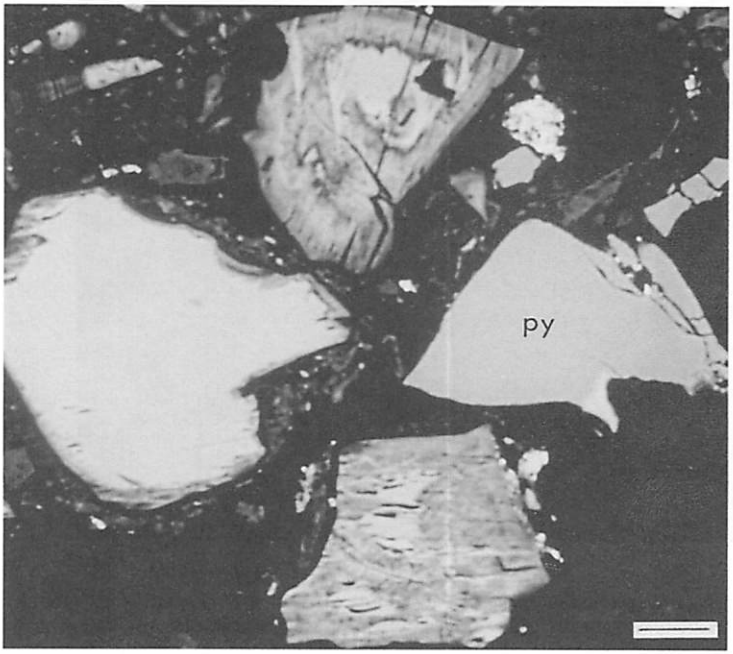

Figure 3.14. Backscattered-electron image of tailings grains in polished section, showing unaltered pyrite (py) and three variably altered grains of pyrrhotite. The top and bottom grains contain only remnants of pyrrhotite, and most of the material is impure marcasite. Electron-microprobe analysis of the bottom grain corresponds to FeS_2, but with a small amount of oxygen also present. Sample is from Joutel, Quebec; bar scale represents 20 μm.

Pyrrhotite in some tailings impoundments has been observed to alter initially to marcasite (Figure 3.5), but in other impoundments the transformation to iron oxyhydroxides is more direct. Pseudomorphism of pyrrhotite grains is common, if not typical; the replacement mineral is usually goethite, but lepidocrocite also has been detected, and pseudomorphism by native sulfur has been observed (Figure 3.7). Thus, various alteration sequences have been noted, *e.g.*, pyrrhotite → marcasite, or pyrrhotite → Fe sulfate → Fe oxyhydroxide, or pyrrhotite → S^o (Figure 3.13). The transformation of pyrrhotite to marcasite may be direct, but more commonly there is an intervening zone of non-sulfide material (Figure 3.6). In many instances the alteration sulfide has a lower reflectance than that of marcasite; one such grain is shown in Figure 3.14. Electron microprobe analysis of the grain corresponds to FeS_2, but with a small amount of oxygen present, possibly indicating fine-scale heterogeneity.

The diversity of products noted in the XPS—AES studies also seems to apply to tailings pyrrhotite. The products formed from pyrrhotite in a tailings impoundment seem to reflect the local micro-environment rather than overall physico-chemical conditions.

3.11. CONCLUSIONS

To date, only a few oxidized, sulfide-rich, decommissioned tailings impoundments have been examined mineralogically. The impoundments have been too few in number and deposit type, and too restricted in climatic setting, to warrant broad statements as to what will occur in oxidizing impoundments in general. Nevertheless, a pattern of mineralogical similarities has emerged with respect to sulfide oxidation and the ensuing products. To date it seems that, if the primary sulfide sources for acid generation are pyrite and pyrrhotite, the principal secondary products are goethite, jarosite, and gypsum, and the main tertiary minerals are gypsum and simple hydrous sulfates of the type $XSO_4.nH_2O$. This pattern has prevailed regardless of whether the tailings are carbonate-rich or carbonate-poor. It has also been observed that the transformation of pyrite in all settings has proceeded directly to goethite-type products; in contrast, pyrrhotite alters in a variety of ways, and marcasite and native sulfur appear as secondary products only in pyrrhotite-bearing tailings. Thus, as pyrrhotite is also much more reactive than pyrite in all tailings settings, it is evident that both the rate of reaction and the pathways of reaction are influenced by pyrite:pyrrhotite ratios rather than total sulfur content of the tailings. This has significant implications in the prediction of AMD because the acid-producing potential of waste solids is generally quantified on the basis of the weight percentage of sulfur in the solids.

In tailings impoundments, the solid-phase controls on pore-water concentrations of various elements are of significant interest and importance to geochemists, but mineralogical work in this area has barely begun. We know, for example, that deposition of secondary covellite strongly influences pore-water concentrations of copper, but there is as yet little knowledge about the intricacies of capture of other elements. In many cases various elements such as Si, Al, S, As, Ni, and Cr have been observed to have a strong affinity for goethite, but solid-solution of these elements, as distinct from the spatial association, has not been demonstrated. In many instances the goethite-affiliated concentrations of elements such as Si and Al are much too high to be accounted for by anything other than the presence of amorphous phases. Perhaps this association accounts for the "amorphous $Al(OH)_3$" that is standard in geochemical calculations; clearly, much more work is needed to clarify and quantify the element associations with goethite. Thus, not only does our knowledge of the general aspects of tailings-oxidation mineralogy need to be broadened, but we need also the details of how the individual minerals, especially the secondary ones, influence the aqueous geochemistry of impoundments.

3.12. ACKNOWLEDGEMENTS

The laboratory studies of tailings were conducted at CANMET, Ottawa, where technical assistance was generously provided by D.R. Owens (microbeam), P. Carrière (X-ray diffraction), and J.M. Greer (lapidary). Much of the work was done in collaboration with D.W. Blowes of the Waterloo Centre for Groundwater Research, University of Waterloo, who provided most of the samples used in the studies. I am also grateful to D.W. Blowes and R.G. Roberts of the University of Waterloo, and J.M. Bigham of The Ohio State University, for critical reading of the draft manuscript.

Chapter 4

Mineralogy of Ochre Deposits Formed by Sulfide Oxidation

Jerry M. Bigham
Department of Agronomy
2021 Coffey Road
The Ohio State University
Columbus, OH 43210-1086 USA

4.1. INTRODUCTION

The oxidative weathering of iron sulfide minerals commonly leads to the formation of ochreous precipitates that are part of a major water-pollution problem in regions with a history of mining for sulfide-bearing coal and ore deposits. Letterman and Mitsch (1978), for example, reported particulate deposition rates of up to 3 g/m2/day in a stream receiving acid coal-mine drainage. Such voluminous blankets of sediment not only have a ruinous impact on native fish populations and benthic communities, but also shorten the effective lifetimes of reservoirs, catchment basins, and wetlands constructed for treatment of acid mine drainage (Fennessy and Mitsch, 1989; Eger *et al.*, 1993; Hedin and Nairn, 1993). Similar accumulations of ochre have been shown to accompany the formation of acid sulfate soils, and to decrease the capacity of subsurface drainage lines installed for the purpose of soil aeration (Bloomfield, 1972; Süsser and Schwertmann, 1983).

Numerous studies have documented the role of mine-drainage ochres in the transport and attenuation of iron and trace elements in surface waters intercepting effluents from adits and waste dumps (*e.g.*, Chapman *et al.*, 1983; Johnson and Thornton, 1987; Filipek *et al.*, 1987; Winland *et al.*, 1991; Fuge *et al.*, 1994; Webster *et al.*, 1994). The natural tendency for these elements to partition into the solid phase through precipitation, sorption, and coprecipitation reactions may be regulated to cleanse wastewaters in commercial treatment systems (*e.g.*, Merrill *et al.*, 1986; Norton *et al.*, 1991); however, the compounds comprising mine-drainage ochres should not be viewed as inert phases under normal conditions. For example, recent studies have demonstrated that diurnal fluctuations in the chemistry of stream systems contaminated with mine drainage may be related to the cyclic dissolution and re-precipitation of ochre deposits caused by photochemically induced oxidation-reduction reactions

(McKnight *et al.*, 1988). Other, more dramatic spatial variations in the geochemical environment (*e.g.*, McKnight and Bencala, 1989; Kimball *et al.*, 1994) may also lead to transformations or changes in the solubilities of mineral phases comprising mine-drainage ochres.

Many quantitative geochemical models for predicting natural water composition are based on chemical equilibria between water and associated solid phases (Nordstrom *et al.*, 1990). Unfortunately, the mineralogy of ochreous precipitates from sulfate-rich mine waters has been oversimplified in most studies of mine drainage. Because of poor crystallinity, such precipitates are commonly referred to in technical articles simply as "amorphous" ferric hydroxide. While it is true that rapid oxidation and hydrolysis of iron may lead to the precipitation of compounds with extremely small particle size (≤10 nm), these materials still represent significant mineralogical diversity. The objectives of this paper are to 1) briefly discuss analytical techniques that have proven useful for the identification and characterization of poorly crystalline products of sulfide oxidation, 2) describe the known range of minerals associated with mine drainage ochres, 3) present a simple case study where analytical techniques and mineral properties can be demonstrated, and 4) summarize our current state of knowledge concerning biogeochemical factors that influence mineral speciation in sulfate-rich waters.

4.2. METHODOLOGY

4.2.1. Sample Collection and Handling

Ochre deposits produced by sulfide oxidation may occur as hardpans in waste dumps (McSweeney and Madison, 1988; Blowes *et al.*, 1991), as soft crusts associated with the seepage and overland flow of mine drainage (Bigham *et al.*, 1992), as sludge in containment/treatment ponds (Milnes *et al.*, 1992), and as loose suspensions of sediment in streams and ditches receiving sulfatic effluents (Karlsson *et al.*, 1988). Consolidated specimens may be relatively easy to secure for laboratory analysis, whereas loose sediments may require access to pumps and the collection of large volumes of material in order to ensure adequate sample size.

Proper treatment of samples following collection depends entirely upon the intended course of study. In all cases, drying at elevated temperatures should be avoided if mineralogical analyses are to be conducted. Drying under such conditions may produce irreversible changes due to the high surface area and poor crystallinity of many mine-drainage ochres. Air drying or freeze drying provide acceptable alternatives. Prior to drying, it may be desirable to remove excess soluble salts by centrifugation, filtration or rapid dialysis. Likewise, it may be possible to reduce or eliminate contamination from detrital mineral particles (*e.g.*, quartz) through the application of

sieve and/or gravity sedimentation techniques. Mineral suites should be simplified as much as possible because of the inherent difficulties involved in analyzing poorly crystalline materials.

4.2.2. *Selective-dissolution Analysis*

Selective-dissolution analysis is a destructive approach that usually includes a suite of chemical extractants designed to exploit the differential dissolution kinetics of minerals occurring in complex mixtures. Ideally, a given dissolution technique should be mineral-specific so that the phase in question is removed quantitatively while leaving other sample constituents unaltered. Strictly speaking, such a separation is impossible with most field samples because they either contain minerals with similar dissolution characteristics or with fairly wide ranges in crystallinity. Nevertheless, selective-dissolution techniques are simple, inexpensive, and may be fairly quantitative if the phases extracted can be verified by other methods of analysis.

Over the past several decades, soil scientists and geologists have developed a number of methods for the selective extraction of Fe oxides (Borggaard, 1988; Chao and Theobald, 1976). Perhaps the best known of these is the dithionite-citrate-bicarbonate (DCB) method of Mehra and Jackson (1960) which takes advantage of the sensitivity of these compounds to reductive dissolution. Numerous variations of this technique have since been proposed (*e.g.*, Coffin, 1963) and new approaches based on chemical reduction are still being developed (*e.g.*, Ryan and Gschwend, 1991). In general, methods utilizing reductive dissolution solubilize Fe occurring as oxides and oxyhydroxides, with minimal impact on other phases (*e.g.*, the silicates). Such methods are generally incapable of distinguishing between different oxide species (*e.g.*, goethite *vs.* hematite).

Methods designed to speciate minerals or phases within the iron oxide/oxyhydroxide group usually involve complexation and/or protonation reactions. In most instances, these methods target poorly crystalline phases and take advantage of naturally accelerated dissolution rates associated with structural disorder. For example, long-term (>90 days) extractions with weak, alkaline solutions of EDTA (a chelating agent) have been proposed for the selective dissolution of "amorphous" Fe oxides in mixed assemblage with silicates or crystalline Fe-oxides (Borggaard, 1982). A more rapid and widely utilized approach for achieving the same goal involves an acid medium with oxalate as the chelating agent. This method was originally proposed by Tamm (1922) and was later modified by Schwertmann (1964). As presently constituted, the technique requires a 2-to-4 hr extraction with 0.2 *M* ammonium oxalate at pH 3 in the dark. Although the sample-solution ratio is not particularly critical, the dissolution reaction is strongly catalyzed both by light (De Endredy, 1963) and by the presence of Fe^{2+} (Fischer, 1972). Thus, minerals such as magnetite and siderite are rapidly dissolved in acid ammonium oxalate (Rhoton *et al.*, 1981). Despite

these limitations, ratios of oxalate-to-dithionite-extractable iron (Fe_o/Fe_d) have been widely used to assess the relative crystallinity of secondary Fe(III) oxides produced by weathering reactions in a variety of surface environments, including mine-drainage systems (Brady *et al.*, 1986; Bigham *et al.*, 1990; Murad *et al.*, 1994).

4.2.3. X-ray and Differential X-ray Diffraction

With proper handling and preparation, well-crystallized minerals formed as a result of sulfide oxidation can commonly be identified readily by X-ray diffraction (XRD) using either Debye-Scherrer or diffractometer techniques. Conventional diffractometers are also useful for the identification of poorly crystallized phases, but analyses must be carried out by slow step-scanning with computer-assisted systems capable of digital data collection and peak-profile analysis. Relatively inexpensive commercial hardware and communications software packages are now available for automation of older XRD systems. X-ray sources yielding CoKα or FeKα radiation are desirable but are not required for analysis of Fe-rich phases so long as the system is equipped with a diffracted-beam monochromator.

The most difficult situations arise when a poorly crystallized phase(s) is present as a minor constituent (<25 wt%) in a sample that also contains well-crystallized components. In these instances, weakly resolved diffraction effects arising from the phase with short-range structural order tend to become "lost" in the background. This problem can be overcome, at least in part, by a combination of XRD and selective-dissolution analysis. Schulze (1981) demonstrated that if a step-scanned XRD pattern obtained from a sample after selective dissolution of all or part of the iron oxide minerals is subtracted from one obtained before extraction (*i.e.*, the original sample), a differential X-ray diffraction (DXRD) pattern of the dissolved fraction can be obtained. He found that goethite or hematite could be detected in a sample containing as little as 1.8 wt % DCB-soluble iron using the DXRD method. Schwertmann *et al.* (1982) subsequently reported that 15 wt % was about the lower limit of detection by DXRD for poorly crystallized ferrihydrite occurring in natural spring deposits and soil samples. The method has also been successfully employed to study the mineralogy of ochre deposits resulting from sulfide oxidation under both natural (Brady *et al.*, 1986) and laboratory conditions (Bhatti *et al.*, 1993).

4.2.4. Mössbauer Spectroscopy

The Mössbauer effect is a nuclear phenomenon involving the resonant absorption of γ-rays. For resonant absorption to occur, there must be limited recoil by both the emitting and absorbing atoms, and the nuclear environments in the source and absorber must be identical. If these environments differ, the energy of the γ-rays must be shifted accordingly, and this is usually accomplished by vibrating the source so as to create a Doppler effect. The Mössbauer isotope of interest in iron-bearing minerals is

^{57}Fe, which has a natural abundance of about 2.19 % (Bancroft, 1973).

In order to generate ^{57}Fe Mössbauer spectra, a ^{57}Co source is used. The ^{57}Co decays by electron capture to ^{57}Fe in an excited state which passes to the ground state with emission of a γ-ray having an energy of 14.41 keV (among others). This γ-ray is generally the most suitable for ^{57}Fe-Mössbauer spectroscopy because it has a low recoil energy and a narrow resonant line-width.

The utility of Mössbauer spectroscopy arises from three major factors. First, the Mössbauer spectrum of an iron mineral is characteristic of that mineral and, with proper interpretation, can be used as a "fingerprint." Secondly, ^{57}Fe-Mössbauer spectroscopy is specific for iron so that analyses may be conducted of iron-bearing compounds in low concentration and without spectral interference from other minerals. Finally, the Mössbauer effect is a nuclear phenomenon and can be used to study finely divided or poorly crystallized materials that may not be responsive to other analytical techniques requiring long-range structural order.

Three parameters, the isomer shift (δ), quadrupole splitting (ΔE_Q), and magnetic hyperfine field (B_i) are commonly extracted from the Mössbauer spectra of iron compounds. The numerical values of these parameters depend upon the type and magnitude of hyperfine interactions that exist between the charge distribution of ^{57}Fe nuclei and extranuclear electric and magnetic fields. Isomer-shift values for Fe^{2+} and Fe^{3+} usually fall within characteristic but separate ranges so that this parameter may be used to determine the oxidation state of iron in a compound. The quadrupole interaction arises when an electric field gradient is imposed on the nucleus resulting in a splitting of the nuclear energy levels and the appearance of a two-line Mössbauer spectrum. The magnitude of this splitting is sensitive to oxidation state, coordination number, and local site distortions. In some iron minerals, the nuclear energy levels of ^{57}Fe may be further split due to interactions with strong, internal magnetic fields. The result is a six-line spectrum wherein the magnitude of the splitting is proportional to the strength of the internal field. Most of the iron oxides are antiferromagnetic, which means that they yield a six-line Mössbauer spectrum because of an antiparallel alignment of equal magnetic moments below a characteristic temperature called the Néel point. Above this temperature, thermal fluctuations prevent the antiparallel alignment of magnetic moments associated with neighboring Fe(III) ions; the oxide behaves as though it is paramagnetic, and its Mössbauer spectrum consists of a doublet.

Additional information about the nuclear environment can be extracted from the Mössbauer line-widths and shapes. Line-widths exceeding about 0.3 mm s^{-1} and significant deviations from Lorentzian shape are indicative of complex conditions in the absorber (Murad, 1988). A good example is the nonideal behavior associated with the phenomenon of superparamagnetic relaxation. This phenomenon is common to small

(<50 nm) iron oxide particles, and is apparently caused by the disruptive effect of the particle surface on long-range magnetic order. Superparamagnetic relaxation averages out the net magnetic field above a certain blocking temperature characteristic of the mineral and the particle size. At or near this temperature, the typical six-line magnetic spectrum "relaxes" to a two-line Mössbauer spectrum characteristic of paramagnetic materials. Relaxation effects of this type can be counteracted by reducing the temperature of the absorber. Because the iron minerals comprising mine drainage ochres typically occur as microcrystals, it is important to utilize a Mössbauer spectrometer equipped with a cryostat so that analyses can be conducted at low temperatures (77 to 4 K).

4.2.5. Other Methods of Analysis

Mineralogical studies of mine-drainage ochres may be facilitated by many different methods of analysis, but several in addition to those already discussed should be mentioned.

a. Color

Perhaps the most striking feature of ochre deposits arising from sulfide oxidation is their bright, yellow-to-red coloration. Many mineralogists are wary of using color as a diagnostic property because of the well-known tendency for pigmentation to vary under the influence of such factors as particle size, aggregation, chemical composition, admixtures, *etc.* There is also a widespread misconception that the color of sediments and other "earthy" materials cannot be measured with any degree of confidence. In fact, the colors of such materials can be measured precisely in the laboratory using diffuse reflectance spectrophotometers (Torrent and Barrón, 1993), and portable tristimulus colorimeters are now available for equally precise determinations in the field (Post *et al.*, 1993). These technical advances, coupled with a better understanding of the spectral characteristics and genesis of minerals comprising ochre deposits (Schwertmann and Cornell, 1991; Schwertmann, 1993; Fanning *et al.*, 1993), should enable useful interpretations concerning not only mineralogy, but also local geochemical conditions to be derived from simple color measurements.

b. Infrared Spectroscopy

Infrared (IR) spectroscopy is a well-known resonance technique wherein spectra originate primarily from the vibrational stretching and bending modes within molecules. It is thus a powerful tool for the study not only of molecular structure, but also of ligand exchange reactions occurring at mineral surfaces. The IR spectrum of a mineral may provide a useful fingerprint for identification purposes, and IR spectroscopy has been the primary analytical tool employed in some studies of the ochreous products from sulfide oxidation (Lazaroff *et al.*, 1982, 1985). In these minerals, diagnostic absorption bands arise primarily from the presence of OH and

SO_4 groups occurring in various configurations.

c. Electron Optical Techniques

Electron optical techniques find natural application in studies of the mineralogy and morphology of the colloidal products resulting from sulfide oxidation. Although particle morphology suffers from many of the same diagnostic uncertainties associated with color, it now seems clear that "typical" morphologies can be assigned to the minerals comprising most mine-drainage ochres. These crystal habits are best observed at the level of resolution afforded by the conventional transmission electron microscope (TEM) and are usually most clearly expressed in samples collected as loose precipitates. The consolidation and/or cementation of ochres into crusts and hardpans seems to have a negative impact on the expression of normal particle morphology. Consequently, morphological analyses of such materials should be viewed with caution. In such cases, selected-area electron diffraction and chemical analyses conducted with a scanning transmission electron microscope may be essential for particle identification.

4.3. MINERALS ASSOCIATED WITH MINE-DRAINAGE OCHRES

The information presented in this section is taken from the technical literature and from studies of specimens collected from an array of mine-drainage environments occurring at various geographic locations. These include mines operated for the production of bituminous coal, lignite, pyrite, silver, copper, and uranium. The aggregate of this information suggests that the major mineral phases associated with mine-drainage ochres include goethite, lepidocrocite, ferrihydrite, schwertmannite, and jarosite. A summary of the major properties of these minerals is presented in Table 4.1.

4.3.1. Goethite α-FeOOH

Goethite is usually considered to be the most stable form of Fe(III) oxide, and it occurs in almost every type of surface environment (Schwertmann and Taylor, 1989; Schwertmann and Fitzpatrick, 1992). In mine-drainage precipitates, goethite is commonly observed as a trace or minor constituent, but is rarely the dominant phase. These goethites have typical, yellowish brown colors with Munsell hues ranging between 7.5 YR and 10 YR. Whereas well-crystallized and/or synthetic goethites commonly display a fibrous or lath-like morphology, those occurring in mine-drainage precipitates usually form short, rod-like particles (Brady *et al.*, 1986, and Figure 4.1a). Typical XRD line-widths at half height are about 1o 2Θ for CoKα radiation (Figure 4.2), corresponding to a particle size of about 15 nm. In contrast to other goethite particles of similar dimensions, which exhibit little reactivity toward ammonium oxalate at pH 3.0, the mine-drainage specimens examined to date have shown moderate solubility in oxalate (Fe_o/Fe_d ratios on the order of 0.3). The reason for this enhanced reactivity is unknown.

Table 4.1. Properties† of minerals encountered in mine-drainage ochres

Mineral Name:	Goethite	Lepidocrocite	Ferrihydrite	Schwertmannite	Jarosite‡
Ideal Formula:	α-FeOOH	γ-FeOOH	~$Fe_5OH_8 \cdot 4H_2O$	$Fe_8O_8(OH)_6SO_4$	$KFe_3(OH)_6(SO_4)_2$
Crystal system	Orthorhombic	Orthorhombic	Trigonal	Tetragonal	Hexagonal
Cell dimensions (Å)	a = 4.608 b = 9.956 c = 3.022	a = 3.88 b = 12.54 c = 3.07	a = 5.08 c = 9.4	a = 10.66 c = 6.04	a = 7.29 c = 17.16
Color	Yellowish brown (7.5YR–10YR)	Orange (5YR–7.5YR)	Reddish brown (5YR–7.5YR)	Yellow (10YR–2.5Y)	Straw yellow (2.5Y–5Y)
Crystal shape	Short rods	Laths	Spherical	Pin-cushion	Pseudocubic
Crystallinity	Moderate	Moderate	Poor	Poor	Good
Most intense XRD spacings (Å)	4.18, 2.45 2.69	6.26, 3.29, 2.47, 1.937	2.54, 2.24, 1.97, 1.73, 1.47	4.86, 3.39, 2.55, 2.28, 1.66, 1.51	5.09, 3.11, 3.08
Major IR bands (cm^{-1})	890, 797	1161, 1026, 753	Nil	1175, 1125, 1055 975, 680, 615	1181, 1080, 1003 628, 493, 472
Néel temp. (K)	400	77	28–115§	75	55–60
Magnetic hyperfine field (T) at:					
295K	38.2	—	—	—	—
77K	50.0	—	≤ 45.1	—	—
4.2K	50.6	46.0	46.5–50.0	45.4	47.0

† Data taken from

Bigham et al. (1990)
Bigham et al. (1992)
Doner & Lynn (1989)
Fanning et al. (1993)
Murad (1988)
Murad et al. (1988)
Murad et al. (1994)
Powers et al. (1975)
Schwertmann (1993)
Schwertmann & Fitzpatrick (1992)
Schwertmann & Taylor (1989)
Takano et al. (1968)

‡ Properties listed are specific to jarosite, but natrojarosite and hydronium jarosite may also occur.

§ Blocking temperature.

Table 4.1. Properties of minerals encountered in mine-drainage ochres.

Well-crystallized specimens of goethite have a Néel temperature of about 400 K and yield a six-line Mössbauer spectrum at room temperature (Table 4.1). By contrast, room-temperature spectra from mine-drainage goethite consists of a doublet, indicating superparamagnetic relaxation that is probably a result of small particle size. At 4.2 K these same goethite samples are magnetically ordered, but they yield hyperfine fields that are slightly smaller than those typical of bulk specimens, thus once again indicating reduced particle dimensions (Murad *et al.*, 1994). Infrared spectra of mine-drainage goethite show diagnostic bands due to OH bending at 890 and 797 cm^{-1}, but may also exhibit additional features arising from surface adsorption of SO_4 (Brady *et al.*, 1986).

4.3.2. *Lepidocrocite* γ-*FeOOH*

Lepidocrocite is a polymorph of goethite that is commonly recognizable in the field by bright orange colors having Munsell hues in the 5 YR to 7.5 YR range, chromas of 6 to 8, and values ≥6 (Schwertmann, 1993). Although lepidocrocite is widespread in surface environments, particularly in soils and recent sediments, observations of the mineral as a product of sulfide weathering are limited. Romberg (1969) reported lepidocrocite as a pseudomorphic replacement product of pyrite; Blowes *et al.* (1991) identified lepidocrocite as a cementing agent in hardpans formed at the depth of active oxidation in sulfide mine tailings, and additional similar occurrences are reported by Jambor (this Volume). Milnes *et al.* (1992) detected poorly crystallized lepidocrocite in an ochreous sludge collected from a retention pond associated with a uranium mine in Australia, and Mann *et al.* (1992) used selected-area electron diffraction to identify microcrystalline lepidocrocite precipitated on the surfaces of microorganisms extracted from waters draining uranium tailings in the Elliot Lake district of Ontario, Canada. Although published XRD and electron optical data are consistent with the data summarized in Table 4.1, little is known about other properties of lepidocrocites from mine-drainage environments.

4.3.3. *Ferrihydrite* ≈ $Fe_5OH_8.4H_2O$

Ferrihydrite has become a popular but often misused synonym for "amorphous" ferric hydroxide. Consequently, it is not surprising to find many references to this mineral in the mine drainage literature (*e.g.*, Nordstrom, 1982a; Filipek *et al.*, 1987; Ferris *et al.*, 1989; Milnes *et al.*, 1992). Ferrihydrite has attracted the attention of physical as well as biological scientists, and its genesis and properties have been the subject of considerable research activity over the past two decades. Much of the resulting literature has been summarized in two recent review articles (Eggleton and Fitzpatrick, 1988; Childs, 1992).

Ferrihydrite occurring in soils and sediments has a rusty, reddish-brown color with Munsell hues in the 5 YR to 7.5 YR range and Munsell values <6 (Schwertmann,

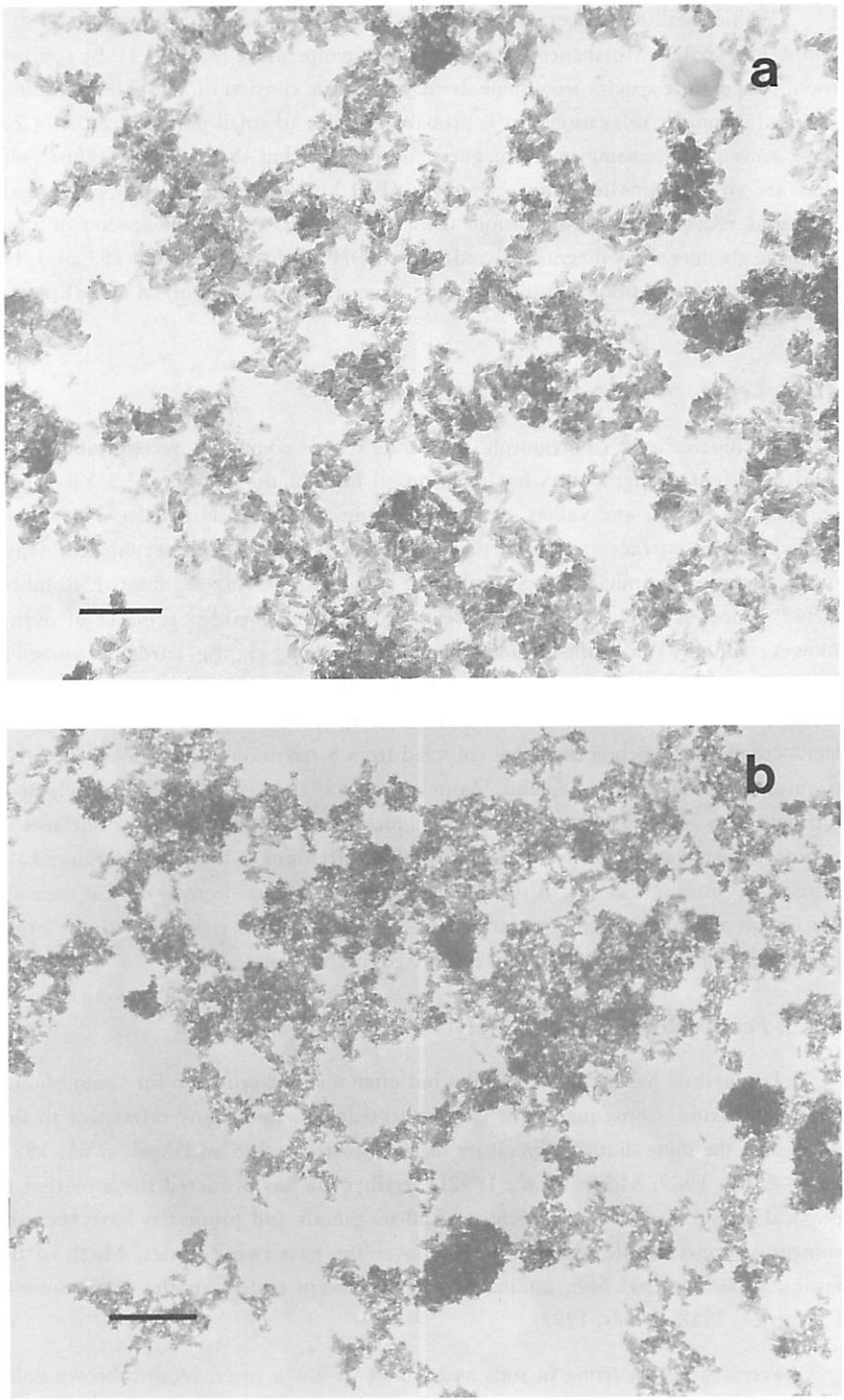
a
b

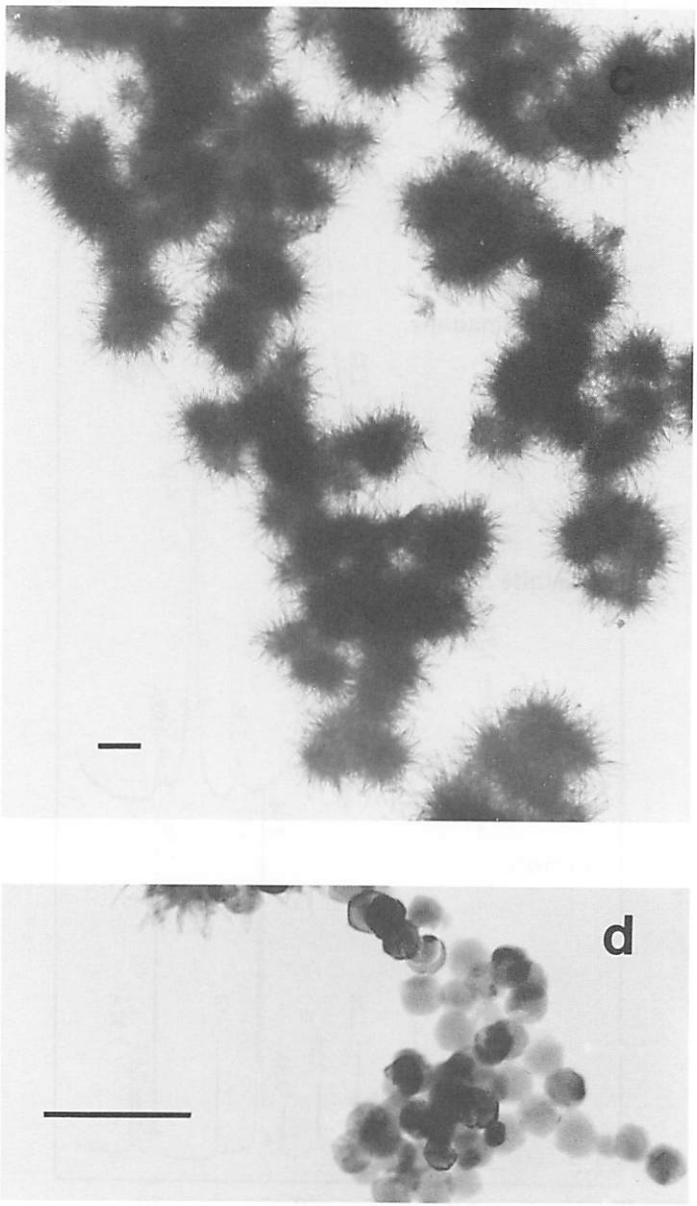

Figure 4.1. Transmission electron micrographs of minerals occurring in mine-drainage ochres: (a) goethite, (b) ferrihydrite, (c) schwertmannite, and (d) jarosite. Scale bar = 0.2 μm.

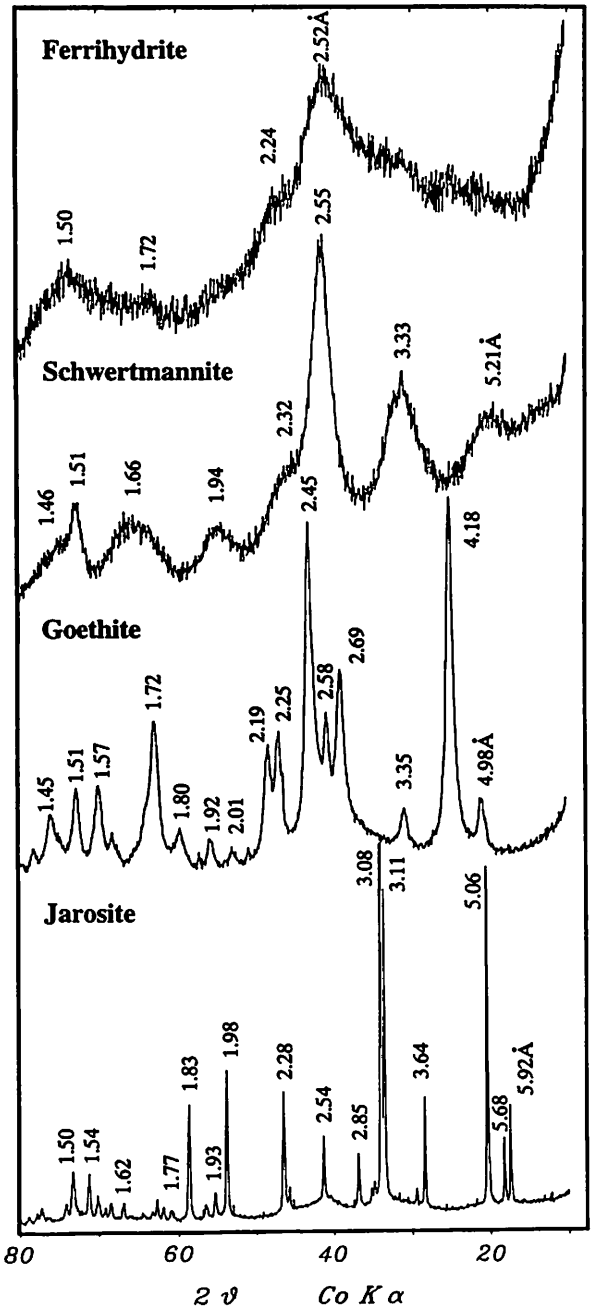

Figure 4.2. Representative X-ray diffraction traces from minerals occurring in mine-drainage ochres (modified from Bigham *et al.*, 1992).

1993). Natural and synthetic samples both usually consist of highly aggregated, spherical particles with diameters in the order of 2 to 6 nm (Figure 4.1b). Consequently, the mineral has high specific surface areas in the range of 200 to 600 m^2/g, and it is readily soluble in both acid ammonium oxalate and DCB so that $Fe_o/Fe_d \equiv 1$. Ferrihydrite is always poorly crystallized, but it can display a range of structural order that gives rise to XRD patterns consisting of anywhere from two (worst crystallized) to six (best crystallized) broad bands (Carlson and Schwertmann, 1981). Most mine-drainage ferrihydrite samples yield two- to four-band profiles (Figure 4.2). Towe and Bradley (1967) originally proposed that ferrihydrite has a defect structure based on that of hematite; however, the structure has remained a point of controversy and several alternative models have also been developed (Harrison *et al.*, 1967; Eggleton and Fitzpatrick, 1988; Drits *et al.*, 1993). The nominal formula for ferrihydrite is commonly taken as $Fe_5HO_8.4H_2O$ (Towe and Bradley, 1967), but Russell (1979) reported on the basis of IR spectroscopy that about half the hydrogen is present as OH, and he suggested the formula $Fe_2O_3.2FeO(OH).2.5H_2O$. Natural specimens also commonly contain up to about 9 wt% Si (Carlson and Schwertmann, 1981; Childs, 1992).

Numerous Mössbauer analyses of ferrihydrite have been conducted. Because of small particle size, natural ferrihydrite is superparamagnetic at room temperature and may remain so down to temperatures as low as 23 K (Murad *et al.*, 1994). Murad *et al.* (1988) observed magnetic blocking temperatures (50 % magnetic order) between 28 and 115 K for ferrihydrite samples of different particle size (Table 4.1). The magnetic hyperfine fields measured for these samples at 4.2 K varied between 50 T for 6-line material and 47 T for 2-line material.

4.3.4. *Schwertmannite* $Fe_8O_8(OH)_6SO_4$

Schwertmannite is a new mineral that has only recently been approved by the Commission on New Minerals and Mineral Names. Its characteristics were originally described by Bigham *et al.* (1990) with subsequent details concerning properties and genesis published elsewhere (Bigham *et al.*, 1992; Murad *et al.*, 1994). In the latter two papers, schwertmannite was referred to indirectly as MDM (mine drainage mineral). The formal description of a type specimen is awaiting publication (Bigham *et al.*, 1994).

Schwertmannite seems to be the most common mineral associated with ochreous precipitates from acid sulfate waters, and its bright yellow color (Table 4.1) probably accounts for the term "yellow boy" that is commonly used by North American miners in reference to acid mine drainage. Like ferrihydrite, schwertmannite is a very poorly crystallized mineral characterized by high specific surface area (100 to 200 m^2/g) and rapid solubility in acid ammonium oxalate. The former is consistent with a unique, "pin-cushion" morphology that is readily observed in particles isolated from loose

precipitates (Figure 4.1c).

Schwertmannite is also easily distinguished from ferrihydrite and other associated minerals by its XRD profile, which consists of eight broad bands for d >1.4 Å (Figure 4.2). Comparisons of this profile with those of synthetic specimens prepared under different geochemical conditions led Bigham *et al.* (1990) to conclude that schwertmannite has a tunnel stucture similar to that of akaganéite, ß-$FeO(OH)_{1-x}Cl_x$ (nominally ß-FeOOH), with SO_4 assuming the position of Cl in the tunnel cavities. The presence of SO_4 is readily confirmed both by infrared spectroscopy (Table 4.1) and by chemical analysis. Natural specimens of schwertmannite contain 10 to 15 wt% SO_4, which translates to an Fe/S mole ratio ranging from 5 to 8 and a structural formula varying between $Fe_8O_8(OH)_6SO_4$ and $Fe_8O_8(OH)_{4.8}(SO_4)_{1.6}$.

Mössbauer data have shown the Fe in schwertmannite to be exclusively trivalent and in octahedral coordination (Murad *et al.*, 1990). The mineral has a Néel temperature of 75 ± 5 K and a saturation magnetic hyperfine field of about 45.5 T at 4.2 K. The former is lower than the Néel temperature of any iron oxide, and the latter is lower by about 1.5 T than those of even the most poorly crystallized ferrihydrites (Table 4.1). The Mössbauer spectra of both paramagnetic and magnetically ordered schwertmannite are asymmetric, indicating multiple environments for Fe^{3+} that presumably arise from the incorporation of SO_4 into the structure. Sulfate probably also inhibits magnetic exchange interactions between neighboring iron atoms and is thereby responsible for the low magnetic ordering temperature and hyperfine field.

4.3.5. Jarosite $KFe_3(OH)_6(SO_4)_2$

Jarosite is a common mineral in acid, high-sulfate environments, usually appearing as straw-colored (Munsell hue of 2.5 Y or yellower and chroma >6) mottles and efflorescences within the saturated or vadose zones of mine tailings and acid sulfate soils (Fanning *et al.*, 1993). Jarosite has often been implicated as an important phase in fresh precipitates from surface waters carrying mine drainage (*e.g.*, Nordstrom, 1982a; Karathanasis *et al.*, 1988), but its importance in this regard has probably been overestimated. Compared with other minerals occurring in mine-drainage ochres, jarosite is usually well-crystallized and easily identified from its characteristic XRD pattern (Figure 4.2). Pseudocubic crystals are commonly observed under the electron microscope (Figure 4.1d), but tabular (Doner and Lynn, 1989) and botryoidal forms (Lazaroff *et al.*, 1985) have also been reported. Mössbauer and magnetic studies (Takano *et al.*, 1968; Afanasev *et al.*, 1974; Powers *et al.*, 1975) have confirmed that jarosite is antiferromagnetic, with a Néel temperature of approximately 55 K, which is lower than those of schwertmannite or any of the iron oxides common to mine drainage (Table 4.1).

Jarosite is the most common member of a family of basic iron sulfates that may

arise by partial replacement or complete substitution of K^+ with other monovalent and some divalent cations. Natrojarosite has been reported to be fairly common in some acid sulfate soils (Ross *et al.*, 1982), and Chapman *et al.* (1983) identified both K and Pb varieties in mine drainage precipitates. Most studies of field samples have lacked sufficient detail to distinguish between species even though investigations of synthetic specimens (*e.g.*, Dutrizac and Kaiman, 1976; Leclerc, 1980) have revealed systematic variations in many diagnostic parameters within the jarosite family of compounds.

4.4. A CASE STUDY OF MINE-DRAINAGE PRECIPITATES IN OGG CREEK, OHIO

Southeastern Ohio sits on the northwest flank of the eastern U.S. coal province. Coal-bearing rocks in this region are of Pennsylvanian and Permian age and yield bitumunious coals with medium (1.1—3.0 %) to high (>3.0 %) sulfur contents. Coal has been extracted in this area since the beginning of the 19th century using both underground and surface mining techniques. The former involved primarily drift mines, many of which have now flooded and become permanent sources of mine drainage. One of the most heavily polluted districts in the state is drained by Moxahala Creek, which is tributary to the Muskingum River. The primary source of coal in this area is the Middle Kittanning (#6) seam, with an average thickness of 1.5 to 2.0 m. Mining continues to the present, but the greatest activity occurred from 1930 through 1960.

From March, 1981, to August, 1982, water and sediment samples were collected from a small, 74.3-km^2 watershed within the Moxahala Basin (39°43'21" N. Lat.; 82°03'42" W. Long.). The watershed, consisting of Black Fork Creek, Ogg Creek, and Bennett Run (Figure 4.3) has experienced both surface and deep mine activity. The latter mines are now abandoned and are the primary source of mine-drainage pollution. Although the sampling in this study was not intensive and did not include basic discharge measurements, the results give a useful snapshot of the local geochemical environment. In addition, fairly detailed analyses of ochreous precipitates collected from the stream beds provide a means of demonstrating the analytical procedures discussed in Section 4.2.

4.4.1. Materials and Methods

Water samples were collected during periods of low stream flow from six sites as shown in Figure 4.3. Sites 1 and 2 represent reference areas upstream from major sources of pollution on Ogg Creek and Bennett Run. Effluent discharged from a buried adit at site 3 was the primary source of pollution in the study area. At its source, the drainage was clear but was in contact with abundant bacterial streamers (Johnson *et al.* 1979). Site 4 was immediately downstream from the entry of this drainage into Bennett Run and was also influenced by approximately 16 ha of unvegetated mine tailings in

the surrounding area. Sites 5 and 6 were located just below and approximately 1 km downstream from the confluence of Bennett Run and Ogg Creek.

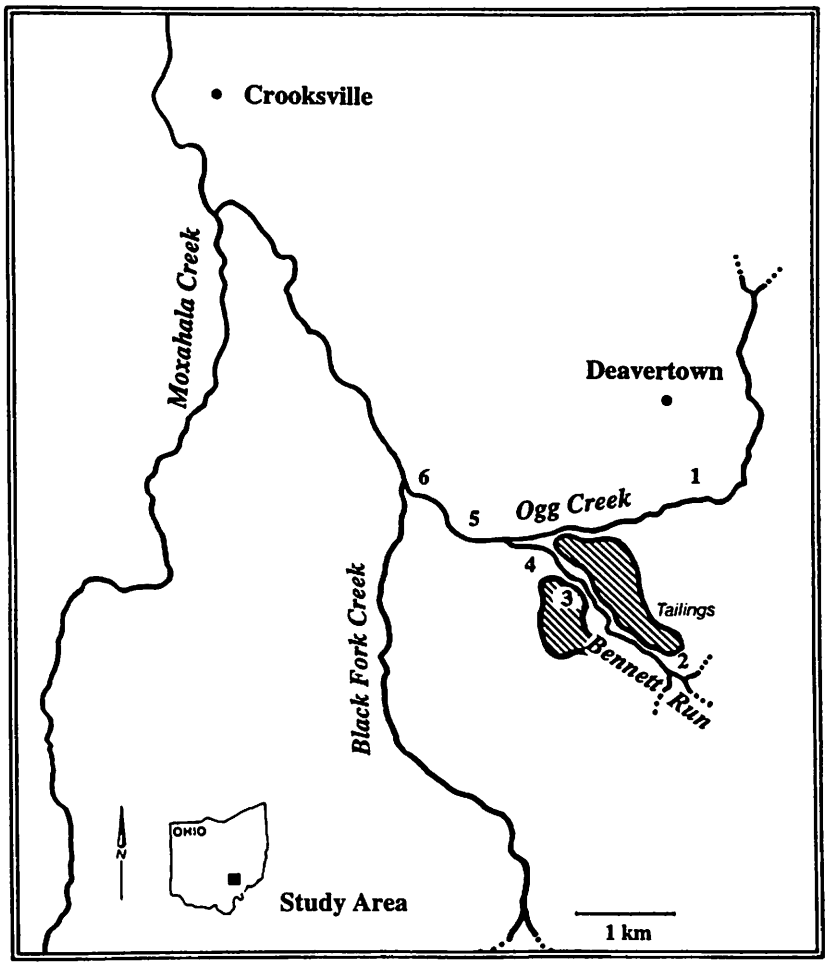

Figure 4.3. Location map for Ogg Creek and Bennett Run.

Three, 500-mL samples of solution were collected from each site during August, 1982. These samples were placed in foil-wrapped, polyurethane bottles, and were transported under ice to the laboratory, whereupon portions were warmed to room temperature and immediately analyzed for pH and Eh. Additional subsamples were filtered through 0.1-μm membranes, and aliquots were immediately analyzed for Fe(II) and total dissolved iron using a procedure modified from that of Stucki (1981). The remaining filtrates were acidified with 2 mL of ultrapure HNO_3 per 125 mL sample

and eventually were analyzed for Al, Ca, Mg, Mn, Na and trace metals by using inductively coupled plasma-emission spectroscopy (ICP). Sulfate in the filtrates was determined by using a standard, turbidimetric method. Finally, total Fe in aliquots of the original (unfiltered) samples was determined according to the method of Stucki (1981) following the addition of a chemical reductant. Percent colloidal Fe was calculated as the difference between total Fe in the unfiltered samples and total Fe passing the 0.1-μm membranes.

In addition to water samples, approximately 60 L of suspension containing a voluminous, yellow preciptate were collected from the stream bed at sites 4 and 5 by using a hand-held pump. In each case, the suspension was allowed to settle, and the supernatant liquid was decanted. The solid phase was then concentrated by centrifugation, washed by dialysis, quick-frozen, and freeze-dried. Both precipitates were analyzed by XRD and selective dissolution, and that from site 5 was further evaluated by Mössbauer, TEM, and other procedures described in detail elsewhere (Brady *et al.*, 1986; Murad *et al.*, 1994).

4.4.2. *Water Chemistry*

Water samples collected from sites 1 and 2 above the area of acid discharge contained background levels of common cations and yielded pH/Eh values typical of streams in the region with normal biological activity (Table 4.2). By contrast, the effluent draining the mine adit at site 3 was acidic and contained high concentrations of Fe, Al, and SO_4. Particulate Fe contents were low, and 95 % of the total dissolved Fe was in the form of Fe(II). Dilution coupled with rapid oxidation, hydrolysis, and precipitation of Fe occurred upon entry of the effluent into Bennett run, as is evident from the data for site 4 (Tables 4.2 and 4.3) and the immediate formation of cloudy, orangish yellow water in the field. This trend was accelerated at site 5 below the confluence with Ogg Creek. At this point, the total dissolved Fe content was one-tenth that of the original effluent, the proportion of Fe(II) had decreased to 0.59, and the content of colloidal Fe had increased to 49% of the total measured. Within an additional kilometer (site 6), the oxidation of Fe was nearly complete, and a decrease in colloidal Fe content suggested that most of the ochreous precipitate had settled to the stream bottom. The modest increase in pH from 2.9 to 3.2 downstream from the mine adit reflects the fact that sandstones and shales are the predominant rock types in the watershed. Consequently, surface waters are not highly buffered.

4.4.3. *Mineralogy*

a. Site 4

An XRD tracing from a random powder mount of the precipitate at site 4 is presented in Figure 4.4. All eight diffraction bands typical of schwertmannite are

Table 4.2. Chemical parameters for waters from Ogg Creek and Bennett Run — August, 1982

Site No.	pH	Eh	SO_4	Al	Ca	Fe	Mg	Mn	Na
		Volts	mg/L						
1	7.3	0.314	31	<1	43	<1	10	<1	18
2	6.8	0.320	32	<1	42	<1	10	<1	20
3	2.9	0.584	4543	343	80	1172	46	4	19
4	2.9	0.646	2000	154	80	273	37	5	31
5	3.1	0.659	1020	87	76	138	26	3	24
6	3.2	0.711	920	74	83	88	27	4	22

Table 4.3. Speciation of iron* in waters from Ogg Creek and Bennett Run — August, 1982

Site No.	Fe (II)	Fe(d)	Fe(t)	Fe(II)/Fe(d)	Colloidal Fe
	mg/L				%
3	1118	1172	1245	0.95	6
4	199	273	329	0.73	17
5	82	138	271	0.59	49
6	9	88	117	0.10	25

* Fe(II) = ferrous iron; Fe(d) = total "dissolved" iron passing a 0.1μm filter; Fe(t) = total iron;

$$\% \text{ Colloidal Fe} = \frac{\text{Fe(t)} - \text{Fe(d)}}{\text{Fe(t)}} \times 100$$

present (see Figure 4.2). In addition, sharp peaks due to the presence of 10.5 wt% detrital minerals (mostly quartz, feldspars, and kaolinite) are clearly expressed. Extraction of the sample with acid ammonium oxalate and DCB yielded 40.5% Fe_o, 40.7% Fe_d, and an Fe_o/Fe_d ratio of 0.99. The total SO_4 content was 13.9%. When these data are corrected for the detrital mineral content of the sample, the results are within the characteristic compositional range for schwertmannite. Consequently, the local geochemical conditions (pH = 2.9; $[SO_4]$ = 2000 mg/L; abundant Fe subject to rapid oxidation and hydrolysis) must be viewed as conducive to the formation of this mineral.

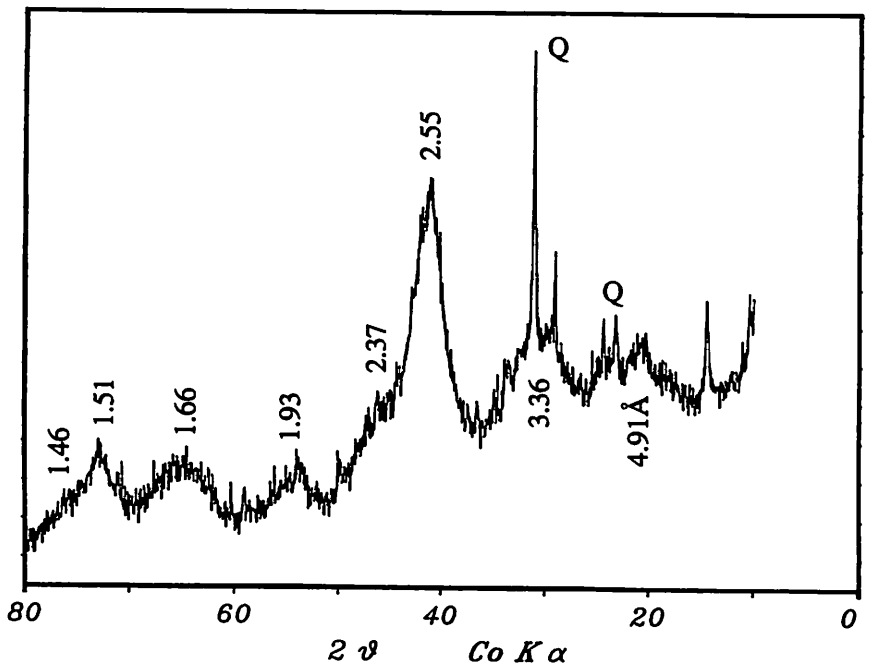

Figure 4.4. X-ray diffraction pattern from precipitate at Site 4.

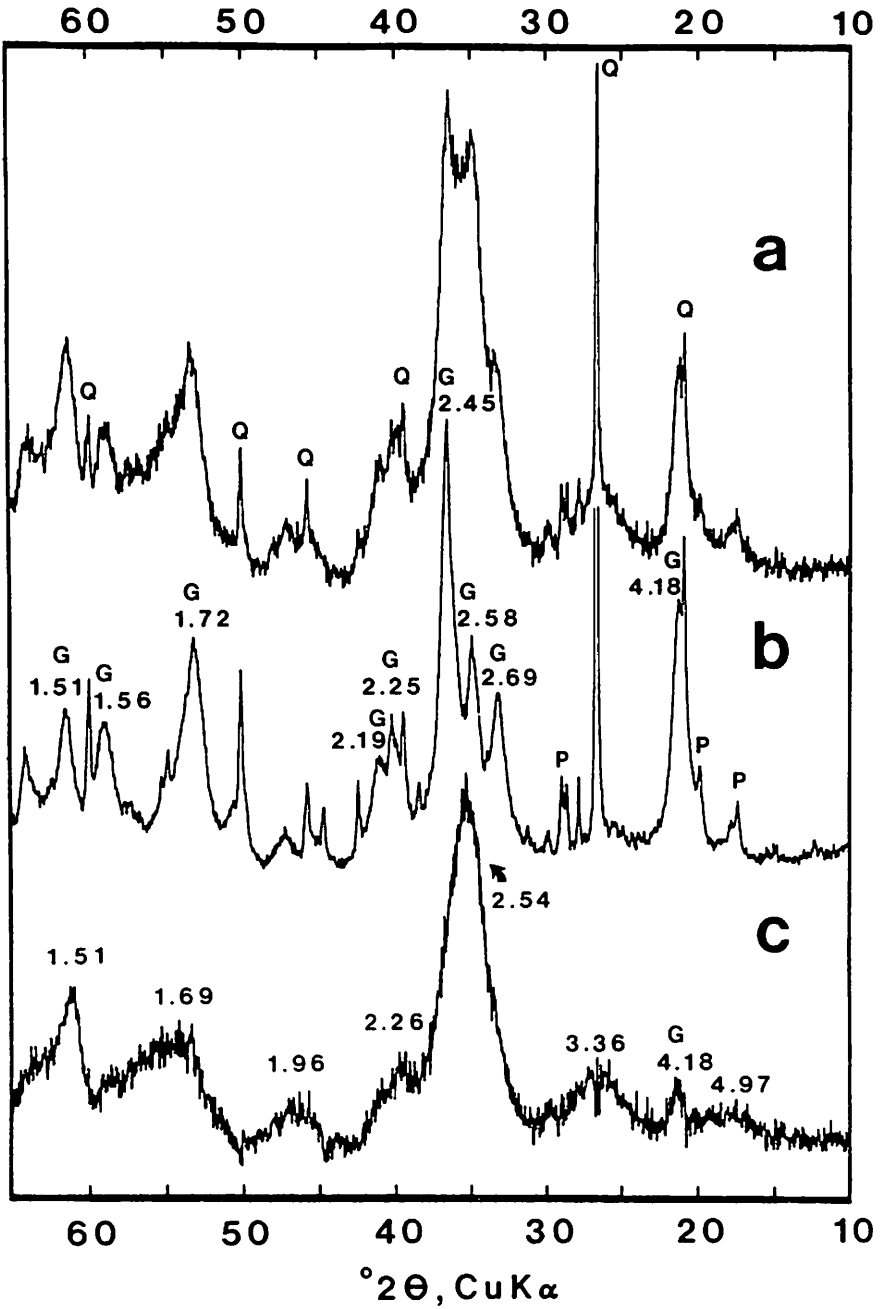

Figure 4.5. X-ray diffraction patterns from precipitate at Site 5: (a) untreated, (b) following 15-min oxalate extraction, (c) after subraction of (b) from (a) (DXRD). G = goethite, Q = quartz, P = phyllosilicates (from Brady *et al.*, 1986).

b. Site 5

The XRD tracing from the precipitate collected at site 5 (Figure 4.5a) is considerably more complicated than that from site 4, indicating that further dilution of the acid mine-effluent with fresh water from Ogg Creek has produced a material with mixed mineralogy. A TEM micrograph of the specimen shows particles with the characteristic "pin-cushion" morphology of schwertmannite together with short, rod-like particles of goethite (Figure 4.6).

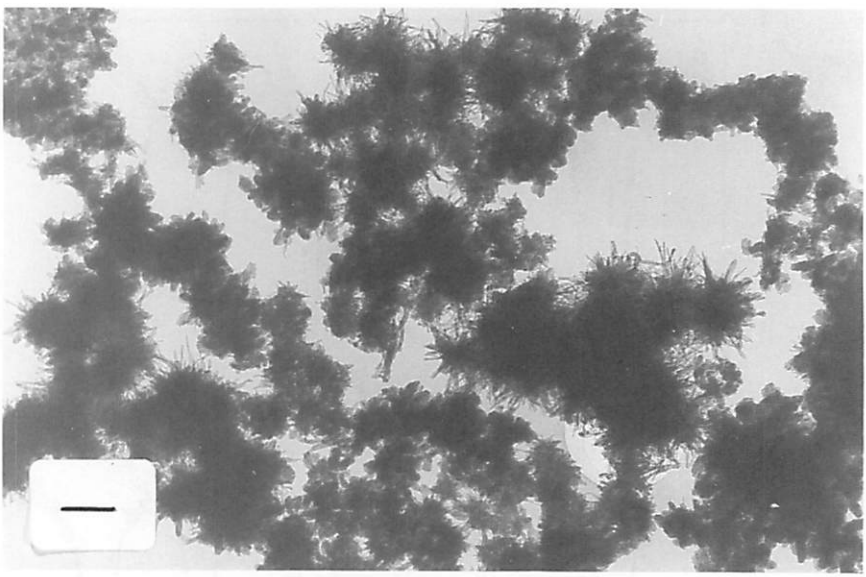

Figure 4.6. Transmission electron micrograph of precipitate at Site 5. Scale bar = 0.2 μm.

To further evaluate the presence of goethite, a subsample of the precipitate was subjected to a rapid, 15-min extraction with acid ammonium oxalate. This treatment removed 78% of the total, DCB-soluble Fe and left a residue consisting of quartz, phyllosilicates, and poorly crystallized goethite (Figure 4.5b). Diffraction effects from the oxalate-soluble component were observed by subtracting the data in Figure 4.5b from that in Figure 4.5a using the technigue of Schulze (1981). The resulting DXRD pattern (Figure 4.5c) is that of schwertmannite with a small contribution from dissolved goethite.

A Mössbauer analysis of the natural (untreated) specimen at 4.2 K (Figure 4.7a) confirms the presence of goethite and schwertmannite. The spectrum consists of two sextets, and a central doublet that is presumably a product of Fe^{3+} in detrital clay minerals. The inner sextet is associated with an average hyperfine field of 45.4 T and arises from schwertmannite. The outer sextet has a magnetic hyperfine field of 49.96 T

and is due to goethite. After a 2-hour oxalate treatment, the inner sextet disappears, leaving only the goethite spectrum and an enhanced paramagnetic doublet (Figure 4.7b). In a paragenetic sense, it is unknown whether the goethite in this sample has formed as a direct preciptate from the contaminated waters of Ogg Creek or is an alteration product of schwertmannite.

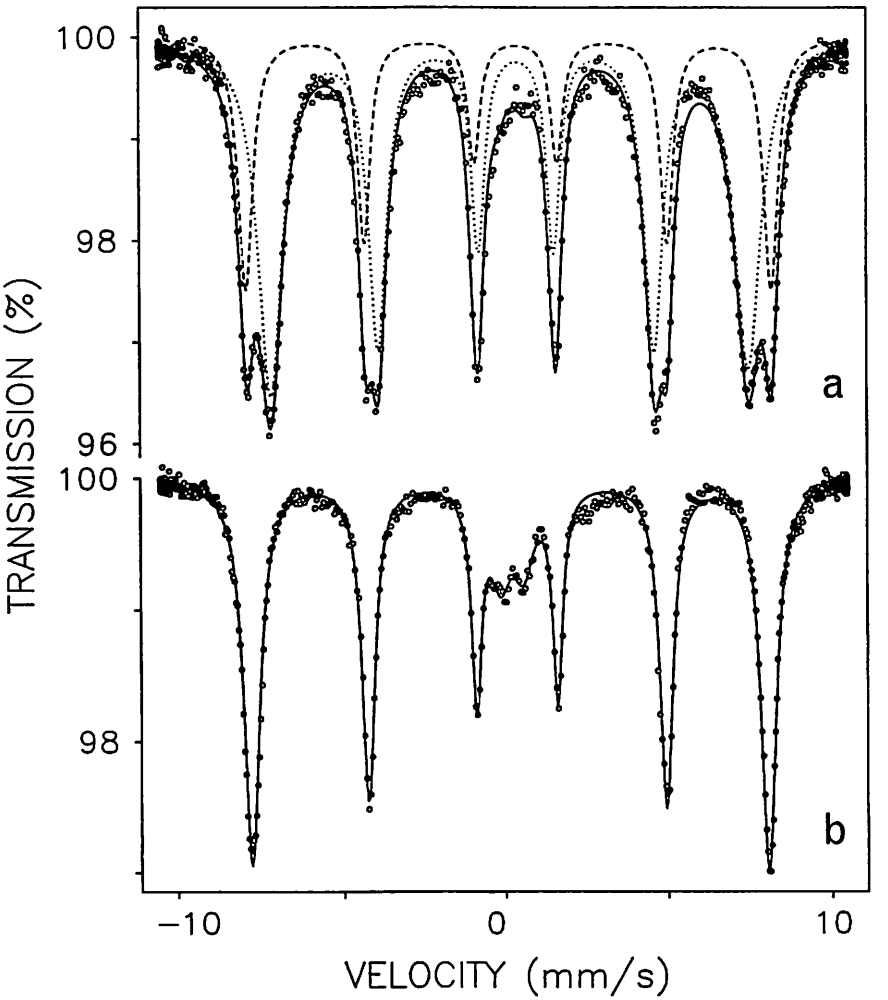

Figure 4.7. Mössbauer spectra taken at 4.2 K of precipitate at Site 5: (a) untreated and (b) following a 2-hour oxalate extraction. Subspectra in the untreated sample are for goethite (broken line) and schwertmannite (dotted line) (from Murad *et al.*, 1994).

4.5. BIOGEOCHEMICAL FACTORS INFLUENCING MINERAL SPECIATION IN OCHRE DEPOSITS

4.5.1. *The Role of Bacteria*

The important role played by acidophilic bacteria, such as *Thiobacillus ferrooxidans*, in the aqueous oxidation of pyrite and related minerals is now widely recognized (*e.g.*, Nordstrom, 1982a). Some controversy remains regarding the ability of bacteria in direct contact with sulfide grain surfaces to initiate the oxidation process through enzymatic pathways, but there is clear evidence that bacteria indirectly catalyze subsequent decomposition reactions by oxidizing aqueous Fe^{2+} whenever the pH of interstitial solutions drops below 4.5. The importance of rapid oxidation under strongly acid conditions is related to the fact that the activity of Fe^{3+} becomes significant at low pH, so that Fe^{3+} replaces O_2 as a primary oxidant. At pH <2.5, a near-steady-state cycling of Fe occurs via the oxidation of primary sulfides by Fe^{3+} and the subsequent bacterial oxidation of regenerated Fe^{2+} (Kleinmann *et al.*, 1981).

Any Fe^{2+} that escapes the cycle of pyrite decomposition may be incorporated into a variety of secondary minerals having a wide array of properties (Nordstrom, 1982a). Ultimately, however, most Fe^{2+} is oxidized, hydrolyzed, and precipitated as one of the "insoluble" mineral phases described in Section 4.3. Almost since its isolation, *Thiobacillus ferrooxidans* has been thought to accelerate the formation of ochreous precipitates associated with acid mine drainage by catalyzing the oxidation of iron (Colmer and Hinkle, 1947). Although Fe-encrusted bacterial remains have been isolated from mine-drainage sediments (Ferris *et al.*, 1989; Mann *et al.*, 1992; Milnes *et al.*, 1992), it is unlikely that the type of mineral produced is controlled by the physiology of the organism. The oxidation of Fe may be biologically induced, and the rate of oxidation may be under metabolic control, but the mineralization process itself is extracellular (Lowenstam and Weiner, 1989). In other words, geochemical parameters such as pH, $[SO_4]$, and $[HCO_3]$ determine the mineralogical fate of Fe once it is oxidized either by biotic or abiotic mechanisms.

4.5.2. *Proton Activity*

Pyrite decomposition is a complicated process involving several reactions that are proton-generating. Consequently, sulfatic mine drainage is usually assumed to be acidic. In fact, the pH of mine drainage may range from less than 2 to as high as 8.5 depending on the stage of the reaction and the geologic setting (Mills, 1985). Bigham *et al.* (1992) studied the mineralogical composition of ochres precipitated from a variety of mine effluents with pH in the range of 2.6 to 7.8 (Figure 4.8). Although they found that goethite occurred over the full range of effluent pH, it was the primary component in only two samples, both of which were formed from solutions with pH >6.0. Slightly acid to alkaline conditions also favored the formation of ferrihydrite, and these results

suggest that ferrihydrite may be more limited in distribution than previously indicated in the mine-drainage literature. A similar conclusion may be reached with regard to jarosite, which was detected in only a few sediments produced under the most acid (pH <3.3) conditions encountered. Brown (1971) has also noted that the solution pH should not exceed 3.0 if jarosite is to remain a stable phase. The most common mineral identified by Bigham *et al.* (1992) was schwertmannite. Schwertmannite was present in more than 60% of the specimens analyzed, and was particularly abundant in precipitates formed from "typical" mine effluents having pH values in the range of 3.0 to 4.0.

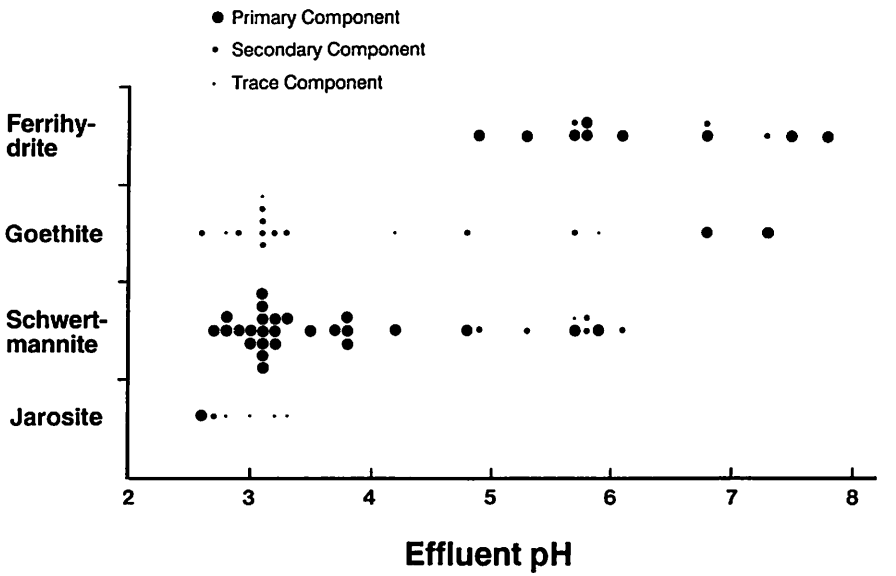

Figure 4.8. Distribution of mine-drainage minerals as a function of effluent pH (modified from Bigham *et al.*, 1992).

4.5.3. Dissolved Sulfate

Sulfate is obviously the most common anion associated with mine-drainage environments, and it is reasonable to expect that the activity of sulfate in solution plays a major role in defining pathways of mineral speciation during ochre formation. Jarosite-type compounds, for example, are easily synthesized from acid solutions containing excess sulfate and suitable concentrations of metal cations (Fe, K, Na, *etc.*) by using either abiotic (Brown, 1970; Dutrizac, 1984) or biotic (Ross *et al.*, 1982; Lazaroff *et al.*, 1982; Grishin *et al.*, 1988) approaches. Critical conditions for the formation of jarosite can also be calculated from available thermodynamic data (*e.g.*, Brown, 1971; Vlek *et al.*, 1974); however, it is not altogether clear what level of sulfate activity is actually required to form jarosite under field conditions. In results reported

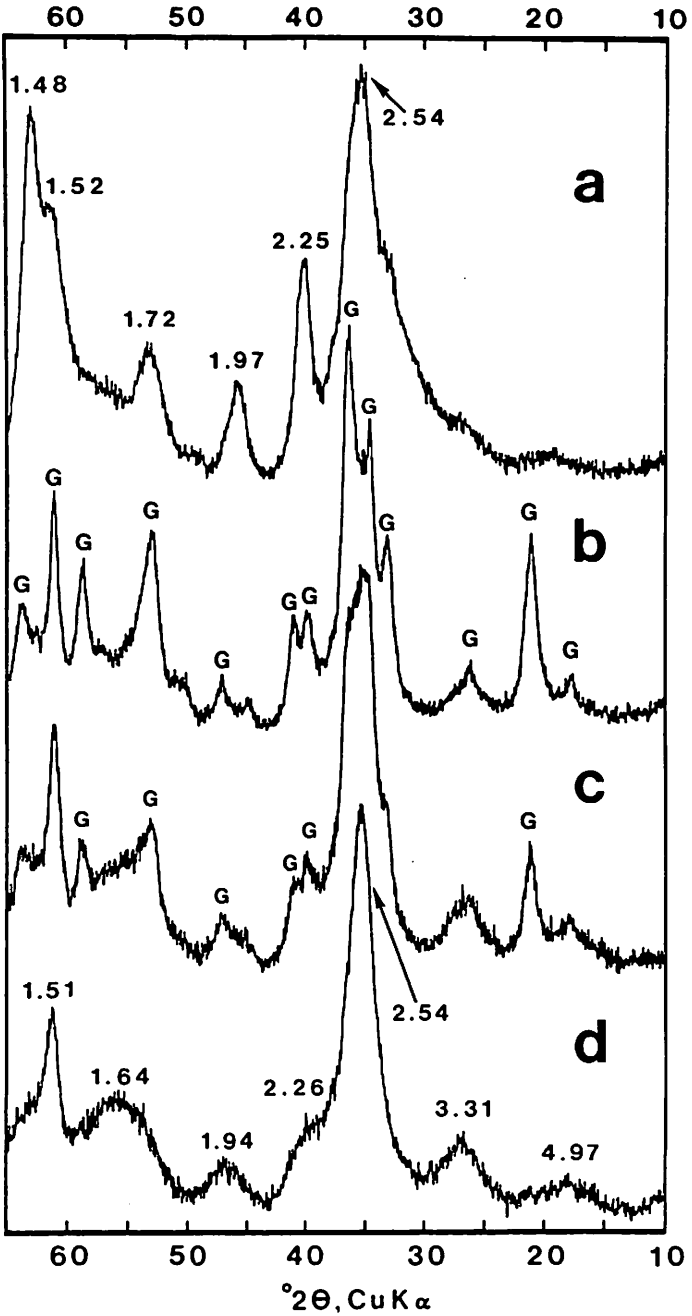

Figure 4.9. X-ray diffraction patterns from synthetic specimens prepared by hydrolysis of ferric nitrate solutions in the presence of (a) 0 mg/L SO_4, (b) 500 mg/L SO_4, (c) 1000 mg/L SO_4, and (d) 2000 mg/L SO_4 (from Brady *et al.*, 1986).

by Bigham *et al.* (1992), jarosite was detected in mine-drainage streams only when [SO4] exceeded 3000 mg/L in the pH range 2.6 to 3.3.

No thermodynamic data are currently available for schwertmannite, but field and laboratory studies suggest that SO_4 concentrations in the range of 1000 to 3000 mg/L are optimal for its formation under the characteristic pH conditions shown in Figure 4.8. Several laboratory studies have also shown SO_4 to enhance the formation of goethite over other iron oxyhydroxides (*e.g.*, lepidocrocite) even though SO_4 is not a structural component of these minerals (Dousma *et al.*, 1979; Brady *et al.*, 1986; Carlson and Schwertmann, 1990). Under field conditions, the precipitation of ferrihydrite seems to be rather insensitive to [SO_4]; however, once ferrihydrite is formed it seems to transform rapidly to goethite in the continued presence of SO_4 (Bigham *et al.*, 1992).

The data presented in Figure 4.9 were taken from an experiment conducted by Brady *et al.* (1986) wherein a series of precipitates were prepared by rapidly hydrolyzing 0.02 *M* $Fe(NO_3)_3$ solutions containing graded amounts of SO_4 (as Na_2SO_4) in the range of 0 to 2000 mg/L. After aging for 30 days in dialysis against distilled H_2O, the precipitates were freeze-dried and analyzed by XRD. When SO_4 was excluded from the hydrolysis solutions, a typical, six-line ferrihydrite was obtained (Figure 4.9a). By contrast, 250-500 mg/L SO_4 facilitated the formation of a poorly crystallized goethite (Figure 4.9b). Further increases in SO_4 to 1000 and 1500 mg/L produced mixtures of goethite and schwertmannite (Figure 4.9c), and only schwertmannite was obtained at 2000 mg/L SO_4 (Figure 4.9d). The XRD patterns shown in Figure 4.9c and d are similar to those presented for the natural materials described in Section 4.4.2. (Figure 4.4 and 4.5a). The natural materials precipitated from drainage waters that had SO_4 concentrations comparable to those utilized in the laboratory synthesis.

4.5.4. Dissolved Carbonate

Most alkaline mine drainage is found in mining districts with abundant limestone or dolomite in the rock column, and the drainage is commonly charged with dissolved carbonate. These conditions might seem to favor the formation of lepidocrocite because procedures for synthesizing this mineral usually involve the oxidation of Fe^{2+} solutions that are buffered in the pH range 5 to 7.5 (Schwertmann and Cornell, 1991). In fact, ferrihydrite and goethite appear to be the normal oxidation products of iron in alkaline mine drainage (Figure 4.8), and this preference is apparently related both to the rate of oxidation and the presence of dissolved carbonate. Whereas rapid oxidation of iron shifts the system toward ferrihydrite, the presence of dissolved carbonate clearly favors goethite.

Both field and laboratory examples are available to demonstrate that goethite

formation is enhanced over lepidocrocite when Fe^{2+} solutions are oxidized in the presence of HCO_3-(Schwertmann and Fitzpatrick, 1977; Fey and Dixon, 1981; Goodman and Lewis, 1981). Recently, Carlson and Schwertmann (1990) observed that the proportion of lepidocrocite to goethite in samples synthesized by oxidizing $FeCl_2$ solutions with air/CO_2 gas mixtures decreased from 100 to 0% as [HCO_3-] increased from 0 to 16 mmol/L (Figure 4.10). These authors also compared infrared spectra from their synthetic specimens with a natural mine-drainage goethite and found that both showed distorted but distinct absorption bands due to CO_3^{2-} (Figure 4.11).

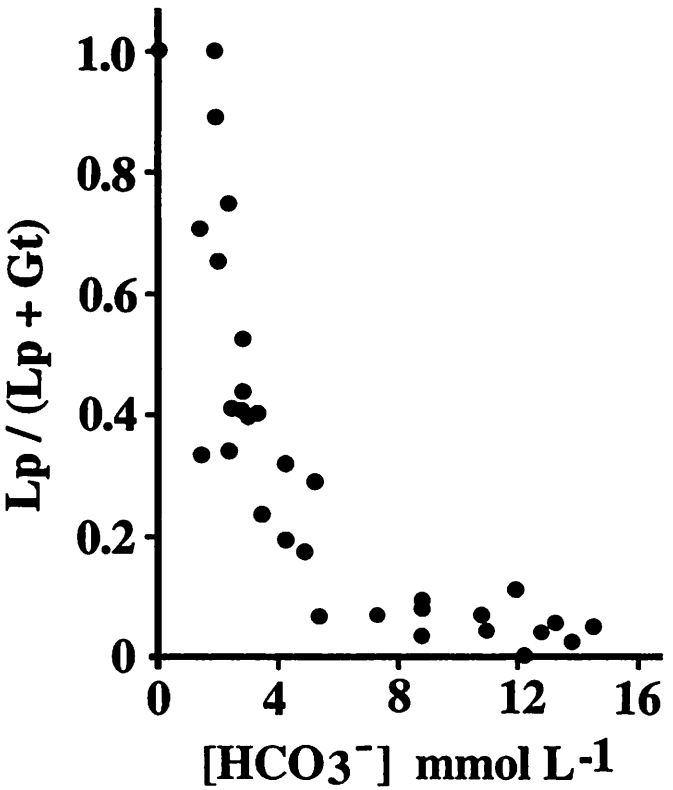

Figure 4.10. Ratio of lepidocrocite to goethite (Lp/Lp + Gt) produced at pH = 6 as a function of [HCO_3-] in solution (modified from Carlson and Schwertmann, 1990).

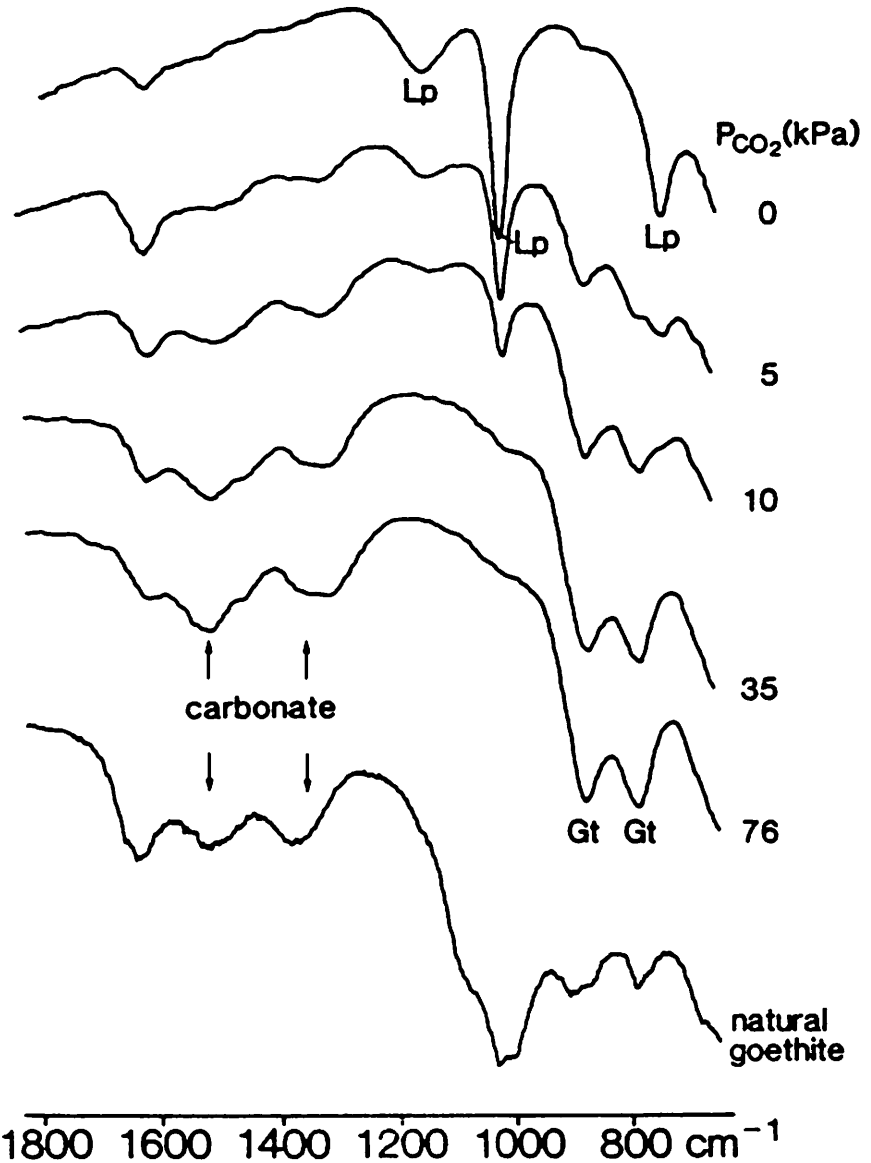

Figure 4.11. Infrared spectra of synthetic specimens prepared at pH 6 and various $P(CO_2)$. Proportion of goethite (Gt) relative to lepidocrocite (Lp) increases from top to bottom. Natural goethite is from mine drainage (from Carlson and Schwertmann, 1990).

4.6. A MODEL FOR MINERAL FORMATION

The previous information regarding mineral speciation in mine-drainage ochres is summarized in Figure 4.12. This "model" is primarily based on field observations and physical data. Consequently, it has a strong kinetic bias with little consideration of solubility controls and other important thermodynamic factors.

According to the proposed model, Fe^{2+} and SO_4^{2-} are released to solution through the bacterially catalyzed decomposition of iron sulfides. A variety of soluble iron sulfates (*e.g.*, melanterite, rozenite) may form as intermediate phases but, ultimately, Fe^{2+} is oxidized and hydrolyzed to form one or more of the minerals associated with mine-drainage ochres. If conditions involving low pH (<3.0), high dissolved SO_4^{2-} (>3000 mg/L), and sustained bacterial activity persist, jarosite or related basic iron sulfates will precipitate in the presence of suitable metal cations. At somewhat higher pH (3.0—4.0) and lower dissolved SO_4^{2-}concentrations (1000 to 3000 mg/L), schwertmannite seems to be the preferred phase. Under these conditions, which are typical of most "acid" mine drainage, bacterial activity is still necessary for rapid oxidation of Fe^{2+}. Slightly acid to alkaline solutions bearing high concentrations of dissolved Fe are conducive to the precipitation of ferrihydrite. Ferrihydrite is clearly a metastable phase whose transformation to other mineral species may be temporarily delayed by contamination of reactive surfaces with organic compounds and adsorbed Si (Childs, 1992). All mineral phases common to ochre deposits are, in fact, transient with respect to goethite, and this is perhaps the most important factor influencing the widespread distribution of goethite in mine-drainage environments. Goethite may also be the primary mineral product formed when low-pH effluents are neutralized by carbonate-charged stream waters.

The proposed model is incomplete with respect to lepidocrocite. Even though lepidocrocite has been documented as a constitutent of ochre deposits associated with sulfide oxidation, the conditions favoring its precipitation are unclear. Synthesis experiments indicate that lepidocrocite formation is favored by the direct, slow oxidation of Fe^{2+}, but is inhibited by low pH, high $[Al^{3+}]$, high $[SO_4^{2-}]$, and high $[HCO_3^-]$. Consequently, it must occupy a rather narrow niche in the total range of mine-drainage environments. Even though the proposed model is not comprehensive, it can perhaps serve as a starting point to understand better the many factors and processes controlling mineral formation in these unique geochemical systems.

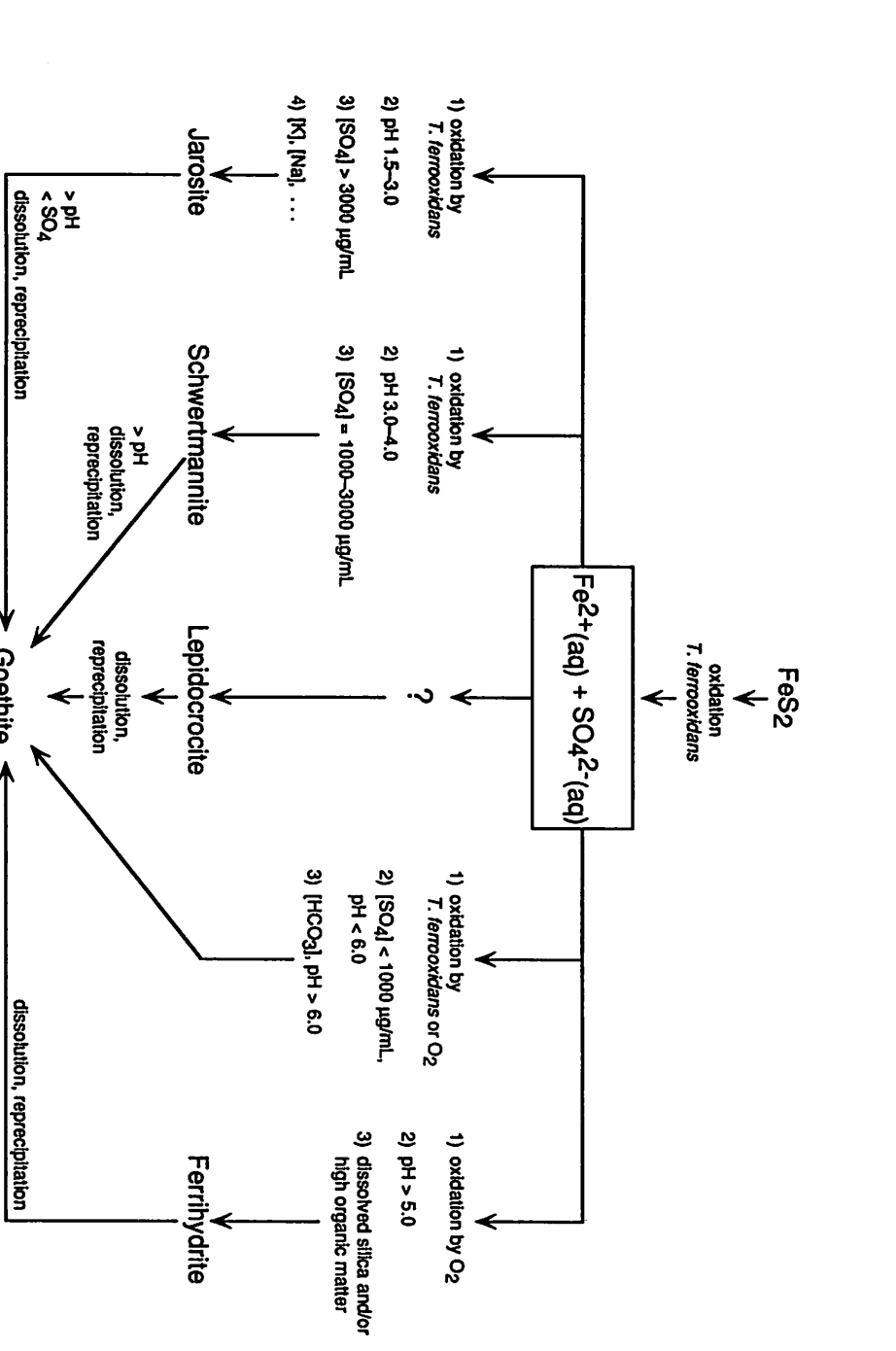

Figure 4.12. Biogeochemical model for the precipitation of various minerals occurring in mine-drainage ochres (modfied from Bigham *et al.*, 1992).

Chapter 5

The Waste-rock Environment

A.I.M. Ritchie
Environmental Science
Australian Nuclear Science and Technology Organization
PMB 1, Menai, NSW 2234 Australlia

5.1. INTRODUCTION

The quantity, chemical composition, and time dependence of polluted drainage from pyritic waste-rock dumps are of considerable concern to environmental regulators and mine operators in many countries around the world. All of these properties reflect the rate of pore-water movement and pore-water chemistry in a dump. The latter, which depends on the pollutant-generation rate within the dump, is driven in turn by the rate of oxidation of pyrite. It is the oxidation of pyrite that is the primary pollutant-generation process. The oxidation rate depends on a number of factors which define the environment within the waste-rock dump, including temperature, pH, oxygen concentration, chemical composition of the pore water, microbial population, and so on. In short, the physico-chemical-microbiological environment within a waste-rock dump determines the pyrite oxidation rate, which in turn determines the physico-chemical-microbiological environment. To predict pollution-generation rates in a waste-rock dump and the consequent chemical composition of pore water, we must know what the environment is and be able to predict what it is or might be when certain conditions are changed.

The environment within a tailings impoundment is determined by similar processes, but there are significant differences between the properties of tailings dams and waste-rock dumps, and these differences have an impact on the environment within each. Chief amongst these is the generally higher height-to-base ratio in a waste-rock dump, and the much coarser run-of-mine material that goes to make up a waste-rock dump. Gas-transport mechanisms, the degree of water saturation, and the intrinsic oxidation rate of the waste material can all be affected by these differences in waste-material properties. This Chapter provides a brief review of the mechanisms and timescales involved in the production of acid drainage from a waste-rock dump, the chemical characteristics of ARD, and the physical characteristics of waste-rock dumps

and the climates in which they are found. This is followed by a review of the interactive processes that determine the physico-chemical environment within a waste-rock dump. Section 5 presents quantitative information on the physico-chemical and microbiological conditions within a waste-rock dump, and Section 6 presents some data on bulk properties of waste-rock dumps. These bulk properties are required both to predict the environmental conditions within a dump, and to quantify oxidation rates. The extents to which these properties vary from place to place in a dump and from dump to dump provide some insight on the impact that dump-construction methods and details of dump composition have on these bulk properties and, by inference, on other bulk properties that define the environment within a dump.

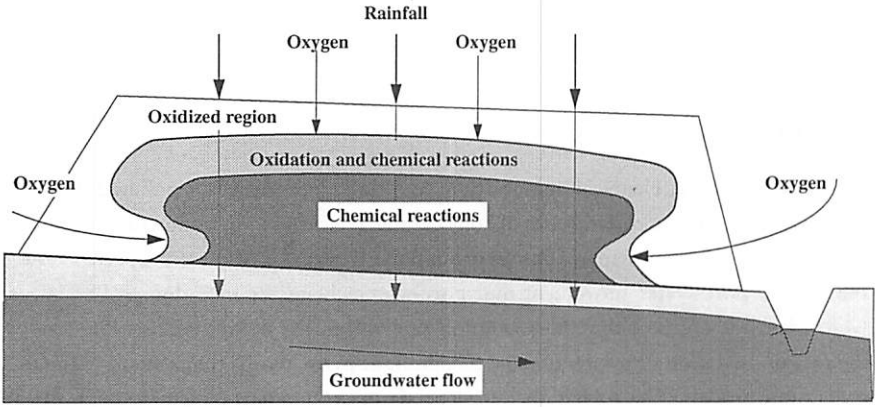

Figure 5.1. Schematic representation of pollutant generation and transport processes in a pyritic waste-rock dump.

5.2. ACID ROCK DRAINAGE

5.2.1. Pollutant Generation

The oxidation of pyrite is the primary pollutant-generation mechanism in pyritic waste dumps. Early in the history of a waste-rock dump there is readily available acid-neutralizing material in the gangue, close to oxidation sites. This means that, at these early times, acid produced in pyrite oxidation is neutralized close to its point of production. Later in the dump's history, when all of this readily neutralizing material has been used up, acid produced at oxidation sites is transported away from its point of production by the movement of pore water within the waste-rock dump. At some point in the lifetime of the waste-rock dump the distribution of oxidation sites and chemical reactions is along the lines of that shown schematically in Figure 5.1. The sizes of the different regions in Figure 5.1 depend very much on the rate at which the dump material oxidizes and on gas-transport mechanisms in the waste-rock dump, as are

discussed in detail in Chapter 8. In particular, the oxidation region can be so large that it encompasses the whole dump, or be only a fraction of a meter thick. Moreover, given the inhomogeneity of the material in waste-rock dumps, these regions can be of different sizes in different parts of the dump.

The general picture then, is that early (years to tens of years) in the history of a waste-rock dump, the chemical composition of the pore water deep in the dump changes with time and depth, depending on the interplay among the pyrite oxidation rate, the distribution of gangue material that reacts quickly with acid, and the rate of pore-water movement. When all of the gangue material that reacts quickly with acid (mainly carbonates) is used up, further neutralization of the acid is effected by slow interaction between oxidation products and other gangue minerals in the dump. The net result is that, whereas early in the history of a waste-rock dump the drainage from the base of the dump may have a near-neutral pH, later the pH may be lower. A characteristic of this later phase is that the chemical composition of drainage water, suitably averaged to remove seasonal fluctuations in infiltration rate, changes very slowly with time over a timescale of tens to hundreds of years.

Table 5.1. Characteristics of acid rock drainage

Property	Typical associated chemical species	Concentration range	Impact
Acidity	Sulfuric acid	pH 2 to 4	mobilization of metal ions
Iron	Ferrous and ferric ion; Ferric oxides, hydroxides; Jarosites	100 to 3000 mg/L	discoloration and turbidity in receiving waters as pH increases and ferric salts precipitate
Heavy metals	Copper, magnesium, zinc, cadmium, mercury, lead, arsenic, radium	1 to 200 mg/L	reduction in aquatic flora and fauna; bioaccumulation; reduction in quality of potable groundwater supplies
Total dissolved salts	Calcium, magnesium, aluminum, sulfate	100 to 30,000 mg/L	reduction in quality of potable groundwater supplies reduction in quality of water supplies for stock

5.2.2. Characteristics of Acid Rock Drainage

It is the later-phase drainage that is generally described as acid rock drainage (ARD) for the obvious reason that a common characteristic is an acid pH in the range 2 to 4. It must be stressed that the chemical composition of ARD depends very much on the mineralogy of the dump material.

Table 5.1 gives some typical characteristics of ARD. If the waste-rock dump results from base-metal mining, or in some cases gold mining, the components of major

concern are the trace metals, both because of their impact on aquatic flora and fauna, and because of their impact on water supplies for stock and human consumption. It must be further stressed that drainage from a waste-rock dump containing pyritic material may not have low pH but still pose an environmental problem. This can be so, for example, if there is sufficient dolomite in the waste rock to neutralize acid production. In such a situation the drainage will be characterized by near-neutral pH, high sulfate levels, and high levels of calcium and magnesium.

The most common and very noticeable manifestation of ARD from a dump is the reddish brown staining associated with the effluent, and which consists of precipitates of, mainly, ferric salts. Apart from being a source of turbidity, these salts do not, as such, represent an environmental problem. Much more insidious with respect to its environmental impact on aquatic flora and fauna is pellucid drainage water containing 1 to 100 mg L^{-1} of such trace metals as copper, zinc, cadmium, and so on. Similarly, there is an unfortunate emphasis on acid generation in pyritic mine wastes. The pH, *per se*, of ARD is not of great concern. Rather, it is the fact that at low pH many trace metals are soluble. In some cases, as indicated above, pyrite oxidation leads to drainage that has near-neutral pH, but in which the levels of such major ions as calcium, magnesium, and sulfate are unacceptably high from an environmental point of view.

Table 5.2. Physical properties of a typical dump of mine waste

Symbol	Definition	Value	Units
L	Dump height	15	m
A	Dump area	25	ha
ρ_r	Bulk density of dump material	1500	kg m^{-3}
ρ_{rs}	Sulfur density as pyrite	30 (2%)	kg m^{-3}
Q_w	Infiltration rate	0.5	m y^{-1}
ε_g	The porosity of the dumped material	0.40	
ε_w	Water-filled porosity at specified infiltration	0.10	
K_S	Saturated hydraulic conductivity of dump	10	md^{-1}
D	Oxygen diffusion coefficient in the dump	$5.0x10^{-6}$	m^2s^{-1}
C_O	Oxygen concentration in air	0.265	kg m^{-3}
ε	Mass of oxygen consumed per unit mass of sulfur oxidized	1.75	
S^*	Mass of oxygen consumed per unit volume and unit time by the dump material	$1x10^{-8}$	kg m^{-3} s^{-1}
ρ_c	Carbonate density	0.6 (0.04%)	kg m^{-3}

5.2.3. Manifestation of ARD

In general, ARD is the drainage from the toe of a waste-rock dump. It must be appreciated that such drainage is a property of the hydrology of the dump and its surroundings, and may represent a small fraction of the water that infiltrates the surface of the dump. Drainage into the local groundwater may well then represent a

major portion of the environmental impact from pollutants generated in the dump. It should further be noted that the quantity of water required to support a significant pollutant-generation rate is quite small (see reaction 1 in Figure 5.4). If a dump with the specifications in Table 5.2 was producing, say, 40 t y^{-1} of copper and the SO_4:Cu ratio in drainage was about 60, then the corresponding sulfate production rate is 2.5 kg m^{-2} y^{-1} sulfate, which requires only 0.23 kg m^{-2} y^{-1} of water (see reaction 1 in Figure 5.4). This is just 0.23 mm y^{-1}. The absence of visible drainage in low-rainfall areas should not be taken to indicate an absence of ARD. It is crucial to quantify the water balance in a waste-rock dump to assess the quantity of polluted drainage contributing to groundwater, and to assess the overall impact this drainage has on groundwater.

During dry periods, osmotic pressure due to salts in the pore water of the waste-rock dump as a consequence of pyritic oxidation can exceed the pore-pressure component due to gravity. When this happens, pore water moves up toward the surface of the dump. This makes available near-surface pollutants that are picked up by surface runoff in the next rainfall event. Runoff from a waste-rock dump can therefore contribute to the pollution load from the dump. The environmental impact of such runoff is very much site-dependent, but generally represents only a few percent of the total pollutant load from the dump (Daniel *et al.*, 1982). Runoff from a waste-rock dump is, however, very visible and, like the iron-staining of classic ARD, may attract more attention than its importance warrants.

5.2.4. Timescales Affecting ARD

As indicated above, and as discussed in more detail in Chapter 8, the primary pollutant-generation process in a waste-rock dump operates on a timescale of tens to hundreds of years. The chemical composition of drainage from the toe of a waste-rock dump is very much a property of the chemical composition of the pore water at the base of the dump. As indicated above, this chemical composition changes at early times (years to tens of years). The timescale depends primarily on the timescale, t_c, for dissolution of mainly carbonates and the transit time, t_w, for water in the dump. These are of the order of:

$$t_c = \frac{\varepsilon_c \rho_c}{S^*} \qquad (1)$$

$$t_w = \frac{\varepsilon_w L}{Q_w} \qquad (2)$$

For a waste-rock dump with the properties listed in Table 5.2 (see also Nomenclature in Section 5.8), these timescales are 2.3 years and 3 years, respectively.

Figure 5.2 shows the pollution load in a waste-rock dump as a function of time

for different infiltration conditions generated by a mathematical simulation of a waste-rock dump. In these simulations the pollutant is sulfate, so the main determinant of the time to peak load is the water transit time. Of note are the long times to peak load, which are of the order of, or greater than, the time over which many mines operate.

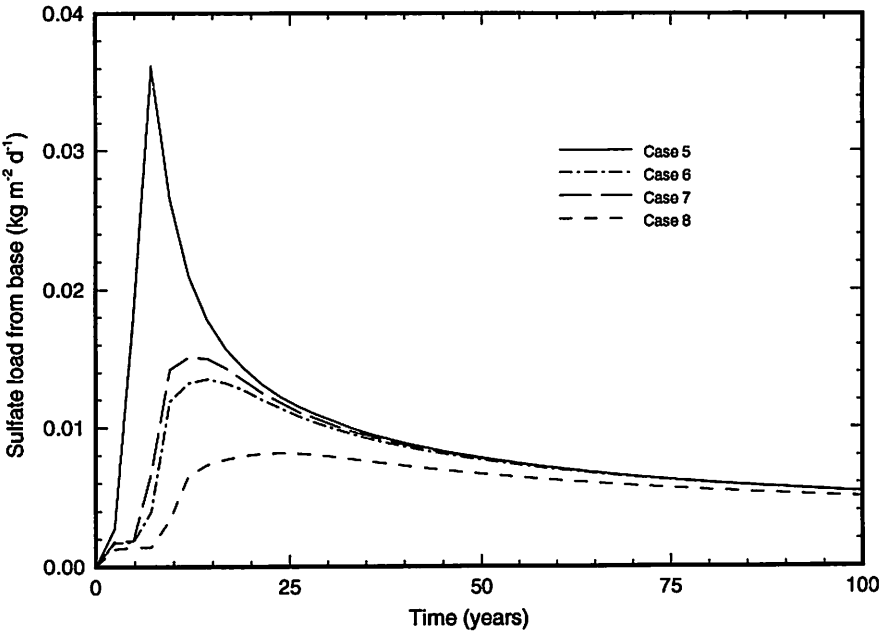

Figure 5.2. Variation with time of the sulfate load at the base of a waste-rock dump 20 m high with four different cover systems.
Case 5 infiltration 4.82 x 10^{-4}m/d
Case 6 infiltration 2.49 x 10^{-4}m/d
Case 7 infiltration 2.70 x 10^{-4}m/d
Case 8 infiltration 1.75 x 10^{-4}m/d

The water transit times are based on the assumption that water flow in the dump is porous flow in that it can be described by Richard's equation (Bear, 1979). There is considerable debate at the moment on the nature of water flow in such a heterogenous system as a waste-rock dump but, for the moment, it is useful to distinguish between the relatively short timescale (a fraction of a day to a few days) for flow at the base of a dump to respond to increased infiltration at its surface, and the relatively long timescale (a fraction of year to a few years) for water to travel through the pore space. These rather different timescales mean that, if there is a rapid change in infiltration at the surface, then flow at the base of the dump follows that change closely (on a timescale of hours or days), the discharge having the chemical characteristics of the pore water at the base of the dump. The pore-water chemistry at the base of the dump changes on a much slower timescale as changes in pore-water concentrations move through the

dump on the timescale of water transit times. Some of the water collected at the toe of a waste-rock dump has flowed down through the dump and then laterally through the near-base of the dump, or through an aquifer below the dump. The water collected at the toe is therefore some integral of the time-dependent concentrations at various parts of the dump base. In this sense, water collected at the toe of a dump is very useful in estimating total pollution loads, and is sometimes essential in estimating the environmental impact of a waste-rock dump, but not very useful in elucidating the pollutant-generation process within the dump.

Figure 5.1 also exposes another potential problem in elucidating the physico-chemical environment in a waste-rock dump. In most waste-rock dumps the central region at the base of the dump is anaerobic or effectively so. The peripheral regions at the base may well not be so, because oxygen is transported into this portion of the dump both by diffusion and by convection. The result is that drainage collected at the toe of the dump may have started under anaerobic conditions typical of a large area of the base of the dump, but has subsequently flowed through a region where oxidizing rather than reduced conditions prevailed.

5.2.5. Water Balance in a Waste-rock Dump

As indicated above, drainage from the toe of a dump can provide an estimate of the integrated pollution load from the dump. To achieve this it is essential that flow and concentration measurements both be carried out. If the load from this drainage point is to be useful in a quantitative way, then it is essential that there be a good estimate of water balance for the dump. Apart from the fact that such a water balance reveals the quantity of the effluent from the dump, which goes into the local groundwater, the balance also reveals sources other than infiltration from precipitation on the dump surface. Such sources can be springs, which generally are a source of unpolluted water, or other minesite features, such as tailings dams, which can be sources of polluted water.

When planning construction of a waste-rock dump, consideration should be given to ensuring that a water balance can readily be determined in the operational and post-operational phases. Any model used to predict pollutant generation from a dump is likely to be calibrated against a measured total load unless the properties of the dump can be so closely specified prior to construction that it is possible to calculate pollutant generation and transport in all parts of the dump.

5.3. PHYSICAL CHARACTERISTICS OF WASTE-ROCK DUMPS

5.3.1. Climatic Locations

ARD is encountered at minesites at locations ranging from a few kilometers from

the equator, to hundreds of kilometers north of the Arctic Circle. Infiltration rates range from about 0.1 to 5 m y^{-1}. The conservative approach in assessing the environmental impact of a mine is to assume that pyrite oxidation proceeds, and pollutants are generated, wherever pyrite is exposed to a sufficiency of oxygen and water. The question of sufficiency is discussed in Section 5.5.

5.3.2. Physical Characteristics of Waste-rock Dumps

The size and shape of waste-rock dumps reflect the scale of the mining operation that creates the waste and the topography of the minesite. A range of heights, areas, and tonnages is given in Table 5.3 together with a range of pyrite contents. In predictive modelling of ARD, a reasonable generic value for the dump height is about 20 m because in many locations the economics of waste-rock disposal lead to dumps of about this height.

Table 5.3. Range of physical properties of waste dumps producing ARD

	Property	Value	Unit
Height	Typical dump	20	m
	Approximate range	2 to 150	m
Area	Typical dump	30	ha
	Approximate range	0.1 to 150	ha
Density	Typical	1500	kg m^{-3}
	Approximate range	1300 to 1900	kg m^{-3}
Sulfur content as pyrite	Typical	2	% w/w
	Approximate range	0.5 to 30	% w/w
Climate type		Tropical to Polar	
Rainfall		0.1 to 5	m y^{-1}
Temperature within dump		-7 to 65	°C
Water content within dump		5 to 25	% v/v

Many dumps are constructed by end-dumping, which leads to some segregation of dump material down the slope at the end of the dump, and also leads to some layering in the dump. These features have given rise to the speculation that the water- and gas-transport properties in waste rock are greatly influenced by the dump structure, particularly the propensity of coarse material to collect at the bottom of the dump end-slope. Such a feature is shown in Figure 5.3a. The material in a ditch dug by a backhoe into the same waste-rock dump is shown in Figure 5.3b for comparison. It can be seen that, although the material comprising the dump is heterogeneous in size, it has the appearance of homogeneity on a scale of a meter or so. The extent to which the structure of the dump has an impact on bulk properties that define transport mechanisms in the dump needs more well-considered investigation. This point is returned to in Section 6.

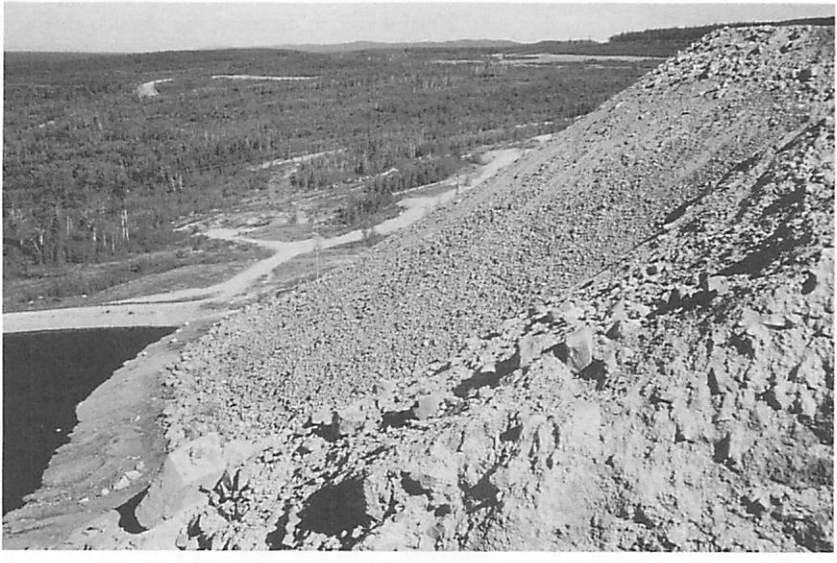

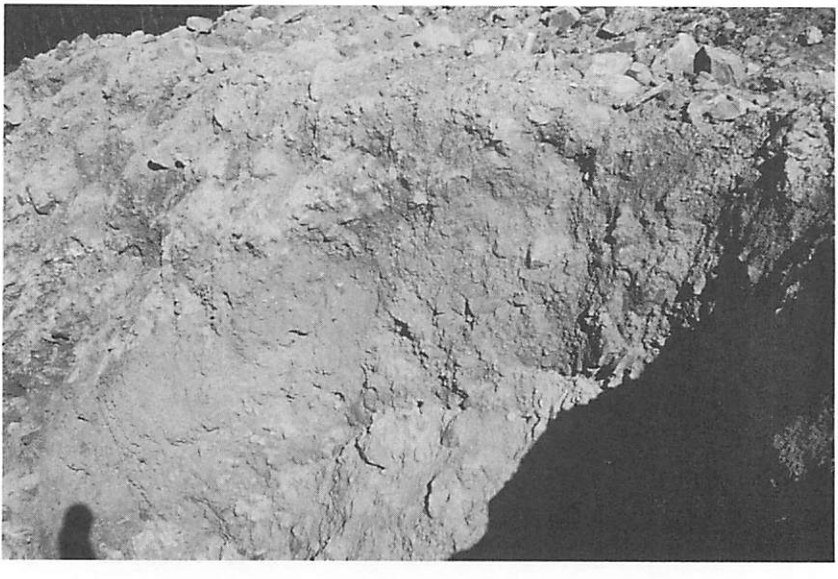

Figure 5.3. Typical appearance of material in a waste-rock dump. (a) Material on the batters; (b) material within the dump.

5.4. BASIC PROCESSES

5.4.1. Chemical Reactions

The chemical reactions that play a major role in dictating the physico-chemical conditions in a waste-rock dump can be considered under the classifications of pyrite oxidation, carbonate dissolution, and gangue-mineral dissolution. The more important reactions in these three classes are given in Figures 5.4, 5.5, and 5.6.

1. $FeS_2+{}^7/_2O_2+H_2O \rightarrow FeSO_4+H_2SO_4$, $\Delta H = 1440\ kJmol^{-1}$
2. $2FeSO_4+H_2SO_4+{}^1/_2O_2 \rightarrow Fe_2(SO_4)_3+H_2O$, $\Delta H = 102\ kJmol^{-1}$
3. $FeS_2+Fe_2(SO_4)_3+2H_2O+3O_2 \rightarrow 3FeSO_4+2H_2SO_4$
4. $MS+Fe_2(SO_4)_3+{}^3/_2O_2+H_2O \rightarrow MSO_4+2FeSO_4+H_2SO_4$
   where MS stands for any metal sulfide

Figure 5.4. Equations of sulfide oxidation.

1. Calcite:
   $CaCO_3+H_2SO_4 \rightarrow CaSO_4+H_2O+CO_2$
2. Dolomite:
   $CaMg(CO_3)_2+2H_2SO_4 \rightarrow CaSO_4+MgSO_4+2H_2O+2CO_2$

Figure 5.5. Equations of the dissolution of carbonate by acid.

The first set (Figure 5.4) shows that oxygen and water are required to oxidize pyrite, that acid and sulfate are oxidation products, and that heat is released. The second set (Figure 5.5) typifies the way in which acid is neutralized by the comparatively fast process of carbonate dissolution, and shows that carbon dioxide is a product of this dissolution. The third set (Figure 5.6) describes in the main the generally slow dissolution of the gangue minerals by the products of oxidation, and the consequent neutralization of acid.

Certain bacteria, principally *Thiobacillus ferrooxidans* (Brierley, 1978), catalyze the oxidation of ferrous iron and increase the rate of this reaction (reaction 2 of Figure 5.4) by a large factor which has been estimated at about 10^5 (Singer and Stumm, 1968). In many situations this leads to a marked increase in the oxidation rate of pyrite at low pH: below a pH of about 4, reaction 3 in Figure 5.4 is much faster than reaction 1. Both in practice and under laboratory conditions, the presence of bacteria speeds up

the oxidation rate of pyrite by factors of between about 10 and 100 (Olson, 1991).

It is shown in Chapter 8 that, in most waste-rock dumps, the intrinsic oxidation rate of the sulfidic component of the dump material determines the size of the oxidation region shown in Figure 5.1: the higher the rate, the smaller the region. It is further shown in Chapter 8 that, with an intrinsic oxidation rate of 1×10^{-8} kg (O_2) m^{-3} s^{-1} and an oxygen diffusion coefficient of about 5×10^{-6} m^2 s^{-1}, the region is about 15 m deep in the early history of a large dump. Because the thickness of the region decreases as $1/S^*$, it follows that in those parts of the dump in which the dominant oxygen transport mechanism is diffusion, any intrinsic oxidation rate greater than about 10^{-7} kg (O_2) m^{-3} s^{-1} is effectively infinitely great with respect to oxygen transport. With this value of intrinsic oxidation rate and the dump parameters of Table 5.2, the thickness of the oxidation region is about 1 m. Thus, in those portions of a large dump where diffusive transport dominates, the oxic region is comparatively small for quite modest values of the intrinsic oxidation rate; conversely, the region in which chemical reactions proceed under essentially reducing conditions is large. It also follows that, unless the tactic is to dramatically decrease the time-scale for complete oxidation of pyrite in the dump, from a practical point of view we are interested only in those processes, be they chemical or microbiological, that change the pyrite oxidation rate below about 10^{-7} kg (O_2) m^{-3} s^{-1}

1. Muscovite dissolution:
   $KAl_2[AlSi_3O_{10}](OH)_2(s)+H^+ + {}^3/_2H_2O \rightarrow K^+ + {}^3/_2Al_2Si_2O_5(OH)_4(s)$
2. Biotite dissolution:
   $KMg_{1.5}Fe_{1.5}AlSi_3O_{10}(OH)_2(s)+7H^+ + {}^1/_2H_2O$
   $\rightarrow K^+ + 1.5Mg^{2+} + 1.5Fe^{2+} + 2H_4SiO^0{}_4 + {}^1/_2Al_2Si_2O_5(OH)_4(s)$
3. Albite dissolution:
   $NaAlSi_3O_8(s)+H^+ + {}^9/_2H_2O \rightarrow Na^+ + 2H_4SiO^0{}_4 + {}^1/_2Al_2Si_2O_5(OH)_4(s)$
4. Anorthite dissolution:
   $CaAl_2Si_2O_8(s)+2H^+ + H_2O \rightarrow Ca^{2+} + Al_2Si_2O_5(OH)_4(s)$
5. K-feldspar dissolution:
   $KAlSi_3O_8(s)+H^+ + {}^9/_2H_2O \rightarrow K^+ + 2H_4SiO^0{}_4 + {}^1/_2Al_2Si_2O_5(OH)_4(s)$
6. Iron precipitation:
   $Fe^{3+} + 3H_2O \rightarrow Fe(OH)_3(s) + 3H^+$

Figure 5.6. Equations of typical gangue reactions.

5.4.2. Gas Transport

Table 5.4 gives the masses of oxygen and water required, according to equation 1 in Figure 5.4, to oxidize all of the pyrite in the dump specified in Table 5.2. It is clear that, whereas the initial water inventory is some ten times more than the amount required to oxidize all of the pyrite, the initial oxygen inventory is about a thousand times too small. It follows that oxygen has to be supplied to support pyrite oxidation in the dump whereas, on the basis of the needs of pyrite oxidation, water does not. The various ways in which oxygen can be transported to oxidation sites in the waste-rock dump are discussed in Chapter 8.

Table 5.4. Masses of oxygen and water required to oxidize the pyrite in the dump

Mass of oxygen required to oxidize pyrite	200,000 t
Mass of oxygen initially in the pore space of the dump	300 t
Mass of water required to oxidize pyrite	32,000 t
Mass of water initially in the pore space of the dump	375,000 t

It is shown in Chapter 8 that, except in special cases or where the intrinsic oxidation rate is low, the overall oxidation rate in the dump is controlled by the rate at which oxygen can be supplied by gas transport to oxidation sites. It follows that, in general, we expect to see gradients in the pore-gas oxygen concentration in a waste-rock dump producing ARD.

The reactions in Figure 5.5 indicate that carbonate dissolution is a source of carbon dioxide. We therefore expect to find carbon dioxide in the pore gas, and gradients in the pore-gas carbon dioxide concentration.

5.4.3. Heat Transport

As the oxidation of pyrite is exothermic, and as the soil-like material of waste-rock dumps is a poor conductor of heat, we expect the temperature in a waster-rock dump to be higher than ambient if the pyrite is oxidizing at an appreciable rate. It is instructive to estimate what this temperature rise might be for the dump specified in Table 5.2.

If for the moment it is assumed that the oxidation rate is uniform throughout the whole volume of the dump and that the system is in pseudo steady state in that pyrite still remains to be oxidized and gas transport rates are rate-controlling, then it follows that the heat source is uniform; it is easy to show that the temperature distribution in such a dump is given by

$$T = 1\text{-}x\ (1\text{-}\alpha) + \frac{S_T\ x\ (1\text{-}x)}{2} \qquad (3)$$

$$S_T = \frac{L^2}{\kappa T_o} \cdot \frac{\delta S^*}{\varepsilon \rho_s c_s} \qquad (4)$$

where $T_o = T_1$ is the temperature of the top surface, T_2 is the temperature of the bottom surface and $a = T_1/T_2$. For $S^* = 1 \times 10^{-8}$ kg (O_2) m^{-3} s^{-1}, which we know from Chapter 8 can be sustained throughout the full height of the dump by diffusive transport of oxygen for typical values of the gas diffusion coefficient and the assumption that the intrinsic oxidation rate is independent of oxygen and pyrite concentrations. In such a case the temperature rise is only about 2 °C. If S^* were some 10 times larger, and if some gas transport mechanism (such as convection) maintained the oxygen levels above zero, then we would expect a temperature rise of about 20 °C.

Thus, if the intrinsic oxidation rate of the dump material is low, temperature rises are expected to be small, and measurement of temperature profiles is not likely to produce data from which the intrinsic oxidation rate can be extracted easily. If the intrinsic oxidation rate is high, temperatures significantly above ambient can be expected, provided that oxygen can be supplied to the oxidation sites, and provided that high temperatures do not decrease the rate of the bacterially catalyzed oxidation process.

Changes in ambient temperature at the surface of the waste-rock dump penetrate into the dump, but are attenuated with depth. A useful expression to describe the space- and time-dependence of the temperature variation from this source, assuming a one-dimensional (1D) description of the dump is adequate, is (Carslaw and Jaeger, 1959):

$$T^*(x, t^*) = \sum_n u_n A_n(x) \cos\left(\omega_n t^* + \theta_n + \Psi_n(x) - \phi_n\right) \qquad (5)$$

where the impressed signal at the surface is

$$T_o(t) = \sum_n u_n \cos\left(\omega_n t^* + \theta_n\right) \qquad (6)$$

and

$$A_n(x) = \left[\frac{\cos h\ 2\beta_n L\ (1\text{-}x) - \cos 2\beta_n L\ (1\text{-}x)}{\cos h\ 2\beta_n L - \cos 2\beta_n L}\right]^{\frac{1}{2}} \qquad (7)$$

$$\beta_n = \left(\frac{\omega_n}{2\kappa}\right)^{\frac{1}{2}} \qquad (8)$$

$$\Psi_n(x) = \tan^{-1}\left[\frac{\tan\beta_n L\,(1-x)}{\tan\beta_n L}\right] \qquad (9)$$

$$\Phi_n(x) = \tan^{-1}\left[\frac{\tan\beta_n L}{\tanh\beta_n L}\right] \qquad (10)$$

Because β_n increases with frequency, and because for large $\beta_n L$, A_n tends to exp-$(\beta_n x)$, changes due to ambient temperatures with frequencies higher than about a month are small except within a meter or so of the dump surface. In most situations the largest component in expression 6 at low frequencies corresponds to annual changes in ambient temperature. Even for annual swings in surface temperature of 30 °C, the amplitude at about 5 m or so from the surface is only 3 °C for typical heat transport properties of the dump material. Thus, changes in ambient temperature lead to significant near-surface temperature variation, but these die out quite rapidly with distance from the dump surface and become insignificant at depths much greater than about 5 m from the surface.

Of concern is the temperature distribution that might be built into the dump during its construction, and the impact this distribution has on the future evolution of temperatures in the dump. The concern can arise where a dump is constructed under very hot or very cold conditions, the question being how long it takes for the initial temperature distribution to vanish. It is readily shown (see for example Carslaw and Jaeger, 1959) that the temperature distribution built into a dump vanishes with a time constant, t_H of the order:

$$t_H = \frac{L^2}{\pi^2 \kappa} \qquad (11)$$

For a dump 15–20 m high, and again assuming typical heat-transport properties for the dump material, the time constant is about 1.5 to 2.5 years.

Rainfall infiltrating the dump leads to heat loss, not so much because the percolating water removes heat, but because it changes the shape of the temperature distribution and this leads to increased heat loss. This is most easily demonstrated, for a large dump in a pseudo steady state, by considering a 1D system with uniform heat source, top surface temperature T_1, and bottom surface temperature T_2:

$$T(x) = 1 + \frac{S_T}{\Lambda_T} x - \left(1 - \alpha + \frac{S_T}{\Lambda_T}\right) \frac{\exp(\Lambda_T x) - 1}{\exp(\Lambda_T) - 1} \qquad (12)$$

$$\Lambda_T = \frac{\rho_w c_w Q_w L}{\rho_s c_s \kappa} \qquad (13)$$

For the special case of $\alpha = 1$, that is, the two surface temperatures are equal, the maximum temperature is at

$$x_{max} = \frac{1}{\Lambda_T} \ln\left(\frac{e^{\Lambda_T} - 1}{\Lambda_T}\right) \qquad (14)$$

For our 15-m-high dump and $Q_w = 0.5$ m y^{-1}:

$$T_{max} = 1.122 \qquad (15)$$

at

$$x_{max} = 0.56 \qquad (16)$$

compared with,

$$T_{max} = 1.125 \qquad (17)$$

at

$$x_{max} = 0.50 \qquad (18)$$

when $Q_w = 0$.

The maximum temperature is reduced and the point at which it occurs is moved in the direction of water flow. This is expected, but note that in the special case $\alpha = 1$, in which percolating water removes no heat because it leaves with the same temperature at which it enters, heat loss is increased by the increased water flow. It is apparent that, at quite modest infiltration rates, water flow through the dump transports a significant quantity of heat and modifies the temperature distribution. In general, the significance of heat transport by water flow can be assessed by comparing the magnitude of $\Lambda_T(\delta T/\delta x)$, which is the heat removed by water movement, and S_T, which is the volume heat source.

The same approach can be used to assess heat transport by gas flow. Numerical calculations (Pantelis and Ritchie, 1991a, 1992) show that when convection is a significant gas transport mechanism in a waste-rock dump, or when advection is used to achieve high overall oxidation rates in a biooxidation heap (Pantelis and Ritchie, 1993), the specific discharge rates associated with gas flow are the order of 10^{-4} to 10^{-3}

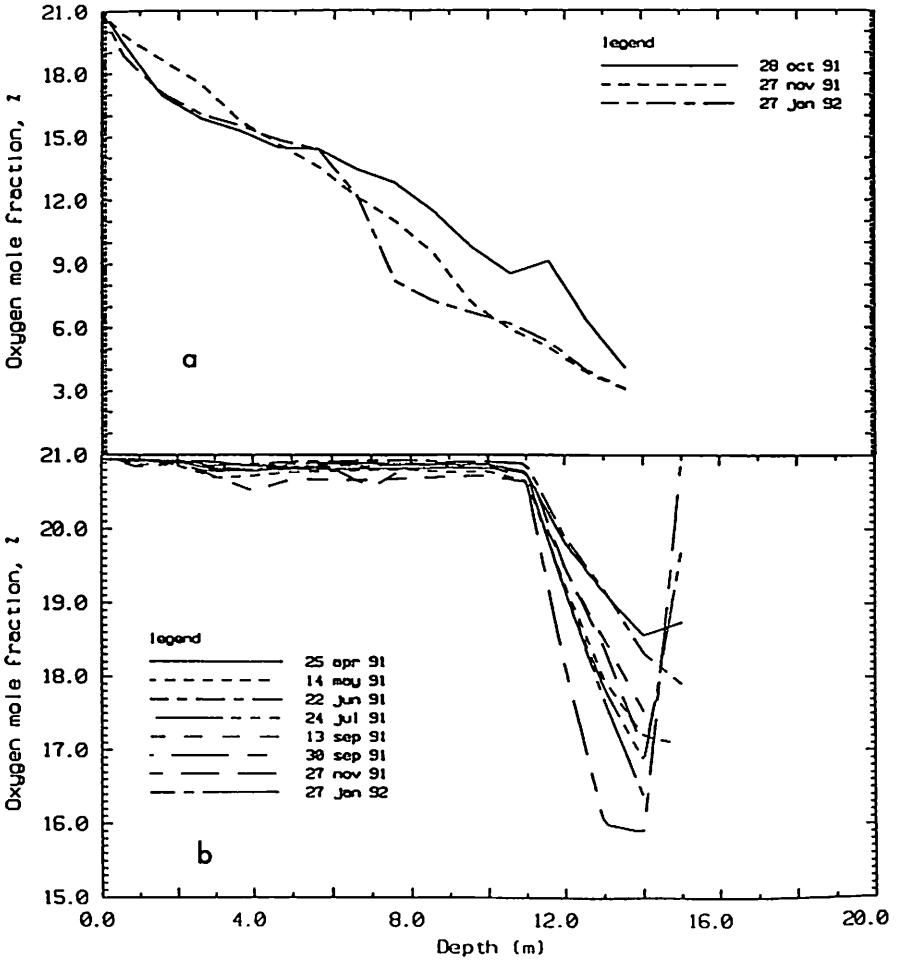

Figure 5.7. Typical pore-gas oxygen-concentration profiles where diffusion is dominant. (a) Relatively uniform oxidation rate over a large portion of the dump; (b) isolated region of oxidation in a large region of low oxidation.

m s^{-1}. These are much larger than the specific discharge rates for water of about 10^{-8} m s^{-1} typically associated with infiltration due to rainfall. Hence, although gas densities are much lower than the density of water, heat transport rates by gas flow in those parts of a waste-rock dump where convection occurs are of the same order of, or greater, than heat transport rates by water flow.

5.4.4. Water Infiltration

It should be stressed that waste-rock dumps are generally unsaturated, except near the base if the underlying material has low hydraulic conductivity. If the underlying material has relatively high hydraulic conductivity, then the waste-rock dump is unsaturated throughout its full height. The unsaturated flow follows from the comparatively low water-infiltration rates occurring at the surface of most waste-rock dumps (about 1×10^{-8} m s^{-1}) and from the relatively high saturated hydraulic conductivity (about 10^{-4} m s^{-1}) of the dump material. The water content in waste-rock dumps, discussed in Section 5.3 below, is typically 5 to 15 volume percent. If the waste-rock dump material is assumed to have the water transport properties of a porous soil then, with an infiltration rate of 0.5 m y^{-1}, water flow rates through the pore space are about 5 m y^{-1} and transit times of water from the top to the bottom of the dump are typically of the order of a few years. Such comparatively long transit times have an impact on the early time-dependence of pollution loads from waste-rock dumps; the long transit times also affect the time-dependent response of pollutant levels in drainage to long-term changes in water infiltration rates engendered by, for example, the emplacement of a cover system.

5.5. THE ENVIRONMENT WITHIN A WASTE-ROCK DUMP

5.5.1. Pore-gas Composition

From the above discussion the oxygen and carbon dioxide concentrations in the pore gas can be expected to vary because there are sinks and sources for these within the waste-rock dump. As a consequence of the absorption and production of these two gases, the concentration of other gases, principally nitrogen and the noble gases normally found in air, also vary. In general, except very close to the dump surface, it is expected that the water-vapor content of the pore gas is in equilibrium with the water in the pore space because gas velocities in the pore space are small (typically 10^{-4} m s^{-1}). Because, as indicated above and as quantified below, the temperature is expected to vary in a waste-rock dump, the absolute water-vapor content of the pore space is also expected to vary.

The source of oxygen in a waste-rock dump is the air at the outer surface of the dump. Oxygen concentrations vary with increasing distance into a dump in a manner

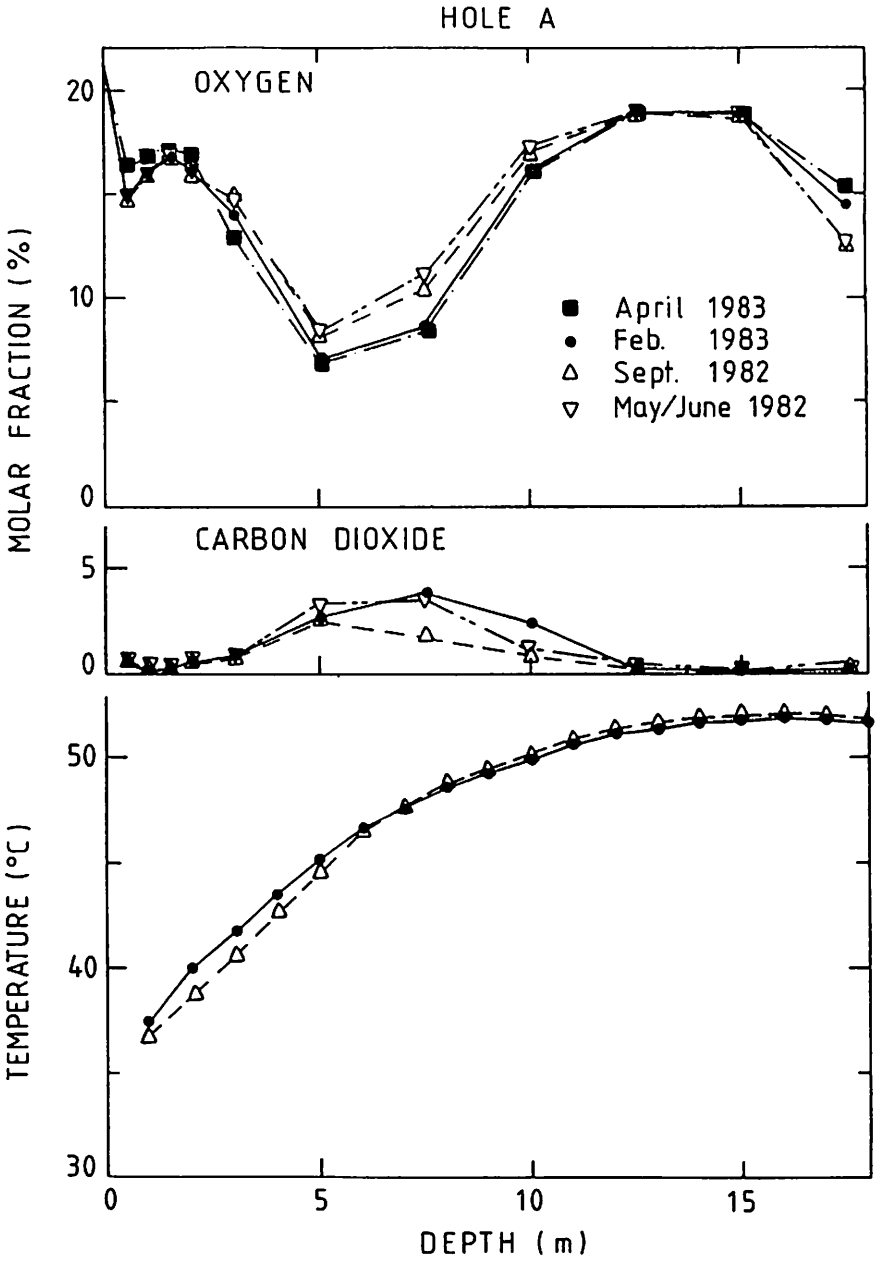

Figure 5.8. Pore-gas oxygen-concentration profile where there is both diffusion and convection.

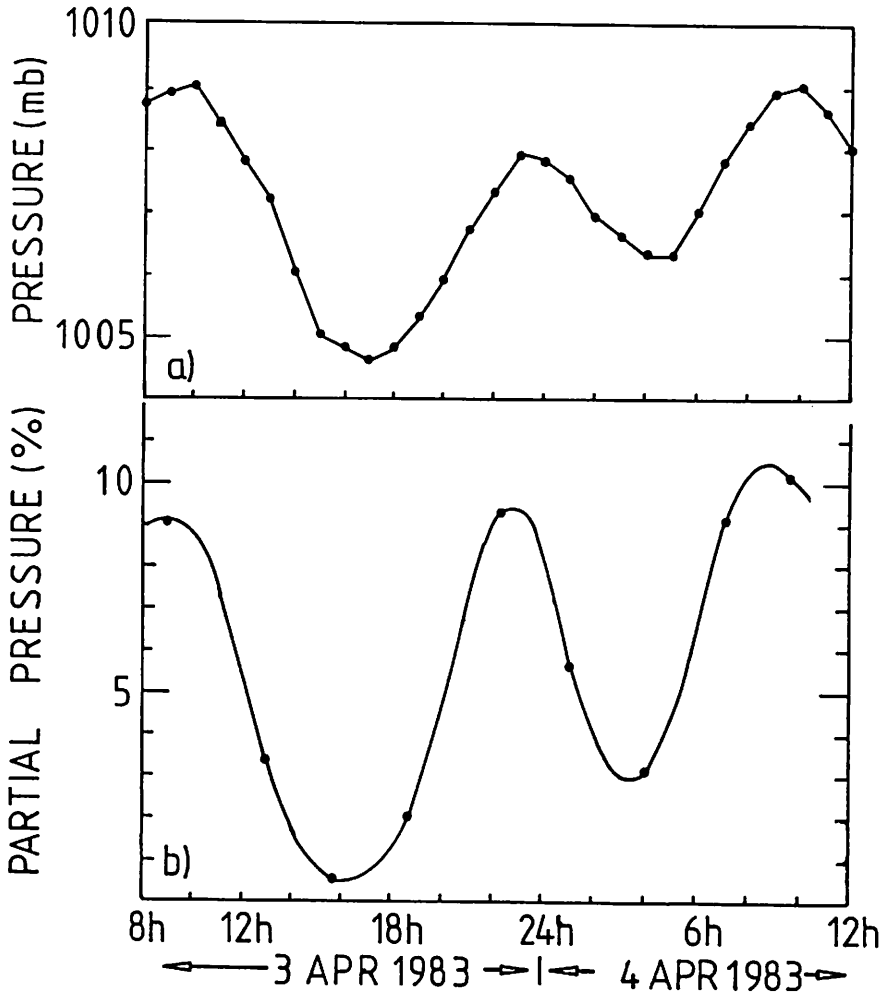

Figure 5.9. A pore-gas oxygen-concentration profile with a marked, systematic, short-time variation.

that depends on the prevailing oxygen transport mechanisms and on the intrinsic oxidation rate. Figure 5.7 shows some oxygen profiles that may be encountered. Figure 5.7a is typical of a dump in which the intrinsic oxidation rate is relatively high, is relatively uniform over an area some tens of meters wide, and in which diffusion is the dominant gas transport mechanism. It should be noted that oxygen concentrations less than 0.2% mole fraction have been measured (Bennett *et al.*, 1992), and values as low as 0.01% mole fraction have been reported (Goodman *et al.*, 1983). The profile in Figure 5.7b is that found if a region of comparatively high intrinsic-oxidation-rate material, some meters in extent, is buried in material of low intrinsic oxidation rate. The large distances over which diffusion is an effective oxygen transport mechanism should be noted in the context of "isolating" pyritic material by selective placement.

The profile of Figure 5.8 is to be expected if gas transport is both by diffusion and by convection. The existence of high oxidation rates in the well-oxygenated lower region is confirmed by elevated temperatures. The carbon dioxide concentration profile, also shown in this Figure, indicates that carbon dioxide and oxygen concentrations tend to be anticorrelated, the reason being that air outside the dump is the source of oxygen because carbon dioxide is produced by chemical reactions within the dump.

The profile in Figure 5.9 emphasizes the need to monitor pore-gas oxygen concentrations on the appropriate timescale. The rapid variation in concentration follows closely the pronounced diurnal variation in atmospheric pressure that applies at the latitude of the minesite where this waste-rock dump is located (Harries and Ritchie, 1985). This particular variation was a consequence of the geometry of the dump at the location of the probe hole and does not represent a mass transport of gas into a large area of the dump.

Carbon dioxide concentrations in the pore space of a waste-rock dump can range up to about 20% mole fraction and are frequently in the range 1—10% (Harries and Ritchie, 1983; Schuman *et al.*, 1992). This is much higher than atmospheric levels of 0.03%. Elevated concentrations of carbon dioxide increase the oxidation rate of pyrite by moderate thermophiles (Norris, 1989); some workers (see for example Holuigue *et al.*, 1987; Beyer *et al.*, 1990) have reported increased growth rate of *Thiobacillus ferrooxidans* with increasing levels of carbon dioxide, but others (*e.g.*, Kelly and Jones, 1978; Norris, 1989) have reported little change up to 7%. Haddadin *et al.* (1993) observed that increased carbon dioxide concentrations increased the pyrite oxidation rates, but that concentrations of 4% were inhibitory to all three of the microbial populations involved in pyrite oxidation in the system studied.

Gases such as sulfur dioxide and hydrogen sulfide might be expected as possible products in the aerobic and anaerobic zones, respectively, of the dump. Although attempts have been made to measure these gases, they have not been found in

significant quantities.

5.5.2. *Temperature*

In waste-rock dumps where there is ARD, temperatures range from a low of about -7 °C (Bell *et al.*, 1991) to a high of about 65 °C. The low temperatures, although surprising in view of the temperature sensitivity of the bacteria that catalyze pyrite oxidation (Ahonen and Tuovinen, 1989, 1991), perhaps emphasize the point that even low pyrite oxidation rates are environmentally significant. The high temperatures are not surprising, as indicated in Section 4.3 above, and are to be expected at quite modest oxidation rates. It does, however, mean that if bacteria are present and are involved in catalyzing the oxidation of pyrite, then the dominant species in the hot regions must be thermophiles. Thermophiles have been isolated from pyritic waste dumps (Marsh and Norris, 1983; Hendy, 1987).

As indicated above, the temperature profile in a dump depends on the rate of heat production from pyrite oxidation, on the heat transport by heat diffusion and gas and water flow, and on changes in ambient temperature at the dump surface. The resulting profile may have the shape shown in Figure 5.8 if the oxidation rate is high, or the shape in Figure 5.10 if the oxidation rate is similar to that which gives the oxygen profile of Figure 5.7a. Here the temperature rise due to the relatively small oxidation rate is swamped by changes in ambient temperature.

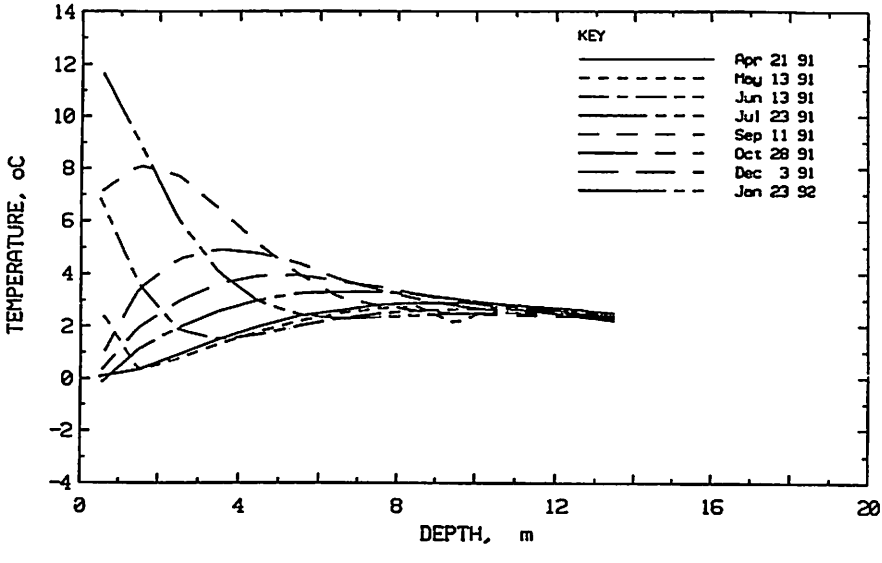

Figure 5.10. Typical temperature profile in a dump in which ambient changes in temperature have a dominant effect.

It is worth emphasizing that a high pore-gas oxygen concentration at a point in a dump may result from either a very low oxidation rate, or from a high oxidation rate together with rapid transport of oxygen to that point. If it is the second, then the temperature at the point will be elevated. Measurements of oxygen and temperature profiles are complementary techniques.

5.5.3. Pore-water Composition

As shown in Chapter 8, the concentration of chemical species in pore water is expected to change as pore water percolates towards the base of the waste-rock dump, with the concentration of conservative species increasing with increasing distance from the dump surface. As discussed in Section 2.4 above, it is the chemical composition of pore water at the base of the waste-rock dump that is of prime interest because this composition is a major factor in determining the water quality of drainage from the dump. It follows that, to obtain a complete picture of the chemical environment in pore water, samples of pore water need to be taken throughout the depth of the dump, from close to the surface to close to the base of the dump. Waste-rock dumps are generally unsaturated over most of their height (Section 4.4), making pore-water sampling difficult technically. The problem is exacerbated when the dump is >10 m high, as this is as high as a column of water can be supported by atmospheric pressure. For these reasons, few data on the chemical composition of pore water within waste-rock dumps are in the literature.

Two techniques for *in-situ* sampling of pore water have been reported. Lysimeters have been installed within a waste-rock dump (Yanful *et al.*, 1993; Bennett *et al.*, 1992; Bennett and Ritchie, 1992) to collect pore water for subsequent analysis. The implementation of such a technique is relatively straightforward in small dumps, about 5 to 10 m high, where a back-hoe can be used to install lysimeters at various depths. Location near the base of a large waste-rock dump is not practical this way, and installation is best done while the dump is being constructed. Care must be taken in designing the lysimeter so that it is an effective collector of pore water in the unsaturated medium (Gibson, 1987).

In the second technique, pore-water samples are collected from the unsaturated zone by vacuum extraction via a hollow porous ceramic cup buried in the waste-rock dump. As the maximum pressure that forces the water from the soil pores is atmospheric, the technique will work only if the capillary suction in the soil pores is less than 10 m, or in practice, to achieve a reasonable pore-water collection rate, less than about 8 m. This technique has been applied in the study a waste-rock dump conducted for Golden Sunlight Mines in Montana, USA (Schaeffer and Associates, 1993). These ceramic cups have been used extensively (Suarez, 1986; Debyle, 1988; Iggy Litaor, 1988) to measure soil suction in the top meter or so in soils, mainly in an agricultural context. In such situations the soil, although unsaturated, generally has a

Table 5.5. Analysis of soil samples from the near surface of a waste-rock dump generating ARD (extracted from Appendix C of Goodman *et al.*, 1981)

Distance from surface (cm)		30	60	90	120	150	180	210	240	248	255	263	270	300	330	338	343	353	360	390	420
Moisture content w/w %		9.3	17	16	15	16	13	14	15	15	14	18	15	14	15	14	15	15	12	18	20
Water-solubles ($x10^3$ppm)		n	n	2.6	1.8	2.5	1.4	0.6	1.9	n	1.2	1.7	1.4	1.4	2.4	2.3	1.1	0.1	1.6	3.1	2.4
pH		3.5	3.2	3.7	3.7	3.2	3.6	3.4	3.6	3.7	3.8	3.5	3.9	4.4	3.9	4.1	3.9	4.0	3.9	3.7	3.1
Soluble metal content (ppm)	Fe	n	n	10	n	n	10	n	210	n	n	n	11	n	n	10	n	n	n	n	n
	Cu	n	n	18	n	n	31	n	n	n	n	n	10	n	n	18	n	n	10	n	n
	Zn	n	n	n	n	n	5	n	n	n	n	n	15	n	n	n	n	n	7	n	n

Note: Sampling taken in March 1977 at end of wet season

Table 5.6. Chemical composition of ARD from some waste-rock dumps

	Chemical Concentrations (mg L^{-1})										
	Al	Ca	Mg	SO_4	Cu	Mn	Zn	Pb	Fe	Flow m^3s^{-1} ($x10^3$)	pH
Cumulative springs from SE of White's dump, Rum Jungle	-	428	7460	34,000	114	56	133	0.44	48	0.32	3.4
Cut-off drain for S.W. dump, Aitik Sweden	45	98	-	640	12.8	-	3.8	-	1.0	133	3.8
Seepage from toe of E. dump Mt. Washington, Canada (Kwong & Ferguson 1990)	19.1	116	11	500	16.5	3.3	0.16	-	1.7	-	4.1

higher moisture content than expected in a waste-rock dump.

The extraction of pore water from samples collected from a waste-rock dump is a direct way of assessing the chemical composition of pore water. The disadvantage is that the measurement is not an *in-situ* one, and generally samples are collected from the near-surface. Drilling into waste rock does not generally provide samples suitable for sampling pore water. Table 5.5 presents some data on water content and chemical composition obtained from sampling dump material.

The chemical composition of drainage water at the toe of a dump is another way to infer the chemistry of pore water within the dump. As discussed above, a drainage-water sample is some integral over space and time of the pore water at the dump base. Although it is not a direct measure of pore-water chemistry in the dump, it can be a guide as to what the pore-water chemistry might be. Table 5.6 presents data on drainage-water chemistry from some waste-rock dumps.

5.5.4. Microbial Ecology

Chapter 7 covers in detail the role of microorganisms in the tailings environment. As much of this applies equally well to the waste-rock-dump environment, just a few points on the microbial ecology will be made here.

As discussed in Section 5.2, elevated temperatures found in some parts of some waste-rock dumps exceed the temperature at which *Thiobacillus spp* are viable. It is therefore not surprising that thermophilic pyrite-oxidizing bacteria have been isolated from waste-rock dumps (Hendy, 1987). Similarly, it is not surprising that various of the *Thiobacillus spp* have been isolated from a variety of waste-rock dumps.

Few studies (Harrison, 1978; Goodman *et al.*, 1981) on the microbial ecology of waste-rock dumps have been conducted. From these the following points are worth emphasizing. Goodman *et al.* (1981) found that the most abundant microorganisms in the top 4 m or so of a dump in which oxidation was known to occur were acidophilic heterotrophs. These were present at levels from 10^3 to 10^6 g^{-1}, with levels of *Thiobacillus ferrooxidans* ranging from 10^2 to 10^4 g^{-1}. In another heap *Thiobacillus ferrooxidans* was present at 10^3 to 10^5 g^{-1} in the top 3 m of a part of the dump where the oxidation rate was high, but no acidophilic heterotrophs were found. McGinness and Johnson (1993) also noted an apparent lack of acidophilic heterotrophs in acid mine waters from a disused pyrite mine. It has been noted before (Ralph, 1979, 1985) that acidophilic heterotrophs are common in dumps in which pyrite is oxidizing, but their role, if any, in pyrite oxidation remains unclear.

In that part of the dump where Goodman *et al.* found acidophilic heterotrophs to be the most abundant microorganisms, the oxidation rate ranged up to about 8×10^{-8} kg (O_2) m^{-3} s^{-1} (Harries and Ritchie, 1981). At the time of sampling, the water

content of the samples was about 15 wt%. Even allowing for this, the *Thiobacillus ferrooxidans* populations of 10^2 to 10^4 g^{-1} are at least two orders of magnitude smaller than the 10^6 to 10^7 mL^{-1} frequently quoted in experiments on the microbially catalyzed oxidation of pyrite (*e.g.*, Olson, 1991). This difference is of about the same order as the difference found between field and laboratory determinations of pyrite oxidation rates as discussed in Chapter 8. As indicated in that Chapter, taking account of the different timescales that apply in waste-rock dumps, it is likely that it is not so much that the low bacterial population causes a low oxidation rate, but that the intrinsic oxidation rate of the dump material is low and limits the size of the bacterial population.

Many waste-rock dumps have large regions in which the pore-gas oxygen concentrations are low. The microbial studies of Goodman *et al.* found *Thiobacillus ferrooxidans* in dump regions where gas profiles indicated that the oxygen concentrations were less than about 0.1% mole fraction. It is of course possible that the microorganisms found there had been transported by the movement of pore water from oxygen-rich regions higher in the dump. It has, however, been detailed by Pronk *et al.* (1992) that *Thiobacillus ferrooxidans* continues to grow under anaerobic conditions by using organic material as a substrate and ferric ion as a terminal electron acceptor. Although such a finding might explain the presence of *Thiobacillus ferrooxidans* in anaerobic regions of a dump, the question of the source of organic material remains unanswered. Moreover, as ferric ion is such a potent oxidizing agent under acid conditions, and because the ultimate oxidant in the creation of ferric ion is oxygen (see reaction 2 of Figure 5.4), we would not expect growth of *Thiobacillus ferrooxidans* much below the oxic zone if ferric ion is the only possible electron acceptor.

5.6. BULK PHYSICAL PROPERTIES OF WASTE-ROCK DUMPS

The gas concentration and temperature profiles in a waste-rock dump depend on the magnitude of a number of physical properties of the dump material, including air permeability, the gas diffusion coefficient, and the thermal conductivity. The appropriate values required for these properties are averages over a representative volume appropriate to the transport of heat and gas in a waste-rock dump in which pyritic material is oxidizing. Measurements of gas and temperature profiles in waste-rock dumps suggest that an appropriate scale is of the order of a meter or a large fraction of a meter.

Techniques to measure these properties of waste-rock dumps need to be appropriate to this scale. Such measurements provide results that can be used not only in predictive modelling or the analysis of profiles to elucidate gas-transport mechanisms and quantifictaion of oxidation rates, but they also can be used to provide insight concerning the extent to which the heterogeneity of the dump affects these bulk properties. Techniques have been developed for the *in-situ* measurement of thermal

Table 5.7. ***In-situ*** **thermal conductivity measurements in waste-rock dump material**

Minesite location	Number of measurement points in waste dump	Range* ($Wm^{-1} K^{-1}$)	Average ($Wm^{-1}K^{-1}$)
Aitik mine, Sweden	8	0.71 – 1.63	1.2 ± 0.4
Heath Steele, Canada	3	1.04 – 1.22	1.2 ± 0.1
Kelian, Kalimantan	7	1.57 – 3.31	2.1 ± 0.6
Rum Jungle, Australia	6	1.77 – 3.12	2.2 ± 0.5

* Experimental error on individual measurements estimated at 3%

Table 5.8. ***In-situ*** **air permeability measurements in waste-rock dump material**

Minesite location	Number of measurement points in waste dump	Range (m^2)
Aitik mine Sweden	27	$(2.6 \pm 0.2)\times10^{-11}$ - $(1.4 \pm 0.1)\times10^{-9}$
Heath Steele, Canada	24	$(1.6 \pm 0.15)\times10^{-10}$ - $(4.7 \pm 0.5\times10^{-9}$
Kelian, Kalimantan	18	$(3.9 \pm 0.1)\times10^{-13}$ - $(9.3 \pm 0.6)\times10^{-10}$
Rum Jungle, Australia	144	$(8.89 \pm 0.19)\times10^{-13}$ - $(1.49 \pm 0.21)\times10^{-9}$

Table 5.9. ***In-situ*** **oxygen diffusion coefficient measurements in waste-rock dump material**

Minesite location	Number of measurement points in waste dump	Range $m^2 s^{-1}$ ($\times 10^6$)
Aitik mine, Sweden	2	(2.25 ± 1.04) - (6.85 ± 1.02)
Heath Steele, Canada	3	(2.65 ± 0.55) - (3.35 ± 0.25)
Woodlawn, Australia	2	(3.49 ± 1.64) - (5.07 ± 0.39)

conductivity (Blackford and Harries, 1985; Bennett *et al.*, 1993b), air permeability (Bennett and Ritchie, 1993), and the gas diffusion coefficient (Bennett *et al.*, 1993a). These techniques have been used to measure the bulk properties at a number of positions in individual waste-rock dumps, and dumps at different minesites. The results are shown in Tables 5.7, 5.8, and 5.9.

The comparatively small variation in the values of these bulk parameters from point to point in the same dump is noteworthy. In this context, it needs to be noted that gas transport in a dump is dominated by diffusion when the air permeability is 10^{-10} m^2 or less (Bennett *et al.*, 1989; Pantelis and Ritchie, 1991a). Also of note is that the variation from dump to dump is about the same as that within a dump. At this stage the results in Tables 5.7, 5.8, and 5.9 are a small data-set, and there is a need for more measurements of the bulk properties of waste-rock dumps. The set does indicate that, at least for the parameters measured, the heterogeneity of the dump material and any layering consequent on the method of dump formation do not carry through in any marked way.

5.7. CONCLUSIONS

Techniques exist to provide data on the temperature and pore-gas-composition profiles in waste-rock dumps. These data indicate that in most waste-rock dumps these profiles are pseudo steady state on a timescale of years to tens of years. The pseudo-steady-state profiles can be perturbed by processes with faster timescales, for example temperature variations due to seasonal variation in ambient temperature. Waste-rock dumps are usually high enough that temperature changes due to seasonal changes in ambient temperature do not penetrate through the whole dump. The pseudo-steady-state profiles reflect the interaction between the oxidation rate of pyritic material in the dump and the transport of oxygen to the oxidation sites, and the interaction between heat released in pyrite oxidation and heat transported by conduction and by water and gas flow in the dump pore-space.

Oxygen concentrations in the pore space range from atmospheric levels of 20.9% mole fraction, down to <0.1% mole fraction. Carbon dioxide concentrations range from atmospheric levels of 0.03%, up to about 20%. Humidity is expected to be close to 100% within the dump pore-space, except very close to the surface. Other gases normally present in air, such as nitrogen and the noble gases, have concentrations that balance the concentrations of oxygen, carbon dioxide, and water vapor.

Temperatures in waste-rock dumps producing ARD range from about 65 °C to about -7 °C. The temperature rise associated with an intrinsic oxidation rate of about 1 x 10^{-8} kg (O_2) m^{-3} s^{-1}, which is high enough to generate pollutants at an environmentally significant rate, is only about 2 °C.

Data on temperature and gas-concentration profiles can be used to evaluate the oxidation rate in a dump; thus, there is a need for more measurements in a range of dumps, not only to provide data on the dump environment, but to quantify the intrinsic oxidation rate in such environments. Such measurements have, for example, shown that waste-rock material in a dump can oxidize at an environmentally significant rate at temperatures close to 0 °C. Such a result seems to be counter to the classical picture that the primary pollutant-generation process is bacterially catalyzed pyrite oxidation.

Oxygen and temperature profiles in a dump provide an early measure of the effectiveness of schemes implemented to reduce oxidation rates in dumps. The profiles also provide a direct way to identify those parts of a dump where the intrinsic oxidation rate is high, and those where it is low. This information can be compared with laboratory-generated results on the oxidation properties of dump material, or used where no such data exist.

A picture of the chemical environment within waste-rock dumps is much less clear. There are two reasons. First, a great deal of attention has been given to the quality of drainage water from waste-rock dumps. Second, the collection of pore water from within an unsaturated system, often tens of meters high, is technically difficult. The attention given to the quality of drainage water is understandable as environmental regulations commonly relate to water quality, but flow rates need to be measured to provide useful quantitative data. Moreover, as loads and concentrations measured at the toe of a dump are some integral over space and time of drainage from various parts of the base of the dump, they do not provide a clear picture of the chemical composition of water in the pore space within the dump. It is this chemical composition and the way it changes with time that dictate the time-dependence of the load from the dump. Just as oxygen and temperature profiles provide timely data on the efficacy of measures to reduce oxidation rates, the chemical composition of pore water would provide timely data on the effectiveness of these measures in reducing the pollution load if suitable, in-dump monitoring techniques were developed.

Similiar to the scarcity of data for the pore-water chemistry, data on water movement through waste-rock dumps are minimal, and for similar reasons. Data on pore-water movement are urgently required to elucidate water transport mechanisms in waste-rock dumps, and the extent to which these mechanisms reflect the structure and method of construction of the dump. *In-situ* measurements to date of the dump bulk properties, thermal conductivity, air permeability, and gas diffusion coefficient, which are important in gas and heat transport, indicate that waste-rock dumps are relatively homogeneous at the scale appropriate for the determination of these properties.

Within a waste-rock dump producing ARD, the relatively extreme environment, which includes wide ranges of temperature, gas composition, and pH, leads to

interesting questions as to the types of microorganism to be found. The identification of a particular microorganism in a waste-rock dump is not very useful unless it can be related to the generation rate of pollutants in a quantitative way. Moreover, it seems possible that it is the microbial ecology rather than individual microorganisms that is the real determinant of pyrite oxidation rates. New genetic techniques should be deployed to evaluate better the types and numbers of bacteria, and to relate these to the oxidation rate. It is also likely that, given the timescale of the various processes that control the oxidation rate in a waste-rock dump, the bacterial population follows rather than dictates the environment within a dump.

5.8. NOMENCLATURE

T^* = Temperature (°C)

T_0 = Some characteristic temperature for normalization

T = T^*/T_0 Dimensionless temperature

x^* = Spatial variable (m)

L = Height of waste rock dump (m)

x = x^*/L = Dimensionless spatial variable

S^* = Intrinsic oxidation rate (kg $(O_2)m^{-3}s^{-1}$)

C_0 = Concentration of oxygen in air (0.265 kg m^{-3})

c_w = Specific heat of water (4.18 x 10^3 $m^2s^{-1}K^{-1}$)

D = Oxygen bulk diffusion coefficient of dump (m^2s^{-1})

S = $(L^2S^*)/C_0D$ = Dimensionless intrinsic oxidation rate

κ = Bulk thermal diffusivity of dump (m^2s^{-1})

ρ_s = Bulk density of dump (kg m^{-3})

δ^w = Density of water (1000 kg m^{-3})

δ = Heat released per mass of reactant oxidized (2.25 x 10^7 J kg^{-1})

ρ_c = Density of fast-reacting acid-consuming material (kg m^{-3})

ε_c = Mass of oxygen used per mass of fast-reacting acid-consuming material (0.60 for calcium carbonate)

ε_w = Fractional volume of dump which is water-filled

ε = Mass of oxygen used per mass of reactant in oxidation reaction (1.75)

c_s = Bulk specific heat of dump (866 $m^2s^{-1}K^{-1}$)

S_T = $(L^2\delta S^*)/(\kappa T_0\, \varepsilon\, \rho_s\, c_s)(s^{-1})$

Λ_T = $(\rho^w c_w Q_w L)/(\rho_s c_s \kappa)$

Q_w= Infiltration rate (ms^{-1})

Chapter 6

Iron-sulfide Oxidation Mechanisms: Laboratory Studies

Ronald V. Nicholson
Waterloo Centre for Groundwater Research
Department of Earth Sciences
University of Waterloo
Waterloo, Ontario N2L 3G1

6.1. INTRODUCTION

Laboratory studies of sulfide mineral oxidation have been conducted for a variety of reasons. Numerous studies have been conducted to address the environmental controls on the rate of oxidation of sulfides in mine wastes. Investigations of iron sulfides in the 1960s and 1970s were focused mainly on the water-quality problems associated with pyritic spoils from coal mines in the eastern United States. Numerous individual laboratory studies resulted in a wide range of results that commonly were inconclusive and confusing regarding the mechanisms controlling pyrite oxidation in natural environments. This early work, however, did help to identify the critical environmental factors that play a role in the rate of sulfide-mineral oxidation, and these factors have been studied more extensively since the early 1980s. Lowson's (1982) literature review contains a fairly comprehensive summary of research on the oxidation of pyrite and other sulfide minerals by molecular oxygen. Lowson's emphasis on the diversity of research results and conflicting values for important controlling parameters may leave many readers confused about the oxidation process. As will be shown, work completed more recently has identified the similarities and consistencies in the results of pyrite oxidation studies.

The main purposes for conducting laboratory studies of sulfide mineral oxidation are: (1) to explore and define the mechanisms controlling the oxidation reactions, including a description of the rate-determining steps; (2) to develop an understanding of the important variables that represent environmental factors in the role of sulfide-mineral oxidation; and (3) to develop predictive models to describe the oxidation process. Although the chemical mechanisms are extremely important in understanding the oxidation reaction, or series of reactions, this manuscript will emphasize the study of environmental factors and the application of laboratory results

to the modelling of this apparently complex process. This report is focused on reactions involving pyrite oxidation. A separate section on pyrrhotite oxidation is also presented, and comparisons with the kinetics of pyrite oxidation are made.

6.2. EFFECT OF ENVIRONMENTAL FACTORS

A wide assortment of variables has been tested to determine their effect on the rate of pyrite oxidation. Two oxidants are important in this process: oxygen and ferric iron (Fe^{3+}). Oxidation of pyrite by dissolved oxygen can be expressed as:

$$FeS_2 + {}^7/_2\, O_2 + H_2O \Rightarrow Fe^{2+} + 2SO_4^{2-} + 2H^+ \qquad (1)$$

where the sulfur component of pyrite is oxidized from S_2^{2-} to SO_4^{2-}, thereby releasing seven electrons per sulfur atom oxidized. In this reaction, the ferrous iron (Fe^{2+}) remains unoxidized. It has been suggested that a number of sulfur intermediates, such as $S_2O_3^{2-}$, polythionates, and elemental sulfur can form during the oxidation process (Goldhaber, 1983), but Moses *et al.* (1987) concluded that these are not important products when oxidation occurs in environments with pH values less than 8. It is evident from Goldhaber's (1983) results that the formation of sulfur intermediates is a function of the rate of reaction, with faster reactions favoring the formation of some intermediates. The analysis also showed that the intermediate products decay rapidly by oxidation to sulfate when the source of pyrite is removed. Therefore, we will assume here that the final oxidation product of pyrite oxidation is SO_4^{2-}. It is known, however, that elemental sulfur can form under field conditions of pyrrhotite oxidation, and the fate of this material is still not clearly understood (Jambor, this Volume).

The second oxidant of pyrite that can be important in mine-waste environments is ferric iron. The reaction with pyrite can be written as:

$$FeS_2 + 14Fe^{3+} + 8H_2O \Rightarrow 15Fe^{2+} + 2SO_4^{2-} + 16H^+ \qquad (2)$$

where fourteen ferric ions are required to provide the electrons necessary to oxidize the two sulfur atoms from S_2^{2-} to SO_4^{2-}. This is a rapid reaction, which was recognized as an extremely important component of the oxidation process at sulfide waste sites (Singer and Stumm, 1970). The Fe^{3+} will not be produced, however, unless oxygen is present as the terminal electron acceptor or the primary oxidant. The source of Fe^{3+} in most sulfide wastes is the cycling of Fe^{2+} in the presence of oxygen as shown in the following reaction:

$$Fe^{2+} + {}^1/_4\, O_2 + H^+ \Rightarrow Fe^{3+} + {}^1/_2\, H_2O \qquad (3)$$

in which a proton is consumed. If this reaction occurs under acidic conditions (pH $\leq$3.5), then a significant quantity of the Fe^{3+} can remain in solution to react with pyrite

as shown in equation (2). When the pH is greater than 3.5, low concentrations of Fe^{3+} are maintained through the precipitation of ferrihydrite or ferric hydroxide, commonly shown in the reaction

$$Fe^{3+} + 3H_2O \Leftrightarrow Fe(OH)_{3(s)} + 3H^+ \qquad (4)$$

in which three moles of H^+ are produced for each mole of Fe^{3+} that is precipitated. Other ferric iron solids such as jarosite $KFe_3(SO_4)_2(OH)_6$, can also form under acidic, oxidizing conditions. However, when oxidation decreases and sulfate levels decline, jarosite can transform to ferric hydroxide solids, thereby releasing stored acidity.

Reactions 1 through 4 may occur simultaneously in nature, and the presence of Fe^{2+} and Fe^{3+} have been noted in tailings pore-waters where oxygen is present (Dubrovsky *et al.*, 1985). Although the cycling of ferrous to ferric iron and back again through the oxidation of pyrite is complex, we will examine separately the significance of each variable that can play a role in the oxidation process. The information will be synthesized and summarized to provide a working kinetic model for pyrite oxidation.

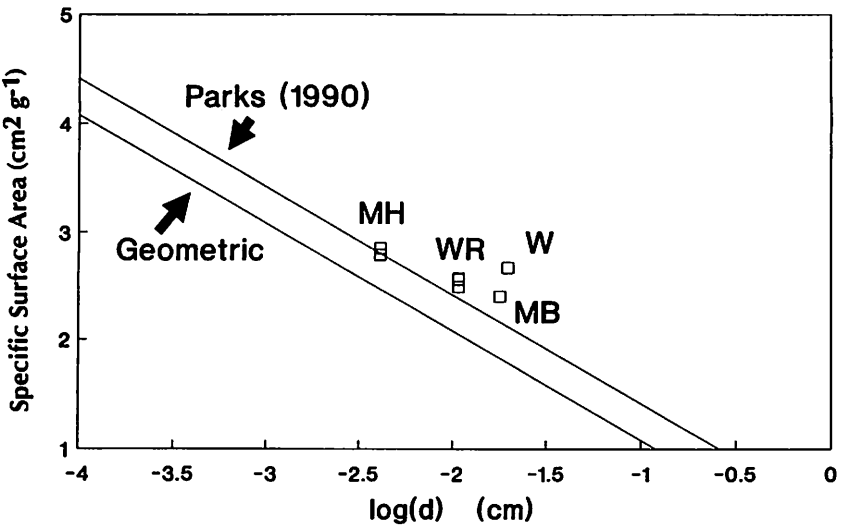

Figure 6.1. Plot of the log of specific surface area *versus* the log of grain diameter.

6.2.1. *Surface Area*

In addition to the presence of oxidants, the available (exposed) surface area of sulfide minerals is probably one of the most important variables controlling the rate of oxidation. Historically, there was some confusion regarding the effect of various pyrite

"types" on the rates of oxidation. Some of this confusion was clarified when it was understood that the morphological forms of pyrite, such as framboidal pyrite, represented material with extremely high available surface areas. Many, if not most, of the laboratory experiments conducted on pyrite to determine oxidation kinetics are performed with crushed and sieved fractions of massive or crystalline pyrite. Typically, the grain-size fractions used are on the order of 50—100 μm in diameter. Crushed material is used in order to provide sufficient surface area so that reaction rates will be rapid enough to monitor in the laboratory.

On the basis of a unit mass, the available surface area of granular material such as tailings is inversely proportional to the grain diameter. Based on simple geometric forms such as a sphere or cube, the specific surface area (A_s) with dimensions [L^2M^{-1}] can be expressed as:

$$A_s = \frac{6}{\rho d} \qquad (5)$$

where ρ is the grain density [M/L^3] and d is the particle diameter [L]. This relationship does not account for irregularities on the grain surfaces and, in recent experiments, measurements of surface area are common. Earlier studies, however, reported mainly grain-size ranges; therefore, equation (5) permits a comparison of grain size with surface-area measurements performed by BET analysis. Such comparisons can be seen in Figure 6.1, in which the simple geometric relationship is shown as the lower line, and the regression of measured BET surface area for quartz grains against grain diameter is shown in the upper line. The regression equation reported by Parks (1990) is

$$\log(A_s) = 0.415 - \log(d) \qquad (6)$$

This equation is similar and parallel to the simple geometric relationship in equation (5) in log-form terms with $\rho = 5\ g \cdot cm^{-3}$ for pyrite giving:

$$\log(A_s) = 0.08 - \log(d) \qquad (7)$$

where it can be readily seen that the difference between the geometric estimate of surface area (equation 7) and the BET-measured surface area (equation 6) have the same slope, with a factor of five (or about 0.3 log units) difference in specific surface areas for any grain size. Data from three studies (Figure 6.1) indicate that measured BET values for pyrite occur at, or slightly above, the regression relationship for quartz sand. In any case, it appears that the BET-measured areas do not differ from the geometric estimates of surface area by more than a factor of four. This means that it may be possible to compare the rates from earlier studies in which BET measurements were not conducted, but in which information on grain diameters is available. It is

convenient to make comparisons of oxidation rates on the basis of unit surface areas, and comparison among various studies provides reasonably consistent results.

All of the recent studies of pyrite oxidation indicate that the rate of reaction is proportional to the available surface area. This has been shown for the same mass of material with different grain diameters, or with increasing mass of same-diameter pyrite particles. An example in Figure 6.2 shows the relationship of oxidation rate to the inverse grain diameter that indicates the proportionality to surface area for a unit mass of pyrite.

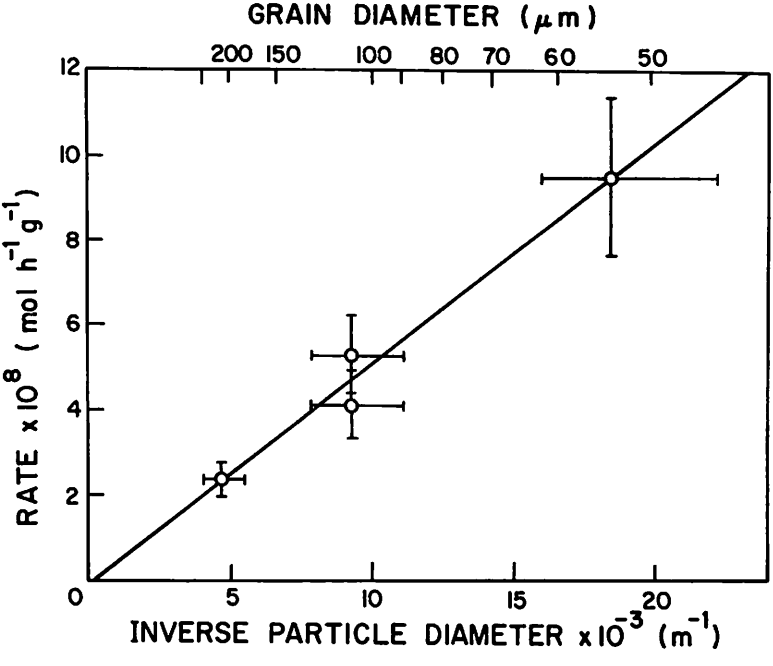

Figure 6.2. Pyrite oxidation rate as a function of inverse grain diameter (from Nicholson, 1984).

Some of the previous confusion regarding the relationship between surface area and oxidation rates seems to have arisen because of inconsistent preparation of the pyrite used in oxidation experiments. It is now well-known that crushing of pyrite and sieving can result in bimodal grain-size distributions (Nicholson *et al.*, 1988). This result is the consequence of large grains of material being coated with fine particles or "dust" from the crushing procedure. Experience with silicate-weathering experiments has shown that improper removal of these fines produces inappropriate rate results that appear non-linear with respect to surface area. The fine-grained material on the larger particle surfaces has a much higher specific surface area and will oxidize more rapidly

than the grain-size fraction that was selected. Therefore, care must be taken to remove or eliminate the fine particles before conducting kinetic experiments. Removal of fines is usually accomplished by repeated washing, either in weak acid solutions or in various solvents such as methanol or acetone. Different washing techniques do not seem to affect the kinetic results. Various washing techniques are described by McKibben and Barnes (1986), Moses *et al.* (1987), Nicholson *et al.* (1988), Rimstidt *et al.* (1994), and others.

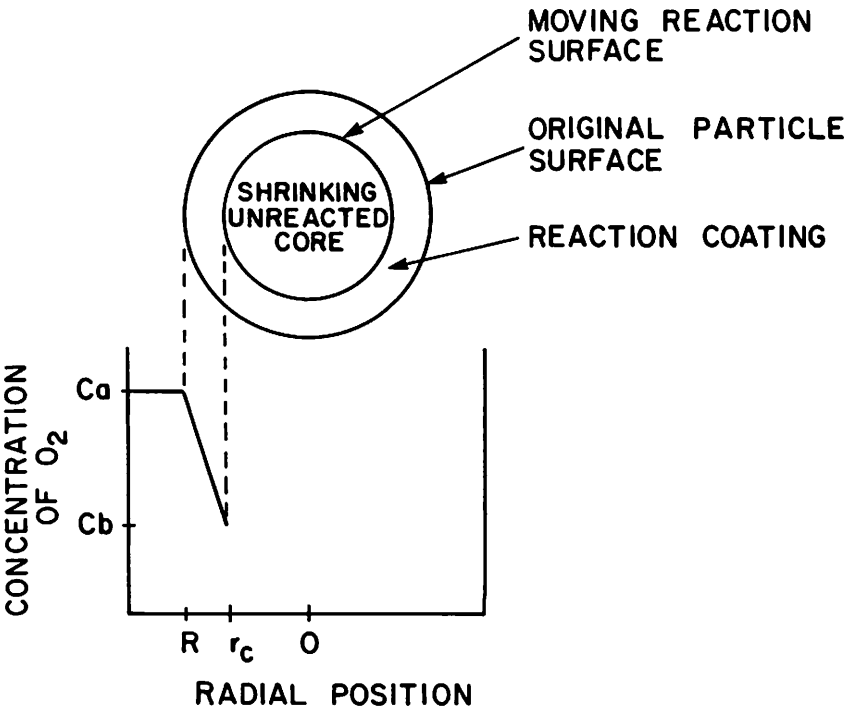

Figure 6.3. Schematic diagram of reacting particle with increasing product layer. The concentration of reactant (*e.g.*, oxygen) from particle surface to bulk solution is shown.

There are other effects related to surface area and exposure of reactive sulfide surfaces to oxidation that are purposefully avoided in the laboratory, but have important implications for predicting rates in field settings. Changes in surface area can occur for "shrinking particles", when significant mass is lost in the oxidation process under acidic conditions. The decrease in particle diameter is related to mass oxidized by the mineral density. This shrinking-particle model was applied to pyrrhotite oxidation column experiments in the laboratory with favorable results (Elberling *et al.*, 1993a).

Under less acid conditions, coatings of ferric hydroxide, known as product layers, can form on the surfaces of iron-sulfide minerals and can result in lower rates that become transport-controlled over time. In studies of homogeneous sulfide particles, the coatings can be described by a "shrinking core" model. The diameter of the reactive particle decreases with time while the product layer thickness increases as shown in Figure 6.3. The rates become restricted by oxygen diffusion through the oxide coating. Although this effect is usually avoided in studies of intrinsic kinetics, Nicholson *et al.* (1988) showed that this mechanism provides a significant control on long-term rates of pyrite oxidation in near-neutral pH solutions. The "shrinking core" model has been used successfully to describe the rates of heap-leaching of copper ores (Cathles, 1979; Shafer *et al.*, 1979).

Finally, laboratory studies of oxidation rates involve careful preparation of solids to assure that all particle surfaces are exposed. Although this can usually be controlled in the laboratory, conditions in the field may include partly exposed particles imbedded in non-reactive materials. This means that the "reactive" surface area in some waste may be poorly defined, and special consideration is required to estimate the reactive surface area. Fortunately, many base-metal tailings represent a simple scenario in which most sulfide grains are homogeneous, with little attachment of unreactive material. However, waste rock can represent very complex mixtures of reactive and non-reactive materials in which the exposed sulfide surfaces are not well-defined. Characterization of intrinsic rates in waste rock is a topic of ongoing research (Ritchie, this Volume).

6.2.2. *Dependence on Oxygen*

The rate-dependence on reactants or products for kinetically controlled reactions can provide information regarding the mechanism of the reaction. A first-order dependence or linear relationship between a reactant concentration and rate suggests that a single-step reaction is rate-controlling. Alternatively, the fractional orders of dependence generally imply mechanisms involving control by sorption or desorption processes. There has been little consensus on the effect of oxygen concentrations: some laboratory results clearly show a linear dependence on $P(O_2)$ (McKay and Halpern, 1958), but many of the more recent studies indicate a fractional order, or apparent fractional order, of dependence (Smith *et al.*, 1968; McKibben and Barnes, 1986; Nicholson *et al.*, 1988). This overall fractional rate-dependence is strongly supported by comparisons among studies as summarized by Williamson (1992) and Williamson and Rimstidt (1992); these authors showed that when dissolved oxygen concentrations and pH are considered as controlling variables, the results of at least three studies agree well. These results, adjusted to rates at pH = 2, and those of Nicholson *et al.* (1988) are shown in Figure 6.4. Williamson and Rimstidt (1992) argued convincingly that the fractional order of dependence on oxygen concentration is strong evidence for sorption of oxygen onto the pyrite surface according to a Freundlich isotherm that indicates a

non-site-specific sorption and possible multi-layers of oxygen on the surface. The results from the four studies shown in Figure 6.4, in which oxygen concentrations vary over six orders of magnitude, seem to support this hypothesis. The rate model proposed by those authors is:

$$\text{Rate} = 10^{-8.19} \frac{[O_2]^{0.50}}{[H^+]^{0.11}} \qquad (8)$$

where $[O_2]$ and $[H^+]$ are the concentrations of dissolved oxygen and protons in mol $\bullet m^{-3}$, respectively, and the rate is given in units of mol $\bullet$ $m^{-2}s^{-1}$. These results are also of practical significance because they suggest that it is possible to predict the non-biologic rate of pyrite oxidation as a function of oxygen concentration, with little concern for study-specific conditions or the environmental levels of oxygen.

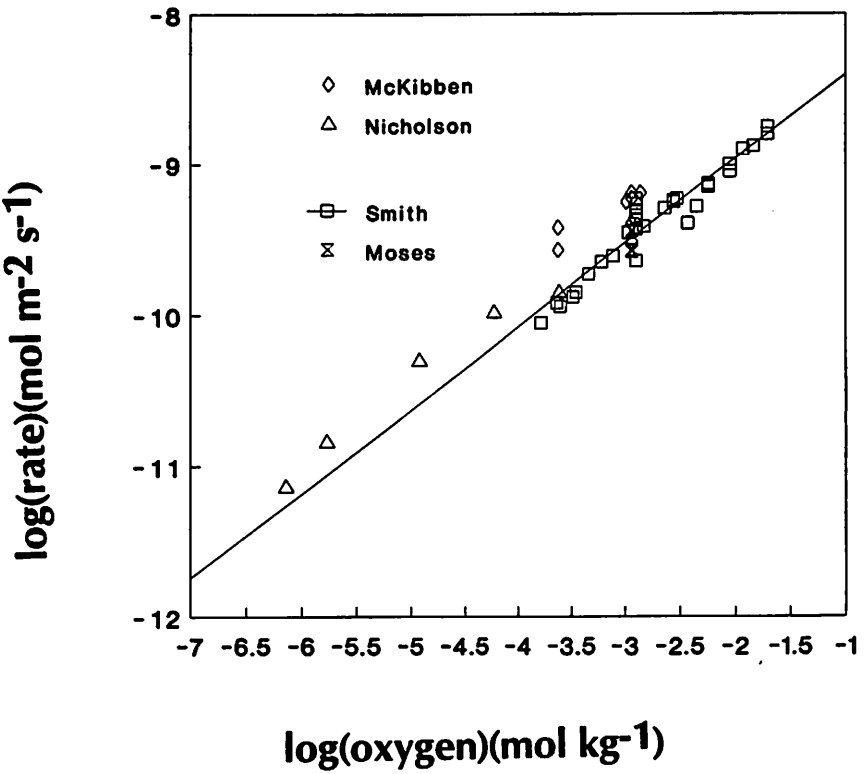

Figure 6.4. Rates of pyrite oxidation as a function of oxygen concentration. Data reported by Williamson and Rimstidt (1992) except those from Nicholson *et al.* (1988).

6.2.3. *Ferric Iron*

The relationship between oxidation rates and the concentration of Fe^{3+} in solution is apparently more complex than that for oxygen. Williamson and Rimstidt (1992) found that the rate of oxidation by Fe^{3+} depended on the presence of oxygen in solution. The authors combined their results with those of McKibben (1984) and Smith *et al.* (1968) to show this effect. During oxidation by Fe^{3+}, the rates are enhanced by the presence of dissolved oxygen at high Fe^{3+}/Fe^{2+}. In effect, the rate of reaction is dependent on the ratio of Fe^{3+} to Fe^{2+} in solution (Williamson and Rimstidt, 1992). However, oxidation rates are faster in the absence of dissolved oxygen at low Fe^{3+}/Fe^{2+} ratios. The rate equation when oxygen is absent is:

$$\text{Rate} = 10^{-8.58} \frac{\left[Fe^{3+}\right]^{0.30}}{\left[Fe^{2+}\right]^{0.47}\left[H^{+}\right]^{0.32}} \qquad (9)$$

where the rate is given in mol • $m^{-2}s^{-1}$. When oxygen is present, the following rate equation describes the data:

$$\text{Rate} = 10^{-6.07} \frac{\left[Fe^{3+}\right]^{0.93}}{\left[Fe^{2+}\right]^{0.40}} \qquad (10)$$

These rates give significantly different results when Fe^{3+} to Fe^{2+} ratios are less than 10^{-2}. Ratios of Fe^{3+} to Fe^{2+} of less than 10^{-2} are values expected in sulfide waste environments. At low Fe^{3+} to Fe^{2+} ratios, the rate is faster in the absence of oxygen than in its presence. Based on these rate laws, it is possible to calculate the approximate rate of oxidation that could occur in a tailings environment containing pyrite. Using concentrations of total Fe^{3+} and total Fe^{2+} found in the pore water in the oxidation zone of a tailings impoundment at Elliot Lake, Ontario (Dubrovsky *et al.*, 1985), a rate of 5 x 10^{-8} mol • $m^{-2}s^{-1}$ was calculated. This value is almost a factor of 100 times than for oxidation by atmospheric oxygen. The calculation assumes that oxygen is present and that $Fe^{2+}/Fe^{3+} = 0.3$, a very high value representing rapid oxidation rates of Fe^{2+} to Fe^{3+} and low pH conditions.

In addition, Williamson and Rimstidt (1992) showed that the rate data for oxidation of pyrite by Fe^{3+} do not conform to a site-specific sorption model. They found that the models showed consistent errors that suggested a systematic lack of fit. They concluded that site-specific sorption as proposed by others (Smith *et al.*, 1968) is not consistent with the data. They also argued that the behavior is more consistent with Freundlich adsorption, which is non-site-specific, and that oxidation of pyrite by ferric iron is not limited by adsorption.

6.2.4. Temperature

The Arrhenius equation is a simple relationship used to describe the dependence of rates on temperature. The rate constant (k) is an exponential function of temperature as:

$$k = A \exp\left[\frac{-E_a}{RT}\right] \qquad (11)$$

where E_a is the activation energy [J • mol^{-1}], A is the pre-exponential factor referred to as the Arrhenius factor [units of k], R is the universal gas constant [J • mol^{-1}K^{-1}], and T is temperature [K]. Although the concept of activation energy can only be used strictly for elementary-type reactions, this simple model applies well to complex reactions such as pyrite oxidation. Agreement among various studies suggests that the activation energy for oxidation of pyrite by oxygen is on the order of about 60—80 kJ • mol^{-1}. The activation energy is found by measuring the rate constant at various temperatures and plotting the results in the form of log(k) *versus* $1/T$; the result is a linear plot with a slope of $-E_a/R$ and a y-intercept of A. A typical plot is shown in Figure 6.5. In this case, the rate at 60 °C (open circle) is lower than expected because oxide coatings reduced initial rates (Nicholson *et al.*, 1988).

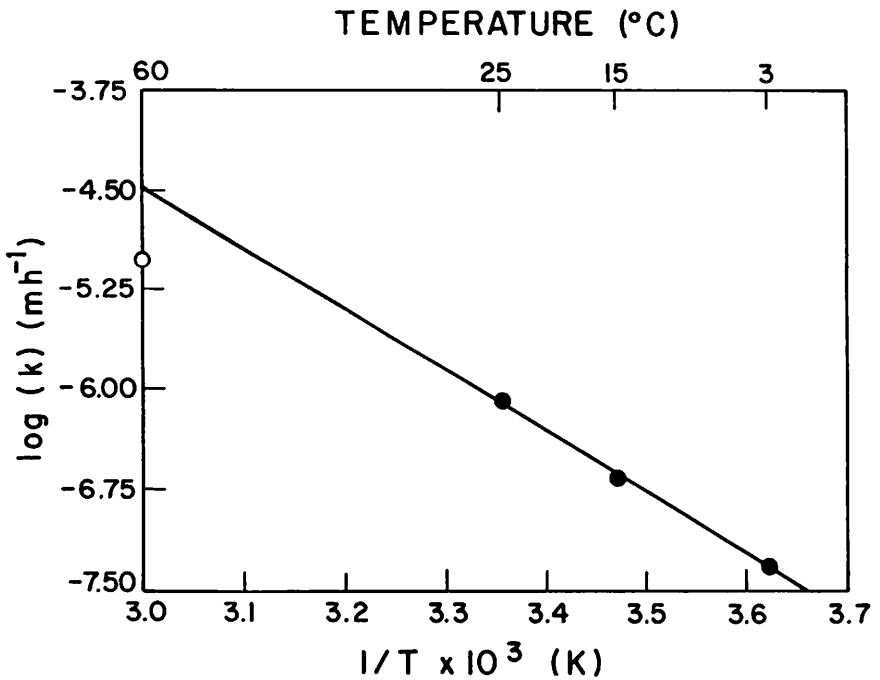

Figure 6.5. An Arrhenius plot for pyrite oxidation (from Nicholson, 1984).

The activation energy is not only a means of predicting the rate variation with temperature, but also provides an indication of the controlling factors in kinetic reactions. When the activation energy is below about 20 kJ • mol^{-1}, the rates are not sensitive to temperature, and this result is indicative of diffusion-controlled reaction rates. Alternatively, higher activation energies suggest that the rate-controlling step is a chemical reaction involving formation or breaking of bonds. The values reported for the activation energy for pyrite oxidation suggest a chemical control of oxidation rates.

6.2.5. Bacteria

It is well-known that the bacterial species *Thiobacillus ferrooxidans* catalyzes the oxidation of pyrite and dissolved ferrous iron. Examples of bacterial effects have been published by many authors (*e.g.*, Mehta and Murr, 1982; Ahonen *et al.*, 1986; Ahonen and Tuovinen, 1991). Historically, it has been suggested that bacterial catalysis can enhance abiotic rates by as much as a factor of 10^4 times, but more recent evidence suggests that increases in rate by a factor of ten to one hundred times for pyrite is more reasonable. The critical role of bacteria is the elimination of the rate-determining step for iron oxidation by oxygen at low pH. This was proposed by Singer and Stumm (1970) and is shown schematically in Figure 6.6. The proposed model shows that oxidation of pyrite results in the formation of SO_4^{2-} and Fe^{2+}, and that the abiotic oxidation of Fe^{2+} to Fe^{3+} by oxygen is a slow, or kinetically hindered, reaction. This step, however, is thermodynamically favorable in the presence of oxygen, and bacteria make use of the energy gap in electron cycling that is required to carry out metabolic processes. It is also known that bacteria play a more direct role in the oxidation of pyrite as the bacilli attach to the solid surfaces where the oxidation process occurs. The bacteria have optimal ranges of conditions for maximum catalysis of the oxidation reaction. The optimum conditions for pH and temperature are on the order of pH = 2.5—3 and 30 °C.

Historically it had been suggested that because bacteria catalyze the reaction at low pH, it would also be possible for bacteria to catalyze the oxidation process either at neutral or elevated pH values. This idea was put forward by those who considered that the initially neutral-pH environments evolve to acidic from the H^+ produced during oxidation of Fe^{2+} and pyrite, and that bacteria play a role in this process. Some effort was put into the search for the neutral-pH "bacteria". It was later shown that even *Thiobacillus ferrooxidans* does not catalyze the oxidation process above pH values of about 4 (Arkesteyn, 1979). The oxidation process, however, does occur above pH values of 4. The only difference is that bacterial catalysis is no longer required because the rates of oxidation are faster and bacteria cannot achieve the same energy production. The kinetic hindrance of the rate-limiting step is eliminated under those pH conditions. The reason for this becomes apparent upon examination of Figure 6.7, which shows the pH dependence of oxidation rates for the oxidation of ferrous iron.

The dependence on pH is related to the second-order effect of OH^-, as was proposed by Singer and Stumm (1968). This is indicated by the slope of +2 in the diagram at pH values above 4. The rates decrease to a near-constant value at pH ≤4.

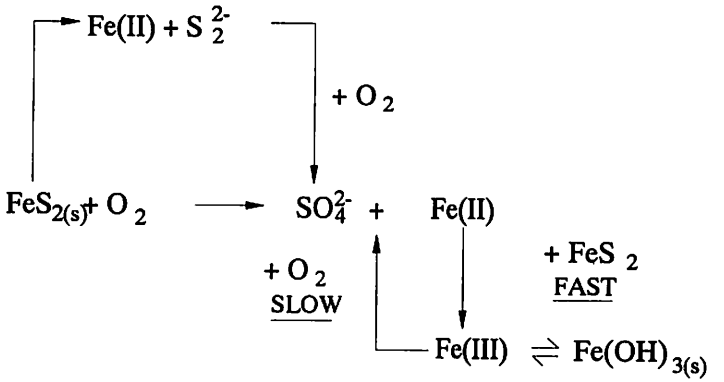

Figure 6.6. The scheme for pyrite oxidation proposed by Singer and Stumm (1970).

It is almost certain that all waste environments will contain *Thiobacillus* bacteria if sulfide minerals are present. Therefore, it should be assumed that biologically-controlled oxidation rates will occur if the appropriate pH conditions are present. This assumption has led some researchers to suggest that enhanced rates of oxidation may be controlled by eliminating or reducing the effect of these bacteria. However, the work of Kleinmann (1979) on bactericides and surfactants suggests that these measures are temporary, and they require multiple applications to be effective in reducing oxidation rates and the subsequent acid mine drainage (AMD) problems. Although there may be utility in preventing short-term oxidation processes, control of bacteria does not seem to be a legitimate approach to long-term elimination of AMD.

6.3. THE CONSISTENCY OF OXIDATION RATES FOR PYRITE

Laboratory studies of pyrite oxidation kinetics are numerous, and many related reviews have been published (Nordstrom, 1982a; Lowson, 1982; de Hann, 1991). The wide variety of results seems to present conflicting mechanisms and rate controls, particularly for oxidation by molecular oxygen. Until recently, there has been little agreement on the observed rates of oxidation, and there have been few attempts to make such comparisons among the studies. One of the fundamental problems has been the inconsistent reporting of reaction rates and, prior to the mid-1980s, the inadequate attention given to the treatment and description of pyrite surfaces used in the experiments. Since the mid-1980s, a better understanding has been gained by

Rate*	pH	Original Rates and Conditions	Corrections Used	Source
8.4	~1	3.11×10^{-4} mol L^{-1} min^{-1} T=110 °C $P(O_2)$=4 atm 40 g/L -270+325 mesh (d=53μm) Figure 6.6	E_a= 57000 J/mol Rate $\propto$ $P(O_2)$ Estimated A_s= 453 cm^2 g^{-1}	1
3.05	2	2.51×10^{-9} mol L^{-1} min^{-1} T=30 °C $P(O_2)$=0.21 A/V=0.94 cm^{-1} (940 cm^2 L^{-1}) Fig. 6.7 (rate in Abstr./1000) -250+125μm (d=176μm) A_s=251 cm^2 g^{-1}	E_a= 57000 J/mol Note: Rates given in text and abstract are a factor of 10^3 higher than those derived from data in Figure 6.7 and should probably be reported in units of millimole m^{-2} s^{-1}	2
3.23	4			
3.55	6	log(rate)=-3.45 (pH=6) log(rate)=-3.26 (pH=7) (μmol m^{-2} s^{-1}) T=23 °C		3
5.50	7			
8.3	~8	7.02×10^{-8} mol h^{-1} g^{-1} T=23±2 °C $P(O_2)$=0.21 -125+90μm (d=108μm)	Estimated A_s=222 cm^2 g^{-1}	4
5.34 (±2.5)			Average (±Std Dev)	

*Rate ($\times 10^{10}$ mol m^{-2} s^{-1})

1. McKay and Halpern (1958)
2. McKibben and Barnes (1986)
3. Moses and Herman (1991)
4. Nicholson et al. (1988)

Table 6.1. Summary of the reported oxidation rates, experimental conditions and estimated rates at 25 °C and $P(O_2)$ of 0.21

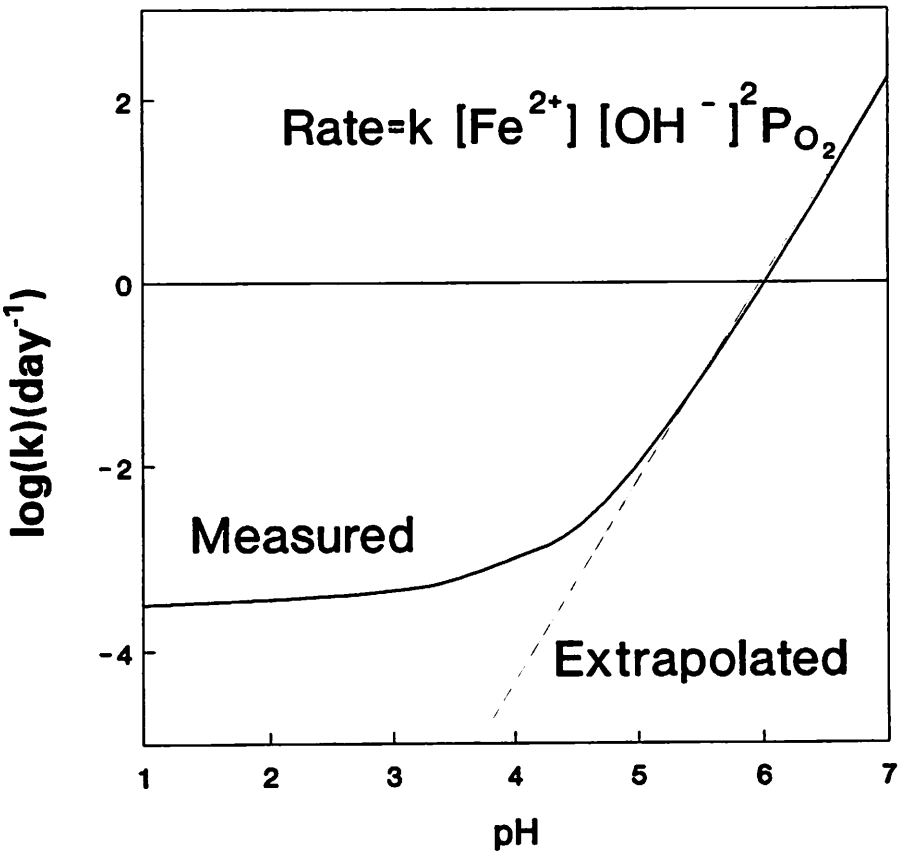

Figure 6.7. Plot of ferrous iron oxidation-rate constant as a function of pH (schematic adapted from Singer and Stumm, 1968).

researchers regarding the experimental controls that are required to obtain reasonable and consistent rate-data. Despite the complex interpretations of pyrite oxidation kinetics, results from different studies can be compared; as seen in Figure 6.4, however, similar dependence on oxygen concentrations was common to at least four studies.

If studies that reported appropriate techniques for grain-size distributions, cleaning, and avoidance of oxygen limitations during the experiments are the only ones considered here, then it is possible to show that rates of reaction are very consistent among a number of different investigations. Oxidation rates from McKay and Halpern (1958), McKibben and Barnes (1986), Nicholson *et al.* (1988), and Moses and Herman (1991) were compared. The results are given in Table 6.1, in which the adjusted rates to standard conditions are shown in the first column and give an average value of $5.0 \pm 2.1 \times 10^{-10}$ mol • $m^{-2}s^{-1}$ from six reported values. The original conditions,

including pH, are shown in the Table for each of the experiments. All reported rates were adjusted, with activation energies, to a standard temperature of 25 °C. Adjustment was also made for oxygen concentration for standard conditions of $P(O_2)$ = 0.21 atm, and surface areas were either estimated from grain-size diameters or given as BET measurements to normalize the rate data. These values were not adjusted for pH levels even though Williamson and Rimstidt (1992) showed clearly that the rates are a function of $(H^+)^{0.11}$. These results suggest consistency even though two of the studies had only estimations for surface areas, and one study was conducted at 110 °C under $P(O_2)$ = 4 atm. These results, as well as those reported by Williamson and Rimstidt (1992), are encouraging in terms of the potential for predicting oxidation rates as a function of surface area, oxygen concentration, temperature, and ferric iron concentrations.

6.4. COMPARISONS WITH PYRRHOTITE OXIDATION

Compared with the number of studies reported for oxidation of pyrite, research on pyrrhotite is relatively sparse. One of the main reasons is the greater abundance and more widespread distribution of pyrite relative to pyrrhotite. Recent attention on pyrrhotite has increased as a result of the recognition that this mineral is as an important waste sulfide in metal mines. It has also been recognized that pyrrhotite oxidizes more rapidly than pyrite; therefore, the potential for environmental impact may be increased in certain environments. Pyrrhotite has the formula $Fe_{1-x}S$ where x can vary from 0.125 (Fe_7S_8) to 0.0 (FeS). The monoclinic form of iron-deficient Fe_7S_8 is one end-member, with intermediate hexagonal and orthorhombic structures of Fe_9S_{10} and $Fe_{11}S_{12}$ progressing to the equimolar FeS phase known as troilite.

The iron-deficiency in its crystal structure may affect the oxidation of pyrrhotite. It has been speculated that iron vacancies in the crystal may be compensated by the presence of Fe^{3+} (Vaughan and Craig, 1978). Using X-ray-photoelectron-spectroscopy (XPS) to analyze the surface of unoxidized pyrrhotite, Pratt *et al.* (1994) present evidence of Fe(III) bonded with sulfide. Mössbauer studies do not support this hypothesis (Levinson and Treves, 1968).

The oxidation of pyrrhotite by oxygen can be written as:

$$Fe_{1-x}S_{(s)} + \left(2 - \frac{x}{2}\right) O_2 + xH_2O \Rightarrow (1-x)Fe^{2+} + SO_4^{2-} + 2xH^+ \qquad (12)$$

in which the stoichiometry of the pyrrhotite affects the relative production of acid. At one extreme, if x = 0 and the formula is FeS, no H^+ will be produced in the oxidation reaction; at the other extreme, the maximum amount of acid will be produced by the iron-deficient Fe_7S_8 phase. Additional acid can also be formed by the oxidation of Fe^{2+} and the subsequent precipitation of ferric hydroxide. The oxidation of pyrrhotite can

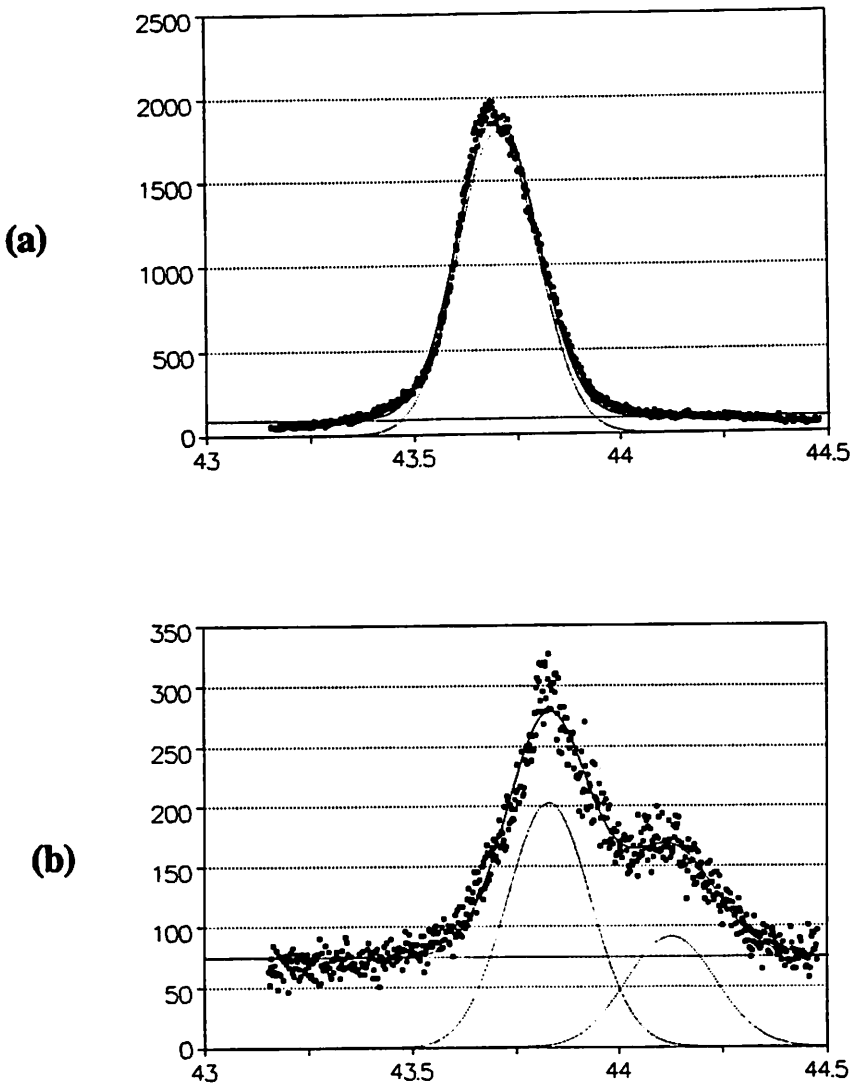

Figure 6.8. An example of XRD spectra showing: (a) pure hexagonal pyrrhotite, and (b) a mixture of monoclinic and hexagonal pyrrhotite.

also involve the formation of elemental sulfur as suggested by Ahonen and Tuovinen (1994):

$$Fe_{1-x}S_{(s)} + \left(\frac{1-x}{2}\right)O_2 + 2(1-x)H^+ \Rightarrow$$
$$(1-x)Fe^{2+} + S^o + (1-x)H_2O \qquad (13)$$

where this reaction consumes acid. It has also been shown that rapid oxidation of pyrrhotite can result in the formation of pyrite (and/or marcasite) (Burns and Fisher, 1990; Fisher and Burns, 1990). The following reaction is suggested:

$$2Fe_{1-x}S + \left(\frac{1}{2} - x\right)O_2 + (2-4x)H^+ \Rightarrow$$
$$FeS_2 + (1-2x)Fe^{2+} + (1-2x)H_2O \qquad (14)$$

Again, this is an acid-consuming reaction and the pyrite and marcasite products are only metastable; in the presence of oxygen, they also will oxidize given time.

The kinetics of pyrrhotite oxidation were examined by Nicholson and Scharer (1994), who reported the effects of pH, temperature, and surface area. The experimental results showed that the rate of pyrrhotite oxidation is proportional to surface area (the area was estimated from grain-size measurements). Three temperatures were studied: 10, 22, and 33 °C. Experiments were conducted at pH values of 2, 3, 4, and 6. The rates were insensitive to pH at temperatures of 10 and 22 °C, but the 33 °C tests showed rate changes by a factor of up to three. This behavior could not be readily explained. In general, Arrhenius behavior was observed at all pH values, but the activation energy differed with pH. The activation energies for pyrrhotite oxidation as well as pyrite oxidation as a function of pH are shown in Table 6.2. For both pyrite and pyrrhotite, the activation energies are observed to be higher for pH values in the range of 6—8 than in the range of 2—4. Although the explanation for this is not clear, Casey and Sposito (1991) suggested that proton adsorption/desorption reactions can contribute up to 50 kJ • mol^{-1} to the experimental activation energy of dissolution reactions for silicate minerals. The hydrogen-ion activity or pH, therefore, may play an important role in the observed activation energy also in the oxidation of sulfide minerals.

Although the pyrrhotite used for the experiments by Nicholson and Scharer (1994) had almost equal ratios of iron and sulfur (Fe_9S_{10}), the effluent solution exhibited SO_4^{2-}/Fe_T ratios of 0.925, 0.83, and 0.76 at pH values of 2, 4, and 6, respectively. This preferential excess of iron in solution suggested that the oxidized pyrrhotite becomes increasingly depleted in Fe, as was suggested by Burns *et al.* (1991); they observed an iron-deficient sulfide surface having the composition Fe_yS, where $y \leq 0.5$. Elemental sulfur may also form, but surface analysis (XPS) suggests that the

reaction surface exhibits a complex iron-sulfide composition (Pratt *et al.*, 1994). Although sulfur release at pH = 2 seems to be nearly stoichiometric, sulfur enrichment in the solid seems probable at higher pH values; this enrichment will affect any prediction of sulfate release rates during the oxidation process. This behavior is quite different than that observed for pyrite oxidation, in which the oxidation products are released stoichiometrically.

pH	Activation Energy (J/mol)	
	Pyrite	Pyrrhotite[c]
2	57,000[a]	58,000
4	57,000[a]	52,000
6		100,000
7–8	88,000[b]	

[a] - McKibben and Barnes (1986)
[b] - Nicholson et al. (1988)
[c] - Nicholson and Scharer (1994)

Table 6.2. Reported activation energies of oxidation of pyrite and pyrrhotite by oxygen at different solution-pH values

The study of pyrrhotite oxidation is further complicated by non-oxidative dissolution under acidic conditions. Dissolution rates that are comparable to rates of pyrite oxidation ($P(O_2)$ = 0.21 and T=25 °C) have been reported for pyrrhotite (FeS — troilite) in sulfuric acid solutions (Tervari and Campbell, 1976). These rates are on the order of 1 x 10^{-9} to 1 x 10^{-10} mol • $m^{-2}s^{-1}$ and agree with a value of about 2 x 10^{-9} mol • $m^{-2}s^{-1}$ at pH = 2 and 25 °C observed by the author (unpublished data). Non-oxidative dissolution requires further attention in the measurement of oxidation rates under acidic conditions. Oxidation of pyrrhotite with a typical value of x = 0.1 (equation 12) generates only one-tenth as much acid as pyrite. However, with oxidation rates of 20 to 100 times those of pyrite, pyrrhotite may play an important role in acid production, especially at early times. Even with less acid produced, pyrrhotite will result in similar if not greater concentrations of oxidation products, iron, and sulfate.

Pyrrhotite differs significantly from pyrite in that the former has several crystallographic structures, including monoclinic (Fe_7S_8), hexagonal (Fe_9S_{10} — $Fe_{11}S_{12}$), and orthorhombic. Preliminary data suggest that the difference in composition and electronic structure implied by crystal type may affect oxidation kinetics. For example, it is well known in metallurgical processing that flotation of monoclinic pyrrhotite is significantly different from that of hexagonal pyrrhotite. Preliminary experiments suggest that the monoclinic form oxidizes more rapidly than the hexagonal form. The pyrrhotite composition can be determined by an X-ray

diffraction (XRD) measurement of the d_{102} value, as was suggested by Arnold and Reichen (1962). The XRD results can be seen in Figure 6.8, in which part (a) indicates a pyrrhotite with the hexagonal structure only, and part (b) represents a mixture of hexagonal and monoclinic structures. Most pyrrhotite samples are mixtures of the monoclinic and hexagonal phases, and it is probable that the form that oxidizes at a more rapid rate is responsible for the observed rates.

There have been suggestions that oxidation rates for mixtures of sulfide minerals differ from those of the individual minerals, exhibiting a galvanic protection effect. Nicholson and Scharer (1994) conducted experiments on physical mixtures of pyrite and pyrrhotite of identical grain sizes to determine whether any electrochemical enhancement (galvanic effects) occurred in such a system. The galvanic action should decrease rates of oxidation for sulfides with a higher rest-potential while increasing rates for those with lower rest-potential. The results of abiotic studies suggest that the observed rate of oxidation in these mixtures is the same as that calculated from the respective fractions of the individual minerals and the rate constants of the pure minerals.

The rates of oxidation for pyrite and pyrrhotite at 25 °C and atmospheric oxygen concentrations indicate that pyrrhotite reacts 20—100 times faster than pyrite. This result is consistent with the higher relative reactivity commonly observed for pyrrhotite in the field. Pyrite, however, produces more acid per mole than pyrrhotite. The higher acid production is related to the greater sulfur content of pyrite.

6.5. MICROSCOPIC *VERSUS* MACROSCOPIC BEHAVIOR

The oxidation of sulfide minerals involves complex mechanisms and pathways. The oxidation of pyrite involves the transfer of up to fifteen electrons per molecule, suggesting that several elementary steps are required for completion. Mössbauer spectroscopy and X-ray photoelectron spectroscopy (XPS) studies have shown that pyrrhotite transformation involves complex intermediates in the solid phase, including possibly pyrite and/or marcasite and some iron-deficient sulfide (Burns *et al.*, 1991). More recent studies of oxidized pyrrhotite by XPS and Auger electron spectroscopy (AES) indicate that the oxidation process is not simple on the microscale: within the solid phase, sulfur-enriched and iron-depleted zones develop near the surface, with concentration gradients towards the unreacted zones (Pratt *et al.*, 1994). Nicholson *et al.* (1990) studied the development of ferric hydroxide coatings on pyrite after long-term oxidation experiments, and demonstrated the formation of oxide coatings that could be measured using AES techniques. The various studies indicate that the oxidation process is indeed complex, and that many unknowns remain regarding specific mechanisms and reaction pathways.

6.6. APPLICATION OF LABORATORY MEASUREMENTS TO MODELLING

The oxidation rates described here can be referred to as intrinsic rates. These are rates based on unit surface area under specific conditions for oxygen concentration, ferric iron concentration, and temperature. Bacterial activity can also be taken into account, but some controlling variables are not readily characterized in all environments. Nonetheless, it is possible to use these laboratory rates to characterize the intrinsic rates of oxidation within mine-wastes.

The key to transferring fundamental kinetic data to field predictions is: (1) the characterization of the sulfide minerals in terms of available surface area per unit volume of waste, and (2) coupling of transport controls for oxygen, temperature controls, and chemical composition of the pore water. Column experiments have shown that short-term predictions of oxidation rates in pyrrhotite wastes representing tailings material agree well with measurements (Elberling *et al.*, 1993b). The prediction of long-term trends in wastes becomes more complex because of the temporal changes in important variables that affect sulfide-mineral oxidation. These include changes in oxygen transport with time, changing surface area with time, variations in temperature for waste rock in particular, and evolution of pore-water chemistry over time. Complex models involving kinetics, mass transport, equilibrium of secondary solid formation, and pore-water migration suggest that reasonable estimates can be obtained for oxidation in tailings (Scharer *et al.*, 1994).

It is evident that, as the physical and chemical environments become more complex, more heterogenous, and more difficult to characterize, the ability to predict water-quality characteristics precisely becomes less and less likely. This is analogous to predicting the transport of contaminants in porous media. Uniform and homogeneous materials provide an ideal environment for such predictions. In contrast, the complex heterogeneous systems that are common in nature are difficult to represent in a deterministic fashion, and predictions of contaminant transport become somewhat probabilistic to the point where stochastic approaches to modelling are highly favored by many experts in the field. The prediction of water quality associated with waste-rock deposits is an example of such a complex and heterogeneous system causing uncertainties in prediction results. It may not be possible to predict actual concentrations at any location within such a complex system. There is hope, however, for the prediction of contaminant-release rates or fluxes on the basis of average behaviors, in this case macroscopic or megascopic behavior representing deposits of waste on a scale of hundreds of meters. The average release rates would equate to chemical loadings in drainage from the water rather than to concentrations at any location within the waste. Scharer *et al.* (1993) describe a model that uses fundamental physicochemical principles and laboratory measured rates to predict loadings from tailings over time. It is felt that the fundamental information gained from laboratory

investigations of sulfide-mineral oxidation can contribute to the overall prediction of these chemical loadings even in such heterogeneous environments.

6.7. ACKNOWLEDGEMENTS

This manuscript benefitted greatly from the critical and careful scrutiny of a knowledgeable anonymous reviewer; for that, many thanks are due. The clarity in the text was significantly enhanced by the careful editorial handling of John Jambor. As usual, errors, omissions, and confusing prose are the responsibility of the author.

Chapter 7

The Nature and Role of Microorganisms in the Tailings Environment

W.D. Gould, G. Béchard & L. Lortie
Environmental Laboratory
CANMET, Department of Natural Resources Canada
555 Booth St., Ottawa, Ontario,
K1A 0G1

7.1. INTRODUCTION

Acid mine drainage (AMD) is considered to be the largest single environmental problem currently facing the mineral industry (Filion and Ferguson, 1989). AMD is characterized by a low pH, a high sulfate content, and the presence of dissolved metals such as iron and aluminum. The oxidation of sulfides such as pyrite and pyrrhotite in tailings ponds, which is responsible for the acidic drainage generated at these sites, can be caused both by chemical and biological reactions. The autotrophic thiobacilli are capable of oxidizing a number of metal sulfides to produce sulfuric acid and solubilize metals (Brierley, 1978; Harrison, 1984; Karavaiko, 1985).

The production of AMD possibly is primarily the result of biological reactions. Nevertheless, there is also potential for the use of biological processes to ameliorate AMD. The use of engineered wetlands or systems based on sulfate-reducing bacteria (SRBs) has been studied for the treatment of AMD.

7.2. BASIC MICROBIOLOGY

The presently accepted classification system for microorganisms divides them into three groups: (1) Archaebacteria, (2) Eubacteria, and (3) Eucaryotes. All bacteria fall into the first two groups, and algae, fungi, and yeasts fall into the third group. At one time the Archaebacteria and the Eubacteria were considered to be in the same group but more recent work, particularly in molecular biology, has shown some fundamental differences between these two groups.

7.2.1. Bacteria

Bacteria are small single-celled organisms whose genetic material (DNA) is circular and not enclosed in a special nuclear membrane. All of the bacteria (Archaebacteria and Eubacteria) are referred to as procaryotes because of this characteristic. A very simplified description of the bacterial cell will show the following components: (1) the cytoplasm, which contains DNA, the protein-synthesizing machinery, and the enzymes for most of the cell's biochemical reactions: (2) the cytoplasmic membrane, which is a semi-permeable membrane surrounding the cytoplasm and is composed primarily of phospholipids; the cytoplasmic membrane controls the entry and exit of various metabolites and is responsible for maintaining the required chemical environment in the cell; (3) the cell wall which provides structural rigidity; and (4) the capsule, composed primarily of polysaccharides, but which varies both amongst different bacteria and also under different growth conditions (Figure 7.1).

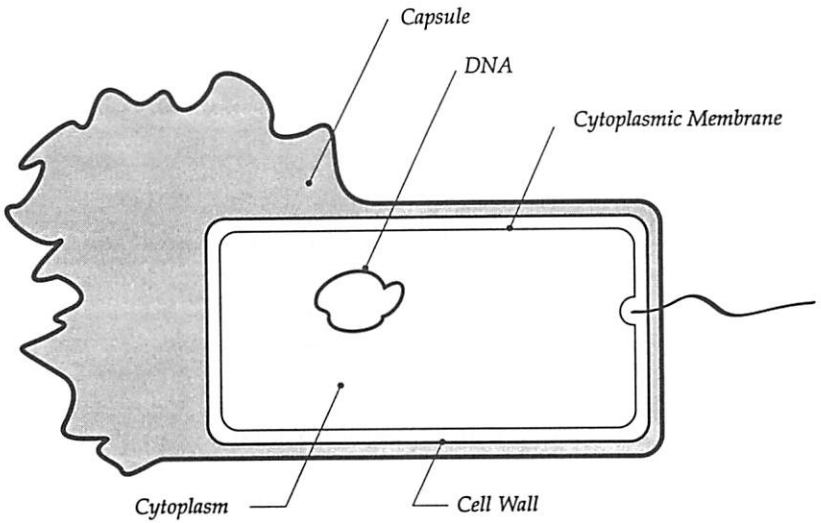

Figure 7.1. A bacterial cell.Tailings Microorganisms.

a. The Eubacteria

Most of the common bacterial species are eubacteria. They can be differentiated into two major groups by a stain (Gram stain) that reacts with cell-wall constituents. Gram-positive bacteria have a fairly thick cell wall with a high proportion of peptidoglycan which imparts rigidity to the cell wall. Peptidoglycan is a polymer composed of repeating units of two amino sugars (N-acetyl glucosamine and N-acetyl muramic acid) that are cross-linked by short peptide links. Gram-negative bacteria have

a much lower percentage of peptidoglycan and also have two membranes, a plasma membrane around the cytoplasm and an outer membrane. Some peptidoglycan occurs between the two membranes.

b. The Archaebacteria

The archaebacteria differ from the eubacteria in a number of ways, such as having no peptidoglycan in their cell walls. The archaebacteria are commonly found in extreme environments and include three groups: (1) methanogens, which are strictly anaerobes that produce methane; (2) extreme halophiles, which require high concentrations of salt for survival; (3) thermoacidophiles, which normally grow in hot acidic environments.

7.2.2. *Fungi*

The fungi are eucaryotic microorganisms and differ significantly from the bacteria. In eucaryotic cells the DNA is linear and is enclosed by a nuclear membrane. The fungi include (1) the yeasts, which are unicellular organisms; (2) molds, which are multicellular and form long tubes called hyphae; and (3) basidiomycetes, which include the mushrooms and white-rot-fungi.

7.2.3. *Metabolic Categories of Bacteria*

a. Carbon and Energy Sources

Heterotrophic bacteria require complex organic compounds as a main carbon source, and obtain energy either by photosynthesis or by oxidizing organic compounds. Autotrophic bacteria have the ability to grow solely on inorganic compounds, with carbon dioxide as the carbon source and photosynthesis or the oxidation of inorganic compounds as the energy source.

b. pH Effects on Growth

In general, bacteria are inhibited by pH values below 5.0 and above 8.0. Fungi are capable of growth over a greater pH range than bacteria, typically from pH 3.0 to 8.0. However, some autotrophic bacteria such as *Thiobacillus ferrooxidans* and *Thiobacillus thiooxidans* can grow at pH values as low as 1.0. Some fungal and bacterial isolates obtained from alkaline soils can grow at pH values between 9.0 and 10.0.

c. Oxygen

Bacteria can be divided into four groups in their response to free oxygen. *Aerobic bacteria* require oxygen for respiration, although some bacteria are able to use alternate electron acceptors in place of oxygen (NO_3^-, NO_2^-, and Fe^{3+}). *Anaerobic bacteria* grow only in the absence of oxygen, and some anaerobes are killed by exposure to oxygen.

Anaerobes are unique in that they can ferment sugars and amino acids to organic acids or alcohols. Some anaerobes are also capable of sulfate reduction. *Facultative anaerobic bacteria* can grow under either aerobic or anaerobic conditions. *Microaerophilic bacteria* are able to grow in the presence of very low concentrations of oxygen.

d. Temperature

Microorganisms are grouped into three main categories in terms of their response to temperature. *Psychrophiles* will grow over the temperature range of 0—25°C, with an optimum near 15 °C. *Mesophiles* will generally grow at temperatures between 10 to 40 °C, with optimum growth in the 25°—40 °C range. Thermophiles are generally found in environments with temperatures between 45 and 90 °C, and optima for growth vary from 50 to 80 °C.

7.3. FORMATION OF ACID MINE DRAINAGE

In Canada, AMD is generated at coal (which can contain pyrite), nickel, zinc, copper, lead, gold, and uranium mines (Mining Association of Canada, 1991) and also at construction sites where sulfide minerals have been exposed (Murray *et al.*, 1988). At mine sites AMD can be generated by either waste rock from mining activities or by the tailings produced during mineral processing. The exact conditions that initiate the acidification process are not completely understood, nor is it yet possible to predict with complete accuracy which sites will become acid-generating. Walsh and Mitchell (1972) suggested that a succession of pH-dependent microbial activities was responsible for establishing the acidic conditions required for growth of the sulfur-and iron-oxidizing bacteria responsible for the production of AMD. Kleinmann *et al.* (1981) postulated that acidification of pyrite occurs in three stages, with abiotic reactions predominating in the first stage (above pH 4.5). The microbial activities that catalyze AMD generation are also associated with the bioleaching of metals (Brierley, 1978; Lundgren and Silver, 1980; McCready and Gould, 1990). At pH values lower than 4.5, iron-oxidizing bacteria such as *Thiobacillus ferrooxidans* catalyze the oxidation of ferrous iron (either as part of a mineral or as a soluble ion) to ferric iron. Production of acid and high metal concentrations (particularly iron) by these mechanisms are the main characteristics of the process of AMD generation.

7.3.1. Thiobacillus Species

In general, the thiobacilli can be described as Gram-negative aerobic autotrophic bacteria capable of oxidizing reduced sulfur compounds (Kuenen *et al.*, 1992). Among the thiobacilli, however, there are exceptions to all of the previously mentioned characteristics. The various species differ from each other in a number of ways, such as compounds oxidized, nutrient requirements, pH optima, and oxygen requirements

(Hutchinson *et al.*, 1969; Tuovinen and Kelly, 1972). Some of the more commonly isolated thiobacilli are discussed in this Chapter.

a. Thiobacillus ferrooxidans

T. ferrooxidans, the most well-characterized of the acidophilic thiobacilli (*i.e.*, those that will grow only at low pH) was first isolated from coal AMD by Colmer and Hinkle (1947). This thiobacillus is an obligate acidophile that has a pH range of 1.0 to 3.5, and an optimum near 2.0. *T. ferrooxidans* is capable of obtaining energy from the oxidation of a number of metal sulfides as well as reduced-sulfur compounds such as thiosulfate, and sulfide and elemental sulfur. *T. ferroxidans* is also able to obtain energy via the oxidation of ferrous iron to ferric iron. These oxidation reactions can be summarized by the following equations:

$$2FeS_2 + 15/2\ O_2 + H_2O \Rightarrow 2Fe(SO_4)_3 + H_2SO_4 \qquad (1)$$

$$2FeSO_4 + 1/2\ O_2 + H_2SO_4 \Rightarrow Fe_2(SO_4)3 + H_2O \qquad (2)$$

At low pH values, the ferric sulfate produced by bacterial oxidation of sulfide minerals can also oxidize and solubilize additional metal ions:

$$2Fe^{3+} + MS \Rightarrow 2Fe^{2+} + M^{2+} + S^o \qquad (3)$$

The elemental sulfur can subsequently be oxidized to sulfuric acid by either *T. ferrooxidans* or other acidophiles.

T. ferrooxidans is a mesophile with a temperature optimum near 35 °C, and with 40 °C the maximum temperature for growth (Tuovinen and Kelly, 1972). Because it is an autotroph it obtains all of its carbon by fixation of CO_2, and only low concentrations of inorganic nitrogen and phosphorus compounds, as well as trace amounts of magnesium, are required. *T. ferrooxidans* has a high tolerance to various metal ions and also to some anions such as the arsenate ion (Tuovinen and Kelly, 1972).

b. Leptospirillum ferrooxidans

L. ferrooxidans is similar to *T. ferrooxidans* and is found in the same habitats but is not as well-characterized. *L. ferrooxidans* grows more slowly and is actively motile, whereas *T. ferrooxidans* is only slightly motile (Harrison, 1984). Leptospirillum-like bacteria are as abundant as *T. ferrooxidans* in acidic environments at temperatures equal to or above 20 °C, but at lower temperatures *T. ferrooxidans* predominates (Sand *et al.*, 1992).

c. Thiobacillus thiooxidans

T. thiooxidans is unable to oxidize iron but does oxidize sulfide, elemental sulfur, thiosulfate, and thiocyanate to sulfuric acid. *T. thiooxidans* is the most acid-

tolerant of the thiobacilli: its pH range for growth is 0.5 to 4.0. It is a mesophile, with optimum growth observed between 25 to 30 °C. It can be isolated from soil, sulfur piles, tailings ponds, and freshwater and marine environments (Kuenen *et al.*, 1992).

d. Thiobacillus thioparus

T. thioparus can oxidize sulfide, thiosulfate, tetrathionate, thiocyanate, and other reduced compounds (Katayama and Kuraishi, 1978; Lyric and Suzuki, 1970a,b). Some strains of *T. thioparus* can also grow chemolithoautotrophically on dimethyl disulfide, dimethylsulfide, dimethylsulfoxide, carbon disulfide, carbonyl sulfide, and methyl mercaptan (Kanagawa and Mikami, 1989; Smith and Kelly, 1988a,b,c). *T. thioparus* is a mesophile, with a pH range of 6.0-8.0 (Kuenen *et al.*, 1992).

e. Thiobacillus denitrificans

T. denitrificans can use nitrate as a terminal electron acceptor for oxidation of reduced sulfur compounds (Justin and Kelly, 1978a,b; Schedel and Truper, 1979). It can grow on either thiosulfate or tetrathionate, and can reduce nitrate or nitrite completely to dinitrogen gas (Justin and Kelly, 1978a,b). *T. denitrificans* is a mesophile, with a pH range of 6.0—8.0 (Kuenen *et al.*, 1992).

f. Thiobacillus novellus

Some species of thiobacilli are facultative chemolithoheterotrophs, capable of growth on either inorganic or organic substrates. *T. novellus* can grow autotrophically on reduced-sulfur compounds such as thiosulfate but can also grow heterotrophically on a wide range of organic acids and sugars (Kuenen *et al.*, 1992). One strain of *T. novellus* even requires the vitamin biotin for growth (Matin *et al.*, 1979). The pH range for growth of *T. novellus* is 6.0—8.0, and the temperature optimum is between 25—30°C.

7.3.2. *Effect of Environmental Variables on Sulfur Oxidation*

Although *T. denitrificans* is the most well-documented of the thiobacilli that utilize nitrate as a terminal electron acceptor, other species of thiobacilli can reduce nitrate to nitrite. Recently it has been shown that *T. ferrooxidans* in the absence of oxygen can use Fe^{3+} as a terminal electron acceptor for the oxidation of sulfide, sulfur and sulfite (Pronk *et al.*, 1991; Sugio *et al.*, 1987, 1988, 1989, 1992). *Desulfurolobus* spp. are extreme thermophiles that can grow aerobically by the oxidation of sulfur with oxygen, or by the anaerobic reduction of sulfur with hydrogen to produce H_2S (Kletzin, 1989). One of the strategies to prevent AMD is to prevent the entry of moisture or oxygen into the tailings. The significance of anaerobic sulfur oxidation in the tailings environment is still uncertain, but when understood in more detail the process may have a role in developing or modifying prevention strategies.

The oxidation of metal sulfides is strongly exothermic, and in warmer climates extremely high temperatures have been observed in the center of ore piles in heap-leach operations. One of the most extreme thermophiles is *Sulfolobus acidocaldarius*, which grows well at temperatures of 60—70 °C (Su and Kelly, 1988). In waste-rock piles in which oxidation rates are higher because of better aeration, hot zones have been observed. Under Canadian conditions it is more likely that temperatures prevailing during most of the year will be lower in tailings ponds than in waste-rock piles. Although *T. ferrooxidans* is considered to be a mesophile, the growth of some strains at lower temperatures has been observed (Ahonen and Tuovinen, 1992; Berthelot *et al.*, 1993; Ferroni *et al.*, 1986). Some isolates have been shown to be capable of iron oxidation and growth at temperatures as low as 2 °C (Leduc *et al.*, 1993). These natural isolates were classified as psychotrophic bacteria because they were able to grow at low temperatures as well as higher temperatures (20—30 °C; Berthelot *et al.*, 1993; Ferroni *et al.*, 1986). Thus, in the natural environment, temperature changes would not seriously disrupt the sulfur-oxidizing activities of *T. ferrooxidans* populations. Ahonen and Tuovinen (1991) calculated activation energies for the oxidation of various minerals by a mixed culture and found different temperature effects on the dissolution rate of each mineral.

Acidophilic heterotrophs can also be isolated from AMD and may survive by utilizing organic compounds excreted by the acidophilic autotrophs (Harrison, 1984). If an exogenous carbon source is present, considerable numbers of acidophilic heterotrophs will be found. The most acidophilic microorganism known to date is a fungus, *Scytalidium acidophilicum*, which has a pH optimum of 1.0 and can grow in the presence of 1.0 N sulfuric acid (Gould *et al.*, 1974). This species has been isolated from uranium-mine drainage, and from soil adjacent to a sulfur pile.

7.4. PREVENTION OF ACID MINE DRAINAGE

7.4.1. Prevention of Acid Mine Drainage During Tailings Disposal

The use of shallow- and deep-water covers has been considered as an option for tailings disposal. Natural lakes used for tailings disposal have shown that the submerged tailings are relatively unreactive and that dissolution of heavy metals from the tailings sediments is minimal. Regulatory agencies, however, are reluctant to approve the use of natural lakes for subaqueous tailings disposal, preferring that man-made lakes be used instead (Feasby, 1993).

Various types of dry covers applied to the surface of tailings have also been considered. Organic matter such as wood waste and municipal compost are being evaluated. The decomposition of the organic material will remove oxygen and also produce soluble organic substrates that can potentially inhibit *T. ferrooxidans*. Another

approach to prevent the access of oxygen to the tailings is to add nutrients in order to establish a microbial biofilm at the surface of the tailings (McCready, 1993). Laboratory column studies have shown that a microbial biofilm can scavenge oxygen, reduce the dissolved oxygen content, and increase the pH of the column effluents, but no field tests using this concept have been initiated to date.

One example of capping an acid-generating material is at the Halifax International Airport, Nova Scotia. The airport is located on a bedrock layer of highly pyritic slate. During construction of a taxiway, approximately 225,000 m^3 of waste rock were deposited in an area covering 7 ha (Murray *et al.*, 1988). The waste rock was capped with a 1-cm layer of salt, a 75-cm layer of compacted clay, and 15 cm of topsoil seeded to grass. The salt layer both inhibits *T. ferrooxidans* and renders the clay less permeable (McCready, 1987). Previous to capping, approximately 250 L/min of effluent at pH 3.2 and containing 400 mg/L Fe were being generated by the waste rock. One year after installation of the clay cap, waste rock was producing only 50 L/min of effluent with an Fe content of 80 mg/L.

Protozoa have been shown to consume large numbers of thiobacilli in pure culture, but these organisms are probably unsuitable as biological control agents. Protozoa require larger population densities of their prey (bacteria) to initiate feeding than are present in the natural environment. Also, protozoa are too large (>25 μm) to enter the interstitial spaces within the tailings to obtain their prey (McCready, 1987).

Using biocides to inhibit sulfur-oxidizing bacteria is another means of preventing AMD, but the use of many bacteriocides is limited because of the potential for leaching of these agents into the environment. At low pH values, anionic surfactants are bacteriocidal. Surfactants alone have a limited lifetime due to dilution and leaching. Slow-release rubber-based surfactant pellets that should extend the effective lifetime of these agents have been developed (Kleinmann *et al.*, 1981; Sobek, 1987).

7.4.2. Treatment of Existing Acid Mine Drainage

Collection and neutralization with lime is the current method for treating existing AMD problems. Some sites, however, will generate acid for hundreds of years, and lime treatment produces a sludge of high volume containing a low percentage of solids. The final volume of lime sludge may exceed the original tailings volume. Perpetual liming is not a sustainable long-term answer for AMD; thus, new technologies are needed. Biological treatment systems offer the possibility of treatment processes that are inexpensive and potentially self-sustaining.

a. Use of Wetlands and Biotrenches for AMD Amelioration

Natural wetlands receiving AMD have been observed to improve the quality of the eventually discharged effluent (Huntsman *et al.*, 1985; Weider and Lang, 1984).

Acidic effluents draining through cattail marshes and peat-moss bogs can have final effluent qualities that are even higher than the quality in unaffected streams (Burris *et al.*, 1984). These observations have encouraged a number of groups to construct artificial wetlands for the treatment of AMD (Kalin and Smith, 1991; Kalin *et al.*, 1991; Kleinmann *et al.*, 1991). In the United States, more than 300 small engineered wetlands have been constructed to treat AMD from coal (Kleinmann, 1989). Artificial wetlands incorporate oxidizing ponds to precipitate iron, followed by ponds generally containing an inorganic source of alkalinity such as limestone. Plants such as sphagnum moss and *Typhus* sp. (cattails) are planted to assist in metal removal (Sancindiver and Bhumbla, 1988). Microorganisms in the sediments also participate in AMD mitigation. Mechanisms involved in AMD mitigation by wetlands are complex, but are being investigated (Dave and Lim, 1989). Design of artificial wetlands has generally been empirical. Most of the wetlands built in the United States do not meet effluent requirements and need a final chemical-treatment step (Kleinmann, 1989).

Water-quality improvements in wetlands occur by a number of mechanisms mediated by plants, microorganisms, and chemical reactions. Wetland plants remove metals from acid water by : (1) adsorption, which includes ion exchange and acting as nucleation centers for precipitation; (2) consumption (plant uptake), and (3) filtration. Plants vary in their capabilities to remove metals; for example, sphagnum mosses have a large surface area and high ion-exchange capacity. Although *Typhus* sp. have low surface areas, they accumulate significant amounts of iron and manganese (Snyder and Aharrah, 1984); the uptake, however, is not large in terms of the quantity of available iron in AMD. One of the most important contributing activities of plants in these systems is to provide nutrients and energy for the microorganisms involved in AMD amelioration during the decomposition of plant tissue. If the annual production of plant biomass is sufficiently high, the wetland AMD treatment system can theoretically be self-sustaining. In a self-sustaining wetland the lifetime of the treatment system will be determined by the rate of sludge accumulation.

In anaerobic zones the removal of metals is mediated by SRBs. In aerobic zones the Fe-and Mn-oxidizing bacteria have been shown to aid in metal removal (Kleinmann and Crerar, 1979; Singer and Stumm, 1970; Stone, 1984). The oxidation of Fe and Mn results in their precipitation as hydroxides, but this process does generate additional acidity. An alternative to wetlands is the use of passive trenches (Béchard *et al.* 1993). In this system AMD flows through decomposing organic matter where aerobic and anaerobic microorganisms interact to neutralize the acidity and precipitate metals, as described in the following section. The main constraints on the use of wetlands and biotrench systems for the treatment of AMD are the slower kinetics of biological processes and the large size of trench or wetland needed to treat a given flow of AMD.

b. Use of Organic-matter Decomposition and Sulfate Reduction for Amelioration of AMD

Microorganisms were first implicated in AMD mitigation when Tuttle *et al.* (1969a) reported an increase in pH and decrease in iron and sulfate concentrations for an acidic stream percolating through a dam composed principally of wood dust. Microbial activity within the dam, and sulfate reduction in particular, were demonstrated. Microorganisms, including *Clostridium*, *Bacillus*, *Desulfovibrio*-type, and *Desulfotomaculum*-type, were isolated from the wood dust. Tuttle *et al.* (1969b) suggested that wood dust could be added to acidic streams to establish anaerobic conditions by forcing oxygen consumption and to provide the necessary nutrients for sulfate reduction. Other authors have since reported on the mitigation of AMD in the presence of SRBs for AMD flowing through wetland-type systems amended with straw (Cairns *et al.* 1988), peat (Eger and Lapakko, 1988), hay (Stark *et al.*, 1988), and compost (Hedin *et al.*, 1988). Cairns *et al.* (1988) reported that AMD with a pH of 2.3 from tailings at a base-metal mine contained no metals and had a pH of almost 6.0 after passage through straw.

In the laboratory, mixed cultures of SRBs having sawdust as the only nutrient were able to reduce the sulfate in acid water at pH 3.0, whereas pure cultures of SRB did not reduce sulfate at a pH lower than 5.5 (Tuttle *et al.*, 1969a). Wakao *et al.* (1979) reported that sulfate reduction by a mixed culture did not occur until the pH had been raised to 4.0—5.2, presumably by other microorganisms. Jongejan (1982) isolated several microorganisms from decaying wood collected from acidic uranium tailings. True cellulolytic microorganisms, as well as organisms noted as "pH-increasers" that could raise the pH enough to initiate sulfate reduction, were isolated. Theoretically, wherever organic matter is available the SRBs, ammonifiers, denitrifiers, methanogens, and Fe- and Mn-reducing bacteria can participate in AMD mitigation under anaerobic conditions (Mills *et al.*, 1989).

SRBs are all strictly anaerobic bacteria which use simple organic compounds as electron donors for the reduction of sulfate, as shown for lactate in the following equation (Widdel, 1988):

$$2CH_3CHOHCOO^- + 3SO_4^{2-} \Rightarrow 6HCO_3^- + 3HS^- + H^+ \qquad (4)$$

SRBs represent a very heterogeneous group, encompassing species that differ morphologically, biochemically, nutritionally, and phylogenetically (Widdel, 1988). SRBs use compounds of low molecular weight as electron donors; such compounds are generally fermentation products resulting from the bacterial degradation of carbohydrates, proteins, and other components of dead biomass. In an ecosystem, the SRBs depend on other microbial populations to supply the needed substrates, as they themselves are unable to use complex organic molecules.

Sulfate reduction produces the proton-scavenging ions HCO_3^- and HS^-. The production of HS^- leads to permanent alkalinity when sulfide escapes from the system as H_2S gas. The lower the pH, the more H_2S released permanently from the system. Sulfide can also be trapped within the system by forming elemental sulfur or by reacting with iron or other metals to form insoluble metal-sulfide precipitates (Hedin *et al.*, 1988).

Production of ammonia may also contribute to the neutralization process. Ammonia can be produced from organic nitrogen by ammonification. Nitrogen in organic matter occurs mainly in the amino form, NH_2^-. Through fermentation and hydrolysis reactions, many enzymes and microorganisms are capable of ammonification, as shown for the urease-catalyzed hydrolysis of urea (Atlas and Bartha, 1987):

$$NH_2CONH_2 + H_2O \Rightarrow 2NH_3 + CO_2 \qquad (5)$$

In acidic to neutral conditions, ammonia is rapidly transformed to ammonium ions:

$$NH_3 + H^+ \Leftrightarrow NH_4^+ \qquad (6)$$

For every ammonia molecule produced, a proton is removed from solution, thereby directly neutralizing AMD. In systems where nitrate is present, a number of anaerobic microorganisms, including some SRBs (McCready *et al.*, 1983) can use nitrate as a final electron acceptor and reduce it to ammonia. Denitrification, which is also referred to as nitrate respiration, is mediated by a number of bacterial species such as *Pseudomonas, Paracoccus, Flavobacterium, Alcaligenes,* and *Bacillus* spp. (Payne, 1981). The nitrate ion is reduced to dinitrogen gas by the following pathway:

$$2NO_3^- \Rightarrow 2NO_2^- \Rightarrow 2NO \Rightarrow N_2O \Rightarrow N_2 \qquad (7)$$

Although the denitrifying bacteria are aerobic microorganisms they can utilize oxidized nitrogen compounds in place of oxygen (Nelson and Knowles, 1978; Terai and Mori, 1975). In AMD containing nitrate, this utilization would contribute to neutralization by consuming protons during the reduction processes (Mills *et al.*, 1989).

Methanogenic bacteria can also participate in AMD mitigation. Methanogens use a limited number of very simple compounds to produce methane: $H_2 + CO_2$, formate, acetate, methanol, and methylated amines (Oremland, 1988). A rise in pH can occur during the reduction of CO_2 with H_2 when methanogenesis occurs in sediments underlying most bodies of water (Mills *et al.*, 1989). Methanogenesis from acetate, the most abundant substrate of methanogenesis in nature, can in theory also participate in AMD mitigation by consuming protons (Vogels *et al.*, 1988):

$$CH_3COO^- + H^+ \Rightarrow CH_4 + CO_2 \qquad (8)$$

Like SRBs, methanogens cannot use complex molecules for growth and depend on

other microbial populations to supply their substrates.

Manganese and iron reduction may also participate in the neutralization process. A great variety of microorganisms can directly reduce manganese and iron by using them as final electron acceptors under anaerobic conditions (Ghiorse, 1988; Lovley and Phillips, 1988). These organisms include heterotrophic bacteria such as *Pseudomonas, Clostridium,* and *Desulfovibrio,* and fungi such as *Penicillium.* The ability to reduce ferric iron is widespread amongst acidophilic heterotrophic bacteria (Johnson and McGuinness, 1991) and has been reported for *Thiobacillus ferrooxidans* growing on elemental sulfur (Brock and Gustafson, 1976). Very little information is available on the mechanisms involved in microbial reduction of iron and manganese. Bell *et al.* (1987) suggested that alkalinity is generated from the dissociation of $Fe(OH)_3$:

$$2Fe(OH)_3 \Leftrightarrow 2Fe^{3+} + 6OH^- \qquad (9)$$

Iron reduction generates ferrous iron, which reacts with sulfide produced by sulfate reduction:

$$2Fe(OH)_3 + SO_4^{2-} + CH_3COO^- + H_2 \Rightarrow FeS + Fe^{2+} + 3OH^- + 2HCO_3^- + 3H_2O \qquad (10)$$

Bell *et al.* (1987) stated that both sulfate and iron reduction are necessary to remove sulfide and iron from solution and also to prevent them from reoxidizing. The iron and sulfur cycles are complex; for example, in ocean sediments thiosulfate is a key intermediate in the sulfur cycle as it can undergo microbially catalyzed oxidation, reduction, and disproportionation reactions (Jorgensen, 1990).

Reactions participating in AMD mitigation are carried out by anaerobic microorganisms that depend on other microbial groups to provide the necessary substrates by breaking down sugars, proteins, and even complex molecules such as cellulose. Cellulose is an unbranched polymer of D-glucose units joined by B-1,4-glycosidic links which can contain from 1, glucose units to over 1, units (Bisaria and Ghose, 1981).

Aerobic degradation by fungi such as *Fusarium solani, Trichoderma reesei,* or *Penicillium funiculosum,* or by bacteria such as *Cellulomonas* sp. can lead to the release of sugars, cellobiose and glucose (Bisaria and Ghose, 1981) which can then be fermented to organic acids by fermentative bacteria. In most systems the aerobic microorganisms are the principal cellulose decomposers.

Anaerobic fermentation of cellulose is an essential component of carbon mineralizaton in marshes, peat bogs, aquatic sediments, sewage digesters, and the ruminant stomach. Much of the work on anaerobic cellulolytic microorganisms has focused on the rumen ecosystem, and all anaerobic cellulolytic fungi known to date have been found in the rumen and the horse cecum (Colberg, 1988). Anaerobic cellulolytic bacteria have been found in other environments such as sewage sludge, soil,

lake sediments, swamps, mud from freshwater, marine and estuarine environments, dairy waste, and anaerobic digesters (Colberg, 1988; Khan and Patel, 1991; Coughlan and Mayer, 1992). Although each of the microbial groups has been shown to play a role in metal removal and pH increase in AMD treatment, the magnitude of contribution of each group and the interrelationships among these bacteria are still not well-understood.

c. Biological Reactor Systems Employing Sulfate Reduction

An alternative method to increase pH and remove metals is to use SRBs in a contained bioreactor. BUDELCO, which operates a zinc refinery in the Netherlands, has developed a pilot-plant system (1.5-3.0 m^3/h capacity) based on sulfate reduction for the removal of sulfate and metals from contaminated groundwater that occurs in the vicinity of their refinery (Scheeren *et al.*, 1992). In its pilot study, BUDELCO used an anaerobic-sludge-blanket reactor in which ethanol was the carbon source and trace amounts of nitrogen and phosphorus were added (Barnes *et al.*, 1992). The final effluent met the requirements for either reuse in the plant or discharge to the environment. The company found that SRBs and methanogens were both required for satisfactory operation. The methanogens degrade the excess acetate produced by the SRBs. The advantages of this system include the greatly reduced space requirements compared to that of wetlands, better process control, and the potential for easier recovery of the metals for reuse. The disadvantage of this type of system is the continuous process-control and maintenance required to operate a bioreactor.

d. Biosorption for Metal Removal

Removal of metals from AMD could potentially be done using microbial biomass. Bacteria (Beveridge and Murray, 1976, 1980), fungi (Tsezos *et al.*, 1989; Venkobachar, 1990), yeasts (Byerley *et al.*, 1987; Huang *et al.*, 1990), algae (Aksu and Kutsal, 1990; Greene *et al.*, 1986; Harris and Ramelow, 1990), and activated sludges (Kasan and Baecker, 1989) have been used for the removal of metal ions from solution. Microorganisms can accumulate metals by passive processes, or via enzymatic reactions in a process known as active transport. The quantities of metals accumulated by passive processes can be one to two orders of magnitude higher than by active processes. Living or non-living microbial cells can sequester metal ions by cation exchange, chelation (Awadalla and Pesic, 1992), or adsorption. The biosorption of uranium by *Rhizopus arrhizus* is mediated by the chitin in the cell wall and occurs in two stages (Tsezos, 1983; Tsezos and Volesky, 1982). Amino groups in the cell-wall chitin act as sites of uranium coordination, which then function as nucleation centers for the deposition of uranyl hydroxide. However, the binding of copper (II) by *Rhizopus arrhizus* occurs via coordination of the copper with one nitrogen-containing ligand and with oxygen atoms filling the remainder of the coordination positions (Tsezos and Mattar, 1986).

The most practical means of contacting a metal-laden effluent with a biomass would be to employ an ion-exchange configuration (Tsezos *et al.*, 1989). Low mechanical strength and small particle size are the two major problems encountered with native biomass (Tsezos *et al.*, 1988, 1989). Microbial biomass can be prepared for pelletization or immobilization by a number of techniques, including: adsorption onto a solid carrier, such as sand (Huang *et al.*, 1990); incorporation into gels or polymeric matrices; binding by various covalent crosslinking agents such as acrylamide (Klein and Vorlop, 1985). Nevertheless, there has yet to be a large-scale demonstration of the use of biosorption for the removal of metals from solution. Biomass can be used for only a limited number of adsorption/desorption cycles and is still too expensive to produce for large-scale metal removal. Until improvements in both the performance of biomass and the economics of production are achieved, the use of reactors containing biomass will be restricted to laboratory studies.

7.5. CONCLUSIONS

AMD is formed by the chemical and bacterial oxidation of metal sulfides. Various sulfur-oxidizing bacteria, principally of the genus *Thiobacillus*, are responsible for AMD generation. In tailings that are neutral or alkaline it is likely that a succession of chemical and bacterial activities, each predominating at different pH ranges, generates the acidic conditions necessary for AMD. Sulfur oxidation requires both oxygen and moisture, but there is some evidence for the oxidation of reduced-sulfur compounds under anaerobic conditions. Sulfur oxidation rates decrease with decreasing temperature, but strains of *T. ferrooxidans* capable of growth at 2 °C have been isolated. Under Canadian conditions, tailings-pond temperatures are generally low, but high temperatures have been observed in waste-rock piles.

The options considered for prevention of the formation of AMD include water covers, dry capping, biocides, and subaqueous disposal of tailings. Wetlands have been used to ameliorate existing AMD flows. The biological activities in wetlands contribute to treatment of AMD by a number of complex mechanisms. Plants and microorganisms can adsorb metals, and sulfate-reducing bacteria can both increase the pH and precipitate metals. Organic material, either added to a biotrench system or produced by plant growth, provides carbon and energy for sulfate-reducing bacteria. The main limitations of wetlands and biotrenches for AMD amelioration are their limited capacity to handle high flow-rates, and their short effective lifetimes.

Biological reactor systems employing sulfate reduction have the advantages of easier control and less space utilization than wetlands, but such systems require constant control and maintenance. Using biosorption as the primary metal-removal technique has not yet been accepted for either metal purification or treatment of AMD.

Future research on the microbiology of AMD should be concentrated in three

areas: (1) the ecology of the sulfur-oxidizing bacteria should be studied in more detail, with the objective of finding new control strategies; (2) additional work is required to understand the processes occurring in wetlands and to scale up the biotrench and wetland-type treatment systems; (3) there is potential for cost-effective technologies using biosorption if new approaches to the preparation of biosorbants are examined.

7.6. ACKNOWLEDGEMENTS

The authors gratefully acknowledge thorough and useful reviews of the manuscript by T. Hynes and G. Tremblay.

7.7. ABBREVIATED GLOSSARY

Classification of bacteria: for example, with Thiobacillus ferrooxidans the first name is the genus name and the second is the species name. If the bacterial isolate has been classified only to the genus level it would be designated as a Thiobacillus sp. If one refers to a group of different bacteria all belonging to the same genus, the designation would be Thiobacillus spp.

DNA: abbreviation for deoxyribonucleic acid, a nucleic acid that is the carrier of genetic information occurring in the cytoplasm and the nucleus, containing phosphoric acid, D-2-deoxyribose, adenine, guanine, cytosine, and thymine.

Electron donor: a compound capable of being reduced by an organism, with the concomitant production of energy.

Exogenous: supplied externally.

Obligate: the microorganism requires a particular set of conditions and will not grow if those conditions are not present.

RNA: abbreviation for ribonucleic acid, a nucleic acid occurring in the cytoplasm and the nucleus, containing phosphoric acid, D-ribose, adenine, guanine, cytosine, and uracil.

Substrate: a substance acted on by an enzyme or utilized by a microbe for growth.

Urease: an enzyme, produced by many fungi and bacteria, that hydrolyzes urea to final products of ammonium hydroxide and ammonium bicarbonate.

Chapter 8

Sulfide Oxidation Mechanisms: Controls and Rates of Oxygen Transport

A.I.M. Ritchie
Environmental Science
Australian Nuclear Science and Technology Organisation
PMB 1, Menai, NSW 2234 Australia

8.1. INTRODUCTION

The oxidation of pyrite is common to the processes of metal extraction in leach heaps, to pre-treatment of refractory gold ores in biooxidation heaps, to the pre-treatment of gold ores in biooxidation tanks, and to pollutant generation from pyritic wastes. In the first three cases there is a desire for economic reasons to achieve high oxidation rates. For this reason there has been a major thrust over the last thirty years or so to maximize pyrite oxidation rates. It must be appreciated, however, that an oxidation consumption rate of 10^{-9} kg m^{-3} s^{-1} in a dump of pyritic material 25 ha in area and 15 m high can produce about 4 t of copper a year if the sulfate copper ratio in drainage from the dump is 50:1. This oxidation rate is 10^3 to 10^4 times lower than the rates sought in mineral treatment, but is still high enough to be environmentally significant. This means that, although some of the mechanisms and concepts are common to both the mineral extraction and environmental situations, some are not. In common to both is the pivotal role of the oxygen supply rate to oxidation sites. It is easy to show that, even at the low oxidation rates that are environmentally significant, the oxygen supply rate can restrict oxidation to a comparatively small region of the pyritic wastes. This has an impact on the time dependence of the pollution load from pyritic wastes, as well as on the magnitude of the load.

The second section of this Chapter contains an overview of the processes of pollutant generation in pyritic wastes, and of the role that oxygen supply plays in controlling the overall oxidation rate within the wastes. A picture is presented of the space dependence of pollutant generation in pyritic wastes and how the picture evolves with time. The emphasis is on waste rock rather than tailings because more oxygen supply mechanisms come into play in waste rock than in tailings. The overview is followed by a more detailed examination of oxygen transport mechanisms in porous

material, and on the set of equations that can be used to quantify the overall oxidation rate in a mass of pyritic material. Of importance here is the non-linear interaction between pyrite oxidation rate and gas, water, and heat transport.

Some simple models of the intrinsic oxidation rate (see Section 8.2.4 for a definition) are presented in Section 8.5, together with the overall oxidation rate and pollutant levels to be expected with each of these models. The attraction of these simple models is that they possess important features of actual intrinsic oxidation rates, and they indicate the impact that the intrinsic oxidation rate has on the time dependence of the overall oxidation rate in a waste-rock dump. They provide a quick, quantitative assessment of the pollutant load that might be expected from a waste-rock dump, and also provide some insight to those features of an actual intrinsic oxidation rate which have an impact on the performance of a waste-rock dump. The last section contains a discussion on how the intrinsic oxidation rate of material in pyritic wastes can be measured. Also presented are some data on intrinsic oxidation rates that have been obtained from such measurements on waste dumps.

8.2. POLLUTANT GENERATION AND TRANSPORT

8.2.1. Overview of the Geochemistry of Pyrite Oxidation

a. Pyrite Oxidation

The equations used to describe the oxidation of pyrite are given in Figure 8.1. Below about pH 3 the oxidation of pyrite by ferric ion (reaction 3 of Figure 8.1) is about ten to a hundred times faster than by oxygen (reaction 1 of Figure 8.1) where there is only a small dependence of rate on pH (Moses *et al.*, 1987). Under abiotic conditions the rate of oxidation of pyrite by ferric ion is controlled by the rate of oxidation of ferrous ion (reaction 2 of Figure 8.1), which decreases rapidly with

1. $FeS_2+{}^7/_2O_2+H_2O \rightarrow FeSO_4+H_2SO_4$, $\Delta H = 1440\ kJmol^{-1}$
2. $2FeSO_4+H_2SO_4+{}^1/_2O_2 \rightarrow Fe_2(SO_4)_3+H_2O$, $\Delta H = 102\ kJmol^{-1}$
3. $FeS_2+Fe_2(SO_4)_3+2H_2O+3O_2 \rightarrow 3FeSO_4+2H_2SO_4$
4. $MS+Fe_2(SO_4)_3+{}^3/_2O_2+H_2O \rightarrow MSO_4+2FeSO_4+H_2SO_4$
   where MS stands for any metal sulfide

Figure 8.1. Equations of sulfide oxidation.

decreasing pH. Certain bacteria, principally *Thiobacillus ferrooxidans*, catalyze the oxidation of ferrous ion and increase the rate of this reaction by a large factor which has been estimated at about 10^5 (Singer and Stumm, 1970). Although this factor is

commonly quoted in discussing the importance of microbial ecology in ARD, in practice the rate of pyrite oxidation under biotic conditions is about ten to a hundred times faster than the abiotic chemical rate (Olson, 1991). Reaction 1 is also catalyzed by bacteria, and it follows that the pH dependence of the oxidation rate in waste-rock dumps may well be overstated.

1. Calcite:
   $CaCO_3+H_2SO_4 \rightarrow CaSO_4+H_2O+CO_2$
2. Dolomite:
   $CaMg(CO_3)_2+2H_2SO_4 \rightarrow CaSO_4+MgSO_4+2H_2O+2CO_2$

Figure 8.2. Equations of the dissolution of carbonate by acid.

Reaction 4 in Figure 8.1 is a general description of the oxidation of other metal sulfides present with pyrite in the waste-dump material. Reaction 1, which is just the sum of reactions 2 and 3, is useful in estimating both the quantities of water and oxygen required to fuel the oxidation of pyrite in waste-rock dumps, and the quantity of heat generated.

It should be stressed that the equations in Figure 8.1 do not describe all of the mechanisms involved in the oxidation of pyrite which, from a chemical and microbiological point of view, is a complex of a set of complex reactions. For example, it has been shown that under both abiotic (Reedy *et al.*, 1991) and biotic conditions (Gould *et al.*, 1989), the majority of oxygen atoms in the sulfate is derived from the water. Thus, although the presence of oxygen or ferric ion is essential as the primary oxidant, water plays a pivotal role in the oxidation process. This role is obscured in equations 1 to 3, which describe the net or overall process.

In the same vein, it has been reported (Pronk *et al.*, 1992) that *Thiobacillus ferrooxidans* can grow under anaerobic conditions by using ferric ion as the terminal electron acceptor. Again the implication is that bacterially catalyzed oxidation of sulfide can proceed in a waste-rock dump even when oxygen is expended. In practice, there needs to be a source of ferric ion. A continuing source requires oxygen as described by reaction 2 in Figure 8.1. Alternatively, the ferric ion can be present in a 'rehabilitated' waste-rock dump as a result of oxidation conditions prior to rehabilitation. In practice, the mechanism allows a small spatial extension of the oxidation region (to be described below), or a relatively short-term extension of pyrite oxidation until the ferric-ion inventory is depleted.

b. Carbonate Dissolution

Carbonate is generally present in waste-rock dump material, usually as calcite,

but sometimes as dolomite. The reactions describing the dissolution of carbonate by acid produced in pyritic oxidation are presented in Figure 8.2. Again, these do not describe the actual mechanism but do indicate the overall reactions from which it is possible to evaluate stoichiometric relations.

An important property of carbonate dissolution is that it is relatively fast compared to the rate of other mechanisms that control pyrite oxidation in waste-rock dumps. A further important property is that carbonate buffers the pH of pore water in the waste-rock dump at a pH near neutral. An important consequence is that, because chemical species containing many of the trace metals which are important pollutants in ARD are not soluble at pH values much above 4.5, trace-metal pollution is absent while the buffering action of carbonate persists. If there is a large fraction of calcite in the dump material, the concentration of gypsum in pore water may rise to a level at which gypsum precipitates. This level is about 600 mg L^{-1} of Ca, and 1300 mg L^{-1} sulfate, depending on the detailed chemical conditions of the pore water. The precipitation of gypsum is part of the formation of "hardpan" layers found in tailings dams (Boorman and Watson, 1976; Blowes *et al.*, 1991). Although this is a noteworthy process in tailings dams and may present a means of "capping" tailings dams in the long term, hardpan formation is less likely in the much coarser material comprising a waste-rock dump.

1. Muscovite dissolution:
   $KAl_2[AlSi_3O_{10}](OH)_2(s)+H^+ + {}^3/_2H_2O \rightarrow K^+ + {}^3/_2Al_2Si_2O_5(OH)_4(s)$
2. Biotite dissolution:
   $KMg_{1.5}Fe_{1.5}AlSi_3O_{10}(OH)_2(s)+7H^+ + {}^1/_2H_2O$
   $\rightarrow K^+ + 1.5Mg^{2+} + 1.5Fe^{2+} + 2H_4SiO^0{}_4 + {}^1/_2Al_2Si_2O_5(OH)_4(s)$
3. Albite dissolution:
   $NaAlSi_3O_8(s)+H^+ + {}^9/_2H_2O \rightarrow Na^+ + 2H_4SiO^0{}_4 + {}^1/_2Al_2Si_2O_5(OH)_4(s)$
4. Anorthite dissolution:
   $CaAl_2Si_2O_8(s)+2H^+ + H_2O \rightarrow Ca^{2+} + Al_2Si_2O_5(OH)_4(s)$
5. K-feldspar dissolution:
   $KAlSi_3O_8(s)+H^+ + {}^9/_2H_2O \rightarrow K^+ + 2H_4SiO^0{}_4 + {}^1/_2Al_2Si_2O_5(OH)_4(s)$
6. Iron precipitation:
   $Fe^{3+} + 3H_2O \rightarrow Fe(OH)_3(s)+3H^+$

Figure 8.3. Equations of typical gangue-dissolution reactions.

c. Gangue Dissolution

Several reactions describing the dissolution of some of the more common gangue materials are presented in Figure 8.3. These reactions have been chosen in part because the minerals are typical constituents of rock, and partly because the reaction rates are slow and likely to be important in the long-term evolution of the chemical composition of pore water in a waste-rock dump. These reactions are responsible for the concentrations of major ions such as Cu, Mg, Na, K, Al, and sulfate in the drainage water. The pH of the pore water depends on the presence of various mineral species and on the rates of reaction. In general, the pH in the drainage water decreases with time as various reactions proceed within the waste-rock dump until pH reaches the 2.0—4.0 range characteristic of ARD. Even if the pH of the drainage from a waste-rock dump remains sufficiently high that trace-metal concentrations are too low to be of environmental significance and the drainage does not have the 'classical' characteristic of ARD, the total dissolved salt (TDS) concentration could be too high to be environmentally acceptable.

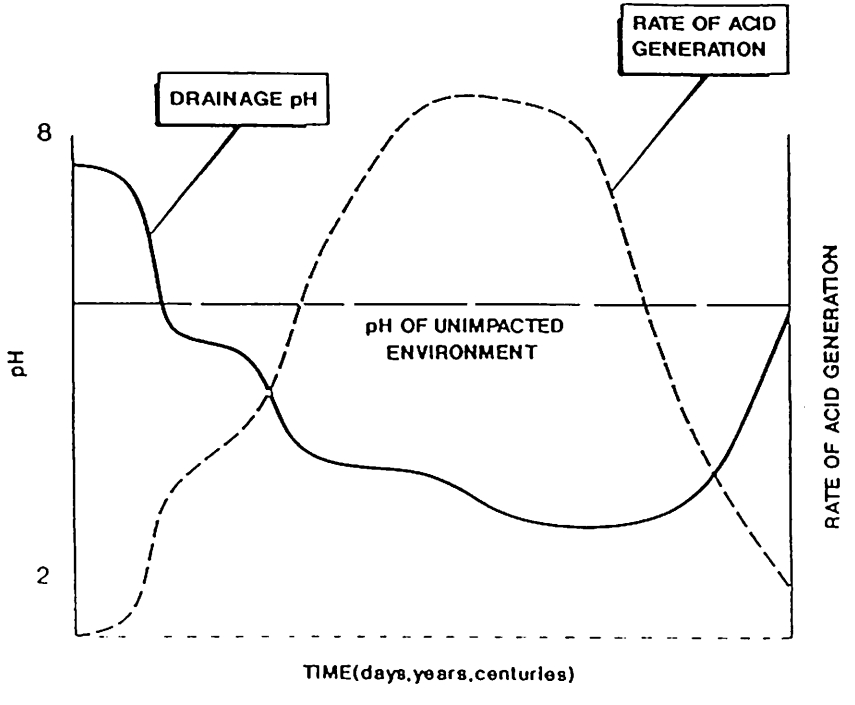

Figure 8.4. Schematic diagram of the evolution of acid drainage (adapted from B.C. AMD Task Force, 1989).

8.2.2. Evolution of ARD

Figure 8.4 shows a schematic diagram of the evolution of acid drainage on the basis of U.S. and Canadian studies as reviewed by the British Columbia AMD Task Force (1989). In this picture the slow initial rate corresponds to the "slow" rate of reaction 1 in Figure 8.1, which is the dominant reaction at high pH. As pyrite oxidation proceeds, the pH decreases in a series of steps, each of which represents the dissolution of a specific buffering species present at that pH (Morin *et al.*, 1988a,b; Morin and Cherry, 1988; Morin, 1988). The mineral species believed responsible for each of the pH plateaux are

- calcium-based carbonate pH 5.5 to 6.4
- aluminum hydroxide pH 4.3 to 5.0
- iron hydroxide and jarosites pH 3.0 to 3.7

With decreasing pH the oxidation rate is thought to increase as both the increasing bacterial population and the increasing effect of reactions 2 and 3 of Figure 8.1 come into play. At some stage the pyrite oxidation rate reaches a maximum, thereafter decreasing as the quantity of readily oxidizable pyrite decreases. Eventually all of the available pyrite is oxidized, and drainage returns to a near-neutral pH.

It should be noted that Figure 8.4 has no numerical scale on the pyrite oxidation rate. This absence largely reflects the small amount of data currently available on oxidation rates within waste-rock dumps. It should also be noted that the description infers that the whole waste-rock dump is acting as a well-stirred chemical reactor, and that largely chemical-based reaction rates dominate the pollution-generation process within a waste-rock dump. It will be shown below that, in reality, the pollutant-generation process in a waste-rock dump is expected to be strongly space-dependent, that the description of a waste-rock dump as a single well-stirred chemical reactor is inappropriate in all but some special cases, and that the dominant rate controls are not chemical or biological.

8.2.3. Rates of Reactions

Table 8.1 is a comparison of pyrite oxidation rates derived from: a set of laboratory experiments with the focus on microbiological mechanisms, a set of laboratory experiments with the focus on chemical mechanisms, and measurements in a waste-rock dump in which oxidation is occurring. The oxidation rates derived from the first two sets of experiments can readily be compared with each other, but there are some reservations in making a direct comparison of results of the first two sets with the third set. The third set results from measurements in a waste-rock dump in which pyrite oxidation is the dominant oxygen-consumption process, and the results represent an

Table 8.1. Comparison of oxygen consumption rates derived from different types of experiment

Type of experiment	Conditions of experiment	Quoted rate	Normalized rate ($kg\ m^{-3}\ s^{-1}$ at a dump pyrite density of 56.3 kg m^{-3})	Reference
Microbiological mechanism	Comparison of results from 8 labs; 1 g pyrite in 50 mL pH 3—3.4, 28 °C	($mg\ Fe\ L^{-1}\ h^{-1}$) range 7.8—17.8 average 12.4 abiotic rate average 0.36	1.9×10^{-5} from biotic average 5.6×10^{-7} from abiotic average	Olson (1991)
Chemical mechanisms	Oxidation in D.O. saturated solutions and ferric solutions; the data quoted are for D.O. solutions, pH 2.2—9.1, 22—25 °C; results normalized to 1 g pyrite in 300 mL	($mmol\ min^{-1}$ SO_4) range 0.021—0.085 average 0.057	3.2×10^{-6} from average rate	Moses et al. (1987)
Measurements in waste-rock dumps	Inferred from temperature profiles measured in a dump pH 2.0—4.0, 35—56 °C	($kg\ m^{-3}\ s^{-1}$) range $0.3—8.8 \times 10^{-8}$	1.0×10^{-8} for model dump	Harries & Ritchie (1981)

Table 8.2. Comparison of chemical kinetic rates for waste-rock minerals

Process	Description	Reaction rate per unit surface area of mineral ($mol\ m^{-2}\ s^{-1}$)
1, Fig. 8.1	pyrite oxidation	5.12×10^{-8}
1, Fig. 8.3	muscovite dissolution	6.32×10^{-12}
2, Fig. 8.3	biotite dissolution	2.57×10^{-9}

oxygen-consumption rate integrated over a large volume. The fact that the third set is from such an integral measurement is one of the points of the comparison. It shows that, in a waste-rock dump which is posing an environmental problem, the oxygen-consumption rates are low and are much lower than might be expected on the basis of laboratory experiments. This is not to say that rates in all heaps of pyritic material are low. If this were so, then the overall oxidation rates sought in biooxidation heaps would be unattainable. Rather, the point is to emphasize that oxygen-consumption rates in a waste-rock dump can be orders of magnitude lower than rates of pyrite oxidation measured in the laboratory and, as will be shown below, the rates have an impact on the space and time dependence of pollutant production in the dump and on the time dependence of polluted drainage from the dump.

In comparison with the slow rate of acid generation in a waste-rock dump, it is reasonable to assume that acid neutralization by acid-consuming materials such as

carbonates will be fast enough to react with acid close to the point of production in the dump, and that this acid neutralization will continue until all such fast-reacting, acid-consuming materials are used up. After that, acid will be transported by water from the point of production to parts of the dump below the point of production. In comparison with carbonate-dissolution rates, most other gangue-dissolution rates are slow. It is beyond the scope of this paper to discuss these rates at length. Table 8.2, however, compares pyrite-oxidation kinetic data (see Nicholson, this Volume) with the kinetic data for the dissolution of the two gangue minerals listed in Figure 8.3. It can be seen that, provided that integration over the surficial mineral-surface area does not greatly affect the relative rates, the rates of these reactions are substantially lower than pyrite oxidation rates.

Table 8.3. Physical properties of a dump of mine waste

Symbol	Definition	Value	Units
L	Dump height	15	m
A	Dump area	25	ha
ρ_r	Bulk density of dump material	1500	kg m^{-3}
ρ_{rrs}	Sulfur density as pyrite	30 (2%)	kg m^{-3}
Q_w	Infiltration rate	0.5	m y^{-1}
ε_g	Gas-filled porosity of the dump material	0.30	
ε_w	Water-filled porosity at specified infiltration	0.10	
K_s	Saturated hydraulic conductivity of the dump	10	m d^{-1}
D	Oxygen diffusion coefficient in the dump	5.0×10^{-6}	m^2 s^{-1}
C_o	Oxygen concentration in air	0.265	kg m^{-3}
ε	Mass of oxygen consumed per unit mass of sulfur oxidized	1.75	

Table 8.4. Masses of oxygen and water required to oxidize the pyrite in the dump

Mass of oxygen required to oxidize pyrite	200,000 t
Mass of oxygen initially in the pore space of the dump	300 t
Mass of water required to oxidize pyrite	32,000 t
Mass of water initially in the pore space of the dump	375,000 t

8.2.4. Rate Controls

In discussing mechanisms that control pollutant-generation rates in pyritic waste-rock dumps, it is helpful to have a specific waste dump in mind. Such a dump, with parameters typical of a waste-rock dump, is specified in Table 8.3. The masses of oxygen and water required to oxidize all of the pyrite in the dump are given in Table 8.4. It is clear that, whereas the water inventory in the dump is some ten times greater than the amount required to oxidize the pyrite, the initial oxygen inventory is about a

thousand times too small. It follows that oxygen has to be supplied to support pyrite oxidation in the dump whereas, on the basis of the stoichiometry of pyrite oxidation, water does not.

There are three mechanisms that transport oxygen from the outer surfaces of a dump to oxidation sites within the dump:

- dissolved in infiltrating rainwater
- diffusive transport through the gas-filled pore space
- advective transport through the gas-filled pore space

As discussed in more detail in Section 4 below, the first mechanism is of negligible significance in most circumstances. Diffusion is a common and significant transport mechanism in waste-rock dumps, and advection in the form of convection has been identified as a gas transport mechanism in waste-rock dumps (Harries and Ritchie, 1985; Lefebvre *et al.*, 1992). It is reasonable to expect that advection driven by pressure gradients consequent on wind-driven airflow over waste-rock dumps would also be a gas transport mechanism, but such an effect has not been quantitatively identified.

Several authors have included gas transport in modelling pyrite oxidation in dumps of pyritic material (Cathles and Schlitt, 1980; Jaynes *et al.*, 1984; Davis and Ritchie, 1986, 1987; Davis *et al.*, 1986; Pantelis and Ritchie, 1991a,b, 1992, 1993). Pantelis and Ritchie used the expression "intrinsic oxidation rate" for the term in the pore oxygen-transport equation that describes the loss of oxygen from the dump pore space by oxidation reactions in the material comprising the dump. It has been shown that, unless the intrinsic oxidation rate of the dump material is low, it is the oxygen transport rates that control the rate at which pyrite oxidizes in a dump. It has further been shown by Pantelis and Ritchie (1991a) that convection is rapidly established in a dump with an air permeability of 10^{-9} m^2 or higher, but diffusion dominates in a dump with an air permeability of 10^{-10} m^2. The air permeability in waste-rock dumps is generally in the range 10^{-12}—10^{-9} m^2 (J.W. Bennett 1993, private communication). Moreover, as convection is established first in the toe of a dump and propagates from there into the main body of a dump (Pantelis and Ritchie, 1992), diffusive transport tends to be the dominant gas transport mechanism in large waste-rock dumps. The interaction of diffusion, convection, and the intrinsic oxidation rate in determining the overall oxidation rate is discussed in more detail in Section 5 below.

It also follows that, in a dump in which diffusive transport dominates, oxidation is confined to a region that starts at the outer surfaces of the dump and propagates inward. The spatial extent of this region depends on the ratio of the intrinsic oxidation rate to the oxygen diffusion coefficient; the larger the ratio the smaller the region until,

at large intrinsic oxidation rates, oxidation in the dump conforms to the simple homogeneous model discussed by Davis and Ritchie (1986) and in Section 5.2 below.

8.2.5. Space and Time Dependence of Pollutant Generation

Figure 8.5 is a schematic diagram of the space dependence of pyrite oxidation and associated chemical reactions in a waste dump in which gas transport is by both diffusion and convection. As shown, there are three distinct regions.

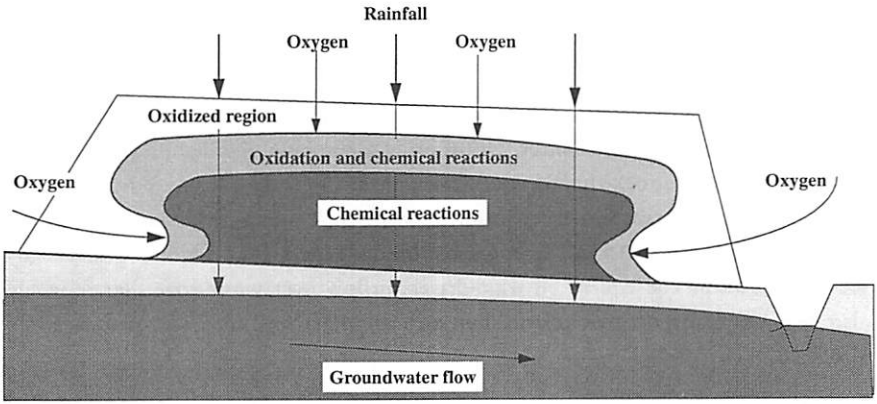

Figure 8.5. Schematic representation of pollutant generation and transport processes in a pyritic waste-rock dump.

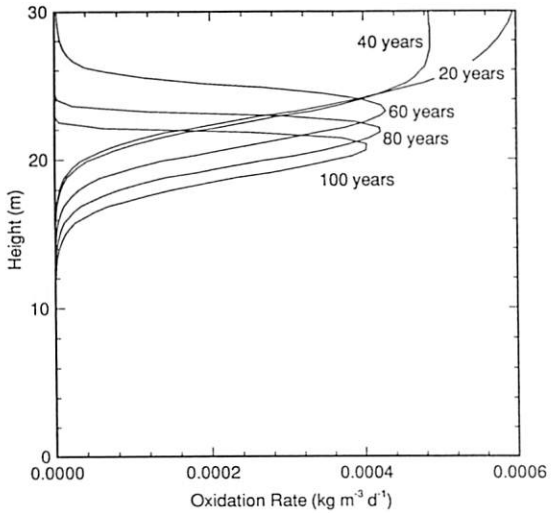

Figure 8.6. Oxidation rates as a function of depth for an uncovered dump at 20-year intervals. The parameters are given in Table 8.6.

In the outer region, all of the oxidizable material has been oxidized. This region is non-reactive from an ARD viewpoint, with no absorption of oxygen and no chemical reactions. In the second region, pyrite is oxidizing and the oxidation products interact with other constituents of the dump material. The lower boundary of this region is defined by the point where the oxygen concentration falls to zero. In the inner region, the only products of pyrite oxidation are those transported down by water infiltrating the dump. If the intrinsic oxidation rate is very low, then the second region can encompass the whole of the waste-rock dump.

The pH of the second region remains high as long as the buffering action of carbonate persists. The timescale for this depends primarily on the magnitude of the intrinsic oxidation rate and the amount of carbonate in the material of the waste-rock dump; the scale can be of the order of years. Thereafter, a pH front propagates down through the inner region at a rate that depends primarily on the acid production rate in the oxidation region, the carbonate concentration in the dump, and on the specific discharge rate of water through the dump. This pH front eventually reaches the base of the dump. Further pH fronts propagate through the dump until the pH at the base of the dump corresponds to a pH at which trace metals are soluble. At this stage, drainage at the base of the dump assumes the characteristics of ARD. It is frequently at this stage that the mine operator realizes that an ARD problem exists. This can be many years after initial construction of the waste-rock dump.

In a dump in which ARD is well-established, there will be a decrease in pH from the top of the second region to its base. In the inner region there will be a pH gradient and a gradient in other chemical species in the pore water from the top of the inner region to the base of the dump. The details of the gradients in the inner region depend on the detailed mineral composition of the dump. It should be noted, however, that the boundaries of the second region typically move sufficiently slowly that pseudo-steady-state conditions can be assumed in chemical modelling of most dumps.

It should be noted that the effluent from the toe of a waste-rock dump is not a direct measure of drainage from the base of the dump. Rather, it is some integral of drainage from a large area of the base; the time dependence of the chemical composition of effluent at the toe is some convolution of the transit times from points at the base of the dump which contribute to drainage at the particular part of the toe where the effluent is sampled. Thus, the chemical composition of such effluent provides only a limited amount of information on pollutant-generation rates within the dump. The fact that effluent from such a point is an integral of drainage from some portion of the waste-rock dump does provide access to some integral properties of pollutant generation if the flow rates, as well as pollutant concentrations, are monitored. It is unfortunate that at many minesites there is a wealth of data on the chemical composition of ARD, but data on flow rates are sparse at best.

Table 8.5: Typical timescales associated with pyritic oxidation in a dump of mine waste

	Intrinsic oxidation rate (kg of oxygen m^{-3} s^{-1})		
	low, 1×10^{-8}	medium, 10×10^{-8}	high, 100×10^{-8}
Time to use up the initial pore-space oxygen	92 d	9.2 d	0.92 d
Time to oxidize all pyrite	166 y	150 y	142 y
Time to oxidize all of the pyrite if the intrinsic oxidation rate is infinitely high		142 y	
Time to completely oxidize a particle 4 mm in diameter assuming a shrinking-core model		66 d	
Time for bacterial population to increase by a factor of one million		about 20 d	
Time for flow at base to respond to an increased infiltration rate at the surface		about 1 d	
Transit time for water from top to base of dump if whole depth is unsaturated		about 3 y	
Transit time for water to pass along the length of the base if the base is saturated		about 5 y	

It is instructive in understanding the dynamics of pollutant production, pollutant transport, and ARD to compare the timescales of the various processes. Some of these are presented in Table 8.5 for the waste-rock dump specified by the data in Table 8.3. The timescale to consume all of the pyrite in the dump is based on the assumption that diffusion is the dominant gas transport mechanism. It should be noted that, at the low oxidation rate of Table 8.5, region two, the region where oxidation and chemical reactions occur, encompasses the whole dump. At the higher rates, oxidation moves through the dump with a $t^{1/2}$ time dependence after an initial transient. It follows that, if the dump were 30 m high rather than 15 m high, the time to oxidize all of the pyrite would increase from about 150 years to 600 years.

These timescales mean that the short-term (days to years) time dependence of the quantity and quality of drainage from the base of a waste-rock dump depends on the height of the dump, water transport mechanisms in the dump, the rate of water infiltration into the top surface of the dump, where and at what rate pyrite oxidation proceeds in the dump, and the concentration of fast-reacting, acid-consuming materials such as carbonates. The long-term (years to tens to hundreds of years) time dependence depends on the relative magnitude of the gas diffusion coefficient and the intrinsic oxidation rate, and on the dissolution rate of gangue minerals. It is also clear that when the ratio of the intrinsic oxidation rate to the diffusion coefficient is high, then the intrinsic oxidation rate is in effect infinitely large and does not need to be known with any precision. This point is quantified in Section 5 below.

Some of the above points are illustrated in Figures 8.6, 8.7 and 8.8, which show results from computer simulations of the effectiveness of different cover systems on a

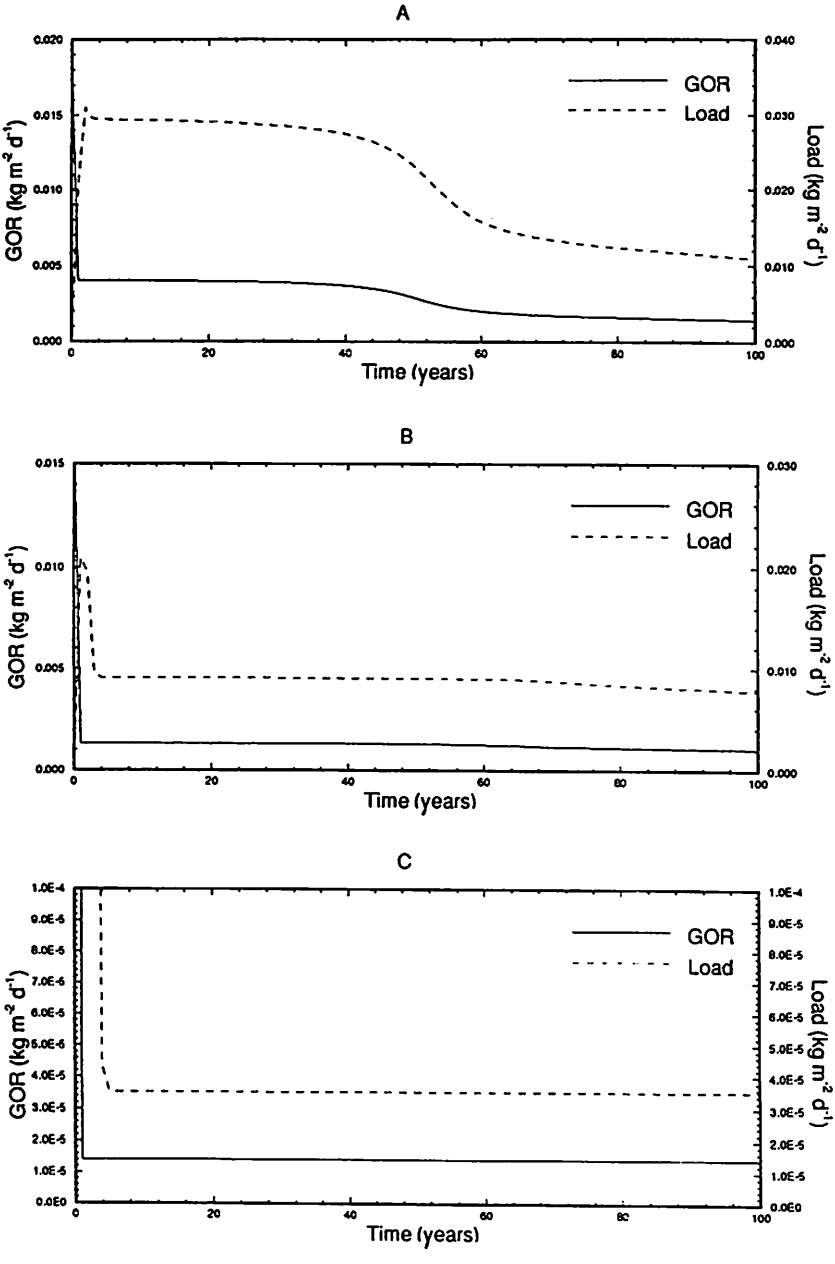

Figure 8.7. The overall oxidation rate (GOR) and sulfate load at dump base as a function of time for three cases. The parameters are given in Table 8.6; (a) uncovered dump; (b) 0.5 m cover, Ks = 0.01 m/d: (c) 1.0 m cover, Ks = 0.001 m/d.

waste-rock dump, using the parameter values presented in Table 8.6. The global oxidation rate is the space-integrated oxidation rate in the dump, and the load is the sulfate load in drainage from the base of the dump, assuming that sulfate is conserved. Figure 8.6 indicates that, even at the low intrinsic oxidation rate used (see Table 8.6), the oxidation rate is confined to a relatively small region of the dump at times greater than about 60 years. Figure 8.7 shows that the effect of the covers, which reduce the oxygen flux into the dump but which do not alter the water infiltration rate, is to reduce the global oxidation rate and the load at early times. The effectiveness of the cover with K_s = 0.01 m d^{-1} at times greater than about 60 years is not great; at these times the oxidized upper layer is just as effective as the cover in reducing the oxygen flux. Figure 8.8 demonstrates just why the cover with K_s = 0.001 m d^{-1} is so effective. The oxidation rate, and hence the pollution-production rate, are greatly reduced because this cover greatly reduces the oxygen flux into the dump. The short-lived peak in the load at early times in Figure 8.6 is just oxidation from the initial oxygen inventory of the dump. For this reason it is unaffected by the covers. The time dependence of this peak reflects water transit times in the dump.

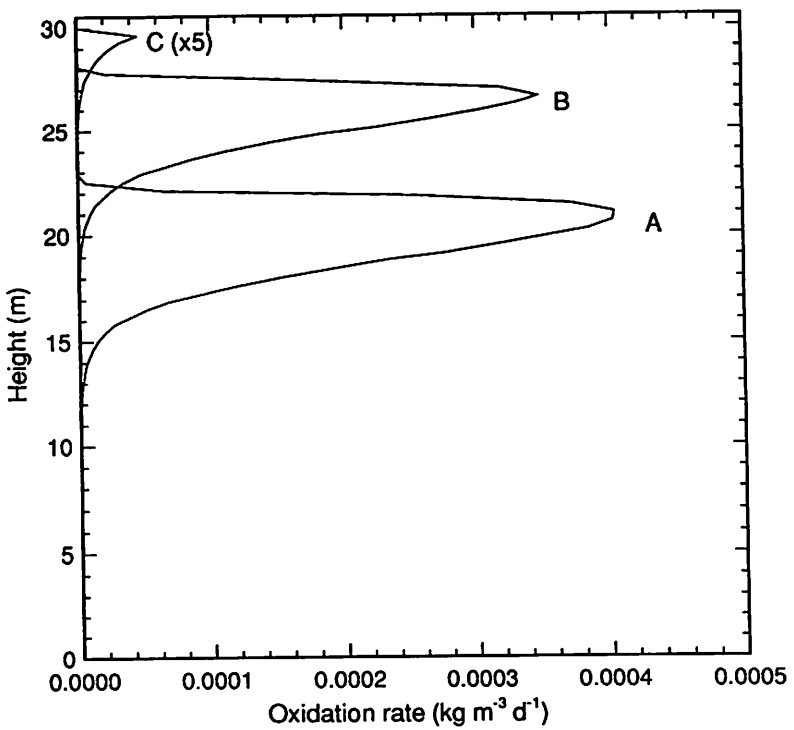

Figure 8.8. Oxidation rate after 100 years as a function of depth for three cases. The parameters are given in Table 8.6; (a) uncovered dump; (b) 0.5 m cover, Ks = 0.01 m/d; (c) 1.0 m cover, Ks = 0.001 m/d.

The schematic representation of the space dependence of pollutant generation in a waste-rock dump (Figure 8.5) assumes homogeneity of the dump material, and the same concept can be applied where the dump is not homogeneous. Given that the appropriate scale for the transport processes important in defining the overall oxidation rate in pyritic wastes is a meter or so, and that the bulk physical properties that determine the magnitude of the transport rates appear not to vary appreciably over a scale of tens of meters (see Chapter 5), it is practical and appropriate to consider a dump as a set of contiguous, homogeneous dumps. This is particularly so when the goal is to assess the effectiveness of rehabilitation strategies rather than to explain detailed variability from one part of a dump to another.

8.3. OXYGEN TRANSPORT MECHANISMS

8.3.1. Oxygen Dissolved in Rainwater

Oxygen dissolved in rainwater infiltrating a waste-rock dump is a source of oxygen for pyrite oxidation within the dump. At 25 °C the saturated dissolved-oxygen concentration in water is about 8 mg/L. At the rainfall infiltration rate given in Table 8.3 the corresponding oxygen flux is 1.3×10^{-10} kg m^{-2} s^{-1}. If this is converted to sulfate according to the stoichiometry of reaction 1 in Figure 8.1, and if sulfate is conserved in the dump, this oxygen flux supports a sulfate concentration of about 14 mg/L. This is very much lower than the sulfate concentrations usually associated with acid rock drainage and indicates that, in the context of acid rock drainage, oxygen-saturated rainwater is not a significant oxygen supply mechanism.

8.3.2. Diffusion Through the Dump Pore Space

Oxygen removed from the dump pore space by pyrite oxidation sets up a concentration gradient in the pore space. Although such gas removal will initially set up a pressure gradient, the gradient is rapidly removed by mass transport of air into the dump. The transport mechanism is then by diffusion of oxygen into the dump in primarily an oxygen — nitrogen gas mixture, and by nitrogen diffusion out of the dump. To estimate the pyrite oxidation rate that can be supported by such a mechanism, it is simplest to assume that the intrinsic oxidation rate is very high. It is then easy to show (see Section 5 below) that the oxidation rate of the sulfidic sulfur is:

$$G(x^*, t^*) = \delta(x^* - x^*(t^*)) \sqrt{\frac{(DC_o \varepsilon \rho_{rs})}{(2t^*)}} \qquad (1)$$

$$X^*(t^*) = \sqrt{\frac{(2DC_o t^*)}{(\varepsilon \rho_{rs})}} \qquad (2)$$

With the dump parameters given in Table 8.3, and again assuming conservation of

sulfate, the sulfate concentration in pore water percolating a 5-year-old dump is 45.8 g/L. The corresponding oxygen flux into the dump at the surface is 4.3×10^{-7} kg m^2 s^1. These quantities indicate that gas diffusion can support oxidation rates at environmentally significant levels. Oxygen concentration profiles that can be ascribed to diffusive gas transport have been observed both in waste-rock dumps and in tailings dams (Harries and Ritchie, 1985; Lefebvre *et al.*, 1992; Blowes *et al.*, 1991).

8.3.3. Convection

Because pyrite oxidation is very exothermic (see reaction 1 in Figure 8.1), and as soil is generally a poor conductor of heat, relatively modest oxidation rates give rise to elevated temperatures in waste-rock dumps. Temperatures of 50—60 °C are not uncommon (Harries and Ritchie, 1981; Lefebvre *et al.*, 1992). The resulting temperature gradients give rise to in-dump density gradients that lead to convective transport of gas and to the rapid replacement of oxygen, consumed in the dump, by air moving in from the surface of the dump. Gas specific-discharge rates are about 5×10^{-5} m s^{-1} at a temperature rise in a dump of about 50—60 °C and an air permeability of 10^{-9} m^2 . At an oxygen density of 0.265 kg m^{-3} in air, the oxygen flux at the dump surface caused by this convective gas flow is 1.3×10^{-5} kg m^{-2} s^{-1}. Although this is a substantially higher flux than the diffusive flux quoted in Section 3.2 above, the convective flux in a large dump generally applies over a much smaller area than does the diffusive flux. It does, however, indicate that convection can be a significant oxygen-supply mechanism. Oxygen concentration profiles which can be ascribed to convective transport have been observed in a number of waste-rock dumps (Harries and Ritchie, 1981; Lefebvre *et al.*, 1992).

8.3.4. Advection

Many waste-rock dumps are constructed on comparatively flat areas. Wind blowing over the dump generates pressure differences in much the same way as those over an aircraft wing. Assuming a wind velocity of 10 ms^{-1} (36 km h^{-1}) and the dump properties of Table 8.3, simple fluid-flow considerations indicate a pressure gradient of about 1 Pa m^{-1} in the region of the dump batters. At an air permeability of 10^{-9} m^2, the gas specific-discharge rates are then about 2×10^{-5} ms^{-1}. This is of the same order as those generated by temperature gradients, and it is therefore reasonable to expect advective gas transport in waste-rock dumps. Such an effect has not been quantitatively identified. A possible reason is that, whereas a temperature gradient in a waste-rock dump persists on a timescale of years, the persistence timescale for wind velocities is more like hours. Because the transit time for gas through a dump under these wind-induced pressure gradients is a few hours or more, this form of advective transport may not last long enough to support a significant oxidation rate.

Table 8.6. The values of the parameters used in computer simulations of cover systems

Quanity	Definition	Value
Q_w	Irrigation rate (md^{-1})	1.5×10^{-3}
L	Height of dump (m)	30
D	Cover layer thickness (m)	case dependent
K_{sw}	Saturated hydraulic conductivity, waste rock ($m\,d^{-1}$)	10
K_{sc}	Saturated hydraulic conductivity, cover (md^{-1})	case dependent
α	Capilary parameter (m^{-1})	= 3.0 (waste material) = 1.0 (cover layer)
ε_s	Volume fraction of dump material (= 1-porosity)	0.6
ρ_s	Bulk density of dump material ($kg\,m^{-3}$)	1500
S_{max}	Maximum intrinsic oxidation rate ($kg\,(O_2)\,m^{-3}s^{-1}$)	2×10^{-8}
ρ_{rs}	Sulfur density as pyrite ($kg\,m^{-3}$)	15

Oxygen Mass Fraction

$$\frac{\partial(\rho_g \omega^g)}{\partial t^*} + \nabla \cdot [\rho_g \underline{v}^g \omega^g - \rho_g D \nabla \omega^g] = -\varepsilon S_S(\omega^g, \omega^s, T^*)$$

Solid Reactant Mass Fraction

$$\rho_s \frac{d\omega^s}{dt^*} = -S_S(\omega^g, \omega^s, T^*)$$

Heat Equation

$$\Sigma_\alpha \rho_\alpha c_\alpha \frac{\partial T^*}{\partial t^*} + \Sigma_\alpha \rho_\alpha c_\alpha \underline{v}^\alpha \cdot \nabla T^* - \nabla \cdot (K_T \nabla T^*) = \delta S_S(\omega^g, \omega^s, T^*)$$

Macroscopic Pore Velocities

$$\varepsilon_\alpha \underline{v}^\alpha = -\frac{K k_{r\alpha}(\varepsilon_\alpha)}{\mu_\alpha}(\nabla p^\alpha + \rho^\alpha g \hat{z}) \quad \alpha = g, w$$

Mass Balance for the Gas and Water Phases

$$\frac{\partial \rho_\alpha}{\partial t^*} + \nabla \cdot (\rho_\alpha \underline{v}^\alpha) = \sigma^\alpha \quad \alpha = g, w$$

where σ^α is a generic source/sink term. The intrinsic density ρ^α is related to the bulk density ρ_α, by the relationship $\rho_\alpha = \varepsilon_\alpha \rho^\alpha$ ($\alpha = g, w, s$). In the above we must have $\Sigma_\alpha \varepsilon_\alpha = 1$. The water and air intrinsic pressures within the porous medium are related by $p^c(\varepsilon_w) = p^g - p^w$, where $p^c(\varepsilon_w)$ is the capillary pressure which is a function of the water volume fraction ε_w. The intrinsic gas density ρ^g is a function of the gas pressure p^g and the temperature T^*.

Figure 8.9. Equations describing heap oxidation (Pantelis, 1993).

8.4. MATHEMATICAL MODELLING OF GAS TRANSPORT

8.4.1. Model Equations

From the discussion in Section 3, the following physical processes need to be considered in quantifying pyrite oxidation rates in pyritic wastes:

- the pore-gas oxygen concentration
- heat transport in the pyritic waste
- gas transport through the pore space of the wastes
- the intrinsic oxidation rate

Furthermore, because water flow through the wastes transports heat, and because changes in the fraction of pore space filled with water changes the gas-filled volume of pore space (thereby changing such dump properties as the gas diffusion coefficient and air permeability), it is necessary also to model water flow through the waste material.

A set of equations describing the above physical transport processes is given in Figure 8.9. A clear advantage of using this set of equations is that the solution provides not only the pyrite oxidation rate, which is the primary pollution source, but also provides the space and time dependence of the temperature and pore-gas oxygen concentrations within the dump. These are both readily measured quantities. Furthermore, such bulk properties of the waste material as the gas diffusion coefficient, the air permeability, and the thermal conductivity, all of which determine gas transport rates and hence oxidation rates, can all be measured *in situ*. A model based on this set of equations is therefore predictive and does not need to be "calibrated". The question of the variability of bulk properties throughout the dump, and the possible impact of such variation on pollutants loads in drainage, are discussed Chapter 5.

8.4.2. The Intrinsic Oxidation Rate

In principle the intrinsic oxidation rate, which is just the rate at which oxygen is consumed by the dump material, is a function of a large number of variables; these include pore-gas oxygen concentration, particle-size distribution, mineral surface area, bacterial population, temperature, pH, ferric ion concentration, and so on. To include the functional dependence of the intrinsic oxidation rate on these variables means that, for consistency, equations describing their dependence on other variables and on dump properties have to be added to the set of equations in Figure 8.9. This makes even more numerically intensive an already numerically intensive calculation. In practice, and as will be discussed in Section 5 below, the overall oxidation rate in a waste-rock dump is comparatively insensitive to detailed changes in the intrinsic oxidation rate unless the intrinsic oxidation rate is very low. Furthermore, and as is again discussed below, the

characteristic timescales for changes in many of these variables are so much shorter than the timescales of others, that the variables with short timescales will follow, in a time sense, the time dependence of the more slowly changing variables. Variables with small characteristic timescales therefore need not be included as variables in the set of model equations. In addition, as there is a very limited amount of experimental data on the intrinsic oxidation rate of run-of-mine waste rock, it is inappropriate to include more detail than is absolutely necessary in the functional dependence of the intrinsic oxidation rate.

In the same vein it is worth stressing that the purpose of modelling pyrite oxidation in a waste-rock dump is not to predict the conditions at each point of the dump; rather, it is to achieve one or other of the following goals:

- identify mechanisms that are important controls on the overall oxidation rate in the dump, and the sensitivity of the overall oxidation rate to the bulk parameters required to quantify these mechanisms
- assist in planning experimental measurement programs to elucidate gas transport mechanisms
- assess the effectiveness of rehabilitation schemes intended to reduce oxidation rates within a waste-rock dump
- assess the effectiveness of dump construction techniques in reducing oxidation rates
- quantify the pollution loads in drainage, particularly the peak load and the time to peak load

It follows that the intrinsic oxidation rate should be of a form that is physically reasonable and which allows the above goals to be achieved.

There are a number of forms of the intrinsic oxidation rate that satisfy these criteria. Two such are the shrinking-core model (SCM) and a model based on Monod kinetics. These are described below together with a third form with properties close to those of the shrinking-core model.

The shrinking-core model of the intrinsic oxidation rate has the form

$$S\,(\omega^g,\ \omega^s,\ T^*) = \frac{3\gamma D_2 \varepsilon_s}{a^2}\,\alpha\,(T^*)\,\rho^g \omega^g \frac{(\rho_s \omega^s)^{\frac{1}{3}}}{\rho_{rs}^{\frac{1}{3}} - (\rho_s \omega^s)^{\frac{1}{3}}} \qquad (3)$$

The intrinsic oxidation rate in this form has the following properties:

- it is proportional to the pore-gas oxygen concentration
- it decreases to zero in a smooth fashion as the oxidizable material is consumed

- it decreases increasingly slowly as the oxidizable material is consumed
- it is high at early stages of oxidation of the particles comprising the dump
- small particles oxidize more rapidly than large particles
- it is infinitely fast when oxidation starts on an unoxidized particle

Most of these features are consistent with an intuitive understanding of how sulfidic material oxidizes in pyritic waste. The last feature is the exception. The infinity can be removed by arguing that all the sulfidic material on the surface of a particle is oxidized by the time the waste material is dumped; therefore, the model is started with a thin oxidized layer on the outer rim of each particle.

The temperature dependence $\alpha(T)$ has been included for completeness. Given the large mass of a waste-rock dump, the temperature profile is a slowly varying property of the dump, reflecting the oxidation rate within the dump rather than that imposed by external influences. The ten-folding length for a temperature wave propagating into a dump, with a frequency of the order of that of the annual variation in surface temperature, is typically about 5 m; thus, even with a swing in surface temperature of ±20 °C from summer to winter, the temperature variation 5 m from the surface is only ±2 °C. Unless the oxidation process is confined to the near-surface of the wastes, as it commonly is in tailings material, the temperature dependence of the intrinsic oxidation rate can therefore be neglected for most waste-rock dumps. Moreover, as discussed below in Section 6.3, the temperature dependence of run-of-mine waste rock can be much less than expected on the basis of laboratory measurements.

An intrinsic oxidation rate based on Monod kinetics takes the form

$$S\,(\omega^g,\ \omega^s,\ T^*) = \varepsilon\rho_g\rho_s\alpha\,(T^*)\sigma_3\frac{\omega^g}{\sigma_1+\omega^g}\frac{\omega^s}{\sigma_2+\omega^s} \qquad (4)$$

With this formulation the intrinsic oxidation rate has the following properties:

- at high values of pyrite and of pore-gas concentration it varies only very slowly with changes in these two variables
- at low values of either the pore-gas oxygen concentration or the pyrite concentration it is effectively proportional to these variables
- the change between the two functional dependencies occurs in a small region of these two variables as defined by the parameters σ_1 and σ_2.

Again, these properties are consistent with those thought applicable to the oxidation of pyrite. It should be noted, however, that with this formulation of the intrinsic oxidation rate neither pyrite nor oxygen is ever completely exhausted. The shrinking-core model, on the other hand, defines an oxidation lifetime for a particle of a given

size so that, with this form of the intrinsic oxidation rate, there a region in the dump where oxidation is complete. In general, this region starts at the dump surface and propagates into the dump as the dump ages. In quantitative terms, the use of expression (4) does in effect lead to an oxidized region, an oxic region, and an anaerobic region as indicated in Figure 8.5.

A much simpler form of the intrinsic oxidation rate that avoids the infinity of the shrinking-core model is

$$S\,(\omega^g,\ \omega^s,\ T^*) = 9.02\,\frac{3\gamma D_2 \varepsilon_s \omega^g \omega^s \rho_{rs}}{a^2} \qquad (5)$$

As can be seen from Figure 8.10, the way the oxygen consumption evolves in time using this form is not very much different from that using the shrinking-core model. Given that the overall oxidation rate is insensitive in many cases to the details of the intrinsic oxidation rate (Pantelis and Ritchie, 1991a), the above form has the attraction of simplicity.

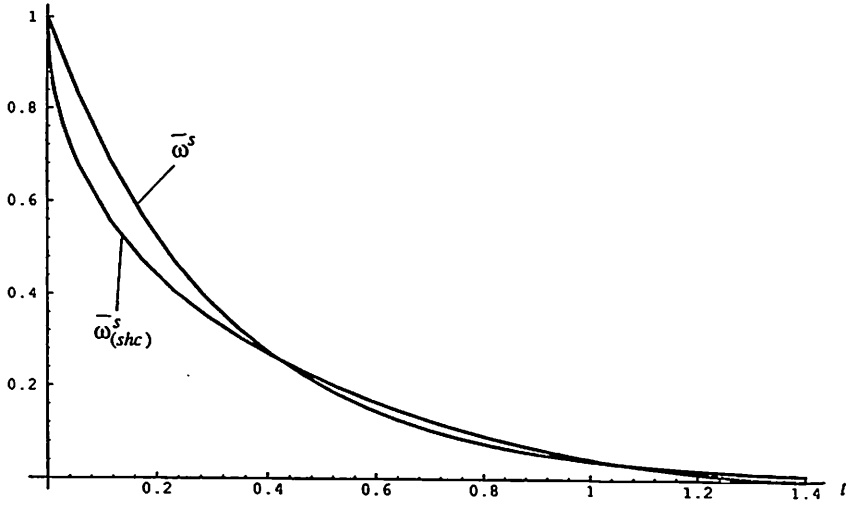

Figure 8.10. A comparison of the normalized sulfur mass fraction, ω^s of (5) with the normalized sulfur mass fraction, $\omega^s_{(shc)}$, of the shrinking-core form (3) (after Pantelis, 1993).

8.4.3. *Typical Timescales in Gas Transport*

Figure 8.11 defines and quantifies the timescales which appear naturally in the model equations describing gas and heat transport in waste-rock dumps. The same timescales will apply in other large pyritic dumps of waste material, such as tailings dams, but the physical form of the dump may preclude one or other of the transport

mechanisms. For example, convection is not likely to be a significant gas transport mechanism in a tailings dam because of the large ratio of area to height.

The longest timescale is that associated with diffusive transport of oxygen in the dump, and the shortest is that for oxidation of a single particle when the shrinking-core model is used to describe the intrinsic oxidation rate. Not surprisingly, Pantelis and Ritchie (1991a,b) have shown that, in a waste-rock dump in which gas transport controls the overall oxidation rate, a reduction in the time to oxidize a particle has little impact on the oxidation rate in the dump as a whole.

The timescale of 1.49 y for convection in Figure 8.11 is for a dump with an air permeability of 10^{-9} m^2, and becomes 14.9 y for an air permeability of 10^{-10} m^2 t. This is still much smaller than the 343-y timescale associated with diffusion. It is therefore noteworthy that Pantelis and Ritchie have shown that diffusive gas transport dominates over convective gas transport in a dump with an air permeability of 10^{-10} m^2 . One reason is that, initially, the only gas transport mechanism is diffusion. The temperature gradients that potentially drive convection are established on a diffusive timescale and are established in the toe of the dump batters. Temperature gradients resulting from ambient temperature changes are not large enough or deep enough in a dump to initiate convection.

Timescale for oxidation of pyrite in a particle

$$t_p = \frac{e\rho_{rs}a^2}{3\gamma D_e e_g C_o}$$

= 0.09 years for 4 mm diameter particle

(Time to completely oxidize a spherical particle is $t_p/2$)

Timescale associated with convection of gas through a heap with a competing chemical reaction

$$t_c = \frac{e\mu_a\rho_{rs}L}{K\rho_o^2 gbT_o C_o}$$

= 1.49 years for 15 m high heap, K = 10^{-9} m^2, T_o = 30 °C

Timescale for diffusion of gas through heap with a competing chemical reaction

$$t_D = \frac{e\rho_{rs}L^2}{C_o D}$$

= 307 years for a 15 m high heap

Timescale for thermal diffusion in a heap

$$t_T = \frac{L^2}{\pi^2 \kappa}$$

=1.45 years for a 15 m high heap

Figure 8.11. Characteristic timescales.

As long as gas specific-discharge rates are very small, heat transport is largely diffusional and the timescale to establish a new temperature distribution is that given in Figure 8.11. The L^2 dependence means that this characteristic timescale increases rapidly with increasing dump height. This long timescale to establish a new temperature distribution is another reason why diffusive gas transport dominates over convective gas transport in many waste-rock dumps. In biooxidation heaps, which are generally smaller than waste-rock dumps and in which every attempt is made to promote convective gas transport (Pantelis and Ritchie, 1993), temperature distributions are established quickly as heat transport by gas flow is significant. These points underscore the interactive nature of gas and heat transport in defining the oxidation rate in a waste-rock dump.

8.5. THE SPACE AND TIME DEPENDENCE OF THE OXIDATION RATE

Temperature and oxygen profiles can be analyzed both to extract the oxidation rate in a region of pyritic material and to determine the dominant gas-transport mechanisms. With this information and data on bulk physical properties of the dumped material, the primary pollution-production rate can be calculated; from this result an estimate can be made of the time dependence of pollution load in drainage from the base of the pyritic material. It is therefore useful to know what temperature and pore-gas oxygen-concentration profiles to expect for different forms of the intrinsic oxidation rate. The intent in the section below is to show the profiles expected for some simple forms of the intrinsic oxidation rate, and how the profiles change as the intrinsic oxidation rate changes. The profiles expected when convection is a significant transport mechanism, and the conditions under which convection occurs, will also be addressed.

8.5.1. The Simple Constant-rate Model (SCRM)

In the SCRM model the intrinsic oxidation rate is independent of pore-gas oxygen concentration and of the pyrite concentration unless these approach zero, whereupon it is assumed that the intrinsic oxidation rate tends to zero. Although this model may seem very simplistic, there is evidence (D.K. Gibson, 1992 private communication) that it applies to some pyritic material. It is also the form to which the intrinsic oxidation rate given by expression (4) tends when σ_1 and σ_2 are very small. Let us further assume that this intrinsic oxidation rate applies in a dump with the physical properties given in Table 8.3. Again for simplicity we assume that the dump was built sufficiently quickly that little or no pore-space oxygen was consumed during the construction phase and, further, that the moisture content of the dump at completion was the equilibrium one for the infiltration rate given. Neither of these two assumptions is crucial.

It is easy to show that if the equations are made dimensionless, $S = 2$, where

$$S = \frac{L^2 S^*}{DC_o} \tag{6}$$

and

$$S^* = IOR \tag{7}$$

is a critical value in the sense that, when $S < 2$, oxidation occurs throughout the pyritic wastes; when $S > 2$, oxidation is confined to a region within the wastes. When $S > 2$, oxidation is confined initially to a region $0 \le x \le x_1$ near the surface of the waste dump until all the pyrite is oxidized. Oxidation then moves to a second region $x_1 \le x \le x_2$ and is confined to that region until again all the pyrite in it is oxidized. This stepping process continues until the oxidation region encompasses the bottom of the wastes (assuming that these are not water-saturated). When the first region is fully oxidized, oxygen diffuses into the lower region and after some time a new concentration profile is established. The characteristic timescale for this is $L^2/(\pi^2 D)$ which, at about 0.15 years using the parameter values in Table 8.3, is much shorter than 170 years for the characteristic timescale of $(\varepsilon\rho_{rs})/S^*$ associated with oxidation of the pyrite. It is therefore legitimate to neglect initially the short time to establish the new profile and to treat the problem as pseudo steady state.

The points x_n are given by Gibson *et al.* (1994):

$$x_n = \sqrt{n}\, x_1 \tag{8}$$

$$x_1 = \sqrt{\frac{2}{S}} \tag{9}$$

Because the intrinsic oxidation rate is independent of oxygen concentration, the same rate applies in all regions, and hence the time to oxidize the pyrite in each region is the same.

The global oxidation rate, however, decreases with time because the regions to which oxidation is confined decreases with each step. At the time, t, oxidation is confined to the region:

$$x_n^* - x_{n-1}^* = (\sqrt{n} - \sqrt{n-1})\sqrt{\frac{2C_o D}{S^*}} \tag{10}$$

and the

$$GOR = \sqrt{2C_o D S^*}\,(\sqrt{n} - \sqrt{n-1}) =$$

$$\sqrt{2C_o D S^*}\left[\sqrt{\frac{S^* t^*}{\varepsilon\rho_{rs}} + 1} - \sqrt{\frac{S^* t^*}{\varepsilon\rho_{rs}}}\right] \tag{11}$$

These points are illustrated in Figure 8.12.

As the ratio S^*/D increases, the global oxidation rate tends to a curve with a $t^{-1/2}$ dependence. As D does not vary by more than a factor of about 2 to 3 in unsaturated wastes (see Chapter 5), the main variable in the ratio S^*/D is the intrinsic oxidation rate. Assuming a dump height of 15 m and a diffusion coefficient in the wastes of 5×10^{-6} m^2 s^{-1}, then $S = 2$ for an intrinsic oxidation rate of 1.1×10^{-8} kg (O_2) m^{-3} s^{-1}. If the intrinsic oxidation rate is ten times greater and the diffusion coefficient remains the same, oxidation is confined to regions within the dump only about 1 m deep and the time dependence of the global oxidation rate is close to $t^{-1/2}$.

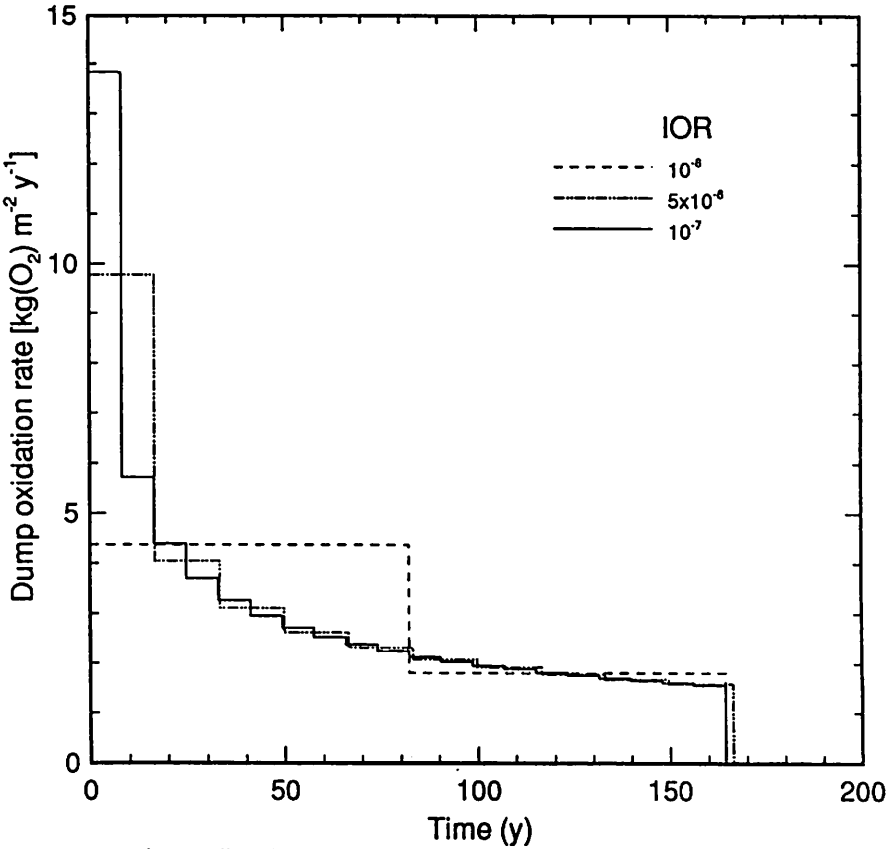

Figure 8.12. The overall oxidation rate (GOR) as a function of time for the simple constant-rate model for three values of the IOR, dump height 20 m, sulfur density 15 kg m^{-3} (after Gibson *et al.*, 1994).

The pore-gas oxygen concentration has the form shown in Figure 8.13a when $S > 2$, and is similar to that in Figure 8.13c. A more rigorous treatment, which includes the time dependence of the gas redistribution at the end of each step (Gibson *et al.*, 1994), confirms the utility of the pseudo-steady-state approach. The pollutant concentration is shown schematically in Figure 8.14a as a function of distance into the

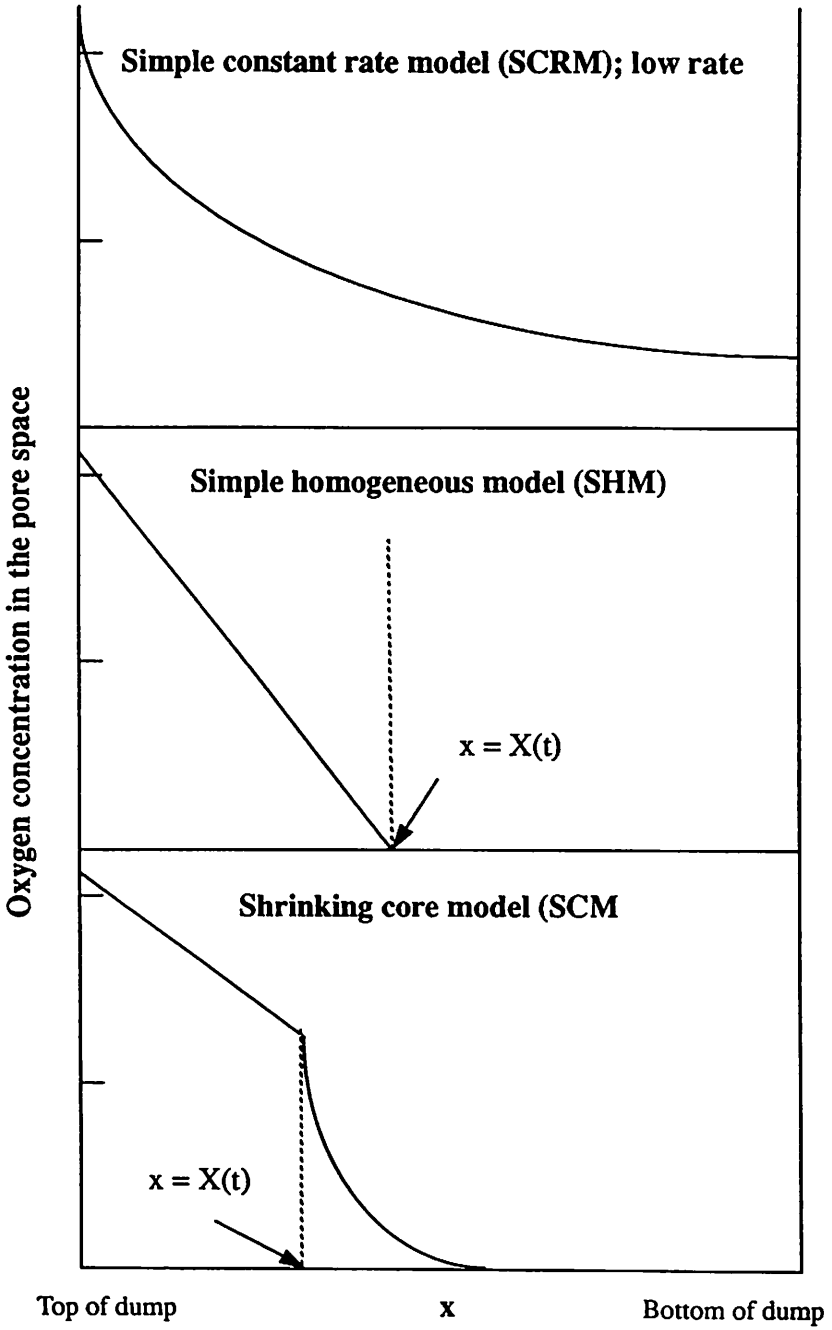

Figure 8.13. Oxygen-concentration profiles for different models of the intrinsic oxidation rate (IOR).

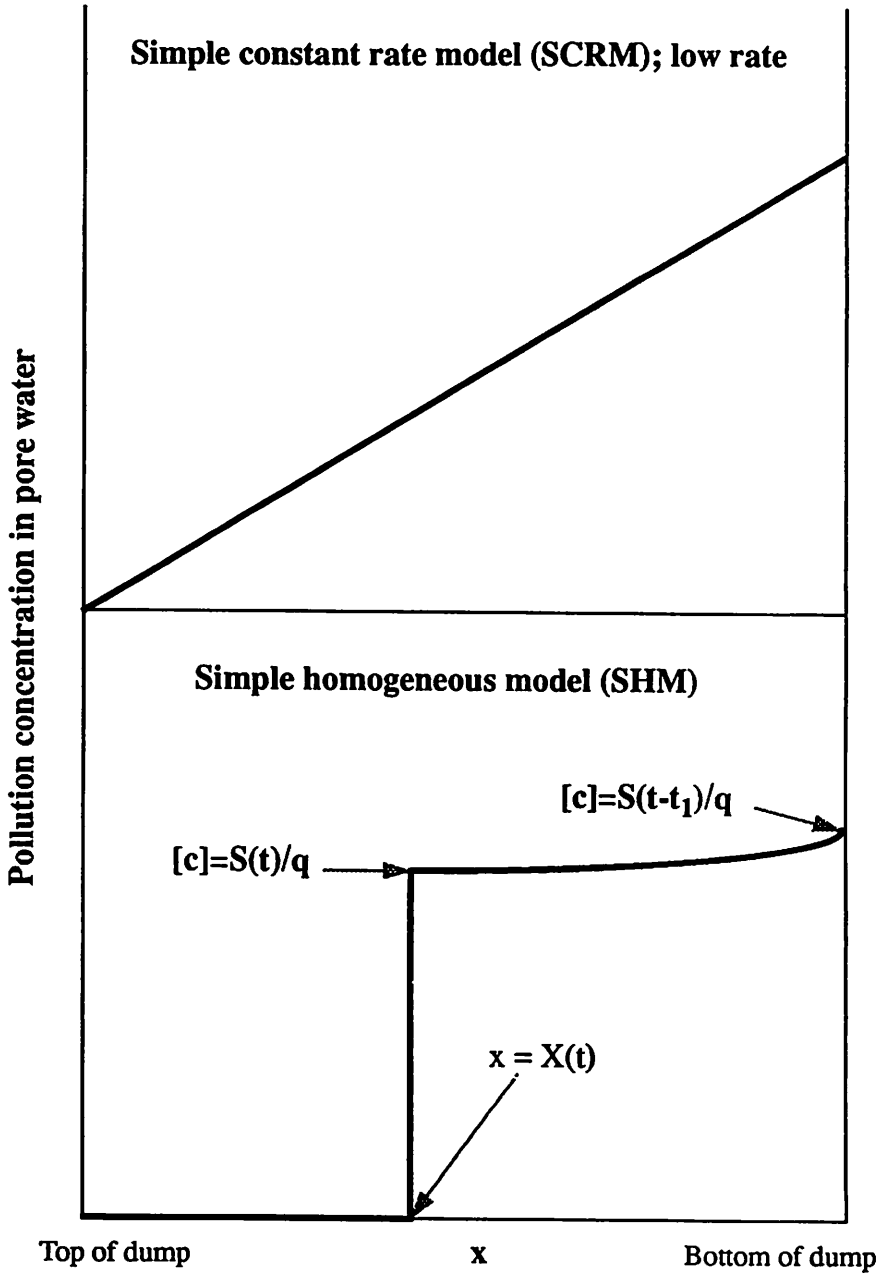

Figure 8.14. Sulfate concentrations in pore water for different models of IOR.

dump for the case where oxidation occurs throughout the dump. The assumption here is that a long enough time has elapsed that any transients associated with the transit time of pollutants through the dump can be neglected. It is also assumed that the pollutant concentrations remain below the solubility limit of the pollutant throughout the depth of the dump.

8.5.2. The Simple Homogeneous Model (SHM)

The SHM model is in effect the simple constant-rate model, but with an infinitely high oxidation rate for the waste material. It should be noted that, in the present context, an "infinitely high" intrinsic oxidation rate is only about 10^{-7} kg (O_2) m^{-3} s^{-1}. In this model it is assumed that the oxidizable material is uniformly distributed through the dump, and that the oxidation rate in the dump is limited by the rate at which oxygen can be supplied to an oxidation front which starts at the surface and moves into the dump. In mathematical terms the model is a classical moving-boundary problem (Crank, 1956), and its properties have been discussed elsewhere (Davis and Ritchie, 1986).

The oxygen concentration takes the form shown in Figure 8.13b, and the oxygen consumption rate in the dump is given by equation (1). The position of the reaction front is given by equation (2). When the reaction front reaches the base of the dump, all of the pyrite in the dump is oxidized; from equation (2), this occurs at time $t_d = 1/2$.

The pollutant concentration is shown schematically in Figure 8.14b, where again it is assumed that enough time has elapsed so that transients associated with the transit time through the dump can be neglected. The slight increase in concentration towards the base of the dump reflects the fact that the pollutant concentration here reflects the rate of pollutant generation at some earlier time which, given the $t^{-1/2}$ dependence of the oxidation rate, is higher at earlier times.

8.5.3. The Shrinking-core Model

As discussed above, the shrinking-core model has the attraction that the intrinsic oxidation rate decreases as the pore-gas oxygen concentration decreases and as the quantity of oxidizable material decreases. Intuitively, this is a property we seek in a realistic intrinsic oxidation rate. The use of such a model to describe oxidation in a waste-rock dump has been studied in some detail by Davis and Ritchie (1986, 1987) and Davis *et al.* (1986). The shrinking-core model gives rise to a moving front in the dump, above which there is no oxidation because all of the oxidizable material has been consumed. In practical terms there is another region below the oxidation region where the oxidation rate is negligibly small. The resulting oxygen concentrations have the form shown in Figure 8.13c.

The location of the upper front $x = X(t)$ in a dump composed of particles of just one size is given by the condition $R = 0$, where R is the position of the reaction front in a particle. This condition can be restated as

$$w(X, t) = \frac{1}{6k} \tag{12}$$

where

$$w(x, t) = \int_0^t u(x, \tau)\, d\tau \tag{13}$$

Application of this condition also allows the ready incorporation of a particle-size distribution into the intrinsic oxidation rate in a natural way because condition 12 is used to test whether or not a particle of a given size has been fully oxidized and no longer contributes to oxygen consumption at that point. The intrinsic oxidation rate then becomes an integral in which the integrand has the form of expression (3), with a weighting function to represent the particle-size distribution. In practice, as the set of equations has to be solved numerically (Davis and Ritchie, 1987), the integral is replaced by a sum; condition (12) is used to select those particle sizes to be included in the sum at a particular point in space and time.

The expression can also be used to quantify the time t_c during which a particle at the surface of the dump continues to oxidize. Because at the surface $w(x,t)$ is just t,

$$t_c = \frac{1}{6k} \tag{14}$$

Another useful expression is

$$t = t_c + \frac{X^2}{2} + t_c\sqrt{\beta}X \tanh\sqrt{\beta}\,(1-x) \tag{15}$$

which can be used to evaluate the position of the moving front $X(t)$, above which all of the pyritic material is oxidized. This expression can also be used to evaluate the time t_d to oxidize the whole heap. This takes the simple form

$$t_d = \frac{1}{2} + t_c \tag{16}$$

This is just the time to oxidize completely the particle at the surface of the dump, t_c, together with the time for the moving front $X(t)$ to travel the full depth of the dump. As the particle size tends to zero, so does t_c, and expression (16) becomes identical to the result given by the simple homogeneous model.

Davis and Ritchie (1986) also showed that oxygen concentration in the region $X(t) \leq x \leq 1$ is approximated by

$$\bar{u}(x, t) = \frac{t_c \cosh\sqrt{\beta}\,(1-x)}{\left[t - \frac{X^2}{2}\right] \cosh\sqrt{\beta}\,(1-x)} \qquad (17)$$

and the global oxidation rate by

$$S(t) = \frac{L\,\varepsilon\rho_{rs}}{\tau_4} \frac{1}{\sqrt{2t - t_c}} \qquad (18)$$

The pore-gas oxygen concentration is shown schematically in Figure 8.13c. It is clear from the form of the global oxidation rate that, at long times, it takes on the $t^{-1/2}$ dependence of the simple homogeneous model. It also follows that, as the particle size tends to zero, the intrinsic oxidation rate of the shrinking-core model tends to that of the simple homogeneous model, t_c tends to zero, and the global oxidation rate has the same form as that of the simple homogeneous model.

In this sense the simple homogeneous model and the simple constant-rate model can be taken as useful extreme cases of the form taken by the intrinsic oxidation rate. It is also apparent from these three simple models that, unless the intrinsic oxidation rate is so low that much of the dump is involved in oxidation, the global oxidation rate tends to a $t^{-1/2}$ dependence after an initial transient. The length of this transient reflects details of the intrinsic oxidation rate, and stems from the way in which oxygen penetrates the surface regions of the dump. The implication is that, in a large mature dump, the global oxidation rate decreases as $t^{-1/2}$ and approaches the form given by equation (1). It is then largely independent of the details or magnitude of the intrinsic oxidation rate. It follows that the pollution load in drainage at the base of a dump, if averaged over, say, a year to remove fluctuation due to short-term fluctuations in infiltration rate, will have this same long-term time dependence. This is the reason why acid rock drainage is a long-term problem and why speeding up oxidation rates in a waste-rock dump is rarely a practical proposition.

8.5.4. Convection

As indicated above, the pollutant-generation rate in a large dump in which diffusion is the dominant gas transport process and in which the intrinsic oxidation rate is low, tends to decrease as $t^{-1/2}$ in the long term. The oxygen concentration decreases from the outer surface into the interior of the dump. The much shorter timescale associated with convective gas transport raises the spectre of high pollution-generation rates, but also opens the possibility of completely oxidizing the pyritic material in a dump in a time period short in comparison with the lifespan of a mining

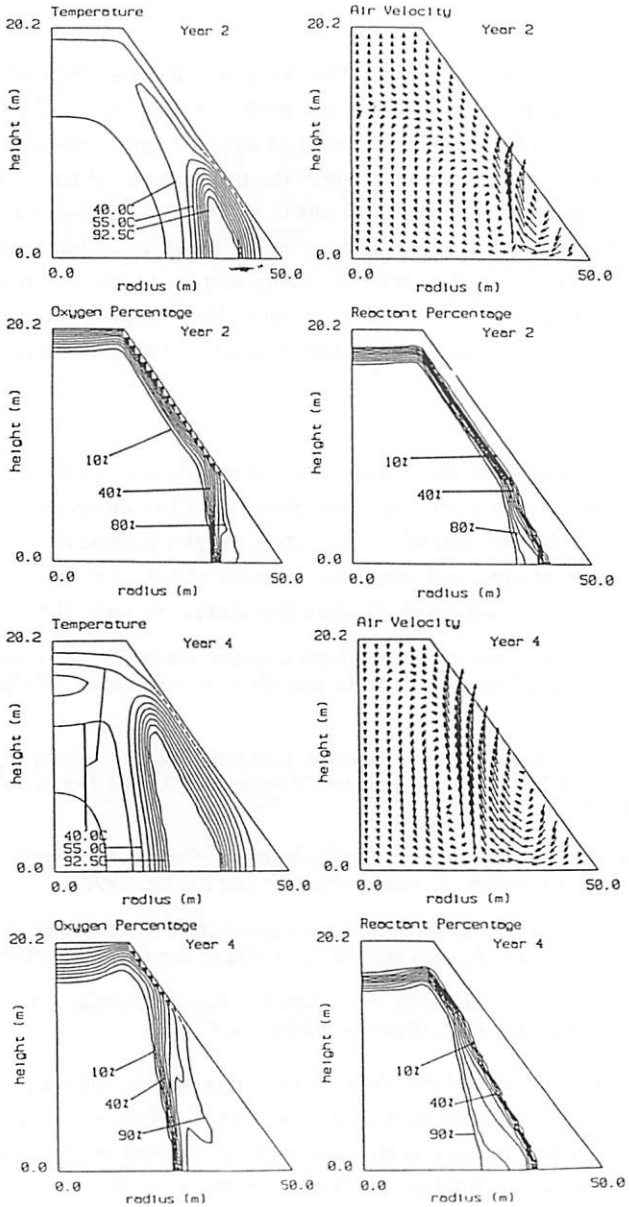

Figure 8.15. Profiles of temperature, gas velocity, fractional concentration of oxygen, and fractional concentration of remaining oxidizable material in a truncated cone-shaped heap at 2 and 4 years. The air permeability is $K = 10^{-9}$ m^2, the IOR is the shrinking-core model with $a = 0.005$ m, the maximum air velocity components are $|V_x|_{max} = 1.6 \times 10^{-5}$ m/s, $|V_z|_{max} = 6.3 \times 10^{-5}$ m/s at 2years, and $|V_r|_{max} = 1.7 \times 10^{-5}$m/s, $|V_z|_{max} = 7.8 \times 10^{-5}$ m/s at 4 years (after Pantelis and Ritchie, 1991b).

operation.

Cathles and his co-workers (1980) have modelled the effect of convection in copper heap-leach piles, and Pantelis and Ritchie (Bennett *et al.*, 1989; Pantelis and Ritchie, 1991a,b, 1992 1993) have modelled diffusion and convection in waste-rock dumps and biooxidation heaps in which the pyritic material has a relatively high intrinsic oxidation rate. The work of Pantelis and Ritchie indicates that oxidation in a newly built waste-rock dump proceeds initially by diffusion but, after some time, convection builds up in the toe of the dump batters. Convective transport of gas penetrates further into the dump as it ages. The evolution of the oxygen and temperature profiles is shown as a function of time for a typical dump in Figure 8.15.

8.5.5. Summary

The dependence of the global oxidation rate on such dump properties as the intrinsic oxidation rate, the air permeability, the gas diffusion coefficient, the infiltration rate, and the thermal conductivity is complex because the various transport processes are interactive and non-linear. Pantelis and Ritchie have shown that the following general principles apply to waste-rock dumps and biooxidation heaps:

- convection is not a significant gas transport mechanism in a dump where the air permeability is 10^{-10} m^2 or less (Pantelis and Ritchie, 1991a,b; Bennett *et al.*, 1989)
- convection is a significant gas transport mechanism in a dump in which the air permeability is 10^{-9} m^2 or more (Pantelis and Ritchie 1991a,b; Bennett *et al.*, (1989)
- convection is most effective in the batters of the dumps; diffusion dominates in the central regions of a dump (Pantelis and Ritchie, 1992)
- the global oxidation rate is very insensitive to increases in the intrinsic oxidation rate (Pantelis and Ritchie 1991a,b; Bennett *et al.*, 1989)
- the global oxidation rate is sensitive to irrigation rates in a dump with a high global oxidation rate (Pantelis and Ritchie 1991b)

It needs to be stressed that these are general principles, and the performance of a waste dump or biooxidation heap needs to be considered on a case-by-case basis. For example, allowing gas entry at the base of the dump and the possibility of forced aeration (Pantelis and Ritchie, 1993) removes the limitation set by diffusion and natural convection on gas transport rates in dumps that are closed to gas transport at the base. In such a situation the high global oxidation rate required can only be achieved at a high intrinsic oxidation rate for the heap material. The intrinsic oxidation rate sought in such cases is of the order of 10^{-6} $kg(O_2)m^{-3}s^{-1}$. Such high values of intrinsic oxidation rate can be achieved (Brierley, 1993).

8.6. FIELD MEASUREMENTS OF THE OXIDATION RATE

8.6.1. General Principles

It is evident from Sections 4 and 5 that the oxygen profile within a large waste-rock dump is pseudo steady state on a timescale of years, except in some special circumstances (see, for example, pronounced diurnal variations; Harries and Ritchie, 1985). If diffusive gas transport dominates over other forms of gas transport in some parts of the dump, and if the intrinsic oxidation rate is low as quantified in Section 5, then the oxygen profile is a reflection of the intrinsic oxidation rate. If, in addition, the variation within the dump can be taken as one-dimensional, as is usually so in large parts of a waste-rock dump, then the pore-gas oxygen concentration is described by the equation

$$\frac{\partial^2 u}{\partial x^2} = S\ (x) \tag{19}$$

$$S\ (x) = \frac{L^2}{DC_o} S\ ^*(x^*) \tag{20}$$

where the variables S and x have been made dimensionless in an obvious way. The task is then, on the basis of measurement of the pore-gas oxygen concentration, to estimate the curvature of the oxygen-concentration profile at a point, and to evaluate the oxygen consumption at that point. It is worth remembering in conducting such an analysis that $\delta u/\delta x = 0$ at the point where the oxygen concentration goes to zero (Elliot and Ockenden, 1982) as a result of oxygen consumption in the dump when the intrinsic oxidation rate is of particular, but useful, form.

As in most waste-rock dumps the rate of heat transport by gas flow is generally small compared to the rate of heat transport by conduction, the direct effect of convective and advective gas flow on the temperature profiles is much less than on pore-gas oxygen profiles. Hence, if it is clear from the shape of the oxygen-concentration profile that gas transport mechanisms other than diffusion are important, then analysis of temperature profiles to extract the intrinsic oxidation rate may be more practical than analysis of oxygen profiles. In one dimension, the temperature within the dump is described by

$$\frac{\partial^2 T}{\partial x^2} = -\frac{\gamma DC_o}{T_o K_T} S\ (x) \tag{21}$$

where again the variables have been made dimensionless. Again the task is to estimate the curvature of the temperature profile from the measured temperature distribution.

The temperature distribution in the waste material is a sum of the temperature distribution due to ambient temperatures and that due to heat sources in the wastes. This aspect is of particular significance near the surface of the wastes, where the temperature profile is commonly dominated by ambient temperatures. As the temperature changes that are due to ambient changes in surface temperature propagate into the dump, they are attenuated at a rate depending on their frequency. In principle, the temperature variation due to ambient changes in temperature is given by the expression (see Chapter 5 for more details)

$$T^*(x, t^*) = \sum_n u_n A_n(x) \cos(\omega_n t^* + \theta_n + \Psi_n(x) - \phi_n) \qquad (22)$$

In practice, the amplitudes of all of the components except those associated with the annual variation are small. Moreover, because the attenuation constant increases with increasing frequency, temperature variations caused by variations on the timescale of a month or less are small a meter or more from the surface. Hence, if temperature measurements are taken approximately monthly over a period of at least a year, the effect of changes in the ambient temperature can readily be taken into account in the data analysis. Similarly, the effect of heat transport by water infiltrating the dump is small and can be readily taken into account.

If convection is significant and it is important to extract the oxidation rate from the region of the dump where convection occurs, then one-dimensional analysis of the measured temperature profiles may not suffice. Because the heat source is proportional to the intrinsic oxidation rate, a simultaneous analysis of temperature and oxygen profiles yields the intrinsic oxidation rate. As such an approach requires an estimate of the curvature of the profiles in the two phases (horizontal as well as the vertical), a large grid of profiles would be required. Analysis of the data is most readily done by accessing a code that evaluates the two-dimensional temperature and oxygen profiles. Such a code is FIDHELM (Pantelis 1993), which solves the set of equations presented in Figure 8.9 and employs at the user's option one of the three forms of the intrinsic oxidation rate discussed in Section 4.2.

The point was made in Section 8.5 that if the intrinsic oxidation rate is much more than about 10^{-7} kg m^{-3} s^{-1} then, in those parts of the dump where diffusion dominates, the overall oxidation rate in the dump and its time dependence tend to that given by the simple homogeneous model. This requires knowledge only of the gas diffusion coefficient and concentration of oxidizable material. It follows that we do not need to measure the intrinsic oxidation rate with great precision; rather, we need to know it within limits in order to achieve the goal of defining an effective rehabilitation strategy. Furthermore, if sulfate is largely conserved within the dump, then the sulfate load from the dump is a measure of the integrated oxidation rate. The measured sulfate load can be used, together with temperature and oxygen concentrations, to indicate

that the oxidation rate of the material in the dump is known with a precision sufficient to assess various rehabilitation options.

8.6.2. *Estimation of the Oxidation Rate from Heat Sources*

The Rum Jungle mine was a uranium-copper producer in the Northern Territory of Australia in the 1950s and 1960s. The ore was removed by an open-cut operation that left three large waste-rock dumps (White's, Dyson's, and Intermediate) when operations stopped in 1971 and the minesite was abandoned (Davy, 1975). The White's and Intermediate dumps have been instrumented (Harries and Ritchie, 1981; Daniel *et al.*, 1982) to allow measurements of the temperature and oxygen concentrations through the dumps. Both dumps were about 20 to 25 m high; White's was the larger, with an area of about 27 ha compared to that of Intermediate's 7 ha.

The climate at the minesite is tropical, with an average of 80% of the mean annual rainfall of 1.5 m falling in the period December to March. The variation in the monthly mean daily temperature is small, varying only between 30 °C in November to 25 °C in July.

Figures 8.16 and 8.17 show typical temperature and pore-gas oxygen profiles measured in two of the dumps. These profiles changed very slowly over a period of some five years, with the most marked change being a slow decrease, about 1 °C y^{-1}, in the highest temperatures (Harries and Ritchie, 1983). It was clear from these profiles that gas transport in much of the dump was by diffusion from the surface, but that convection occurred in one large region of each of the dumps (Bennett *et al.*, 1988). The temperature profiles were analyzed assuming one-dimensional heat transport to extract the heat-source distribution and hence the oxidation-rate distribution at a number of points in both dumps (Harries and Ritchie, 1981, 1987). The effect of the variable ambient temperature was accounted for, as was the effect of rainwater infiltrating the dump. The heat-source distributions are shown in Figure 8.18. Using a heat output of 1.29 J kg^{-1} released in the oxidation of pyrite, the corresponding values of intrinsic oxidation rate range from about 0.3 kg m^{-3} s^{-1} to 8.8 x 10^{-8} kg m^{-3} s^{-1}. The lower limit of detection of this technique under the experimental conditions in that situation was about 0.02 x 10^{-8} kg m^{-3} s^{-1}.

8.6.3. *Estimation of Oxidation Rates from Oxygen-concentration Profiles*

The Aitik minesite is in the north of Sweden, about 100 km north of the Arctic Circle. The mine is operated by Boliden Minerals AB and is Europe's largest copper mine. It is an open-cut operation producing about 14 million tonnes of waste rock a year. The waste-rock dumps have been constructed by end-dumping from trucks and flattening by bulldozers. The dumps are typically 35 m high and currently cover a total

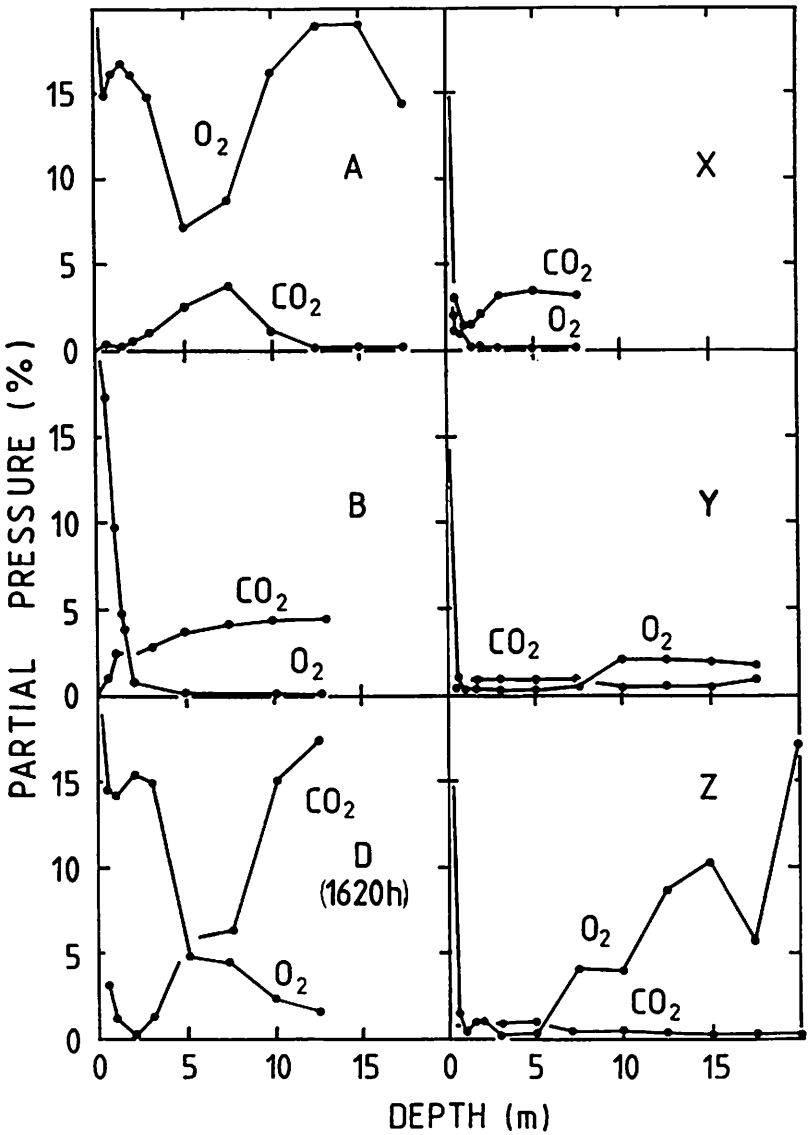

Figure 8.16. Oxygen and carbon dioxide concentrations as a function of depth in White's (locations A, B, D) and Intermediate (locations X, Y, Z) waste-rock dumps at the Rum Jungle minesite (after Harries and Ritchie, 1983).

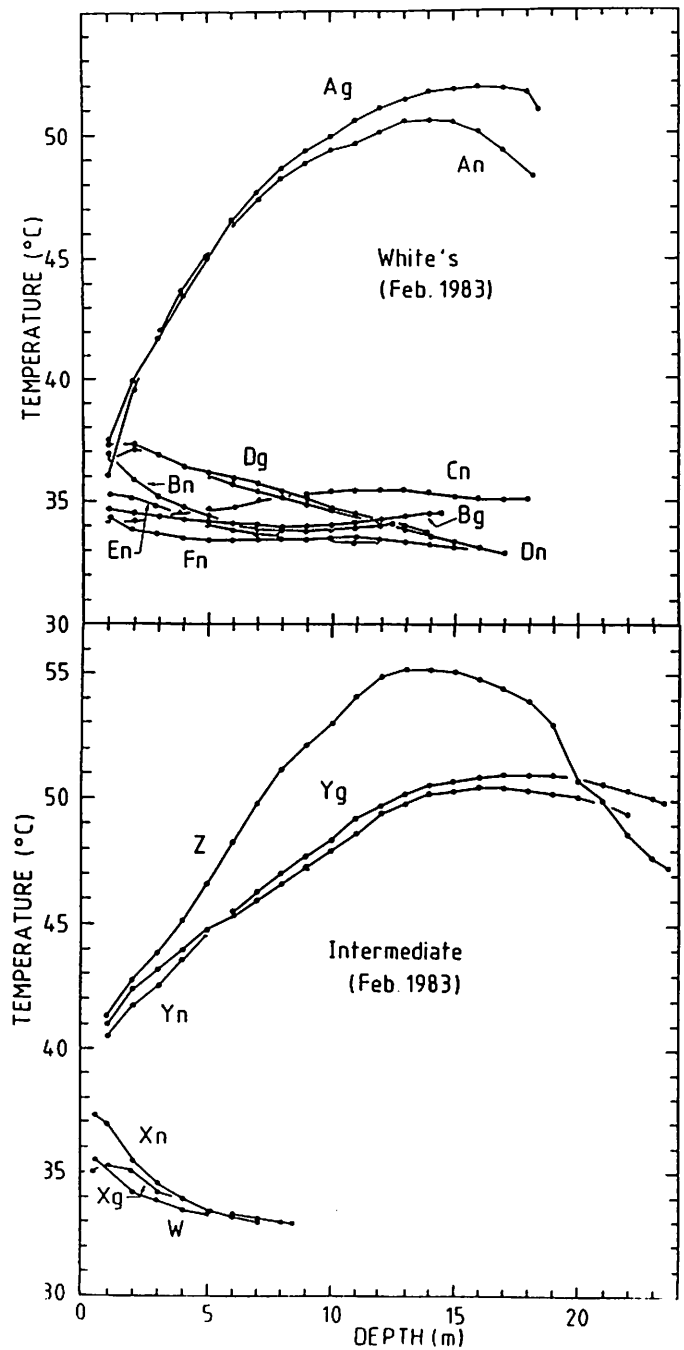

Figure 8.17. Temperature profiles in White's and Intermediate waste-rock dumps at the Rum Jungle minesite (after Harries and Ritchie, 1983).

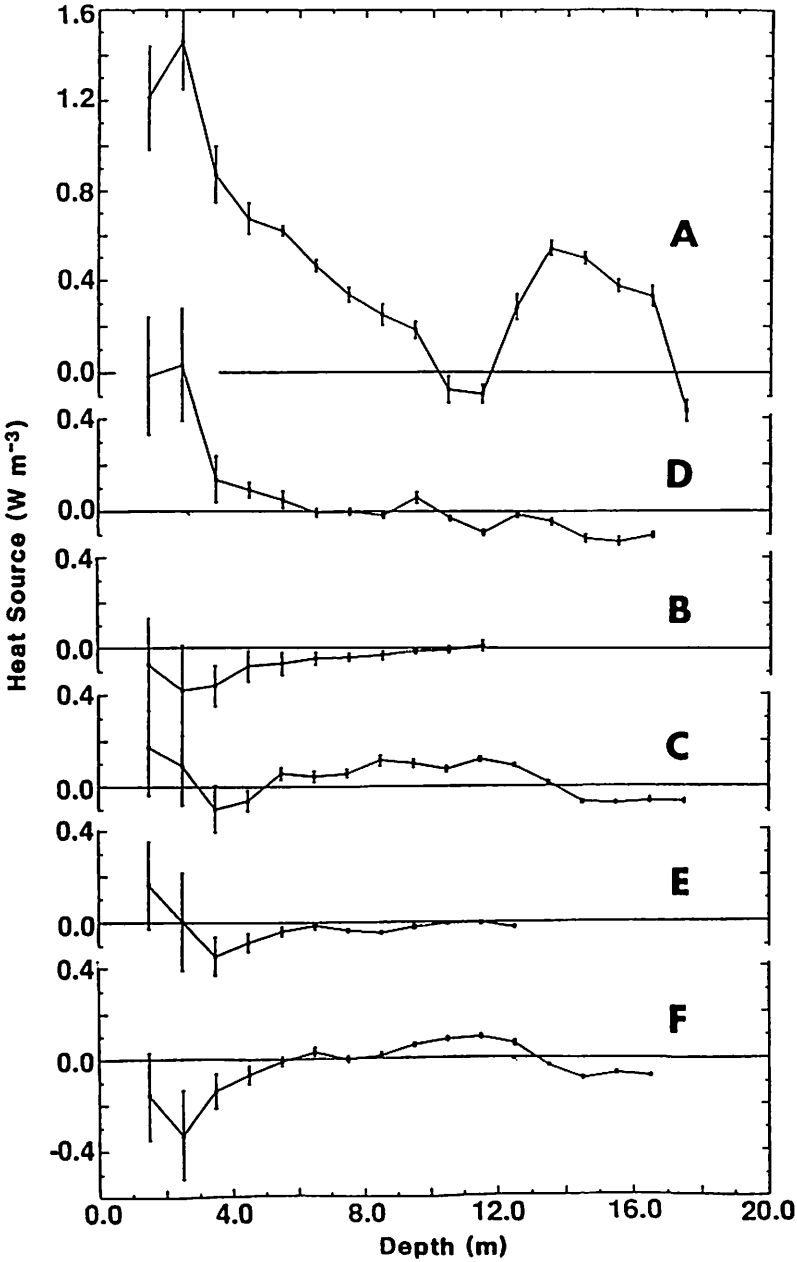

Figure 8.18. Heat-source distribution calculated from temperature profiles measured in the period March 1979 to September 1983 at locations in White's waste-rock dump at the Rum Jungle minesite (after Harries and Ritchie, 1987).

area of about 300 ha. The average annual temperature at the site is close to 0 °C, ranging from about 15 °C in July to about -15 °C in January. The average precipitation is 680 mm/yr, with a net infiltration into the waste rock of about 500 mm/yr (Axelsson *et al.*, 1992). From about the middle of October to the middle of April, precipitation is mainly in the form of snow which melts over a period of a few weeks, usually in May.

Instrumentation was installed to allow measurement of temperature and pore-gas composition in a 1.5-ha portion of a waste-rock dump with an area of about 130 ha. Instrumentation to measure flow rates and pollutant concentrations was also installed in a cut-off drain that collected effluent from the dump. More details of the dump and the installations are given by Bennett *et al.* (1994).

Oxygen profiles in the region of the monitored dump fell into one of the following three categories:

1. Profiles where the oxygen concentration decreased significantly with increasing depth into the dump;
2. Profiles where the oxygen concentration decreased very slowly with increasing depth into the dump;
3. Profiles where the decrease in oxygen concentration was generally very small, but where there was a sharp fall followed by a sharp rise in the concentration over a distance of a few meters.

Examples of profiles for categories 1 and 3 are shown in Figure 8.19. Temperature profiles measured in one of the probe holes are shown in Figure 8.20. These profiles are typical of all temperature profiles measured in the portion of the monitored dump.

The shape of the oxygen-concentration profiles and the clear lack of any significant heating within the waste-rock dump indicate that, where the levels of oxygen are close to atmospheric, there is little oxygen consumption by the dump material, and where there is a significant gradient, diffusion is the dominant gas-transport mechanism. The oxygen profiles show a variability from month to month, even in those parts of the dump where it is clear from the oxygen-concentration profiles that oxygen is being consumed at the highest rate. Detailed analysis of these profiles (Bennett *et al.*, 1994) show that some of this time dependence is seasonal and can be ascribed to a very small temperature dependence in the oxygen-consumption rate (about a 30% increase in the range 0—17 °C). Analysis of the oxygen-concentration profiles in the portion of the dump that had the highest oxygen-consumption rate yielded an intrinsic oxidation rate of about 1×10^{-8} kg m^{-3} for material comprising the top 9 m where the dump was about 15 m high. The data were consistent with the assumption that the intrinsic oxidation rate of this material was independent of oxygen concentration in the range 10 to 21% mole fraction.

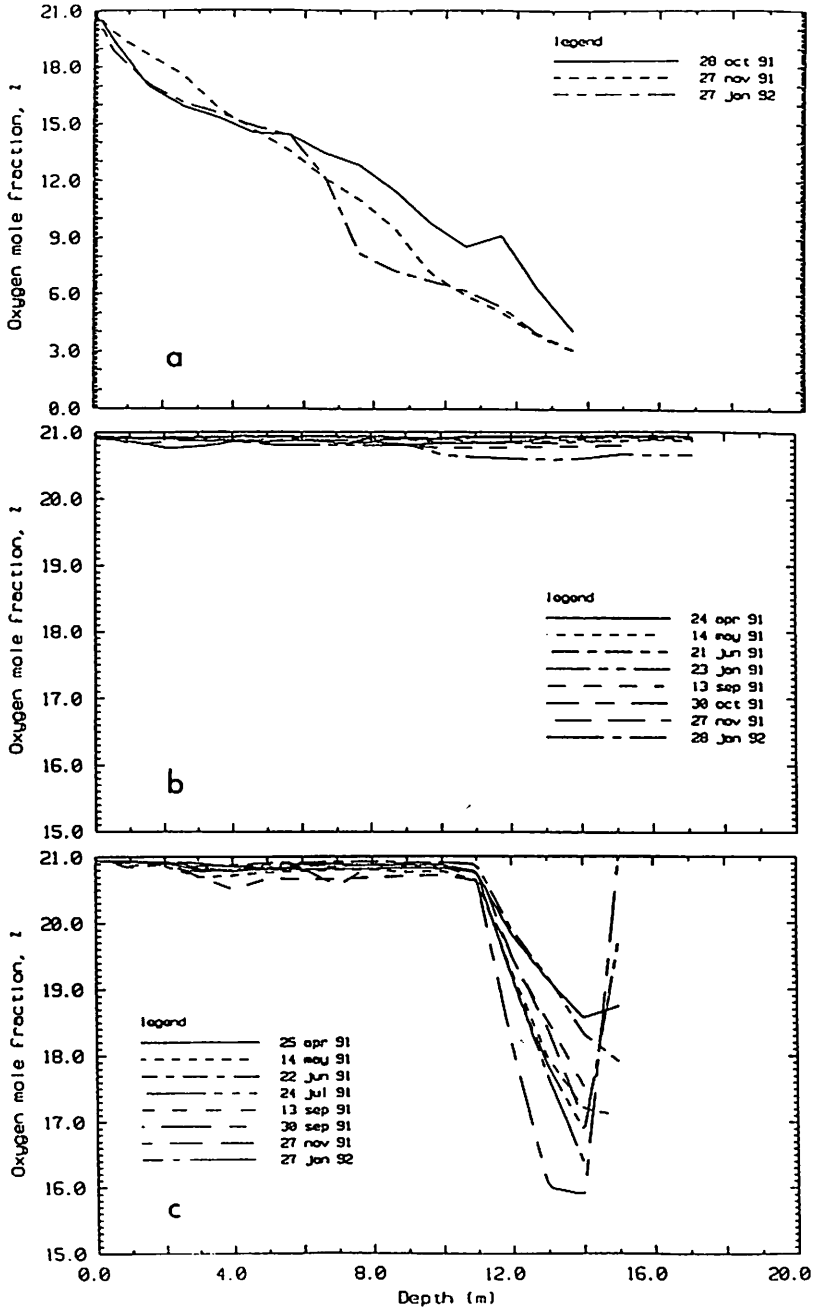

Figure 8.19. Oxygen profiles in a waste-rock dump at the Aitik minesite, showing the three types of profiles: (a) a region of "high" IOR; (b) a region of very low IOR; (c) a pod of "high" IOR material in a region of very low IOR.

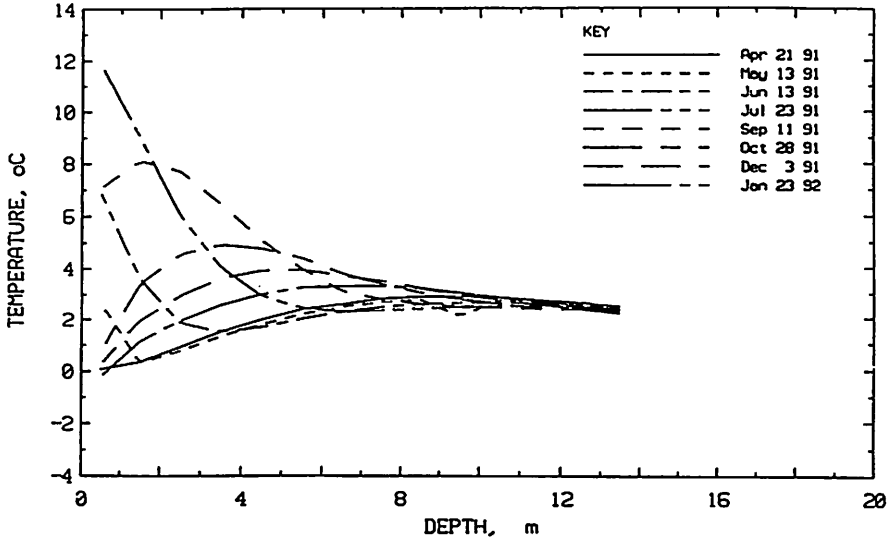

Figure 8.20. Temperature profiles in a waste-rock dump at the Aitik minesite.

The oxygen flux into those regions of the dump where the intrinsic oxidation rate was high averaged 15 x 10^{-8} kg m^{-2} s^{-1}, compared with 0.25 x 10^{-8} kg m^{-2} s^{-1} in those regions where the intrinsic oxidation rate was generally low. The implication was that the contribution to the pollutant load in drainage from the latter regions was about 60 times less than that from regions of the dump containing material with an intrinsic oxidation rate of about 1 x 10^{-8} kg m^{-3} s^{-1}. The annual pollution load evaluated from flow rates and concentration levels in the cut-off drain were consistent with the assumption that some 20% of the dump material had the high intrinsic oxidation rate, and 80% had the vanishingly low intrinsic oxidation rate. It should be noted that the analysis of Section 5 shows that, when the intrinsic oxidation rate is low and gas transport is dominated by diffusion, the global oxidation rate increases with the square root of the intrinsic oxidation rate. This means that, if there are regions in the dump where the intrinsic oxidation rate is substantially higher than 1 x 10^{-8} kg m^{-3} s^{-1}, the conclusion that material having a high intrinsic oxidation rate comprises a comparatively small fraction of the total material in the dump will not be much changed.

8.6.4. Other Minesites

A comprehensive set of oxygen and temperature measurements has been made in some waste-rock dumps at the Heath Steele minesite in New Brunswick, Canada. The waste-rock dumps are comparatively small, with masses ranging from 3,250 tonnes to

235,700 tonnes, and heights from 3.4 m to 10.5 m. In such dumps, temperature changes due to ambient changes in temperature appear through the whole depth of the dump. To date, only qualitative conclusions have been reached on gas and heat transport in these dumps (Bell *et al.*, 1991). Oxidation of the dump material is apparent both from temperature and oxygen-concentration profiles. It seems likely that wind-driven advection is also a gas transport mechanism in these dumps. Quantitative analysis is expected to be available in 1994 (MEND Annual Report, 1992). A waste-rock dump at Mines Doyon in Quebec, Canada, has been instrumented to measure oxygen and temperature profiles (Gelinas *et al.*, 1992).

8.6.5. Data on Intrinsic Oxidation Rates

At this juncture there are little data on oxidation rates measured in large dumps of pyritic waste or from measurements that purport to be on run-of-mine wastes. Table 8.7 is a compilation of data on oxidation rates for run-of-mine material. Of interest is the last entry, which is for material in a large column in which the oxidation rate was measured directly (Bennett *et al.*, 1993a) from the rate of oxygen consumption rather than being inferred from the concentration of chemical species in drainage. It can be seen that this laboratory-measured rate is very much of the same order as that measured in the field for the dump material.

Another feature of the rates in Table 8.7 is that all are very much of the same order of magnitude and much lower than the "laboratory" measured rates in Table 8.1. There are two points to emphasize. First, the magnitude of the oxidation rates listed in Table 8.7 indicates that the intrinsic oxidation rate will be a large determinant in the early (years to tens of years) time dependence of the pollution load from the waste-rock dump (Gibson *et al.*, 1994, and Chapter 5). Second, the scaling-up of laboratory-measured intrinsic oxidation rates to those appropriate to run-of-mine waste rock must incorporate factors that account for the 2 orders of magnitude difference between the two types of results. Given the magnitude of the difference, and given that it is only if the intrinsic oxidation rate is less than about 1×10^{-7} kg m^{-3} s^{-1} that we need to know it with any precision, it may in practice be more cost-effective to measure the intrinsic oxidation rate directly in run-of-mine material.

It must be stressed that the rates listed in Table 8.7 cannot be typical of all bulk pyritic material. If they were, then it would be impossible to achieve the overall oxidation rates required to pre-treat some refractory gold ores in biooxidation heaps. That such treatment is indeed practical has been demonstrated by Brierley (1993). A technique to overcome the limitations in the rate of oxygen supply in such heaps has been quantified by Pantelis and Ritchie (1993).

Table 8.7. Measured intrinsic oxidation rates

Minesite	Entity	Reference	$kg(O_2)m^{-3}s^{-1}$
Rum Jungle, Australia	waste-rock dump	Harries & Ritchie (1981)	$(0.3 \text{ to } 8.8) \times 10^{-8}$
Norwich Park, Australia	coal rejects	*	$(0.3 \text{ to } 2.2) \times 10^{-8}$
Woodlawn, Australia	waste-rock dump	**	$(0.2 \text{ to } 2.7) \times 10^{-8}$
Aitik, Sweden	waste-rock dump	Bennett et al. (1993)	$(0.3 \text{ to } 4.3) \times 10^{-8}$
Aitik, Sweden	large columns	Bennett et al. (1993	1.4×10^{-8}

* personal communication from J.W. Bennett and Y. Tan, 1993
** personal communication from Y. Tan, 1993

8.7. CONCLUSIONS

The intrinsic oxidation rate defines the primary pollutant-production rate in a waste-rock dump. If the rate is high, and high is about 1×10^{-7} kg m^{-3} s^{-1}, then the overall oxidation rate is determined predominantly by the rate at which oxygen can be transported to oxidation sites within the waste-rock dump. If the rate is less than about 10^{-7}, then relatively large regions of the dump will be involved in oxidation, and the magnitude of the intrinsic oxidation rate will be a major control on the early time (years to tens of years) behavior of the pollution load from the dump.

Measurements in waste-rock dumps have shown that gas transport by diffusion is observed in many dumps, and that gas transport by convection is observed in some. Advective gas transport generated by, for example, wind blowing over a waste-rock dump, is a possible mechanism but has not been observed quantitatively. Convective gas transport is not likely to be significant in a dump unless the air permeability of the dump material is greater than about 10^{-9} m^2. Convection, if it occurs, starts in the batters of the dump and penetrates into the dump from there. In a large dump, oxidation is generally dominated by diffusive transport in the central regions of the dump.

Oxygen and temperature profiles reflect the oxidation rate and gas transport mechanisms in a dump. Analysis of measured profiles has been used to evaluate the intrinsic oxidation rate of deposited waste-rock dump material. The measurements yield values ranging from <0.3 to about 9.0×10^{-8} kg m^{-3} s^{-1}. These are low compared to values from measurements of pyritic oxidation rates in the laboratory, but are certainly large enough to be environmentally significant. Such is the large difference between the intrinsic oxidation rate derived from field measurements and those from laboratory measurements on crushed samples that there must be some doubt that all of the factors which need to be applied to crushed samples to scale up to run-of-mine material can be taken into account adequately. This is particularly so if scaling up yields values greater than about 10^{-7} kg m^{-3} s^{-1}, as then there is no need to know the

intrinsic oxidation rate with any precision because, in most waste-rock dumps, gas transport rates then control the primary pollution-production rates. Such is not the case when steps are taken, such as in biooxidation heaps, to ensure that gas transport rates are not rate-limiting. Such steps include ensuring that the air permeability is high, or constructing the heap to ensure that the bottom of the heap is open to gas flow.

Oxygen and temperature profiles in pyritic wastes are easily measured with inexpensive instrumentation once an appropriately constructed probe hole has been installed. As both these parameters are closely related to the pyrite oxidation rate, which is the primary pollutant-generation mechanism, they provide a direct and rapid indicator of the effectiveness of measures adopted to reduce the oxidation rate in pyritic mine-wastes. In this sense, monitoring these parameters provides more timely and more easily interpreted information on the effectiveness of rehabilitation, both in the short and in the long term, than does monitoring of drainage-water quality.

8.8. ACKNOWLEDGEMENTS

I thank the following for insightful discussions, access to recent data, and hard work at various times: Dr John Bennett, Dr Andrew Garvie, Dr David Gibson, Dr Garry Pantelis, Dr Yunhu Tan, Mr Norman Clark, Mr Alan Boyd, Mr Arthur Dixon, Mr Warren Hart, Mr William Plotnikoff and Mr Viphakone Sisoutham. I also appreciate the clarification of some of the chemical mechanisms, which has resulted from discussions with Dr Paul Brown, Dr Josick Comarmond, and Dr Richard Lowson.

8.9. NOMENCLATURE

T^* = temperature (°C)
T_o = some characteristic temperature for normalization
T = T^*/T_o dimensionless temperature
x^* = spatial variable (m)
L = height of waste-rock dump (m)
x = x^*/L dimensionless spatial variable
S^* = intrinsic oxidation rate (kg $(O_2)m^{-3}s^{-1}$)
S_S = oxidation rate of oxidizable material (kg $(O_2)m^{-3}s^{-1}$)
C_o = concentration of oxygen in air (0.265 kg m^{-3})
c_w = specific heat of water (4.18 x 10^3 $m^2s^{-2}K^{-1}$)
D = oxygen bulk diffusion coefficient of dump (m^2s^{-1})
S = $(L^2S^*)/C_oD$ = dimensionless intrinsic oxidation rate
κ = bulk thermal diffusivity of dump (m^2s^{-1})
ρ_s = bulk density of dump (kg m^{-3})
δ = heat released per mass of reactant oxidized (2.25 x 10^7J kg^{-1})

ε = mass of oxygen used per mass of reactant in oxidation reaction (1.75)

c_s = bulk specific heat of dump (886 $m^2s^{-1}K^{-1}$)

Q_w = infiltration rate (ms^{-1})

b = thermal coefficient of expansion of air (3.4 x 10^{-3})

D_2 = diffusion of oxygen in solid (m^2s^{-1})

$\rho\, ^a{}_0$ = density of air at t_0

ρ_α = bulk density of α phase; g = gas, w = water, s =solid

ρ^α = intrinsic density of α phase

ρ_α = $\varepsilon_\alpha \rho^\alpha$

ρ_{rs} = initial bulk density of reactant (kg m^{-3})

ε_α = volume fraction of α phase; g = gas, w = water, s =solid

$u(x,t)$ = dimensionless oxygen concentration

$u(x,t)$ = expression for $u(x,t)$ corresponding to $(w(x,t)$

ωg = mass fraction of oxygen in gas phase

ω^s = mass fraction of oxidizable material in solid phase

$w(x,t)$ = defined by equation (13)

$w(x,t)$ = approximate solution for $w(x,t)$

γ = a proportionality constant encompassing both Henry's Law and the Gas Law (0.03)

$X^*(t^*)$ = position of planar moving front within dump (m)

X = X^*/L = dimensionless position of planar moving front

β = $6k$

τ_3 = $a^2\varepsilon\, \rho_{rs}/(\gamma\varepsilon_s C_o)$

τ_4 = $L^2\varepsilon\, \rho_{rs}/(DC_o)$

t^* = time variable (s)

t = t^*/τ_4 = dimensionless time variable

k = $1/k_2$

k_2 = τ_3/τ_4

K = intrinsic air permeability of the dump (m^2)

$k_{rg}(\varepsilon_g)$ = relative air permeability of the dump; *in-situ* measurement of air permeability yields the product $Kk_{rg}(\varepsilon_g)$

K_T = bulk thermal conductivity of the dump ($W\, m^{-1}\, K^{-1}$)

K_s = saturated hydraulic conductivity of the dump (ms^{-1} or md^{-1})

a = radius of a particle (m)

t_c = time for the particle at the surface to oxidize completely (s)

t_d = time for the dump to oxidize completely (s)

t_p = timescale for oxidation of a particle (s)

t_C = timescale for convection of a gas through a dump (s)

t_D = timescale for diffusion of a gas through a dump (s)

t_T = timescale for thermal diffusion in a dump (s)

Chapter 9

Secondary Minerals and Acid Mine-water Chemistry

C.N. Alpers
U.S. Geological Survey, Room W-2233, 2800 Cottage Way
Sacramento, California 95825

D.W. Blowes
Waterloo Centre for Goundwater Research, University of Waterloo
Waterloo, Ontario N2L 3G1

D.K. Nordstrom
U.S. Geological Survey, 3215 Marine Street
Boulder, Colorado 80303

J.L. Jambor
Department of Earth Sciences, University of Waterloo
Waterloo, Ontario N2L 3G1

9.1. INTRODUCTION

Waters associated with mines and mining waste are geologically unusual fluids and are of interest to geochemists because they accentuate certain types of water—rock interactions. Rates of mineral weathering are greatly accelerated during mining and mineral processing. In particular, the increased accessibility of oxygen enhances the rates of sulfide-oxidation reactions, which produce sulfuric acid and result in highly acidic waters with elevated metal concentrations.

Secondary minerals can form during weathering when solubility products are exceeded in the weathering solutions, so that states of mineral saturation or supersaturation are achieved. Mineral precipitation can take place at the surface of a mineral undergoing incongruent dissolution, or can take place in response to a number of processes that affect the weathering solutions including oxidation, dilution, mixing, evaporation, and neutralization.

Both the formation and the dissolution of secondary minerals can affect the composition of waters associated with sulfide-bearing mine wastes. For example, the formation of insoluble minerals such as anglesite ($PbSO_4$) can cause significant attenuation of metals close to the source of sulfide oxidation, thereby preventing significant exposure to ecosystems. On the other hand, soluble sulfate minerals formed in arid and semi-arid environments can store metals and acidity during dry periods and then release them during wet periods. This type of cycle can result in dramatic seasonal variations in metal concentrations, with undesirable impacts on biota.

In this Chapter the composition of secondary minerals commonly associated with sulfide mine-wastes are reviewed, and the geochemical and hydrologic processes that contribute to the formation and dissolution of these minerals are discussed. Some examples are given of aqueous speciation—saturation computations for water samples from sites at which secondary minerals are known to occur. This type of computation is a form of geochemical modelling that can be used to evaluate the role of secondary minerals in controlling metal solubility.

9.2. SECONDARY MINERALS AND THEIR RELATIVE SOLUBILITY

Secondary minerals have a wide range in solubility. In the following sections, minerals are discussed in groups, generally starting with the most soluble and progressing toward the least soluble. The groups are: soluble sulfates, less-soluble and insoluble sulfates, metal oxides and hydroxides, carbonates, and secondary sulfides. In addition, there is a section on miscellaneous minerals including arsenates, phosphates, and halides.

Some information is given regarding occurrences of the minerals, generally limited to the direct experience of the authors. Several available reference books and papers contain considerable additional information and references on occurrences, crystallography, crystal chemistry, and other properties of secondary minerals which are known to form in mine-waste environments (*e.g.*, Bandy, 1938; Palache *et al.*, 1951; Sabelli and Trosti-Ferroni, 1985; Williams, 1990).

9.2.1. Soluble Sulfates: Iron Minerals

Pyrite (FeS_2) and pyrrhotite ($Fe_{1-x}S$) are the most abundant sulfide minerals in mine wastes, so it is not surprising that their oxidized equivalents, iron-sulfate minerals, are among the most abundant secondary minerals in this environment. The geochemistry of iron in the weathering environment is complicated by having both a ferrous (Fe^{II}) and a ferric (Fe^{III}) oxidation state. Table 9.1 lists the end-member compositions of some iron-sulfate minerals, including Fe^{II} sulfates, Fe^{III} sulfates, and mixed Fe^{II}-Fe^{III} sulfates. All of the minerals listed in Table 9.1 are highly soluble; they

form as efflorescent salts from waters containing iron and sulfate, the products of pyrite and pyrrhotite oxidation, by a combination of processes that includes evaporation and Fe^{II} oxidation. The Fe^{II} sulfates occur commonly, whereas the Fe^{II}-Fe^{III} sulfates are known from many fewer localites. Copiapite is the most common of the Fe^{II}-Fe^{III} sulfates; bilinite and voltaite are extremely rare. Among the Fe^{III} sulfates, coquimbite is the most common.

Table 9.1. Selected soluble iron-sulfate minerals

	Mineral	Formula	Color
Fe^{II}			
	melanterite	$Fe^{II}SO_4.7H_2O$	pale blue-green
	ferrohexahydrite	$Fe^{II}SO_4.6H_2O$	white
	siderotil	$Fe^{II}SO_4.5H_2O$	white
	rozenite	$Fe^{II}SO_4.4H_2O$	white
	szomolnokite	$Fe^{II}SO_4.H_2O$	white, green
	halotrichite	$(Fe^{II})Al_2(SO_4)_4.22H_2O$	white, green
Mixed Fe^{II}-Fe^{III}			
	copiapite	$Fe^{II}Fe_4^{III}(SO_4)_6(OH)_2.20H_2O$	yellow
	bilinite	$Fe^{II}Fe_2^{III}(SO_4)_4.22H_2O$	orange
	römerite	$Fe^{II}Fe_2^{III}(SO_4)_4.14H_2O$	brown, pink
	voltaite	$K_2Fe^{II}{}_5Fe_4^{III}(SO_4)_{12}.18H_2O$	black, green
Fe^{III}			
	coquimbite	$Fe_2^{III}(SO_4)_3.9H_2O$	purple, white
	kornelite	$Fe_2^{III}(SO_4)_3.7H_2O$	pink
	rhomboclase	$HFe^{III}(SO_4)_2.4H_2O$	cream
	ferricopiapite	$Fe_5^{III}(SO_4)_6O(OH).20H_2O$*	yellow, orange

* Sabelli and Trosti-Ferroni (1985)

At pH values below about 4, ferric iron is the dominant oxidant of pyrite (Nordstrom, 1982a), by the reaction

$$FeS_2 + 14Fe^{3+} + 8H_2O \Rightarrow 15Fe^{2+} + 2SO_4^{2-} + 16H^+ \qquad (1)$$

Probably the most common of the minerals in Table 9.1 is melanterite $Fe^{II}SO_4.7H_2O$, which forms by combining the first two products of reaction (1). Pure melanterite is pale blue-green, and can occur as stalactites in open mine-tunnels (*e.g.*, Richmond mine, Iron Mountain, California; Alpers and Nordstrom, 1991), or as pore-filling cement in the hardpan layer of sulfide tailings (*e.g.*, Heath Steele, New Brunswick; Blowes and Jambor, 1990). Inclusion of orange-brown Fe^{III}-rich pore water or Fe-hydroxide minerals in melanterite can cause an apparent dark green color, but

the color of the inclusion-free mineral remains pale blue-green.

All of the iron-sulfate minerals listed in Table 9.1 are hydrous compounds, with 1 to 22 waters of hydration per mole. As a result, each mineral has a stability range defined by temperature and water activity (or relative humidity). With increasing temperature and/or decreasing water activity, melanterite may dehydrate to rozenite $Fe^{II}SO_4.4H_2O$ or szomolnokite $Fe^{II}SO_4.H_2O$. The presence of solid-solution substitutions can have an effect on the product. For example, Jambor and Traill (1963) noted that, under identical conditions, copper-free melanterite dehydrated to rozenite, but copper-bearing melanterite transformed to the pentahydrate, siderotil. It should be noted that the preservation of potentially unstable hydrous minerals is facilitated by immersing the samples in mineral oil, which retards dehydration and deliquescence reactions by sharply reducing contact with the atmosphere.

The stoichiometrically simple Fe^{III}-sulfate salts are coquimbite $Fe^{III}_2(SO_4)_3.9H_2O$, and the rare minerals quenstedite $Fe_2^{III}(SO_4)_3.10H_2O$, kornelite $Fe_2^{III}(SO_4)_3.7H_2O$, and lausenite $Fe_2^{III}(SO_4)_3.6H_2O$. Coquimbite is a relatively common oxidation product of pyrite in highly oxidized environments. In the underground workings of the Richmond mine at Iron Mountain, California, kornelite occurs together with szomolnokite at temperatures of 45—50 °C; these less-hydrous phases are more stable at elevated temperatures caused by the exothermic nature of pyrite oxidation. Such temperatures occur in some massive-sulfide workings and within actively oxidizing waste-rock and leaching, piles (*e.g.*, Cathles, 1994; Guo and Parizek, 1994).

An alternative way to write the formula for rhomboclase $HFe^{III}(SO_4)_2.4H_2O$, is $(H_3O)Fe^{III}(SO_4)_2.3H_2O$, indicating the presence of the hydronium ion. For the latter formula, an overall reaction to form this mineral by pyrite oxidation would be

$$FeS_2 + 2O_2 + 3H_2O \Rightarrow (H_3O)Fe(SO_4)_2 \cdot 3H_2O \qquad (2)$$

showing that the acidity from pyrite oxidation (*e.g.*, equation 1) could be stored in solid form until released by subsequent rhomboclase dissolution. Rhomboclase is known from relatively few localities (*e.g.*, Iron Mountain, California; Alpers and Nordstrom, 1991), but possibly it occurs in trace amounts as a receptor for hydronium ions when acid-sulfate waters are evaporated to dryness.

Römerite is a mixed-valence iron-sulfate mineral that forms relatively late in the evolution of evaporating mine-water from the Richmond mine at Iron Mountain (C. Maenz, personal communication, 1994). Crystalline römerite is brown. A fine-grained pink phase that forms as an alteration product of other Fe-sulfate minerals in the laboratory gives a weak X-ray diffraction pattern for römerite, suggesting that this mineral may be stable relative to other Fe sulfates at laboratory conditions. Römerite has been noted to occur in coal spoils (Cravotta, 1994) and in base-metal mine-waste

settings (Alpers and Nordstrom, 1991).

Voltaite is distinct among the iron-sulfate minerals listed in Table 9.1 because it has essential K in its structure. Although rare, it forms abundant, distinctive aggregates of dark green-to-black octahedral crystals in the Richmond mine at Iron Mountain (Alpers and Nordstrom, 1991). Copiapite and ferricopiapite generally occur as fine-grained yellow crusts. These minerals are occasionally mistaken for jarosite (discussed in a later section) or native sulfur.

Halotrichite, pickeringite, and bilinite are end-member minerals of the halotrichite group of general formula $A^{II}B_2^{III}(SO_4)_4.22H_2O$. The divalent site *A* can be filled by Mg, Fe^{II}, Mn and other transition metals, and the trivalent site *B* is filled by Fe^{III}, Al, or Cr. Halotrichite-group minerals may occur as very fine acicular needles, or as blanket-like aggregates; microscopically filiform aggregates have been observed as white blooms on sulfate-bearing mine wastes, and halotrichite *per se* is known to occur on coal spoils and coal outcrops. Natural occurrences of soluble iron-sulfate minerals in coals and sulfide ores have been described by numerous authors (*e.g.*, Kossenberg and Cook, 1961; Bol'shakov and Ptushko, 1971; Cody and Biggs, 1973; Zodrow and McCandlish, 1978; Zodrow *et al.*, 1979; Raymond *et al.*, 1983, Wiese *et al.*, 1987).

9.2.2. *Soluble Sulfates: Other Elements*

Many elements other than iron can form soluble sulfate minerals. Some of the more common phases and their end-member formulas are listed in Table 9.2. As with the iron sulfates, the various hydration states for each metal sulfate have stability fields that are a function of temperature and water activity.

Table 9.2. Some soluble sulfate minerals

Mineral	Formula	Mineral	Formula
epsomite	$MgSO_4.7H_2O$	anhydrite	$CaSO_4$
hexahydrite	$MgSO_4.6H_2O$	retgersite	$NiSO_4.6H_2O$
goslarite	$ZnSO_4.7H_2O$	chalcanthite	$CuSO_4.5H_2O$
bianchite	$ZnSO_4.6H_2O$	alunogen	$Al_2(SO_4)_3.17H_2O$
gunningite	$ZnSO_4.H_2O$	mirabilite	$Na_2(SO_4).10H_2O$
gypsum	$CaSO_4.2H_2O$	thenardite	$Na_2(SO_4)$

Formation of the end-member phases in Table 9.2, with the exception of the Ca sulfates, takes place from weathering solutions with relatively low concentrations of Fe^{2+}. Otherwise, the divalent metals such as Cu, Zn, Ni, Mg, and Mn are likely to be incorporated as solid-solution components of Fe^{II}-bearing salts. For example, the following melanterite compositions were determined for stalactites from the Richmond

mine at Iron Mountain (Alpers *et al.*, 1994): $Fe_{.930}Zn_{.035}Cu_{.019}Mg_{.016}SO_4.7H_2O$ (mean of three analyses), and from another sample, $Fe_{.534}Zn_{.281}Cu_{.142}Mg_{.043}SO_4.7H_2O$ (mean of two analyses). No discrete Zn, Cu, or Mg sulfate phases were observed in association with these melanterites.

There are two distinct mechanisms that can lead to the formation of non-Fe^{II}-bearing sulfates in mines and mine-waste environments. Oxidation of deposits (or portions thereof) rich in base-metal sulfides containing Cu and Zn with only minor amounts of Fe sulfide present can result in Fe^{2+}-poor waters that may precipitate sulfate minerals such as those in Table 9.2. An alternative process is the oxidation of sulfide deposits containing Fe sulfides, which leads to the formation of Fe^{2+}-rich waters (*e.g.*, reaction 1) also containing other base metals. Metal sulfate minerals in Table 9.2 may precipitate from these waters after the predominant Fe^{2+} is removed from solution, *e.g.*, by oxidation to Fe^{3+} and precipitation as Fe^{III} oxide or hydroxide minerals (see Section 9.2.4.).

Nickel sulfates that form in the weathering environment are morenosite $NiSO_4.7H_2O$, regersite $NiSO_4.6H_2O$ (tetragonal), and nickel-hexahydrite (monoclinic, isomorphous with members of the hexahydrite group). None of these minerals has yet been found associated with mine wastes. Solid solution of Ni^{2+} substituting for *X* in the $XSO_4.nH_2O$ minerals (Tables 9.1 and 9.2) is expected to occur, but has not yet been documented.

9.2.3. *Less Soluble Sulfate Minerals*

a. Alunite-jarosite Group

The alunite-jarosite goup consists of a large number of isostructural rhombohedral minerals with the general formula $AB_3^{3+}(SO_4)_2(OH)_6$, where the *A* site is filled by monovalent K, Na, H_3O, NH_4, Ag, or 1/2 Pb, and the *B* site is filled by trivalent Fe or Al. End-member formulas corresponding to various combinations of *A* and *B* are given in Table 9.3.

Table 9.3. Less soluble sulfates: some minerals of the alunite group

Mineral	Formula	Mineral	Formula
jarosite	$KFe_3^{III}(SO_4)_2(OH)_6$	alunite	$KAl_3(SO_4)_2(OH)_6$
natrojarosite	$NaFe_3^{III}(SO_4)_2(OH)_6$	natroalunite	$NaAl_3(SO_4)_2(OH)_6$
hydronium jarosite	$(H_3O)Fe_3^{III}(SO_4)_2(OH)_6$	ammonioalunite	$(NH_4)Al_3(SO_4)_2(OH)_6$
ammoniojarosite	$(NH_4)Fe_3^{III}(SO_4)_2(OH)_6$	osarizawaite	$PbCuAl_2(SO_4)_2(OH)_6$
argentojarosite	$AgFe_3^{III}(SO_4)_2(OH)_6$	beaverite	$PbCuFe_2^{III}(SO_4)_2(OH)_6$
plumbojarosite	$Pb_{0.5}Fe_3^{III}(SO_4)_2(OH)_6$		

The derivative phases beaverite and osarizawaite have one mole of Cu^{II} on the *B* site, with the resulting charge imbalance satisfied with a full mole of Pb on the *A* site rather that 1/2 mole as in plumbojarosite. Other members of the alunite family not shown in Table 9.3 include minamiite and its derivatives, which contain 1/2 mole of Ca or Ba on the *A* site (Li *et al.*, 1992). Alunite and the other Al-bearing members of the alunite-jarosite group can form either hydrothermally or during weathering. Hydrothermal alunite is an essential component of the acid-sulfate (or advanced argillic) alteration type (Meyer and Hemley, 1967) which is abundant in epithermal systems and in the upper levels of some porphyry copper deposits (*e.g.*, El Salvador, Chile: Gustafson and Hunt, 1975; La Escondida, Chile: Alpers and Brimhall, 1988, 1989). The same duality of genesis applies to jarosite, although hydrothermal occurrences are much rarer than those by weathering. Considerable effort has gone into distinguishing alunite and jarosite formed under hydrothermal (hypogene) *versus* weathering (supergene) conditions, for the purposes of metal prospecting. Such efforts include stable isotopes (Rye *et al.*, 1992) and unit-cell dimensions calculated from powder X-ray diffraction patterns (Stoffregen and Alpers, 1992).

Alunite-jarosite minerals of supergene origin are commonly found in the weathered zone of sulfide ore deposits; therefore, it is reasonable to suppose that the deposition of these phases will affect the chemistry of weathering solutions. However, apparent supersaturation of surface waters with respect to alunite and jarosite is commonly observed when speciation—saturation analysis is performed (*e.g.*, Nordstrom, 1977, 1982b; Chapman *et al.*, 1983; van Breemen, 1985). This suggests that kinetic barriers may prevent the rapid precipitation of alunite, jarosite, and related minerals. Alunite has been observed to be actively forming at a small number of localities, including naturally acidic lakes in southeastern Australia (Alpers *et al.*, 1992; Long *et al.*, 1992), and in an acid mine-water mixing with a CO_2-rich, saline spring discharge in Colorado. These observations suggest that the presence of high ionic strength may help to overcome kinetic barriers to alunite precipitation.

Supersaturation of weathering solutions is less likely to occur for jarosite than for alunite. Thermodynamic calculations of saturation indices should take into account the fact that jarosite-gorup minerals formed during weathering tend to incorporate 10 to 20 mole percent H_3O on the *A* site (Kubisz, 1964; Brophy and Sheridan, 1965; Dutrizac, 1983). For example, Alpers *et al.* (1989) described the solubility of a jarosite solid solution $[K_{0.75}(H_3O)_{0.20}Na_{0.05}]Fe_3(SO_4)_2(OH)_6$ from acid mine-water aged 12 years. The erroneous assumption of end-member compositions in saturation-index calculations can lead to errors of more than one order of magnitude with regard to apparent supersaturation (Alpers *et al.*, 1989).

b. Other Hydroxy-sulfate Minerals

Table 9.4 gives formulas for a number of other hydroxy-sulfate minerals of Fe^{III}

and Al. Nordstrom (1982b) provided a detailed discussion of mineral solubility and stability relations in the Al_2O_3-SO_3-H_2O system. The minerals jurbanite and basaluminite have been found in mine-drainage settings, but the most common phase in this system seems to be an amorphous (or poorly crystalline) Al hydroxy-sulfate of basaluminite stoichiometry (Nordstrom *et al.*, 1984). A common setting for the occurrence of such an aluminous precipitate is the confluence of an acidic (pH <5), Al-rich surface water with a neutral water that brings the confluent pH to >5.

Table 9.4. Other less-soluble iron- and aluminum-sulfate minerals

Mineral	Formula	Mineral	Formula
fibroferrite	$Fe^{III}(SO_4)(OH).5H_2O$	jurbanite	$Al(SO_4)(OH).5H_2O$
amarantite	$Fe^{III}(SO_4)(OH).3H_2O$	hydrobasaluminite	$Al_4(SO_4)(OH)_{10}.12\text{-}36H_2O$
schwertmannite	$Fe_8^{III}O_8(SO_4)(OH)_6$	basaluminite	$Al_4(SO_4)(OH)_{10}.H_2O$

The geochemistry of ferric iron has certain parallels to that of aluminum, including the occurrence of poorly crystalline hydroxy-sulfate phases. Schwertmannite, an iron oxyhydroxide with essential sulfate, is derived structurally from akaganéite, an iron oxyhydroxide with essential chloride (Bigham *et al.*, 1990; Murad *et al.*, 1994; Bigham, this Volume).

Copper also occurs commonly as hydroxy-sulfate minerals of intermediate solubility. Antlerite and brochantite (Table 9.5) are characteristic green-colored copper minerals that occur in oxidized zones. The hydrated minerals with brochantite stoichiometry (*e.g.*, wroewolfite) are much less common.

Table 9.5. Other less-soluble sulfate minerals

Mineral	Formula
celestite	$SrSO_4$
anglesite	$PbSO_4$
barite	$BaSO_4$
antlerite	$Cu_3(SO_4)(OH)_4$
brochantite	$Cu_4(SO_4)(OH)_6$
langite, wroewolfeite	$Cu_4(SO_4)(OH)_6.2H_2O$
posnjakite	$Cu_4(SO_4)(OH)_6.H_2O$

The alkali-earth elements generally form poorly soluble to insoluble sulfate minerals. The most notoriously insoluble mineral of this type is barite $BaSO_4$, which is used in various analytical schemes as a medium for quantitative precipitation of sulfate from solution. Anglesite $PbSO_4$, was mentioned previously as a relatively insoluble compound that is responsible for the attenuation of lead close the source of sulfide

oxidation in many base-metal deposits (*e.g.*, Waite Amulet, Quebec; Blowes *et al.*, 1991). The solid solution of $RaSO_4$ in other alkali-earth sulfate minerals, including barite and celestite, provides an important mechanism for the attenuation of radium, which carries a significant amount of the radiation in wastes from uranium mining (Landa, 1980; Langmuir and Melchior, 1985).

9.2.4. Metal Oxides and Hydroxides: Iron and Aluminum

Some other similarities between the geochemistry of ferric iron and aluminum are that the two metals have a trivalent charge, similar ionic radii, and form minerals of similar structure and composition. An important difference between the aqueous geochemistry of these elements is the pH at which hydrolysis occurs. The first hydrolysis reaction of aluminum can be written as

$$Al^{3+}_{(aq)} + H_2O \Leftrightarrow Al(OH)^{2+}_{(aq)} + H^+ \qquad (3)$$

Reaction (3) has a log K_3 of -5.00 ± 0.04 at 25 °C, 1 bar, and the standard state of infinite dilution (Nordstrom and May, 1989). For ferric iron, the first hydrolysis reaction

$$Fe^{3+}_{(aq)} + H_2O \Leftrightarrow Fe(OH)^{2+}_{(aq)} + H^+ \qquad (4)$$

has a log K_4 of -2.2 (Nordstrom *et al.*, 1990) at standard conditions. The mass-action expressions corresponding to reactions (3) and (4) are:

$$K_3 = \frac{[AlOH^{2+}][H^+]}{Al^{3+}} \qquad (5)$$

and

$$K_4 = \frac{[FeOH^{2+}][H^+]}{Fe^{3+}} \qquad (6)$$

where brackets denote aqueous activity. Inspection of equations (5) and (6) reveals that equal activities of $Al(OH)^{2+}$ and Al^{3+} are achieved at $[H^+] = K_3$, or a pH = -log K_3 = pK_3 = 5.0. Similarly, equal activites of $Fe(OH)^{2+}$and Fe^{3+} are achieved at $[H^+] = K_4$, or pH = -logK_4 = pK_4 = 2.2.

The minerals in Table 9.6 are among the most common of the oxide, hydroxide, and oxyhydroxides of iron and aluminum. Not all of the minerals in Table 9.6 are observed to form readily during weathering. Rather, the table is constructed to emphasize the similarities and differences between the geochemistry of ferric iron and alumium. Thermodynamic phase relations in the Al_2O_3—H_2O and Fe_2O_3—H_2O systems are complicated by a large number of metastable phases with similar solubility.

Table 9.6. Iron and aluminum oxide and hydroxide minerals

Mineral	Formula	Mineral	Formula
hematite	α-Fe_2O_3	corundum	Al_2O_3
maghemite	γ-Fe_2O_3	diaspore	AlO(OH)
magnetite	$FeO.Fe_2O_3$	boehmite	AlO(OH)
goethite	α-FeO(OH)	gibbsite	$Al(OH)_3$
akaganéite	β-FeO(OH,Cl)	bayerite	$Al(OH)_3$
lepidocrocite	γ-FeO(OH)	doyleite	$Al(OH)_3$
feroxyhyte	δ-FeO(OH)	nordstrandite	$Al(OH)_3$
ferrihydrite	$Fe_5HO_8.4H_2O$, or $5Fe_2O_3.9H_2O$		

Efforts to determine stable and metastable phase relations in the Al-O-H system are not straightforward because (Hemingway and Sposito, 1989) "... no single study contains all the information necessary to support the chosen interpretations." According to Hemingway and Sposito (1989), diaspore AlO(OH) is stable relative to the Al-hydroxide phases (*i.e.*, gibbsite, bayerite) in the Al_2O_3 system at 25 °C, 1 bar. Slow growth kinetics of diaspore and gibbsite result in the control of aluminum solubility at pH values above 5.0 by a reaction that mimics gibbsite solubility (Nordstrom and Ball, 1986). Such a reaction may be caused by reversible solubility with a poorly crystalline to amorphous phase of gibbsite or similar composition, or by a surface reaction involving the exchange of Al^{3+} and $3H^+$ on any mineral surface containing aluminum.

The Fe_2O_3—H_2O system is similarly complicated. Hematite and goethite solubilities and stabilities are sufficiently close that grain size and surface Gibbs free energy have an important influence on the phase stability. With regard to coarse-grained minerals, goethite appears to be stable relative to hematite (Langmuir, 1969, 1971, 1972). Both goethite and hematite have slow growth kinetics at surficial temperatures, so the initial solid products from the hydrolysis of Fe^{3+} are poorly crystalline, metastable phases such as ferrihydrite (Chukhrov *et al.*, 1973; Russell, 1979) or microcrystalline goethite.

Leached cappings and gossans represent the *in situ* oxidized equivalents of porphyry-copper and massive-sulfide deposits, respectively. The mineralogy of iron in the oxidized zones of these deposits is dominated by hematite, goethite, and jarosite. The early literature dating back to the 1920s (*e.g.*, Locke, 1926; Tunell, 1930) documented the observations that "deep maroon to seal brown" hematitic iron oxide tends to remain in rocks after oxidation of supergene chalcocite-bearing ores, which

formed as the enrichment product of copper—iron sulfide protores. Increasing amounts of goethite and jarosite correlate with progressively higher ratios of pyrite:chalcocite at depth (Loghry, 1972; Alpers and Brimhall, 1989). The texture of the iron oxides (or "limonites") also changes systematically from indigenous (in original sulfide cavities) to transported (outside sulfide cavities and in fractures) with increasing pyrite content prior to oxidation (Blanchard, 1968; Loghry, 1972) due to increased acidity and iron mobility after pyrite oxidation.

Although the chemical reaction betwen goethite and hematite (equation 7) involves only water and not free hydrogen ions,

$$Fe_2O_3 + H_2O \Leftrightarrow 2FeO(OH) \qquad (7)$$

pH can have an effect on the relative formation of these phases because of kinetic effects. Ferrihydrite has been shown to be the necessary precursor to hematite, to which it transforms by solid-state dehydration reaction (Schwertmann, 1985a,b, and references therein). As this transformation takes place in the presence of water, there is a competing tendency for ferrihydrite to dissolve back into solution and for the ferric iron to precipitate as fine-grained goethite. Schwertmann and Murad (1983) demonstrated that ferrihydrite aged in solutions with a wide spectrum of pH values showed considerable variation in terms of the resulting proportions of hematite and goethite. Goethite was the dominant phase below pH = 6 and above pH = 11; maximum hematite production occurred at pH = 8. These results are relevant to iron in soils, which show increasing proportions of hematite to goethtite with increasing pH in the range of 4 to 6 (*e.g.*, Kämpf and Schwertmann, 1982).

Other dissolved ions may also play an important role in determining goethite *versus* hematite formation and preservation. For example, the presence of Ca and Mg in solution has been found to favor the precipitation of hematite rather than goethite, and dissolved sulfate can suppress goethite formation completely under certain conditions (*e.g.*, Torrent and Guzman, 1982). The presence of Cu^{2+} can catalyze the oxidation of Fe^{2+} to Fe^{3+} by oxygen (Thornber, 1985), leading to the precipitation of ferrihydrite-like solids which may convert to hematite if aged under favorable conditions.

Aluminum has been observed to substitute into goethite and hematite, to maximum concentrations of 33 mole % AlO(OH) and 14 mole % Al_2O_3, respectively (Yapp, 1983; Schultze, 1984; Tardy and Nahon, 1985; Schwertmann, 1985a). Although both iron and aluminum are highly soluble in acid mine waters, the authors are unaware of any data showing significant aluminum substitution in iron-oxide minerals formed in mine-drainage settings. It is possible that high sulfate concentrations commonly found in acid mine drainage have some effect on minimizing the aluminum content of the resulting iron precipitates.

9.2.5. Oxides and Hydroxides: Other Elements

Ferric oxide, oxyhydroxide, and hydroxysulfate precipitates have been noted at numerous mine-waste sites (Bigham, this Volume). Although geochemical measurements and thermodynamic calculations also indicate conditions favorable for the formation of other metal oxide and hydroxide phases in mine wastes, the authors know of no location where the occurrence of these phases in tailings has been confirmed through mineralogical techniques. The absence of these metal-bearing oxides or hydroxides in mine wastes suggests that other mechanisms limit the concentrations of dissolved metals in mine-waste environments. Field and laboratory studies suggest that coprecipitation or adsorption reactions are the most likely mechanisms of metal attenuation in the absence of discrete sulfate- or carbonate-bearing precipitates. Determination of metal-removal mechanisms in systems in which adsorption or coprecipitation reactions are dominant is an area of active research. Leckie *et al.* (1980) noted that it is difficult to distinguish between coprecipitation and adsorption reactions in some environments in which ferric oxyhydroxide phases are actively precipitating. Farley *et al.* (1985) proposed that a continuum exists between the mechanisms of adsorption and precipitation, and suggested that similar theoretical tools can be used to describe both adsorption and surface precipitation.

The extent of adsorption and coprecipitation is controlled by the intensity of the coulombic attraction between the oxide surface and the dissolved ion, and by the intensity of intermolecular bonds that are formed at the mineral surface. The degree of dissolved-metal adsorption and binding to ferrric oxyhydroxide surfaces is dependent on the mineralogical composition of the ferric oxyhydroxide surface and the solution characteristics, including pH, ionic strength, and the concentrations of competing cations and ligands (Davis *et al.*, 1978).

The dependence on pH and ionic strength has been attributed to variations in surface charge that result from changes in the degree of protonation of water molecules coordinated with the metal-oxide surface (Schindler, 1981). As the metal oxide is immersed in solution, water molecules orient and bind to the surface, offsetting the inherent surface charge. Dissociation and protonation of these water molecules occur in a manner that is analogous to the dissociation and protonation of water molecules in the bulk solution. Variations in the protonation of bound water molecules result in changes in the surface charge, and therefore in varying affinities for dissolved metals.

Ions attracted to mineral surfaces participate in complexation reactions or ligand-exchange reactions with surface species. Reactions at the mineral surface can be described by association constants that are analogous to those used to describe the formation of aqueous complexes (Westall, 1986). Numerous mathematical models have been developed to describe the electrostatic attraction and chemical bonding of dissolved metals to mineral surfaces (Davis *et al.*, 1978; Hohl *et al.*, 1980; Dzombak

and Morel, 1986). Although these mathematical models are based on different conceptualizations of the oxide—water interface, several are able to describe well the laboratory adsorption data (Westall and Hohl, 1980), indicating a need to characterize the nature of metal binding at the mineral surface. Current research focuses on developing more accurate descriptions of the adsorption mechanism at the mineral surface (Dzombak and Morel, 1991), and on the application of adsorption models to natural materials (Honeyman, 1984; Fuller *et al.*, 1993; Waychunas *et al.*, 1993).

a. Formation of Nickel Hydroxides

The most widespread secondary mineral of nickel in ore deposits is violarite Ni_2FeS_4, but a variety of secondary sulfates, carbonates, and combinations that include Ni with other elements is known. For secondary oxides or hydroxides, however, only three minerals have been characterized (Table 9.7): bunsenite NiO, theophrastite $Ni(OH)_2$, and jamborite $(Ni^{2+},Ni^{3+},Fe)(OH)_2(OH,S,H_2O)$ (Morandi and Dalrio, 1973). No discrete secondary nickel hydroxide or oxide phases have been found in tailings impoundments or as acid mine drainage (AMD) precipitates. It could be argued, as in the case for aluminum, that secondary nickel hydroxides are likely to be X-ray amorphous, as occurs with laboratory precipitates unless special precautions are taken. Energy-dispersion analyses of altered tailings, however, do not show nickel to be sufficiently concentrated to indicate the presence of a discrete secondary nickel phase, regardless of whether it is crystalline or amorphous.

Table 9.7. Some other oxide and hydroxide minerals, and native metals

Mineral	Formula	Mineral	Formula
pyrolusite	MnO_2	cuprite	Cu_2O
hausmannite	Mn_3O_4	delafossite	$CuFeO_2$
manganite	γ-MnO(OH)	bunsenite	NiO
pyrochroite	$Mn(OH)_2$	theophrastite	$Ni(OH)_2$
todorokite	$(Mn^{II},Ca,Mg)Mn_3{}^{IV}O_7.H_2O$	jamborite	$(Ni^{2+},Ni^{3+},Fe)(OH)_2(OH,S,H_2O)$
rancieite	$(Ca, Mn^{II})Mn_4{}^{IV}O_9.3H_2O$	native copper	Cu
tenorite	CuO	native silver	Ag

The Copper Cliff tailings area at Sudbury, Ontario, contains millions of tonnes of tailings from the processing of Ni and Cu ore, with the metals occurring predominantly as pentlandite and chalcopyrite, respectively. The precipitation of secondary nickel in these tailings provides a good example of what has been found to occur for nickel and several other elements, such as Si and Al, in an oxidizing tailings environment. Figure 9.1 shows a backscattered-electron image of the remnants of a large grain of pyrrhotite, surrounded by its alteration products. In the accompanying X-ray image for Fe, the pyrrhotite grain is outlined well because of its high Fe content; the surrounding alteration material is also rich in Fe, and is predominantly goethite.

The whiteness of the dot-maps reflects the element concentrations, and as the ideal formulas for pyrrhotite and goethite have similar Fe contents (63.5 and 62.8 wt%, respectively), they should also have a similar whiteness. The pattern for goethite, however, is considerably weaker because it has been "diluted", probably mainly by excess H_2O, but also by the presence of appreciable quantities of Si and Al (not shown). As well, the X-ray map for S shows that the goethite is S-bearing, probably as sulfate. The X-ray map for Ni reveals that the pyrrhotite is slightly nickeliferous, and that Ni is dispersed in the surrounding goethite.

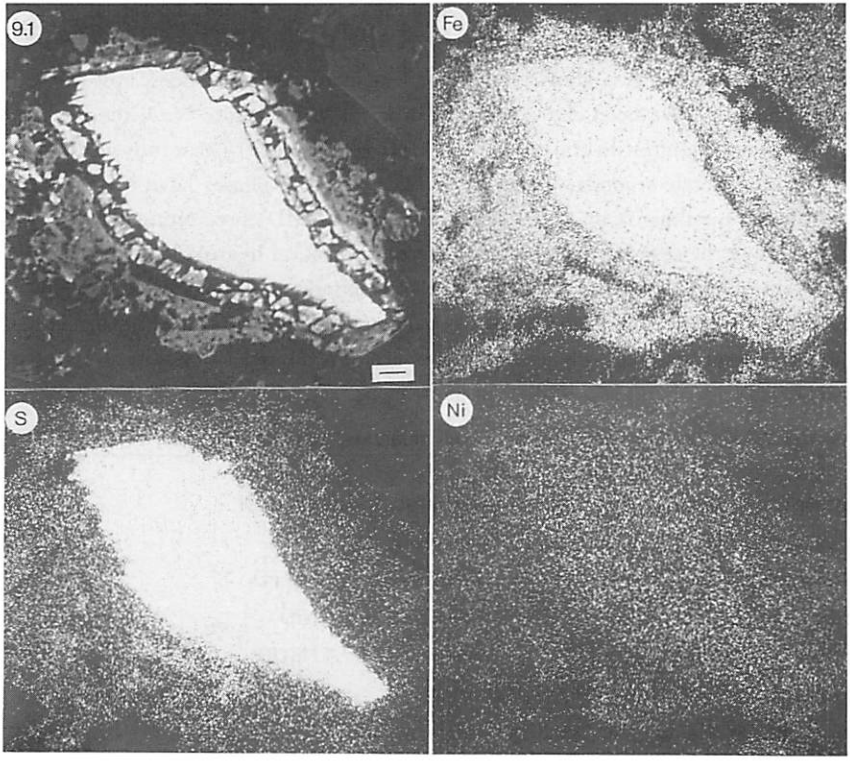

Figure 9.1. Backscattered-electron image of a margin-altered grain of pyrrhotite in a polished section of tailings from Copper Cliff, Ontario. Corresponding X-ray maps show the distributions of Fe, S, and K. Bar scale represents 10 μm.

Not all pyrrhotite or goethite is nickeliferous, but all pentlandite is. Nevertheless, the same picture emerges when pentlandite alteration rims are examined. The geochemical and mineralogical results suggest that part of the nickel remains in solution, a small part is taken up by vermiculite and associated mixed-layer phyllosilicates that form by the alteration of biotite, possibly some occurs as the expected but as-yet-undetected violarite, and the bulk is deposited with goethite.

b. Coprecipitation of Other Metals

The coprecipitation of other elements in association with secondary hydrous Fe oxides follows the same pattern as that described above for nickel. Some examples of the association are given for tailings from the Delnite minesite, which is a former gold producer in the Timmins area of northern Ontario. Examples from any of the impoundments examined to date could have been chosen to illustrate the element associations with oxyhydroxides, but Delnite was selected because arsenopyrite is present in the tailings, and significant amounts of pore-water arsenic generated by the dissolution of arsenopyrite and arsenic-bearing pyrite were precipitated with goethite.

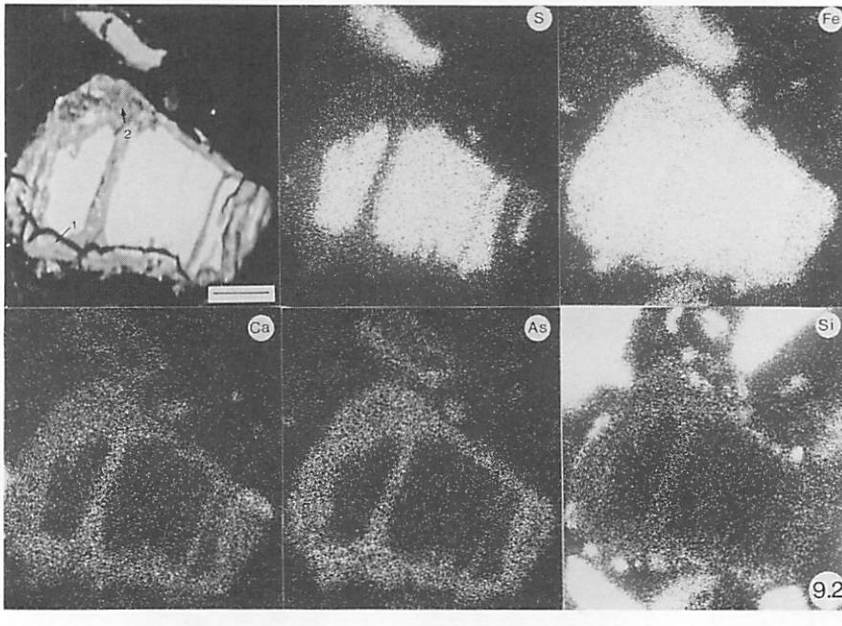

Figure 9.2. Backscattered-electron (BSE) image of a pyrrhotite grain, rimmed and veined by arsenic-rich goethite, in a polished section of tailings from the Delnite impoundment, Ontario. Arrows point to microprobe-analyzed areas as given in Table 9.8. X-ray maps for S, Fe, Ca, As, and Si match the BSE image. Smaller, less altered grain above the pyrrhotite is pyrite. Bar scale represents 10 μm.

Figures 9.2, 9.3, and 9.4 show iron oxyhydroxide rims that surround grains of pyrrhotite. As X-ray diffraction patterns of rims and bulk, altered grains from Delnite consistently indicate the presence of goethite, but no other iron oxyhydroxides, the rims are referred to here as goethite. Each of the pyrrhotite grains in Figures 9.2, 9.3, and 9.4 is accompanied by corresponding X-ray dot-maps to show the distributions of S, Fe, Ca, As, and Si. The distribution patterns are similar in indicating an association of Ca, As, Si, and a small amount of sulfate with the goethite. Figure 9.4 has a partly replaced grain of arsenopyrite, and its rim has element associations similar to those for

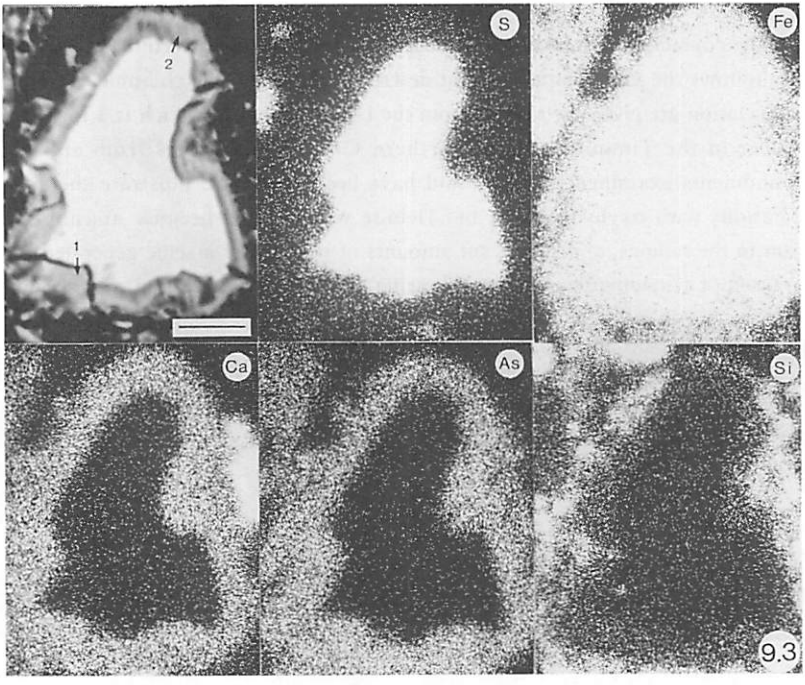
2
1
S
Fe
Ca
As
Si
9.3

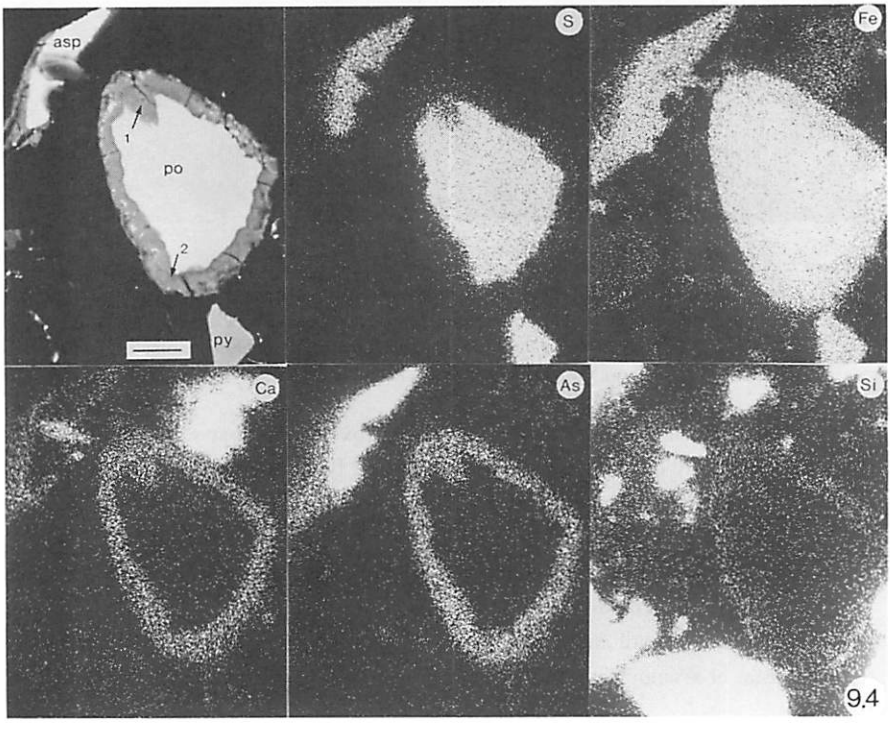
asp
1
po
2
py
S
Fe
Ca
As
Si
9.4

the rims on pyrrhotite.

Electron-microprobe analyses of the rims are given in Table 9.8. The results show that the sum of Ca, Si, As, and S (as oxides) ranges from 12.7 to 19.5 wt%, and averages 16.4 wt%. Substitutions of these elements at such magnitudes cannot be accommodated in the goethite structure. The arsenic content alone is much too high to be structurally incorporated, thus indicating a physical rather than a solid-solution association. The calcium content is too low to suggest the presence of a calcium arsenate, but the presence of an iron arsenate is a possibility. As no iron arsenate has been identified mineralogically, the phase is assumed to be amorphous. This assumption is reasonable in that, unlike the association of iron with other anions, iron and arsenic commonly combine to form poorly crystalline to amorphous compounds in oxidation zones.

Table 9.8. Electron microprobe analyses of goethite rims, Delnite mine, Ontario

		Figure 9.2		Figure 9.3		Figure 9.4	
		area 1	area 2	area 1	area 2	area 1	area 2
wt%	Fe_2O_3	74.6	73.1	75.1	74.8	73.8	68.9
	CaO	2.1	1.4	3.2	3.4	3.4	3.1
	SiO_2	1.5	1.7	0.0	0.9	0.9	0.9
	As_2O_5	7.2	7.4	10.0	10.6	10.9	13.0
	SO_3	3.5	2.2	2.7	2.7	2.2	2.5
	sum	88.9	85.8	91.9	92.4	91.2	88.4

Figure 9.3. BSE image and corresponding X-ray maps for a pyrrhotite grain and alteration rim, as in Figure 9.2. Bar scale represents 10 μm.

Figure 9.4. BSE image and corresponding X-ray maps for a pyrrhotite grain and its alteration rim, as in Figure 9.2. Also present are a smaller arsenopyrite grain (asp), and a small pyrite grain (py). The X-ray map for As shows that the arsenic concentrations in the goethite around the arsenopyrite and pyrrhotite are similar. Bar scale represents 10 μm.

The above example illustrates the significant role that goethite and other iron oxyhydroxides, especially ferrihydrite, can play in acting as "sinks" for various elements in an AMD environment. In a vertical oxidation zone, such as occurs in a tailings impoundment, the sink-type goethite is more amenable to dissolution than is pure goethite. With prolonged oxidation the dissolution—precipitation cycle is repeated so that the various elements gradually move downward in the oxidizing zone.

9.2.6. Carbonate Minerals

Acid neutralization by carbonate minerals is discussed by Blowes and Ptacek (this Volume). Table 9.9 lists various carbonate minerals; the most common in ore deposits and mine wastes are calcite, siderite, dolomite, and ankerite. All of the hydroxyl-bearing carbonates in Table 9.9 are secondary minerals formed by the oxidation of Zn-Cu-Pb ores.

Table 9.9. Some carbonate minerals

Rhombohedral

Mineral	Formula
calcite	$CaCO_3$
magnesite	$MgCO_3$
siderite	$FeCO_3$
rhodochrosite	$MnCO_3$
smithsonite	$ZnCO_3$
otavite	$CdCO_3$
gaspeite	$NiCO_3$
sphaerocobaltite	$CoCO_3$

Orthorhombic

Mineral	Formula
aragonite	$CaCO_3$
strontianite	$SrCO_3$
witherite	$BaCO_3$
cerussite	$PbCO_3$

Double

Mineral	Formula
dolomite	$CaMg(CO_3)_2$
kutnohorite	$CaMn(CO_3)_2$
ankerite	$Ca(Fe,Mg)(CO_3)_2$
minrecordite	$CaZn(CO_3)_2$

Hydroxyl

Mineral	Formula
malachite	$Cu_2(CO_3)(OH)_2$
azurite	$Cu_3(CO_3)_2(OH)_2$
hydrocerussite	$Pb_3(CO_3)_2(OH)_2$
hydrozincite	$Zn_5(CO_3)_2(OH)_6$
aurichalcite	$(Zn,Cu)(CO_3)_2(OH)_6$

9.2.7. Supergene and Diagenetic Sulfides

The supergene enrichment process is important to mine-waste geochemistry from two points of view: (1) it is necessary to recognize whether ores and associated wastes may be enriched or partly enriched, as the resulting mineralogy and its oxidation properties will be distinct from primary ores and protores, and (2) enrichment

processes may become established in oxidizing waste-piles, resulting in redistribution of iron, copper, sulfur, and other elements.

Alteration of copper- and nickel-sulfide deposits results in significant enrichment of ore grades by a process involving oxidation and leaching above the water table, followed by transport of metals to a zone of more reducing conditions where secondary sulfides are formed. Table 9.10 lists the formulas of some of the copper and nickel minerals found in the supergene environment. The recent paper by Sato (1992) provides a discussion of metastable sulfide assemblages and their persistence in the oxidized zone. Reviews of supergene copper enrichment have been given by Bateman (1950), Anderson (1955), Brimhall and Crerar (1987), and Alpers and Brimhall (1989). Supergene nickel enrichment is described by Thornber (1975, 1985).

Table 9.10. Some supergene sulfide minerals

Mineral	Formula	Mineral	Formula
chalcocite	Cu_2S	spionkopite	$Cu_{1.39}S$
djurleite	$Cu_{31}S_{16}$	yarrowite	$Cu_{1.12}S$
digenite	$(Cu,Fe)_{1.8}S$	covellite	CuS
anilite	$Cu_{1.75}S$	violarite	Ni_2FeS_4
geerite	$Cu_{1.60}S$	millerite	NiS

Diagenesis represents the chemical, physical, and mineralogical changes that occur when sediments are buried. The diagenetic environment is generally reducing, and can be a favorable site for the reduction of sulfate and the formation of secondary sulfide minerals. Iron-sulfide minerals reported from this environment are listed in Table 9.10. Secondary iron sulfides formed in diagenetic environments are almost always fine grained, and some occur in raspberry-shaped aggregates known as framboids. There is an abundant literature on geochemical processes related to formation of sulfide minerals in the diagenetic environment, especially in tidal marshes. Some of the key publications are by Berner (1964, 1967a,b, 1980, 1984), Howarth (1979), Luther *et al.* (1982), Howarth and Giblin (1983), Canfield (1989), and Canfield and Des Marais (1991, 1993).

Iron is usually the most abundant transition metal and therefore is the most likely metal to combine with H_2S formed by sulfate reduction to produce secondary sulfides in diagenetic environments. Other divalent metals present in pore water will also tend to form sulfide minerals, as indicated in Table 9.11. The relative solubility of metal sulfides, starting from the most soluble is: MnS > FeS > NiS ~ ZnS > CdS ~ PbS > CuS > HgS (DiToro *et al.*,1991). The fixation of metals in anoxic wetlands and lake bottoms may be related to the formation of diagenetic metal sulfides.

Table 9.11. Diagenetic sulfide minerals

Mineral	Formula	Symmetry
amorphous FeS	FeS (with coprecipitated Zn, Cd, Mn, Cu, Ni, As)	—
mackinawite	$(Fe,Ni)_9S_8$	tetragonal
smythite	$(Fe,Ni)_9S_{11}$	trigonal
greigite	$Fe^{II}Fe_2^{III}S_4$	cubic
pyrite	FeS_2	cubic
marcasite	FeS_2	orthorhombic

Conventional lime neutralization tends to form hydroxide and carbonate phases as the pH is raised by addition of CaO or $Ca(OH)_2$. A high-density-sludge process involves the addition of H_2S as a way to fix metals as secondary sulfides. The resulting sludge has improved dewatering properties. The high-density-sludge process has been chosen at Iron Mountain, California, for treatment of AMD so that the available disposal capacity for sludge in an open pit can be more efficiently utilized (U.S. EPA, 1992).

9.2.8. Miscellaneous Minerals: Arsenates, Phosphates, Halides

Secondary arsenates, phosphates, and halide minerals can form naturally in oxidized zones of *in-situ* sulfide deposits as well as in weathered zones of tailings and waste rock. Some of the more common minerals are listed in Table 9.12. The most common arsenate mineral is probably scorodite $Fe^{III}AsO_4.2H_2O$, which forms as an alteration product of arsenopyrite. Mansfieldite $AlAsO_4.2H_2O$ is the aluminum analogue to scorodite and can be found in aluminum-rich environments such as the advanced argillic alteration at Summitville, Colorado (R. Stoffregen, personal communication). The solubility of scorodite has been discussed by Dove and Rimstidt (1985), Robbins (1987), and Nordstrom and Parks (1987).

Another relatively common group of arsenate minerals is the beudantite group, isostructural with alunite and jarosite. The arsenate ion AsO_4^{3-} contains the most oxidized form of arsenic, $As^{(v)}$. Substitution in beudantite of AsO_4^{3-} for one of the sulfate groups in jarosite creates a charge imbalance which is satisfied by the presence of a full mole of Pb on the *A* site, similar to that which occurs in beaverite (Table 9.3.).

Substitution of phosphate PO_4^{3-} for SO_4^{2-} in alunite has a similar effect as for arsenate, resulting in the corkite group of minerals (Table 9.12). Other phosphate-bearing members of the extended alunite group are svanbergite, woodhouseite, and crandallite, which tend to contain Sr and (or) Ca rather than Pb. The source for phosphate in these phases is likely the destruction of primary apatite by sulfuric acid

solutions (Stoffregen and Alpers, 1987). An excellent example of compositional variability in supergene alunite-jarosite-beudantite-corkite assemblages in gossans was presented by Scott (1987). Other discussions of gossan mineralogy, textures, and geochemistry are given by Blain and Andrew (1977), Andrew (1980), and Boyle (1994).

Table 9.12. Selected phosphate, arsenate, and halide minerals

Mineral	Formula
vivianite	$Fe_3^{II}(PO_4)_2.8H_2O$
strengite	$Fe^{III}(PO_4).2H_2O$
variscite	$Al(PO_4).2H_2O$
berlinite	$Al(PO_4)$
crandallite	$CaAl_3(PO_4)_2(OH)_5.H_2O$
svanbergite	$SrAl_3(PO_4)(SO_4)(OH)_6$
woodhouseite	$CaAl_3(PO_4)(SO_4)(OH)_6$
corkite	$PbFe_3^{III}(PO_4)(SO_4)(OH)_6$
pyromorphite	$Pb_5(PO_4)_3Cl$
pseudomalachite	$Cu_5(PO_4)_2(OH)_4.H_2O$
scorodite	$Fe^{III}(AsO_4).2H_2O$
mansfieldite	$Al(AsO_4).2H_2O$
pharmacosiderite	$KFe_4^{III}(AsO_4)_3(OH)_4.6\text{-}7H_2O$
beudantite	$PbFe_3^{III}(AsO_4)(SO_4)(OH)_6$
chlorargyrite	Ag(Cl,Br,I)
bromargyrite	AgBr
boleite	$Pb_{26}Ag_9Cu_{24}Cl_{62}(OH)_{48}$
atacamite paratacamite	$Cu_4Cl_2(OH)_6$

Other common phosphate minerals of aluminum and iron may form when acidic water containing Al and Fe mix with phosphate-rich waters. An example is waters with high nutrients such as sewage effluent.

Supergene halides have been exploited as a high-grade surficial weathering product of sulfide ores. Many halide minerals are quite soluble, whereas others such as chlorargyrite are extremely insoluble. Halides tend to persist only in extremely dry climates, and may be present as ephemeral phases in the dry season where Cl, B, or I are present from natural causes (*e.g.*, sea spray) or anthropogenic factors (*e.g.*, road salt).

9.3. DETERMINATION OF SOLUBILITY CONTROL

The precipitation and dissolution of secondary minerals can effectively limit the maximum aqueous concentrations of dissolved metals associated with inactive mine wastes. The approach to equilibrium can be described by the saturation index (*S.I.*) through the relationship

$$S.I. = \log \frac{I.A.P.}{K_{sp}} \qquad (8)$$

where *I.A.P.* is the ion activity product determined from observed solution concentrations following the appropriate activity and speciation calculations, and K_{sp} is the theoretical solubility product adjusted to the observed water temperature. An *S.I.* <0 indicates water undersaturated with respect to a mineral phase, *S.I.* >0 indicates supersaturation, and *S.I.* = 0 indicates equilibrium conditions. Equilibrium conditions with respect to an observed mineral phase suggest that precipitation or dissolution of that phase controls the dissolved concentrations of the components contained in the phase.

Solubility controls on aqueous concentrations of dissolved metals have been inferred at many mine sites. An example is the Heath Steele mine tailings impoundment, near Newcastle, New Brunswick (Boorman and Watson, 1976; Blowes *et al.*, 1991, 1992, 1994). Oxidation of the sulfide-rich tailings has released high concentrations of dissolved metals to the tailings pore-waters, including up to 60 g/L Fe(II), 95 g/L SO_4, 6 g/L Zn, and 15 g/L Pb. Geochemical calculations conducted using PHRQPITZ (Plummer *et al.*, 1988) and MINTEQA2 (Allison *et al.*, 1990) indicated that pore-water samples collected from near the depth of a cemented hardpan layer approach saturation with respect to melanterite $FeSO_4.7H_2O$, gypsum $CaSO_4.2H_2O$, and anglesite $PbSO_4$ (Blowes, 1990). Mineralogical study has confirmed the presence of these phases in the shallow tailings near the depth of the hardpan layer.

Precipitation and dissolution of the sulfate-bearing secondary minerals melanterite, gypsum, and anglesite are rapid and seem to limit the dissolved concentrations of Fe(II), Ca, Pb, and SO_4. Melanterite is a soluble sulfate mineral, and high concentrations of Fe(II) >60 g/L are observed. Gypsum is less soluble, and dissolved concentrations of Ca are consistently <800 mg/L. Anglesite is relatively insoluble, and relatively low concentrations of Pb (<20 mg/L) are maintained by anglesite solubility. In contrast to anglesite, one of the more common zinc-bearing sulfate minerals, goslarite $ZnSO_4.7H_2O$, is very soluble, and dissolved Zn concentrations in excess of 6 g/L are observed in the shallow tailings. Below the hardpan layer the carbonate content of the tailings pore-water approaches saturation with respect to siderite $FeCO_3$ (Ptacek and Blowes, 1994). The occurrence of siderite in the tailings has been confirmed through mineralogical study.

Precipitation and dissolution reactions can have both beneficial and detrimental effects in mine wastes. Precipitation of relatively insoluble minerals, such as anglesite, can maintain low concentrations of dissolved metals in the tailings pore-water while an increasing mass of the metal accumulates in the tailings solids. After the most intense period of sulfide oxidation and dissolved-metal release has passed, the dissolution of secondary precipitates can contribute dissolved metals to the tailings pore-waters for long periods of time. Dissolution of secondary minerals may result in increases in the concentrations of dissolved metals if the concentration of the anion contained in the mineral decreases. This may occur in a tailings impoundment as the rate of sulfide oxidation slows and SO_4 concentrations decrease. In this situation, there is potential for increases in dissolved-metal concentrations.

9.4. CONCLUDING REMARKS

This Chapter has reviewed several groups of secondary minerals that influence water chemistry in the vicinity of mine wastes. Soluble sulfate minerals of iron and other transition metals form readily from acid-sulfate drainage in virtually all climates during periods of drying. Evaporation is clearly an important mechanism in the formation of these salts and is most likely to occur at interfaces between saturated and unsaturated conditions in the presence of air.

Rapid dissolution of soluble salts occurs during wetting events and can result in significant increases in certain metal concentrations (*e.g.*, Cu, Al) during high-flow flushing events, with severe effects on ecosystems. Aqueous speciation—saturation computations can aid in interpretation of water chemistry by indicating the minerals likely to dissolve or to precipitate from water of a known composition.

Less-soluble sulfate minerals, including the hydroxy-sulfate minerals of the alunite-jarosite group, can also incorporate transition metals in solid-solution substitution. These minerals, because of their relatively slow dissolution rates, are less likely than the soluble sulfates to affect water quality adversely.

Iron and aluminum oxyhydroxide and hydroxysulfate minerals commonly precipitate from acid drainage in response to a variety of reactions, most commonly either by neutralization in response to mineral hydrolysis (see Ptacek and Blowes, this Volume) or by mixing with waters of higher pH. Oxidation of iron from Fe^{2+} to Fe^{3+} is also an important factor in the formation of secondary iron minerals. The mineralogy of secondary Fe^{III} precipitates is complex and depends on solution composition, pH, temperature, and the rate of Fe^{2+} oxidation.

Concentrations of transition metals (*e.g.*, Cu, Zn, Cd, Ni) and semi-metals (*e.g.*, As) in acid drainage are commonly affected by sorption and coprecipitation with hydrous Fe^{III} oxides. Substantial progress has been made in modelling metal sorption

processes on monomineralic substrates in the laboratory, but much work remains to be done in the quantitative application of sorption models to complex natural systems.

9.5. DISCLAIMER

This Chapter is not an authorized publication of the U.S. Geological Survey and has not received approval from the Director.

Chapter 10

Acid-neutralization Mechanisms in Inactive Mine Tailings

David W. Blowes
Waterloo Centre for Groundwater Research
Department of Earth Sciences
University of Waterloo
Waterloo, Ontario N2L 3G1

Carol J. Ptacek
National Water Research Institute
Environment Canada
Burlington, Ontario L7R 4A6

10.1. INTRODUCTION

The oxidation of sulfide minerals and consequent release of acid in tailings impoundments can last for decades to centuries. When H^+ released by sulfide oxidation contacts carbonate- hydroxide-, and other base-containing solids, a sequence of pH-buffering reactions occurs. Acid-neutralization reactions result in an increase in the pore-water pH. This increase in pH is frequently accompanied by the precipitation of metal-bearing hydroxide and hydroxysulfate minerals that remove dissolved metals from the moving water within the tailings pores. Acid-neutralization and mineral-precipitation reactions that occur at the location of sulfide oxidation can decrease the rate of oxidation through the formation of inhibitory mineral coatings. Acid-neutralization reactions that occur at and downgradient of the location of sulfide oxidation can decrease the rate of transport of H^+ and dissolved metals away from the source area.

The dissolution of carbonates and simple-hydroxide minerals is generally rapid relative to transport rates, and the tailings pore-water commonly attains near-equilibrium conditions with respect to these solids. Dissolution of carbonates releases alkali and metal cations, including Ca, Mg, Fe, and Mn. These cations participate in the formation of secondary solids, including simple hydroxide solids, which, in some cases, can later dissolve and contribute to acid neutralization. Accompanying the

equilibrium dissolution of carbonate and hydroxide minerals is the slower dissolution of aluminosilicate minerals. Throughout the duration of dissolution of carbonate and hydroxide minerals, aluminosilicate minerals also are dissolving, are consuming H^+ ions, and are contributing base cations (Ca, Mg, Fe(II)), alkali elements (Na, K), and dissolved Si and Al to the tailings pore-water. In general, aluminosilicate dissolution is not rapid enough to attain equilibrium between the tailings pore-water and the aluminosilicate solids. As the readily soluble carbonate and hydroxide minerals are depleted, however, the significance of acid neutralization by the more stable aluminosilicate minerals becomes evident.

Tailings impoundments and underlying aquifers are complex hydrogeological environments (Robertson, this Volume) that are characterized by a large number of dissolved constituents and a number of potentially reactive minerals, each contributing to the chemical evolution of the tailings pore-water. Predictions of the temporal effects of acid-neutralization reactions on the release and transport of H^+ and dissolved metals require knowledge of the physical setting of the impoundments, the mineralogy of the pH-buffering solids, and an understanding of the sequential nature of pH-buffering reactions, as well as information on how these reactions proceed under conditions of dynamic flow. The results of field studies indicate that acid neutralization in mine wastes and underlying aquifers occurs through a complex series of reactions (Smyth, 1981; Morin, 1983; Dubrovsky, 1986; Morin *et al.*, 1988a; Blowes, 1990; Blowes and Jambor, 1990; Blowes *et al.*, 1994). It is necessary to investigate the benefits and effects of these pH-buffering reactions because of the variety of metal-bearing sulfide minerals present in base- and precious-metal tailings impoundments, and because the mobilities of many of the metals derived from oxidation of these sulfide minerals varies with changing pH.

10.2. PHYSICAL CHARACTERISTICS OF MINE-TAILINGS ENVIRONMENTS

10.2.1. Tailings Impoundments

The physical hydrogeology of tailings impoundments is described by Robertson (Chapter 1). The interaction between the physical flow-system and geochemistry of the tailings impoundment is illustrated schematically in Figure 10.1. Sulfide-oxidation reactions occur in the vadose zone of the impoundment where oxygen diffusion through the partly water-saturated tailings is rapid. Sulfide-oxidation reactions release H^+, SO_4, Fe(II) and other metals to the infiltrating water. Simulations conducted using the model of Davis and Ritchie (1986) indicate that, under conditions typical of tailings impoundments in central and eastern Canada, sulfide-oxidation reactions will continue for periods of decades to centuries (Blowes, 1990). The concentrations of dissolved constituents in the vadose zone, however, will vary depending on: the sulfide content of

the tailings, the rate of oxygen transport into the tailings, the rate of sulfide oxidation and metal release, the velocity of groundwater moving through the tailings, and the extent of attenuation of dissolved species within the tailings. In general, the rate of sulfide oxidation and dissolved-metal release is greatest shortly after tailings deposition ends, because O_2 gas can diffuse rapidly across the short distance between the tailings surface and the depth of active sulfide oxidation. As the near-surface sulfide minerals are depleted, the rate of sulfide oxidation slows as the length of the O_2-gas diffusion path increases. Also, because the diffusivity of the tailings material decreases as the moisture content increases, the rate of oxidation slows in the increasingly water-saturated tailings present deeper in the impoundment (Blowes and Jambor, 1990).

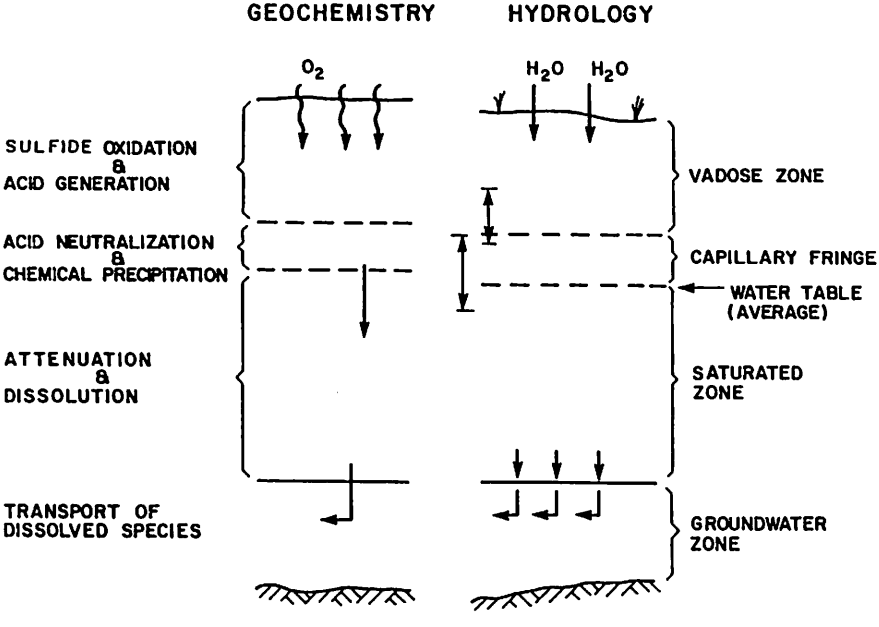

Figure 10.1. Dominant hydrogeologic and geochemical processes controlling metal migration in mine wastes.

The changing rate of sulfide oxidation is evident in the distribution of dissolved sulfate observed in many impoundments. For example, field measurements of dissolved-sulfate concentrations made at the Copper Cliff tailings area near Sudbury, Ontario show maximum concentrations of sulfate at depths between 2 m and 5 m below the tailings surface (Fig. 10.2; Coggans *et al.*, 1994). Comparison of these sulfate concentrations with the groundwater ages determined using tritium concentrations (Robertson, this Volume) suggests that the maximum sulfate concentrations were derived from sulfide-oxidation reactions occurring shortly after tailings deposition ceased. Comparison of the sulfate concentrations observed at the Copper Cliff site to

the distribution of low-pH conditions shows that the effect of acid-neutralization reactions in the low-pH conditions are limited to the shallow zones of the tailings.

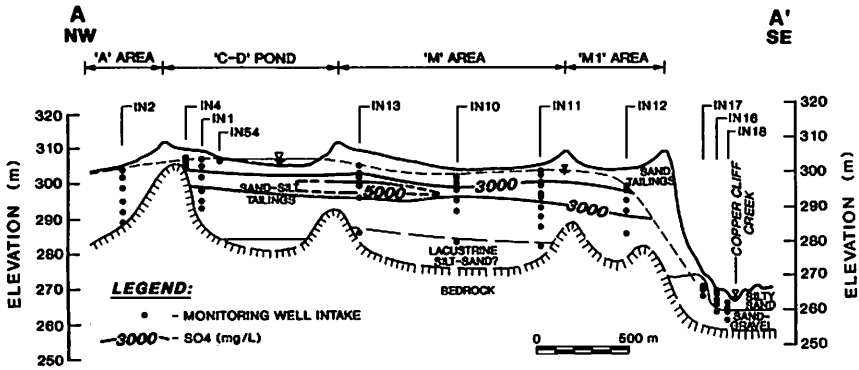

Figure 10.2. Concentrations of dissolved SO_4 along a north-south cross-section of the Copper Cliff mine-tailings impoundment.

10.2.2. Aquifers

Tailings-derived discharge water, containing high concentrations of dissolved constituents as a result of sulfide-oxidation reactions, may be released directly to surface-water bodies, or may infiltrate into underlying aquifers. When released to underlying aquifers, further attenuation of sulfide-oxidation products may occur as the tailings-derived water migrates through the aquifer material. Attenuation of sulfide-oxidation products may be enhanced by the longer residence time available within the aquifer and by changes in the aquifer mineralogy. Because attenuation reactions occur not only in the tailings, but also in the surrounding geological materials, predictions of acid and metal migration rates require consideration of the groundwater flow paths, the duration of contact between the tailings discharge-water, and reactive solid phases contained in the tailings and in underlying and adjacent aquifers.

10.3. ACID-PRODUCTION MECHANISMS AND RATES IN TAILINGS

The principal reactions that generate H^+ are the oxidation of sulfide minerals, oxidation of Fe^{2+} and hydrolysis of Fe^{3+}, and precipitation of metal hydroxide and hydroxysulfate phases. The most common sulfide minerals in base- and precious-metal mine tailings are pyrite FeS_2, and pyrrhotite $Fe_{(1-x)}S$. The oxidation of pyrite produces two moles of H^+ for each mole of pyrite oxidized through the reaction:

$$FeS_2 + 7/2\ O_2 + H_2O \Rightarrow Fe^{2+} + 2SO_4^{2-} + 2H^+ \qquad (1)$$

Subsequent oxidation of Fe^{2+}, and hydrolysis and precipitation of $Fe(OH)_3$, produce an additional two moles of H^+, resulting in the overall reaction:

$$FeS_2 + 15/4\ O_2 + 7/2\ H_2O \Rightarrow Fe(OH)_3 + 2\ SO_4^{2-} + 4\ H^+ \qquad (2)$$

The precipitation of other Fe(III)-bearing phases, such as goethite α-FeOOH, or schwertmannite $Fe_8O_8(OH)_6SO_4$ (Bigham *et al.*, 1990; Bigham, this Volume) may occur, releasing differing amounts of H^+. Alternatively, Fe^{3+} may be consumed through further oxidation of sulfide minerals, *e.g.*

$$FeS_2 + 14\ Fe^3 + 8\ H_2O \Rightarrow 15Fe^{2+} + 2SO_4^{2-} + 16^+ \qquad (3)$$

In many tailings impoundments, particularly those resulting from the concentration and recovery of nickel, pyrrhotite is the most abundant sulfide mineral. Oxidation of pyrrhotite may proceed to completion through the reaction:

$$Fe_{(1-x)}\ S + (2-x/2)\ O_2 + xH_2O \Rightarrow (1-x)\ Fe^{2+} + SO_4^{2-} + 2xH^+ \qquad (4)$$

or may proceed to partial completion, generating Fe^{2+} and elemental S^0 through the reaction:

$$Fe_{(1-x)}S + (2-2x)Fe^{3+} \Rightarrow (3-3x)\ Fe^{2+} + S_{(S)}^0 \qquad (5)$$

This elemental S^0 may be subsequently oxidized to SO_4^{2-}. Partial oxidation of pyrrhotite, resulting in accumulation of $S^0_{(S)}$, has been observed at several tailings sites, including two Ni mine-tailings impoundments (Coggans *et al.*, 1994; Jambor and Owens, 1993), and a Cu-Zn mine-tailings impoundment (Jambor, 1987c; Blowes and Jambor, 1990).

In the zone of active sulfide oxidation, in the near-surface zone of the tailings where oxygen transport by gas-phase diffusion is rapid, the weathering of sulfide minerals may be complete (equation 2), resulting in the formation of stable secondary precipitates such as goethite, or incomplete, with some of the Fe derived from the initial sulfide remaining in solution as dissolved Fe^{2+} (equation 1). Ferrous-iron-bearing sulfate and hydroxide minerals are relatively soluble. As a result, dissolved Fe^{2+} concentrations contained in tailings pore water may be high (up to 70 g/L; Blowes *et al.*, 1991). This dissolved Fe^{2+} is displaced along groundwater flow-paths and is ultimately discharged to the surface-water flow system, where oxidation to Fe^{3+} and precipitation of ferric oxyhydroxide phases result in the generation of H^+ in the surface-water bodies (Figure 10.3; Dubrovsky *et al.*, 1984a; Coggans *et al.*, 1994).

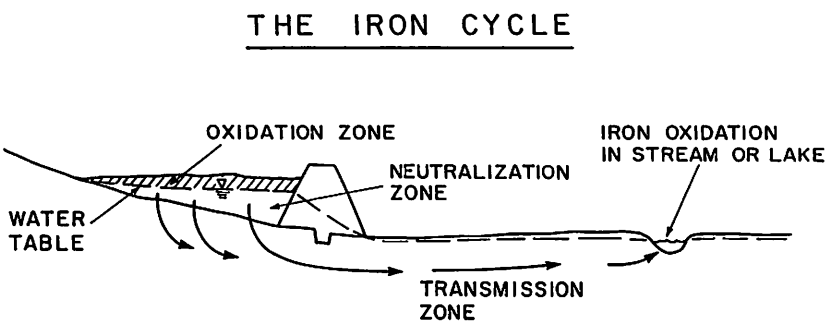

Figure 10.3. Schematic cross-section of tailings impoundment showing cycling of Fe along a flowpath.

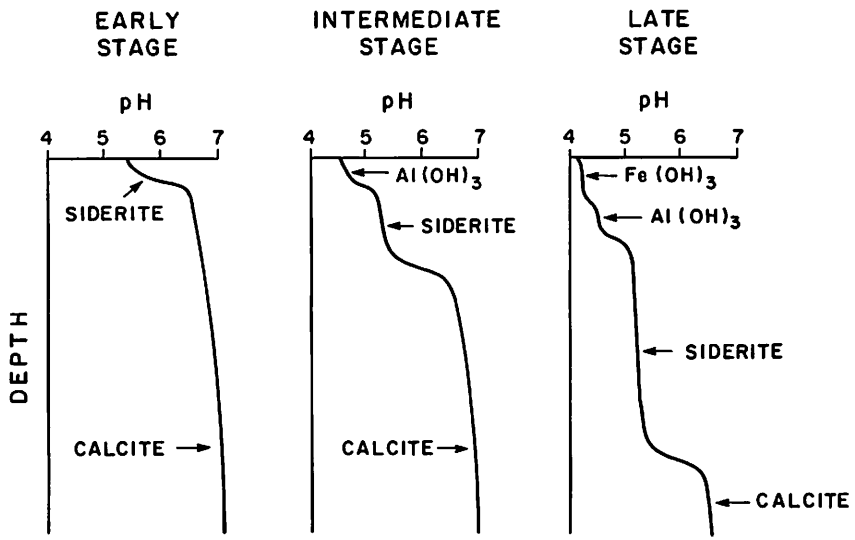

Figure 10.4. Development of pH-buffering zones during early, intermediate, and late stages of sulfide oxidation.

10.4. IMPORTANT ACID-NEUTRALIZATION REACTIONS

The principal acid-neutralization mechanisms in inactive mine-tailings impoundments are carbonate-mineral dissolution, hydroxide-mineral dissolution, and aluminosilicate-mineral dissolution (Table 10.1). Unlike sulfide-oxidation reactions, many acid-neutralization reactions are independent of gas-phase O_2 concentrations. Acid-neutralization reactions can occur along the groundwater flowpath throughout the tailings impoundment and underlying aquifers, limited only by the availability of

acid-consuming mineral phases. These H^+-consuming reactions result in the general increase in pH with increasing depth that is observed at many tailings impoundments (Figure 10.4; Dubrovsky *et al.*, 1984a; Morin *et al.*, 1988a; Blowes and Jambor, 1990; Blowes *et al.*, 1991; Coggans *et al.*, 1994). Consequently, the water present near the base of tailings impoundments, or present in aquifers underlying the impoundments, is usually near-neutral in pH, but may contain high concentrations of potentially acid-generating Fe^{2+}.

Field studies conducted at a number of impoundments indicate that there are series of equilibrium pH-buffering reactions controlling the pH of the tailings pore water (Smyth, 1981; Dubrovsky *et al.*, 1984a; Blowes and Jambor, 1990; Johnson, 1993; Blowes *et al.*, 1994). These series are similar to those which Morin *et al.* (1988a) observed in a plume of tailings-derived water moving outward from beneath the Nordic Main uranium-tailings impoundment near Elliot Lake, Ontario, at which the sequence follows the order: calcite dissolution, siderite dissolution, $Al(OH)_3$ dissolution, and $Fe(OH)_3$ dissolution. Each of these mechanisms is discussed in greater detail below.

Mineral	Formula
Carbonates	
Calcite	$CaCO_3$
Dolomite	$CaMg(CO_3)_2$
Siderite	$FeCO_3$
Ankerite	$Ca(Fe,Mg)(CO_3)_2$
Hydroxides	
Gibbsite[1]	$Al(OH)_3$
Ferrihydrite[1]	$Fe(OH)_3$
Goethite	α-FeOOH
K-Jarosite	$KFe_3(SO_4)_2(OH)_6$
Aluminosilicates	
Chlorite	$(Mg,Al,Fe)_6(Si,Al)_4O_{10}(OH)_8$
Muscovite	$KAl_2(Si_3Al)O_{10}(OH,F)_2$
Alakali Feldspars	$(K,Na)AlSi_3O_8$
Plagioclase Feldspars	$NaAlSi_3O_8-CaAl_2Si_2O_8$
Pyroxene Group	
Amphibole Group	

[1] Or equivalent amorphous phases

Table 10.1. Principal pH-buffering phases in mine-tailings impoundments

10.5. pH-BUFFERING SEQUENCES IN MINE TAILINGS

10.5.1. Carbonate Dissolution

The most significant of the pH-buffering reactions in mill tailings involve the dissolution of carbonate minerals (Table 10.1). Reactions involving carbonate-mineral dissolution in mine wastes are among the few that have the potential to maintain the near-neutral pH conditions required to prevent the extensive release and transport of dissolved metals. Carbonate-dissolution reactions follow the general form for calcite:

$$CaCO_3 + H^+ \Leftrightarrow Ca2^+ + HCO_3^- \qquad (6)$$

These reactions consume carbonate minerals and H^+, release dissolved cations to the tailings pore water, and increase pore-water alkalinity concentrations. At many tailings impoundments the first indication of sulfide-oxidation reactions is a sharp increase in the pore-water or discharge-water alkalinity.

Depletion of carbonate minerals in the low-pH zone of tailings impoundments is observed at many field sites. An increase in solid-phase carbonate content is generally accompanied by an increase in pore-water pH as carbonate neutralization affects the tailings pore water. In general, the order of carbonate depletion begins with calcite, which is followed by dolomite, ankerite, and siderite. This order of depletion is controlled partly by equilibrium mass-action constraints and by kinetic limitations. Calcite dissolution proceeds rapidly. In most locations, the rate of dissolution is sufficient to maintain near-equilibrium conditions with respect to calcite, and to maintain the pore-water pH in the range 6.5—7.5. Dissolution of dolomite is slower, and disequilibrium is commonly observed. Disequilibria, and near-equilibrium conditions, have been observed for siderite.

In the initial stages of sulfide oxidation and acid generation, the dissolution of calcite, the most soluble of the normally occurring carbonate minerals, is favored. Under the intermediate-pH conditions developed in the carbonate-dissolution zone, the precipitation of amorphous and crystalline metal-hydroxide solids and carbonates is favored. Under intermediate-pH conditions, the activity of hydroxide is sufficiently high to lead to the precipitation of sparingly soluble hydroxide solids through reactions of the form:

$$Me^{n+} + nOH^- \Leftrightarrow Me(OH)_{n(s)} \qquad (7)$$

where *Me* represents a metal cation, and *n* is the stoichiometric coefficient. Dissolution of calcite (equation 6) also releases HCO_3^- to the tailings pore water, which, combined with the Fe^{2+} released by sulfide oxidation, can lead to saturation or supersaturation with respect to those carbonates with solubilities lower than that of calcite. For example, precipitation of siderite through a reaction of the form (Morin and Cherry,

1986; Ptacek and Blowes, 1994):

$$HCO_3^- + Fe^{2+} \Leftrightarrow FeCO_3 + H^+ \qquad (8)$$

has been suggested to be an important reaction that limits dissolved Fe concentrations at tailings sites. Geochemical studies conducted at a number of impoundments and in aquifers affected by tailings discharge-water (Morin and Cherry, 1986; Dubrovsky, 1986; Blowes *et al.*, 1991; Johnson, 1993; Coggans *et al.*, 1994; Blowes *et al.*, 1994) have shown that the tailings pore-water and groundwater are supersaturated or near-saturated with respect to siderite. In an aquifer receiving tailings discharge, Morin and Cherry (1986) postulated that precipitation of secondary siderite may decrease groundwater concentrations of dissolved Fe(II) and may result in the accumulation of a secondary acid-neutralizing buffer. Morin and Cherry were unable to isolate secondary siderite in the aquifer solids, possibly because of oxidation of siderite during sample handling, or because the quantities anticipated to have precipitated were below the analytical detection limit. At a TiO_2 recovery plant, where the geochemical environment is very similar to that occurring at mine-tailings sites, the formation of secondary siderite and ferroan calcite was observed in a calcite-bearing aquifer receiving acidic Fe^{2+}-bearing discharge water (Ho *et al.*, 1984; Wajon *et al.*, 1985). The presence of secondary siderite in tailings environments where primary siderite is absent in the tailings or aquifer solids has not been observed directly, but is inferred through geochemical calculations of siderite saturation indices. At sites where siderite comprises a significant proportion of the primary carbonate content of the tailings, supersaturation or near-saturation with respect to siderite has been observed, but the occurrence of secondary siderite has not been confirmed (Blowes *et al.*, 1991, 1994).

Following the depletion of calcite, the pore-water pH declines abruptly, and the pore water becomes near-saturated or slightly undersaturated with respect to siderite. The dissolution of siderite, including primary and secondary forms, is inferred. As siderite dissolves, the pH is buffered to between 4.8 and 6.3. Under these moderate-pH conditions resulting from siderite dissolution, adsorption or coprecipitation of many dissolved metals is favored, resulting in continued removal of these elements from the moving water.

10.5.2. Hydroxide Dissolution

In the calcite- and siderite-buffered zones the precipitation of metal hydroxides or hydroxysulfates, including gibbsite, amorphous $Al(OH)_3$, amorphous $Fe(OH)_3$, ferrihydrite, goethite, and schwertmannite, is favored, leading to the accumulation of these solids as cements or grain coatings. Ferric iron contained in these phases is derived from the sulfide-oxidation reactions occurring in the shallow tailings. Dissolved Al is derived from the dissolution of aluminosilicate minerals. As acid generation continues, and the carbonate minerals are depleted, the pH declines abruptly until the

dissolution of the next pH buffer in the series, $Al(OH)_3$, is favored. Dissolution of $Al(OH)_3$ buffers the pH to values between 4.0 and 4.3. When $Al(OH)_3$ is completely consumed the pH again declines, favoring the dissolution of $FeOH_3$, and resulting in pH values that fall below 3.5. These pH-buffering reactions, dissolution of $Al(OH)_3$ and $Fe(OH)_3$, have also been observed to be near-equilibrium reactions under the flow regimes observed at typical tailings sites.

10.5.3. Aluminosilicate Dissolution

Under very low-pH conditions, after all carbonates and simple hydroxides are depleted, the dissolution of aluminosilicate minerals becomes an important acid-neutralization mechanism. Evidence for aluminosilicate dissolution is the increase in Si and Al concentrations in the tailings pore water. Dissolution of aluminosilicate minerals is frequently slower than the rate of movement of tailings pore water, leading to the development of pore-water compositions that are undersaturated with respect to the aluminosilicate minerals in the tailings. The principal groups of aluminosilicate minerals present in tailings are summarized in Table 10.1. Dissolution of aluminosilicates may occur congruently, to result in complete solubilization, or incongruently, to result in the depletion of the original mineral and formation of a second, more stable, mineral. The extent of acid neutralization resulting from each aluminosilicate-dissolution reaction depends on the degree of completion of the reaction. In addition, as sulfide oxidation and acid generation continue, products from initial incongruent-dissolution reactions may dissolve, resulting in additional acid neutralization.

10.6. FIELD OBSERVATIONS OF ACID NEUTRALIZATION

In the 1980s and 1990s, detailed geochemical studies were conducted at field sites in central and eastern Canada to investigate the mechanisms of sulfide oxidation, acid neutralization, and metal attenuation in tailings impoundments, and to interpret the effects of these mechanisms in the context of the hydrogeologic flow regime. The following examples are derived from field studies conducted at the old and new Heath Steele Zn-Pb tailings impoundments in New Brunswick (Figure 10.5; Blowes, 1990; Blowes *et al.*, 1991, 1994), and the Nickel Rim Ni-Cu tailings impoundment in northern Ontario (Figure 10.5; Johnson, 1993). The Heath Steele tailings contain approximately 85 wt% sulfide minerals, predominantly pyrite, and 3 wt% carbonate minerals (expressed as $CaCO_3$). The Nickel Rim tailings average 3 wt% sulfides, principally pyrrhotite, and 0.1—0.2 wt % carbonate minerals (expressed as $CaCO_3$). At both sites, sulfide oxidation and acid generation have led to the development of low-pH pore water containing high concentrations of dissolved SO_4, Fe, and other metals near the tailings surface. As this low-pH water infiltrates downward into the tailings, a series of acid-neutralization reactions occurs, leading to a general increase in pore-water pH and removal of dissolved metals with increasing depth.

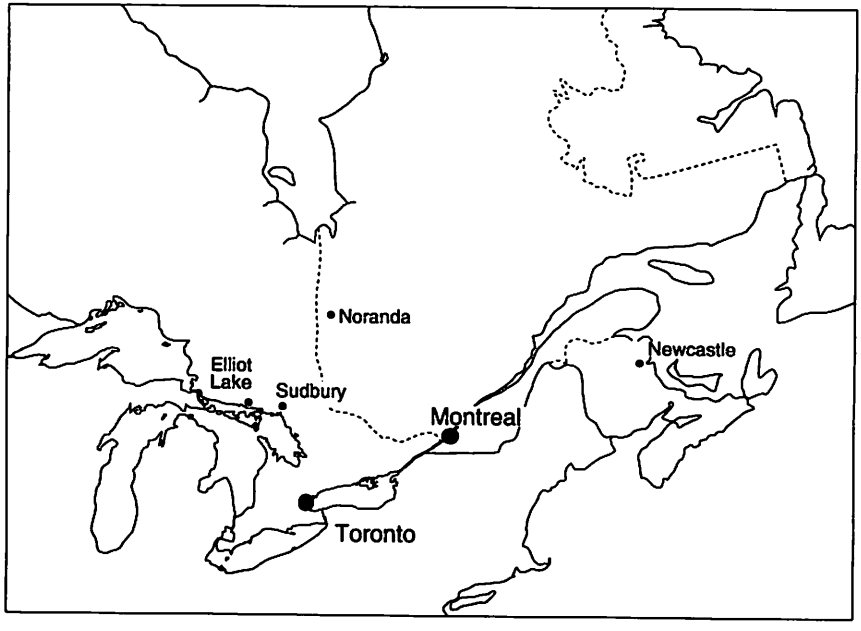

Figure 10.5. Location of study areas.

10.6.1. Heath Steele Tailings

Mineralogical study of the Heath Steele tailings indicates that the tailings, as deposited, contain calcite, dolomite and siderite (Chen and Petruk, 1980). Examination of tailings collected from the impoundment confirmed the presence of abundant dolomite and siderite, but only trace amounts of calcite (Jambor and Blowes, 1989, 1992). Measurements of the pore-water composition in the old Heath Steele tailings impoundments (Figure 10.6), coupled with geochemical calculations, suggest that as H^+ is released by sulfide-oxidation reactions, the tailings pore-water becomes undersaturated with respect to calcite and dolomite, leading to their dissolution and to buffering of the pore-water pH to between 6.5 and 7.5 (Figure 10.7). Geochemical equilibrium calculations suggest that the precipitation of siderite, $Al(OH)_3$, and $Fe(OH)_3$ is favored as calcite and dolomite dissolve. When calcite is completely consumed, the pore-water pH declines abruptly, favoring dissolution of the primary siderite present as gangue material. Although geochemical calculations suggest the formation of secondary siderite, no secondary siderite was detected during the mineralogical study (Jambor and Blowes, 1989, 1992).

After siderite is completely consumed, the pH again declines abruptly until the dissolution of the next pH buffer in the series, $Al(OH)_3$, is favored. Dissolution of $Al(OH)_3$ buffers the pH to values between approximately 4.0 to 4.3. Although geoche-

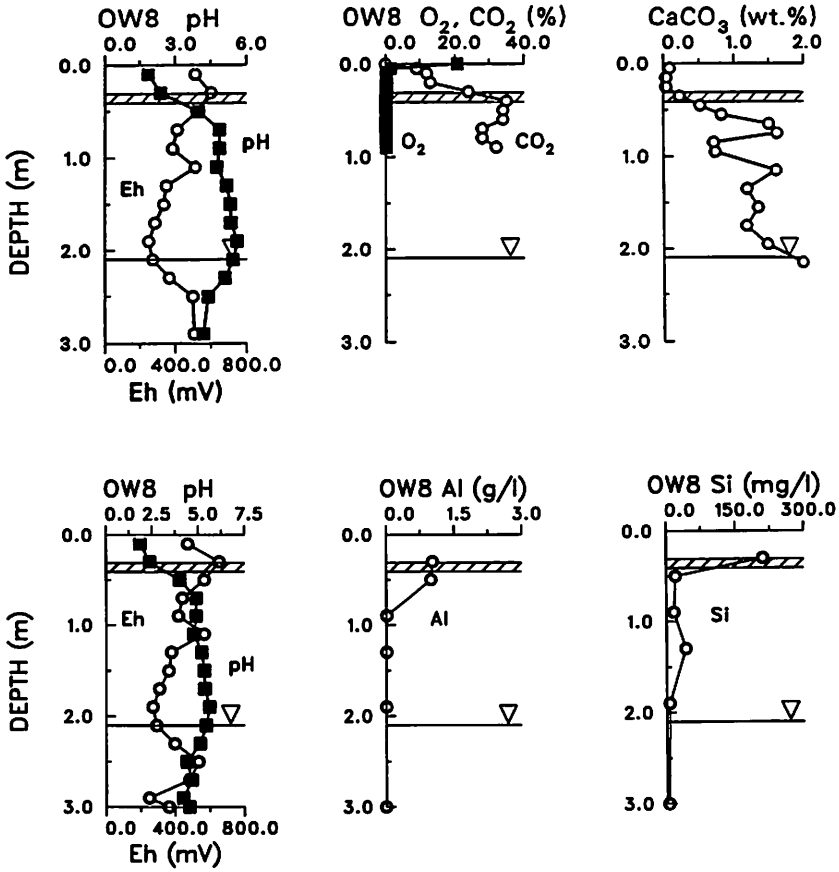

Figure 10.6. Pore-water pH, Eh, and concentrations of dissolved constituents in the old Heath Steele tailings impoundment, New Brunswick.

mical calculations suggest the formation of an $Al(OH)_3$ phase, none was detected during the mineralogical study. The mineralogical study did indicate the presence of two aluminum hydroxysulfate precipitates. One of these precipitates had an approximate stoichiometry $(Fe,Al)_{2.00}(SO_4)_{3.09}$. With this formula ratio as a guide, the Debye-Scherer X-ray pattern was identified as that of alunogen $Al_2(SO_4)_3 \cdot 17H_2O$. The other phase remains to be identified. Because of the uncertainty concerning the identity of these phases, their role in pH buffering cannot be discerned. For calculation purposes, the simpler aluminum hydroxide phase $Al(OH)_3$ was assumed to be the dominant pH-buffer. This example illustrates the need for coupled geochemical and mineralogical study and the need for the refinement of our conceptual model of the geochemical evolution of mill-tailings impoundments. When the pore water becomes undersaturated with respect to $Al(OH)_3$, the pH declines, favoring the dissolution of

$Fe(OH)_3$ and other ferric hydroxide and hydroxysulfate minerals, resulting in pH values that are less than 3.5. The mineralogical study indicates that goethite is the most abundant ferric-iron-bearing precipitate. Lesser amounts of jarosite and ferrihydrite are present in the tailings (Jambor and Blowes, 1989, 1992). The dissolution of ferric oxyhydroxides buffers the pore-water pH in the range between 2.5 and 3.5. In the shallow portion of the tailings there is a paucity of ferric hydroxide precipitates, giving the thirty-year old Heath Steele impoundment the appearance of fresh, unweathered tailings. In this zone the pH ranges from 0.8—1.5, and geochemical calculations indicate undersaturation with respect to all of the ferric-iron-bearing minerals observed in the deeper tailings.

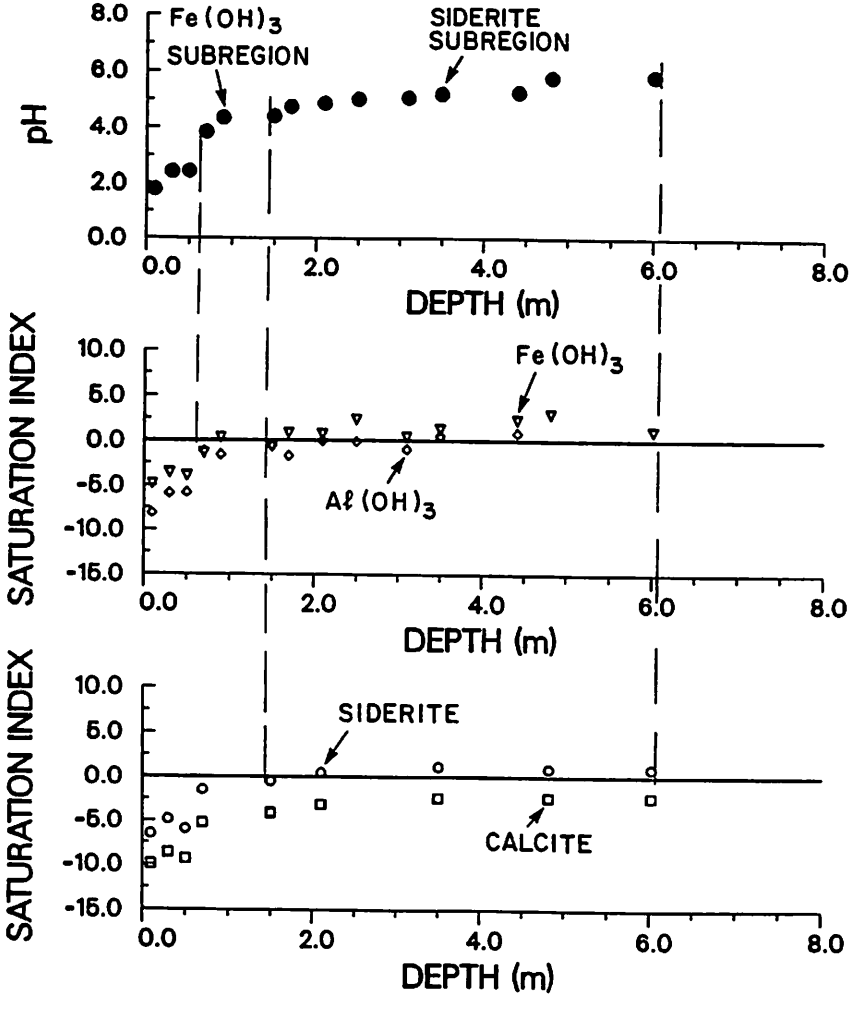

Figure 10.7. Mineral-saturation indices, calculated using MINTEQA2, versus depth, for water samples collected from the old Heath Steele tailings impoundment.

Further buffering of the pore-water pH by aluminosilicate dissolution at the Heath Steele site is evident from the high aqueous concentrations of dissolved Al and Si (up to 2,500 mg/L and 200 mg/L, respectively) under very low-pH water conditions (pH <1.5); as well, there has been the depletion of aluminosilicate solids near the tailings surface. Mineralogical study (Jambor and Blowes, 1989, 1992) indicated that a diverse silicate gangue, including chlorite, stilpnomelane, muscovite, quartz, and an Fe-bearing amphibole, is present in samples collected 80—100 cm below the tailings surface. Samples from the upper 30 cm, however, contain a less varied silicate gangue, and are extensively depleted in chlorite, stilpnomelane, and amphibole relative to the deeper samples (Figure 10.8). These observations suggest that aluminosilicate-dissolution reactions are contributing to acid neutralization at Heath Steele, and as sulfide oxidation continues it is anticipated that the zone of aluminosilicate removal will become more extensive, and the zone of very low-pH water will expand.

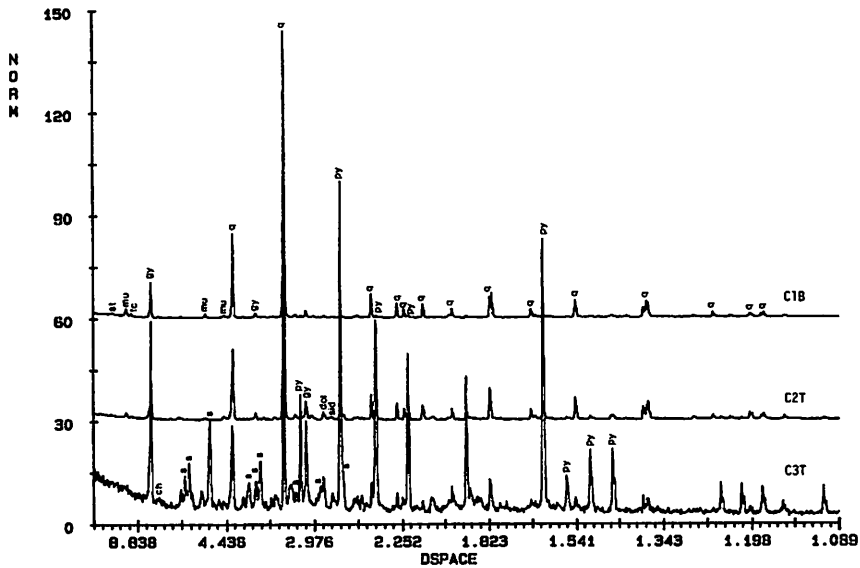

Figure 10.8. X-ray diffraction patterns *versus* depth for tailings solids collected from the old Heath Steele tailings impoundment.

10.6.2. Nickel Rim Tailings

Complete development of the equilibrium pH-buffering sequence and its effect on the mobility of dissolved metals are illustrated, in two dimensions, by observations made at the Nickel Rim Ni-Cu tailings impoundment near Sudbury, Ontario (Figure 10.9; Johnson, 1993). At this site, sulfide oxidation in the vadose zone has released H^+ to the tailings water, resulting in low-pH (2.1 <pH <3.5) conditions near the tailings surface. Interaction with H^+-consuming minerals has resulted in the progressive

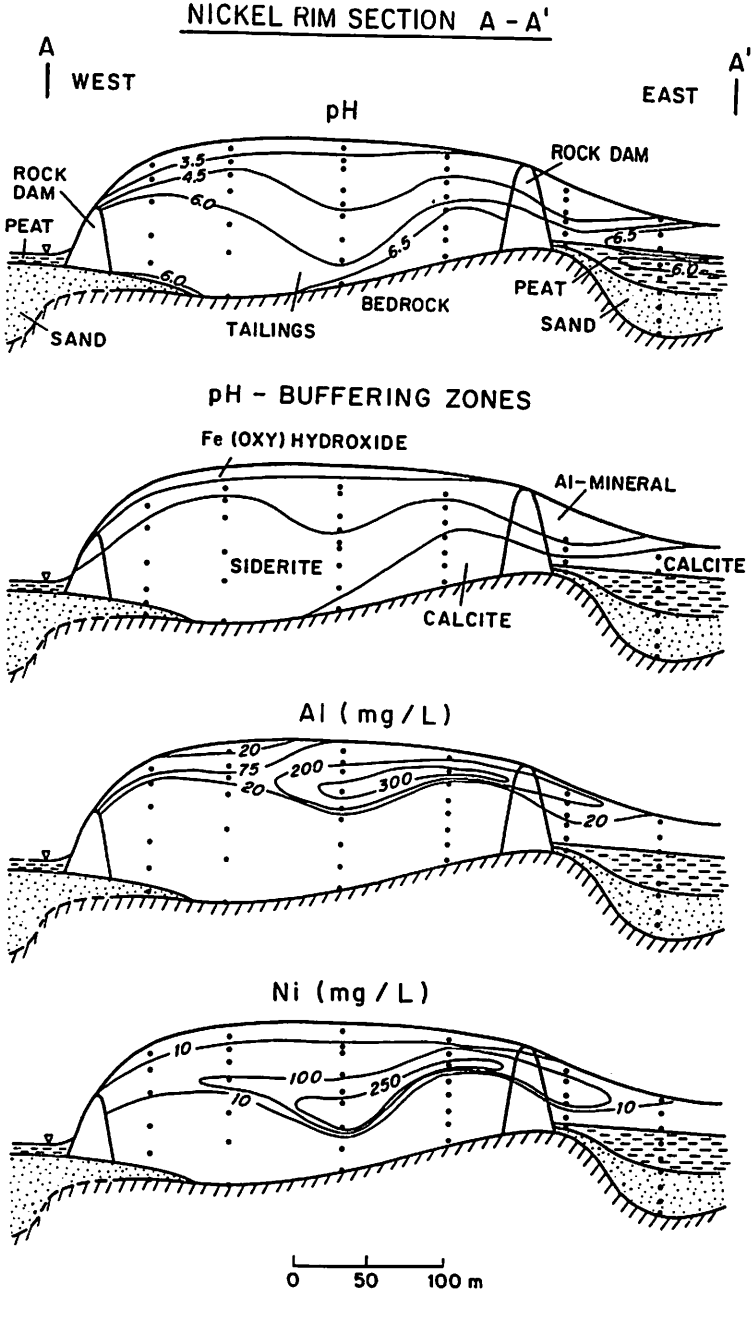

Figure 10.9. Values of pH, pH-buffering zones, and pore-water concentrations of Al and Ni in the Nickel Rim tailings impoundment near Sudbury, Ontario.

increase in pH with increasing depth. Geochemical calculations conducted using MINTEQA2 indicate that the pore water approaches or attains equilibrium with respect to $Fe(OH)_3$, $Al(OH)_3$, siderite, and calcite, forming a series of pH-buffering zones moving downward from the tailings surface. The pH-buffering zones in Figure 10.9 are labelled according to the dominant pH-buffering process. Irregularities in the shapes of these pH-buffering zones are likely the result of variations in the pore-water velocity, composition of the tailings solids, and rates of acid generation.

At the Nickel Rim site, the pH of the tailings pore-water has a strong effect on the movement of dissolved Al and Ni in the impoundment (Figure 10.9). At the interface between the Al-mineral pH-buffering zone and the siderite pH-buffering zone, the concentration of dissolved Al decreases sharply. For example, at sampling nest NR2, located in the central part of the impoundment, the dissolved-Al concentration decreases from >1,150 mg/L to <10 mg/L within a 1-m interval. In this interval the pH increases from ~4 to ~5.8. Geochemical calculations conducted using MINTEQA2 indicate that the water samples from this location are saturated or slightly undersaturated with respect to amorphous $Al(OH)_3$, and are supersaturated with respect to the crystalline aluminum hydroxide mineral gibbsite. These observations suggest that Al is removed from solution through the precipitation of an aluminum hydroxide or hydroxysulfate phase.

The concentration of dissolved Ni is also strongly dependent on the pore-water pH, showing a sharp decrease from >250 mg/L to <10 mg/L as the pH increases to above 5.8 within the siderite pH-buffering zone. Geochemical calculations conducted using MINTEQA2 suggest that the water at this depth is consistently undersaturated with respect to all of the secondary nickel-bearing hydroxide and hydroxysulfate phases included in the MINTEQA2 database. It is inferred, therefore, that Ni is removed from solution through adsorption or coprecipitation with the secondary ferric oxyhydroxide precipitates. Mineralogical study of the tailings solids indicated that goethite, which occurs near the surface of the impoundment, is Ni-bearing (Jambor and Owens, 1993), thereby supporting the idea that Ni is removed from the tailings pore water through adsorption or coprecipitation reactions.

10.6.3. Other Tailings Impoundments

Sequences of similar pH-buffering zones have been indicated to occur at a number of tailings impoundments, including the Nordic Main uranium tailings impoundment (Dubrovsky *et al.*, 1984a), the Waite Amulet Cu-Zn tailings impoundment (Blowes and Jambor, 1990), and the Copper Cliff Ni-Cu tailings impoundment (Coggans *et al.*, 1994). At these sites, the amount of time required to deplete a given mineral phase, and the relative thicknesses of the zones which were developed, are dependent on the original mass of solid-phase buffers contained in the gangue materials and on the initial mass of sulfide minerals. At sites at which the H^+

generated by sulfide oxidation is less than the acid consumed by carbonate-mineral dissolution, such as at the Delnite site (Blowes, 1990; Jambor and Blowes, 1991), the pore-water pH is controlled completely by carbonate-mineral dissolution, and this dissolution limits the development of the remaining pH-buffering zones.

10.7. MODELLING ACID-NEUTRALIZATION MECHANISMS IN MINE WASTES

The complexity of the interactions between the large number of dissolved constituents in the tailings pore waters and the large quantity of tailings solids makes it difficult to determine *a priori* the changes in pH and metal-ion mobility that are likely to occur as sulfide oxidation proceeds. Equilibrium geochemical-speciation modelling of tailings pore water and mineralogical analysis of tailings solids can be used to delineate the principal reactions that contribute to pH buffering and metal attenuation. Incorporation of the observed pH-buffering and metal-controlling reactions into an equilibrium solute-transport model permits calculations for estimating the rates of migration of dissolved metals. Using the multicomponent reactive-solute transport model MINTRAN (Frind *et al.*, 1994; Walter *et al.*, 1994a), simulations were conducted to estimate the migration of low-pH conditions through an underlying aquifer affected by acidic tailings water, and the effect of the conditions on the transport of dissolved metals (Frind *et al.*, 1994; Walter *et al.*, 1994b; Frind and Molson, this Volume). MINTRAN couples the geochemical speciation mass-transfer model MINTEQA2 (Allison *et al.*, 1990) with an efficient two-dimensional solute-transport model (Frind *et al.*, 1990). A detailed description of MINTRAN is provided by Frind and Molson (this Volume). The model, as applied in this study, includes only equilibrium reactions and is limited, therefore, to conditions in which the local-equilibrium assumption applies.

The simulations were based loosely on the description of the plume of tailings-derived water moving through an unconfined aquifer underlying the Nordic Main uranium tailings impoundment (Morin *et al.*, 1988a). The aquifer characteristics, tailings-water compositions, and background-water compositions were selected to be similar to those at the field site. The aqueous components and initial mineral reserves included in the simulation are similar to those observed by Morin and Cherry (1988). The dissolved metals observed at the Nordic site include Al, Fe(II) and Fe(III). Important mineral phases include calcite, siderite, gibbsite, gypsum, amorphous silica, and ferrihydrite. To enhance the generality of our simulation, we added higher concentrations of Pb, Cr, and Mn, and the associated mineral phases anglesite, cerussite, amorphous chromium hydroxide, and rhodochrosite. This selection of phases was based on observations we made at other field sites. In the model simulation, low-pH tailings water infiltrated into the source area of the aquifer for 24 years. The source area covers 10 m $< x <$ 30 m at the water table. The water-table boundary receives a

flux of 0.142 m/yr, the downgradient boundary has a constant head of 13.6 m, and the left and lower boundaries are impermeable. The hydraulic conductivity is 2.5 x 10^{-6} m/s, the porosity is 0.3, and the longitudinal and transverse dispersivities are 3.00 m and 0.03 m, respectively.

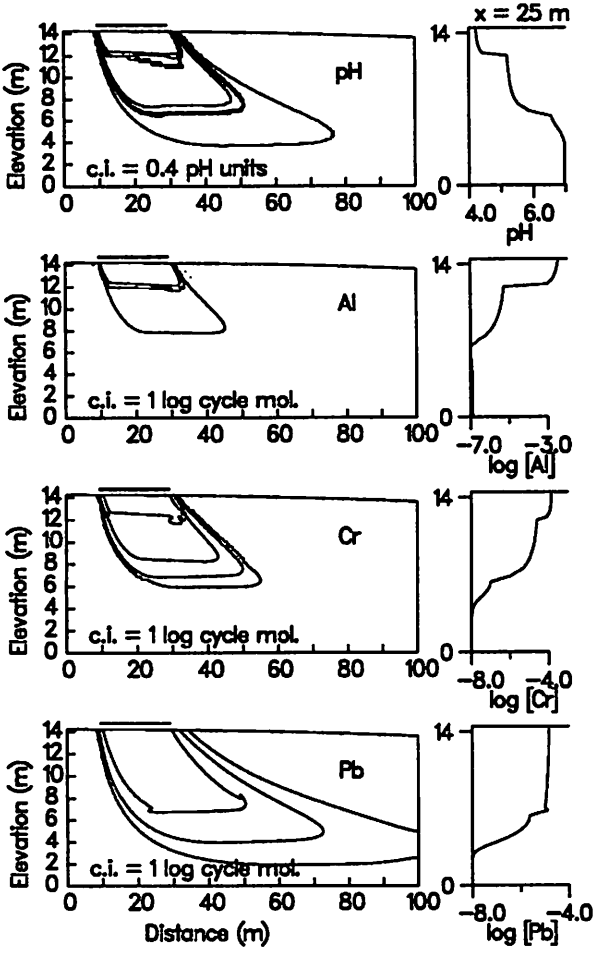

Figure 10.10. Simulated distributions of pH and concentrations of dissolved Al, Cr, and Pb in an aquifer receiving acidic discharge from a tailings impoundment at 24 years.

The results of the simulations (Figures 10.10 and 10.11) show the development of a low-pH plume moving outward from the source area. Figure 10.10 shows contours and vertical profiles at x = 25 m for pH and dissolved Al, Cr, and Pb; Figure 10.11 shows solid-phase distributions for the associated mineral phases. The pH plume contains a series of pH plateaus similar to those observed in field studies (Figure 10.10). Far from the source, the pH ranges from 7.0 to 6.5 and is near equilibrium

with respect to calcite, siderite, and gibbsite. In this region of the aquifer, calcite is dissolving and siderite and gibbsite are accumulating. Closer to the source, the pH decreases sharply as the calcite initially present in the aquifer is depleted. At this front, the water becomes undersaturated with respect to calcite, and the pH decreases from 6.5 to 5.5 (Figure 10.10) until equilibrium with respect to the second pH-buffering mineral (siderite) is attained. As siderite dissolves, the mass of gibbsite continues to increase. Near the source, the pH decreases again as the primary and secondary siderites present in the aquifer are depleted. At this front, the pH decreases from 5.2 to 4.3 (Figure 10.10) and equilibrium with respect to gibbsite controls the pH from this point to the source. In this final region, the pH varies from 4.3 to 4.1.

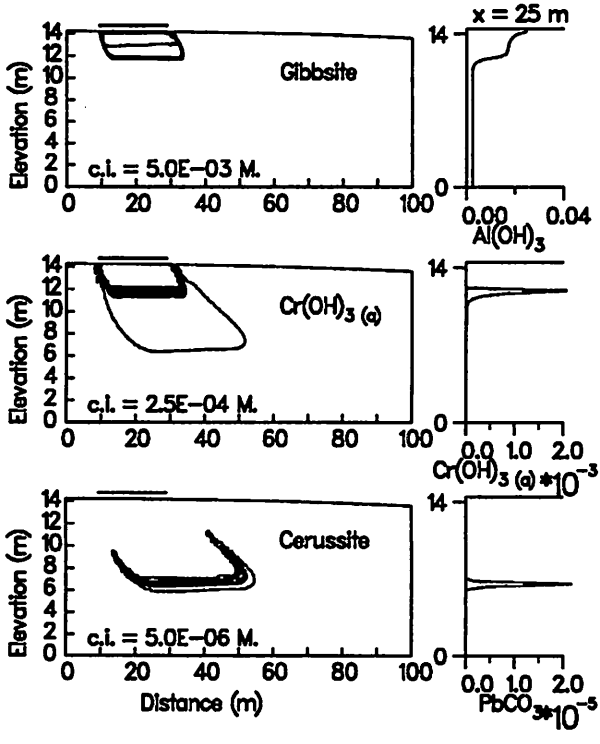

Figure 10.11. Simulated distributions of solid-phase masses of gibbsite, amorphous $Cr(OH)_3$, and cerussite in an aquifer receiving acidic discharge at 24 years.

The pH of the plume water affects the concentrations of the dissolved metals Al, Cr, and Pb, assumed to be present in the plume. The secondary phases allowed to precipitate and dissolve include gibbsite, amorphous chromium hydroxide $Cr(OH)_3$, and cerussite $PbCO_3$. The mobilities of Al and Cr are dependent directly on the pH of

the plume water, whereas the mobility of Pb is dependent on the activity of CO_3^{2-}, and is therefore indirectly dependent on the plume-water pH. The dissolved concentrations of Al and Cr show sharp decreases (Figure 10.10) that correspond with the changes in pH accompanying the siderite- and calcite-dissolution fronts. These decreases are sufficient to lower the concentration of Cr to below the recommended concentration for drinking water (<0.05 mg/L; OMOE, 1983) and to lower the Al concentration to below the maximum recommended for the protection of freshwater aquatic life (0.005 mg/L; CCREM, 1987). The decreases in dissolved Cr and Al are accompanied by increases in the masses of gibbsite and $Cr(OH)_3$ retained in the aquifer (Figures 10.10 and 10.11). The total mass of $Cr(OH)_3$ is much less than the mass of gibbsite; the greatest accumulation of $Cr(OH)_3$ occurs at the siderite-dissolution front. Lead is removed from the plume water through the precipitation of cerussite at the calcite-dissolution front. Lead concentrations, however, remain above the recommended drinking water limit (<0.05 mg/L, OMOE, 1983) downstream of the cerussite-precipitation front. Frind and Molson (this Volume) present the results of simulations of the conditions in the aquifer after the period of sulfide oxidation, at which time the sulfide minerals have been depleted or an effective sulfide-oxidation control put in place. These simulations show that the low solubilities of the metal-bearing precipitates are sufficient to maintain low concentrations of dissolved metals. The aqueous concentrations of all the metals considered, except Pb, decrease to below current regulatory guidelines shortly after the source of acidic drainage is terminated. These calculation results suggest that metals precipitated in the aquifer would be effectively immobilized if effective sulfide-oxidation controls were implemented.

10.8. IMPLICATIONS OF ACID-NEUTRALIZATION REACTIONS

10.8.1. Role of Acid Neutralization in Determining Sulfide-oxidation Rates

Acid-consuming reactions affect both the rate of sulfide oxidation and the distribution of sulfide-oxidation products between the tailings pore water and solid-phase precipitates. Numerous studies have concluded that the rate of sulfide oxidation in mine-waste piles and heap-leach systems is controlled by the supply of oxidant to the mineral surface (Cathles, 1979; Davis and Ritchie, 1986; Nicholson *et al.*, 1990). Processes that limit the supply of oxidant are transport through the mine-waste pile to the depth of active oxidation, and diffusion of oxidants (O_2 or Fe^{3+}) through oxide coatings that surround unaltered sulfide cores (Davis and Ritchie, 1986). Nicholson *et al.* (1990) concluded that transport of oxygen through alteration rims surrounding pyrite grains controlled the rate of pyrite oxidation in an experimental study conducted under near-neutral pH conditions. In the field, Blowes and Jambor (1990) and Coggans *et al.* (1994) observed well-developed alteration rims, composed of goethite and jarosite, surrounding sulfide grains under low pH ($3.5 < pH < 4.5$) conditions. No

alteration rims were observed by Blowes *et al.* (1994) on sulfide grains present under the very low-pH conditions (pH <1.5) present at the Heath Steele impoundment. This pattern suggests that the formation of secondary alteration rims may be a primary control on the rate of sulfide oxidation in all but the most extreme low-pH settings.

10.8.2. Role of Acid Neutralization in Determining Metal Release

The field observations made at tailings impoundments that have similar sulfide contents but variable carbonate-mineral contents suggest that the location of H^+ consumption is important in determining the potential for metal release and future acid production. The Nordic uranium tailings impoundment near Elliot Lake, Ontario, and the Delnite gold-mine tailings impoundment at Timmins, Ontario, both contain approximately 5 wt% sulfide minerals, principally as pyrite. The carbonate content of the Nordic tailings is generally <0.1 wt% as $CaCO_3$, whereas the carbonate content of the Delnite tailings is >20 wt%. At the Nordic site, the pH in the vadose zone is low ($1 < pH < 4$), and much of the Fe^{2+} released through pyrite oxidation remains in solution, resulting in pore-water Fe concentrations that exceed 20,000 mg/L at some locations (Dubrovsky *et al.*, 1984b). This water is being displaced down through the tailings and laterally through an underlying aquifer in which the water is neutralized along the groundwater flow-path. Concentrations of dissolved Fe^{2+}, however, remain high along the flow path. Acidic conditions are generated as this ferrous-rich water discharges to the surface-water flow system down-gradient from the tailings impoundment. At the Delnite site, the pH in the vadose zone has remained high ($6 < pH < 8$), favoring precipitation of Fe oxyhydroxide minerals, predominantly goethite, near the location of sulfide oxidation (Jambor and Blowes, 1991). As a result of goethite precipitation, Fe concentrations are generally <50 mg/L (Blowes, 1990). These Fe concentrations represent an acid-generating potential that is less than the acid-consuming potential of the pore-water alkalinity; therefore, no acidity is generated as this water is discharged to the surface-water flow system. The importance of maintaining high carbonate contents in the vadose zone of the tailings impoundments is thus illustrated. At both sites, acid-neutralization reactions have produced pore waters near the base of the impoundments that are near-neutral in pH, but the high concentrations of dissolved Fe^{2+} in the Nordic pore water represent a high acid-generating potential in contrast to the low acid-generating potential at Delnite.

10.9. CONCLUSIONS

A series of acid-neutralization reactions controls the pore-water pH at four inactive mine tailings impoundments: the Waite Amulet Cu-Zn tailings impoundment (Blowes and Jambor, 1990), the Heath Steele Pb-Zn tailings impoundment (Blowes *et al.*, 1991), the Copper Cliff Ni-Cu tailings impoundment (Coggans *et al.*, 1994) and the Nickel Rim Ni-Cu tailings impoundment (Johnson, 1993). Sequential calcite/dolomite

dissolution, siderite dissolution, $Al(OH)_3$ dissolution, and $Fe(OH)_3$ dissolution, are the same as the pH-buffering sequence observed in the Nordic uranium tailings impoundment near Elliot Lake, Ontario (Dubrovsky, 1986) and in a plume of tailings-derived water adjacent to the Nordic impoundment (Morin *et al.*, 1988a). The sequence of pH-buffering reactions observed at these inactive tailings impoundments results in the development of a series of pH regions that controls the mobility of several dissolved trace metals, including Al, Cr, Ni, and Pb. The zones of pH-buffering and metal attenuation are described well by a model which couples solute transport mechanisms with equilibrium geochemical reactions. Simulations conducted using this model suggest that, in tailings impoundments with large masses of acid-consuming materials, some of these metals may be retained in the tailings or underlying aquifers throughout the duration of acid release. Field observations suggest that the ferric oxyhydroxide coatings which form on sulfide minerals in all but extremely acidic tailings impoundments are probably an important control on the rate of sulfide oxidation and acid generation. The precipitation of ferric oxyhydroxides under high-pH conditions is sufficient to maintain low concentrations of dissolved Fe^{2+} at the Delnite minesite near Timmins, Ontario. The formation of ferric oxyhydroxide coatings, and the precipitation of ferric-iron-bearing precipitates is favored under the high-pH conditions present in carbonate-buffered tailings impoundments. These observations illustrate the benefits of maintaining a high carbonate:sulfide ratio in the shallow tailings through the selective addition of carbonate minerals during the late stages of tailings deposition or through the extraction of sulfide minerals and the production of low-sulfur tailings.

Chapter 11

The Geochemistry of Cyanide in Mill Tailings

Adrian Smith
Kea Pacific Holdings Inc.
North Vancouver, B.C.
V7R 2M9

11.1. INTRODUCTION

In this review of the geochemistry of cyanide in mill tailings, the basis of an understanding of cyanide behavior is established through a description of some fundamental cyanide chemistry, after consideration of the extraction-process chemistry for precious metals from ore in which cyanide is a vital ingredient. This description is followed by a translation of the cyanide chemistry basic to geochemical reactions and processes. The application of these processes and reactions forms the root of the evaluation of cyanide geochemistry in mill tailings and the migration of cyanide from mill tailings into the natural environment. Between the basic chemistry of cyanide and final application to cyanide geochemistry in mill tailings and cyanide migration, a caveat is inserted by way of a discussion of the widespread difficulties of cyanide analysis and the problems of obtaining reliable data on which sound technical assessment of cyanide behavior can be based.

11.2. CYANIDE CHEMISTRY

11.2.1. Extraction and Recovery of Precious Metals

For almost one hundred years, cyanide solutions have been used to extract gold and silver from ores. Gold dissolution from ore by using cyanide solutions is a two-stage process, known as cyanidation, which is summarized in the reaction described by Elsner's equation:

$$4Au + 8NaCN + O_2 + 2H_2O \Leftrightarrow 4NaAu(CN)_2 + 4NaOH \qquad (1)$$

The reaction with silver is similar. In the absence of other metals that form cyanide complexes, relatively weak cyanide solutions can be used for this process to extract either gold or silver, as both form strong complexes with cyanide. Ores, however,

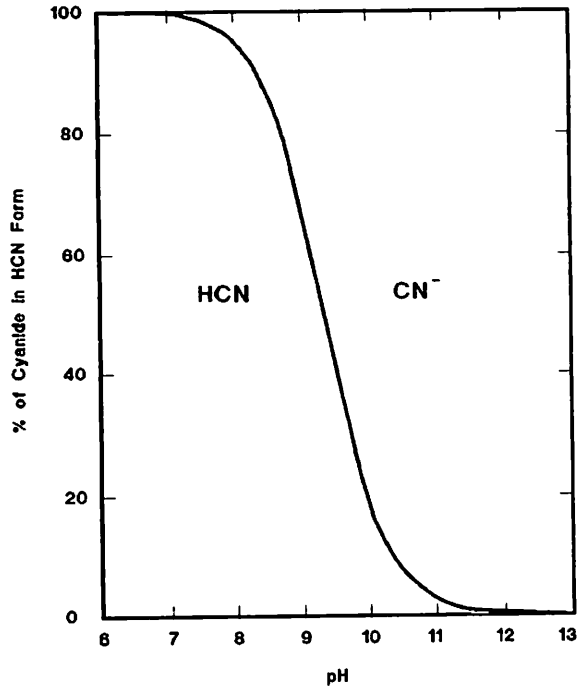

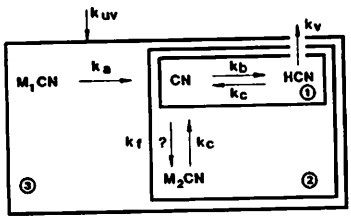

where

M_1 = strong complexing transition metal (TM). e.g., iron

M_2 = other "weak" TM, e.g., copper, zinc, etc.

k_{uv} = additional influence of (k_{uv}) ultraviolet degradation

k_a, k_b, k_c, k_d, k_f = rate constants transformation

k_v = volatilization mass transfer coefficient (loss to atmosphere) (L/t)

Now can add, if neccessary, cyanate reaction, for example:

1. $HCN \longrightarrow CN \longrightarrow M_2CN$
2. $2HCN + O2 \ (+ \text{ catalyst}) \longrightarrow 2HCNO$
   $2CN + O2 \ (+ \text{ catalyst}) \longrightarrow 2CNO$

Mass Balance (MCN, FCN, TCN)

1. $\frac{d(MCN)}{dt} = -K_a(MCN) - K_{uv}(MCN)$ where $_{uv}$ influenced
   or $- k_a(MCN)$ where not.
2. $\frac{d(FCN)}{dt} = -k_a(MCN) + k_{uv}(MCN) - \frac{k_v}{z}(HCN)$
   where Z is related to volume and area for volatization
   $Z = \frac{V\ (m^3)}{A\ (m^2)} = m$
3. $\frac{d(TCN)}{dt} = -\frac{k_v}{z}(HCN)$ where there is no k_{uv} ultraviolet degradation of MCN

Figure 11.1. (Top) Relationship between HCN and cyanide with pH.
Figure 11.2 (Bottom) Interrelationships in cyanide chemistry: conceptualization of FCN, WAD, and TCN.

contain many metallic species, particularly from the first-row transition series of metals in the periodic table, that react with cyanide to form metallo-cyanide complexes; these result in higher cyanide consumption rate and a residual solution bearing a whole range of cyanide species and complexes. For example, Table 11.1 gives approximate extraction rates for a range of metals from sulfide ores, many of which are commonly associated with gold mineralization.

Table 11.1. Solubility of metal sulfide minerals in cyanide solutions (after Scott and Ingles, 1987).

Mineral	Formula	Percent Extraction of Metal
Sphalerite	ZnS	18.4(1)
Chalcocite	Cu_2S	90.2(2)
Chalcopyrite	$CuFeS_2$	5.6(Cu)(2)
Bornite	Cu_5FeS_4	70.0(Cu)(2)
Enargite	Cu_3As_4	65.8(Cu)(2)
Tetrahedrite	$(Cu,Fe)_{12}Sb_4S_{13}$	21.9(Cu)(2)
Metallic copper	Cu	9.0(2)

Notes: (1): 2.0 g/L NaCN solution (at 45 °C)
(2): 1.0 g/L NaCN solution (at 23 °C)

Concurrent with the formation of metallo-cyanide complexes is the formation of thiocyanate (SCN) and cyanate (CNO) complexes. Such formation is enhanced in the presence of free-sulfur species or sulfides which are relatively reactive, such as pyrrhotite ($Fe_{1-x}S$).

Gold is recovered from the cyanidation solution generally using cementation with zinc (the Merrill-Crowe process) or adsorption on activated carbon; there are, however, many variants of each of these two procedures. Remaining after gold extraction is a solution bearing cyanide, metallo-cyanide complexes, cyanates, thiocyanates, and other chemical species dissolved from the ore.

11.2.2. Chemistry of Cyanidation Solutions

Cyanide compounds in cyanidation solutions and mineral-processing effluents include free cyanide, the alkali-earth salts, and the metal cyanide complexes formed with gold, mercury, zinc, cadmium, silver, copper, nickel, iron, and cobalt. These compounds may be classified into five general categories, as shown in Table 11.2. The discussion of cyanidation solution-chemistry is based on the summary by Smith and Mudder (1991).

Table 11.2. Classification of cyanide and cyanide compounds in cyanidation solutions on the basis of their stability (after Scott and Ingles, 1987).

	Classification	Compound
1.	Free cyanide	CN^-, HCN
2.	Simple compounds	
	a) readily soluble	NaCN, KCN, $Ca(CN)_2$, $Hg(CN)_2$
	b) neutral insoluble salts	$Zn(CN)_2$, $Cd(CN)_2$, CuCN, $Ni(CN)_2$, AgCN
3.	Weak complexes	$Zn(CN)_4^{2-}$, $Cd(CN)_3^-$, $Cd(CN)_4^{2-}$
4.	Moderately strong complexes	$Cu(CN)_2^-$, $Cu(CN)_3^{2-}$, $Ni(CN)_4^{2-}$, $Ag(CN)_2^-$
5.	Strong complexes	$Fe(CN)_6^{4-}$, $Co(CN)_6^{4-}$, $Au(CN)_2^-$, $Fe(CN)_6^{3-}$

a. Free Cyanide

The term free cyanide is confined to two species, the cyanide ion (CN^-) and hydrocyanic acid or hydrogen cyanide (HCN). The relative proportion of these two forms depends upon the pH of the system. The reaction between cyanide ion and water is expressed by the following equation:

$$CN^- + HOH \Leftrightarrow HCN + OH^- \qquad (2)$$

At any particular pH and temperature, the system is in equilibrium and the relative amounts of each can be determined from the following expression:

$$K_a = \frac{[H^+][CN^-]}{[HCN]} = 2.03 \times 10^{-10},\ pKa = 9.31\ (at\ 20\ °C) \qquad (3)$$

Figure 11.1 presents this relationship in graphical form. In natural waters with a pH below 8.3, cyanide is present predominantly as HCN.

b. Simple Cyanide Compounds

The simple cyanides are the salts of hydrocyanic acid (*i.e.*, KCN and NaCN), which dissolve completely in solution to produce free alkali-earth cations and cyanide anions, for example:

$$NaCN \Rightarrow Na^+ + CN^- \qquad (4)$$

$$Ca(CN)_2 \Rightarrow Ca^{2+} + 2\ CN^- \qquad (5)$$

The CN^- then reacts with water to form HCN, the extent of which depends upon the pH of the solution.

The simple cyanides are electrically neutral (the positive charges of the metal ion balance exactly with the negative charges of the cyanide ions) and are capable of existing in solid form. The simple cyanide compounds are water-soluble and dissociate or ionize readily and completely to yield free cyanide (as defined above) and the alkali-earth cation.

Table 11.3. Metal-cyanide complex ions in order of decreasing stability in water (after Caruso, 1975).

Name	Formula	Dissociation Constant
Hexacyanoferrate (III) or ferrocyanide	$[Fe(CN)_6]^{3-}$	1.0×10^{-52}
Hexacyanoferrate (II) or ferrocyanide	$[Fe(CN)_6]^{4-}$	1.0×10^{-47}
Tetracyanomercurate (II)	$[Hg(CN)_4]^{2-}$	4.0×10^{-42}
Tricyanocuprate (I)	$[Cu(CN)_3]^{2-}$	5.0×10^{-28}
Tetracyanonickelate (II)	$[Ni(CN)_4]^{2-}$	1.0×10^{-22}
Dicyanosilverate (I)	$[Ag(CN)_2]^{-}$	1.0×10^{-21}
Tetracyanocadminate (II)	$[Cd(CN)_4]^{2-}$	1.4×10^{-17}
Tetracyanozincate (II)	$[Zn(CN)_4]^{2-}$	1.3×10^{-17}

Note: The Roman numerals indicate the oxidation state of the metal atom.

Table 11.4. Free cyanide concentration released at various levels of a metal cyanide complex (after Caruso, 1975).

Complex(1,2)	1 mg/L	10 mg/L	100 mg/L	1,000 mg/L	100,000 mg/L
$[Hg(CN)_4]^{2-}$	0.00002	0.00003	0.000045	0.00007	0.00018
$[Ag(CN)_2]^{-}$	0.00009	0.00002	0.0004	0.0009	0.0041
$[Cu(CN)_3]^{2-}$	0.0003	0.00054	0.00097	0.0017	0.0054
$[Fe(CN)_6]^{3-}$	0.0002	0.0032	0.0004	0.0006	0.0012
$[Fe(CN)_6]^{4-}$	0.0012	0.0016	0.0022	0.0031	0.0061
$[Ni(CN)_4]^{2-}$	0.135	0.215	0.340	0.539	1.324
$[Cd(CN)_4]^{2-}$	(3)	2.30	3.64	5.77	14.49
$[Zn(CN)_4]^{2-}$	(3)	2.26	3.59	5.68	14.28

Notes: (1): All values in mg/L.
(2): Free cyanide levels calculated at pH = 7 and 25 °C.
(3): Calculations indicate that at this dilution the two complexes are completely ionized.

c. Cyanide Complexes, Except Strong Complexes

These compounds are cyanide-complexed with cadmium, copper, nickel, silver, and zinc. The complexes form in a step-wise manner, with successively higher cyanide contents as the cyanide concentration of the solution is increased. The stability of these cyanides varies according to the metal ion involved, with zinc and cadmium forming the weakest complexes. The dissociation constants and order of metal-complex stability are presented in Table 11.3.

The rates of chemical dissociation of cyanide complexes are affected by several factors, including the intensity of light, water temperature, pH, total dissolved solids, and complex concentration. The dissociation constants can be utilized to calculate the concentration of free cyanide present in solution in equilibrium with these complexes. Table 11.4 presents the equilibrium concentrations of free cyanide produced at various complex concentrations dissolved in water at pH = 7.0 and 25 °C (Caruso, 1975). The very low concentrations of free cyanide produced demonstrate the stability of complexes under ambient conditions.

These metallo-cyanide complexes within this group will generally report in the analysis of weak acid-dissociable cyanide (WAD). This means that the cyanide can be liberated from the complex by reflux in a mildly acidic solution buffered at pH 4.5.

d. Iron Cyanide Complexes

Cyanide reacts with iron to form stable octahedral complexes, including hexacyanoferrate II (or ferrocyanide), in which the iron is in the reduced state with a valence of +2. Ferrocyanide, which is the usual form in solution at ambient redox potentials, is readily oxidized to ferricyanide (or hexacyanoferrate III). In ferricyanide, iron is present in the oxidized ferric form with a valence of +3.

From an environmental viewpoint, iron cyanides (*i.e.*, the hexacyanoferrates) require special attention due to their extreme stability in the absence of light and their tendency to dissociate in its presence. Considerable controversy has evolved concerning the relative toxicity of the iron cyanides upon their photolitic degradation. Although these complexes resist natural degradation until free cyanide and the more readily degradable metal cyanides have dissipated, the complexes may be capable of releasing hydrogen cyanide when exposed to intense ultraviolet radiation.

The hexacyanoferrates undergo a much broader range of reactions than do the other metal cyanide complexes, and their solution chemistry has been studied more thoroughly. Ferrocyanide and ferricyanide both form stable salts with other metals without undergoing exchange of the cyanide ligand. Similarly, ferrocyanide is readily and reversibly oxidized to ferricyanide, although the cyanide content remains unaffected.

Table 11.5. Solubilities of ferrocyanides and ferricyanides (after Huiatt et al., 1982).

Name	Formula	Solubility, g/L (T °C)
Ammonium ferricyanide	$(NH_4)_3Fe(CN)_6$	very soluble
Ammonium ferrocyanide	$(NH_4)_4Fe(CN)_6.3H_2O$	soluble
Barium ferrocyanide	$Ba_2Fe(CN)_6.6H_2O$	1.7 g (15°)
Cadmium ferrocyanide	$Cd_2Fe(CN)_6.xH_2O$	insoluble
Calcium ferrocyanide	$Ca_2Fe(CN)_6.12H_2O$	868 g (25°)
Cobalt ferrocyanide	$Co_2Fe(CN)_6.xH_2O$	insoluble
Copper (I) ferricyanide	$Cu_2Fe(CN)_6$	insoluble
Copper (II) ferricyanide	$Cu_3[Fe(CN)_6]_2.14H_2O$	insoluble
Copper (III) ferrocyanide	$Cu_2Fe(CN)_6.xH_2O$	insoluble
Iron (II) ferricyanide	$Fe_3[Fe(CN)_6]_2$	insoluble
Iron (III) ferricyanide	Fe $Fe(CN)_6$	—
Iron (II) ferrocyanide	$Fe_2Fe(CN)_6$	insoluble
Iron (III) ferrocyanide	$Fe_4[Fe(CN)_6]_3$	insoluble
Lead ferricyanide	$Pb_3[Fe(CN)_6]_2.5H_2O$	slightly soluble
Magnesium ferrocyanide	$Mg_2Fe\ (CN)_6.12H_2O$	330 g
Manganese (II) ferrocyanide	$Mn_2Fe(CN)_6.7H_2O$	insoluble
Nickel ferrocyanide	$Ni_2Fe(CN)_6.xH_2O$	insoluble
Potassium ferricyanide	$K_3Fe(CN)_6$	330 g (4+°)
Potassium ferrocyanide	$K_4Fe(CN)_6.3H_2O$	278 g (12°)
Silver ferricyanide	$Ag_3Fe(CN)_6$	0.00066 (20°)
Silver ferrocyanide	$Ag_4Fe(CN)_6.H_2O$	insoluble
Sodium ferricyanide	$Na3Fe(CN)_6.H_2O$	189 g (0°)
Sodium ferrocyanide	$Na_4Fe(CN)_6.10H_2O$	318.5 g (20°)
Strontium ferrocyanide	$Sr_2Fe(CN)_6.15H_2O$	500 g
Thallium ferrocyanide	$Tl_4Fe(CN)_6.2H_2O$	3.7 g (18°)
Tin (II) ferrocyanide	$Sn_2Fe(CN)6$	insoluble
Tin (VI) ferrocyanide	$SnFe(CN)6$	insoluble
Zinc ferrocyanide	$Zn_2Fe(CN)6$	insoluble

Ferrocyanide can be formed by addition of a soluble ferrous salt or freshly-prepared ferrous hydroxide to a solution containing free cyanide. In practice, the reaction seems to be limited to pH values below about 9.0. There is evidence that dissociation of the complex occurs rapidly above this pH value. The addition of excess ferrous iron increases the amount of complex formed. There is some evidence that a large excess of ferrous iron, coupled with a pH below 4.0, would precipitate other metal cyanide complexes as well. In spite of its larger stability constant, ferrous iron will not displace zinc, copper, or nickel from their cyanide complexes. Ferricyanide cannot be formed directly in solution from ferric iron and cyanide, probably because of the greater insolubility of ferric hydroxide; the formation of ferricyanide is primarily the result of the oxidation of ferrocyanide.

The hexacyanoferrates are classified as "inert" complexes, in that their chemical stability results from extremely slow rates of dissociation and very low solubilities. Although the precipitated iron cyanides present in mining solutions and wastes are mainly in the mixed ferro-and/or ferri-forms, other relatively insoluble- metal iron cyanide compounds do exist. A compilation of the solubilities of various iron cyanide complexes is shown in Table 11.5.

In the presence of ultraviolet light, photolysis and hydrolysis cause a water molecule to displace one of the cyanide moieties in the complex. On prolonged exposure to ultraviolet light, ferrocyanide and ferricyanide have been shown to release up to 85% and 49% of their cyanide content, respectively (Broderius and Smith, 1980); however, these experiments involved closed systems and very high levels of ultraviolet radiation when compared to natural systems.

The hexacyanoferrate II and III salts are formed by the reactions of the hexacyanoferrate ions and the corresponding cation. In the case of ferrocyanide, if alkali-earth-metals ions are present, the resulting precipitate will usually contain the alkali as well, commonly as a double salt. Ferricyanides are less subject to this phenomenon.

All of the alkali and alkaline-earth hexacyanoferrates are soluble in water, except that barium hexacyanoferrate II is only moderately soluble. All of the alkali and alkaline-earth salts of hexacyanoferrate II are insoluble in alcohol.

The heavy-metal salts of hexacyanoferrate II (ferrocyanide) are insoluble and precipitate in water. Because the corresponding acid is rather highly dissociated, the solubility of these precipitates, in the absence of metal-complexing ligands, is not greatly affected by changes in pH over the range pH 2 to pH 11.

In the case of those metals that form strong cyanide or amine complexes, such as cadmium, copper, nickel, and silver, the precipitates either dissolve or fail to form in solutions that contain excess cyanide ions or free ammonia. The complexes can again precipitate, however, if the pH is lowered to a point where the concentrations of these ligands are insufficient to maintain the metal complex.

Ferrocyanide and ferricyanide form an oxidation-reduction couple. Although the reaction $Fe(CN)_6^{3-} + e^- \Leftrightarrow Fe(CN)_6^{4-}$ does not itself involve the hydrogen ion, it is nevertheless pH-dependent due to the difference in dissociation of the corresponding acids and in the relative proportion of the two free ions at pH values below 7. As a result, ferrocyanide is more easily oxidized in neutral than in acid solutions. Ferricyanide is reported to be reduced to hexacyanoferrate II by cyanide, and would be readily reduced during the Merrill-Crowe precipitation step used for gold recovery (Williams, 1915). Hexacyanoferrate II is not oxidized by air in alkaline solutions in the absence of light or catalysts.

e. Other Cyanide-related Compounds

As a result of cyanidation, various cyanide-related compounds are formed in solution, including thiocyanate, cyanate, and ammonia. The presence of thiocyanate (*i.e.*, SCN^-) in cyanidation solutions results from the reaction of cyanide with labile sulfur atoms (for example, from polythionates or thiosulfates), either during pre-aeration or during leaching. The labile sulfur may originate directly from the attack of lime or cyanide on pyrrhotite, or be formed by the air-oxidation of sulfide ions released by dissolution of the readily soluble metal-sulfide minerals.

The thiocyanate ion and cyanide are classified chemically as pseudohalogens (*i.e.*, they have properties similar to chloride, bromide, and iodide), and can form insoluble ionic salts with silver, mercury, lead, copper and zinc. Thiocyanate is chemically and biologically degradable, with the metabolic byproducts being ammonium ion, carbonate, and sulfate. The primary environmental concerns associated with thiocyanate include its toxicity and its breakdown products (*i.e.*, ammonia), which may be toxic if present in sufficient levels.

Many oxidants (chlorine, ozone, oxygen, and hydrogen peroxide) convert cyanide to cyanate. The mechanisms for the dissolution of gold involve formation of hydrogen peroxide as part of the initial step, and it is possible that the cyanate present in the cyanide leach solutions arises as a result of peroxide attack on cyanide. In addition, cyanate under acidic conditions slowly hydrolyzes to ammonia and carbonate. At room temperature, cyanide and thiocyanate react slowly with water to form ammonia, formate ion, and/or carbonate. The reaction rate increases with temperature.

Free ammonia forms soluble amine complexes with many heavy metals, including copper, nickel, silver and zinc. The hydrolysis constant for the free ammonia-ammonium ion equilibrium is 1.86×10^{-10} at 10 °C (pKa = 9.73). As a result, the presence of ammonia in cyanidation solutions can inhibit the precipitation of these metals at basic pH values above 9.0, the pH range generally suitable for the precipitation of many metal hydroxides.

11.3. CYANIDE ANALYSIS

11.3.1. Introduction

Despite its critical importance, the analysis for cyanide in mining-related solutions remains a source of concern and confusion, both to operators and regulators. In the United States, the current status and applicability of methods of cyanide analysis to mining solutions are in a state of flux. Effluent discharge standards for cyanide are being codified in permits at levels below the practical quantification limits (PQL) of

cyanide analysis in mining effluents, despite acknowledgment and a considerable database to indicate that there are major problems with the determination of such values. It is imperative that the interpretation of cyanide migration data be tempered with an understanding of the reality of problems of cyanide analysis.

The present state of uncertainty will continue until some fundamental review is made of the practical aspects of cyanide analysis. Certain pronouncements by regulatory agencies on application of the "cyanide-amenable-to-chlorination" method as being applicable to mining-related solutions is cause for further concern about the status of cyanide analytical methods. Rather than being a reiteration of various studies on the analysis of cyanide (for example, Conn 1981), this section of the Chapter is focused on those methods considered most appropriate for cyanidation solutions. This does not imply that the methods described are without their problems and interferences, nor that they are universally applicable. It is that these methods have found successful application in specific cases in a mining environment.

11.3.2. Sample Preservation

The preservation and storage of samples, critical to the success of any analytical program, is a concern when dealing with samples for cyanide analysis. Methods of preservation have been developed for most commonly analyzed parameters. Little information, however, is available to define the effect of preservation on cyanide-sample integrity, or to define any interfering effect the preservative may have on a particular analysis.

Immediate analysis of the sample is the most desirable approach. The sample should be refrigerated immediately at 4 °C and should be analyzed as soon as possible. All other means are somewhat less appropriate or accurate, but nonetheless are commonly employed. The best approach is to utilize chemical preservatives only when necessary, only when they are known to be compatible with the method of analysis, and only when the preservative has been shown acceptable in the particular application under consideration.

Some of the issues and relationships with respect to sample preservation and cyanide can be illustrated by reference to two recent studies. In the first example (Table 11.6), a comparative evaluation of weak-acid-dissociable (WAD) cyanide analysis on refrigerated, non-preserved samples and samples stabilized with sodium hydroxide to pH 12 or greater shows that non-preservation was successful in retaining the WAD cyanide components in the sample if the sample was refrigerated and analyzed in a little more than 24 hours (Damon *et al.*, 1991).

The second example (Table 11.7) is from an evaluation of the effects of the use of preservatives on total, WAD, and free-cyanide analyses using two separate

Table 11.6. Comparison of WAD-cyanide values from preserved and unpreserved samples (after Damon *et al.*, 1991).

Sample No.	WAD Cyanide (mg/L) Unpreserved (held 24 hours)*	WAD Cyanide (mg/L) Preserved by addition of sodium hydroxide (held 6 days)
1	0.04	0.05
2	0.04	0.08
3	0.09	0.09
4	0.11	0.08
5	0.03	0.08
6	0.03	0.05
7	0.02	0.04
8	0.02	0.02
9	0.08	0.09
10	0.48	0.41
11	1.52	1.40
12	1.92	1.81
13	2.30	2.12
14	2.22	2.06
15	1.97	1.41
16	1.80	1.68
17	1.77	1.72

*Refrigerated at 4 °C.

Table 11.7. Effects of the use of preservatives for oxidants and sulfides on cyanide analysis (after Damon et al., 1991; all values in mg/L).

	Laboratory A	Laboratory B
Total Cyanide		
Unfixed	1.80	2.30
Fixed for sulfide	1.80	2.20
Fixed for oxidants	1.30	2.30
Fixed for oxidants and sulfides	2.00	2.10
WAD Cyanide		
Unfixed	0.10	0.18
Fixed for sulfide	0.11	0.22
Fixed for oxidants	0.35	0.45
Fixed for oxidants and sulfides	0.75	0.72
Free Cyanide		
Unfixed	0.03	0.07
Fixed for sulfide	0.04	0.04
Fixed for oxidants	0.11	0.08
Fixed for oxidants and sulfides	0.02	0.10

laboratories for quality assurance purposes. Samples were treated to remove potential interferences by oxidants (fixed for oxidants) by the incremental addition of sodium arsenite and for the removal of potential interferences by sulfide (fixed for sulfides) by the addition of cadmium nitrate. In practice, the samples were unlikely to have contained any residual oxidants and were shown not to contain any detectable levels of sulfides. The data show considerable variability, with the WAD-cyanide samples being most affected by the addition of preservatives. The cumulative effect of adding both the preservatives on the WAD-cyanide values is particularly striking. In the case of free-cyanide values, it is difficult to assess whether the preservatives skew the analysis, as the replication of the analytical method at this level is poor.

11.3.3. Analytical Procedures

Selection of a method of cyanide analysis should involve the following considerations:

- complete characterization of the solution to be analyzed, with particular emphasis on the species of cyanide present and potential interfering components.
- knowledge of the basic chemistry of cyanides
- awareness of the strengths and weaknesses of the method for a given set of conditions
- understanding of the capabilities of equipment, and operator expertise and experience
- knowledge of the potential treatments to obviate or reduce the effect of interferences
- recognition of the fact that treatment to reduce an interference may be an interference itself

In the context of the above considerations, the following analytical methods require discussion with respect to their utility for analysis of cyanidation solutions:

- distillation method for total cyanide, USEPA Method 9010/9012 (USEPA, 1986) or similar, but including alternative finishes to the colorimetric method
- standard method 4500-CN/ASTM Method C distillation methods for weak-acid-dissociable cyanide
- picric acid colorimetric method for weak-acid-dissociable cyanide
- silver nitrate titrimetric method for free cyanide at levels above 10-20 ppm

In addition, the cyanide-amenable-to-chlorination method is discussed, not because of the appropriateness of the application of this method to mining solutions, but because it is one of the few methods recognized by federal agencies in the United States for cyanide analysis. A fuller discussion of the following methods and their applicability to mining-related solutions is given in Smith and Mudder (1991):

- ion-selective electrode for free cyanide and as a finish to distillation methods
- ion chromatographic method for individual cyanide species and complexes
- "reactive" cyanide by USEPA (1986) test method section 7.3.3.2 in support of reactivity criteria for cyanide in waste materials

Table 11.8. Comparison of total cyanide analyses by manual (USEPA Method 9010) and autoanalyzer (USEPA Method 9012): values in µg/L (after Smith and Mudder, 1991).

Sample #	Total Cyanide (Autoanalyzer)	Total Cyanide (Manual)
1	90	14
2	80	<5
3	1610	<5
4	2780	13
5	780	<5
6	1200	5
7	560	<5
8	2520	20
9	1900	15
10	1090	<5
11	620	40
12	1550	16
13	1770	<5

Table 11.9. Comparison of autoanalyzer and non-autoanalyzer analyses for total cyanide in a mining effluent* (after Smith and Mudder, 1991).

Date		Laboratory A (Non-auto)	Laboratory B (Non-auto)	Laboratory C (Autoanalyzer)
16	Unfixed	1.80	2.30	7.60
	Fixed **	1.80	2.20	7.50
17	Unfixed	2.20	2.10	6.40
	Fixed **	2.00	2.20	6.60
18	Unfixed	2.10	2.50	6.80
	Fixed **	2.30	2.70	6.50

*Data in mg/L; anticipated cyanide value was about 2 mg/L.
**"Fixed", treated to remove sulfide from the sample.

a. Total Cyanide by Distillation

Cyanide, as hydrogen cyanide, is released by a one-hour reflux distillation of the sample with a strong acid at a pH value less than pH 2; the hydrogen cyanide is collected in a sodium hydroxide scrubber solution. The cyanide so collected is quantified by titrimetric, colorimetric, or ion-selective electrode techniques, as for WAD cyanides. The USEPA Method 9010 (manual) and 9012 (autoanalyzer) use a colorimetric finish to the analysis (USEPA, 1986). In this procedure the cyanide is converted to cyanogen chloride with chloramine-T at a pH value of less than pH 8, the color being developed by the addition of pyridine-barbituric acid. This method is subject to a number of common potentially severe interferences, notably thiocyanates, and sulfides and other sulfur species. These interferences, however, are treatable to a certain extent, and the detection limits under favorable conditions are excellent. The total-cyanide method will recover all cyanide species with the exception of cobaltous cyanides. Ion chromatographic techniques are available for the determination of cobalt cyanide complexes. Although these interferences are treatable, the treatment may affect the final result.

Lower limits of detection are reported to be 2.0 ± 1 μg/L (Ingersoll *et al.*, 1981), with a relative standard deviation above 10 μg/L of less than 10%. In a single laboratory, using mixed industrial/domestic waste samples in the range of 0.06 to 0.60 mg/L CN^-, the respective standard deviations were +0.005 to +0.094. USEPA (1986), using known concentrations of 0.28 and 0.62 mg/L CN, reported recoveries of 85% and 102%, respectively. ASTM (1985) suggests a sensitivity limit of 0.1 mg/L CN.

If performed by skilled personnel, the manual total-cyanide method is probably the best of the available methods for cyanide determinations. Although the reliability of the autoanalyzer version of the method is accepted by the USEPA, there are cases where the autoanalyzer method has been shown to give erroneous results on samples verified using the manual distillation. Table 11.8 gives comparative values for total-cyanide determinations on effluent from a gold/sulfide project in the United States over a six-month period. With anticipated values of total cyanide being in the 5—20 μg/L range, the manual distillation data are seen to be far more representative than the equivalent autoanalyzer results. A second example (Table 11.9) is from a comparative study of three laboratories, two of which used a manual distillation method on samples of effluent from a heap-leach project in the United States. Here the cyanide values are two orders of magnitude higher than the first example, yet the autoanalyzer data are still in error, about three times the values seen in the manually determined samples. These two examples suggest that, if the autoanalyzer technique is proposed for routine determination of total cyanide, a comparative study should be made with manual distillation data to ensure that the autoanalyzer method is appropriate for the sample matrix being evaluated.

In research conducted in the Homestake mine analytical laboratory, it was noted that the total-cyanide method using sulfuric acid in the presence of thiocyanate resulted in a positive error, probably due to the breakdown of thiocyanate promoted by the acid (Whitlock *et al.*, 1981a). The positive interference resulting from thiocyanate is important when considering low and environmentally important levels of cyanide and monitoring of an effluent for compliance purposes. Although the presence of cyanide may be noted through analysis, resulting in an apparent permit violation, the cyanide may not be present in reality.

b. Cyanide Amenable to Chlorination

The cyanide-amenable-to-chlorination method was widely used in the past, prior to the development of the WAD-cyanide procedures. Both methods measure the same cyanide species, although the cyanide-amenable-to-chlorination method is more time-consuming as it involves two total-cyanide determinations (*i.e.*, one before and one after a chlorination step), with the attendant compounding of errors such an approach produces.

In recent years, the WAD-cyanide method has superseded the amenable-to-chlorination method and has become widely accepted by the mining industry and many state regulatory agencies, both for monitoring and compliance purposes, because of recognition of the problems with the cyanide-amenable-to-chlorination method. Unfortunately, the USEPA still only recognizes the cyanide-amenable-to-chlorination method in discharge permits, although the WAD-cyanide method has been accepted on occasions. The recoveries of cyanide with the cyanide-amenable-to-chlorination method are incomplete for a number of species and appear to be concentration-dependent (Ingersoll *et al.*, 1981). Ecological Analysts Inc. (1979) reported poor accuracy and precision with the method, with susceptibility to a wide range of interferences.

c. WAD Cyanide by Distillation

The two most popular versions of this WAD-cyanide method are that from "Standard Methods" (16th edition 1985, Method 412-H, p. 344; 17th edition 1989, 4500-CN Method I, p. 4—38) and the ASTM Method C (ASTM, 1985). The method involves the evolution and collection of hydrogen cyanide by reflux distillation for one hour, with the sample buffered at pH 4.5 using an acetate buffer. This is followed by estimation of the cyanide liberated in the distillation using titrimetric, colorimetric, or ion-specific electrode techniques.

The method recovers all free cyanide and weakly complexed cyanides, for example cadmium and nickel cyanides, but will not dissociate and recover hydrogen cyanide from strongly complexed forms such as iron and cobalt cyanide. The WAD-cyanide method is generally less susceptible than other cyanide analytical methods to interference by either thiocyanate or sulfides. The lower limits of detection are similar

to total-cyanide methods, although the procedure is more reliable at environmental concentrations of cyanide. Precision is listed as linear, expressed as 0.085 x cyanide concentration + 0.0032 for reagent water. Conn (1981) reported a 7.5% relative standard deviation at the 0.08 mg/L as CN level.

d. Picric Acid Method for WAD Cyanide

The picric acid colorimetric method for WAD cyanide is included in this section as it has been shown to be a relatively reliable and accurate method down to about 0.5 mg/L cyanide in solution. The method involves developing color with picric acid in the presence of nickel, followed by heating over a water bath for 20 minutes prior to measurement using a visible-range spectrophotometer.

As an example of the use of the picric acid method for WAD cyanide, Brohm Mining Corporation, South Dakota, USA, evaluated the applicability of the picric acid method to solutions from their heap-leach pads. The data in Table 11.10 show that there is generally little difference between WAD-cyanide values determined by the picric acid and ASTM Method C WAD-cyanide analytical protocols for these solutions. This result is consistent with previous experience which has indicated that the picric acid procedure is a reliable analytical method, capable of providing quantitative evaluations of WAD cyanide down to 0.50 mg/L. Prior to implementing the picric acid method for compliance purposes, its accuracy and reproducibility should be confirmed independently on a site-specific basis using an outside commercial laboratory.

e. Free Cyanide by Titration with Silver Nitrate

The silver nitrate titration method is used for the determination of free cyanide or as a finish to the total-cyanide distillation method. The process involves titrating a known volume of sample with a standard silver nitrate solution, forming silver cyanide in the process. The end point, the presence of excess silver nitrate when all the free cyanide has reacted, is estimated using a dimethylaminobenzalrhodamine indicator. The solution must be maintained at a high pH value with sodium hydroxide to prevent hydrogen cyanide volatilization.

f. Ion-selective Electrode for Free Cyanide

In a similar manner to the silver nitrate titration, the cyanide-ion-specific electrode can be used both to determine free cyanide only in solution and as a finish for the distillation method for total cyanide. The method involves the direct measurement, using an expanded-scale pH or voltmeter, of the response of the electrode to the cyanide in solution against a reference electrode. A calibration curve is prepared using standard additions of a known cyanide solution. It is important to match the matrix of the standard solutions with that of the test solution where the presence of a potential interfering species is suspected, a common issue with mining-related effluents. The cyanide-ion-specific electrode itself often becomes "poisoned" in effluent solution

bearing sulfide species, with coatings forming on the electrode junction. These coatings require removal in order to attain credible results.

Table 11.10. Comparison of leach and rinse effluent WAD cyanide analyses

Sample Date	Sample I.D.	Picric Acid WAD Cyanide (mg/L)	ASTM Method C WAD Cyanide (mg/L)
4/11/90	Barren Solution	220	224
4/11/90	Cell #5 Effluent	193	199
4/11/90	Column D Effluent	169	170
4/11/90	Column C Effluent	172	171
4/11/90	Column B Effluent	177	173
5/31/90	Column A Effluent	11.8	11.7
5/31/90	Column B Effluent	11.2	11.2
5/31/90	Column C Effluent	11.5	11.3
5/31/90	Column D Effluent	12.4	12.2
5/31/90	Cell #5 Effluent	16.5	16.5
6/28/90	Column B Effluent	0.25	0.17
6/28/90	Column C Effluent	0.11	0.07
6/28/90	Column D Effluent	0.21	0.13
6/28/90	Cell #5 Effluent	2.7	2.8
6/28/90	Neutralization Pond Effluent	0.13	0.11

Source: ASCI/SRK (1990)
Notes: April data: leach cycle
May/June data: rinse cycle

g. Ion Chromatographic Method

Ion chromatography has been used by many researchers for the separation of several metal cyanide complexes. Various methods and conditions give good to poor recovery of the loosely complexed metal cyanides. Indirect determination of cyanide by ion chromatography has been successfully demonstrated by several researchers.

A method developed by Koch (1983) claims detection of trace quantities of free cyanide by electrochemical means at 1 µg/L to 1000 µg/L, and a standard deviation better than 1%. Rocklin and Johnson (1983) have also developed a method using electrochemical detection of free cyanide from easily-dissociated-metal cyanide complexes. Simultaneous determination of cyanide and sulfide was successfully demonstrated. Pohlandt *et al.* (1983) and Pohlandt (1984a,b; 1985) have shown good recovery of the easily-dissociated-metal cyanide complexes as well as complexes of nickel, cobalt, iron, and gold conductometrically. Copper cyanide was detected photometrically along with nickel cyanide. The method distinguishes between the two cobalt and iron forms, which is significant in industrial applications. Ultraviolet irradiation of more refractory metals is also utilized.

h. "Reactive" Cyanide by USEPA Test Protocol

The USEPA defines the hazardous characteristic of reactivity with respect to cyanide for a waste as "waste that, when exposed to pH conditions between 2 and 11.5, can generate toxic gases, vapors or fumes to present a danger to human health or the environment." The current action level (1992) triggering this classification is 250 mg/kg waste. The method involves placing a small mass of the sample in sulfuric acid, such that the resultant pH is about 2, and passing a stream of nitrogen over the sample for 30 minutes. The concentration of hydrogen cyanide collected from the nitrogen gas stream in a sodium hydroxide scrubber is determined. Based on recent experience, it is difficult to know how data obtained by this method equates to other cyanide analytical results. Adding sulfuric acid to the material down to pH 2 will cause precipitation of some metal-cyanide complexes, which will redissolve slowly only over the pH range 2—4.5. Cyanide from these complexes will not report to the nitrogen stream. For example, some recent unpublished data indicated that a particular sample with a total cyanide of 900 mg/L, 90 mg/L WAD cyanide, and 15 mg/L free cyanide had a reactive cyanide value, when corrected for sample mass and scrubber solution volume, of less than 1 mg/L.

11.3.4. Analytical Interferences

Associated with any analytical procedure are interferences, both positive and negative, which affect both the precision and accuracy of that method. All of the methods discussed previously are affected by interferences to various degrees. This section contains a brief discussion of the various interferences, as well as a discussion of the research directed towards quantification of various interferences.

In summary, the WAD-cyanide procedure, which measures the weakly complexed forms of cyanide, is least affected by interferences, whereas the total-cyanide method (and, as a consequence, the cyanide-amenable-to- chlorination method), the ion-selective electrode, and the titrimetric method for free cyanide are susceptible to many interferences. The principal species that cause interference in cyanide analyses are:

- oxidizing agents
- sulfides
- thiocyanate
- nitrite and nitrate
- carbonates
- thiosulfates, sulfates, and other related sulfur compounds
- metals

a. Oxidizing Agents

Oxidizing agents, as a general rule, are a negative interference in cyanide analysis as they continue to decompose cyanide in the sample during storage, handling or other

manipulation. Common oxidizers in mining solutions are chlorine, oxygen, ozone, and hydrogen peroxide.

The only valid means of control is immediate removal of the oxidizers. The common test for oxidizers (ASTM, 1985) is to use potassium iodide – starch paper moistened with acetate buffer. If oxidizers are present, the most widely accepted means of treatment is to add 0.1 g/L increments of sodium arsenite with re-testing. Other reagents for removal of oxidizers are mentioned in the literature, but all of these may cause problems in analysis: sodium thiosulfate, sodium hydrogen sulfite, ascorbic acid, oxalic acid, and stannous chloride. Kelada *et al.* (1984) preferred sodium arsenite and oxalic acid. As a general rule, a positive test for sulfide would establish that oxidizers are not present in the solution.

b. Sulfides

Along with thiocyanate, sulfides are one of the most common interferences found in mining process or discharge waters. Free sulfides are normally only present in solutions with oxygen deficiency (Brickell, 1981).

Oxidized products of sulfides convert cyanide to thiocyanate rapidly at elevated pH. Csikai and Barnard (1983) and Yoshida *et al.* (1983), have demonstrated that sulfide evolves through the cyanide analysis as hydrogen sulfide. This interference is normally removed by precipitation in the formation of insoluble sulfides. Luthy *et al.* (1978), reported on precipitation studies. Precipitants commonly used are lead and cadmium carbonates, lead acetate, cadmium nitrate, bismuth citrate, and bismuth nitrate. In addition, oxidants such as permanganate are utilized to destroy residual sulfides.

c. Thiocyanate

Thiocyanate is a common interference to many of the methods. Thiocyanate is generated in solution by the reaction of sulfides in ores, or process solutions, with cyanide added to the solutions. Thiocyanate under acidified conditions, in the presence of a strong oxidant will convert to free cyanide with oxidation of the sulfur to oxysulfur anions. Under these conditions, determined cyanide values will be higher than appropriate, with the rise in value difficult if not impossible to quantify. The phenomena of elevated cyanide values has been documented by Barton *et al.* (1978), Csikai and Barnard (1983), Conn (1981), and Whitlock *et al.* (1981a), as well as many others. The presence of 0.2 mg/L as thiocyanate can contribute as much as 0.01 mg/L cyanide (Barton *et al.*, 1978). Higher concentrations of thiocyanate can negate any meaningful attempt at accurate analysis of trace or environmental levels of cyanide.

Under strong-acid reflux-distillation procedures the conversion of thiocyanate to sulfide is not rapid but proceeds throughout distillation with hydrogen sulfide transferred to the absorber. This occurrence is a major problem to the total-cyanide

and cyanides-amenable-to-chlorination methods. In less acidic distillations (*i.e.*, weak-acid-dissociable cyanides or modified Roberts-Jackson), thiocyanate interference is at a minimum. It has also been postulated that thiocyanate or its decomposition products will react with chloramine-T in the color-development step, producing a positive interference. Several researchers have included a cadmium compound trap to precipitate sulfide products that are passing to the absorber. Barton *et al.* (1978) used zinc acetate in mildly acidic solutions to inhibit the decomposition of thiocyanate.

Whitlock *et al.* (1981b) demonstrated that, when using the USEPA total-cyanide method for cyanidation process solutions of high thiocyanate concentration, the substitution of phosphoric acid for sulfuric acid lessened the concentration of sulfur products in the absorber and led to more accurate cyanide values. With cyanide standards in deionized water, the phosphoric acid substitution yielded improved reliability when compared with the sulfuric acid method.

d. Nitrite and Nitrate

Both nitrite and nitrate may be considered as potential interferences to many of the methods at levels as low as 25 mg/L as nitrate. Nitrites may form HCN during distillation and affect the total-cyanide method and cyanide-amenable-to-chlorination method, as well as the method for cyanates. Although the interferences are usually positive, addition of nitrate to samples containing total cyanide has resulted in negative interferences as well. Kelada *et al.* (1984), and ASTM (1985) recommend sulfamic acid addition of 2 g/L to the sample prior to distillation to obviate the interference of nitrate and/or nitrite.

e. Carbonates

Under strongly acidic conditions of distillation, carbonates in high concentration cause excessive gassing and may reduce the NaOH content of the absorber. Pre-analysis of sample alkalinity will produce information concerning this potential problem.

f. Thiosulfates, Sulfites, and Other Related Sulfur Compounds

Many different types of sulfur compounds are formed by decomposition during distillation, including hydrogen sulfide, sulfur dioxide, and sodium sulfite. Thiosulfate breaks down to form elemental sulfur and sulfurous acid with liberation of SO_2 during distillation. This decomposition bleaches colorimetric finish and reduces cyanide recovery (Conn, 1981). Weak-acid distillations are less subject to this interference, and some researchers add as much as 50 g of lead carbonate to the absorber, followed by filtration of the absorber solution. This filtration may also lower cyanide recoveries. Other analysts have used potassium iodide – starch paper to test for an excess of chloramine-T, given that SO_2 forms Na_2SO_3 which consumes the chloramine-T used in the colorimetric step.

Samples can be pre-treated with hydrogen peroxide as a treatment for sulfites. However, an excess of hydrogen peroxide will rapidly oxidize cyanide and reduce the recovery values. Makhija and Hitchen (1979) have presented methods for titrimetric determinations of sulfite, thiosulfate, and polythionates in mining effluents.

g. Metals

Certain metals at high concentration may interfere with cyanide analysis in a number of the methods. Mercuric and copper chlorides added as catalysts may inhibit analysis, particularly if thiocyanate is present. Mercury, due to high volatility, may diffuse to the absorber and cause a negative interference (Kelada *et al.*, 1984; Barton *et al.*, 1978). Metals such as iron, cobalt, and mercury may interfere with simple cyanide methods by forming more stable complexes that cannot be quantified by the method, thus reducing the reported cyanide value.

11.3.5. Effects of Interferences on Cyanide Recovery in Selected Methods

The research of Ingersoll *et al.* (1981) included the organization of data expressing the effects of various interferences on selected methods. His work is a significant reference guide to the methods and includes a number of tables summarizing the various interferences.

Data from the Homestake Mining Company (1981, unpublished) are an example of evaluating interferences by spiking a complex mining-process-solution. One significant concept when dealing with an interference was to limit the sample size to the lowest concentration of cyanide acceptable for analysis in order to dilute the concentration of potential interfering components of the sample.

The following general conclusions were drawn:

- ascorbic acid treatments to reduce oxidizing agents should not exceed 30 mg/L excess ascorbic acid
- thiosulphate acts as a negative interference to cyanide analysis (total) at concentrations as low as 25 mg/L
- sulfide that gains access to the absorption solution may cause positive or negative interference with colorimetric procedures at very low concentrations
- thiocyanate is a major interference to the total-cyanide distillation method, usually resulting in high cyanide values; however, decomposition is not predictable and the mechanism is uncertain
- bisulfite seems to be a primary negative interference with the potential for some degree of cyanide destruction. Residual bisulfite is an interference
- sulfur species interference may be minimized by the following treatments:
  - sulfide precipitation from the sample
  - distillation of smallest possible sample
  - sulfide precipitation from the absorption solution
  - increased levels of chloramine-T in the colorimetric procedure

11.4. CYANIDE GEOCHEMISTRY

11.4.1. Introduction

Some appreciation of the basic chemistry of cyanide is an important building block in the appreciation of cyanide geochemistry. Next, a solid phase is introduced, either the ore or gangue material leached by cyanide in a tank or on a pad, or the subsite geological material (*i.e.*, soil or aquifer material) for geochemical interaction with the cyanide-bearing solutions.

The physical and chemical properties of the natural material can greatly influence cyanide geochemistry. Ores, rocks, and soils contain to a greater or less extent silicates, aluminosilicates, clay minerals, sulfides, carbonates, and oxides (*e.g.*, iron and manganese more commonly) as mineral phases, plus organic matter, water, and gases in some cases. These are the potential reactants with the cyanide solutions in slurry leaching, in the tailings impoundments, in the leaching heap, or in the subsite soils and aquifer materials. The solid components can control the solution chemistry with regard to alkalinity or acidity (pH control), buffering capacity, and degree of oxidation or reduction (redox potential), resulting in ion-exchange adsorption or chemical reaction in the cyanide solution (*i.e.*, precipitation of insoluble species).

In order to use the knowledge of cyanide chemistry and relate it to the analytical data (total cyanide, WAD cyanide, and free cyanide), one needs a concept of their inter-relationship. Figure 11.2, modified by Smith (1988b) from Simovic *et al.* (1985), takes a geochemical system, such as found in a tailings/heap-leach system, with both "strong" and "weak" metal complexes and relates these complexes to cyanide hydrolysis and HCN volatilization. The contribution of each to the "free" cyanide, WAD cyanide, and total-cyanide analysis is shown. Clearly, this expression of cyanide inter-relationships is rather simple, but it is an effective tool for combining the theoretical cyanide chemistry with the actual analytical values used everyday in industry.

11.4.2. Degradation Mechanisms of Cyanide

In natural environments there are eight mechanisms of cyanide degradation that merit discussion. These are:

-complexation
-cyanide-complex precipitation
-adsorption
-oxidation to cyanate
-volatilization
-biodegradation
-formation of thiocyanate and
-hydrolysis/saponification

a. Complexation

Ford-Smith (1964) reported that 28 elements are capable of forming complexes with cyanide, with 72 metal-cyanide complexes possible. The solubilities of these complexes range from very soluble to insoluble. However, some of these compounds are not very stable and will decompose to release free cyanide. The toxicity of metal-cyanide complexes is generally due to the dissociation of the complex into free cyanide.

At a pH of 4.5, some of the metal-cyanide complexes typically found in cyanidation solutions (for example, zinc and copper) may dissociate into free cyanide to various degrees and at various rates. These are the so-called weak-acid-dissociable metal-cyanide complexes.

The tightly bound iron-cyanide complexes may produce free cyanide by photochemical decomposition under favorable conditions; there is some question as to the significance of this decomposition to surface-water toxicity under realistic conditions (Doudoroff, 1980). Although the formation of metal-cyanide complexes does not completely eliminate the toxicity of cyanide, it does effect a substantial reduction in such toxicity. Metal-cyanide complexes are also intermediates to formation of more-stable compounds that remove free cyanide from the environment (*i.e.*, ferrocyanide precipitates and the oxidation to cyanate). For example, Milne (1950) suggested the use of nickel to form complexes as a method for the disposal of free and complex cyanides in electroplating wastes. Kunz *et al.* (1979) described a process where copper was complexed with cyanide to enhance the adsorption and oxidation of cyanide on activated carbon. Bishop and Wright (1977) received a patent for an electrochemical cyanide-oxidation process using nickel to enhance the process.

The environmental significance of complexation/chelation of cyanide with transition metals is that it is relatively rapid and it occurs wherever soluble species of these metals are present, such as found in soils and ores. Complexation/chelation reduces the toxicity of free cyanide and acts as a intermediary to reduce cyanide mobility via adsorption on organic and inorganic surfaces, or precipitation of ferrocyanide metal salts. Based on the relative abundance of metal species in natural soils, it is expected that the majority of metal-cyanide reactions occurring in the soil will be with iron.

The complexation of cyanide can have two very diverse affects on cyanide mobility in soils. If cyanide complexes with iron it is less able than free cyanide to adsorb on surfaces; hence, cyanide mobility can be increased, as demonstrated by Fuller (1984). If free transition metals such as iron, copper, or nickel are present, however, a ferrocyanide precipitate will cause the cyanide species to be tied up with the soil. On the other hand, if cyanide chelates as a weak-acid-dissociable metal complex, chelation will enhance adsorption of cyanide on organic carbon, metal oxides, feldspar, and clay

surfaces.

b. Cyanide-complex Precipitation

The ferrocyanide ion [$Fe(CN)_6^{4-}$] and the ferricyanide ion [$Fe(CN)_6^{3-}$] form insoluble salts with iron, copper, nickel, manganese, lead, zinc, cadmium, tin, and silver as stated by Weast (1969). Typically within the soil environment, oxidation-potential conditions would result in the formation of ferrocyanide precipitates. In addition, the iron-cyanide complexes can react with thiocyanate to form an even more stable complex if sulfur is present in the soil.

Hendrickson and Daignault (1973) demonstrated that ferro- and ferricyanide complexes will precipitate with iron, copper, magnesium, cadmium, and zinc through a broad range of pH (from 2 to 11). At higher pH, however, the precipitation is more complete. Stoichiometric additions of transition materials removed >90% of the ferro- or mixed ferro-ferric complexes. At high oxidation potentials where only ferricyanide complexes are present, however, precipitation only removed about 60 to 90% of the ferricyanide. This result indicates that, over a broad range of pH and oxidation potentials, iron-cyanide metal complexes will precipitate if sufficient free transition metals are available.

c. Adsorption

Adsorption is another mechanism that attenuates cyanide in soils. Alesii and Fuller (1976) conducted tests with free cyanide in water, potassium ferricyanide in water, and free cyanide in landfill leachate to determine cyanide mobility in various types of soils. The test results indicated that soils having high concentrations of hydrous oxides of iron and manganese retained cyanide best.

Studies conducted for the U.S. EPA in the mid-1970s on the leachate pollutant-attenuation properties of soils indicated that soils containing aluminum minerals attenuated cyanide better than other soils (Alesii and Fuller, 1976; Fuller, 1977, 1978, 1984). Nevertheless, Towill *et al.* (1978), in reviewing the environmental effects of cyanide, found that free cyanide ions are not strongly adsorbed or retained by soils irrespective of the presence of aluminosilicate minerals (Murrmann and Koutz, 1972). Alesii and Fuller (1976) concluded from their tests that soils with a high anion-exchange capacity would likely attenuate cyanide. Soils with a high anion-exchange capacity typically contain kaolin clay, chlorite, gibbsite clay, and/or iron and aluminum oxides. Conversely, soils containing predominantly strong cation-exchanging materials (*i.e.*, montmorillonite), were predicted to have a lesser effect.

As is well known in precious-metals leaching, organic materials will adsorb or react with cyanide. Carbonaceous materials in ore slurries will adsorb free cyanide and limit precious-metal recovery. It has been shown that cyanide is first adsorbed, then catalytically oxidized (Bernardin, 1973). The presence of copper, cadmium, zinc, or

nickel ions in solution results in the formation of metal-cyanide complexes, which enhances the adsorptive capacity of carbon.

Chatwin and Trepanowski (1987) found that the magnitude of cyanide adsorption in sub-soils was correlated with the organic carbon content of the soil. Apparently, cyanide adsorbs on soil organic matter and becomes bound or is subsequently oxidized to cyanate. Free cyanide has also been found to adsorb on the surface of clays and feldspar (Chatwin, 1990); the results indicate that this mechanism is dependent not only on the mineralogy of the soil, but on the solution chemistry as well. It was found also that metals that form weak acid-dissoluble cyanide complexes, such as copper and nickel, enhanced the adsorption process.

d. Oxidation to Cyanate

Cyanide can be converted to cyanate according to the following simplified reaction:

$$HCN + 1/2\ O_2 \Rightarrow HCNO \qquad (6)$$

Hydrogen cyanate and cyanate ions are significantly less toxic than HCN. Cyanide conversion to cyanate has been demonstrated when cyanide is in the presence of strong oxidizers (*i.e.*, ozone, hydrogen peroxide, and hypochlorite). Ultraviolet light, in conjunction with catalysts such as titanium dioxide, cadmium sulfide, and zinc oxide, has been shown to convert cyanide to cyanate (Frank and Bard, 1977). It is theorized that the ultraviolet light causes the catalyst to convert oxygen in solution to ozone, which promptly reacts with the cyanide (Miles, 1981). In recent work it has been found that cyanide can be converted to cyanate in the soil on the surface of organic and inorganic materials (Chatwin, 1990).

The thermodynamics of the cyanide – cyanate reaction, as seen in Figure 11.3, indicate that cyanate should be the predominant species under natural conditions. However, it has been found to be difficult to oxidize cyanide to cyanate under natural ambient conditions. A strong oxidant such as ozone, hydrogen peroxide, or chlorine is required to drive this reaction. Bacterial enzymes or catalytic surfaces of titanium dioxide, zinc sulfide, and carbon have been found necessary to promote this oxidation.

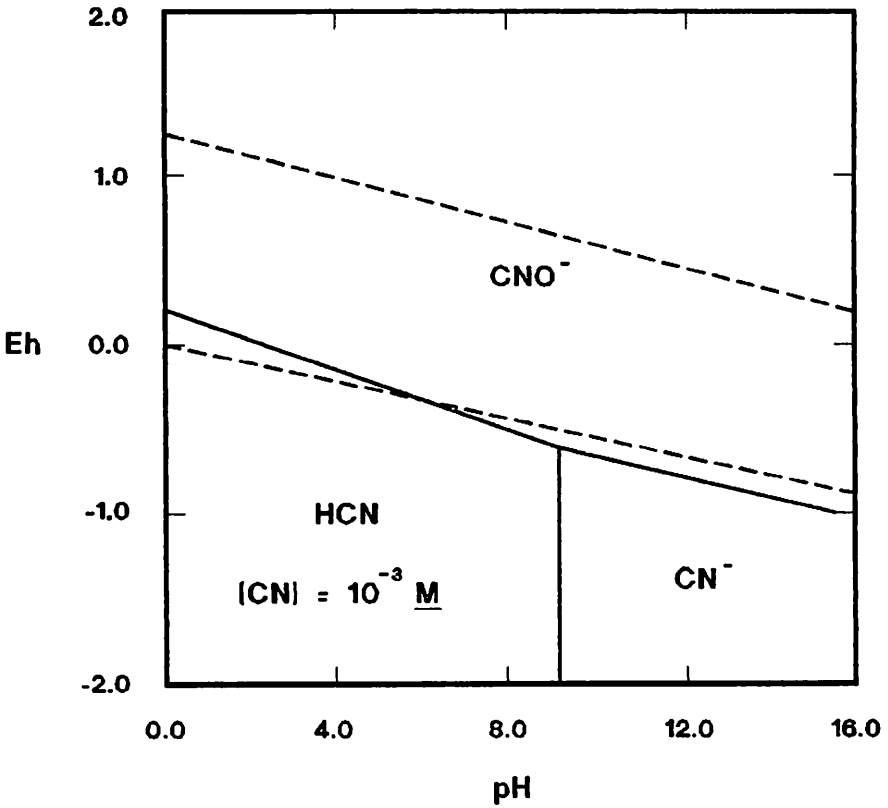

Figure 11.3. Eh-pH diagram for the CN—H_2O system at 25 °C (after Smith, 1988b).

e. Volatilization

Hydrogen cyanide (HCN), also known as hydrocyanic acid, is a colorless gas or liquid with a boiling point of 25.7 °C and a vapor pressure of 100 kPa at 26 °C (Huiatt *et al.*, 1982). The equilibrium hydrolysis reaction between cyanide ion and water occurs according to the following reaction:

$$CN^- + H_2O \Leftrightarrow HCN + OH^- \qquad (7)$$

At a pH of 9.36, which is the pK value, the activities of HCN and CN- ion are equal, as shown in Figure 11.1. At lower pH values at 20 °C, the majority of cyanide exists as HCN (*i.e.*, 69.6% at pH 9, 95.8% at pH 8, and 99% at pH 7). Thus, at neutral pH most of the free cyanide will be in the form HCN. Hence, in soils or other natural geochemical systems, where the pH of cyanide solutions is neutralized to lower pH values, the HCN concentration could be high. For example, in tests performed by Chatwin and Hendrix (1988) on a suite of arid subsoil samples, the soil pH ranged

from 4.5 to 8.9. Should free cyanide be present in contact with these soils, it would result in solutions where the HCN content would be >70%. However, cyanide readily volatilizes in contact with the atmosphere.

Dodge and Zabbon (1952) and The Chester Engineers (1977) identified pH, temperature, interfacial surface area, pressure, concentration, and degree of agitation as factors affecting cyanide volatilization. Palaty and Horokova-Jakubu (1959), cited in Simovic *et al.* (1985), also studied volatilization of cyanide from simple cyanide solutions. They identified the same variables that affected cyanide volatilization as had Dodge and Zabbon (1952).

Whereas cyanide volatilization from surface waters is well-understood, cyanide volatilization from soils is more difficult to understand. Nevertheless, Chatwin and Hendrix (1988) used unsaturated column tests to measure HCN volatilizing from soil surfaces.

f. Biodegradation

Towill *et al.* (1978) reported that cyanide salts move only a short distance through soil before being biologically converted under aerobic conditions to nitrates (microbial degradation to ammonia, NH_3, then conversion to nitrate, NO_3^-) or fixed by trace metals through chelation. The vast majority of this attenuation was attributed to biodegradation.

Strobel (1967) tested both sterile and non-sterile soils to determine their effect on cyanide. The non-sterile soil degraded cyanide, whereas the sterile soil did not appreciably alter cyanide. Fuller (1984) reported that cyanide up to 200 ppm was readily converted to fertilizer nitrogen in the soil. In fact, plants responded to cyanide applications nearly identically as they did to sodium nitrate or ammonium nitrate, both common components of fertilizers.

Cyanide biodegradation is currently being utilized to treat industrial wastewater in two separate processes. Homestake Mining Co. at Lead, South Dakota, utilizes bacteria to treat its wastewater prior to discharge and ICI Bioproducts detoxifies cyanide with a strain of the fungus, Fusarium lateritium.

Biodegradation under anaerobic conditions is not nearly as prolific as under aerobic conditions. The limit for effective anaerobic degradation of cyanide was found by Coburn (1949) to be 2 mg/L cyanide. Above this concentration, the cyanide was found to be toxic to the anaerobic microorganisms. Below 2 mg/L, there is evidence that degradation occurs in certain soluble cyanides, yielding nitrogen gas, N_2 (Huiatt *et al.*, 1982).

g. Formation of Thiocyanate

Free cyanide has been shown to react with various forms of sulfur in the

environment to form thiocyanate. Thiocyanate is relatively non-toxic, in comparison with cyanide. According to IEC (1979), the two forms of sulfur most likely to react with cyanide are polysulfides (S_2) and thiosulfate (S_2O_3). They react according to the following equations:

$$S_x^{2-} + CN^- \Leftrightarrow [S_{(x-1)}]^{2-} + SCN^- \qquad (8)$$

$$S_2O_3^{3-} + CN^- \Leftrightarrow SO_3^{2-} + SCN^- \qquad (9)$$

In neutral to basic solutions, polysulfides and thiosulfates are oxidation products of sulfides, the latter being abundant in minerals. These products therefore could possibly be present in oxidizing environments, such as the vadose zone in soils. The concentrations of polysulfides and thiosulfate in a soil are strongly dependent on the sulfur content and the Eh-pH conditions in that soil.

McGill *et al.* (1985) conducted bench tests on various sulfur-bearing ore minerals to determine if they caused the formation of thiocyanate (at a pH of 10). The laboratory results indicated that chalcopyrite, chalcocite, pyrrhotite, and free sulfur contributed a significant portion of their sulfur content to thiocyanate production, whereas "pure" iron sulfides contributed a lesser, yet significant, portion. The sulfur contained in sphalerite and pyrite was relatively non-reactive with the cyanide.

h. Hydrolysis/Saponification of HCN

As the system pH falls, HCN can be hydrolyzed to give formate, as either formic acid or ammonium formate according to the following reactions:

$$HCN + 2H_2O \Rightarrow NH_4COOH \text{ (ammonium formate)} \qquad (10)$$

or

$$HCN + 2H_2O \Rightarrow NH_3 + HCOOH \text{ (formic acid)} \qquad (11)$$

The system pH will determine the extent of formation of each compound, a lower pH favoring formic acid formation.

Hoecker and Muir (1987) tested high-temperature hydrolysis of cyanide in autoclaves, and developed kinetic data for this reaction. By extrapolating these data to room temperature, a rate for cyanide hydrolysis to ammonium formate of 4% per month was estimated. This rate is similar to the 2% per month that was obtained by DuPont (Longe and DeVries, 1988). Thus, this is not a rapid cyanide-degradation mechanism. However, it would be effective under a variety of conditions, including those found in saturated aquifers, particularly where the system is relatively anaerobic.

11.5. CYANIDE GEOCHEMISTRY IN MILL-TAILINGS SYSTEMS

11.5.1. Introduction

The natural degradation of cyanide process-solutions in mill tailings requires an examination of the behavior of cyanide both prior to and after their exit to the tailings impoundment. The net effect of the cyanide held within the mill tailings is strongly dependant on the reactions that occur above, below, as well as within the mill tailings themselves. Accordingly, an evaluation of these three physical systems is appropriate, each one of which may be affected by the geochemistry of solid phases (mill tailings, the natural liner, and the subsoil geologic materials):

- the mill-tailings supernatant and associated process-solution ponds
- the tailings pore-fluids and tailings solids
- the mobile tailings pore-fluid, which becomes "seepage" that interacts, to a greater or lesser extent, with the natural liner materials or with the subsite geological materials if the impoundment is unlined

Each system is a truly complex geochemical problem to unravel, but it is possible to produce an adequate and workable explanation of each system and how it affects the cyanide chemistry on a general basis.

11.5.2. Reactions in the Tailings Supernatant and Associated Process-water Ponds

The major mechanism of natural cyanide degradation in surface ponds is volatilization of HCN. The pH of the pond is lowered by uptake of carbon dioxide from the air and from rainwater saturated with carbon dioxide. This drop in pH induces a change in the CN^-/HCN balance (Figure 11.1), thereby increasing HCN volatilization.

Data by Schmidt *et al.* (1981) illustrate cyanide losses and transformation related to water depth, season, and temperature for two ponds at a mine in northern Canada. Figure 11.4 illustrates:

- cyanide (total) decay irrespective of pond depth, although there is a slight time lag for the deeper pond section
- cyanide transformation to cyanate, followed by subsequent cyanate loss from the poolwater
- a slight increase in thiocyanate, followed by substantial decay, particularly in the shallow pond

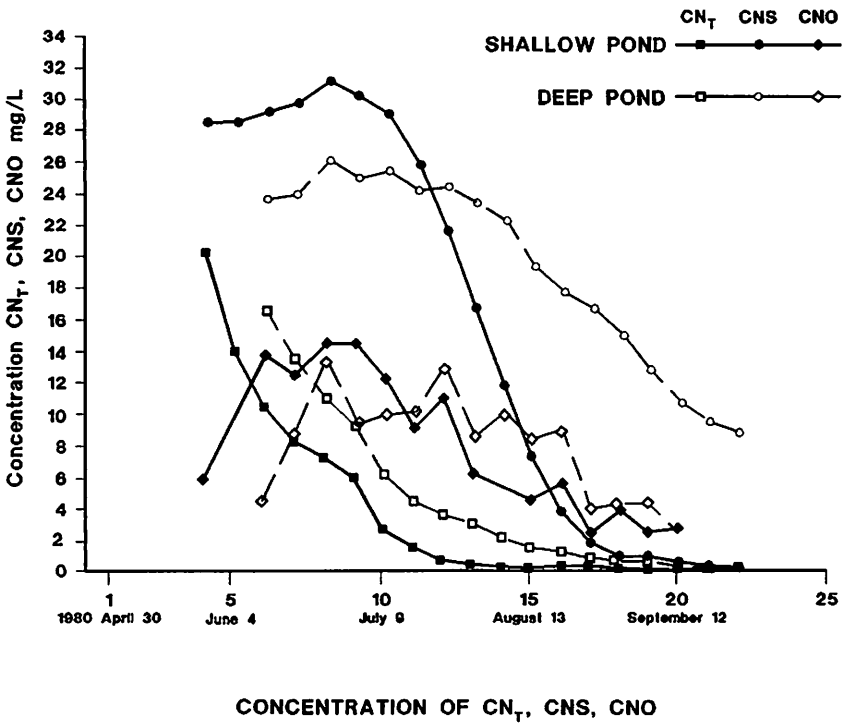

Figure 11.4. Concentration of CN_{total}, CNS, and CNO in deep and shallow sections of a pond.

At first glance this work seems to disagree with the prior studies by Dodge and Zabbon (1952), who found that cyanide volatilization was dependent upon the ratio of solution area to depth in stagnant solutions. In ponds, however, there is a natural mixing caused by the convective currents that are separated by differences in pond temperature with depth, and by temperature differences between the air and water.

Longe and DeVries (1988) utilized this temperature-induced, convective mixing in their chemical-equilibrium pond model, which also assessed the cyanide degradation due to cyanide — copper precipitation. For an arid location (Yuma, Arizona) at various seasons, the following results were obtained:

- maximum time for 200 ppm WAD cyanide solution to degrade to 2.6 ppm was 6 months
- minimum time for 200 ppm WAD cyanide solution to degrade to 2.6 ppm was 3 months
- winter clean-up was more rapid than summer clean-up due to temperature-induced convection currents carrying CO_2-rich, cyanide-lean solution to the bottom of the pond
- almost all of the copper was precipitated as CuCN, rather than dissociating or

precipitating as malachite
- copper content had little effect on the rate of cyanide loss
- the chemistry model predicted final pH values approaching 5.0

Simovic *et al.* (1985) and Zaidi *et al.* (1987) attempted to quantify cyanide losses in process ponds in Canada. They developed a numerical model that predicts cyanide removal, and the model has been validated against actual pond data. The volatilization of HCN from surface waters is the dominant mechanism for natural cyanide degradation; 90% of the free cyanide was removed by volatilization, and an additional 10% was removed by chemical oxidation (Simovic *et al.*, 1985). Cyanide degradation was found to follow a first-order reaction with respect to free cyanide and cyano-metal complexes of zinc, nickel, copper, and iron. Temperature and aeration have the most significant effect on the volatilization rate of free cyanide and most metal cyanide complexes studied. Simovic *et al.* (1985) found also that ultraviolet radiation has a significant effect on the stability and degradation of iron-cyanide complexes in the surface ponds.

Bench-scale laboratory data were fitted to a mathematical model which considered volatilization of free cyanide and dissociation of the metal-cyanide complexes. The model fit the experimental data of single-metal cyanide complexes well, with correlation coefficients of 0.93 to 0.99 (Simovic *et al.*, 1985). Validation of the natural degradation model for predicting the degradation of cyanide in impoundments has been performed by Environment Canada. The model has been used to predict the degradation of cyanide in pilot and full-scale batch and dynamic systems.

As the Environment Canada and DuPont models are validated by comparison with measurements from actual field conditions, they will become useful in predicting the rate of natural treatment of process solutions in ponds. The models will also be helpful in assessing the potential risk of cyanide release and the monitoring time required for decommissioned and inactive process-facilities.

Cyanide degradation mechanisms described in the prior section on surficial ponds are applicable to tailings ponds. Typically, tailings slurries and solutions upon discharge from the mill are at pH 10 or above. As these slurries or solutions "age" in the impoundment, the pH value is reduced due to rainfall and carbon dioxide uptake. As the pH value is lowered, the HCN concentration in the tailings solution increases and volatilization occurs (see Figure 11.1).

Surface effects have been shown to contribute to a large proportion of cyanide loss in mill tailings systems in South Africa (Smith *et al.*, 1984). Discharge concentrations from a conventional (non-CIP) mill showed cyanide concentrations decreasing from about 20 mg/L cyanide in the tailings supernatant to less than 2 mg/L in the tailings porewater. Such values are common. Discharge from CIP/CIL plants at 200—250 mg/L free cyanide or more results in pool concentration of cyanide anywhere

in the range of 20—50 mg/L or less, throughout the world (*e.g.*, Australia, Brazil, Canada, New Zealand, South Africa, and the United States).

11.5.3. Reactions of Cyanide within the mill tailings Mass

a. Geochemical Systems

The tailings mass comprises a series of geochemical systems, all of which may or may not be present at different mill tailings facilities, and whose extent may also vary. These geochemical systems and the general groups of geochemical reactions associated with them can be divided into:

- mill tailings beaches and pool: dilution/concentration/oxidation reactions
- oxidized tailings zone: precipitation/coprecipitation reactions or solution by acidification due to secondary oxidation
- reduced tailings zone: resolution due to reduction in valence state, or precipitation of insoluble phase, *i.e.*, sulfides
- drains/underdrains/penstocks/decant structures: oxidation and precipitation

The last division, which may not (and should not) contain tailings solids, can induce a change in system geochemistry. For example, air access through a underdrainage blanket under the mill tailings mass may change the redox potential of that system, local to the drain.

Fundamental questions, still the subject of much debate, are where in such a system are the cyanide "losses" occurring and is there any loss of cyanide within the tailings or heap-leach mass? The term "loss" is somewhat of a misnomer. Transformation of cyanide to cyanate or thiocyanate is termed a "loss of cyanide", but large concentrations or masses of cyanate or thiocyanate can be of environmental significance in themselves. Also, the formation of iron-cyanide complexes reduces significantly the toxicity of the solutions, but the complexes are still considered in the total cyanide mass-balance.

b. Cyanide Data from Case Histories

It is worth examining certain practical test and field data dealing with actual mill tailings and tailings facilities where the behavior of cyanide has been evaluated in various climatic regimes and parts of the world. Residual cyanide values in mill tailings are a source of substantial (though perhaps often somewhat unwarranted) concern to regulatory agencies. Lack of data on cyanide "loss" or transformation within the mill tailings mass itself is commonly cited, and in many cases the data show the presence of residual cyanide levels after significant time intervals (Hendrix *et al.*, 1985). The extent to which these levels are a real risk to the environment is questionable, however. In this respect, the following work on mill tailings and tailings impoundments illustrates some of the issues.

The work of Smith *et al.* (1984) shows profiles of pore-water quality in mill tailings systems. Table 11.11 shows the variation with depth of total cyanide within a tailings facility, and shows that low residual values of cyanides are present throughout the tailings profile. Table 11.12 relates concentration to overall chemistry within the tailings for the oxidized, intermediate, and reduced zones in the tailings mass. It is interesting to note the low values of cyanide in the reduced zone (<1 mg/L total cyanide), and the large number of samples examined (n = 149).

Smith *et al.* (1985) developed data derived from pre-operational test work for gold tailings from the Cannon mine, Washington State, USA. The geochemical effects of hydrogeochemical reduction and rainwater leaching of the mixed tailings are shown in Table 11.13. In the chemically reduced case, cyanide levels decreased to <0.05 mg/L, due to thiocyanate formation, and rainwater leaching reduced the total cyanide from >300 mg/L to about 57 mg/L as total cyanide, of which about 2.5 mg/L is free cyanide.

Smith (1987) developed data from test work on the Ridgeway mine pilot-plant tailings in South Carolina. These data show the loss of cyanide levels over time and during leaching with rainwater. The data in Table 11.14 show that copper and cobalt are lost from the aqueous phase of the system at an enhanced rate as compared with their leach rate.

Table 11.11. Cyanide profile in interstitial water in a decommissioned mill-tailings impoundment, Witwatersrand, Republic of South Africa (after Smith *et al.*, 1984)

Borehole	Piezometer No.	Depth m(1)	Total CN mg/L(2)
A	1	11	0.16
	2	17	0.21
	3	25	0.57
B	1	27	1.54
	2	30	0.16
	3	47	<0.01(3)
C	1	18	0.22
	2	22	2.92
	3	26	0.35
D	1	19	N/S(4)
	2	24	1.09
	3	28	1.86

(1): Total height of tailings impoundment, 32 m (104 ft).
(2): Cyanide discharge concentration varied between 8—19 mg/L during operation.
(3): Samples taken below 32 m are in the sediments below the impoundment.
(4): N/S, no sample.

Table 11.12. Chemistry of oxidized, intermediate, and reduced zones in mill-tailings impoundments (mean values), Witwatersrand, South Africa, after twenty years (after Smith *et al.*, 1984).

Zone	pH	TDS	SO_4	Total Fe	Mn	Total CN
Oxidized zone, 0—3 m	6.6	3350	1850	47	4	0.6
Intermediate zone, 3—15m	6.6	3600	2210	21	11	2.0
Reduced zone, 15—35 m	6.6	2850	1600	8	20	0.9

(1): pH; units otherwise in mg/L. Sample total = 149
(2): Total cyanide in near-surface groundwater below impoundment was 0.8 mg/L (meanvalue).

Table 11.13. Cyanide chemistry of "mixed" tailings and flotation tailings liquid, Cannon mine, Washington State (after Smith *et al.*, 1985).

Parameter	Mixed-Tailings Supernatant	Reduced Mixed-Tailings Supernatant
pH value (units)	7.17	5.17
Total dissolved solids	4230	N/A
Total cyanide	284	<0.05
Free cyanide	0.35	<0.05
Iron	10	1100
Cobalt	0.33	0.55
Copper	0.03	<0.01
Mercury	0.0024	0.0062
Silver	<0.01	<0.01

Note: All values in mg/L, except pH.

Table 11.14. Time/cyanide-concentration dependency of copper and cobalt cyanide in pore water interstitial to mill tailings, Ridgeway mining project, South Carolina (after Smith, 1987).

Parameter	Original tailings pore water (mg/L)	Leached sample at time T1 (mg/L)	Leached sample at time T2 (mg/L)
Total cyanide	170	2.66	0.90
	408	1.9	0.09
Free cyanide	170	0.92	0.04
	408	1.4	0.09
Cobalt	0.73	<0.1	<0.1
	2.21	0.05	0.05
Copper	1.81	0.04	<0.01
	6.34	0.04	<0.01

Note: T2 = T1 x 2

c. Overall Effects in Mill Tailings

Kidd (1988) and Burden and Kidd (1987) developed data on the Golden Cross and the Macraes project, New Zealand, showing overall cyanide degradation, both in the tailings pool and in the tailings mass. Mudder and Goldstone (1989) described and compared cyanide degradation, both in tailings decant-water and in the entrained tailings pore-water, from test data at the Golden Cross mine, New Zealand. For the mill tailings testing, tailings samples were sealed in cannisters and opened sequentially over time. Test results for the decant are given in Table 11.15, and those for the tailings pore-water are in Table 11.16. Whereas the total cyanide levels remained stable, WAD-cyanide levels decreased rapidly, particularly in the decant water (6.8 ppm to 0.33 ppm in 28 days), presumably by precipitation and degradation. Similar data are given by Smith *et al.* (1984) for mill tailings facilities in South Africa, by Smith (1988b) for gold-tailings projects worldwide, and by Caldwell and Smith (1985) for projects in the U.S.A.

Table 11.15. Cyanide decay in mill-tailings decant, Golden Cross project, New Zealand (after Mudder and Goldstone, 1989).

Exposure Time	pH	Total CN	WAD CN
Initial	10.2	29.4	6.8
1 day	8.0	29.4	—
3 days	8.2	30.0	—
7 days	8.2	30.0	—
14 days	8.0	31.9	—
28 days	7.3	32.0	0.33

Note: All values in mg/L unless otherwise stated.

Table 11.16. Cyanide decay in mill-tailings pore water, Golden Cross project, New Zealand (after Mudder and Goldstone, 1989).

Parameter	Initial	1 Week	2 Weeks	4 Weeks	8 Weeks	12 Weeks
pH	10.2	9.7	9.1	9.8	9.8	9.0
SO2	2525	2525	2530	2370	2370	2390
Ca	858	858	858	858	808	805
Total hardness (as $CaCO_3$)	2140	2140	2140	2140	2013	2008
Total CN	29.4	29.4	31.3	25.5	27	25
WAD CN	6.8	6.6	5.5	3.8	2.1	1.51
Cd	0.1	<0.01	<0.01	<0.01	<0.01	<0.01
Co	0.33	0.25	0.2	—	—	—
Cu	5	4.3	2.9	2.1	0.53	0.16
Fe	8.7	8.9	9	9.3	9.3	9.5
Zn	0.01	0.03	0.01	<0.01	0.01	0.01
Pb	<0.1	<0.1	<0.1	<0.1	—	—
Mn	0.02	0.02	<0.01	0.01	0.02	0.02
Ag	0.04	0.01	0.01	0.02	0.02	0.02
Cr	0.02	—	—	<0.02	—	—
Hg	0.0002	<0.0001	<0.0001	<0.0001	—	—

Note: All values in mg/L unless otherwise stated.

11.5.4. Cyanide Reactions within Natural Liners and Geologic Subsite Materials

In most subsite geologic systems below mill tailings facilities, unless the facility was sited in a swamp or a lake, there is a continuous increase of the moisture content and a continuous decrease of oxygen potentially available with depth below the interface of the tailings and the geologic materials. In the case of liner materials of natural soil, the presence of oxygen and ambient moisture content may depend on a variety of factors including, but not limited to:

- the hydraulic head on the liner
- the extent and efficiency of underdrains below the mill tailings

Two factors, oxygen content and moisture content, have a significant influence on cyanide geochemistry and degradation behavior in the natural liner or subsite

geologic system. Cyanide-reaction mechanisms particularly susceptible to changes in soil moisture and oxygen content are volatilization and biodegradation. These mechanisms are significant because they have been shown to be the two most effective processes for changing the concentration of cyanide, *i.e.*, a cyanide degradation or "loss" mechanism in the vadose or unsaturated soil zone (Chatwin and Hendrix, 1988). The rate of cyanide degradation in the unsaturated or vadose zone is seen to be more rapid than that found in the saturated zone. Cyanide chemical and geochemical reactions which are effectively degradation mechanisms in natural soil liners and geologic materials are:

- the *in-situ* hydraulic conductivity and porosity of the liner
- the mineralogy of the liner
- volatilization
- biodegradation
- adsorption and precipitation
- hydrolysis

a. Cyanide Volatilization

Two major factors control volatilization in natural materials. First is the solution pH, which controls cyanide hydrolysis to HCN and has been discussed previously. The second factor is the availability of continuous vapor path, by which the HCN vapor can migrate from the cyanide solution (Chatwin, 1990).

Other properties upon which cyanide volatilization in natural materials is dependent are the cyanide solubility in water, HCN vapor pressure, and cyanide concentration in the solution. Material properties that affect the HCN volatilization include: water content, sorptive and diffusion characteristics of the soil, and bulk properties of the material such as organic-matter content, porosity, density, and clay content. Meteorological parameters that would affect HCN volatilization are airflow rate over the material, humidity, and temperature.

Cyanide in natural materials may be partitioned among the entrained water, entrained air, and the material solid phase. Considered as a whole, a natural material represents all three phases of matter rather than one. The atmosphere constitutes another air compartment which is distinct from the entrained air. The rate of volatilization of a HCN molecule from a sorption site on the solid phase in the natural material (or in solution in the entrained water) to the vapor phase in entrained air, and then to the atmosphere, is dependent on the physical and chemical properties of both HCN and the material, and on the process of moving from one phase to another.

b. Biological Degradation

Normally, in the upper, oxidized portions of the soil where the conditions are aerobic, biological processes may consume cyanide and generate cyanate (Towill *et al.*,

1978). The hydrogen cyanate is in turn hydrolyzed into ammonia and carbon dioxide. Immediately below the mill tailings mass, however, the entrained air in the natural liner or the subsite geologic material may be depleted in oxygen and may have limited capacity to support aerobic reactions involving cyanide.

From testing of saturated and unsaturated soils, Chatwin and Trepanowski (1987) found that the oxidation of cyanide is almost 25 times more effective in unsaturated soils than in saturated soils; the unsaturated soils had substantial bacterial growth (10^9 counts per gram) *versus* none in the saturated soils. This result is consistent with the studies by Fuller (1984) in his comparison of aerobic and anaerobic cyanide removal in soil. Coburn (1949) found the toxic limit for effective anaerobic degradation of cyanide to be about 2 mg/L in a waste stream.

c. Adsorption and Precipitation

Two mechanisms that seem equally effective, both under saturated and unsaturated conditions, are precipitation and adsorption. These two mechanisms are placed together because they are difficult to separate; in a natural soil or geologic-material/cyanide-solution system where the cyanide concentration is in hundreds of mg/L, it is extremely difficult to determine if the cyanide is being removed as a precipitate, as an insoluble ferrocyanide, or as cyanide adsorbing on material surfaces in the soil.

In tests with free-cyanide solution in natural materials, it has been found that cyanide attached to solid particles correlates well with soil organic-carbon content. Western U.S. subsoils tested by Chatwin and Trepasowski (1987) showed organic-carbon contents ranging from 0.1 to 1.2%, with a mean of 0.6%. The organic carbon in the soil was found to adsorb about 12 mg/L cyanide from a 130 mg/L solution as it travelled 0.3 m (1 ft) through the soil, or about 0.5 g of free cyanide adsorbed per gram of contained organic carbon. Additional studies with pure mineral components (Chatwin and Hendrix, 1988) indicated that free cyanide will also adsorb on inorganic surfaces such as clays and feldspars; the combined removed cyanide varied from about 20 to 80% of the input concentration of cyanide.

d. Hydrolysis

As the system pH falls, HCN can be hydrolyzed to give formate, as either formic acid or ammonium formate. The system pH will determine the extent of formation of each compound, a lower pH favoring formic acid formation.

In summary, cyanide degradation occurs in saturated natural materials in many different environments. Cyanide reacts and is "lost" from the solution phase of the system, both in field observations and laboratory data. For example, data from Witwatersrand, South Africa (Smith *et al.*, 1984), show a distinct lack of impact from tailings seepage in terms of cyanide, whereas the evidence of seepage impact from other

species is present in groundwater around and below gold-tailings facilities.

Quantification of the effects of hydrogeochemical attenuation has been made in overall studies. A detailed study of cyanide "loss" by dilution, degradation (decay), and geochemical attenuation was given by Smith and Brown (1986) for the proposed spent-ore disposal site at the Annie Creek mine, South Dakota. Table 11.17 illustrates partition coefficients for cyanide attenuation in a variety of subsite materials. Partition coefficients, although expressed in units of mL/g, relate to the mass of cyanide that can be removed from solution per unit mass of solid-phase material; the coefficients are nominally independent of the actual concentration of cyanide in the reacting solution. There is clearly variation in cyanide reactions with differing types of material, with the weathered materials (*i.e.*, clay and slate) being better cyanide attenuators than the basal limestone.

Although the migration mechanisms for HCN escape from the groundwater operate slowly, it is not necessary for the HCN to leave the soil, but just to leave the aquifer so as to decrease

groundwater concentrations of cyanide. Hence, substantial amounts of HCN can be trapped or isolated in the capillary fringe or soil above the aquifer and not report in an analysis of the groundwater. As long as a storm event or precipitation does not drive the isolated cyanide back down into the groundwater, the cyanide can be slowly removed by biological degradation or hydrolysis to formate in the unsaturated zone.

It should be stressed that there needs to be a distinction made between the overall cyanide degradation or decay in soils/rocks and the geochemical/hydrogeochemical decay of cyanide. If the decay component of volatilization is removed, some subsite soils or other geological material may have little or no capacity for cyanide degradation. For example, geochemical studies of a cemented conglomerate material below a tailings facility in the United States showed that, when tested in an inert (argon-rich) environment with no available pathway for gas losses, there was no appreciable cyanide decay in the system (Smith 1989, unpublished data).

Table 11.17. Attenuation calculation summary: distribution coefficients (mL/g), Wharf Resources Annie Creek mine, South Dakota (after Smith and Brown, (1986).

Material	Sample	Pore Volume	Total Cyanide	Free Cyanide	Arsenic
Clay	1.1	1	1.95	3.42	430
		3	4.0	8.12	-
	1.2	1	1.30	1.48	426
		3	10.81	33.31	-
Shale	2.1	1	0.66	0.69	-
		4	1.93	0.84	667
	2.2	1	0.65	0.93	334
		4	1.26	1.04	65.10
Rubble	3.1	1	1.25	1.93	98.88
		3	0.93	1.33	-
	3.2	1	1.60	2.41	98.80
		3	0.83	1.18	-
Limestone	4.1	1	9.06	0.03	-
		3	0.09	0.04	-
	4.2	1	0.06	0.03	-
		3	0.07	0.07	-

Chapter 12

A Geochemical Study of the Main Tailings Impoundment at the Falconbridge Limited, Kidd Creek Division Metallurgical Site, Timmins, Ontario

Tom A. Al, David W. Blowes, John L. Jambor
Waterloo Centre for Groundwater Research
University of Waterloo
Waterloo, Ontario
N2L 3G1

12.1. INTRODUCTION

The Kidd Creek mine is approximately 20 km north of Timmins, Ontario (Figure 12.1) and ore from the mine is milled and refined at the Kidd Creek metallurgical complex 25 km east of Timmins. The ore consists mainly of chalcopyrite, sphalerite, galena, and pyrite in massive ore, and chalcopyrite in stringers. The orebody was discovered in November, 1963, and commercial production commenced in November 1966. By the end of 1973 the mine had produced 22.5 million tonnes of ore grading 9.73% Zn, 1.53% Cu, 0.39% Pb, and 146 g/t Ag, and reserves were about 85 million tonnes (Walker and Mannard, 1974). Production peaked at 12,400 tonnes per day (tpd) in 1985 and has since declined to approximately 10,000 tpd. Reserves at the end of 1991 were 37.2 million tonnes averaging 5.08% Zn, 3.45% Cu, 0.15% Pb, and 63 g/t Ag (Giancola, 1992).

Tailings at the Kidd Creek site are deposited as a thickened slurry in a conical pile (Robinsky, 1975, 1979; Robinsky *et al.*, 1991). The initial tailings, which contain about 17 wt% (6.4 vol %) solids, are pumped from the mill to a thickener at which excess mill discharge-water is separated, and the tailings slurry is upgraded to 62 wt% (35.3 vol %) solids. The thickened tailings are pumped through a series of spigots along an elevated central road, and are discharged into a 1200-ha impoundment (Figure 12.1). The resulting conical tailings pile is currently 13 m high and 4000 m in diameter, and contains approximately 100 million tonnes of tailings. The tailings consist of 10 to 25 wt% pyrite, 1 to 2 wt% pyrrhotite, 1 to 2 wt% combined sphalerite

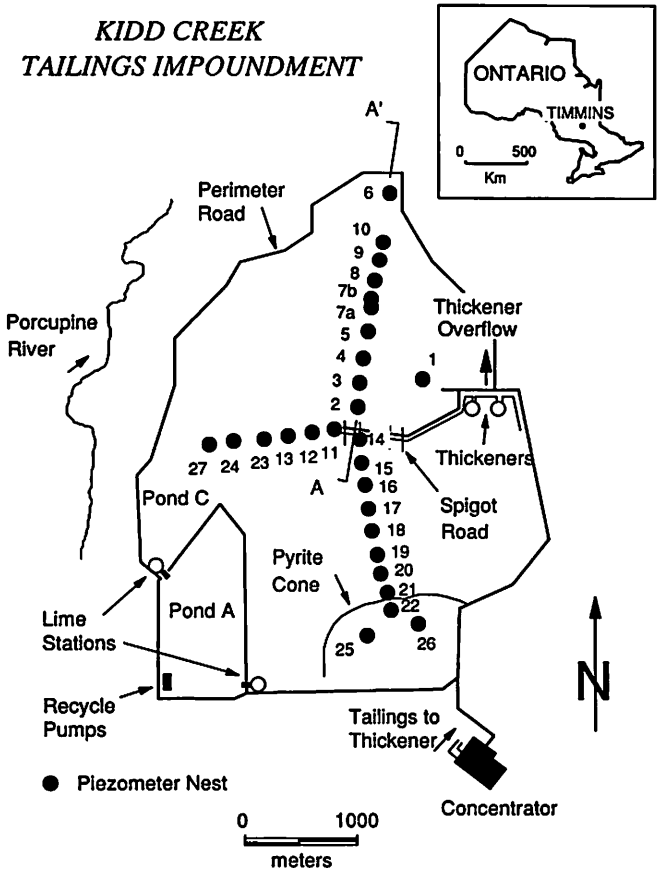

Figure 12.1. Plan of the Kidd Creek tailings impoundment showing the locations of piezometer nests.

and chalcopyrite, 75 to 85 wt% gangue minerals, in which quartz and various silicates are predominant, with 7—8 wt% carbonate minerals and traces of numerous other minerals (Table 12.1).

The zinc refining process used at Kidd Creek requires the removal of dissolved Fe from acidic Zn- and Fe(III)-SO_4 solutions. Removal is achieved by adding Na and increasing the pH, resulting in the precipitation of natrojarosite $NaFe_3(SO_4)_2(OH)_6$ (Scott and Dienstbach, 1990). The monovalent cation site in the natrojarosite precipitate, although dominated by Na, also contains substantial quantities of H_3O^+ and minor to trace quantities of K, Pb, and other elements in solid solution (Scott *et al.*, 1986; Jambor and Owens, 1992). The natrojarosite residue was collected in a dedicated, lined settling pond until 1985, and thereafter has been co-disposed with the

Table 12.1. Tailings mineralogy (after Jambor et al., 1993)

Mineralogy		wt%
quartz	SiO_2	48.7
chlorite	$(Mg,Fe,Al)_6(Al,Si)_4O_{10}(OH)_8$	21.4
pyrite	FeS_2	12.5
siderite (and Fe oxides)	$FeCO_3$	4.9
muscovite	$KAl_2(Si_3Al)O_{10}(OH)_2$	3.3
dolomite	$CaMg(CO_3)_2$	3.1
natrojarosite	$[Na_{0.75}K_{0.01}(H_3O)_{0.24}]Fe_3(SO_4)_2(OH)_6$	1.5
pyrrhotite	$Fe_{1-x}S$	1.4
albite	$NaAlSi_3O_8$	0.8
amphibole*	$(W,X,Y)_{7-8}(Z_4O_{11})_2(OH)_2$	0.5
gypsum	$CaSO_4.2H_2O$	0.5
chalcopyrite	$CuFeS_2$	0.5
sphalerite	(Zn,Fe)S	0.3
cassiterite**	SnO_2	0.2
stilpnomelane	$(K,Na)(Fe,Al)_{10}Si_{12}O_{30}(O,OH)_{12}$	<0.5
Total		99.6

* W=Ca,Na±K; X=Mg,Fe^{2+}±Mn^{2+}; Y=Fe^{3+},Ti,Al; Z=Si,Al
** includes traces of galena and tennantite-tetrahedrite

tailings. The refinery produces approximately 250 tpd of natrojarosite residue, which amounts to 2.5 wt% of the total tailings solids.

The goal of the present study is to characterize the geochemical interactions among the tailings pore water, pore gas, and solids, so that the results of the research can assist in the prediction of the quality of the future effluent. The evolution of the pore-water quality in the tailings will be affected by geochemical reactions such as sulfide oxidation, and by groundwater flow within the tailings impoundment, which contributes to solute transport.

12.2. OBJECTIVES

The principal objectives of the study were (1) to characterize the tailings pore-water chemistry with the aim of defining changes in the pore-water composition relative to that of the mill discharge-water; (2) to determine the geochemical mechanisms that are responsible for changes in the tailings pore-water composition through time, (3) to use the data obtained from the geochemical sampling during two consecutive years to determine the relative importance of the various mechanisms on

the evolution of the pore-water quality, and to characterize the regime of groundwater flow within the tailings. When the results of the first set of geochemical samples were obtained there were indications that dissolution of the natrojarosite residue was occurring and was affecting the pore-water quality. Natrojarosite is thermodynamically unstable in the reduced conditions within sulfide-rich tailings (Alpers *et al.*, 1989; Brown, 1971; Dutrizac, 1980; Kershaw and Pickering, 1980). Thus, the additional objective of determing whether natrojarosite is stable in the tailings impoundment was introduced. One of the concerns was the possibility that the Fe(III) released by natrojarosite dissolution would cause anaerobic oxidation of the sulfides in the impoundment:

$$14[Na_{0.75}K_{0.01}(H_3O)_{0.24}]Fe_3(SO_4)_2(OH)_6 + 3FeS_2 \Rightarrow \qquad (1)$$

$$21/2Na^+ + 7/50K^+ + 84/25H_3O^+ + 34SO_4^{2-} + 45Fe^{2+} + 36(OH)^- + 24H_2O$$

12.3. METHODS OF INVESTIGATION

Samples of the pore water, from surface to the silt/clay underlying the tailings, were collected along three sections that extended from the central spigot road to the perimeter road (Figure 12.1). Data were collected from twenty-five sample sites on the main tailings cone. Core samples were collected from most piezometer-nest sites for analysis of the mineralogy and the solid-phase major and trace-element compositions. The samples were collected between August 1991 and July 1993. Sample sites on the main tailings were selected to be representative of the most oxidized to the least oxidized tailings. This was accomplished by selecting sites where the time between the most recent tailings disposal and the geochemical sampling varied from approximately two weeks (KC14 — least oxidized) to 7 years (KC1 — most oxidized).

12.3.1. Tailings Pore-water—Vadose Zone

Pore water from the vadose zone at all sites was sampled by collecting cores in thin-walled aluminum casing, 7.62 cm in diameter. The cores were cut into lengths of 20 to 25 cm, and pore water was squeezed from each section using a method similar to that described by Patterson *et al.* (1978), as modified by Smyth (1981). This method minimizes oxidation of Fe(II) by atmospheric oxygen during sample collection. All pH and E_H measurements were done in the field. Determinations of pore-water pH and E_H were made at least three times during the collection of each sample to obtain results that were reproducible to within ± 0.05 pH units and ± 20 mV. The pH electrode (Orion Ross combination pH electrode, Model 815600) was calibrated with standard buffers at pH 4 and 7, and the E_H electrode (Orion platinum redox electrode, Model 96-7800) was checked regularly with Zobell's solution (Garrels, 1960). Sample volumes of 40 to 80 mL were obtained from most core sections. Samples were filtered

through 0.45-μm cellulose acetate filters, then were split into two volumes. One of the sub-samples was acidified with 12 *N*, analytical grade HCl to pH <1 for cation analysis, and the unacidified sub-sample was used for anion analysis. All samples were refrigerated until they were analyzed. The acidified pore-water samples were analyzed for Ag, Al, As, Ba, Ca, Cd, Co, Cr, Cu, Fe, K, Mg, Mn, Na, Ni, Pb, Rb, Se, Si, Sr, and Zn by atomic absorption spectroscopy. Some of the samples were analyzed by inductively coupled plasma-emission spectrometry. The unacidified samples were analyzed by ion chromatography to determine the concentrations of Cl, NO_3, PO_4, and SO_4. Most of the determinations were done at the Water Quality Laboratory at the University of Waterloo, and some were analyzed by the analytical laboratory at the Kidd Creek metallurgical site. Pore-water alkalinity was determined in the field on sub-samples of 3 to 10 mL using methyl red, bromcresol green indicator (Greenberg *et al.*, 1992) and a Hach Chemical Company digital titrator.

12.3.2. Tailings Pore-water — Saturated Zone

Pore water from the saturated zone was collected with a peristaltic pump, in polyethylene lines, from polyethylene-lined stainless steel or PVC, single-completion drive-point piezometers installed at regular intervals of 1 to 2 m between the water table and the base of the tailings. The method of sample collection from single-completion drive-point piezometers is similar to that used by Dubrovsky *et al.* (1984a) and Coggans *et al.* (1991). The stainless steel piezometers have a screened interval that is 15 cm long and 1.25 cm in diameter; the screened interval in the PVC piezometers is 15 cm long and 3.2 cm in diameter. All piezometers were bailed dry prior to sampling. Measurements of pH and E_H were made in a sealed flow-through cell, maintained at groundwater temperature of 5 to 10 °C. Samples were filtered with 0.45-μm cellulose acetate filters and were split into two sub-samples. One of the sub-samples was acidified, and the other was left unacidified. The samples were refrigerated until they were analyzed. Groundwater temperatures were measured with a thermistor probe in the piezometer tip after the sample was collected. Alkalinity determinations were made on all samples using 25- to 100-mL sub-samples using a Hach Chemical Company digital titrator and by potentiometric titration.

12.3.3. Tailings Solids

Core samples were collected at most sites using 7.62-cm-diameter aluminum tubing and a gas-powered impact drill. The cores were cut into sections 20 to 25 cm long, and were frozen at the field site. In the laboratory the cores were cut in half along the tube axis, and a sample of the tailings was collected from the most undisturbed, central portion of the core. The samples were then oven-dried at approximately 150°C. Major-element analyses for SiO_2, Al_2O_3, Fe_{total}, CaO, MgO, MnO, Na_2O, K_2O, TiO_2, and P_2O_5, as well as the trace elements Ba, Sr, and Y, were conducted on lithium-

metaborate fused beads by inductively coupled argon-plasma atomic-emission spectrometry. Trace-element analyses for Pb, Zn, Cu, Ni, Co, Cr, V, and As were conducted by X-ray fluorescence with pressed-powder pellets. Total carbon was determined using a Leco induction furnace with an infrared detector. The carbon analytical results are expressed as wt% carbonate minerals. The conversion from the analytical total carbon content is done by assuming that all of the carbon in the tailings is present in the form of carbonate minerals with an average formula of $(Ca_{0.2}Fe_{0.73}Mg_{0.06}Mn_{0.01})CO_3$ determined from data in Jambor *et al.* (1993b).

12.3.4. Hydrogeology

Characterization of the regime of pore-water flow within the tailings required the measurement of hydraulic conductivity (K), hydraulic head (ϕ), and the water-table elevation at all of the piezometer-nest locations within the tailings impoundment. Measurements of K were conducted in more than 100 piezometers by the method described by Hvorslev (1951). The results were compared with values of K calculated with the grain-size technique of Hazen (1892). Values obtained from the two methods were within one order of magnitude. Measurements of vertical and horizontal hydraulic gradients were made by measuring ϕ in all of the piezometers installed in the saturated zone. Transient variation in ϕ was recorded by repeated measurements over a two-year period. The water-table elevation at each piezometer nest was taken as the water level in the shallowest piezometer. The groundwater flow within the tailings was modelled with a steady-state, two-dimensional, cross-sectional finite-element program (FLONET; Guiger *et al.*, 1992). The model iterates on the position of the water table when the top boundary condition is specified as a recharge boundary. In this way, the measured field data (K, ϕ, and water-table elevation) were used to calibrate the model to obtain the observed water-table and hydraulic-head configuration.

12.4. RESULTS AND DISCUSSION

12.4.1. Pore Water

Pore-water data from four piezometer-nest locations (KC1, KC3, KC11, and KC14) are referred to in discussing the pore-water effects of sulfide oxidation and natrojarosite co-disposal with the tailings. During the following discussion, the reader should refer to the geochemical data for the four piezometer nests in Figures 12.2, 12.3, 12.4 and 12.5. At piezometer nest KC1 (Figure 12.1), limited tailings deposition has occurred for the past seven years, and the tailings near the surface are affected by sulfide oxidation to a depth of 20 to 40 cm. Tailings at piezometer nest KC3 are near the point of discharge, and the nearly continuous deposition at this site prior to the initial sampling in 1991 has limited the extent of sulfide oxidation. The water table has remained near the surface at KC3 because of continued deposition nearby;

Table 12.2. Mill discharge-water composition

		1991	1992	Average
Cations (mg/L)	Ca	654	684	669
	Mg	10.5	12.7	11.6
	Mn	0.95	3.08	2.11
	Na	47.3	50.3	48.8
	K	25.7	20.4	23.1
	Al	<0.02	<0.02	<0.02
	Fe	0.05	<0.05	<0.05
	Zn	0.55	9.06	4.81
	Cu	0.07	0.31	0.19
	Ni	0.07	0.15	0.11
	Co	0.05	0.10	0.08
	Cd	1.23	0.16	0.70
	As*	<3.0	3.5	1.8
Anions (mg/L)	SO_4	1520	1780	1650
	Cl	24.4	624.6	24.5
	HCO_3	15.0	50.4	32.7

Samples collected from the tailings thickener overflow. Natrojarosite is added to the tailings prior to thickening.

* Concentration in $\mu g/L$

Table 12.3. Elemental concentration ranges for 3 geochemical zones at sites KC1 and KC3

		Zone 4	Zone 3	Zone 2
KC1				
	Depth (m)	0-0.6	0.6-3.0	3.0-6.0
	Na	885-911	447-861	71-84
	K	29-56	45-58	19-31
	Ca	432-454	433-486	444-450
	Mg	483-3190	270-773	155-247
	Mn	1.6-641	0.7-4.7	0.7-1.0
	Fe	266-991	1-239	2-8
	Al	0-71	-	-
	Zn	2.3-6210	0.4-5.3	0.4-0.5
	Pb	0.27-1.93	0-0.24	-
	Cu	0-38.0	-	-
	Cd	0-33.2	-	-
	Co	0.1-27.1	-	-
	Cr	0-0.3	-	-
	Ni	0.1-5.4	-	-
	As (μg/L)	126-353	0-146	-
	SO_4	5180-27100	3000-5410	1860-2470
	HCO_3	0-141	64-239	91-136
KC3				
	Depth (m)	0-0.2	0.2-6.0	6.0-10.0
	Na	983	550-1460	88-123
	K	89	44-78	16-28
	Ca	451	369-496	451-484
	Mg	706	170-359	71-175
	Mn	22	1.0-11.7	0.8-1.5
	Fe	330	74-512	8-19
	Al	-	-	-
	Zn	4.7	0.65-7.2	0.2-0.4
	Pb	0.14	0.1-0.2	-
	Cu	-	-	-
	Cd	-	-	-
	Co	0.11	-	-
	Cr	-	-	-
	Ni	0.1	-	-
	As (μg/L)	38.8	15.0-106.0	3-22
	SO_4	6240	2970-5580	1660-3740
	HCO_3	540	221-372	48-58

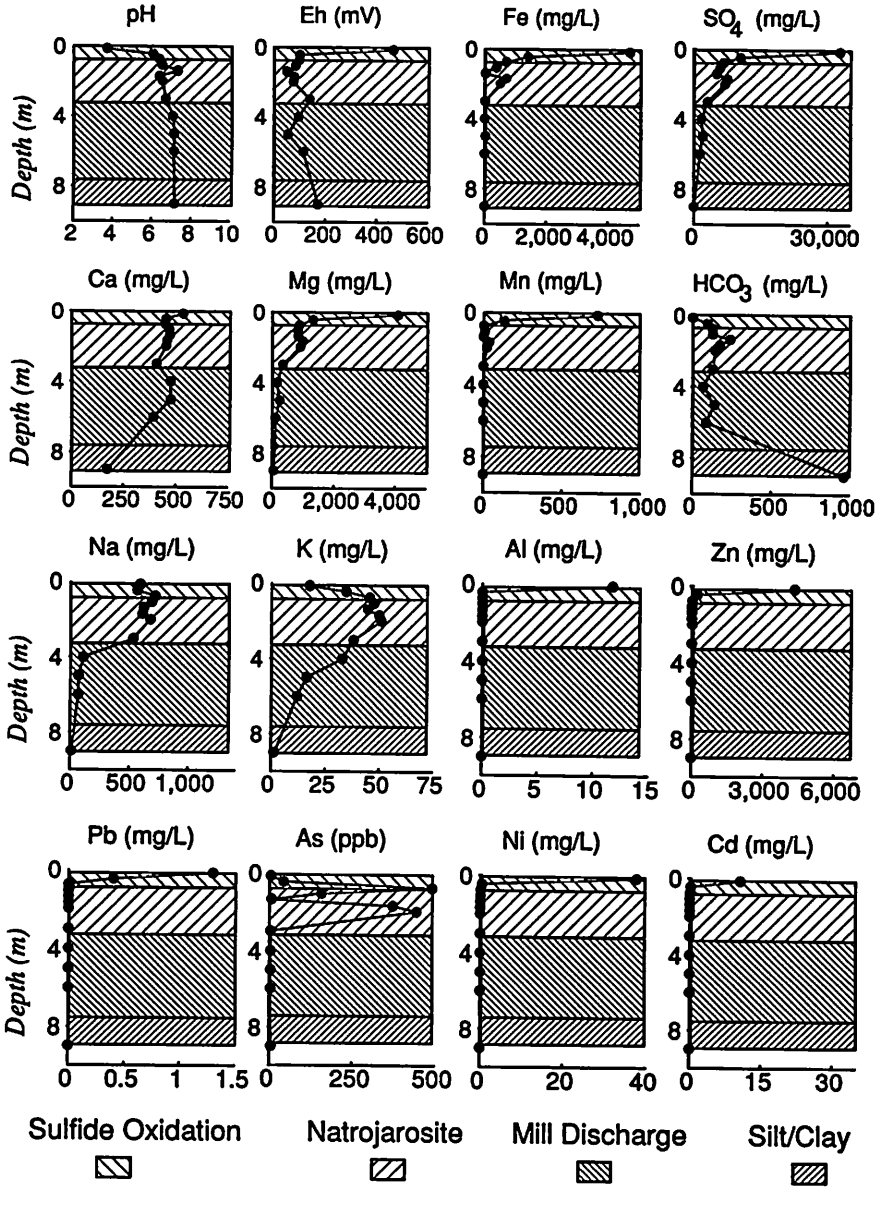

Figure 12.2. Pore-water geochemical data from the 1993 sampling at piezometer nest KC1.

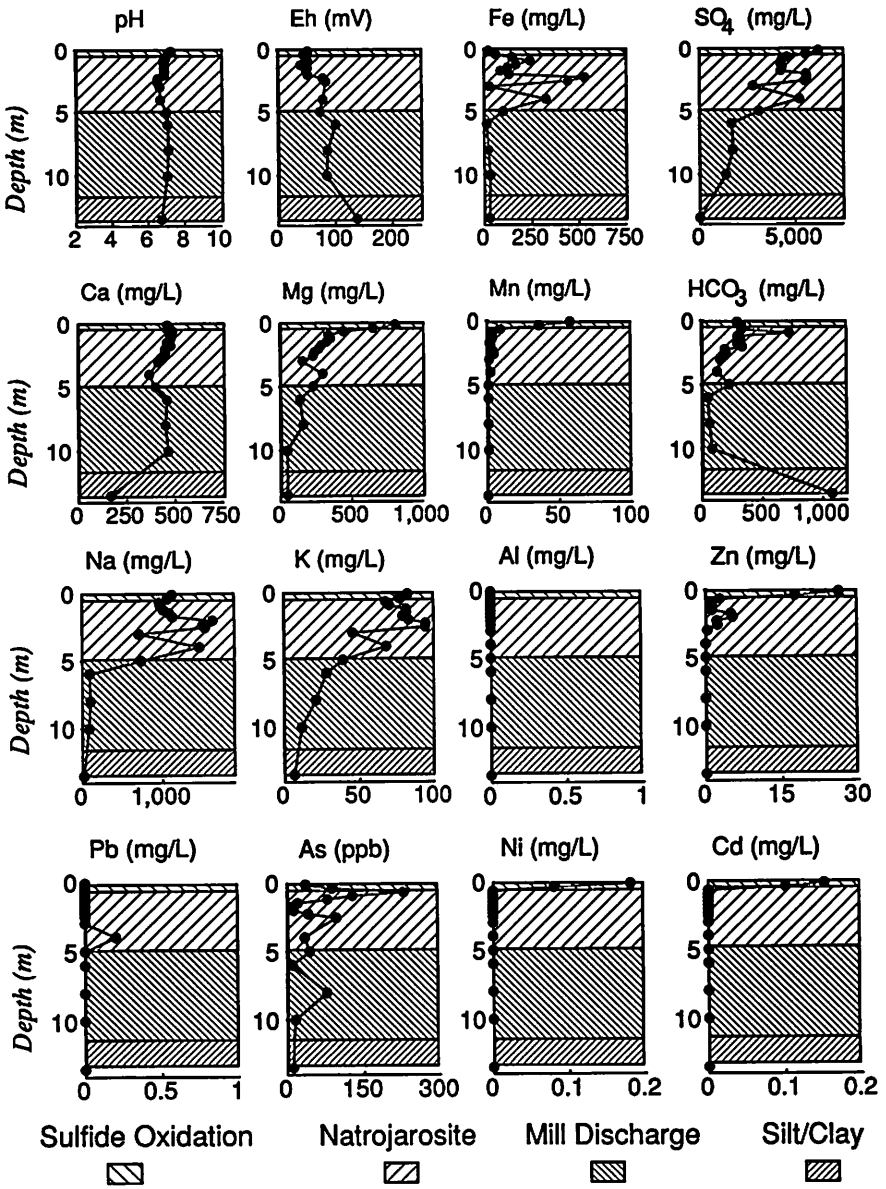

Figure 12.3. Pore-water geochemical data from the 1993 sampling at piezometer nest KC3.

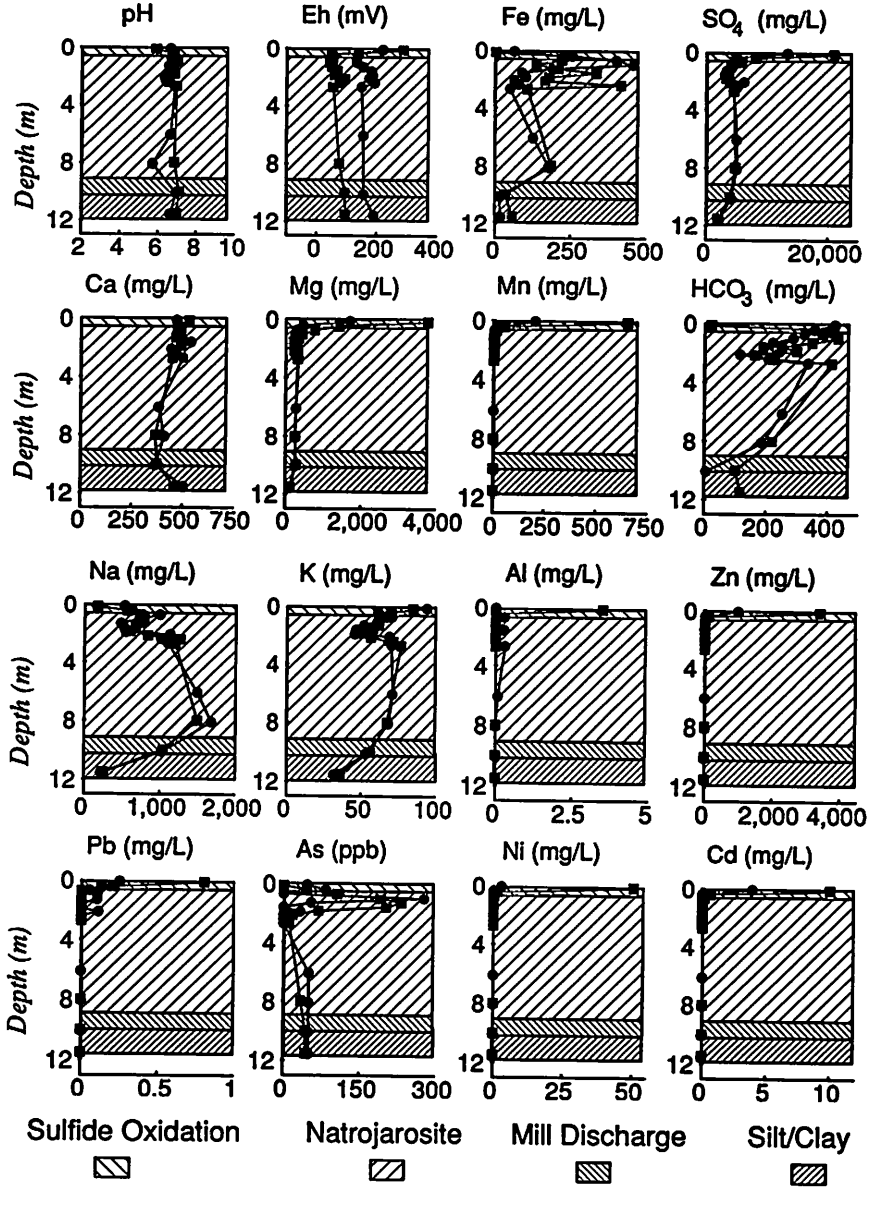

Figure 12.4. Pore-water geochemical data from the 1992 (dots) and 1993 (squares) sampling at piezometer nest KC11.

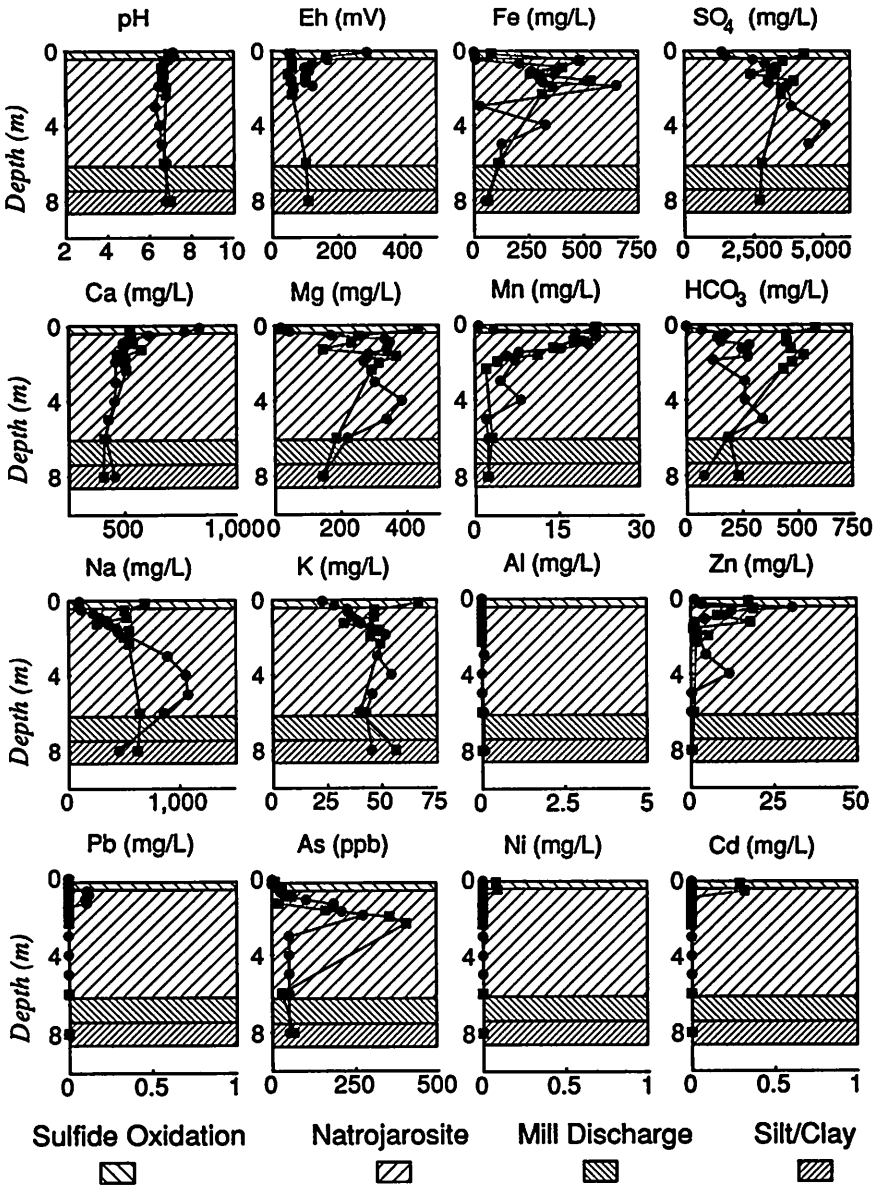

Figure 12.5. Pore-water geochemical date from the 1992 (dots) and 1993 (squares) sampling at piezometer nest KC14.

consequently, there is very little evidence of sulfide oxidation. Tailings had been deposited at site KC11 until eighteen months prior to sampling in 1992. When tailings deposition ceased at KC11, the water table at this site declined to maximum depths of between 6 and 7 meters during the dry summer months due to proximity to the permeable spigot road (Figure 12.1). As a result of the lower water table, the moisture content of the tailings at the surface declined more than at other sites. The surface has been exposed at KC11 since 1991, and the surface samples from 1992 and 1993 record the evolution of geochemical characteristics attributable to sulfide oxidation. The initial sampling (1992) at KC14 was completed within one week of the cessation of tailings deposition, and these samples represent the initial chemical condition for pore water within the tailings impoundment. Follow-up sampling was done at this site in 1993, and comparison of the 1993 results with the data from 1992 reveals the changes that have occurred in the pore-water geochemistry subsequent to tailings deposition.

Comparison is made between the pore-water composition from the tailings and the composition of the present mill-discharge water (Table 12.2). The pore-water chemistry at all sites defines four zones which represent pore water from: (1) the underlying varved silt/clay, (2) the deep tailings unaffected by natrojarosite disposal, (3) shallow to intermediate depths where natrojarosite disposal has affected the pore-water chemistry, and (4) surface samples where sulfide oxidation has had an impact on the pore-water chemistry. Table 12.3 shows the range of concentrations of the metals and anions in the three zones within the tailings from two representative profiles.

a. Varved Silt/Clay Underlying the Tailings

At most sites the samples from the deepest one or two piezometers are distinctive in that there are unusually high alkalinity and low SO_4 concentrations. In some cases the Ca concentrations decrease significantly in these deep samples. In this interval the concentrations of other metals are low to undetectable, the pH is between 6 and 7.5, and the E_H is generally between 100 and 200 mV. In this zone the samples are thought to be of pore water from the varved silt/clay soil underlying the tailings. Cluster analysis, using the partitioned cluster method (Wilkinson, 1990), was performed on pore-water geochemical data from most of these piezometers to support this inference. The analysis was conducted with two clusters, one to represent tailings and another to represent the clay substrate. The chosen variables were Ca, SO_4, and HCO_3: Ca and SO_4 were selected because the mill discharge-water, which forms the tailings pore-water, is near saturation with respect to gypsum $CaSO_4.2H_2O$, and HCO_3 was selected because high pore-water alkalinity occurs in many of the deep samples and in samples from piezometers within the clay, outside the impoundment. Almost all of the samples from the deepest piezometers at each nest were distinguishable from the overlying samples by the cluster-analysis method, thus suggesting that these piezometers are located within a different geochemical environment.

It is uncertain what chemical mechanism is responsible for the unusually high alkalinity in these deep samples. Acid-neutralization reactions are an unlikely mechanism as there is no apparent source of acidity. One possible mechanism is sulfate reduction:

$$1/2SO_4^{2-} + CH_2O \Rightarrow 1/2HS^- + 1/2H^+ + HCO_3^- \qquad (2)$$

The submerged forest undergrowth at the base of the tailings could contribute organic material for growth of heterotrophic, sulfate-reducing bacteria. At most sites, high alkalinity concentrations coincide with very low SO_4 concentrations; if the samples are from the underlying soil, however, the low SO_4 may also be a natural characteristic of the soil.

b. Mill Discharge-water Zone

In the deep pore water within the tailings there are low concentrations of Fe, Mg, Mn, Na, K, Zn, Pb, As, HCO_3, and SO_4; most other metals are below detection. The pH is near-neutral and the E_H is between 100 and 200 mV. The pore-water composition in this zone is similar to that of the mill discharge-water. There has been very little change in the pore-water composition in this zone since the tailings were deposited, suggesting that the solid phases present within these tailings are relatively stable. As an aid to determining the mechanisms controlling the pore-water composition in this zone, an equilibrium geochemical speciation model (MINTEQA2; Allison *et al.*, 1991) was used to model the pore-water speciation and to calculate saturation indices for relevant mineral phases.

In general, geochemical calculations of saturation indices (Figures 12.6 to 12.9) indicate that the pore water in this zone is slightly undersaturated to saturated with respect to calcite $CaCO_3$, and dolomite $CaMg(CO_3)_2$, thus suggesting that these minerals may be dissolving and contributing Ca, Mg, and HCO_3 to the pore water. The pore water in this zone is commonly slightly undersaturated to saturated with respect to siderite $FeCO_3$, is slightly undersaturated to slightly supersaturated with respect to $Fe(OH)_3$, and is supersaturated by several orders of magnitude with respect to goethite α-FeO(OH) and lepidocrocite γ-FeO(OH). These saturation indices suggest that the pore-water ferric-iron concentration is controlled by precipitation and dissolution of $Fe(OH)_3$. The pore water in this zone is undersaturated with respect to jarosite $KFe_3(SO_4)_2(OH)_6$, natrojarosite $NaFe_3(SO_4)_2(OH)_6$, and hydronium jarosite $H_3OFe_3(SO_4)_2(OH)_6$. In general, the pore water throughout the tailings is saturated with respect to gypsum; as this mineral has been detected by X-ray diffraction in most of the tailings samples (Jambor *et al.*, 1993b), the inference is that gypsum precipitation controls the pore-water concentrations of Ca and SO_4.

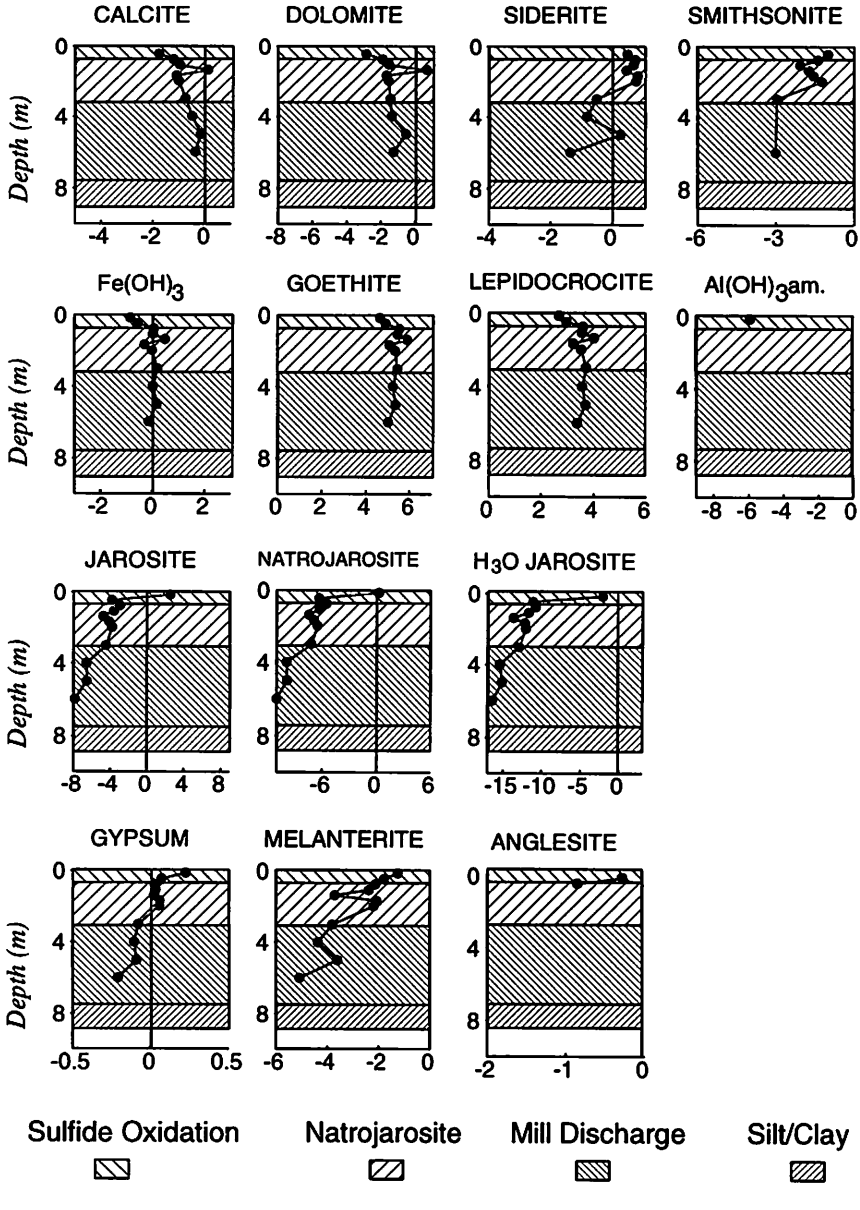

Figure 12.6. Saturation indices calculated with MINTEQA2 for geochemical date from the 1993 sampling at piezometer nest KC1.

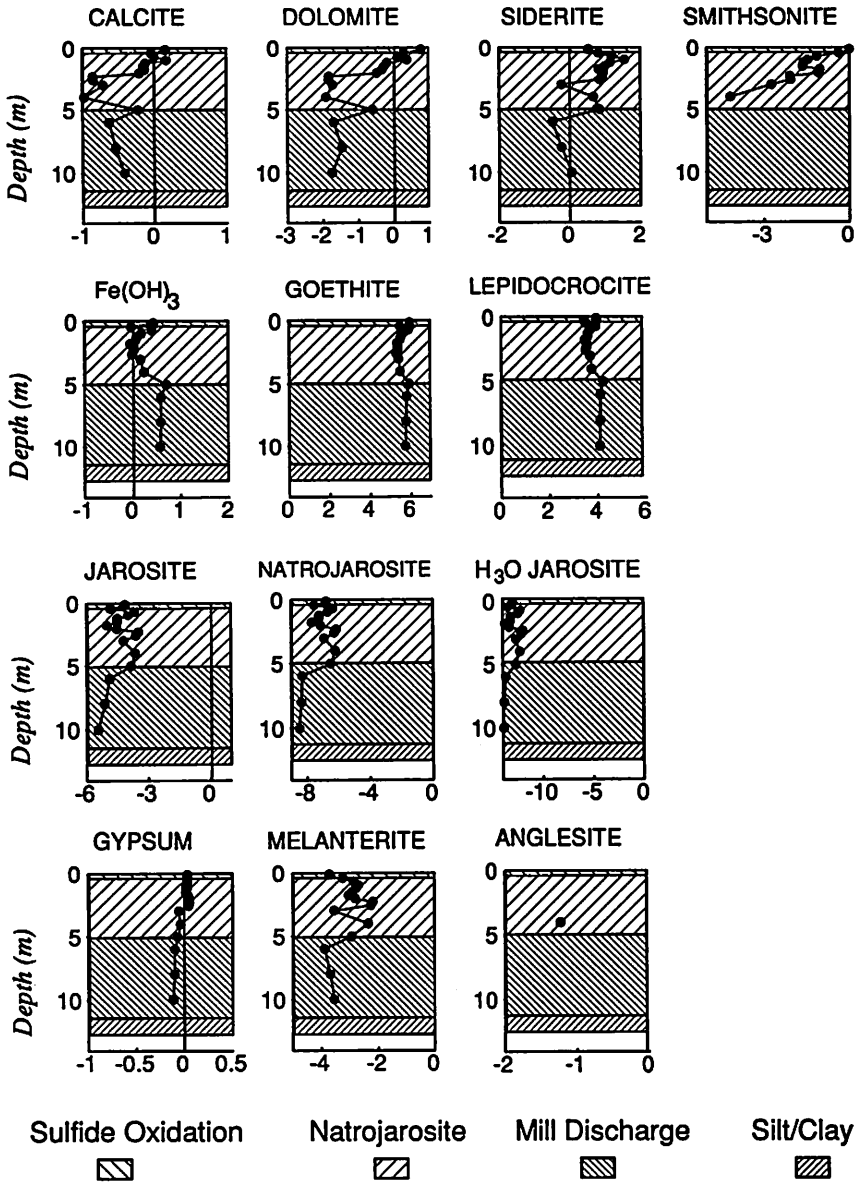

Figure 12.7. Saturation indices calculated with MINTEQA2 for geochemical date from the 1993 sampling at piezometer nest KC3.

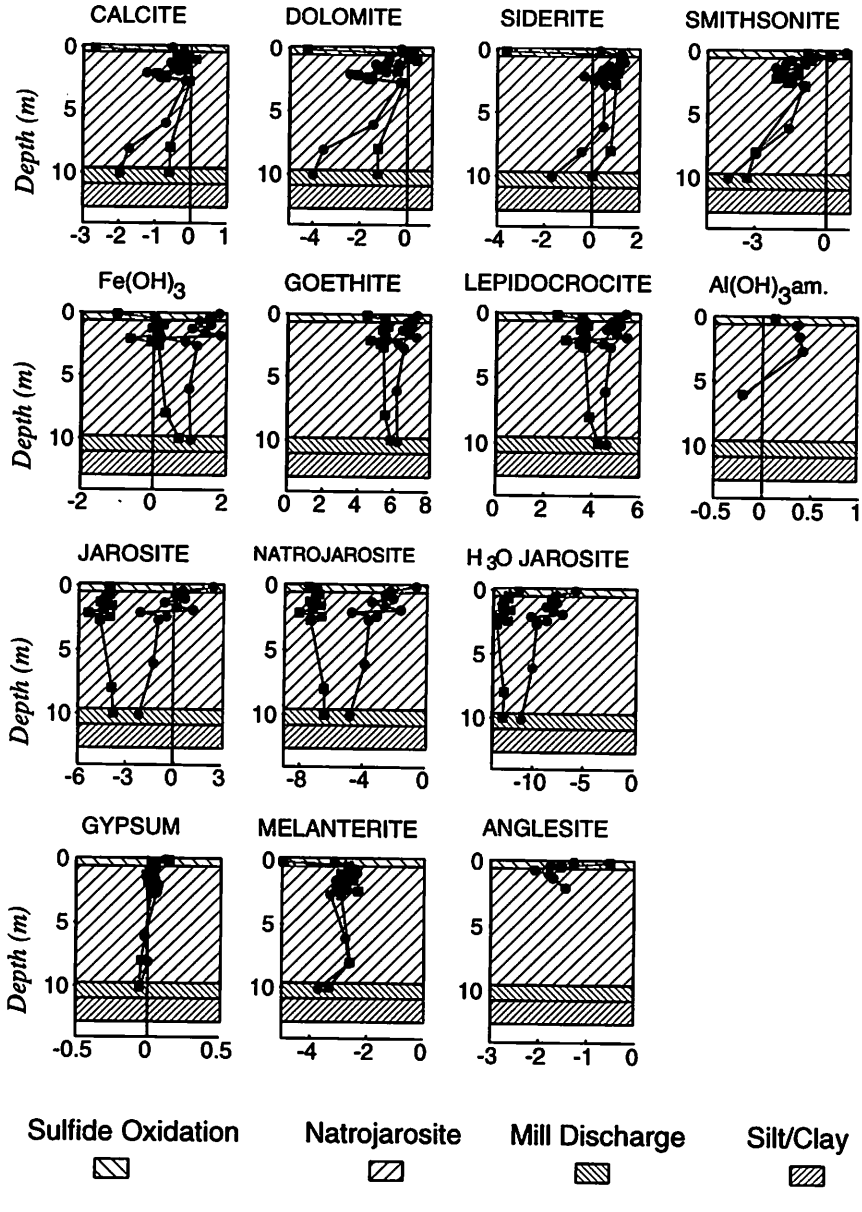

Figure 12.8. Saturation indices calculated with MINTEQA2 for geochemical data from the 1992 (dots) and 1993 (squares) sampling at piezometer nest KC11.

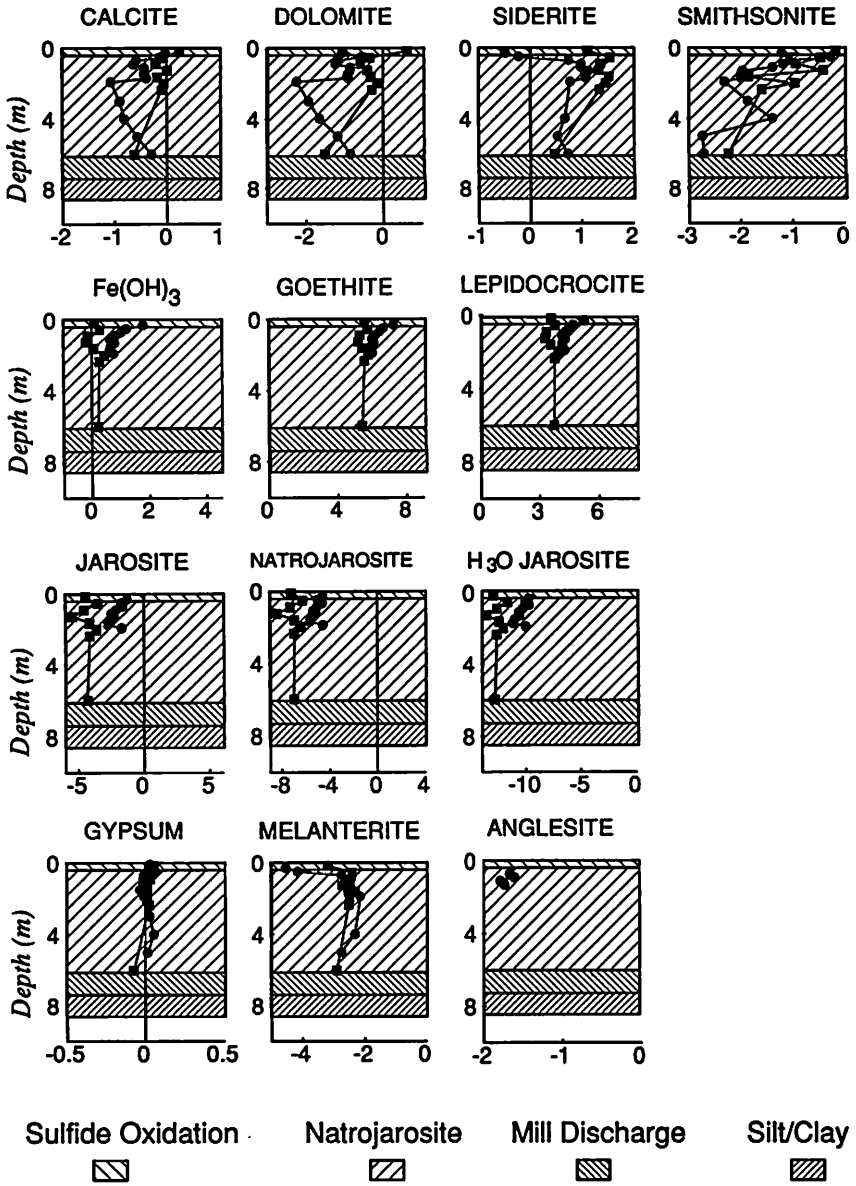

Figure 12.9. Saturation indices calculated with MINTEQA2 for geochemical data from the 1992 (dots) and 1993 (squares) sampling at piezometer nest KC14.

Table 12.4. Analyses of natrojarosite residue (Jambor and Owens, 1992)

	RANGE Min.	Max.	MEAN	σ	MINERALOGICAL SITE
Na	1.91	2.97	2.37	0.25	natrojarosite
K	0.06	0.16	0.10	0.03	natrojarosite
Ca	0.07	0.30	0.15	0.05	gypsum
Mg	0.05	0.11	0.08	0.02	Mg sulfate
Zn	3.93	8.04	6.69	1.21	Zn ferrite, natrojarosite, Zn sulfate
Cd	0.03	0.08	0.05	0.01	Zn ferrite
In*	370.	1242.	728.	210.	natrojarosite
Pb	0.72	2.97	1.63	0.54	plumbojarosite, anglesite
Ag*	151.	511.	308.	90.	natrojarosite, Ag sulfate
Cu	0.12	0.49	0.34	0.09	covellite, Cu sulfate
Fe	25.30	31.80	28.53	1.65	natrojarosite, Zn ferrite
S	8.58	24.60	12.36	4.82	S°
As	0.08	0.32	0.16	0.06	natrojarosite
SO_4	25.22	31.41	27.77	1.83	natrojarosite, various sulfate salts
H_2O	26.06	36.82	32.00	2.97	

$n = 17$
* g/kg, all other values in wt%
Small amounts of Mn, Sn, Al, and SiO_2 occur in the residue from MnO_2 and Mn sulfate, cassiterite, natrojarosite, "silica gel" and quartz, respectively. Silica gel is the amorphous hydrated-alumina-silica product of the acid leaching of chlorite.

c. Natrojarosite-affected Zone

At intermediate to shallow depths within the tailings, a third zone displays increased concentrations of Fe, Mg, Mn, Na, K, Zn, Pb, As, HCO_3, and SO_4. The thickness of this zone varies throughout the tailings cone, but is thickest (8 to 10 m) at the apex of the cone, near the spigot road, and thins outward to the perimeter (<0.25 m). In this zone the concentrations of Fe, Mg, Mn, Na, K, Pb, Zn, As, HCO_3, and SO_4 increase. Among the principal constituents in the Kidd Creek natrojarosite are Fe, Na, K, Pb, and SO_4. Sodium is the principal occupant of the monovalent cation site, with substitution of smaller amounts of $(H_3O)^+$ and K (Table 12.4). The high concentrations of Na and K in the pore water in this zone are best explained by the dissolution of natrojarosite. The only alternative sources of these cations within the tailings are the more stable silicate minerals albite, muscovite, stilpnomelane, and amphibole, and the presence of low concentrations of Na and K in the mill discharge-water zone at depth suggests that these minerals are relatively stable in contact with the mill discharge-water. The ratios of Na to K in the tailings pore-water in this zone range from 10 to 20, similar to the average Na/K ratio of 23.7 in natrojarosite samples from the natrojarosite disposal pond (Jambor and Owens, 1992). Similarly, the increased concentrations of Fe, SO_4, and Pb, which are significant components of the natrojarosite (Table 12.4), can be attributed to natrojarosite dissolution. The increased

concentrations of As in the pore water at this depth also may have resulted from natrojarosite dissolution. Minor solid-solution incorporation of As in jarosite at Kidd Creek and elsewhere is well-known (Dutrizac and Dinardo, 1983; Scott *et al.*, 1986; Dutrizac and Jambor, 1987). Increased concentrations of Zn and As also may be due to retention of Zn and As in the aqueous phase during co-disposal (Jambor and Owens, 1992). Chemical analyses of the bulk natrojarosite residue average 0.165 wt% As and 6.69 wt% Zn (Table 12.4). The increased concentrations of Mg, Mn, and HCO_3 in the natrojarosite-affected zone (Table 12.3) may be the result of carbonate-mineral dissolution following natrojarosite dissolution:

$$[Na_{0.75}K_{0.01}(H_3O)_{0.24}]Fe_3(SO_4)_2(OH)_6 + 3H_2O \Rightarrow \qquad (3)$$

$$3/4Na^+ + 1/100K^+ + 24/100H_3O^+ + 2SO_4^{2-} + 3Fe(OH)_3 + 3H^+$$

$$H^+ + (Ca_{0.2},Mg_{0.06},Fe_{0.73},Mn_{0.01})CO_3 \Rightarrow HCO_3^- + (Ca_{0.2}Mg_{0.06}Fe_{0.73}\,Mn_{0.01})^{2+} \qquad (4)$$

The change in pore-water composition that results from natrojarosite disposal can be observed in the geochemical data. Throughout the summer of 1992, new tailings were deposited at the surface of KC14 to KC21 along the southern line of piezometer nests (Figure 12.1). The pore-water geochemistry from that year displays a gradual increase with depth in the concentrations of Na, K, Fe, Mg, Mn, Zn, HCO_3, and SO_4 (*e.g.*, Figure 12.5, 1992 data). The new tailings at the surface display pore-water concentrations that are similar to those of the mill discharge-water, but with increasing depth (and age), natrojarosite dissolution causes the concentrations of natrojarosite-related components to increase. Subsequent sampling in 1993 at KC14 (Figure 12.5) showed that the pore-water concentrations of these components near the surface had increased to levels characteristic of concentrations within the natrojarosite-affected zone, in which natrojarosite had been in contact with the pore water for more than a year.

In this zone, Cu, Ni, Co, Cd, Se, Cr, Ag, Ba, Al, NO_3, and PO_4 remain at, or below their detection limits. There is commonly a slight decrease in E_H in this zone. In the tailings pore-water, the dominant redox-sensitive species are Fe(II) and Fe(III). The decrease in E_H may be caused by increased activities of Fe^{2+} that result from natrojarosite dissolution, and the subsequent oxidation of pyrite (equation 1). This reaction consumes Fe(III) and produces Fe(II), resulting in a decrease in E_H.

In general within this zone, geochemical calculations using MINTEQA2 (Figures 12.6 to 12.9) indicate that the pore water is undersaturated with respect to calcite and dolomite, and is slightly supersaturated with respect to siderite. The pore water within this interval is generally undersaturated with respect to carbonate minerals of Zn, Mn, Cd and other metals. These results suggest that H^+ generated by natrojarosite dissolution (equation 3) may be consumed by the dissolution of calcite and dolomite

(equation 4). Morin *et al.* (1988a) inferred that precipitation of siderite occurred as a consequence of pH-buffering by calcite dissolution in an aquifer affected by acidic Fe- and SO_4-rich tailings drainage-water near Elliot Lake, Ontario. The observed supersaturation with respect to siderite and undersaturation with respect to calcite and dolomite is consistent with that inference. Geochemical calculations also indicate that the pore water is undersaturated with respect to jarosite, natrojarosite, and hydronium jarosite, suggesting that natrojarosite dissolution, through reactions expressed in equations 1 or 3, is favored. The water in this zone is generally supersaturated with respect to goethite and lepidocrocite, and is very close to saturation with respect to $Fe(OH)_3$. Near-saturation with respect to $Fe(OH)_3$ suggests that $Fe(OH)_3$ may be precipitating as Fe(III) is released by natrojarosite dissolution.

Reactions 1 and 3 are possible reaction paths for natrojarosite dissolution. By comparing the products from each reaction with the pore water geochemical data, we can qualitatively determine which reaction is more favorable. Reactions 3 and 4, combined, result in a pore-water Na/Fe mole ratio ~1, with all of the Fe derived from the carbonate minerals. Reaction 4 describes the dissolution of carbonate minerals with the average cation composition of Kidd Creek carbonate minerals determined from data in Jambor *et al.* (1993b). The average was determined from the variable amounts of calcite, dolomite, ankerite, and siderite (general order of increasing abundance) that were detected. Based on reaction rates determined by Plummer *et al.* (1978) and Busenberg and Plummer (1982), and on observations of the rate of dissolution of crystalline hydrothermal siderite (Ptacek, 1992), acid-neutralization by carbonate minerals should consume calcite, followed by dolomite, and siderite. If reaction 3 is favored and Fe-poor carbonate minerals are the first to dissolve (equation 4), then the expected Na/Fe mole ratio will be >1. Reaction 1 results in a pore-water Na/Fe mole ratio of ~0.25. The average Na/Fe mole ratio of the pore water from the natrojarosite-affected zones at KC1 and KC3, respectively, are 6.55 and 9.10, suggesting that reaction 3 is the favored reaction.

Natrojarosite dissolution causes partial consumption of the acid-neutralization capacity of the tailings solids. The total carbonate content consumed by the co-disposal of 3 wt% natrojarosite has been estimated with the assumptions that 100% of the natrojarosite dissolves, that 75% contributes Fe(III) to the precipitation of ferric hydroxide (reaction 3), and that 25% contributes Fe(III) to the oxidation of pyrite (reaction 1). The 3 wt% natrojarosite (30 kg/t, or 62 mol/t) contributes 139.5 mol/t of Fe(III) to the precipitation of ferric hydroxide, which generates 139.5 mol/t H^+. The oxidation of pyrite generates 32 mol/t OH^-, resulting in a net production of 107.5 mol/t H^+. Neutralization of this H^+ by carbonate-mineral dissolution (reaction 4), assuming a combined carbonate-mineral composition of $(Ca_{0.2}Fe_{0.73}Mg_{0.06}Mn_{0.01})CO_3$, consumes 11.91 kg/t of carbonate or 0.67 wt%. The initial carbonate content of the Kidd Creek tailings is approximately 7 wt%, so the co-disposal of 3 wt% natrojarosite

with the tailings can be expected to consume approximately 9.6% of the total carbonate acid-neutralization capacity. However, mineralogical studies indicate that not all of the natrojarosite has dissolved and, as a result, the estimate of carbonate-mineral consumption is probably high.

d. Sulfide Oxidation Zone

At several of the sites there is a surficial zone in which concentrations of Mg, Mn, Zn, Pb, and SO_4 have increased. In addition, only in this zone within the tailings are there detectable concentrations of metals such as Al, Cu, Cd, Co, Ni, and Cr. All sites that display these characteristics have one thing in common — all have been exposed to the atmosphere for more than six months. This exposure to the atmosphere allows oxygen to diffuse into the unsaturated portion of the tailings and to cause oxidative dissolution of the sulfide minerals such as pyrite:

$$FeS_2 + 15/4O_2 + 7/2H_2O \Rightarrow Fe(OH)_3 + 2SO_4^{2-} + 4H^+ \qquad (5)$$

At sites that have little visible evidence of sulfide oxidation (*e.g.*, KC3), the early geochemical indications of sulfide oxidation are the increased pore-water concentrations of Zn, Mg, Mn, HCO_3, and SO_4. Increases in the Zn concentration may be the result of oxidation of sphalerite. The increased concentrations of Mg, Mn, and HCO_3 in the pore water are probably a result of the neutralization of the H^+ generated by sulfide oxidation, through carbonate-mineral dissolution (reaction 4). As sulfide oxidation proceeds, the pore-water pH decreases from approximately 6.5 to 5.5 (KC11 from 1992 to 1993); occasionally during dry periods, however, the alkalinity of the pore water decreases to below detection at the surface and the pH drops below the carbonate-buffered levels (*e.g.*, KC1) despite the presence of carbonate minerals in the tailings. The depleted alkalinity and low pH suggest that the rate of carbonate-mineral dissolution is slow relative to the rate of H^+ production by sulfide oxidation. From mineralogical studies and analyses of total inorganic carbon it was determined that dolomite and siderite are present in this interval. The geochemical characteristics of the most advanced sulfide oxidation zones (*e.g.*, KC1) include: pH ranging between 2.5 and 5.5, E_H between 300 and 600 mV probably because of the increased solubility of Fe^{3+} at low pH, and high pore-water concentrations of Mg, Mn, Fe, Cd, Co, Cu, Pb, Zn, Ni, Cr, Al, and SO_4.

In general, geochemical modelling of the pore-water chemistry from this zone (Figures 12.6 to 12.9) indicates that the pore water is undersaturated with respect to all of the carbonate minerals; thus, the trend should be to dissolution of these minerals. The pore water in this zone is locally saturated to supersaturated with respect to jarosite, is commonly saturated with respect to natrojarosite, and is undersaturated with respect to hydronium jarosite. The saturation indices of the ferric iron hydroxide and oxyhydroxide phases are lowest in this interval, a result of the low pH. The pore water in this zone also approaches saturation with respect to anglesite $PbSO_4$.

Anglesite, precipitated from tailings pore water, has been observed at the Heath Steele tailings impoundment, New Brunswick (Boorman and Watson, 1976; Blowes, 1990).

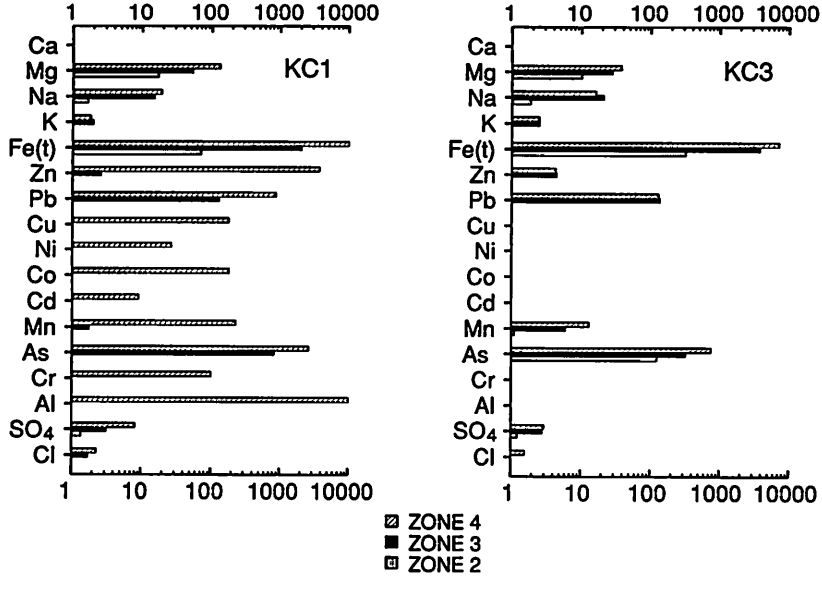

Figure 12.10. Average pore-water compositions from the mill discharge-water zone (zone 2), the natrojarosite-affected zone (zone 3), and the sulfide-oxidation zone (zone 4), normalized to the present mill discharge-water composition from Table 12.2.

e. Comparison with Mill Discharge-water Chemistry

To illustrate the changes in pore-water chemistry that occur subsequent to tailings disposal, with and without the addition of natrojarosite, the 1991 geochemical data from KC1 and KC3 have been normalized to the respective concentrations in the present mill discharge-water. KC1 was chosen as a site that displays the effects of sulfide oxidation, whereas in KC3 the effects of natrojarosite are evident from the pore-water chemistry, but there is little evidence of sulfide oxidation at the surface. In Figure 12.10 the average pore-water compositions at KC1 and KC3 for the mill discharge-water-like zone, the natrojarosite-affected zone, and the sulfide-oxidation zone are normalized to the present mill discharge-water composition from Table 12.2. The mill discharge-water-zone pore water displays slight increases of Mg, Na, Fe, and SO_4 relative to the present mill discharge-water but, except for Fe, these differences could be a result of temporal variation in the mill discharge-water composition. The natrojarosite-affected pore water displays similar patterns at KC1 and KC3: Na, K, Fe, Mg, Mn, Zn, Pb, As, and SO_4 show increased concentrations relative to the present mill discharge-water. The release of metals to the pore water has been greatest in the sulfide oxidation zone. The pore-water pH is low because of the effects of sulfide

oxidation, and increases in the concentrations of Mg, Fe, Zn, Pb, Cu, Ni, Co, Cd, Mn, As, Cr, Al, and SO_4 occur as a result of the dissolution of mineral phases such as carbonates and aluminosilicates, and the oxidative dissolution of sulfide minerals.

12.4.2. Tailings Solids

All of the whole-rock data display spatial heterogeneity with respect to the distribution of components. The distribution of the major elements and many of the trace elements is controlled by the mineralogy of the tailings, and the data reflect the variable mineralogy of the mill feed through time. Major-element or trace-element trends with depth are not evident, except when variations in elemental ratios are considered. At KC3, a vertical core from surface to 10.5 m — almost the entire thickness of the tailings (~12 m at this site) — shows significant increases in the ratios of Na/K, Na/Si, and Na/Al in the shallow tailings above 3 to 4 m depth (Figure 12.11).

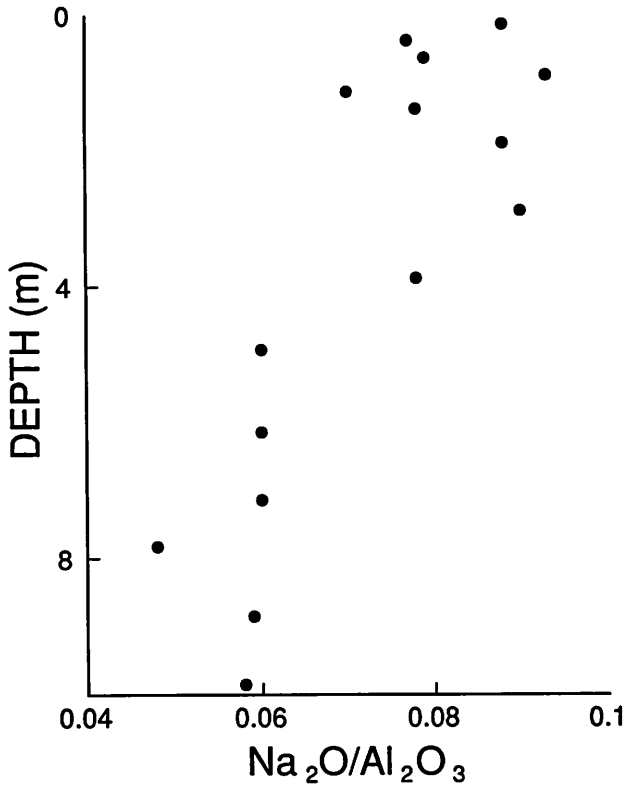

Figure 12.11. Whole-rock Na_2O/Al_2O_3 ratios from a section through the tailings at site KC3. The elevated ratios above 4-m depth represent the interval in which natrojarosite has been co-disposed with the tailings.

The higher ratios at KC3 are similar to the ratios displayed in the samples from shallow cores at the other sites that were sampled (KC1, KC10, KC11, and KC27). The high Na/K, Na/Al, and Na/Si ratios in the shallowest tailings occur where natrojarosite has been co-disposed with the tailings. In the deepest tailings that were deposited prior to natrojarosite co-disposal, Na in the tailings would be contained predominantly in plagioclase, and to a lesser extent, in hornblende and other K-bearing aluminosilicate minerals. The co-disposal of natrojarosite in the upper tailings causes a significant increase in the Na content of the tailings without significantly increasing Al, Si, or K. The increased ratios of Na to Al, Si, or K is therefore an indicator of the depths at which natrojarosite occurs.

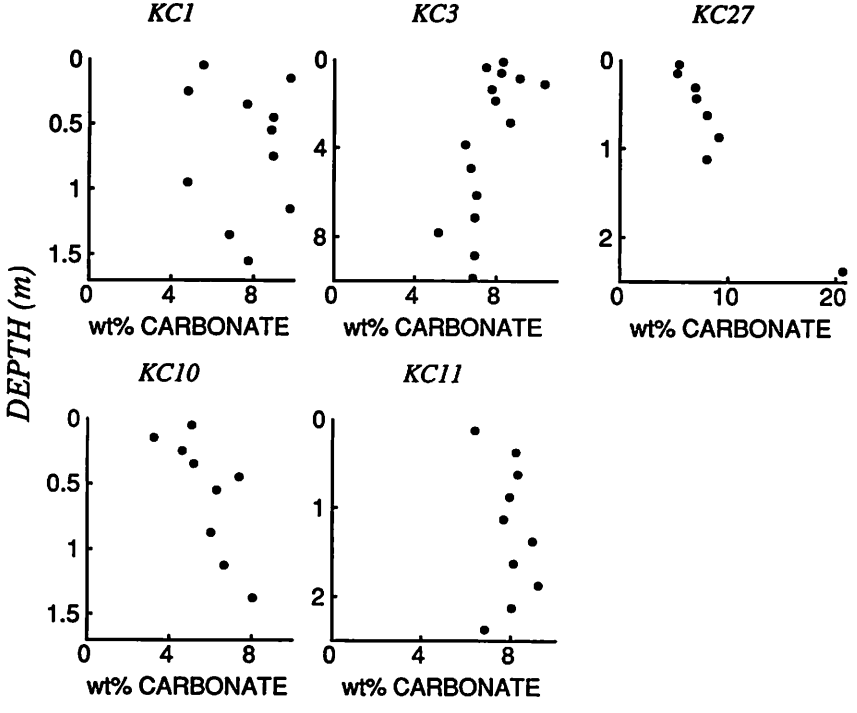

Figure 12.12. Equivalent wt% of carbonate minerals ($[Ca_{0.2}Fe_{0.73}Mg_{0.06}Mn_{0.01}]CO_3$) in the tailings, calculated from analyses of total carbon.

The whole-rock total-carbon results, expressed as wt% carbonate minerals, are shown in Figure 12.12. The average carbonate-mineral content of the tailings is approximately 7 wt%, which is in good agreement with the results obtained by Jambor *et al.* (1993b; Table 12.1). The distribution of carbonate minerals is heterogeneous throughout the tailings and ranges from 4 to 10 wt%. At KC1 the carbonate-content variation is greatest, with no apparent trends in the distribution *versus* depth. Data

from a profile between surface and 10 m depth at KC3 display slightly greater carbonate-mineral contents in the tailings above 4 m depth (8 to 10 wt%) than in the lower section (5 to 8 wt%). There are trends toward increasing carbonate-mineral content with depth at KC10 and KC27. At KC11 the distribution is relatively uniform, near 8 wt%, with a minimum carbonate content of approximately 6.5 wt% in the shallowest sample. The deepest sample at KC 27 contains >20 wt% carbonate minerals. This sample is from the varved silt/clay underlying the tailings. Farkas and Curtis (1991) described similarly high carbonate-mineral contents in samples from the soil underlying the tailings.

Studies of sulfide-rich tailings deposits at Elliot Lake, Ontario, Noranda, Quebec, Bathurst, New Brunswick, and Sudbury, Ontario have documented depletion of carbonate minerals in the near-surface tailings (Blowes, 1990; Blowes *et al.*, 1991). The depletion results from acid-neutraiization reactions which cause carbonate-mineral dissolution (equation 4). The large variation in the carbonate-mineral content of the tailings obscures the possible trends toward surficial depletion of carbonate minerals. Nevertheless, the average carbonate mineral content is approximately 7 wt% (Figure 12.12) and at KC1, where low-pH pore water has been generated by sulfide oxidation, the carbonate-mineral content is approximately 4.5 wt% near the surface. Similarly, at KC11, where the pH of the pore water in 1993 was 5.5, the carbonate-mineral content near the surface is slightly lower than in the deeper samples. The same trend seems to be present at piezometer nests KC10 and KC27, which are located at the perimeter of the tailings cone, where pore water discharges (see Section 12.4.3). Oxidation of Fe(II) in the discharging water may generate acid by the reaction

$$Fe^{2+} + 1/4O_2 + 5/2H_2O \Rightarrow Fe(OH)_3 + 2H^+ \qquad (6)$$

Acid generated in this way may be responsible for the weak trend toward depletion of carbonate minerals near the surface at these sites.

12.4.3. Hydrogeology

The thickened tailings-disposal method employed at Kidd Creek inhibits grain-size segregation in the slurry, which is of common occurrence during conventional tailings disposal (Robinsky *et al.*, 1991). The narrow distribution of hydraulic conductivity displayed by the tailings (Figure 12.13) is a reflection of the relatively uniform grain-size distribution. Hydraulic conductivity measurements range between 5 x 10^{-9} to 1 x 10^{-6} m/s. There is a trend toward decreasing K with depth (Figure 12.14) which may be due to consolidation of the tailings. The lowest values of K (<1.0 x 10^{-8} m/s) are obtained from the deepest piezometers, which are thought to be installed within the underlying varved silt and clay (Section 12.4.1a). In general, measurements of ϕ display (1) downward gradients in the central area of the impoundment, near the apex of the conical tailings pile, (2) slightly downward and lateral gradients along the

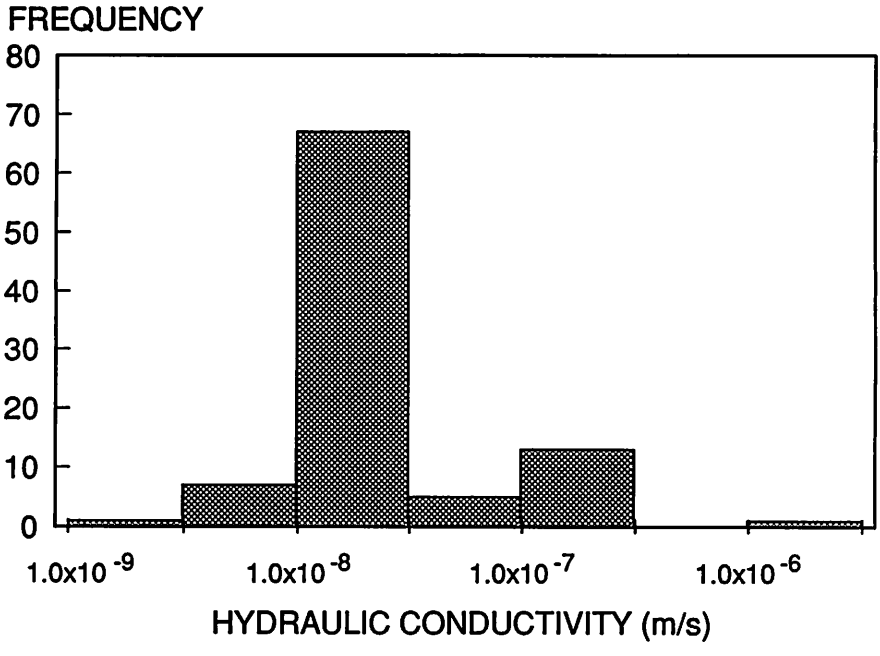

Figure 12.13. Distribution of hydraulic conductivity (m/s) from field measurements.

slopes of the pile, and (3) upward gradients in the area of flat-lying tailings around the periphery of the cone. The downward gradients near the apex of the cone are divergent; gradients near the permeable spigot-road (Figure 12.1) are directed downward and converge toward the road, but at greater radial distance from the road the gradients are directed downward and diverge outward, toward the perimeter of the impoundment.

Changes in the water-table position were monitored closely in 1992. In May of 1992, after the snow-melt, the water table was at the surface throughout the impoundment. By the end of May, the water table had reached a state of dynamic equilibrium in which the depth to the water table varied from 5 m (±1m) near the spigot road, to approximately 1.5 m (+0.5/-1 m) in the peripheral flat-lying areas. Short-term wetting and drying events cause the water-table elevation to fluctuate during the summer, fall, and winter. The uniform grain-size distribution of the tailings permits the formation of a thick capillary fringe when the water table declines in the spring. Moisture-content profiles measured during a week-long dry period in late July are shown in Figure 12.15 for sites near the spigot road (KC14), and at the periphery of the tailings cone (KC24). The profiles indicate that the tailings have maintained saturation to within 0.3 to 0.4 m from the surface, whereas the water table has declined to 6.5 m at KC14 and 1.75 m at KC24.

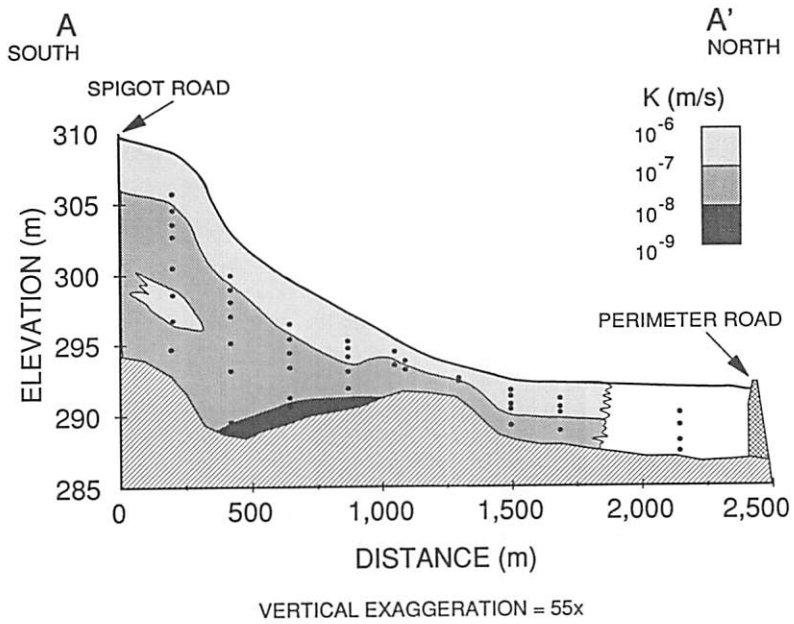

Figure 12.14. Cross-section of the tailings (along A-A' in Figure 12.1), showing the spatial distribution of hydraulic conductivity. The black dots represent piezometer locations.

Figure 12.15. (below) Volumetric moisture-content profiles measured with a neutron moisture probe (CPN Model 503DR Hydroprobe).

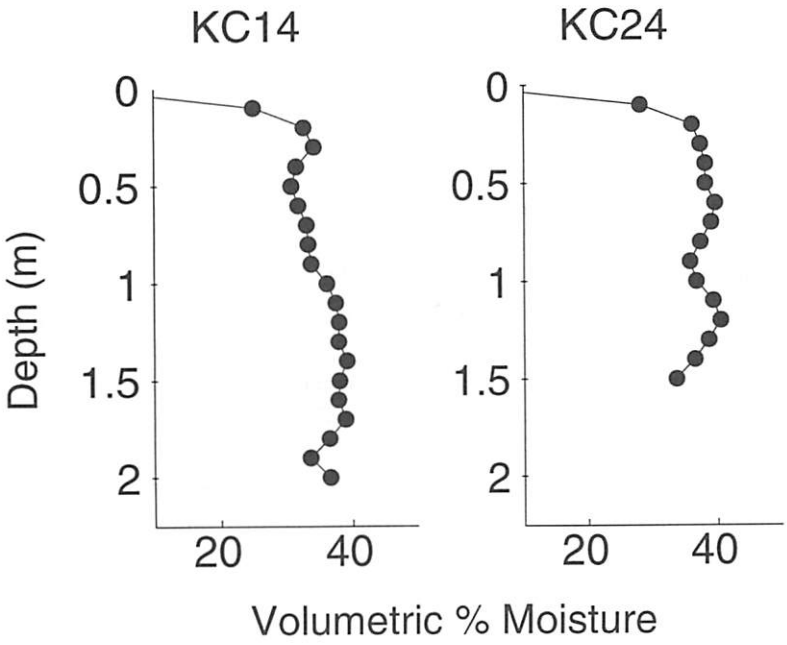

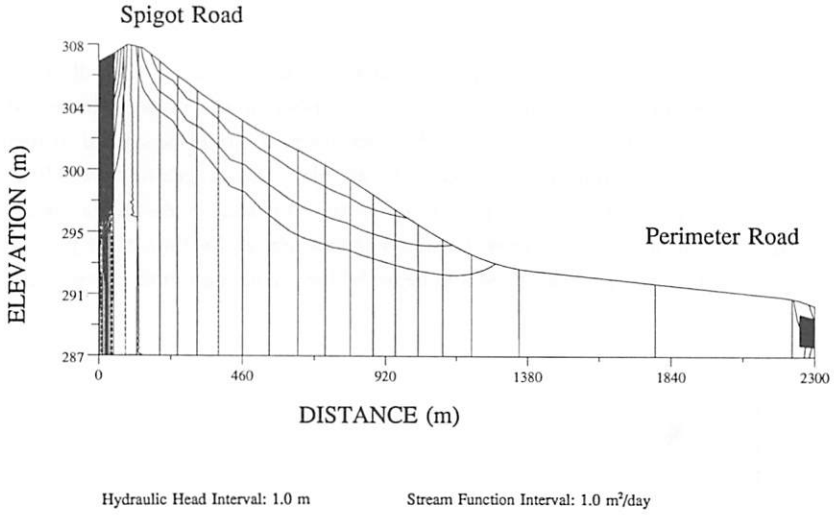

Figure 12.16. Steady-state flownet for the tailings along A-A' in Figure 12.1. The near-vertical lines represent contours of hydraulic head, and the curved lines represent the boundaries of stream tubes.

The groundwater flow-model was calibrated to match data collected during May, 1992. A flownet generated from the model is shown in Figure 12.16. The character of the flow net suggests that flow within the tailings is dominated by infiltration in the central area, from which there is outward and radial flow to the discharge in the flat peripheral area. The flow-net features also suggest that some groundwater flow from the apex of the cone is toward the permeable central spigot road; this trend is consistent with the observations of the hydraulic-head gradients near the road. Pore water flowing into the spigot road from the elevated central tailings, in the spring while the water table is high, would provide an explanation for the observed discharge of water from the sides of the spigot road onto the tailings at lower elevations along the road. The maximum pore-water velocities (approximately 0.5 m/y) calculated by the model occur in the region of downward flow near the apex of the tailings cone. This velocity is consistent with independent measurements of pore-water velocity made from solute tracers derived from natrojarosite dissolution. The depth of natrojarosite occurrence within the tailings has been established (Jambor *et al.*, 1993b) at the piezometer nests along section A-A' (Figure 12.1). The vertical pore-water velocity within the tailings is obtained by determining the difference between the depth of natrojarosite occurrence and the depth of the natrojarosite-affected zone, and dividing by the time since the beginning of co-disposal with the tailings (6.5 years). The maximum velocity determined by this method is approximately 0.6 m/y (Figure 12.17). The vertical pore-water velocity declines to zero at approximately 1000 m from the center of the cone, consistent with the flow-model indication that pore water discharges

beyond a radius of 900 m.

Knowledge of the regime of groundwater flow within the tailngs will in several ways aid the future planning for decommissioning of the impoundment. If an infiltration barrier were to be considered as necessary, it would be critical to identify areas where recharge and discharge occur. Future plans for revegetation would require knowledge of potential fluxes of pore water to the root zone in discharge areas. It is possible that future pore-water will be acid-generating, and estimates of pore-water flux obtained from the modelling would be useful for predicting future H^+ release.

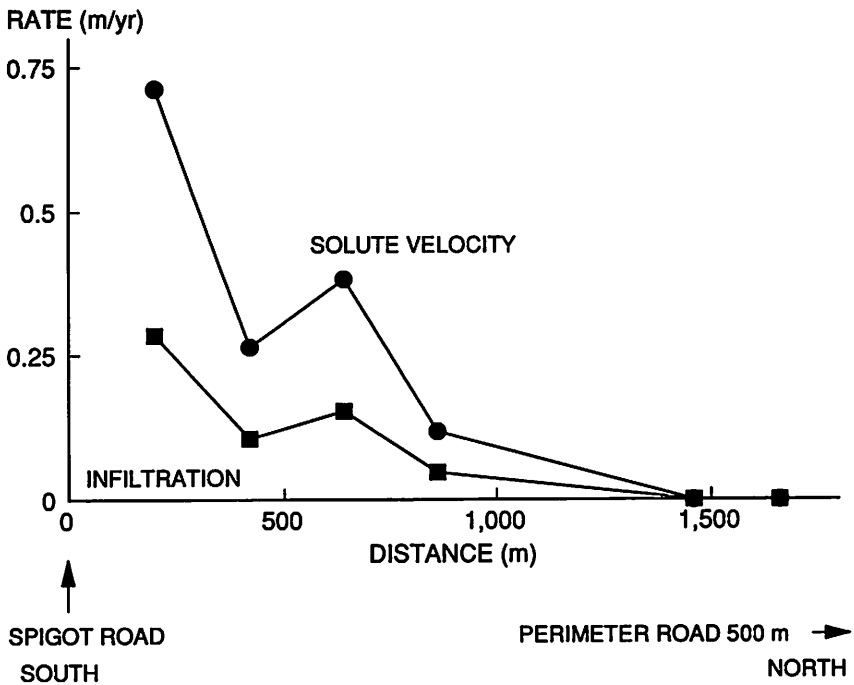

Figure 12.17. Vertical pore-water velocities and infiltration fluxes calculated from the displacement of Na downward from the maximum depth that natrojarosite has been detected (Jambor *et al.*, 1993).

12.5. CONCLUSIONS

Four zones can be defined from the pore-water geochemistry of the Kidd Creek tailings. In the deepest samples, which are thought to be from the varved silt/clay underlying the tailings, the pore water contains the lowest concentrations of metals and sulfate, and the highest alkalinity concentrations. The deepest pore water within the tailings displays pore-water metal and sulfate concentrations that mimic the composition of the present mill discharge-water. This zone, the second, is interpreted to

represent mill discharge-water disposed with tailings prior to 1985, when natrojarosite co-disposal with the tailings was initiated. The third zone occurs at shallow to intermediate depths in the tailings, and is marked by increased concentrations of Na, K, Mg, Mn, Fe, Zn, Pb, As, HCO_3, and SO_4 that resulted from the dissolution of natrojarosite. In the fourth zone, pore-water samples from the surface at several sites display further increases in the concentrations of Mg, Mn, Fe, Zn, Pb, As, and SO_4, in addition to increased concentrations of Al, Cd, Co, Cr, Cu, and Ni that resulted from sulfide oxidation.

The co-disposal of natrojarosite with sulfide-rich tailings at Kidd Creek introduces the natrojarosite to a neutral-pH and low-E_H environment in which the natrojarosite is thermodynamically unstable. Natrojarosite disposed with the tailings at Kidd Creek is interpreted to be dissolving. Geochemical modelling suggests that conditions favoring natrojarosite dissolution are present throughout most of the tailings impoundment. Mineralogical studies indicate that a significant mass of natrojarosite remains in the tailings, representing a long-term source of components such as Na, K, Fe, Pb, and SO_4.

The effects of natrojarosite dissolution on the pore-water composition can be distinguished from the effects of sulfide oxidation. Dissolution of the natrojarosite bulk residue has increased the pore-water concentrations of Na, K, Fe, Pb, As, and SO_4 directly, and has increased the concentration of Mg, Mn, Fe, and HCO_3 indirectly through carbonate-mineral dissolution. Increases in Zn concentration result primarily from the large amounts of zinc that are retained within the aqueous phase of the natrojarosite bulk residue. Sulfide oxidation generates low-pH conditions in the pore water and further increases the concentrations of Mg, Mn, Fe, Zn, Pb, As, and SO_4, as well as increasing the concentrations of Al, Cd, Co, Cr, Cu, and Ni. Sulfide oxidation also causes the dissolution of carbonate minerals, thereby initially increasing the pore-water concentration of HCO_3; continued oxidation, however, will consume the carbonate-mineral acid-neutralization capacity of the tailings and will subsequently deplete the pore-water alkalinity.

Sulfide oxidation has been limited by continuous tailings deposition on the main tailings cone. Variability in the initial carbonate content of the tailings has obscured any obvious indications that sulfide oxidation at the surface has depleted the carbonate-mineral content through acid-neutralization processes. Low-pH pore water with high concentrations of metals such as Fe, Zn, Pb, Co, and Cd has developed near the surface at several sites as a consequence of sulfide oxidation.

Groundwater within the tailings flows outward from the elevated central portion of the cone, toward the perimeter of the impoundment. Flow is predominately vertically downward in the central area. At increasing radial distance the flow becomes horizontal, and at ~1000 m radial distance from the center of the impoundment the

pore water discharges to the peripheral, flat-lying area of tailings. Characterization of the flow regime within the tailings should help in future planning for decommissioning.

12.6. ACKNOWLEDGEMENTS

This geochemical and hydrogeological study of the Kidd Creek tailings was initiated at the request of Falconbridge Limited, Kidd Creek Division. Funding for the work was provided by Falconbridge Limited, Kidd Creek Division.

Chapter 13

Remediation and Prevention of Low-quality Drainage from Tailings Impoundments

D.W. Blowes
Waterloo Centre for Groundwater Research
University of Waterloo,
Waterloo, Ontario N2L 3G1

C.J. Ptacek
National Water Research Institute
Environment Canada
867 Lakeshore Road
Burlington, Ontario L7R 4A6

J.L. Jambor
Waterloo Centre for Groundwater Research
University of Waterloo,
Waterloo, Ontario N2L 3G1

13.1. INTRODUCTION

Since recognition of the problems of acidic and low-quality drainage associated with tailings impoundments, the mining industry has attempted to develop reliable techniques for the prediction, remediation, and prevention of these problems. The development of these techniques requires an understanding of the complex interactions among the hydrogeological, geochemical, mineralogical, and microbiological characteristics of tailings impoundments, as have been described in the preceding chapters of this Volume. Understanding these interactions has led to the development and testing of innovative approaches for the disposal and treatment of mine tailings. As our understanding improves, additional techniques undoubtedly will be put forward.

Robertson (1987) reviewed the abatement techniques that had been developed to date, and prepared a cost-benefit comparison for the various approaches, which were

grouped into three broad categories: (a) collection and treatment of tailings-derived discharge, (b) infiltration controls, and (c) sulfide-oxidation controls. An alternative abatement approach not included in the above is to promote the reduction of sulfate and the subsequent precipitation of low-solubility sulfide minerals at a depth within the tailings under conditions at which these minerals will remain stable. The effluent from many tailings impoundments in North America is collected and treated prior to discharge from the minesite. Acceptable effluent quality is achieved, but the capital and consumable costs associated with perpetual maintenance of treatment facilities are sufficiently large that the development of alternative prevention and abatement techniques is highly desirable.

13.2. REMEDIATION OF EXISTING SOURCES OF ACIDIC DRAINAGE

At many locations mining has been active for several decades. Although mine wastes at these locations were deposited according to the best practices available at the time of disposal, many of these wastes are now the source of low-quality drainage waters. At many of these sites the period of most intense sulfide oxidation and associated release of dissolved metals has passed, but transport of sulfide-oxidation products through the tailings or underlying aquifers will continue for several decades (*e.g.*, Coggans *et al.*, 1994). Remedial programs for these sites focus on the collection and treatment of tailings-derived discharge or on reducing the infiltration and movement of recharge water through the tailings. At tailings impoundments in which sulfide oxidation is in its early stages, it is beneficial to inhibit these reactions through the use of sulfide-oxidation controls, such as saturated soil covers or organic-carbon covers, to inhibit oxygen ingress. For older tailings areas in which the peak period of sulfide oxidation has passed, a potential alternative remediation approach is to install sulfate-reducing porous reactive walls in the path of plumes of tailings-derived water.

13.2.1. Collection and Treatment

Collection and treatment facilities are in place at many tailings sites throughout North America. Conventional water-treatment plants vary from relatively simple, to automated, computer-controlled facilities. Even relatively primitive facilities in some instances can provide an effective control on the release of acidic drainage and dissolved metals. The cost of maintenance of these facilities, however, is large and there is a strong desire to develop and implement alternative treatment systems. A relevant example of the costs associated with conventional treatment systems is that the annual expenditure for lime for the Noranda-group companies alone is on the order of $5 million (Kuyucak *et al.*, 1991). Moreover, the disposal of low-density sludge residues has become an environmental concern, both in terms of disposal and in the potential release of dissolved metals through subsequent leaching.

Alternative passive-treatment systems which have been proposed include downstream polishing or metal scavenging by using wetlands, woodwaste, or peat. These passive-treatment systems may be enhanced through the use of anoxic limestone drains to precondition water prior to discharge to the wetland systems (Hedin and Watzlaf, 1994). Other proposals focus on concentrating the beneficial biological activity observed in a wetland within a constructed facility. For many years wetlands and peat bogs have been recognized as areas of metal accumulation (Kalin and van Everdingen, 1987; Ritcey, 1989; Brown, 1991; Machemer and Wildeman, 1992). Passive treatment of acidic coal-mine drainage by constructed wetlands has been demonstrated to be efficient and effective. In the Appalachian region of the United States more than 400 wetland systems were treating low-quality drainage waters derived from coal minesites (Kleinmann *et al.*, 1991). In addition, the use of constructed wetlands for treatment of drainage from base- and precious-metal mine-tailings impoundments has been proposed (Kleinmann *et al.*, 1991; Gould *et al.*, this Volume). Passive polishing by downstream wetland requires the establishment and maintenance of wetlands that not only will remain stable over long periods, but will also survive the metal loadings associated with base- and precious-metal tailings. As metal loadings from many tailings impoundments are expected to increase over future decades (Blowes and Jambor, 1990; Blowes *et al.*, 1994; Coggans *et al.*, 1994), the wetland must withstand both current and future loadings to be suitable as a long-term treatment system. One of the major concerns with this concept is the gradual infilling of the wetland basin and the potential for the remobilization of contaminants associated with the tailings impoundment.

The mechanisms resulting in the immobilization of dissolved metals in wetlands have been the focus of much research in recent years. Kleinmann *et al.* (1991) noted that a significant attenuation of dissolved metals results from the bacterially catalyzed reduction of sulfate to sulfide and the accompanying reprecipitation of metal sulfides through reactions of the form:

$$CH_2O + SO_4^{2-} \Rightarrow HS^- + HCO^-_3 + H^+ \qquad (1)$$

$$Me^{2+} + HS^- \Rightarrow MeS_{(s)} + H^+ \qquad (2)$$

where CH_2O represents a labile source of organic carbon, and *Me*S represents an amorphous or poorly crystalline sulfide precipitate. These reactions increase the pH and alkalinity of the tailings discharge-water, and decrease the concentrations of dissolved metals. In wetlands, organic carbon is supplied and replenished through the annual growth of wetland plants and their degradation in the wetland. Sulfate, Fe(II), and other dissolved metals are supplied by the captured acid mine drainage-water.

Isolation of the controlling reactions in wetland systems has resulted in the proposal and development of treatment systems in which mine drainage-water is

directed through continuous-flow reactors. Dvorak *et al.* (1991) proposed that mine drainage-water be directed through continuous-flow reactors containing solid-phase organic carbon to induce sulfate reduction and precipitation of metal sulfides. The results of pilot-scale experiments demonstrated significant decreases in the concentrations of SO_4 and the dissolved metals Fe, Zn, Mn, Ni, and Cd; these decreases were accompanied by increases in effluent pH and alkalinity. Dvorak *et al.* indicated that scaling up of the reactors to treat acidic drainage from minesites is economically feasible. A further variation of this continuous-flow system is the use of a sulfate-reduction treatment zone, followed by treatment using an anoxic limestone layer (Kepler and McCleary, 1994).

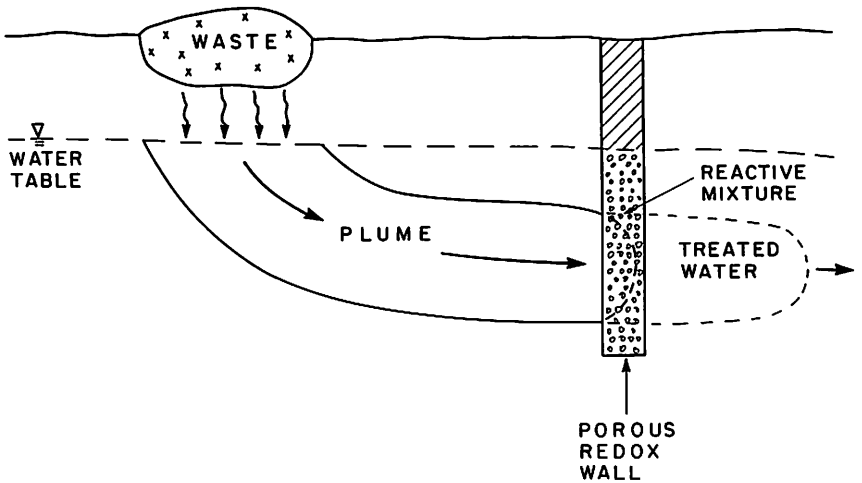

Figure 13.1. Schematic diagram of a porous reactive wall for *in-situ* treatment of contaminated groundwater.

Plumes of tailings-derived water moving in aquifers affected by mine-tailings impoundments are anaerobic, the pH is near neutral, and the temperature is relatively constant throughout the year (Morin, 1983; Bain, 1994). These conditions are well-suited for the *in-situ* treatment of mine drainage-water. Blowes and Ptacek (1992a, 1994) proposed intercepting Fe(II)- and SO_4-laden groundwater prior to discharge to the surface-water flow system through the use of porous reactive walls containing labile organic carbon (Figures 13.1, 13.2). Treatment using these porous walls requires that the contaminant be sufficiently reactive for the reaction to proceed as the plume of contaminated water passes through the wall. The wall material also must be sufficiently reactive during the limited residence time of the contaminant plume, and the wall material must be sufficiently stable so its lifespan is economically competitive with other treatment systems. Preliminary experiments, conducted using potential wall components, suggest that the sulfate-reduction and metal-sulfide precipitation reactions

proceed rapidly enough that treatment of tailings-derived water by sulfate-reducing reactive walls is feasible (Figure 13.3). To examine the potential for treatment of tailings-derived waters using reactive walls under field conditions, a test cell has been installed in the path of a plume of tailings-derived water at the Nickel Rim minesite near Sudbury, Ontario.

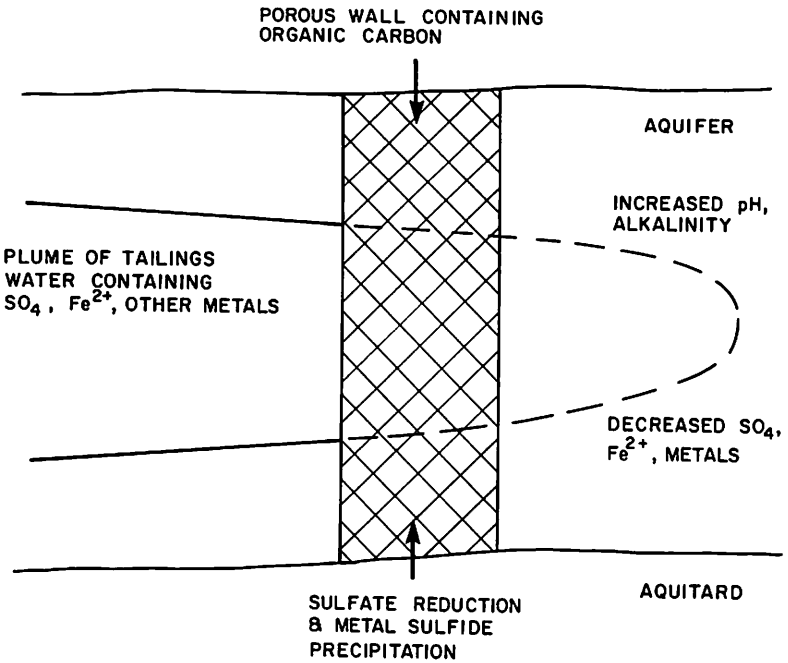

Figure 13.2. Schematic diagram showing relevant reactions for treatment of tailings water containing SO_4, Fe(II), and other metals.

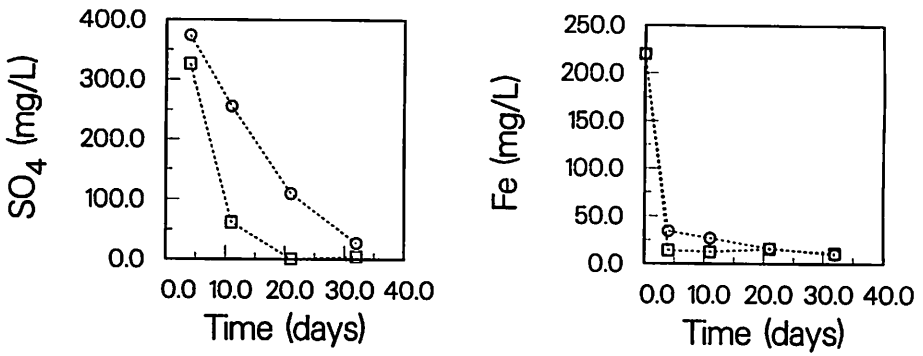

Figure 13.3. Removal of SO_4 and iron using mixtures of organic-carbon sources as a function of time. Circles represent results for mixtures with low concentrations of added calcite and squares represent results for mixtures with high concentrations of added calcite.

13.2.2. Infiltration Controls

Although numerous design strategies to restrict the movement of tailings pore-water from the impoundment to adjacent groundwater and surface-water flow systems have been proposed, the most effective strategy to control the movement of tailings pore-water from the impoundment is to restrict the entry of meteoric waters, surface water, and groundwater into the impoundment. This in turn will reduce the quantity of tailings-derived seepage leaving the impoundment (Robertson, 1987).

Entry of groundwater and surface water into the tailings can be avoided by appropriate site selection. Where suitable impoundment locations are not available, or where tailings are already placed in an undesirable location, the use of synthetic liners, cutoff walls, and diversion trenching may be considered. Infiltration of meteoric water can also be restricted by surface contouring and by emplacement of low-permeability covers, either of natural geologic or synthetic materials, over the tailings. Optimal cover design would provide a barrier both to infiltration of meteoric water and to atmospheric O_2.

Although it is desirable to limit the entry of meteoric water, groundwater, and surface water into tailings areas, this may not be economically feasible given the large areas (> 200 ha) of many tailings impoundments. In these cases it may still be desirable to restrict the movement of tailings water into underlying aquifers to prevent degradation of aquifer-water quality and to direct tailings-derived water to collection points prior to treatment. Cutoff walls, diversion trenching, and impermeable barriers can be used to direct flowing groundwater toward *in-situ* treatment zones (Figure 13.4; Starr and Cherry, 1994) or toward surface treatment systems.

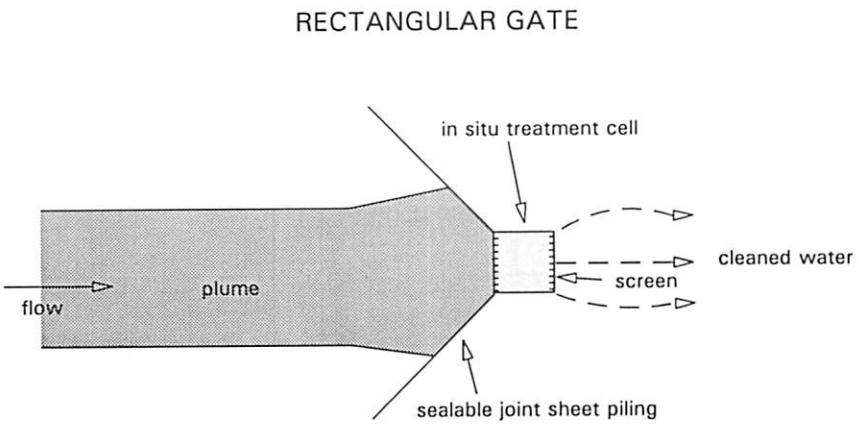

Figure 13.4. Schematic diagram showing funnel-and-gate design for *in-situ* treatment of mine-tailings water, as described by Starr and Cherry (1994).

13.2.3. Sulfide-oxidation Controls

Abatement techniques that limit sulfide oxidation are bactericidal controls, precipitates that coat sulfide surfaces, and O_2-diffusion barriers. The first involves attempts to inhibit the naturally occurring sulfide-oxidizing bacteria through the use of bactericides applied either directly to the tailings surface or as an intimate mixture with the tailings in the impoundment (Erickson and Ladwig, 1985). In the absence of these bacteria the rate of sulfide-mineral oxidation decreases as the pH decreases, and the concentrations of dissolved metals remain low. Preliminary results using this approach have been encouraging, but the bactericides currently available require continual reapplication (Sobek, 1987). The requirement for continual reapplication suggests that bactericides may be better suited to short-term disposal sites, such as locations where tailings are temporarily exposed during impoundment construction.

The second type of oxidation control armors the sulfide mineral surface with a coating of an insoluble, non-reactive precipitate, thereby isolating the sulfide mineral from oxidants (*e.g.*, O_2 and Fe^{3+}). Among the various armoring phases that have been proposed are ferric phosphate (Huang and Evangelou, 1994), and ferric oxyhydroxides (Ahmed, 1991). Huang and Evangelou (1994) observed decreased rates of sulfide oxidation in samples amended with PO_4^{3-} compared to control samples. In field settings ferric oxyhydroxide rims are observed on altered sulfide minerals (Blowes and Jambor, 1990; Jambor and Blowes, 1991). Studies which model sulfide oxidation in mine wastes using "shrinking core" models (Davis and Ritchie, 1986; Davis *et al.*, 1986) assume that similar coatings affect the rate of sulfide oxidation. These field and modelling studies suggest that the observed oxidation rates in the presence of these altered rims remain sufficiently high to represent an environmental concern. To be an effective remedial system the armoring coating must maintain rates below those observed for naturally occurring alteration.

The third type of sulfide-oxidation control restricts the entrance of gas-phase O_2 into the impoundment by placing a diffusion barrier between the atmosphere and the reactive sulfide tailings. Several approaches to the barrier technique have been proposed, including dry covers composed of fine-grained materials, which may be layered to maintain high water contents and low O_2-diffusion coefficients (Collin and Rasmuson, 1986; Sodermark and Lundgren, 1988; Rasmuson and Collin, 1988; Nicholson *et al.*, 1989; Yanful and St. Arnaud, 1991); covers composed of synthetic low O_2-diffusivity materials (Sodermark and Lundgren, 1988; Malhotra, 1991); or covers containing O_2-consuming materials (Reardon and Poscente, 1984; Reardon and Moddle, 1985; Broman *et al.*, 1991; Tassé *et al.*, 1994).

Covers constructed of fine-grained material rely on the moisture-retaining characteristics of these materials to maintain high moisture contents several meters above the water table (Collin and Rasmuson, 1986; Nicholson *et al.*, 1989, 1991;

Yanful *et al.*, 1994). Because of the moisture-retaining capabilities of fine-grained materials, it is possible to layer these materials (silt- and clay-size sediments) over coarser grained tailings and maintain a saturated or near-saturated condition several meters above the water table (Figure 13.5).

Covers which include synthetic layers have also been proposed (Sodermark and Lundgren 1988). A cover incorporating a synthetic layer constructed of 25 cm of Cefill flyash-stabilized concrete was installed over a waste-rock pile at the Bersbo site in Sweden (Figure 13.6; Lundgren and Lindahl, 1991). Such covers are expensive to construct (Sodermark and Lundgren, 1988) and may be susceptible to cracking after installation due to desiccation or to subsidence (Collin, 1987). Collin (1987) conduced a sensitivity analysis which indicated that cracks in soil covers would lead to the oxidation of the underlying sulfide minerals. Based on this analysis, it was recommended that soil covers be protected from root penetration, frost action, and desiccation. The effectiveness of covers for tailings areas relies on their long-term integrity. Because covers are located on the tailings surface, they are at the location most susceptible to erosion.

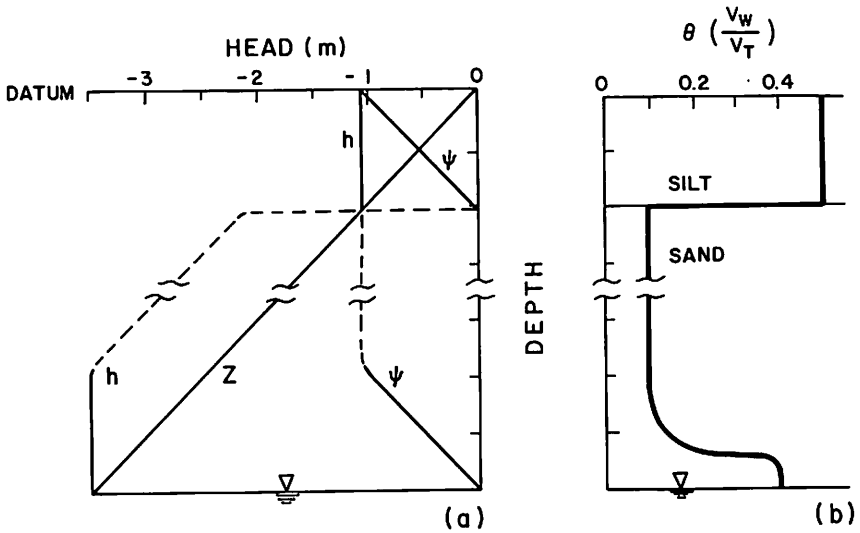

Figure 13.5. Hypothetical head distribution and expected moisture contents through a silt and an underlying coarse sand layer (Nicholson, 1984).

In addition to covers with low O_2-diffusion characteristics, several authors have proposed covers which consume O_2 (Reardon and Poscente, 1984; Blenkinsopp, 1991; Broman *et al.* 1991; Tassé *et al.*, 1994). Covers rich in organic carbon in the form of woodwaste, sewage sludge, and industrial byproducts have been proposed. The intent is to consume O_2 by reaction with organic carbon, preventing O_2 contact with the underlying sulfide minerals (Figure 13.7). Several studies (*e.g.*, Tassé *et al.*, 1994) have

demonstrated that these covers are able to consume O_2, illustrating their potential effectiveness. Reardon and Poscente (1984) calculated the mass of organic carbon required for covers composed of wood waste to serve as long-term prevention of acidic drainage. They concluded that the mass of organic carbon required was prohibitive, and alternative techniques were suggested. Pierce *et al.* (1994) proposed the use of composted sewage sludge as a potential tailings cover. Advantages of its use include its fine-grained nature, high organic-carbon content, and high-pH condition.

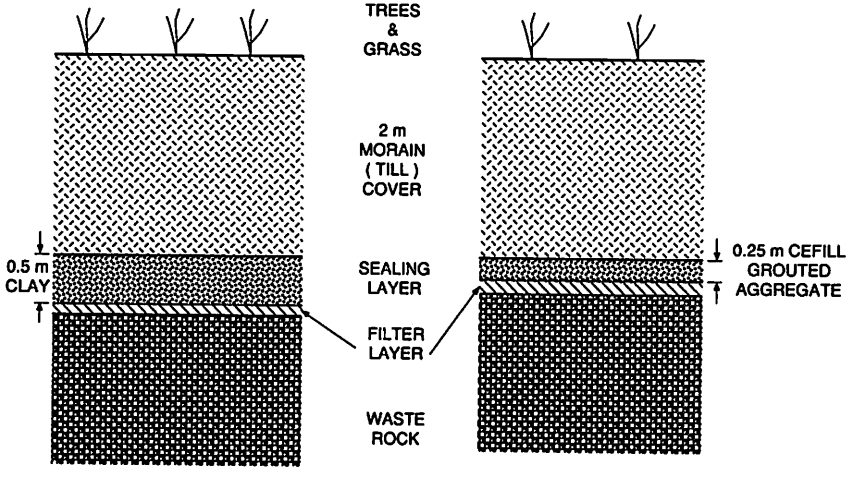

Figure 13.6. Composition of cover materials placed over the Bersbo waste-rock pile. (a) shows the addition of a clay sealing layer, and (b) shows the addition of a Cefill sealing layer to limit sulfide oxidation.

As with all tailings covers, organic-carbon covers must be applied shortly after tailings deposition has ended. Unlike other dry covers, however, organic-carbon covers have the potential to release high concentrations of organic acids to the tailings surface. Interaction between these organic acids and ferric oxyhydroxide minerals precipitated during previous periods of oxidation has the potential to result in reductive dissolution of the ferric oxyhydroxides through reactions of the form

$$4Fe(OH)_3 + CH_20 + 7H^+ \Rightarrow 4Fe^{2+} + HCO^-_3 + 10H_2O \quad (3)$$

These reactions will also release trace and heavy metals adsorbed on, or coprecipitated with these ferric oxyhydroxides. Ribet *et al.* (1994) conducted reductive leaching experiments that demonstrated that significant masses of metals were present in the shallow, altered zone of the Nickel Rim tailings impoundment in a form that was susceptible to attack by reductive dissolution (Figure 13.7).

An alternative to the use of dry covers is the use of wet covers. This is achieved by disposal of tailings into deep lakes (*e.g.*, Pedersen *et al.*, 1993), or by the

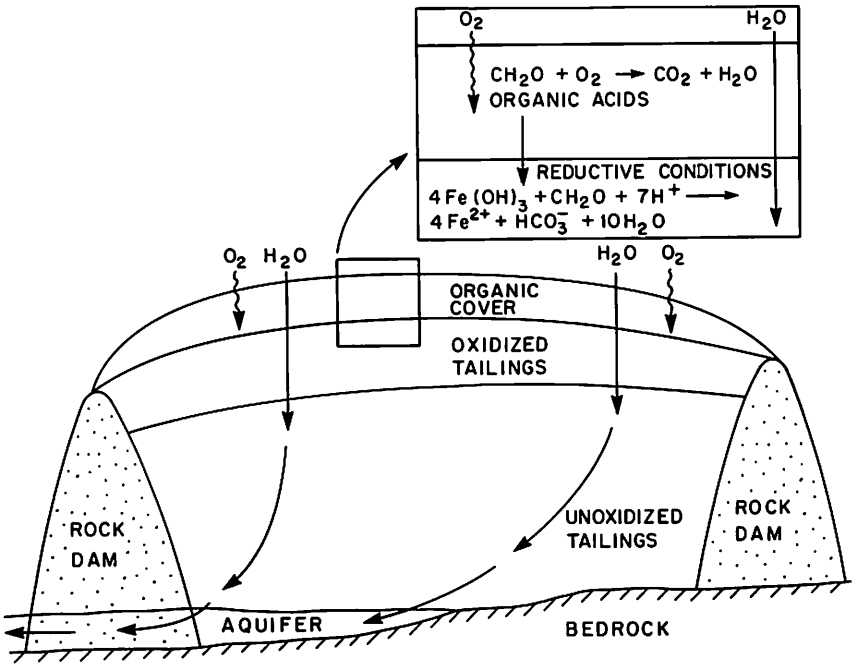

Figure 13.7. Schematic diagram of a tailings impoundment covered with organic matter.

construction of wet covers on existing tailings impoundments (*e.g.*, Robertson, 1992). Wet covers can be established either as ponded water maintained behind a water-retention dam, or as a bog on the tailings surface (Kalin and van Everdingen, 1987). In all of these cases, O_2 ingress into the tailings is limited by the slow diffusion of O_2 through the cover. The establishment of a bog on the tailings surface may also lead to the development of reducing conditions in the cover overlying the tailings, similar to the conditions encountered in natural bogs, which would further lessen the movement of O_2 into the tailings. An attempt to establish bog deposits on an existing tailings surface required that water continually be added to the tailings surface to maintain water-saturated conditions. Without the addition of water the tailings drained due to their coarse-grained nature and the high permeability of the sediments underlying the tailings (Michelutti, 1988). In this case the presence of the bog cover decreased the aqueous concentrations of dissolved metals, but increased the total metal loadings because of the large volume of water that was added to the test plot. In other hydrogeologic settings establishment of bogs on tailings surfaces may be more effective. In all cases, the emplacement of a wet cover on the tailings surface will increase the hydraulic gradient across the dam. Many tailings dams were designed to be permeable in order to allow the tailings to drain and consolidate, and thereby enhance the structural stability of the impoundment. The maintenance of saturated conditions in

such impoundments may reduce the stability of the dam and increase the potential of catastrophic dam failure. In addition to the potential for diminished dam stability, the imposition of a large hydraulic gradient through a tailings impoundment would increase the flow of water through the tailings and into the adjacent groundwater or surface aquatic environments.

To be most effective, O_2-diffusion barriers should be put in place shortly after tailings deposition has ended. The rate of sulfide oxidation is greatest in the early stages of tailings weathering because at this time the sulfide-mineral surfaces are pristine and the O_2-diffusion path length is short. As oxidation proceeds the sulfide minerals are armored by the precipitation of alteration products, and the length of the diffusion path increases. Simulations conducted by Johnson (1993) for the Nickel Rim tailings using the model of Davis and Ritchie (1986), showed that the peak period of oxidation occurs shortly after tailings deposition ends. The rate then declines quickly to a relatively low value, but continues to decline for several years. The depletion of sulfides in the shallow tailings has the effect of developing an expanding silt-size cover on the surface of the tailings. Field determination of Fe and SO_4 concentrations from the Nickel Rim site show maximum Fe and SO_4 concentrations occur 5 m to 8 m below the tailings surface. These higher concentrations represent Fe and SO_4, derived from oxidation shortly after tailings disposal has ended, that has been displaced into the deeper tailings by infiltrating rain and snowmelt. Concentrations of Fe and SO_4 from the vicinity of the tailings surface are lower, indicating that the rate of oxidation has declined.

13.2.4. Prevention of Sulfide Oxidation

The recognition that existing tailings-management programs have the potential to generate low-quality drainage for long periods has lead to alternative proposals for tailings management. These proposals include, but are not limited to, disposal of tailings in deep lakes, separation of sulfide minerals for separate disposal, disposal of tailings as a thickened slurry with improved moisture-retaining capabilities, and enhanced sulfate-reduction within tailings impoundments through the addition of solid-phase organic carbon.

Deep-water disposal of tailings has several advantages. The tailings are located at the base of the flow system and are thereby isolated from the effects of erosion and catastrophic dam failure. The sulfide content is isolated from atmospheric O_2 by a thick water cover, limiting oxidation to the mass of O_2 dissolved in the overlying water cover (approximately 9 mg/L at 25 °C and atmospheric O_2 concentrations and pressures). Studies of tailings deposited in lakes in northern Canada suggest that sulfide minerals are stable in deep lake environments, and that the concentrations of dissolved metals associated with these wastes are low (Pedersen *et al.*, 1993, 1994).

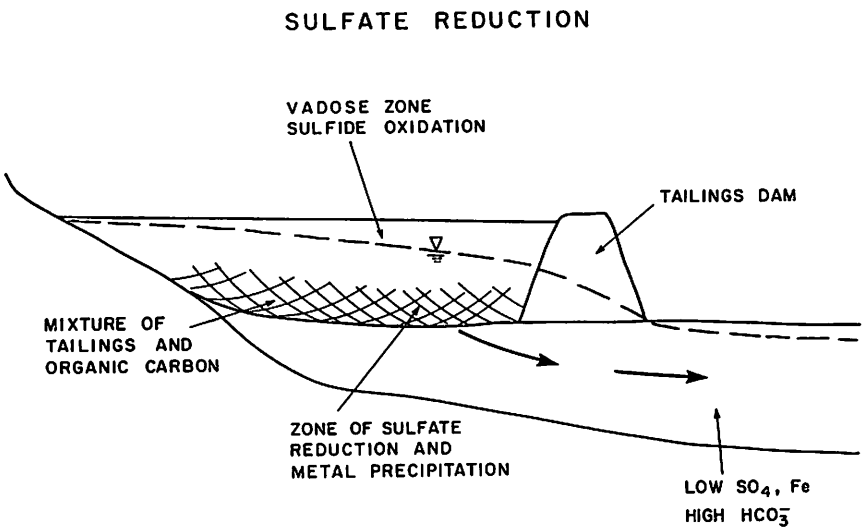

Figure 13.8. Addition of organic carbon dispersed throughout the tailings to enhance sulfate reduction and precipitation of sulfide minerals.

Concentration of sulfide minerals can be achieved by more completely extracting the sulfide minerals in the final stage of flotation in a mill. The separation process would result in two tailings streams, a large-volume low-sulfur tailings product and a smaller volume sulfide-rich portion of the tailings. The sulfur-rich portion of the tailings must be handled in a manner that will prevent contact with atmospheric O_2. The larger volume of low-sulfur tailings may be disposed of by conventional techniques, or may be used for backfill, dam construction, or other surface construction applications.

Separation of the sulfide portion of the tailings represents "geochemically engineering" the tailings properties to beneficial conditions for long-term disposal. Amendments made to the tailings represent an alternative form of geochemical engineering. Addition of organic carbon to tailings as they are deposited in the impoundment was proposed by Blowes (1990) and Blowes and Ptacek (1992b). The addition of organic carbon enhances sulfate-reduction reactions and reprecipitation of metal sulfides. If the organic-carbon-rich zone is located below the equilibrium water-table position (Figure 13.8), the reprecipitated sulfide minerals will be isolated from atmospheric O_2 by the overlying tailings solids and water column.

Mass-balance calculations conducted by Blowes (1990) suggest that it is feasible to add sufficient organic carbon to stabilize much of the Fe and SO_4 contained in a tailings impoundment which has low to moderately high sulfide contents (5—20 wt %

S). The volume of organic carbon required for higher sulfide contents, however, is prohibitive. As a result, this approach is not well-suited to the sulfide-rich tailings derived from some base-metal mining operations.

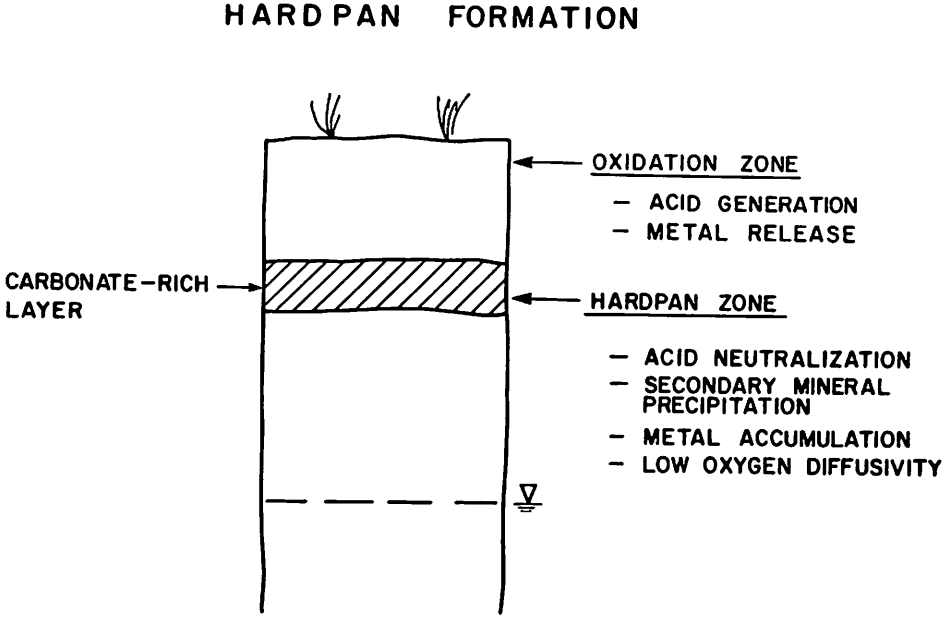

Figure 13.9. Geochemical blending of tailings to promote chemical precipitation of a low-O_2-diffusivity barrier within an impoundment.

In contrast to geochemically engineering a tailings-management system, it has been proposed that the physical hydrogeological characteristics of the tailings be modified as they are deposited in the impoundment. Two of the proposed alternatives are thickened tailings deposition (Robinsky, 1975, 1978; Robinsky *et al.*, 1991), and the intentional formation of cemented "hardpan" layers (Blowes *et al.*, 1991; Ahmed, 1994). Deposition of thickened tailings prevents the segregation of grain sizes that is observed in conventional tailings areas (Robinsky *et al.*, 1991; Robertson, this Volume); thus, the tailings are poorly sorted and have unique moisture-retaining characteristics that result in an extensive tension-saturated zone above the water table. Tension-saturated zones measured at Kidd Creek tailings, at which the thickened-tailings disposal technique is employed, extend > 4 m above the water table.

The oxygen diffusion coefficient of unconsolidated materials is dependent on the moisture content. Empirical equations have been developed to describe the relationship between gas diffusion coefficients and the gas-filled porosity of unconsolidated

sediments. Reardon and Moddle (1985) developed the equation

$$D(O_2) = 3.98 \cdot 10^{-5}[(\varepsilon - 0.05)/0.95]^{1.7}\, T^{3/2} \qquad (4)$$

where $D(O_2)$ is the diffusion coefficient for O_2 gas, ε is the air-filled porosity, and T is the temperature in Kelvin. This relationship indicates that the rate of the diffusion of gas-phase O_2 through saturated tailings is much less than through unsaturated tailings. The large tension-saturated zone observed in thickened tailings deposits (Woyshner and St. Arnaud, 1994; Al *et al.*, 1994a) limits the zone of rapid oxidation to near the tailings surface.

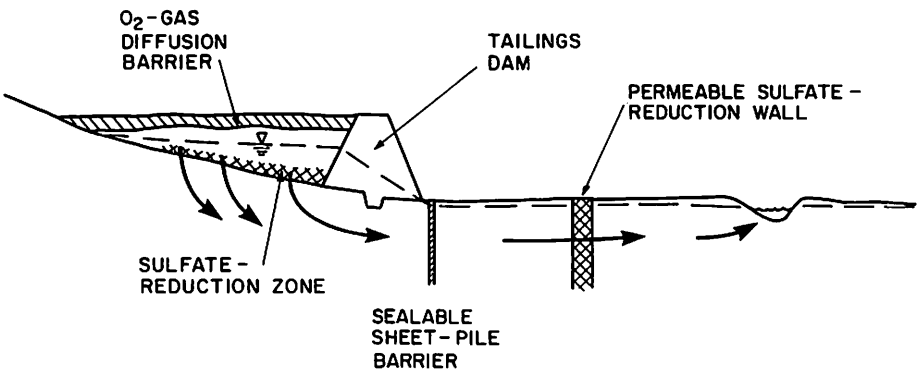

Figure 13.10. Schematic diagram showing the use of a combination of treatment techniques including a low-O_2-gas diffusion barrier, a sulfate-reduction treatment zone in the tailings, an impermeable-sheet-pile barrier, and a permeable sulfate-reduction wall installed along the groundwater flowpath.

The occurrence of cemented or "hardpan" layers has been documented at many mine-waste sites (Boorman and Watson, 1976; McSweeny and Madison, 1988; Blowes *et al.*, 1991). The formation of those layers inhibits the diffusion of pore gases into and out of tailings impoundments. Blowes *et al.* (1991) proposed enhancing the formation of these layers through the selective layering of tailings during the late stages of deposition (Figure 13.9). Ahmed (1994) proposed the addition of $FeSO_4$ solutions to enhance the formation of cemented layers. Although the formation of cemented layers has been proposed by several authors, it has yet to be demonstrated on a field scale.

For sites where extremely low release rates are required, a combination of prevention and treatment techniques can be used (Figure 13.10). For example, geochemical blending of the tailings with organic carbon to promote sulfate reduction below the water table can be used in conjunction with a O_2-gas diffusion barrier. Other techniques, such as the use of a sealable sheet-pile barrier or a permeable reaction wall

installed in the path of the plume can be used in the event one of the previous techniques should fail.

13.3. CONCLUSIONS

Conventional approaches to tailings deposition ensure the structural stability of inactive tailings impoundments. Although revegetation programs stabilize the tailings with respect to aeolian and water erosion, these programs do little to prevent sulfide-mineral oxidation or the transport of dissolved constituents through inactive tailings. Programs intended to remediate the environmental effects of existing tailings areas include collection and treatment of drainage waters using conventional water-treatment facilities, and passive downstream treatment using constructed wetlands or porous reactive walls. To date, of these options, only conventional treatment systems have been demonstrated to be effective for metal-mine wastes at the field scale.

Sulfide-oxidation controls include the use of bactericides, surface armoring processes, and O_2-diffusion barriers. Bactericides have been demonstrated to be useful over short time periods, but their ability to prevent sulfide oxidation over long periods has yet to be demonstrated. Surface-armor systems result in the precipitation of inert coatings on sulfide minerals. The stability of these coatings over the long term, and their effectiveness relative to natural surface coatings, are not yet known.

Oxygen-diffusion barriers, including water covers, layered soil covers, and synthetic covers have been demonstrated to limit O_2 gas diffusion over short time periods (months to years) in field settings. The ability of these barriers to prevent sulfide oxidation over the longer term (decades to centuries) remains unknown. Further testing is required.

Among the various techniques to prevent the oxidation of sulfide minerals under current study, deep-water disposal seems to be most thoroughly evaluated. Separation of sulfide-rich and sulfide-poor tailings is technically feasible, but the environmental benefits of this process have yet to be evaluated. The benefits of thickened-tailings disposal and the addition of organic carbon during tailings deposition are currently being examined at the field and laboratory scale.

References

ACKER, J.G. & BRICKER, O.P. (1992): The influence of pH on biotite dissolution and alteration kinetics at low temperature. *Geochim. Cosmochim. Acta* 56, 3073-3092.

AFANASEV, A.M., GOROBCHENKO, V.D., KULGAWCZUK, D.S. & LUKASHEVICH, I.I. (1974): Nuclear γ-resonance in iron sulphates of the jarosite group. *Phys. Stat. Solidi* A 26, 697-701.

AHMED, S.M. (1991): Electrochemical and surface chemical methods for the prevention of the atmospheric oxidation of sulphide tailings and acid generation. *In* Proceedings Second Internat. Conf. Abatement Acidic Drainage 2, 305-319. MEND Secretariat, Ottawa, Ontario.

_____ (1994): Surface-chemical methods of forming hardpan in pyrrhotite tailings and prevention of the acid mine drainage. *In* Internat. Land Reclamation Mine Drainage Conf. & Third Internat. Conf. Abatement Acidic Drainage 2, 57-66. U.S. Dept. Interior, Bureau of Mines Special Publication SP 06A-94.

AHONEN, L. & TUOVINEN, O.H. (1989): Microbiological oxidation of ferrous iron at low temperatures. *Appl. Environ. Microbiol.* 55, 312-316.

_____&_____ (1991): Temperature effects of bacterial leaching of sulphide minerals in shake flask experiments. *Appl. Environ. Microbiol.* 57, 138-145.

_____& _____ (1992): Bacterial oxidation of sulfide minerals in column leaching experiments at suboptimal temperatures. *Appl. Environ. Microbiol.* 58, 6-66.

_____ & _____(1994): Solid-phase alteration and iron transformation in column bioleaching of a complex sulfide ore. *In* Environmental Geochemistry of Sulfide Oxidation (C.N. Alpers & D.W. Blowes, eds.). *Am. Chem. Soc. Symp. Series* 550, 79-89.

_____, HILTUNEN, P. & TUOVINEN, O.H. (1986): The role of pyrrhotite and pyrite in the bacterial leaching of chalcopyrite. *In* Fundamental and Applied Biohydrometallurgy (R.W. Lawrence, R.M.R. Branion & H.G. Ebner, eds.). Elsevier, Amsterdam, Holland 13-22.

AKSU, Z. & KUTSAL, T. (1990): A comparative study for biosorption characteristics of heavy metal ions with C. vulgaris. *Environ. Technol.* 11, 979-987.

AL, T.A., BLOWES, D.W. & JAMBOR, J.L. (1994a): The pore-water geochemistry of the Cu-Zn mine tailings at Kidd Creek, near Timmins, Ontario, Canada. *In* Internat. Land Reclamation Mine Drainage Conf. & Third Internat. Conf. Abatement Acidic Drainage 2, 208-217. U.S. Dept.

Interior, Bureau of Mines Special Publication SP 06A-94.

_____, _____, _____ & SCOTT, J.D. (1994b): The geochemistry of mine-waste pore water affected by the combined disposal of natrojarosite and base-metal sulphide tailings at Kidd Creek, Timmins, Ontario. *Can. Geotech. J.* (accepted).

ALESII, B.A. & Fuller, W.H. (1976): The mobility of three cyanide forms in soil. *U.S. Environmental Protection Agency Report* EPA-600/9-76-015.

ALLISON, J.D., BROWN, D.S. & NOVA-GRADAC, K.J. (1990): *MINTEQA2/ PRODEFA2, A Geochemical Assessment Model for Environmental Systems: Version 3 User's Manual.* Environmental Research Laboratory, Office of Research and Development, U.S. Environmental Protection Agency, Athens, Georgia.

_____, _____ & _____ (1991): MINTEQA2 /PRODEFA2, a geochemical assessment model for environmental systems: version 3.0 user's manual. *U.S. Environmental Protection Agency Report* EPA/600/3-91/021.

ALPERS, C.N. & BRIMHALL, G.H. (1988): Middle Miocene climatic change in the Atacama Desert of northern Chile: Evidence from supergene mineralization at La Escondida. *Geol. Soc. Am. Bull.* 100, 1640-1646.

_____ & _____ (1989): Paleohydrologic evolution and geochemical dynamics of cumulative supergene metal enrichment at La Escondida, Atacama Desert, northern Chile. *Econ. Geol.* 84, 229-255.

_____ & NORDSTROM, D.K. (1991): Geochemical evolution of extremely acid mine waters at Iron Mountain, California: Are there any lower limits to pH? *In* Proceedings Second Internat. Conf. Abatement Acidic Drainage 2, 321-342.

_____, _____ & BALL, J.W. (1989): Solubility of jarosite solid solutions precipitated from acid mine waters, Iron Mountain, California. *Sci. Geol. Bull.* 42, 281-298.

_____, _____ & THOMPSON, J.M. (1994): Seasonal variations of Zn/Cu ratios in acid mine water from Iron Mountain, California. *In* Environmental Geochemistry of Sulfide Oxidation (C.N. Alpers & D.W. Blowes, eds.). *Am. Chem. Soc. Symposium Series* 550, 324-344.

_____, RYE, R.O., NORDSTROM, D.K., WHITE, L.D. & KING, B.-S. (1992): Chemical, crystallographic, and isotopic properties of alunite and jarosite from acid hypersaline Australian lakes. *Chem. Geol.* 96, 203-226.

ANBEEK, C. (1992a): Surface roughness of minerals and implications for dissolution studies. *Geochim. Cosmochim. Acta* 56, 1461-1469.

_____ (1992b): The dependence of dissolution rates on grain size for some fresh and weathered feldspars. *Geochim. Cosmochim. Acta* 56, 3957-3970.

ANDERSON, C.A. (1955): Oxidation of copper sulfides and secondary sulfide enrichment. *Econ. Geol. 50th Anniv. Vol.*, 324-340.

ANDERSON, M.P. & WOESSNER, W.W. (1992): *Applied Groundwater Modeling.* Academic Press, New York.

ANDREW, R.L. (1980): Supergene alteration and gossan textures of base-metal ores in southern Africa. *Minerals Sci. Engineering* 12, 193-215.

_____ (1984): The geochemistry of selected base-metal gossans, southern Africa. *J. Geochem. Expl.* 22, 161-192.

APPELO, C.A.J. & WILLEMSEN A. (1987): Geochemical calculations and observations on saltwater intrusion, I. A combined geochemical/mixing cell model. *J. Hydrology* 94, 313-330.

ARKESTEYN, G.J.M.W. (1979): Pyrite oxidation by *Thiobacillus ferrooxidans* with special reference to the sulfur moiety of the mineral. *Antonie van Laeurvenhoek (Microbiology)* 45, 423-435.

ARNOLD, R.G. & REICHEN, L.E. (1962): Measurement of the metal content of naturally occurring, metal-deficient hexagonal pyrrhotite by an *x*-ray spacing method. *Am.Mineral.* 47, 105-111.

ASCI/SRK (1990): An Evaluation of the Effectiveness of Rinsing Procedures on Cyanide Removal from Spent Heap Leach Ore: Brohm Mining Corporation, Lead, South Dakota, USA. Report for State of South Dakota, Sept. 1990.

ASTM (1985): Section II, Water and Environmental Technology. Am. Soc. Testing Materials, Vol. 11.02.

ATLAS, R. M. & BARTHA, R. (1987): *Microbial Ecology.* 2nd ed. Benjamin/Cummings Publ. Co., Menlo Park, California.

AWADALLAH, F.T. & PESIC, B. (1992): Biosorption of cobalt with the AMTTM metal removing agent. *Hydrometall.* 28, 65-8.

AXELSSON, C. L., BYSTROM J., HOLMEN, J. & JANSSON, T. (1992): Efterbe handling au sand manasin och grubergsupplag i Aitik, Hydrogeologiska fortsattningar for atgardsplan. *Golder Geosystem AB, Report* 927-1801 (in Swedish).

BAIN, J.G. (1994): *Hydrogeochemistry of a Sand Aquifer Affected by Acid Mine Drainage at the Nickel Rim Mine Tailings, Sudbury, Ontario.* M.Sc. thesis, University of Waterloo, Waterloo, Ontario.

BANCROFT, G.M. (1973): *Mössbauer Spectroscopy: An Introduction for Inorganic Chemists and Geochemists.* McGraw-Hill, London, 252 pp.

BANDY, M.C. (1938): Mineralogy of three sulphate deposits of northern Chile. *Am. Mineral.* 23, 669-759.

BARNES, L.J., JANSSEN, F.J., SCHEEREN, P.J.H., VERSTEEGH, J.H. & KOCH, R.O. (1992): Simultaneous microbial removal of sulphate and heavy metals from waste water. *Trans. Inst. Mining Metall.* 101, C181-C187.

BARTON, P.J., HAMMER, C.A. & KENNEDY, D.C. (1978): Analysis of cyanides in coke plant wastewater effluents. *J. Water Pollution Control Fed.* 50, 234-239.

BATEMAN, A.M. (1950): *Economic Mineral Deposits.* John Wiley & Sons, New York, 245-287.

BATES, R.L. & JACKSON, J.A., editors (1980): *Glossary of Geology*, 2nd ed. Am. Geol. Inst., Falls Church, Virginia.

BEAR, J. (1972): *Dynamics of Fluids in Porous Media.* American Elsevier, New York.

_____ (1979): *Hydraulics of Groundwater.* McGraw-Hill, New York.

BÉCHARD, G., RAJAN, S. & GOULD, W.D. (1993): Characterization of a microbiological process for the treatment of acidic drainage. *In* Biohydrometallurgical Technologies (A.E. Torma, M.L. Apel & C.L. Brierley, eds.). Proc. Internat. Biohydrometall. Symp., Jackson Hole, Wyoming, Aug. 22-25, 1993. Vol. 2, 277-286.

BELL, A.V., SURGES, L. & GROSKOPF, G.R. (1991): An update of the acid waste rock field trials at Heath Steele Mines, New Brunswick. *In* Proceedings Second Internat. Conf. Abatement Acidic Drainage 3, 321-340. MEND Secretariat, Ottawa, Ontario.

BELL, P.E., MILLS, A.L. & HERMAN, J.S. (1987) Biogeochemical conditions favoring magnetite formation during anaerobic iron reduction. *Appl. Environ. Microbiol.* 53, 261-2616.

BENNETT, J.W. & RITCHIE, A.I.M., (1992): The installation of monitoring sites in waste rock at the Aitik Mine site August-September (1991). *Austral. Nuclear Sci. Technology Org. Report* ANSTO/C263.

_____ & _____ (1993): Field procedures manual; measurement of gas permeability. *Austral. Nuclear Sci. Technology Org. Report* ANSTO/C317.

_____, COMARMOND, M.J. & RITCHIE A.I.M. (1993a): Oxidation rates of

Aitik dump material: column studies. *Austral. Nuclear Sci. Technology Org. Report* ANSTO/C337.

_____, GARVIE, A.M. & RITCHIE, A.I.M. (1993b): Field procedures manual; measurement of gas diffusion coefficients. *Austral. Nuclear Sci. Technology Org. Report* ANSTO/C318.

_____, GIBSON, D.K., RITCHIE, A.I.M., TAN, Y., BROMAN, P.G. & JÖNSSON, H. (1994): Oxidation rates and pollution loads in drainage correlation ofmeasurements in a pyritic waste rock dump. *In* Proceedings Third Internat. Conf. Abatement Acidic Drainage Pittsburgh, Pennsylvania (accepted).

_____, HARRIES, J.R. & RITCHIE, A.I.M. (1988): Rehabilitation of waste rock dumps at the Rum Jungle mine site. *In* Mine Drainage and Surface Mine Reclamation, Vol. 1. *U.S. Bureau Mines Inf. Circ.* 9183, 104-108.

_____, _____ & _____ (1992): Chemical activity and water balance of overburden heaps. *In* Rum Jungle Rehabilitation Project Monitoring Report 1986-88 (M. Kraatz & R.J. Applegate, eds.). *Conservation Commission of the Northern Territory Tech. Report* 51, Ch. 7.

_____, _____, PANTELIS, G. & RITCHIE, A.I.M. (1989). Limitations on pyrite oxidation rates in dumps set by air transport mechanisms. *In* Proceedings Internat. Symp. on Biohydrometallurgy (J. Salley, R.G.L. McCready & P.L. Wichlacz, eds.). *CANMET Report* SP89-10, 551-561. Dept. Energy Mines Resources Canada.

_____, RITCHIE, A.I.M. & TAN, Y. (1993c): Field procedures manual: measurement of thermal conductivity. *Austral. Nuclear Sci. Technology Org. Report* ANSTO/C319.

_____, RITCHIE, A.I.M. & TAN, Y. (1993d): The temperature dependence of pyrite oxidation rates in waste rock at the Aitik Mine. *Austral. Nuclear Sci. Technology Org. Report* ANSTO/C335.

BERNARDIN, F.E. (1973): Cyanide detoxification using adsorption and catalytic oxidation on granular activated carbon. *J. Water Pollution Control Fed.* 45, 221-222.

BERNER, R.A. (1964): Distribution and diagenesis of sulfur in some sediments from the Gulf of California. *Marine Chem.* 1, 17-140.

_____ (1967a): Thermodynamic stability of sedimentary iron sulfides. *Am. J. Sci.* 265, 773-785.

_____ (1967b): Diagenesis of iron sulfide in recent marine sediments. *Assoc. Advancement Sci. Publ.* 83, 268-272.

_____ (1980): *Early Diagenesis: A Theoretical Approach.* Princeton University Press, Princeton, New Jersey.

BERTHELOT, D., LEDUC, L.G. & FERRONI, G.D. (1993): Temperature studies of iron-oxidizing autotrophs and acidophilic heterotrophs isolated from uranium mines. *Can. J. Microbiol.* 39, 384-388.

BEVERIDGE, T.J. & MURRAY, R.G.E. (1976): Uptake and retention of metals by cell walls of Bacillus subtilis. *J. Bacteriol.* 127, 152-1518.

_____ & _____ (1980): Sites of metal deposition in the cell wall of Bacillus subtilis. *J. Bacteriol.* 141, 876-887.

BEYER, M., KLEIN, J., VAUPEL, K. & WIEGARD, D. (1990): Microbial coal desulphurization: Calculation of costs. *Bioprocess. Eng. 5*, 97-101.

BHATTI, T.M., BIGHAM, J.M., CARLSON, L. & TUOVINEN, O.H. (1993): Mineral products of pyrrhotite oxidation by Thiobacillus ferrooxidans. *Appl. Environ. Microbiol.* 59, 1984-1990.

BIGHAM, J.M., CARLSON, L. & MURAD, E. (1994): Schwertmannite, a new iron oxyhydroxysulfate from Pyhäsalmi, Finland, and other localities. *Mineral. Mag.* (accepted).

_____, SCHWERTMANN, U. & CARLSON, L. (1992): Mineralogy of precipitates formed by the biogeochemical oxidation of Fe(II) in mine drainage. *In* Biomineralization Processes of Iron and Manganese : Modern and Ancient Environments (H.C.W. Skinner & R.W. Fitzpatrick, eds.). Catena Verlag, Cremlingen-Destedt, Germany, 219-232.

_____, _____, _____ & MURAD, E. (1990): A poorly crystallized oxyhydroxysulfate of iron formed by bacterial oxidation of Fe(II) in acid mine waters. *Geochim. Cosmochim. Acta* 54, 2743-2758.

BIRCH, W.D., PRING, A., RELLER, A. & SCHMALLE, H.W. (1993): Bernalite, Fe(OH)3, a new mineral from Broken Hill, New South Wales: Description and structure. *Am. Mineral.* 78, 827-834.

BISARIA, V.S. & CHOSE, T.K. (1981): Biodegradation of cellulosic materials: substrates, microorganisms, enzymes and products. *Enzyme Microb. Technol.* 3, 9-14.

BISHOP, E. & WRIGHT, D.T. (1977): Oxidation of Cyanides. U.S. Patent 4,024,037. *Chem. Abstracts* 87, 31152b.

BLACKFORD, M.G. & HARRIES, J.R. (1985): A heat source probe for measuring thermal conductivity in waste rock dumps. *Austral. Atomic Energy Commission Report* AAEC/E609.

BLAIN, C.F. & ANDREW, R.L. (1977): Sulfide weathering and evaluation of gossans in mineral exploration. *Minerals Sci. Engineering* 9, 119-149.

BLAIR, R.D. (1981): *Hydrogeochemistry of an Inactive Pyritic Uranium Tailings Basin, Nordic Mine, Elliot Lake, Ontario.* M.Sc. thesis, University of Waterloo, Waterloo, Ontario.

BLANCHARD, R. (1968): Interpretation of leached outcrops. *Nevada Bureau Mines Bull.* 66, 196 pp.

BLENKINSOPP, S.A. (1991): The use of biofilm bacteria to exclude oxygen from acidogenic mine tailings. *In* Proceedings Second Internat. Conf. Abatement Acidic Drainage 1, 369-377. MEND Secretariat, Ottawa, Ontario.

BLOOMFIELD, C. (1972): The oxidation of iron sulphides in soils in relation to the formation of acid sulphate soils, and of ochre deposits in field drains. *J. Soil Sci.* 23, 1-16.

BLOWES, D.W. (1990): *The Geochemistry, Hydrogeology and Mineralogy of Decommissioned Sulfide Tailings: A Comparative Study.* Ph.D. thesis, University of Waterloo, Waterloo, Ontario.

_____ & JAMBOR, J.L. (1990): The pore-water geochemistry and the mineralogy of the vadose zone of sulfide tailings, Waite Amulet, Quebec, Canada. *Applied Geochem.* 5, 327-346.

_____, _____ APPLEYARD, E.C., REARDON, E.J. & CHERRY, J.A. (1992): Temporal observations of the geochemistry and mineralogy of a sulfide-rich mine-tailings impoundment, Heath Steele Mines, New Brunswick. *Expl. Mining Geol.* 1, 251-264.

_____, _____, CHERRY, J.A. & REARDON, E.J. (1994): The geochemical evolution of a sulfide-rich mine-tailings impoundment, Heath Steele, New Brunswick, Canada. *Appl. Geochem.* (accepted).

_____ & PTACEK, C.J. (1992a): Geochemical remediation of groundwater by permeable reactive walls: Removal of chromate by reaction with iron-bearing solids. *In* Proceedings Subsurface Restoration Conf., 3rd Internat. Conf. Ground Water Qual. Research, June 21-24, 1992, Dallas, Texas, 214-216.

_____ & _____ (1992b) Treatment of mine tailings. US Patent.

_____ & _____ (1994): Redox curtain for groundwater remediation. US Patent.

_____, REARDON, E.J., JAMBOR, J.L. & CHERRY, J.A. (1991): The formation and potential importance of cemented layers in inactive sulfide mine

tailings. *Geochim. Cosmochim. Acta* 55, 965-978.

BOL'SHAKOV, A.P. & PTUSHKO, L.L. (1971): Alteration products of melanterite from Nikitov mercury ore deposits. *Internat. Geol. Review* 13, 849-854.

BOORMAN, R.S. & WATSON, D.M. (1976): Chemical processes in abandoned sulfide tailings dumps and environmental implications for Northeastern New Brunswick. *CIM Bull.* 69, No. 772, 86-96.

BORGGAARD, O.K. (1982): Selective extraction of amorphous iron oxides by EDTA from selected silicates and mixtures of amorphous and crystalline iron oxides. *Clay Minerals* 17, 365-368.

_____ (1988): Phase identification by selective dissolution techniques. *In* Iron in Soils and Clay Minerals (J. W. Stucki, B. A. Goodman & U. Schwertmann, eds.). NATO ASI Ser. C., 217, 83-98. D. Reidel Publ. Co., Dordrecht, Holland.

BOYLE, D.R. (1994): Oxidation of massive sulfide deposits in the Bathurst Mining Camp, New Brunswick. *In* Environmental Geochemistry of Sulfide Oxidation (C.N. Alpers & D.W. Blowes, eds.). *Am. Chem. Soc. Symp. Series* 550, 535-550.

BRADY, K.S., BIGHAM, J.M., JAYNES, W.F. & LOGAN, T.J. (1986): Influence of sulfate on Fe-oxide formation: Comparisons with a stream receiving acid mine drainage. *Clays Clay Minerals* 34, 266-274.

BRAITHWAITE, R.S.W., KAMPF, A.R., PRITCHARD, R.G. & LAMB, R.P.H. (1993): The occurrence of thiosulfates and other unstable sulfur species as natural weathering products of old smelting slags. *Mineral. Petrology* 47, 255-261.

BRICKELL, R.H. (1981): Chemistry of cyanide solutions. Presented at *Cyanide and the Gold Mining Industry.* Technical Seminar, Ottawa, Ontario, Jan. 22-23, 1981. Environment Canada.

BRIERLEY, C.L. (1978): Bacterial leaching. CRC Critical Rev. *Microbiol.* 6, 207-262.

BRIERLEY, J.A. & LUINSTRA, L. (1993): Biooxidation—heap concept for pretreatment of refractory gold ore. *In* Biohydrometallurgical Technologies (A.E. Torma, J.E. Weyward & V.I. Lakshmanan, eds.). Proc. Internat. Biohydometallurgy Symp., Jackson Hole, Wyoming. Vol. 1, 437-448.

BRIMHALL, G.H. & CRERAR, D.A. (1987): Ore fluids: Magmatic to supergene. *Reviews in Mineralogy* 17, 235-321.

BRION, D. (1980): Etude par spectroscopie de photoelectrons de la degradation superficielle de FeS_2, $CuFeS_2$, ZnS et PbS a l'air et dans l'eau. *Applications Surface Sci.* 5, 133-152.

BRITISH COLUMBIA ACID MINE DRAINAGE TASK FORCE (1989): *Draft Acid Rock Drainage Technical Guide. Volume 1 Technical Guide.* B.C. Ministry of Energy Mines and Petroleum Resources, Victoria, B.C.

BROCK, T.D. & GUSTAFSON, J. (1976): Ferric iron reduction by sulfur- and iron-oxidizing bacteria. *Appl. Environ. Microbiol.* 33, 567- 571.

BROCK. T.P., SMITH, D.W. & MADIGAN, M.T. (1984): *Biology of Microorganisms.* Prentice-Hall, Englewood Cliffs, New Jersey, 847 pp.

BRODERIUS, S. & SMITH, L. (1980): *U.S. Environmental Protection Agency,* Grant No. R805291.

BROMAN, P.G., HAGLUND, P. & MATTSSON, E. (1991): Use of sludge for sealing purposes in dry covers-Development and field experiences. *In* Proceedings Second Internat. Conf. Abatement Acidic Drainage 1, 515-528. MEND Secretariat, Ottawa, Ontario.

BROPHY, G.P. & SHERIDAN, M.E. (1965): Sulfate Studies IV. The jarosite-natrojarosite-hydronium jarosite solid solution series. *Am. Mineral.* 50, 1595-1607.

BROWN, A. (1991): Proposal for the mitigation of acid leaching from tailings using a cover of muskeg peat. *In* Proceedings Second Internat. Conf. Abatement Acidic Drainage 2, 517-527. MEND Secretariat, Ottawa, Ontario.

BROWN, G. (1980): Associated minerals. *In* Crystal Structures of Clay Minerals and Their X-ray Identification (G.W. Brindley & G. Brown, eds.). Mineralogical Society, London, UK, 361-410.

BROWN, J.B. (1970): A chemical study of some synthetic potassium-hydronium jarosites. *Can. Mineral.* 10, 696-703.

_____ (1971): Jarosite-goethite stabilities at 25 °C, 1 atm. *Mineralium Deposita* 6, 245-252.

BUCKLEY, A.N. & WOODS, R.W. (1983): An X-ray photoelectron spectroscopic investigation of the tarnishing of bornite. *Austral. J. Chem.* 36, 1793-1804.

_____ & _____ (1984a): An X-ray photoelectron spectroscopic study of the oxidation of chalcopyrite. *Austral. J. Chem.* 37, 2403-2413.

_____ & _____ (1984b): An X-ray photoelectron spectroscopic study of the oxidation of galena. *Applications Surface Sci.* 17, 401-414.

_____ & _____ (1985a): X-ray photoelectron spectroscopy of oxidized pyrrhotite surfaces. *Applications Surface Sci.* 20, 472-480.

_____ & _____ (1985b): X-ray photoelectron spectroscopy of oxidized pyrrhotite surfaces. *Applications Surface Sci.* 22, 280-287.

_____ & _____ (1987): The surface oxidation of pyrite. *Applications Surface Sci.* 27, 437-452.

BURDEN, R.J. & KIDD, C.H. (1987): The environmental fate of cyanide in gold mine process tailings. Proceedings Ann. Conf. AIMM, Nelson, New Zealand.

BURNETT, R.D. & FRIND, E.O. (1987): Simulation of contaminant transport in three dimensions 2. Dimensionality effects. *Water Resources Research* 23, 695-705.

BURNS, R.G. & FISHER, D.S. (1990): Iron-sulfur mineralogy of Mars: Magmatic evolution and chemical weathering products. *J. Geophys. Research* 95, 14415-14421.

_____, VAUGHAN, D.J. & ENGLAND, K.E.R. (1991): Spectroscopic investigations of oxidized pyrrhotite surfaces. *Geol. Soc. Am. Ann. Meeting Program Abstracts* 23, A146.

BURRIS, J.E., GERBER, D.W. & McHERRON, L.E. (1984): Removal of iron and manganese from water by sphagnum moss. *In* Treatment of Mine Drainage by Wetlands (J.E. Burris, ed.). Contrib. No. 264, Department of Biology, The Pennsylvania State University, Pittsburg, Pennsylvania.

BUSECK, P.R., editor (1992) Minerals and reactions at the atomic scale: transmission electron microscopy. *Reviews in Mineralogy* 27, 500 pp.

BUSENBERG, E. & PLUMMER, L.N. (1982): The kinetics of dissolution of dolomite in CO_2-H_2O systems at 1.5 to 65 °C and 0 to 1 atm PCO_2. *Am. J. Sci.* 282, 45-78.

_____ & _____ (1992): Use of chlorofluorocarbons (CCl_3F and CCl_2F_2) as hydrologic tracers and age-dating tools: the alluvium and terrace system of central Oklahoma. *Water Resources Research* 28, 2257-2283.

BYERLEY, J.J., SCHARER, J.M. & CHARLES, A.M. (1987): Uranium (VI) biosorption from process solutions. *Chem. Eng. J.* 36, B49-B57.

CAIRNS, J., KALIN, M. & SCRIABLO, R. (1988): *Microbiological Aspects of Organic Matter in Extreme Acidic Conditions on Base Metal Tailings.* Final Report. DSS File No. 7SQ.2344-8-951. CANMET, Dept. Energy, Mines Resources Canada.

CALDWELL, J. & SMITH, A. (1985): Material Considerations in the Design of

Downstream Embankments for Tailings Impoundments. *Mining Sci. Tech.* 3. Elsevier, Amsterdam, Holland.

CANFIELD, D.E. (1989): Sulfate reduction and oxic respiration in marine sediments: Implications for organic carbon preservation in euxinic environments. *Deep-Sea Research* 36, 121-138.

_____ & Des MARAIS, D.J. (1991): Aerobic sulfate reduction in microbial mats. *Science* 251, 1471-1473.

_____ & _____ (1993): Biogeochemical cycles of carbon, sulfur, and free oxygen in a microbial mat. *Geochim. Cosmochim. Acta* 57, 3971-3984.

CARLSON, L. & SCHWERTMANN, U. (1981): Natural ferrihydrites in surface deposits from Finland and their association with silica. *Geochim. Cosmochim. Acta* 45, 421-429.

_____ & _____ (1990): The effect of CO_2 and oxidation rate on the formation of goethite versus lepidocrocite from an Fe(II) system at pH 6 and 7. *Clay Minerals* 25, 65-71.

CARSLAW, H.S. & JAEGER, J.C. (1959): *Conduction of Heat in Solids.* Clarendon Press, Oxford, UK.

CARUSO, S.G. (1975): *The Chemistry of Cyanide Compounds and Their Behavior in the Aquatic Environment.* Carnegie-Mellon Institute of Research, Pittsburg, Pennyslvania.

CASEY, W.H. & SPOSITO, G. (1991): On the temperature dependence of mineral dissolution rates. *Geochim. Cosmochim. Acta* 56, 3825-3830.

CATHLES, L.M. (1979): Predictive capabilities of a finite difference model of copper leaching in low grade industrial sulfide waste dumps. *Math. Geol* 11, 175-191.

CATHLES, L.M. (1994): Attempts to model the industrial-scale leaching of copper-bearing mine waste. *In* Environmental Geochemistry of Sulfide Oxidation (C.N. Alpers & D.W. Blowes, eds.). *Am. Chem. Soc. Symposium Series* 550, 123-131.

_____ & SCHLITT. W.J. (1980): A model of the dump leaching process that incorporates oxygen balance, heat balance, and two-dimensional air convection. *In* Leaching and Recovering Copper from As-mined Materials (W.J. Schlitt, ed.). Soc. Mining Eng. A.I.M.E., 9-27

CCREM (Canadian Council of Resource and Environment Ministers) (1987): Freshwater aquatic life. *In* Canadian Water Quality Guidelines, 1-54.

CHAO, T.T. & THEOBALD, P.K. Jr. (1976): The significance of secondary iron and manganese oxides in geochemical exploration. *Econ. Geol.* 71,

1560-1569.

CHAPMAN, B.M., JONES, D.R. & JUNG, R.F. (1983): Processes controlling metal ion attenuation in acid mine drainage streams. *Geochim. Cosmochim. Acta* 47, 1957-1973.

CHAPMAN, N.A., McKINLEY, I.G., SHEA, M.E. & SMELLIE, J.A., editors (1992a): The Poços de Caldas project: natural analogues of processes in a radioactive waste repository, Part I. *J. Geochem. Expl.* 45, 1-603.

_____, _____, _____, & _____ (1992b): The Poços de Caldas project: natural analogues of processes in a radioactive waste repository, Part II. *J. Geochem. Expl.* 46, 1-146.

CHAPUIS, R.P. (1988): Shape factors for permeability tests in boreholes and piezometers. *Ground Water* 27, 647-654.

CHATWIN, T.D. (1990): Cyanide Attenuation/Degradation in Soil. Final Report, Resource Recovery and Conservation Company, Salt Lake City, Utah.

_____ & HENDRIX, J. (1988): The fate of cyanide in soils. Randol Gold Forum 88, Scottsdale, Arizona, February 23-24, 1988, p. 343.

_____ & TREPANOWSKI, J.J. (1987): Utilization of soils to mitigate cyanide releases. Proceedings Third Western Reg. Conf. on Precious Metals, Coal and Environment. Rapid City, South Dakota, Sept. 23-26, 1987, p. 151.

CHEN, T.T. & PETRUK, W. (1980): Mineralogy and characteristics that affect recoveries of metals and trace metals from the ore at Heath Steele Mines, New Brunswick. *CIM Bull.* 73, No. 823, 167-179.

CHERRY, J.A., GILLHAM, R.W., ANDERSON, E.G. & JOHNSON, P.E. (1983): Migration of contaminants at a landfill: a case study, 2, groundwater monitoring devices. *J. Hydrology* 63, 31-49.

_____, BLACKPORT, R.J., DUBROVSKY, N.M., GILLHAM, R.W., LIM, T.P., MURRAY, D., REARDON, E.J. & SMYTH, D.J.A. (1980): Subsurface hydrology and geochemical evolution of inactive pyritic tailings in the Elliot Lake uranium district, Canada. *In* Proceedings Third Symp. Uranium Mill Tailings Management, Dept. Civil Engineering, Colorado State University, Fort Collins, Colorado, 353-385.

CHILDS, C.W. (1992): Ferrihydrite: A review of structure, properties and occurrence in relation to soils. *Zeitz. Pflanzenernähr. Bodenk.* 155, 441-448.

CHUKHROV, F., ZVIJAGIN, B.B., GORSHKOV, A.I., ERILOVA, L.P. & BALASHOVA, V.V. (1973): Ferrihydrite. *Izv. Akad. Nauk SSSR Ser. Geol.* 44, 23-33.

COBURN, S.E. (1949): Limits for toxic wastes in sewage treatment. *Sewage Works J.* 21, 522-524.

CODY, R.D. & BIGGS, D.L. (1973): Halotrichite, szomolnokite, and rozenite from Dolliver State Park, Iowa. *Can. Mineral.* 11, 958-970.

COFFIN, D.E. (1963): A method for the determination of free iron in soils and clays. *Can. J. Soil Sci.* 43, 7-17.

COGGANS, C.J. (1992): *Hydrogeology and Geochemistry of the INCO Ltd., Copper Cliff, Ontario, Mine Tailings Impoundments.* M.Sc. thesis, University of Waterloo, Waterloo, Ontario.

_____, BLOWES, D.W. & ROBERTSON, W.D. (1991): The hydrogeology and geochemistry of a nickel-mine tailings impoundment, Copper Cliff, Ontario. *In* Proceedings Second Internat. Conf. Abatement Acidic Drainage 4, 1-26. MEND Secretariat, Ottawa, Ontario.

_____, _____, _____ & JAMBOR, J.L. (1994): The hydrogeochemical evolution of a nickel mine tailings impoundment, Copper Cliff, Ontario. *Reviews in Econ. Geol.* (accepted).

COLBERG, P.J. (1988): Anaerobic microbial degradation of cellulose, lignin, oligolignols, and monoaromatic lignin derivatives. *In* Biology of Anaerobic Microorganisms (A.J.B. Zehender, ed.). John Wiley & Sons, New York, 333-372.

COLLIN, M. (1987): *Mathematical Modelling of Water and Oxygen Transport in Layered Soil Covers for Deposits of Pyritic Mine Tailings.* Licentiate Treatise, Royal Institute of Technology, Stockholm.

_____ & RASMUSON, A. (1986): Distribution and flow of water in unsaturated layered cover materials for waste rock. *National Swedish Environmental Protection Board, Report* 3088.

COLMER, A.R. & HINKLE, M.E. (1947): The role of microorganisms in acid mine drainage: A preliminary report. *Science* 106, 253-256.

CONN, K. (1981): Cyanide analysis in mine effluents. Presented at Cyanide and the Gold Mining Industry. Technical Seminar, Ottawa, Ontario, Jan. 22-23, 1981. Environment Canada.

CORNELL, R.M. (1991): Simultaneous incorporation of Mn, Ni and Co in the goethite (α-FeOOH) structure. *Clay Minerals* 26, 427-430.

COUGHLAN, M.P. & MAYER, F. (1992): The cellulose-decomposing bacteria and their enzyme systems. *In* The Prokaryotes (A. Balows, H.G. Truper, M. Dworkin, W. Harder & K.-H Schleife, eds.). 2nd ed., Vol. 1. Springer-Verlag, New York, 460-516.

CRANK, J.C. (1956): *The Mathematics of Diffusion.* Oxford Clarendon Press, Oxford, UK.

_____ (1975): *The Mathematics of Diffusion.* Oxford University Press, London, UK.

CRAVOTTA, C.A. III (1994): Secondary iron-sulfate minerals as sources of sulfate and acidity. *In* Environmental Geochemistry of Sulfide Oxidation (C.N. Alpers & D.W. Blowes, eds.). *Am. Chem. Soc. Symposium Series* 550, 345-364.

CSIKAI, N.J. & BARNARD, A.J., Jr. (1983): Determination of total cyanide in thiocyanate-containing wastewaters. *Anal. Chem.* 55, 1677-1682

DAMON, L., SMITH, A. & MUDDER, T. (1991): *Geochemical Study of Leach Pad Cyanide Neutralization.* Brohm Mining Company, Lead, South Dakota.

DANIEL, J.A., HARRIES, J.R. & RITCHIE, A.I.M. (1982): *Runoff and Seepage from Waste Rock Dumps Containing Pyritic Material.* Hydrology and Water Resources Symposium, Melbourne May 1982. Institution of Engineering Australia.

DAUS, A.D., FRIND E.O. & SUDICKY, E.A. (1985): Comparative error analysis in finite-element formulations of the advection_dispersion equation. *Advances Water Resources* 8, 86-95.

DAVE, N.K. & LIM, T.P. (1989): Wetlands and their role in treating acid mine drainage. A literature review. CANMET Division Report MSL 89-17 (LS). Dept. Energy Mines Resources Canada.

DAVE, N.K., LIM, T.P., SIWIK, R.S. & BLACKPORT, R. (1986): Geophysical and biohydrogeochemical investigations of an active sulfide tailings basin, Noranda, Quebec, Canada. *In* 1986 Natl. Symp. on Mining, Hydrology, Sedimentology and Reclamation, Univ. of Kentucky, Lexington, Kentucky, 13-19.

DAVIDSON, R.M. (1990): Natural oxidation of coal. *IEA Coal Research* IEACR/29, 11-76.

DAVIS, G.B. & RITCHIE, A.I.M. (1986): A model of oxidation in pyritic mine wastes. I. Equations and approximate solution. *Appl. Math. Modelling* 10, 314-322.

_____ & _____ (1987): A model of oxidation in pyrite mine wastes. 3. import of particle size distribution. *Appl. Math. Modelling* 10, 417-422.

_____, DOHERTY, G. & RITCHIE, A.I.M. (1986): A model of pyrite oxidation in mine wastes. II. Comparison of numerical and approximate solutions.

Appl. Math. Modelling 10, 323-329.

_____, JAMES, R.O. & LECKIE, J.O. (1978): Surface ionization and complexation at the oxide/water interface. I. Computation of electrical double layer properties in simple electrolytes. *J. Colloid Interface Sci.* 63, 480-499.

DAVIS, J.A. & HEM, J.D. (1989): The surface chemistry of aluminum oxides and hydroxides. *In* Environmental Geochemistry of Aluminum (G. Sposito, ed.). CRC Press, Boca Raton, Florida, 185-219.

DAVY, D.R., editor (1975): Rum Jungle environmental studies. *Austral. Atomic Energy Commision Report* AAEC/365.

DE ENDREDY, A.S. (1963): Estimation of free iron oxides in soils and clays by a photolytic method. *Clay Minerals Bull.* 5, 209-217.

De HAAN, S.B. (1991): A review of the rate of pyrite oxidation in aqueous systems at low temperature. *Earth Sci. Rev.* 31, 1-10.

De MARSILY, G. (1986): *Quantitative Hydrogeology.* Academic Press Inc., San Diego,California.

DEBYLE, N.V., HENNES, R.W. & HART, G.E. (1988): Evaluation of ceramic cups for determining soil solution chemistry. *Soil Sci.* 146, 130-36.

DEER, W.A., HOWIE, R.A. & ZUSSMAN, J. (1962): Rock-forming Minerals 5, 118-121. Longmans, London, UK.

DiTORO, D.M., MAHONY, J.D., HANSON, D.J., SCOTT, K.J., HICKS, M.B., MAYR, S.M. & REDMOND, M.S. (1990): Toxicity of cadmium in sediments: the role of acid volatile sulfide. *Environ. Toxicol. Chem.* 9, 1487-1502.

DODGE, B.F. & ZABBON, W. (1952): Disposal of plating room wastes IV. Batch volatilization of hydrogen cyanide from aqueous solutions of cyanides. *Plating* 39, 381-384.

DOMENICO, P.A. & SCHWARTZ, F.W. (1990): *Physical and Chemical Hydrogeology.* John Wiley & Sons, New York.

DONER, H.E. & LYNNE, W.C. (1989): Carbonate, halide, sulfate and sulfide minerals. *In* Minerals in Soil Environments (J. B. Dixon & S. B. Weed, eds.). Soil Sci. Soc. Am., Madison, Wisconsin, 279-330.

DOUDOROFF, P. (1980): *A Critical Review of Recent Literature on the Toxicity of Cyanides to Fish.* Am. Petroleum Inst., Washington, D. C.

DOUSMA, J., DEN OTTELANDER, D. & DE BRUYN, P.L. (1979): The influence of sulfate ions on the formation of Fe(III) oxides. *J. Inorg.*

Nuclear Chem. 41, 1565-1568.

DOVE, P.M. & RIMSTIDT, J.D. (1985): The solubility and stability of scorodite, $FeAsO_4.2H_2O$. *Am. Mineral.* 70, 838-844.

DOWN, C.G. & STOCKS, J. (1977): Methods of tailings disposal. *Mining Mag.* 136, 345-359.

DREVER, J.I. & ZOBRIST, J. (1992): Chemical weathering of silicate rocks as a function of elevation in the southern Swiss Alps. *Geochim. Cosmochim. Acta* 56, 3209-3216.

DRITS, V.A., SAKHAROV, B.A., SALYN., A.L. & MANCEAU, A. (1993): Structural model for ferrihydrite. *Clay Minerals* 28, 185-207.

DUBROVSKY, N.M. (1986): *Geochemical Evolution of Inactive Pyritic Tailings in the Elliot Lake Uranium District.* Ph.D. thesis, University of Waterloo, Waterloo, Ontario.

_____, CHERRY, J.A., REARDON, E.J. & VIVYURKA, A.J. (1984a): Geochemical evolution of inactive pyritic tailings in the Elliot Lake uranium district: 1. The groundwater zone. *Can. Geotech. J.* 22, 110-128.

_____, MORIN, K.A., CHERRY, J.A. & SMYTH, D.J.A. (1984b): Uranium tailings acidification and subsurface contaminant migration in a sand aquifer. *Water Pollut. Research J.* 19, 55-89.

DUTRIZAC, J.E. (1980): The physical chemistry of iron precipitation in the zinc industry. *In* Lead-Zinc-Tin '80 (J.M. Cigan, T.S. Mackey & T.J. O'Keefe, eds.). TMS-AIME, Warrendale, Pennsylvania, 532-564.

DUTRIZAC, J.E. (1983): Jarosite-type compounds and their application in the metallurgical industry. *In* Hydrometallurgy—Research, Development, and Practice (K. Osseo-Asare & J.D. Miller, eds.). TMS-AIME, Warrendale, Pennsylvania, 531-551.

DUTRIZAC, J.E. (1984): The behavior of impurities during jarosite precipitation. *In* Hydrometallurgical Process Fundamentals (R.G. Bautista, ed.). Plenum Publ., New York, 125-169.

_____ & DINARDO, O. (1983): The co-precipitation of copper and zinc with lead jarosite. *Hydrometallurgy* 11, 61-78.

_____ & JAMBOR, J.L. (1987): The behaviour of arsenic during jarosite precipitation: arsenic precipitation at 97 °C from sulphate or chloride media. *Can. Metall. Quart.* 26, 91-101.

_____ & KAIMAN, S. (1976): Synthesis and properties of jarosite-type compounds. *Can. Mineral.* 14, 151-158.

DVORAK, D.H., HEDIN, R.S., EDENBORN, H.M. & GUSTAFSON, S.L. (1991): Treatment of metal-contaminated water using bacterial sulfate-reduction: Results from pilot-scale reactors. *In* Proceedings Second Internat. Conf. Abatement Acidic Drainage 1, 301-314. MEND Secretariat, Ottawa, Ontario.

DZOMBAK, D.A. & MOREL, F.M.M. (1986): Sorption of cadmium on hydrous ferric oxide at high sorbate/sorption ratios: equilibrium, kinetics and modeling. *J. Colloid Interface Sci.* 112, 588-598.

_____ & _____ (1990): *Surface Complexation Modeling: Hydrous Ferric Oxide.* John Wiley & Sons, Toronto, Ontario, 393 pp.

EBERHART, J.P. (1991) *Structural and Chemical Analysis of Materials.* John Wiley & Sons, 545 pp.

ECOLOGICAL ANALYSTS, INC. (1979): Cyanide: An Overview and Analysis of the Literature on Chemistry, Fate, Toxicity and Detection in Surface Waters. Prepared for Inter-industry Cyanide Group.

EGER, P. & LAPAKKO, K. (1988): Nickel and copper removal from mine drainage by a natural wetland. *In* Mine Drainage and Surface Reclamation, Vol. 1. U.S. Bureau Mines Inf. Circ. 9183, 31-39.

_____, MELCHERT, G., ANTONSON, D. & WAGNER, J. (1993): The use of wetland treatment to remove trace metals from mine drainage. *In* Constructed Wetlands for Water Quality Improvement (G. A. Moshiri, ed.). Lewis Publ., Ann Arbor, Michigan, 171-178.

EGGLESTON, C.M. & HOCHELLA, M.F., Jr. (1994): Atomic and electronic structure of PbS {100} surfaces and chemisorption—oxidation reactions. *In* Environmental Geochemistry of Sulfide Oxidation (C.N. Alpers & D.W. Blowes, eds.). *Am. Chem. Soc. Symp. Series* 550, 201-222.

EGGLETON, R.A. & FITZPATRICK, R.W. (1988): New data and a revised structural model for ferrihydrite. *Clays Clay Minerals* 36, 111-124.

ELBERLING, B., NICHOLSON, R.V. & DAVID, D. (1993a): Field evaluation of sulfide oxidation rates. *Nordic Hydrol.* 24, 323-338.

_____, _____, REARDON, E.J. & TIBBLE, P. (1993b): Evaluation of sulfide oxidation rates: A laboratory study comparing oxygen flux and rates of oxidation product release. *Can. Geotech. J.* (accepted).

ELLIOT, C.M. & OCKENDEN, J.R. (1982): *Weak Variational Methods for Boundary Problems.* Pitman Advanced Publishing Program, London, UK.

ERICKSON, P.M. & LADWIG J. (1985): *Control of Acid Formation by*

Inhibition of Bacteria and by Coating Pyrite Surfaces. Final Report to the West Virginia Dept. of Natural Resources, 68 pp.

FANNING, D.S., RABENHORST, M.C. & BIGHAM, J.M. (1993): Colors of acid sulfate soils. *In* Soil Color (J. M. Bigham & E. J. Ciolkosz, eds.). Soil Sci. Soc. Am., Madison, Wisconsin, 91-108.

FARKAS, A. & CURTIS, L. (1991): Mineralogical and Chemical Investigation of Sulfide Tailings from the Kidd Creek Mine, Timmins, Ontario. Unpublished report for Falconbridge Limited.

FARLEY, K.J., DZOMBAK, D.A. & MOREL, F.M.M. (1985): A surface precipitation model for the sorption of cations on metal oxides. *J. Colloid Interface Sci.* 106, 226-242.

FARRAH, H., HATTON, D. & PICKERING, W.F. (1980): The affinity of metal ions for clay minerals. *Chem. Geol.* 28, 55-68.

FEASBY, D.G. (1993): The mine environment neutral drainage (MEND) program. *CIM Bull.* 86, No. 971, 71 (Abst.).

FELMY, A.R., GIRVIN, D.C. & JENNE, E.A. (1983): MINTEQ: A Computer Program for Calculating Aqueous Geochemical Equilibria. U.S. Environmental Protection Agency, Washington, D.C.

FENNESSY, M.S. & MITSCH, W.J. (1989): Treating coal mine drainage with an artificial wetland. *J. Water Pollution Control Fed.* 61, 1681-1701.

FERRIS, F.G., TAZAKI, K. & FYFE, W.S. (1989): Iron oxides in acid mine drainage environments and their association with bacteria. *Chem. Geol.* 74, 321-330.

FERRONI, G.D., LEDUC, L.G. & TODD, M. (1986): Isolation and temperature characterization of psychrotrophic strains of Thiobacillus ferrooxidans from the environment of a uranium mine. *J. Gen. Appl. Microbiol.* 32, 169-175.

FEY, M.V. & DIXON, J.B. (1981): Synthesis and properties of poorly crystalline hydrated aluminous goethites. *Clays Clay Minerals* 29, 91-100.

FILION M.P. & FERGUSON, K. (1989): Acid mine drainage research in Canada. *In* Proc. 6th Ann. Meet. of BIOMINET (R.G.L. McCready, ed.). October 5, 1989, Laval, Québec. CANMET Publication 89-90, 27-44. Dept. Energy Mines Resources Canada.

FILIPEK, L.H., NORDSTROM, D.K. & FICKLIN, W.H. (1987): Interaction of acid mine drainage with waters and sediments of West Squaw Creek in the West Shasta Mining District, California. *Environ. Sci. Technol.* 21, 388-396.

FISCHER, W.R. (1972): Die Wirkung von zweiwertigem Eisen auf Lösung und Umwandlung von Eisen(III)-hydroxiden. *In* Pseudogley and Gley (E. Schlichting & U. Schwertmann, eds.).Verlag Chemie, Weinheim, Germany, 37-44.

FISHER, D.S. & BURNS, R.G. (1990): Pyrrhotite oxidation: Mechanism of acid weathering. *Geol. Soc. Am. Ann. Meeting Program Abstracts* 22, 207.

FITZPATRICK, E.A. (1984): *Micromorphology of Soils.* Chapman & Hall, New York, 433 pp.

FLANN, R.C. & & LUKASZEWSKI, G.M. (1970): The oxidation of pyrrhotite in ores and concentrates. Presentation at Austral. Inst. Mining Metall., Regional Mtg., Tennant Creek, Australia (in Ritcey 1989).

FLEISCHER, M. & MANDARINO, J. (1991): Glossary of Mineral Species. The Mineralogical Record Inc., Tucson, Arizona, 256 pp.

FORD-SMITH, M. (1964): The Chemistry of Complex Cyanides: A Literature Review. Her Majesty's Stationery Office, London, UK.

FRANK, S.N. & BARD, A.J. (1977): Heterogeneous photocatalytic oxidation of cyanide ion in aqueous solutions with TiO_2 powder. *J. Am. Chem. Soc.* 99, 303-304.

FREEZE, R.A. & CHERRY, J.A. (1979): Groundwater. Prentice-Hall, Englewood Cliffs, New Jersey, 604 pp.

FREYBERG, D.L. (1988): An exercise in ground-water model calibration and prediction. *Ground Water* 26, 350-360.

FRIEDMAN, G.M. (1959): Identification of carbonate minerals by staining methods. *J. Sedimentary Petrology* 29, 87-97.

FRIND, E.O. (1993): Lecture Notes, EARTH 456: Groundwater Modelling (Numerical Methods). Dept. Earth Sciences, University of Waterloo, Waterloo, Ontario.

_____ & MATANGA, G.B. (1985): The dual formulation for contaminant transport modelling 1. Review of theory and accuracy aspects. *Water Resources Research* 21, 159-169.

_____ & MOLSON, J.W. (1989): On the relevance of the transport parameters in predictive modelling of groundwater contamination. *In* Proceed. Internat. Symposium on Groundwater Management and Quality. Benidorm, Spain. IAHS Press, UK, Publication No. 188.

_____, BLOWES, D.W., MOLSON, J.W. & PTACEK, C.J. (1994): Simulation of multicomponent reactive transport in groundwater. *In* International Symposium on Transport and Reactive Processes in Aquifers. ETH,

Zurich, Switzerland, April 11-15.

_____, DUYNISVELD, W.H.M., STREBEL, O. & BOETTCHER, J. (1990): Modeling of multicomponent transport with microbial transformation in groundwater: The Fuhrberg case. *Water Resources Research* 26, 1707-1719.

_____, MATANGA, G.B. & CHERRY, J.A. (1985): The dual formulation for contaminant transport modelling 2. The Borden Aquifer. *Water Resources Research* 21, 170-181.

FUGE, R., PEARCH, F.M., PEARCE, N.J.G. & PERKINS, W.T. (1994): Acid mine drainage in Wales and influence of ochre precipitation on water chemistry. *In* Environmental Geochemistry of Sulfide Oxidation (C. N. Alpers & D. W. Blowes, eds.). *Am. Chem. Soc. Symp. Series* 550, 261-274.

FULLER, C.C., DAVIS, J.A. & WAYCHUNAS, G.A. (1993): Surface chemistry of ferrihydrite: Part 2. Kinetics of arsenate adsorption and coprecipitation. *Geochim. Cosmochim. Acta* 57, 2271-2282.

FULLER, W. (1977): Movement of selected metals, asbestos and cyanide in soils: applications to waste disposal problems. U.S. Environmental Protection Agency Report EPA-600/1-77-020.

_____ (1978): Investigation of landfill leakage pollutant attenuation by soils. U.S. Environmental Protection Agency Report EPA-600/2-78-158.

_____ (1984): Cyanides in the environment with particular attention to the soil. *In* Cyanide and the Environment (D.J. van Zyl, ed.). Colorado State University, Fort Collins, Colorado, Vol. 1, 19-46.

GARRELS, R.M. (1960): *Mineral Equilibria at Low Temperature and Pressure.* Harper & Brothers, New York.

GELINAS, P., LEFEBVRE, R. & CHOQUETTE, M. (1992): Monitoring of acid mine drainage in a waste rock dump. *In* Environmental Issues and Waste Management in Energy and Minerals Production (K. Singhal et al., eds.). Balkema, Rotterdam, Holland, 747-756.

GERTH, J. (1990): Unit-cell dimensions of pure and trace metal-associated goethites. *Geochim. Cosmochim. Acta* 54, 363-371.

GHIORSE, W.C. (1988): Microbial reduction of manganese and iron. *In* Biology of Anaerobic Microorganisms (A.J.B. Zehnder, ed.). John Wiley & Sons, New York, 315-331.

GIANCOLA, D., editor (1992): *Canadian Mines Handbook 1992-1993.* Southam Business Communications Inc., Don Mills, Ontario.

GIBSON, D.K. (1987): Mathematical study of lysimeter. *Austral. Nuclear Sci. Technology Org. Report* ANSTO/E666.

_____, PANTELIS, G. & RITCHIE, A.I.M. (1994): The relevance of the intrinsic oxidation rate to the evolution of polluted drainage from a pyrite waste rock dump. *In* Proceedings Internat. Conf. Abatement Acid Drainage, Pittsburg, Pennsylvania (accepted).

GILLHAM, R.W. (1984): The capillary fringe and its effect on water table response. *J. Hydrology* 67, 307-324.

GIOVANOLI, R. & CORNELL, R.M. (1992): Crystallization of metal-substituted ferrihydrites. Zeits. Pflanzenernähr. Bodenk. 155, 455-460.

GOLDHABER, M.B. (1983): Experimental study of metastable sulfur oxyanion formation during pyrite oxidation at pH 6-9 and 30 °C. *Am. J. Sci.* 283, 193-217.

GOLDICH, S.S. (1938): A study in rock weathering. *J. Geol.* 46, 17-38.

GOODMAN, A.E., BABIJ, T. & RITCHIE, A.I.M. (1983): Leaching of a sulphide ore by *Thiobacillus ferrooxidans* under anaerobic conditions. *In* Recent Progress in Biohydrometallurgy (G. Rossi & A.E. Torma, eds.). Assoc. Mineraria Sarda, Iglesias, Italy, 361-376.

_____, KHALID, A.M. & RALPH, B.J. (1981): Microbial ecology of Rum Jungle, Part 1. Environmental study of sulphidic overburden dumps, experimental heap-leach piles and tailings dam area. *Austral. Atomic Energy Commission Report* AAEC/E531.

GOODMAN, B.A. (1986): Adsorption of metal ions and complexes on aluminosilicate minerals. *In* Geochemical Processes at Mineral Surfaces (J.A. Davis & K.F. Hayes, eds.). *Am. Chem. Soc. Symposium Series* 323, 342-361.

_____ & LEWIS, D.G. (1981): Mössbauer spectra of aluminous goethites (_-FeOOH). *J. Soil Sci.* 32, 351-363.

GOULD, W.D., FUJIKAWA, J.I. & COOK, F.D. (1974): A soil fungus tolerant to extreme acidity and high salt concentrations. *Can. J. Microbiol.* 20, 123-127.

_____, McCREADY, R.G.L., RAJAN, S. & KROUSE, H.R. (1989): Stable isotope composition of sulfate produced during bacterial oxidation of various metal sulfides. *In* Proceedings Internat. Symp. Biohydrometallurgy (J.D. Alley, R.G.L. McCready & P.L. Wichlacz, eds.). *CANMET Report* SP 89-10, 81-92. Dept. Energy Mines Resources Canada.

GRAEME, R.W. (1981): Famous mineral localities: Bisbee, Arizona. *Mineral. Record* 12, 258-319.

GREENBERG, A.E., CLESCERI, L.S., EATON, A.D. & FRANCON, M.H., editors (1992): *Standard Methods for the Examination of Waste and Wastewater.* 18th ed., published jointly by American Public Health Association, American Water Works Association and Water Environment Association.

GREENE, B., HENZL, M.T., HOSEA, J.M. & DARNALL, D.W. (1986): Elimination of bicarbonate interference in the binding of U (VI) in mill-waters to freeze dried Chlorella vulgaris. *Biotechnol. Bioeng.* 28, 764-767.

GRISHIN, S.I., BIGHAM, J.M. & TUOVINEN, O.H. (1988): Characterization of jarosite formed upon bacterial oxidation of ferrous sulfate in a packed-bed reactor. *Appl. Environ. Microbiol.* 54, 3101-3106.

GUIGIER, N., MOLSON, J., FRIND, E. & FRANZ, T. (1992): *FLONET: Two-dimensional Steady-state Flownet Generator. Version 1.02.* Waterloo Hydrogeologic Software, Waterloo, Ontario.

_____, _____, _____ & _____ (1994): *FLONET User Guide.* Waterloo Centre for Groundwater Research and Waterloo Hydrogeologic Software, University of Waterloo, Waterloo, Ontario.

GUO, WEIXING & PARIZEK, R.R. (1994): Field research on thermal anomalies indicating sulfide-oxidation reactions in mine spoil. *In* Environmental Geochemistry of Sulfide Oxidation (C.N. Alpers & D.W. Blowes, eds.). *Am. Chem. Soc. Symposium Series* 550, 645-657.

GUSTAFSON, L. & HUNT, J. (1975): The porphyry copper deposit at El Salvador, Chile. *Econ. Geol.* 70, 857-912.

HADDADIN, J., MORIN, D., OLLIVIER, P. & FICK, M. (1993): Effect of different carbon dioxide concentration on ferrous iron and pyrite oxidation by a mixed culture of iron and/or sulfur-oxidizing bacteria. *Enzyme Microbiol. Technology* 15, 832-841.

HARRIES, J.R. & RITCHIE, A.I.M. (1981): The use of temperature profiles to estimate the pyritic oxidation rate in a waste rock dump from an open-cut mine. *Water Air Soil Pollution* 15, 405-423.

_____ & _____ (1983): The microenvironment within waste rock dumps undergoing pyritic oxidation. *In* Recent Progress in Biohydrometallurgy (G. Rossi & A.E. Torma, eds.). Assoc. Minereria Sarda, Iglesias, Italy, 377-392.

_____ & _____ (1985): Pore gas composition in waste rock dumps undergoing

pyritic oxidation. *Soil Sci.* 140, 143-152.

_____ & _____ (1987): The effect of rehabilitation on the rate of oxidation of pyrite in a mine waste dump. *Env. Geochem. Health* 9, 27-36.

HARRIS, P.O. & RAMELOW, G.J. (1990): Binding of metal ions by particulate biomass derived from Chlorella vulgaris and Scenedesmus quadricauda. *Environ. Sci. Technol.* 24, 22-228.

HARRISON, A.P. (1978): Microbial succession in mineral leaching in an artificial coal spoil. *Appl. Environ. Microbiol.* 36, 861-869.

_____ (1984): The acidophilic thiobacilli and other acidophilic bacteria that share their habitat. *Ann. Rev. Microbiol.* 38, 265-292.

HARRISON, P.M., FISCHBACK, F.A., HOY, T.G. & HAGGIS, G.M. (1967): Ferric oxyhydroxide core of ferritin. *Nature* 216, 1188-1190.

HAWTHORNE, F.C. (1993): Minerals, mineralogy and mineralogists: past, present and future. *Can. Mineral.* 31, 253-296.

HAZEN, A. (1892): Some physical properties of sands and gravels. *Massachusetts State Board of Health Annual Report*, 539-556.

HEDIN, R.S. & NAIRN, R.W. (1993): Contaminant removal capabilities of wetlands constructed to treat coal mine drainage. *In* Constructed Wetlands for Water Quality Improvement (G. A. Moshiri, ed.). Lewis Publ., Ann Arbor, Michigan, 187-195.

HEDIN, R.S. & WATZLAF, G.R. (1994): The effects of anoxic limestone drains on mine water chemistry. *In* Internat. Land Reclamation Mine Drainage Conf. & Third Internat. Conf. Abatement Acidic Drainage 1, 185-194, U.S. Dept. Interior, Bureau of Mines Special Publication SP 06A-94.

_____, HYMAN, D.M. & HAMMACK, R.W. (1988): Implications of sulphate-reduction and pyrite formation processes for water quality in a constructed wetland: preliminary observations. *In* Mine Drainage and Surface Reclamation, Vol. 1. U.S. *Bureau Mines Inf. Circ.* 9183, 382-388.

HENDRICKSON, T. & DAIGNAULT, L. (1973): Treatment of complex cyanide compounds for reuse or disposal. U.S. Environmental Protection Agency Report EPA R2-73-269.

HENDRIX, J., NELSON, J. & AHMADIANTEHRAN, M. (1987): Cyanide in precious metals mill tailings impoundments. SME-AIME Fall Meet., September.

HENDY, N.A. (1987): Isolation of thermophilic iron-oxidizing bacteria from sulphidic waste rock. *J. Industrial Microbiol.* 1, 389-392.

HO, G.E., MURPHY, P.J., PLATELL, N. & WAJON, J.E. (1984): Iron removal from TiO_2-plant acidic wastewater. *J. Environ. Eng.* **110**, 828-846.

HOCHELLA, M.F., JR. & WHITE, A.F., editors (1990): Mineral-water interface geochemistry. *Reviews in Mineralogy* **23**, 603 pp.

HOECKER, W. & MUIR, D. (1987): Degradation of cyanide. Presented at Research and Development in Extractive Metallurgy. AIMM, Adelaide Branch, Australia, May, 1987.

HOHL, H., SIGG, L. & STUMM, W. (1980): Characterization of surface chemical properties of oxides in natural waters. *In* Particulates in Water (M.C. Kavanaugh & J.O. Leckie, eds.). *Am. Chem. Soc. Advances in Chemistry Series* **186**, 1-31.

HOLUIGUE, L., HERRARA, L., PHILIPS, O.M., YOUND, M. & ALLENDE, J.F. (1987): CO_2 fixation by mineral leaching bacteria: Characteristics of the ribulose bisphosphate carhoxylase-oxygen use of Thiobacillus ferrooxidans. *Biotechnol. Appl. Biochem.* **9**, 497-505.

HONEYMAN, B.D. (1984): *Cation and Anion Adsorption at the Oxide/Solution Interface in Systems Containing Binary Mixtures of Adsorbents: An Investigation of the Concept of Adsorptive Additivity.* Ph.D. thesis, Stanford University, Stanford, California.

HOWARTH, R.W. (1979): Pyrite: Its rapid formation in a salt marsh and its importance in ecosystem metabolism. *Science* **203**, 49-51.

_____ & GIBLIN, A. (1983): Sulfate reduction in the salt marshes at Sapelo Island, Georgia. *Limnol. Oceanogr.* **28**, 70-82.

HUANG, C.-P., HUANG, C.-P. & MOREHART, A.L. (1990): The removal of Cu (II) from dilute aqueous solutions by Saccharomyces cerevisiae. *Water Res.* **24**, 433-439.

HUANG, X. & EVANGELOU, V.P. (1994): Suppression of pyrite oxidation rate by phosphate addition. *In* Environmental Geochemistry of Sulfide Oxidation (C.N. Alpers & D.W. Blowes, eds.). Am. Chem. Soc. Symp. Series **550**, 562-573.

HUIATT, J.L., KERRIGAN, J.E., OLSON, F.A. & POTTER, G.L. (1982): Proceedings of a cyanide workshop, *Cyanide from Mineral Processing.* U.S. Bureau of Mines, Salt Lake City, Utah, February 2-3.

HUNT, C.E. (1991): Strategies and practices for handling mine wastes at the Sudbury operations of INCO Limited. *In* Residues and Effluents—Processing and Environmental Considerations (R.G. Reddy, W.P. Imrie & P.B. Queneau, eds.). TMS, Warrendale, Pennsylvania, 89-94.

HUNTSMAN, B.E., KLEINMANN, R.L.P. & TIERMAN, T.O. (1985): Hydrologic and geochemical considerations in maintaining man-made wetlands constructed for acid mine drainage abatement. *In* Wetlands and Water Management on Mined Lands (R.P. Brooks, ed.). Conf. Proceedings, The Pennsylvania State University, Pittsburg, Pennsylvania.

HUTCHINSON, M., JOHNSTONE, K.I. & WHITE, D. (1969): Taxonomy of the genus Thiobacillus: the outcome of numerical taxonomy applied to the group as a whole. *J. Gen. Microbiol.* 57, 397-41.

HUYAKORN, P. & PINDER, G. (1983): Computational Methods in Subsurface Flow. Academic Press, New York.

_____, SPRINGER, E.P., GUVANASEN, V. & WADSWORTH, T.D. (1986): A three-dimensional finite element model for simulating water flow in variably saturated porous media. *Water Resources Research* 22, 1790-1808.

HVORSLEV, M.J. (1951): Time lag and soil permeability in groundwater observations. *U.S. Army Corps of Engineers, Bulletin* 36. Waterways Experiment Station, Vicksburg, Mississippi.

IEC, CONSULTANTS Ltd. (1979): *Polysulphides for Conversion of Cyanides to Thiocyanate in Gold Mining Effluents.* Fisheries and Environment Canada, Burlington, Ontario, 38p.

IGGY LITAOR, M. (1988): Review of soil solution samplers. *Water Resources Research* 24, 727-733.

INGERSOLL, D., HARRIS, W.E., BOMBERGER, D.G. & COULSON, D. (1981): Development and evaluation of procedures for the analysis of simple cyanides, total cyanide, and thiocyanate in water and wastewater. U.S. Environmental Protection Agency Report EPA-600/u-83-054.

JAMBOR, J.L. (1986): Detailed mineralogical examination of alteration products in core WA-20 from Waite Amulet tailings. *CANMET Division Report* MSL 86-137(IR). Dept. Energy Mines Resources Canada.

_____ (1987a): Character and depth of oxidation of the reactive acid tailings at the Waite Amulet minesite, Noranda, Quebec. *CANMET Division Report* MSL 87-97(IR). Dept. Energy Mines Resources Canada.

_____ (1987b): Geology and origin of the orebodies in the Lucky Strike area. *In* Buchans Geology, Newfoundland (R.V. Kirkham, ed.). *Geol. Surv. Can. Paper* 86-24, 75-106.

_____ (1987c): Mineralogical and chemical investigation of cores from piezometric sites in Waite Amulet tailings, Noranda, Quebec. *CANMET Division Report* MSL 87-32(IR). Dept. Energy Mines Resources Canada.

_____ & BLOWES, D.W. (1989): Mineralogical examination of tailings from the Heath Steele mill, Newcastle area, New Brunswick. *CANMET Division Report* MSL 89-137(IR). Dept. Energy Mines Resources Canada.

_____ & _____ (1990): Major-element variations in the reactive sulfide-rich tailings at the Waite Amulet minesite, Noranda area, Quebec, Canada. *In* Process Mineralogy IX (W. Petruk, R.D. Hagni, S. Pignolet-Brandom & D.M. Hausen, eds.). TMS, Warrendale, Pennsylvania, 511-523.

_____ & _____ (1991): Mineralogical study of low-sulphide, high-carbonate, arsenic-bearing tailings from the Delnite minesite, Timmins area, Ontario. *In* Proceedings Second Internat. Conf. Abatement Acidic Drainage 4, 173-198. MEND Secretariat, Ottawa, Ontario.

_____ & _____ (1992): Examination of possible mineral dissolution in the low-pH zone of the Heath Steele old tailings impoundment, Bathurst-Newcastle area, New Brunswick. *CANMET Division Report* MSL 92-83(IR). Dept. Energy Mines Resources Canada.

_____ & BOYLE, R.W. (1965): Aplowite and moorhouseite, new cobalt sulphate minerals from Walton, Nova Scotia. *Can. Mineral.* 8, 166-171.

_____ & OWENS, D.R. (1992): Mineralogical characterization of process products and secondary phases in the Kidd Creek jarosite impoundment, Timmins, Ontario. *CANMET Division Report* MSL 92-29 (CR). Dept. Energy Mines Resources Canada.

_____ & _____ (1993): Mineralogy of the tailings impoundment at the former Cu-Ni deposit of Nickel Rim Mines Ltd., eastern edge of the Sudbury Structure, Ontario. *CANMET Division Report* MSL 93-4(CF). Dept. Energy Mines Resources Canada.

_____ & TRAILL, R.J. (1963): On rozenite and siderotil. *Can. Mineral.* 7, 751-763.

_____, OWENS, D.R. & BLOWES, D.W. (1992): Examination of possible mineral dissolution in the low-pH zone of the Heath Steele old tailings impoundment, Bathurst_Newcastle area, New Brunswick. *CANMET Division Report* MSL 92-83(IR). Dept. Energy Mines Resources Canada.

_____, _____ & CARRIÈRE, P. (1993a): Environmentally related mineralogy of tailings at the Agnico-Eagle minesite, Joutel, Quebec. *CANMET Division Report* MSL 93-56. Dept. Natural Resources Canada.

_____, _____, _____ & LASTRA, R. (1993b): Mineralogical investigation of tailings and associated waste products, and the distribution of natrojarosite in the Kidd Creek main tailings cone, Timmins, Ontario. *CANMET Division Report* MSL 93-20(CR). Dept. Energy Mines Resources Canada.

JAYNES, D.B., ROGOWSKI, A.S.S. & PIONKE, H.B. (1984): Acid mine drainage from reclaimed coal strip mines. 1. Model description. *Water Resources Research* 20, 233-242.

JOHNSON, C.A. & THORNTON, I. (1987): Hydrological and chemical factors controlling the concentrations of Fe, Cu, Zn and As in a river system contaminated by acid mine drainage. *Water Research* 21, 359-365.

JOHNSON, D.B. & MCGUINNESS, S. (1991): Ferric iron reduction by acidophilic heterotrophic bacteria. *Appl. Environ. Microbiol.* 57, 27-211.

_____, KELSON W.I. & JENKINS, D.A. (1979): Bacterial streamer growth in a disused pyrite mine. *Environ. Pollution* 18, 107-118.

JOHNSON, M.L. (1994): The tetrahedrite zoo and the tetrahedrite bestiary: possible, impossible, and improbable endmembers. *Mineral. Record* 25, 74.

JOHNSON, N.E., CRAIG, J.R. & RIMSTIDT, J.D. (1986): Compositional trends in tetrahedrite. *Can. Mineral.* 24, 385-397.

JOHNSON, R.H. (1993): *The Physical and Chemical Hydrogeology of the Nickel Rim Mine Tailings, Sudbury, Ontario.* M.Sc. thesis, University of Waterloo, Waterloo, Ontario.

JONGEJAN, A. (1982): Observations on the microbial cellulose degradation process that decreases water acidity. CANMET Division Report MRP/MSL 82-113(J). Dept. Energy Mines Resources Canada.

JORGENSEN, B.B. (1990): A thiosulfate shunt in the sulfur cycle of marine sediments. *Science* 249, 152-154.

JUSTIN, P. & KELLY, D.P. (1978a): Growth kinetics of Thiobacillus denitrificans in anaerobic and aerobic chemostat culture. *J. Gen. Microbiol.* 17, 123-13.

_____ & _____ (1978b): Metabolic changes in Thiobacillus denitrificans accompanying the transition from aerobic to anaerobic growth in continuous chemostat culture. *J. Gen. Microbiol.* 107, 131-137.

KAKOVSKY, I.A. & KOSIKOV, Ye. M. (1975): Study of the kinetics of oxidation of some sulfide minerals. *Obogashch. Rud.* 20, 18-21 (in Russia).

KALIN, M. & SMITH, M.P. (1991): Biological amelioration of acidic seepage streams. *In* Proceedings 2nd Internat. Conf. Abatement Acidic Drainage, Vol. 1, 355-368. MEND Secretariat, Ottawa, Ontario.

_____, CAIRNS, J. & McCREADY, R.G.L. (1991): Ecological engineering methods for acid mine drainage treatment of coal wastes. *Resources Conserv. Recycling* 5, 265-275.

KALIN, M. & VAN EVERDINGEN, R.O. (1987): Ecological engineering: Biological and geochemical aspects. Phase I experiments. Seminar/Workshop, 23-26 March, 1987, Halifax, Nova Scotia, 565-590.

KAMPF, N. & SCHWERTMANN, U. (1982): Goethite and hematite in a climosequence in southern Brazil and their application in classification of kaolinitic soils. *Geoderma* 29, 27-39.

KANAGAWA, T. & MIKAMI, E. (1989): Removal of methanethiol, dimethyl sulphide, dimethyl disulphide, and hydrogen sulphide from contaminated air by Thiobacillus thioparus TK-m. *Appl. Environ. Microbiol.* 55, 555-558.

KARATHANASIS, A.D., EVANGELOU, V.P. & THOMPSON, Y.L. (1988): Aluminum and iron equilibria in soil solutions and surface waters of acid mine watersheds. *J. Environ. Qual.* 17, 534-543.

KARAVAIKO, G.I. (1985): Lithotrophic bacteria in the oxidation and leaching of sulphide minerals. *In* Microbiological Processes for the Leaching of Metals from Ores. State-of-the-art Review (A.E. Torma, ed.). United Nations Environment Programme, 6-69.

KARLSSON, S., ALLARD, B. & HÅKANSSON, K. (1988): Characterization of suspended solids in a stream receiving acid mine effluents, Bersbo, Sweden. *Appl. Geochem.* 3, 345-356.

KASAN, H.C. & BAECKER, A.A. (1989): An assessment of toxic metal biosorption by activated sludge from the treatment of coal-gasification effluent of a petrochemical plant. *Water Res.* 23, 795-800.

KATAYAMA, Y. & KURAISHI, H. (1978): Characteristics of Thiobacillus thioparus and its thiocyanate assimilation. *Can. J. Microbiol* 24, 804-810.

KELADA, N.P., LUE-HING, C. & CHAVICH, J.A. (1984): Cyanide thiocyanate speciation and removal of thiocyanate and other interferences. *In* Cyanide and the Environment. (D.J. van Zyl, ed.). Colorado State University, Fort Collins, Colorado. Vol. 1, 114-142.

KELLY, D.P. & JONES, C.A. (1978): Factors affecting metabolism and ferrous ion oxidation in suspensions and batch cultures of *Thiobacillus ferrooxidans:* Relevance to ferric ion leach solution regeneration. *In* Metallurgical Applications of Bacterial Leaching and Related Microbiological Phenomena (L.E. Murr, A.E. Torma & J.A. Brierley, eds.). Academic Press, New York, 19-44.

KEPLER, D.A. & McCLEARY, E.C. (1994): Successive alkalinity-producing systems (SAPS) for the treatment of acidic mine drainage. *In* Internat. Land Reclamation Mine Drainage Conf. & Third Internat. Conf.

Abatement Acidic Drainage 1, 195-204, U.S. Dept. Interior, Bureau of Mines Special Publication SP 06A-94.

KERSHAW, M. & PICKERING, R. (1980): The jarosite process—phase equilibria. *In* Lead-Zinc-Tin '80 (J.M. Cigan, T.S. Mackey & T.J. O'Keefe, eds.). TMS—AIME, Warrendale, Pennsylvania, 565-582.

KERTH, M. & WIGGERING, H. (1990): The weathering of colliery spoil in the Ruhr : problems and solutions. *In* Reclamation, Treatment and Utilization of Coal Mining Wastes (A.K.M. Rainbow, ed.). Balkema, Brookfield, Vermont, 417-424.

KHAN, A.W. & PATEL, G.B. 1991. Cellulose degradation by mesophilic anaerobic bacteria. *In* Biosynthesis and Biodegradation of Cellulose (C.H. Haigler & P.J. Weimer, eds.). Marcel Dekker Inc., New York (355-375).

KIDD, C.H. (1988): Prediction of solute transport from gold mine tailings, Coromandel, New Zealand. *Proceedings 3rd Internat. Mine Water Conf.*, Melbourne, Australia.

KIMBALL, B.A., BROSHEARS, R.E., MCKNIGHT, D.M. & BENCALA, K.E. (1994): Effects of instream pH modification on transport of sulfide-oxidation products. *In* Environmental Geochemistry of Sulfide Oxidation (C. N. Alpers & D. W. Blowes, eds.). *Am. Chem. Soc. Symp. Series* 550, 224-243.

KINZELBACH, W. (1986): *Groundwater Modelling.* Elsevier, Amsterdam.

KLEIN, J. & VORLOP, K.D. (1985): Immobilization techniques-cells. *In* Comprehensive Biotechnology (M. Moo-Young, ed.). Pergamon Press, New York, Vol. 2, 203-224.

KLEINMANN, R.L.P. (1979): *The Biogeochemistry of Acid Mine Drainage and a Method to Control Acid Formation.* Ph.D. thesis, Princeton University, Princeton, New Jersey.

_____ (1989): Acid mine drainage. U.S. Bureau of Mines researches and develops control methods for both coal and metal mines. *Eng. Mining. J.* 19, 16I-16N.

_____ & CRERAR, D. (1979): *Thiobacillus ferrooxidans* and the formation of acidity in simulated coal mine environments. *Geomicrobiol. J.* 1, 373-388.

_____, _____ & PACELLI, R.R. (1981): Biogeochemistry of acid mine drainage and a method to control acid formation. *Mining Eng.* 33, 300-306.

_____, HEDIN, R.S. & EDENBORN, H.M. (1991): Biological treatment of mine

water-an overview. *In* Proceedings 2nd Internat. Conf. Abatement Acidic Drainage 4, 27-43. MEND Secretariat, Ottawa, Ontario.

KLETZIN, A. (1989): Coupled enzymatic production of sulfite, thiosulfate, and hydrogen sulfide from sulfur: purification and properties of a sulfur oxygenase reductase from the facultatively anaerobic archaebacterium Desulfurolobus ambivalens. *J. Bacteriol.* 171, 1638-1643.

KNAUSS, K.G. & WOLERY, T.J. (1989): Muscovite dissolution kinetics as a function of pH and time at 70 °C. *Geochim. Cosmochim. Acta* 53, 1493-1501.

_____, NGUYEN, S.N. & WEED, H.C. (1993): Diopside dissolution kinetics as a function of pH, CO_2, temperature, and time. *Geochim. Cosmochim. Acta* 57, 285-294.

KOCH, W.F. (1983): The determination of trace levels of cyanide by ion chromatography with electrochemical detection. *J. Research National Bureau Standards* 88, 157-161.

KONIKOW, L.F. (1986): Predictive accuracy of a ground-water model : Lessons from a post audit. *Ground Water* 24, 173-184.

_____ & BREDEHOEFT, J.D. (1992): Ground-water models cannot be validated. *Adv. Water Resources* 15, 75-83.

KOSSENBERG, M. & COOK, A.C. (1961): Weathering of sulphide minerals in coal: production of ferrous sulphate heptahydrate. *Mineral. Mag.* 32, 829-830.

KRUSEMAN, G.P. & De RIDDER, N.A. (1970): Analysis and evaluation of pumping test data. Internat. Inst. Land Reclamation and Improvement, Wageningen, The Netherlands, *Bull.* 11, 187 pp.

KUBISZ, J. (1964): Minerals of the alunite-jarosite group. *Polska Akad. Nauk. Prace Geol.* 22, 1-93 (in Polish).

KUNENEN, J.G., ROBERTSON, L.A. & TUOVINEN, O.H. (1992): The genus Thiobacillus, Thiomicrospira, and Thiosphaera. *In* The Prokaryotes (A. Balows, H.G. Truper, M. Dworkin, W. Harder & K.H. Schleifer, eds.). 2nd ed., Vol. 3, 2638-2657.

KUNZ, R. G., CASEY, J.P. & HUFF, J.E. (1979): Refinery cyanides, a regulatory dilemma. *Hydrocarbon Processing* 5, 98-106.

KUYUCAK, N., SHEREMATA, T.W. & WHEELAND, K.G. (1991): Evaluation of improved lime neutralization processes. *In* Proceedings Second Internat. Conf. Abatement Acidic Drainage 2, 517-527. MEND Secretariat, Ottawa, Ontario.

KWONG, Y.T.J. (1991): Acid generation in waste rock as exemplified by the Mount Washington minesite, British Columbia, Canada. *In* Proceedings Second Internat. Cong. Abatement Acidic Drainage 1, 175-190. MEND Secretariat, Ottawa, Ontario.

_____ & FERGUSON, K.D. (1990): Water chemistry and mineralogy at Mount Washington: Implications to acid generation and metal leaching. *In* Acid Mine Drainage: Designing for Closure. (J.W. Gadsby, J.A. Malick & S.J. Day, eds.). Bitech Publishers, Vancouver, British Columbia, 217-230.

_____ & VAN STEMPWOORT, D.R. (1994): Attenuation of acid rock drainage in a natural wetland system. *In* Environmental Geochemistry of Sulfide Oxidation (C.N. Alpers & D. W. Blowes, eds.). *Am. Chem. Soc. Symp. Series* 550, 382-392.

LAFLAMME, J.H.G. (1990): The preparation of materials for microscopic study. *Mineral. Assoc. Can. Short Course* Vol. 17, 37-68.

LANDA, E. (1980): Isolation of uranium mill tailings and their component radionuclides from the biosphere: some earth science perspectives. *U.S. Geol. Survey Circular* 814, 32 pp.

LANGMUIR, D. (1969): The Gibbs free energies of substances in the system Fe-O_2-H_2O-CO_2. *U.S. Geol. Surv. Prof. Paper* 650-B, 180-184.

_____ (1971): Particle size effect on the reaction goethite = hematite + water. *Am. J. Sci.* 271, 972.

_____ (1972): Correction : Particle size effect on the reaction goethite = hematite + water. *Am. J. Sci.* 272, 972.

_____ & MELCHIOR, D.C. (1985): The geochemistry of Ca, Sr, Ba, and Ra sulfates in some deep brines from the Palo Duro Basin, Texas. *Geochim. Cosmochim. Acta* 49, 2423-2432.

LAZAROFF, N., SIGAL, W. & WASSERMAN, A. (1982): Iron oxidation and precipitation of ferric hydroxysulfates by resting Thiobacillus ferrooxidans cells. *Appl. Environ. Microbiol.* 43, 924-938.

_____, MELANSON, L., LEWIS, E., SANTORO, N. & PUESCHAL, C. (1985): Scanning electron microscopy and infrared spectroscopy of iron sediments formed by Thiobacillus ferrooxidans. *Geomicrobiol. J.* 4, 231-268.

LECKIE, J.O., BENJAMIN, M.M., HAYES, K.F., KAUFMAN, G. & ALTMANN, S. (1980): Adsorption/coprecipitation of trace elements from water with iron oxyhydroxide. Report **EPRI RP-910-1**. Electric Power Research Institute, Palo Alto, California.

LECLERC, A. (1980): Room temperature Mössbauer analysis of jarosite-type compounds. *Phys. Chem. Minerals* 6, 327-334.

LEDUC, L.G., TREVORS, J.T. & FERRONI, G.D. (1993): Thermal characterization of different isolates of Thiobacillus ferrooxidans. FEMS Microbiol. Lett. 18, 189-194.

LEFEBVRE, R., GÉLINAS P. & ISABEL, D. (1992): Heat transfer analysis applied to acid mine drainage production in a waste rock dump, La Mine Doyon (Quebec). Internat. Assoc. Hydrogeol., Hamilton, Ontario, May.

LENSING, H.J., VOGT M. & HERRLING B. (1994): Modelling of biologically mediated redox processes in the subsurface. *J. Hydrology* (accepted).

LEPPERT, D. (1990): Heavy metal sorption with clinoptilolite zeolite: Alternatives for treating contaminated soil and water. *Trans. Soc. Mining Metall. Expl.* 288, 604-608.

LETTERMAN, R.D. & MITSCH, W.J. (1978): Impact of mine drainage on a mountain stream in Pennsylvania. *Environ. Pollution* 17, 53-73.

LEVINSON, L.M. & TREVES, D. (1968): Mössbauer study of magnetic structure of Fe_7S_8. *J. Phys. Chem. Solids* 29, 2227-2231.

LI, GEJING, PEACOR, D.R., ESSENE, E.J., BROSNAHAN, D.R. & BEANE, R.W. (1992): Walthierite, $Ba_{0.5}\square_{0.5}Al_3(SO_4)_2(OH)_6$, and huangite, $Ca_{0.5}\square_{0.5}Al_3(SO_4)_2(OH)_6$, two new minerals of the alunite group from the Coquimbo region, Chile. *Am. Mineral.* 77, 1275-1284.

LIU, C.W. & NARASIMHAN, T.N. (1989): Redox controlled multiple-species reactive chemical transport: 1. Model development. *Water Resources Research* 25, 868-882.

LOCKE, A. (1926): *Leached Outcrops as Guides to Copper Ores.* Williams & Wilkins, Baltimore, Maryland, 166 pp.

LOGHRY, J.D. (1972): *Characteristics of Favorable Cappings from Several Southwestern Porphyry Copper Deposits.* M.Sc. thesis, Univ. Arizona, Tucson, Arizona.

LONG, D.T., FEGAN, N.E., McKEE, J.D., LYONS, W.B., HINES, M.E. & MACUMBER, P.G. (1992): Formation of alunite, jarosite and hydrous iron oxides in a hypersaline lake system: Lake Tyrrell, Victoria, Australia. *Chem. Geol.* 96, 183-202.

LONGE, G.K. & DeVRIES, F.W. (1988): Some recent considerations on the natural disappearance of cyanide. Presented at *Economics and Practice of Heap Leaching in Gold Mining.* Cairns, Queensland, Australia, August.

LOVELEY D.R. & PHILLIPS, E.J.P. (1988): Novel mode of microbial energy

metabolism: organic carbon oxidation coupled to dissimilatory reduction of iron or manganese. *Appl. Environ. Microbiol.* 54, 1472-148.

LOWENSTAM, H.A. & WEINER, S. (1989): *On Biomineralization.* Oxford University Press, Oxford, UK, 324 pp.

LOWSON, R.T. (1982): Aqueous oxidation of pyrite by molecular oxygen. *Chem. Rev.* 82, 461-497.

LUCKNER, L. & SCHESTAKOW, W.M. (1991): Migration Processes in the Soil and Groundwater Zone. (English translation), VEB Deutscher Verlag fur Grundstoffindustrie, Leipzig. Lewis Publishers Inc., Chelsea, Michigan.

LUNDGREN, T. & LINDAHL, L-A. (1991): The efficiency of covering the sulphidic waste rock at Bersbo, Sweden. *In* Proceedings Second Internat. Conf. Abatement Acidic Drainage 3, 239-255. MEND Secretariat, Ottawa, Ontario.

LUNDGREN, D.G. & SILVER, M. (1980): Ore leaching by bacteria. *Ann. Rev. Microbiol.* 34, 263-283.

LUTHER, G.W., GIBLIN, A., HOWARTH, R.W. & RYAN, R.A. (1982): Pyrite and oxidized mineral phases formed from pyrite oxidation in salt marsh and estuarine sediments. *Geochim. Cosmochim. Acta* 46, 2665-2669.

LUTHY, R.G., BRUCE, S.G., WALTERS, R.W. & NAKLES, D.V. (1978): Identification and reactions of cyanide and thiocyanate in coal gasification wastewaters. *U.S. Dept. Energy Sixth Quarterly Report* FE-2496-23.

LYRIC, R.M. & SUZUKI, I. (1970a): Enzymes involved in the metabolism of thiosulfate by Thiobacillus thioparus. I. Survey of enzymes and properties of sulfite:cytochrome C oxidoreductase. *Can. J. Biochem.* 48, 334-343.

_____ & _____ (1970b): Enzymes involved in the metabolism of thiosulfate by Thiobacillus thioparus. II. Properties of adenosine-5'-phosphosulfate reductase. *Can. J. Biochem.* 48, 344-354

MACHEMER, S.D. & WILDEMAN, T.R. (1992): Adsorption compared with sulfide precipitation as metal removal processes from acid mine drainage in a constructed wetland. *J. Contam. Hydrol.* 9, 115-131.

MAKHIJA, L. & HITCHEN, A. (1979): The titrimetric determination of sulfate, thiosulfate and polythionates in mining effluents. *Anal. Chem. Acta* 105, 375-382.

MALHOTRA, V.M. (1991): Fibre-reinforced high-volume fly ash shotcrete for controlling aggressive leachates from exposed rock surfaces and mine tailings. *In* Proceedings Second Internat. Conf. Abatement Acidic

Total Envir. 132, 27-41.

McINTYRE, N.S. (1984): Modern methods of surface analysis and microanalysis *Mineral. Assoc. Can. Short Course* Vol. 10, 169-195.

McKAY, D.R. & HALPERN, J. (1958): A kinetic study of the oxidation of pyrit in aqueous suspension. *AIME Transactions* 212, 301-309.

McKIBBEN, M.A. (1984): *Kinetics of Aqueous Oxidation of Pyrite by Ferric Iron Oxygen and Hydrogen Peroxide from pH 1-4 and 20-40* °C. Ph.D thesis, Pennsylvania State University, University Park, Pennsylvania.

_____ & BARNES, H.L. (1986): Oxidation of pyrite in low temperature acidi solutions: Rate laws and surface textures. *Geochim. Cosmochim. Act* 50, 1509-1520.

McKNIGHT, D.M. & BENCALA, K.E. (1989): Reactive iron transport in a acidic mountain stream in Summit County, Colorado: A hydrologi perspective. *Geochim. Cosmochim. Acta* 53, 2225-2234.

_____, KIMBALL, B.A. & BENCALA, K.E. (1988): Iron photoreduction an oxidation in an acidic mountain stream. *Science* 240, 637-640.

McSWEENEY, K. & MADISON, F.W. (1988): Formation of a cemente subsurface horizon in sulfidic minewaste. *J. Environ. Qual.* 17, 256-262

MEHRA, O.P. & JACKSON, M.L. (1960): Iron oxide removal from soils an clays by a dithionite-citrate system buffered with sodium bicarbonate. *I Clays* and *Clay Minerals*, Proc. 7th. Natl. Conf., 1958 (A. Swinefor ed.). Pergamon Press, Washington, D.C., 317-327.

MEHTA, M. & MURR, L.E. (1982): Kinetic study of sulfide leaching by galvani interaction between chalcopyrite, pyrite, and sphalerite in the presence o *Thiobacillus ferrooxidans* (30 °C) & thermophilic microorganisms (5 °C). *Biotechnol. Bioeng.* 24, 919-940.

MEND (1989): Field sampling manual for reactive sulphide tailings. Min Environment Neutral Drainage, Report 4.1.1. *CANMET*, Dept. Natur Resources Canada, Ottawa.

_____ (1991): New methods for determination of key mineral species in aci generation prediction by acid-base accounting. Mine Environmer Neutral Drainage, Report 1.16.1c. *CANMET*, Dept. Natural Resourc Canada, Ottawa.

_____ (1992): *MEND Annual Report.* MEND Secretariat, CANMET Ottaw Canada

MERRILL, D.T., MANZIONE, M.A., PETERSON, J.J., PARKER, D.S., CHOV W. & HOBBS, A.O. (1986): Field evaluation of arsenic and seleniu

Total Envir. 132, 27-41.

McINTYRE, N.S. (1984): Modern methods of surface analysis and microanalysis. *Mineral. Assoc. Can. Short Course* Vol. 10, 169-195.

McKAY, D.R. & HALPERN, J. (1958): A kinetic study of the oxidation of pyrite in aqueous suspension. *AIME Transactions* 212, 301-309.

McKIBBEN, M.A. (1984): *Kinetics of Aqueous Oxidation of Pyrite by Ferric Iron, Oxygen and Hydrogen Peroxide from pH 1-4 and 20-40* °C. Ph.D. thesis, Pennsylvania State University, University Park, Pennsylvania.

_____ & BARNES, H.L. (1986): Oxidation of pyrite in low temperature acidic solutions: Rate laws and surface textures. *Geochim. Cosmochim. Acta* 50, 1509-1520.

McKNIGHT, D.M. & BENCALA, K.E. (1989): Reactive iron transport in an acidic mountain stream in Summit County, Colorado: A hydrologic perspective. *Geochim. Cosmochim. Acta* 53, 2225-2234.

_____, KIMBALL, B.A. & BENCALA, K.E. (1988): Iron photoreduction and oxidation in an acidic mountain stream. *Science* 240, 637-640.

McSWEENEY, K. & MADISON, F.W. (1988): Formation of a cemented subsurface horizon in sulfidic minewaste. *J. Environ. Qual.* 17, 256-262.

MEHRA, O.P. & JACKSON, M.L. (1960): Iron oxide removal from soils and clays by a dithionite-citrate system buffered with sodium bicarbonate. *In Clays* and *Clay Minerals*, Proc. 7th. Natl. Conf., 1958 (A. Swineford, ed.). Pergamon Press, Washington, D.C., 317-327.

MEHTA, M. & MURR, L.E. (1982): Kinetic study of sulfide leaching by galvanic interaction between chalcopyrite, pyrite, and sphalerite in the presence of *Thiobacillus ferrooxidans* (30 °C) & thermophilic microorganisms (55 °C). *Biotechnol. Bioeng.* 24, 919-940.

MEND (1989): Field sampling manual for reactive sulphide tailings. Mine Environment Neutral Drainage, Report 4.1.1. *CANMET,* Dept. Natural Resources Canada, Ottawa.

_____ (1991): New methods for determination of key mineral species in acid generation prediction by acid-base accounting. Mine Environment Neutral Drainage, Report 1.16.1c. *CANMET,* Dept. Natural Resources Canada, Ottawa.

_____ (1992): *MEND Annual Report.* MEND Secretariat, CANMET Ottawa, Canada

MERRILL, D.T., MANZIONE, M.A., PETERSON, J.J., PARKER, D.S., CHOW, W. & HOBBS, A.O. (1986): Field evaluation of arsenic and selenium

removal by iron coprecipitation. *J. Water Pollution Control Fed.* 58, 18-26.

MERRINGTON, G. & ALLOWAY, B.J. (1993): Leaching characteristics of heavy metals from three historical Pb-Zn mine tailings heaps in the United Kingdom. *Trans. Inst. Mining Metall.* 102, A75-A82.

MEYER, C.A. & HEMLEY, J.J. (1967): Wall-rock alteration. *In* Geochemistry of Hydrothermal Ore Deposits (H.L. Barnes, ed.). Holt, Rinehart & Winston, New York, 166-235.

MICHELUTTI, R.E. (1988): Minimizing metal contaminated seepages from high sulphide mine tailings by establishing a marsh cover. *In* Proceedings Internat. Conf. on Control of Environ. Problems from Metal Mines, June, 1988, Roros, Norway, 15 pp.

MILES (1981): A study of the photocatalytic effects of aqueous suspensions of platinized semiconductor materials on the reaction rates of candidate redox reactions. *National Aeronautics and Space Administration Report* LAR-13171.

MILLS, A.L. (1985): Acid mine waste drainage: Microbial impact on the recovery of soil and water ecosystems. *In* Soil Reclamation Processes (R. L. Tate & D. A. Klein, eds.). Marcel Dekker, Inc., New York, 35-80.

_____, BELL, P.E. & HERLIHY, A.T. (1989): Microbes, sediments and acidified water: the importance of biological buffering. *In* Acid stress and Aquatic Microbial Interactions (S.S. Roa, ed.). CRC Press, Boca Raton, Florida, 1-19.

MILNE, O. (1950): Equilibria in dilute cyanide waste solutions. Sewage Industrial Wastes 22, 902-911.

MILNES, A.R., FITZPATRICK, R.W., SELF, P.G., FORDHAM, A.W. & MCCLURE, S.G. (1992): Natural iron precipitates in a mine retention pond near Jabiru, Northern Territory, Australia. *In* Biomineralization Processes of Iron and Manganese—Modern and Ancient Environments (H.C.W. Skinner & R.W. Fitzpatrick, eds.). Catena Verlag, Cremlingen-Destedt, Germany, 233-261.

MINING ASSOCIATION OF CANADA (1991): Environmental Challenges to the Mining Industry. Submitted to the House of Commons Standing Committee on Energy, Mines and Resources, Ottawa, September, 1991.

MOLSON, J.W. (1988): *Three-dimensional Numerical Simulation of Groundwater Flow and Contaminant Transport at the Borden Landfill.* MSc. thesis, University of Waterloo, Waterloo, Ontario.

MORANDI, N. & DALRIO, G. (1973): Jamborite: A new nickel hydroxide

mineral from the northern Apennines, Italy. *Am. Mineral.* 58, 835-839.

MORIN, K.A. (1983): *Prediction of Subsurface Contaminant Transport in Acidic Seepage from Uranium Tailings Impoundments.* Ph.D. thesis, University of Waterloo, Waterloo, Ontario.

_____ (1988): Physical and chemical hydrogeology of uranium tailings in Canada and the United States of America. *In* Proceedings Internat. Groundwater Symp., Internat. Assoc. Hydrogeologists, Halifax, Nova Scotia (C.L. Lim, ed.), 175-188.

_____ & CHERRY, J.A. (1986): Trace amounts of siderite near a tailings impoundment, Elliot Lake, Ontario, and its implication in controlling contaminant migration in a sand aquifer. *Chem. Geol.* 56, 117-134.

_____ & _____ (1988): Migration of acid groundwater seepage from uranium tailings impoundments, 3. Simulation of the conceptual model with application to seepage area A. *J. Contam. Hydrology* 2, 323-342.

_____, _____, DAVE, N.K., LIM, T.P. & VIVYURKA, A.J. (1988a): Migration of acidic groundwater seepage from uranium-tailings impoundments, 1. Field study and conceptual hydrogeochemical model. *J. Contam. Hydrology* 2, 271-303.

_____, _____, _____, _____ & _____ (1988b): Migration of acidic groundwater seepage from uranium-tailings impoundments, 2. Behaviour of radionuclides in water. *J. Contaminant Hydrology* 2, 305-322.

MOSES, C.O. & HERMAN, J.S. (1991): Pyrite oxidation at circumneutral pH. *Geochim. Cosmochim. Acta* 55, 471-482.

MOSES, C.O., NORDSTOM, D.K., HERMAN, J.S. & MILLS A.A. (1987): Aqueous pyrite oxidation by dissolved oxygen and ferric iron. *Geochim. Cosmochim. Acta* 51, 1561-1571.

MUDDER, T.I. & GOLDSTONE, A. (1989): The recovery of cyanide from slurries. *In* Randol Conference Gold and Silver Recovery Innovations Phase IV Workshop. Sacramento, California, November.

MUIR, I.J. & NESBITT, H.W. (1992): Controls on differential leaching of calcium and aluminum from labradorite in dilute electrolyte solutions. *Geochim. Cosmochim. Acta* 56, 3979-3985.

_____, _____ & PRATT, A.R. (1993): Surface oxidation of arsenopyrite upon exposure to air and water. *Geol. Assoc. Can. Mineral. Assoc. Can. Program Abs.*, A84.

MURAD, E. (1988): Properties and behavior of iron oxides as determined by Mössbauer spectroscopy. *In* Iron in Soils and Clay Minerals (J.W. Stucki,

B.A. Goodman & U. Schwertmann, eds.). NATO ASI Ser. C., Vol. 217, 309-350. D. Reidel Publ. Co., Dordrecht, Holland.

_____, BIGHAM, J.M., BOWEN, L.H. & SCHWERTMANN, U. (1990): Magnetic properties of iron oxides produced by bacterial oxidation of Fe^{2+} under acid conditions. *Hyperfine Interactions* 58, 2373-2376.

_____, BOWN, L.H., LONG, G.J. & QUIN, T.G. (1988): The influence of crystallinity on magnetic ordering in natural ferrihydrites. *Clay Minerals* 23, 161-173.

_____, SCHWERTMANN, U., BIGHAM, J.M. & CARLSON, L. (1994): Mineralogical characteristics of poorly crystallized precipitates formed by oxidation of Fe^{2+} in acid mine sulfate waters. *In* Environmental Geochemistry of Sulfide Oxidation (C.N. Alpers & D.W. Blowes, eds.). *Am. Chem. Soc. Symposium Series* 550, 190-200.

MURRAY, D.P. (1977): Pit slope manual, supplement 10-1. *CANMET REPORT* 77-31. Dept. Energy Mines Resources Canada.

MURRAY, E.W., GOUDEY, S.P., McCREADY, R.G.L. & SALLEY, J. (1988): Laboratory and field testing of salt-supplemented clay cap as an impermeable seal over pyritic slates. *In* Mine Drainage and Surface Mine Reclamation Vol. 1. *U.S. Bureau Mines Inf. Circ.* 9183, 52-58.

MURRAY, J.W. (1979): Iron oxides. *Reviews in Mineralogy* 6, 47-98.

MURRMANN, R.P. & KOUTZ, F.R. (1972): Role of soil chemical processes in reclamation of wstewater applied to land. *In* Wastewater Management by Disposal on the Land. U.S. Army Cold Regions Research Eng. Lab. Special Report 171, 48-76.

NARASIMHAN, T.N., WHITE A.F. & TOKUNAGA, T. (1986): Groundwater contamination from an inactive uranium mine tailings pile, 2. Application of a dynamic mixing model. *Water Resources Research* 22, 1820-1834.

NELSON, L.M. & KNOWLES, R. (1978): Effect of oxygen and nitrate on nitrogen fixation and denitrification by Azospirillum brasilense grown in continuous culture. *Can. J. Microbiol.* 24, 1395-143.

NEUMAN, S.P. & WITHERSPOON, P.A. (1972): Field determination of the hydraulic properties of leaky multiple-aquifer systems. *Water Resources Research* 8, 1284-1298.

NICHOLSON, R.N., GILLHAM, R.W. & REARDON, E.J. (1990): Pyrite oxidation in carbonate-buffered solutions. 2. Rate control by oxide coatings. *Geochim. Cosmochim. Acta* 54, 395-402.

NICHOLSON, R.V. (1984): *Pyrite Oxidation in Carbonate-buffered Systems: Experimental Kinetics and Control by Oxygen Diffusion in Porous Medium.* Ph. D. thesis, University of Waterloo, Waterloo, Ontario.

_____, AKINDUNNI, F.F., SYDOR, R.C. & GILLHAM, R.W. (1991): Saturated tailings covers above the water table: The physics and criteria for design. *In* Proceedings Second Internat. Conf. Abatement Acidic Drainage 1, 443-460. MEND Secretariat, Ottawa, Ontario.

_____ & SCHARER, J.M. (1994): Laboratory studies of pyrrhotite oxidation kinetics. *In* Environmental Geochemistry of Sulfide Oxidation (C.N. Alpers & D.W. Blowes, eds.). *Am. Chem. Soc. Symp. Series* 550, 14-30.

_____, GILLHAM, R.W., CHERRY, J.A. & REARDON, E.J. (1989): Reduction of acid generation in mine tailings through the use of moisture-retaining cover layers as oxygen barriers. *Canadian Geotech. J.* 26, 1-8

_____, _____, & REARDON, E.J. (1988): Pyrite oxidation in carbonate-buffered solutions: 1. Experimental kinetics. *Geochim. Cosmochim. Acta* 52, 1077-1085.

_____, _____ & _____ (1990): Pyrite oxidation in carbonate-buffered solutions: 2. Rate control by oxide coatings. *Geochim. Cosmochim. Acta* 54, 395-402.

NICKEL, E.H. & DANIELS, J.L. (1985): Gossans. *In* Handbook of Strata-bound and Stratiform Ore Deposits (K.H. Wolf, ed.). Vol. 13, 261-390. Elsevier Science Publishers.

NORDSTROM, D.K. (1977): *Hydrogeochemistry and Microbiological Factors Affecting the Heavy Metal Chemistry of an Acid Mine Drainage System.* Ph.D. thesis, Stanford University, Stanford, California.

_____ (1982a): Aqueous pyrite oxidation and the consequent formation of secondary iron minerals. *In* Acid Sulfate Weathering. Soil Sci. Soc. Am., Madison, Wisconsin, 37-46.

_____ (1982b): The effect of sulfate on aluminum concentrations in natural waters: some stability relations in the system Al_2O_3-SO_3-H_2O at 298 K. *Geochim. Cosmochim. Acta* 46, 681-692.

_____ & BALL, J.W. (1986): The geochemical behavior of aluminum in acidified surface waters. *Science* 232, 54-56.

_____ & MAY, H.M. (1989): Aqueous equilibrium data for mononuclear aluminum species. *In* Environmental Geochemistry of Aluminum (G. Sposito, ed.). CRC Press, Boca Raton, Florida, 29-53.

_____ & MUNOZ, J.L. (1986): *Geochemical Thermodynamics.* BlackwellScientific Publications, Boston, Massachusetts.

_____ & PARKS, G.A. (1987): Solubility and stability of scorodite, $FeAsO_4.2H_2O$: Discussion. *Am. Mineral.* 72, 849-851.

_____, BALL, J.W., ROBERTSON, C.E. & HANSHAW, B.B. (1984): The effect of sulfate on aluminum concentrations in natural waters: II. Field occurrences and identification of aluminum hydroxysulfate precipitates. *Geol. Soc. Am. Program Abstracts* 16(6), 611.

_____, PLUMMER, L.N., LANGMUIR, D., BUSENBERG, E., MAY, H.M., JONES, B.F. & PARKHURST, D.L. (1990): Revised chemical equilibrium data for major water-mineral reactions and their limitations. *In* Chemical Modelling in Aqueous Systems II (D.C. Melchior & R.L. Bassett, eds.). Am. Chem. Soc. Symp. Series 416, 398-413.

NORRIS, P.R. (1989): Factors affecting bacterial mineral oxidation: the example of carbon dioxide in the context of bacterial diversity. *In* Proceedings Internat. Symp. on Biohydrometallurgy (J. Salley, R.G.L. McReady & P.L. Wichlacz, eds.). *CANMET Report* SP 89-10, 3-14. Dept. Energy Mines Resources Canada.

NORTON, G.A., RICHARDSON, R.G. & MARKUSZEWSKI, R. (1991): Precipitation of jarosite compounds as a method for removing impurities from acidic wastes from chemical coal cleaning. *Environ. Sci. Technol.* 25, 449-455.

OLSON, G.J. (1991): Rate of bioleaching by *Thiobacillus ferrooxidans*; results of an interlaboratory comparison. *Appl. Environ. Microbiol.* 57, 642-644.

OMOE (Ontario Ministry of the Environment) (1983): *Ontario Drinking Water Objectives.* Ontario Ministry Environment Tech. Report, Toronto, Ontario.

OREMLAND, R.S. (1988): Biogeochemistry of methanogenic bacteria. *In* Biology of Anaerobic Microorganisms (A.J.B. Zehnder, ed.). John Wiley & Sons, New York, 641-705.

PALACHE, C., BERMAN, H. & FRONDEL, C. (1951): The System of Mineralogy, *Vol.* 2. J. Wiley & Sons, New York, 1124 pp..

PALATY, J. & HOROKOVA-JAKUBU, M. (1959): *The Course and Rate of Removal of Cyanides from Water under Natural Conditions*, Vol. 3, Part 1. Faculty of Technology of Fuel and Water, Prague, Czech Republic.

PALMER, C.M. (1992): *Principles of Contaminant Hydrogeology.* Lewis Publishers, Chelsea, Michigan, 211 pp.

PANTELIS, G. (1993): FIDHELM: Description of model and users guide. *Austral. Nuclear Sci. Technology Org.* Report ANSTO/M123.

_____ & RITCHIE, A.I.M., (1991a): Macroscopic transport mechanisms as a rate-limiting factor in dump leaching of pyritic ores. *Appl. Math. Modelling* 15, 136-143.

_____ & _____ (1991b): Rate controls on the oxidation of pyritic materials imposed by the upper temperature limits on the bacterially catalysed process. *FEMS Microbiol. Reviews* 11, 183-190.

_____ & _____ (1992): Rate limiting factors in dump leaching of pyritic ores. *Appl. Math. Modelling* 16, 553-560.

_____ & _____ (1993): Optimizing oxidation rates in heaps of pyritic material. *In* Biohydrometallurgical Technologies (A.E. Torma, M.L. Apel & C.L. Brierley, eds.). Proceedings Internat. Biohydrometallurgy Symp., Jackson Hole, Wyoming, 1, 731-738. TMS.

PARFITT, R.L., RUSSELL, J.D. & FARMER, V.F. (1975): Confirmation of the surface structures of goethite (α-FeOOH) and phosphated goethite by infrared spectroscopy. *J. Chem. Soc. Faraday Trans.* 72, 1082-1087.

_____, VAN DER GAAST, S.J. & CHILDS, C.W. (1992): A structural model for natural siliceous ferrihydrite. *Clays Clay Minerals* 40, 675-681.

PARKHURST, D.L., THORSTENSON, D.C. & PLUMMER, L.N. (1980): PHREEQE: a computer program for geochemical calculations. *U.S. Geol. Surv. Water-Resources Invest.Report* 80-60.

_____ & GRAY, W. (1977): *Finite Element Simulation in Surface and Subsurface Hydrology.* Academic Press, New York.

PARKS, G.A. (1990): Surface energy and adsorption at mineral—water interfaces: An introduction. *Reviews in Mineralogy* 23, 133-175.

PATTERSON, R.J., FRAPE, S.K., DYKES, L.S. & McLEOD, R.A. (1978): A coring and squeezing technique for the detailed study of subsurface water chemistry. *Can. J. Earth Sci.* 15, 162-169.

PAYNE, W.J. (1981): Denitrification. John Wiley & Sons, New York.

PEDERSEN, T.F., McNEE, J.J., MUELLER, B., FLATHER, D.H. & PELLETIER, C.A. (1994): Geochemistry of submerged tailings in Anderson Lake, Manitoba: Recent results. *In* Internat. Land Reclamation Mine Drainage Conf. & Third Internat. Conf. Abatement Acidic Drainage 1, 288-296. U.S. Dept. Interior, Bureau of Mines Special Publication SP 06A-94.

_____, MUELLER, B., McNEE, J.J. & PELLETIER, C.A. (1993): The early diagenesis of submerged sulphide-rich tailings in Anderson Lake,

Manitoba. *Canadian J. Earth Sci.* 22, 133-135.

PICKERING, W.F. (1989): The competing roles of dissolution, sorption and complex formation in element mobilisation. *In* Weathering: Its Products and Deposits. Volume 1. Processes. Theophrastus Publications, Athens, Greece, 259-305.

PIERCE, W.G., BELZILE, N., WISEMAN, M.E. & WINTERHALDER, K. (1994): Composted organic wastes as anaerobic reducing covers for long term abandonment of acid-generating tailings. *In* Internat. Land Reclamation Mine Drainage Conf. & Third Internat. Conf. Abatement Acidic Drainage 2, 148-157. U.S. Dept. Interior, Bureau of Mines Special Publication SP 06A-94.

PLUMLEE, G. (1993): The environmental geology of mineral deposits. *In* The Environmental Geochemistry of Mineral Deposits, Short Course Notes. Soc. Econ. Geol. Seminar, Denver, Colorado, April 13-16, 1993.

_____ (1994): Environmental geology models of mineral deposits. *SEG Newsletter* 16, 5-6.

PLUMMER, L.N., PARKHURST, D.L., FLEMING, G.W. & DUNKLE, S.A. (1988): A computer program incorporating Pitzer's equations for calculation of geochemical reactions in brines. *U.S. Geol. Survey WRI Report* 88-4153.

_____, WIGLEY, T.M.L. & PARKHURST, D.L. (1978): The kinetics of calcite dissolution in CO_2-water systems at 5° to 60°C and 0.0 to 1.0 atm CO_2. *Am. J. Sci.* 278, 179-216.

POHLANDT, C. (1984a): The determination of cyanide in hydrometallurgical process solutions and effluents by ion chromatography. *Council for Mineral Technology Report* M128. Randburg, South Africa.

_____ (1984b): The determination of cyanides in the hydrometallurgical processing of gold. *In* Cyanide and the Environment (D.J. van Zyl, ed.). Colorado State University, Fort Collins, Colorado, Vol. 1, 105-107.

_____ (1985): Chromatographic separation and determination of stable metal cyanide complexes in gold processing solution. *S. African J. Chem.* 38, 110-114.

_____, JONES, E. & LEE, A. (1983): A critical evaluation of methods applicable to the determination of cyanides. *J. S. African Inst. Mining Metall.* 83, 11-19.

POST, D.F., BRYANT, R.B., BATCHILY, A.K., HUETE, A.R., LEVINE, S.J., MAYS, M.D. & ESCADAFAL, R. (1993): Correlations between field and laboratory measurements of soil color. *In* Soil Color (J.M. Bigham &

E.J. Ciolkosz, eds.). Soil Sci. Soc. Am., Madison, Wisconsin, 35-49.

POST, J.E. & BUCHWALD, V.F. (1991): Crystal structure refinement of akaganéite. *Am. Mineral.* 76, 272-277.

POWERS, D.A., ROSSMAN, G.R., SCHUGAR, H.J. & GRAY, H.B. (1975): Magnetic behavior and infrared spectra of jarosite, basic iron sulfate, and their chromate analogs. *J. Solid State Chem.* 13, 1-13.

PRATT, A.R., MUIR, I.J. & NESBITT, H.W. (1993a): Surface analytical studies of pyrrhotite reacted with H_2O, H_2SO_4 and HCl. *Geol. Assoc. Can - Mineral. Assoc. Can. Program Abs.*, A85.

_____, _____ & _____ (1993b): Surface analytical studies of pyrrhotite fractured under high vacuum and reacted with air. *Geol. Assoc. Can. - Mineral. Assoc. Can. Program Abs.*, A85.

_____, _____ & _____ (1994): X-ray photoelectron and auger electron spectroscopic studies of pyrrhotite and mechanisms of air oxidation. *Geochim. Cosmochim. Acta* 58, 827-842.

PRONK, J.T., DE BRUYN, J.C., BOS, P. & KUENEN, J.G. (1992): Anaerobic growth of Thiobacillus ferrooxidans. *Appl. Environ. Microbiol.* 58, 2227-2230.

_____, LIEM, K., BOS, P. & KUENEN, J.G. (1991): Energy transduction by anaerobic ferric iron respiration in *Thiobacillus ferrooxidans*. *Appl. Environ. Microbiol.* 57, 263- 268.

PTACEK, C.J. (1992): *Experimental Determination of Siderite Solubility in High Ionic-strength Aqueous Solutions.* Ph.D. thesis, University of Waterloo, Waterloo, Ontario.

_____ & BLOWES, D.W. (1994): Influence of siderite on the geochemistry of inactive mine tailings impoundment. p. 172-189. *In* Environmental Geochemistry of Sulfide Oxidation (C.N. Alpers & D.W. Blowes, eds.). Am. Chem. Soc. Symp. Series 550, 172-189.

QUIN, T.G., LONG, G.L., BENSON, C.G., MANN, S. & WILLIAMS, R.J.P. (1988): Influence of silicon and phosphorus on structural and magnetic properties of synthetic goethite and related oxides. *Clays Clay Minerals* 36, 165-175.

RALPH, B.J. (1979): Oxidative reactions in the sulphur cycle. *In* Biogeochemical Cycling of Mineral-forming Elements (P.A. Trudinger & D.J. Swaine, eds.). Elsevier, Amsterdam, Holland, 369-400.

_____ (1985): Geomicrobiology and the new biotechnology. *Dev. Industrial Microbiol.* 26, 32-59.

RASMUSON, A. & COLLIN, M. (1988): Mathematical modelling of water and oxygen transport in layered soil covers for deposits of pyritic mine tailings. *In* Proceedings Internat. Conf. Control Environ. Problems from Metal Mines, June, 1988, Roros, Norway, 32 pp.

RAYMOND, R., Jr., BISH, D.L. & GOOLEY, R. (1983): Occurrence of szomolnokite in Kentucky No. 14 coal and possible implications concerning formation of iron sulfides in peats and coals. *In* Mineral Matter in Peat: Its Occurrence, Form, and Distribution (R. Raymond, Jr. & M.J. Andrejko, eds.). Los Alamos National Lab., Los Alamos, New Mexico, 159-167.

REARDON, E.J. & MODDLE, P.M. (1985): Gas diffusion coefficient measurements on uranium mill tailings: Implications to cover layer design. *Uranium* 2, 111-131.

_____ & POSCENTE, P.J. (1984): A study of gas composition in sawmill waste deposits. *Reclam. Revegetation Research* 3, 109-128.

REEDER, R.J. (1983): Crystal chemistry of the rhombohedral carbonates. *Reviews in Mineralogy* 11, 1-47.

REEDY, B.J., BEATTIE, J.K. & LOWSON, P.J. (1991): A vibrational spectroscopic ^{18}O tracer study of pyrite oxidation. *Geochim. Cosmochim. Acta* 55, 1609-1614..

RHOTON, F.E., BIGHAM, J.M., NORTON, L.D. & SMECK, N.E. (1981): Contribution of magnetite to oxalate-extractable iron in soils and sediments from the Maumee River Basin of Ohio. *Soil Sci. Soc. Am. J.* 45, 645-649.

RIBET, I., PTACEK, C.J., BLOWES, D.W. & JAMBOR, J.L. (1994): The potential for metal release by reductive dissolution of weathered mine tailings. *J. Contam. Hydrol.* (accepted).

RICHARDSON, S. & VAUGHAN, D.J. (1989a): Arsenopyrite: a spectroscopic investigation of altered surfaces. *Mineral. Mag.* 53, 223-229.

_____ & _____ (1989b): Surface alteration of pentlandite and spectroscopic evidence for violarite formation. *Mineral. Mag.* 53, 213-222.

RIMSTIDT, J.D., CHERMAK, J.A. & GAGEN, P.M. (1994): Rates of reaction of galena, sphalerite, chalcopyrite, and arsenopyrite with Fe(III) in acidic solutions. *In* Environmental Geochemistry of Sulfide Oxidation (C.N. Alpers & D.W. Blowes, eds.). *Am. Chem. Soc. Symp. Series* 550, 2-13.

RITCEY, G.M. (1989) *Tailings Management.* Elsevier Science Publ. Co. New York, 969 pp.

ROBBINS, R.G. (1987): The solubility and stability of scorodite, $FeAsO_4.2H_2O$: discussion. *Am. Mineral.* 72, 842-844.

ROBERTSON, A.M. (1987): Proc. 11th Annual British Columbia Mine Reclamation Symp., April, 1987, Campbell River, British Columbia.

ROBERTSON, J. (1992): Subaqueous disposal: a promising method for the effective control of reactive waste materials. In 24th Annual Operator's Conference of the Canadian Mineral Processors, Paper 3, 10 pp. Can. Inst. Mining Metall. Petroleum, Montreal, Quebec.

ROBERTSON, W.D. (1992): *Atmospherically-derived Sulphate and Tritium in Sandy Recharge Areas of Central Canada.* Ph.D. thesis, University of Waterloo, Waterloo, Ontario.

_____ & CHERRY, J.A. (1989): Tritium as an indicator of recharge and dispersion in a groundwater system in central Ontario. *Water Resources Research* 25, 1097-1109.

ROBINSKY, E. (1975): Thickened discharge: a new approach to tailings disposal *CIM Bull.* 68, No. 764, 47-53.

_____ (1978): Tailings disposal by the thickened discharge method for improved economy and environmental control. *In* Tailings Disposal Today, Proceedings Second. Internat. Tailings Symp., Denver, Colorado 2, 75-92.

_____ (1979): Tailings disposal by the thickened discharge method for improved economy and environmental control. *In* Tailings Disposal Today (G.O. Argall, ed.). Miller Freeman Publications, San Francisco, California, 76-92.

_____, BARBOUR, S.L., WILSON, G.W., BORDIN, D. & FREDLUND, D.G. (1991): Thickened sloped tailings disposal: an evaluation of seepage and abatement of acid drainage. *In* Proceedings Second Internat. Conf. Abatement Acid Drainage 1, 529-550. MEND Secretariat, Ottawa, Ontario.

ROCKLIN, R. & JOHNSON, E. (1983): Determination of cyanide, sulfide, iodide and bromide by ion chromatography with electrochemical detection. *Anal. Chem.* 55, 4-7.

ROMBERG, I.B. (1969): Lepidocrocite at Rossvatn, north-Norway, an example of pseudomorphism after pyrite cubes. *Norsk. Geol. Tids.* 49, 251-256.

ROSS, G.J. & WANG, C. (1982): Lepidocrocite in a calcareous, well-drained soil. *Clays Clay Minerals* 30, 394-396.

_____, IVARSON, K.C. & MILES, N.M. (1982): Microbial formation of basic

iron sulfates in laboratory systems and in soils. *In* Acid Sulfate Weathering (J.A. Kittrick, D. S. Fanning & L.R. Hossner, eds.). Soil Sci. Soc. Am., Madison, Wisconsin, 77-94.

RUSSELL, J.D. (1979): Infrared spectroscopy of ferrihydrite: Evidence for the presence of structural hydroxyl groups. *Clay Minerals* 14, 109-114.

_____, PATERSON, E., FRASER, A.R. & FARMER, V.C. (1975): Adsorption of carbon dioxide on goethite (α-FeOOH) surfaces, and its implications for anion adsorption. *J. Chem. Soc. Faraday Trans.* 71, 1621-1630.

RUTHERFORD, G.K., DIMMA, D., VAN LOON, G.W. & BRECK, W.G. (1982): The pedological properties of tailings derived from three mining operations in the Sudbury area, Ontario, *Canada. J. Environ. Quality* 11, 511-518.

RYAN, J.N. & GSCHWEND, P.M. (1991): Extraction of iron oxides from sediments using reductive dissolution by titanium(III). *Clays Clay Minerals* 39, 509-518.

RYE, R.O., BETHKE, P.M. & WASSERMAN, M.D. (1992): The stable isotope geochemistry of acid-sulfate alteration *Econ. Geol.* 87, 225-262.

SABELLI, C. & TROSTI-FERRONI, R. (1985): A structural classification of sulfate minerals. *Periodico Mineral.* 54, 1-46.

SANCINDIVER, J.C. & BHUMBLA, D.K. (1988): Effects of cattails (Typha) on metal removal from mine drainage. *In* Mine Drainage and Surface Mine Reclamation, Vol. 1. *U.S. Bureau Mines Inf. Circ.* 9183, 359-369.

SAND, W., ROHDE, K., SOBOTKE, B. & ZENNECK, C. (1992): Evaluation of *Leptospirillum ferrooxidans* for leaching. *Appl. Environ. Microbiol.* 58, 85-92.

SARVESWARA RAO, R.K., DAS, R.P. & RAY, H.S. (1991): Study of leaching of multimetal sulphides through an interdisciplinary approach. *Mineral. Process. Extr. Metall. Rev.* 7, 209-233 (in Merrington & Alloway, 1993).

SATO, M. (1992): Persistency-field Eh-pH diagrams for sulfides and their application to supergene oxidation and enrichment of sulfide ore bodies. *Geochim. Cosmochim. Acta* 56, 3133-3156.

SCHAEFFER & ASSOCIATES (1993): Golden Sunlight Mines West Dump Hydrology Study. Construction Report. Bozeman, Montana.

SCHARER, J.M., ANNABLE, W.K. & NICHOLSON, R.V. (1993): WATAIL 1.0 user's manual: A tailings basin model to evaluate transient water quality of acid mine drainage. Report to Falconbridge Ltd. and MEND- Ontario.

_____, NICHOLSON, R.V., HALBERT, B. & SNODGRASS, W.J. (1994): A computer program to assess acid generation in pyritic tailings. *In* Environmental Geochemistry of Sulfide Oxidation (C.N. Alpers & D.W. Blowes, eds.). *Am. Chem. Soc. Symp. Series* 550, 132-152.

SCHEDEL, M. & TRUPER, H.G. (1979): Purification of Thiobacillus denitrificans siroheme sulfite reductase and investigation of some molecular and catalytic properties. *Biochim. Biophys. Acta* 568, 454-467.

SCHEEREN, P.J.H., KOCH, R.O., BUISMAN, C.J.N., BARNES, L.J. & VERSTEEGH, J.H. (1992): New biological treatment plant for heavy metal-contaminated groundwater. *Trans. Inst. Mining Metall.* 11, C188-C197.

SCHINDLER, P.W. (1981): Surface complexes at oxide-water interfaces. *In* Adsorption of Inorganics at Solid-Liquid Interfaces (M.A. Anderson & A.J. Rubin, eds.). Ann Arbor Science, Ann Arbor, Michigan, 1-49.

SCHMIDT, J.W., SIMOVIC, L. & SHANNON, E. (1981): Natural degradation of cyanides in gold milling effluents. Presented at Cyanide and the Gold Mining Industry. Technical Seminar, Ottawa, Ontario, Jan. 22-23, 1981. Environment Canada.

SCHOTT, J. & BERNER, R.A. (1983): X-ray photoelectron studies of the mechanism of iron silicate dissolution during weathering. *Geochim. Cosmochim. Acta* 47, 2233-2240.

_____, _____ & SJÖBERG, E.L. (1981): Mechanisms of pyroxene and amphibole weathering : I. Experimental studies of iron-free minerals. *Geochim. Cosmochim. Acta* 45, 2123-2135.

SCHUILING, R.D. (1992): Goslarite: threat or promise for the environment of the Geul Valley? *J. Geochem. Expl.* 42, 383-386.

SCHULTZE, D.G. (1984): The influence of aluminum on iron oxides VIII. Unit-cell dimensions of Al-substituted goethites and estimation of Al from them. *Clays Clay Minerals* 32, 36-44.

SCHULZ, H.D. & REARDON E.J. (1983): A combined mixing cell/analytical model to describe two-dimensional reacting solute transport for unidirectional groundwater flow. *Water Resources Research* 19, 493-502.

SCHULZE, D.G. (1981): Identification of soil iron oxide minerals by differential x-ray diffraction. *Soil Sci. Soc. Am. J.* 45, 437-440.

_____ & SCHWERTMANN, U. (1984): The influence of aluminium on iron oxides: X. Properties of Al-substituted goethites. *Clay Minerals* 19, 521-539.

SCHUMAN, G., CARUCCIO, F.T. & BRADHAM, W.S. (1992): Assessment of factors affecting pyrite reactivity. *U.S. Government Report* PB 92-140227.

SCHWARTZ, F.W., editor (1990): *Ground Water Models : Scientific and Regulatory Applications.* National Academy of Sciences.

SCHWERTMANN, U. (1964): Differenzierung der Eisenoxide des Bodens durch Extraktion mit Ammoniumoxalat-Lösung. *Zeits. Pflanzenernähr. Düng. Bodenk.* 105, 194-202.

_____ (1985a): The effect of pedogenic environments on iron oxide minerals. *In* Advances in Soil Science (B.A. Stewart, ed.). Springer-Verlag, New York, 1, 171-200.

_____ (1985b): Occurrence and formation of iron oxides in various pedoenvironments. *In* Iron in Soils and Clay Minerals (J.W. Stucki, B.A. Goodman & U. Schwertmann, eds.). D. Reidel Publ. Co., Boston, Mass. NATO Advanced Study Institute Series C, 217, 267-308.

_____ (1993): Relations between iron oxides, soil color, and soil formation. *In* Soil Color (J.M. Bigham & E.J. Ciolkosz, eds.). Soil Sci. Soc. Am., Madison, Wisconsin, 51-69.

_____ & CORNELL, R.M. (1991): Iron Oxides in the Laboratory. Verlag Chemie, Weinheim, Germany, 137 pp.

_____ & FITZPATRICK, R.W. (1977): Occurrence of lepidocrocite and its association with goethite in Natal soils. *Soil Sci. Soc. Am. J.* 41, 1013-1018.

_____ & _____ (1992): Iron minerals in surface environments. *In* Biomineralization Processes of Iron and Manganese—Modern and Ancient Environments (H.C.W. Skinner & R.W. Fitzpatrick, eds.). Catena Verlag, Cremlingen-Destedt, Germany 7-30.

_____ & MURAD, E. (1983): The effect of pH on the formation of goethite and hematite from ferrihydrite. *Clays Clay minerals* 31, 277-284.

_____ & TAYLOR, R.M. (1977): Iron oxides. *In* Minerals in Soil Environments. Soil Sci. Soc. Am., Madison, Wisconsin, 145-180.

_____ & _____ (1989): Iron oxides. *In* Minerals in Soil Environments (J.B. Dixon & S.B. Weed, eds.). Soil Sci. Soc. Am., Madison, Wisconsin, 379-438.

_____, GASSER, U. & STICHER, H. (1989): Chromium-for-iron substitution in synthetic goethites. *Geochim. Cosmochim. Acta* 53, 1293-1297.

_____, SCHULZE, D.G. & MURAD, E. (1982): Identification of ferrihydrite in soils by dissolution kinetics, differential x-ray diffraction, and Mössbauer

spectroscopy. *Soil Sci. Soc. Am. J.* 46, 869-875.

SCOTT, J.D. & INGLES, J. (1987): *State-of-the-Art Processes for the Treatment of Gold Mill Effluents.* Mining, Mineral, and Metallurgical Processes Division, Industrial Programs Branch, Environment Canada, Ottawa, Ontario, March.

SCOTT, J.D., DONYINA, D.K.A. & MOULAND, J.E. (1986): Iron — the good with the bad — Kidd Creek zinc plant experience. *In* Iron Control in Hydrometallurgy (J.E. Dutrizac & A.J. Monhemius, eds.). Ellis Horwood, Chichester, UK, 657-675.

SCOTT, K.D. (1987): Solid solution in, and classification of, gossan-derived members of the alunite-jarosite family, northwest Queensland, Australia. *Am. Mineral.* 72, 178-187.

SHAFER, J.L., WHITE, M.L. & CAENEPEEL, C.L. (1979): Application of the shrinking core model for copper oxide leaching. *Mining Eng.*, February, 165-171.

SIMOVIC, L., SNODGRASS, W.J., MURPHY, K.L. & SCHMIDT, I.W. (1985): Development of a model to describe the natural degradation of cyanide in gold mill effluents. *In* Cyanide and the Environment (D.J. van Zyl, ed.). Colorado State University, Fort Collins, Colorado, Vol. 2, 413-432.

SINGER, P.C. & STUMM, W. (1968): Kinetics of the oxidation of ferrous iron. *In* Proceedings Second Symp. Coal Mine Drainage Research. Bituminous Coal Research Inc., Monroebille, Pennsylvania, 12-34.

_____ & _____ (1970): Acidic mine drainage: The rate-determining step. *Science* 167, 1121-1123.

SMITH, A. (1985): *Applied Hydrogeochemistry in Mining Wastes Disposal.* Proc. Dunham-Durham Symposium, Durham, UK. Special Vol. IMM, London, UK.

_____ (1987): *Testimony to Department of Health and Environmental Control.* South Carolina, Permit No. SC 0041378 Appeal Hearing, Columbia, South Carolina, December, 1987.

_____ (1988a): Cyanide degradation and detoxification. *In* Introduction to Evaluation, Design and Operation of Precious Metal Leaching Projects (D. van Zyl, Hutchinson & Kiel, eds.). SME_AIME, 293-305.

_____ (1988b): *The Management of Cyanide in the Gold Mining Industry.* Seminar Proceedings, Australian Groundwater Consultants, Australia, November.

_____ & BROWN, A. (1986): The potential for cyanide migration from the Annie

Creek processing facility. Report 1086/2 to Wharf Resources (USA) Inc., SRK, Lakewood, Colorado, November.

_____, DEHRMANN, A. & PULLEN, R. (1984): The effects of cyanide-bearing, gold tailings disposal on water quality in Witwatersrand, South Africa. *In* Cyanide and the Environment (D.J. van Zyl, ed.). Colorado State University, Fort Collins, Colorado, Vol. 1, 221-229.

_____, MOORE, D. & CALDWELL, J. (1985): Prediction of groundwater impact of tailings disposal. *In* Hazardous Wastes in Ground Water: a Soluble Dilemma (B. Hitchon & M. Trudell, eds.). Proceedings 2nd Annual Can./Am. Conference on Hydrogeology. National Water Well Assoc., Dublin, Ohio, 215-218.

SMITH, A.C.S. & MUDDER, T.I. (1991): *Chemistry and Treatment of Cyanidation Wastes.* Mining Journal Press, London, UK, 365 pp.

SMITH, E.E., SVANKS, K. & SHUMATE, K. (1968): Sulfide to sulfate reaction studies. *In* Proceedings Second Symp. on Coal Mine Drainage Research. Bituminous Coal Research Inc., Monroebille, Pennsylvania, 1-11.

SMITH, K.L. & EGGLESTON, R.A. (1983): Botryoidal goethite: a transmission electron microscope study. *Clays Clay Minerals* 31, 392-396.

SMITH, N.A. & KELLY, D.P. (1988a): Isolation and physiological characterization of autotrophic sulphur bacteria oxidizing dimethyl disulphide as sole source of energy. *J. Gen. Microbiol.* 134, 147-1417.

_____ & _____ (1988b): Mechanism of oxidation of dimethyl disulphide by Thiobacillus thioparus strain E6. *J. Gen. Microbiol.* 134, 331-339.

_____ & _____ (1988c): Oxidation of carbon disulphide as the sole source of energy for the autotrophic growth of Thiobacillus thioparus strain TK-m. *J. Gen. Microbiol.* 134, 341-348.

SMYTH, D.J.A. (1981): *Hydrogeological and Geochemical Studies above the Water Table in an Inactive Uranium Tailings Impoundment near Elliot Lake, Ontario.* M.Sc. project, University of Waterloo, Waterloo, Ontario.

SNYDER, C. & AHARRAH, E.C. (1984): The influence of the Typha community on mine drainage. *In* Proceedings Symp. on Surface Mining, Hydrology, Sedimentology and Reclamation, Lexington, Kentucky, 149-153.

SOBEK, A.A. (1987): The use of surfactants to prevent AMD in coal refuse and base metal tailings. *In* Proceedings of an Acid Mine Drainage Workshop, Halifax, Nova Scotia, March 1987. Environment Canada, Ottawa, 357-390.7

SODERMARK, B. & LUNDGREN, T. (1988): The Bersbo project – The first full scale attempt to control acid-mine drainage in Sweden. *In* Proceedings Internat. Conf. Control Environ. Problems from Metal Mines, June, 1988, Roros, Norway, 17 pp.

SOLOMON, D.K., POREDA, R.J., SCHIFF, S.L. & CHERRY, J.A. (1992): Tritium and helium-3 as groundwater-age tracers in the Borden Aquifer. *Water Resources Research* 28, 741-755.

STANDARD METHODS FOR THE EXAMINATION OF WATER AND WASTEWATER (1989): 17th Edition, Am. Public Health Assoc-Am. Water Works Assoc.-Water Pollution Control Federation, Washington, D.C.

STARK, L.R., KOLBASH, R.L., WEBSTER, H.J., STEVENS, S.E.Jr., DIONIS, K.I. & MURPHY, E.R. (1988): The Simco #4 wetlands: biological patterns and performance of a wetland receiving mine drainage. *In* Mine Drainage and Surface Reclamation, Vol. 1. *U.S. Bureau Mines Inf. Circ.* 9183, 332-344.

STARR, R.C. & CHERRY, J.A. (1994): In situ remediation of contaminated groundwater: The funnel-and-gate system. *Groundwater* (submitted).

STIERS, W. & SCHWERTMANN, U. (1985): Evidence for manganese substitution in synthetic goethite. *Geochim. Cosmochim. Acta* 49, 1909-1911.

STOFFREGEN, R.E. & ALPERS, C.N. (1987): Svanbergite and woodhouseite in hydrothermal ore deposits: products of apatite destruction during advanced argillic alteration. *Can. mineral.* 25, 201-211.

_____ & _____ (1992): Observation on the unit-cell dimensions, H_2O contents, and δD values of natural and synthetic alunite. *Am. Mineral.* 77, 1092-1998.

STONE, R.W. (1984): The presence of iron and manganese-oxidizing bacteria in natural and simulated bogs. *In* Treatment of Mine Drainage by Wetlands (J.E. Burris, ed.). Contrib. No. 264, Department of Biology, The Pennsylvania State University.

STROBEL, G.A. (1967): Cyanide utilization in soil. *Soil Sci.* 103, 299-302.

STUCKI, J.W. (1981): The quantitative assay of minerals for Fe^{+2} and Fe^{+3} using 1,10-phenanthroline: II. A photochemical method. *Soil Sci. Soc. Am. J.* 45, 638-641.

SU, W.-W. & KELLY, R.M. (1988): Effect of hyperbaric oxygen and carbon dioxide on heterotrophic growth of the extreme thermophile *Sulfolobus acidocaldarius*. *Biotechnol. Bioeng.* 31, 750-754.

SUAREZ. D.L. (1986): A soil water extractor that minimizes CO_2 degassing and pH errors. *Water Resources Research* 22, 876-880.

SUDICKY, E.A. (1986): A natural gradient experiment in solute transport in a sand aquifer: spatial variability of hydraulic conductivity and its role in the dispersion process. *Water Resources Research* 22, 2069-2082.

_____ & HUYAKORN, P.S. (1991): Contaminant migration in imperfectly known heterogeneous groundwater systems. *In* Reviews of Geophysics, Supplement. U.S. National Report to International Union of Geodesy and Geophysics 1987-1990. Am. Geophys. Union, Washington, D.C., 240-253.

_____ & McLAREN, R.G. (1992): The Laplace Transform Galerkin technique for large scale simulation of mass transport in discretely-fractured porous formations. *Water Resources Research* 28, 499-514.

SUGIO, T., KATAGIRI, T., MORIYAMA, M., ZHEN, Y.L., INAGAKI, K. & TANO, T. (1988): Existence of a new type of sulfite oxidase which utilizes ferric ions as an electron acceptor in Thiobacillus ferrooxidans. *Appl. Environ. Microbiol.* 54, 153-157.

_____, _____, INAGAKI, K. & TANO, T. (1989): Actual substrate for elemental sulfur oxidation by sulfur:ferric ion oxidoreductase purified from Thiobacillus ferrooxidans. *Biochim. Biophys. Acta* 973, 25-256.

_____, MIZUNASHI, W., INAGAKI, K. & TANO, T. (1987): Purification and some properties of sulfur:ferric ion oxidoreductase from Thiobacillus ferrooxidans. *J. Bacteriol.* 169, 4916-4922.

_____, WHITE, K.J., SHUTE, E., CHOATE, D. & BLAKE, R.C. II. (1992): Existence of a hydrogen sulfide:ferric ion oxidoreductase in iron-oxidizing bacteria. *Appl. Environ. Microbiol.* 58, 431-433.

SÜSSER, P. & SCHWERTMANN, U. (1983): Iron oxide mineralogy of ochreous deposits in drain pipes and ditches. Zeits. *Kulturtechnik Flurbereinigung* 24, 386-395.

SWANSON, E.A., STRONG, D.F. & THURLOW, J.G., editors (1981): The Buchans orebodies: fifty years of geology and mining. *Geol. Assoc. Can. Special Paper* 22, 350 pp.

TAKANO, M., SHINJO, T., KIYAMA, M. & TAKADA, T. (1968): Magnetic properties of jarosites, $RFe_3(OH)_6(SO_4)_2$ (R = NH_4, Na or K). J. Phys. Soc. Jap. 25, 902.

TAMM, O. (1922): Eine Methode zur Bestimmung der anorganischen Komponenten des Gelkomplexes in Boden. *Medd. Stat. Skogsförsöks* 19, 385-404.

TARDY, Y. & NAHON, D. (1985): Geochemistry of laterites, stability of Al-goethite, Al-hematite, and Fe^{3+}-kaolinite in bauxites and ferricretes. *Am. J. Sci.* 285, 865-903.

TASSÉ, N., GERMAIN, M.D. & BERGERON, M. (1994) Composition of interstitial gases in wood chips deposited on reactive mine tailings. *In* Environmental Geochemistry of Sulfide Oxidation (C.N. Alpers & D.W. Blowes, eds.). Am. Chem. Soc. Symp. Series 550, 631-634.

TAYLOR, R.K. (1973): Compositional and geotechnical characteristics of a 100-year-old colliery spoil heap. *Trans. Inst. Mining Metall.* 82, A1-A4.

_____ & HARDY, R.G. (1974) Sulphate species in colliery spoil banks. *Trans. Inst. Mining Metall.* 83, A123-A126.

TERAI, H. & MORI, T. (1975): Studies on phosphorylation coupled with denitrification and aerobic respiration in Pseudomnonas denitrificans. *Bot. Mag.* 38, 231-244.

TERVARI, P.H. & CAMPBELL, A.B. (1976): Dissolution of iron sulfide (troilite) in aqueous sulfuric acid. *J. Phys. Chem.* 80, 1844-1848.

THE CHESTER ENGINEERS (1977): Report on the Lower Monogahela River Study : Water Quality Conditions, Point and Nonpoint Source Waste Loads Allocations. Vols. 1 and 2. Prepared for U.S. Steel Corp., Corapolis, Pennsylvania.

THERRIEN, R. (1992): *Three-dimensional Analysis of Variably-saturated Flow and Transport in Discretely-fractured Porous Media.* Ph.D. thesis, University of Waterloo, Waterloo, Ontario.

THOREZ, J. (1989): Between the crystal and the solutions: a graphical overview of the passage to, from and of the clay minerals in the lithosphere during weathering. *In* Weathering: Its Products and Deposits. Volume 1. Processes. Theophrastus Publications, Athens, Greece, 49-120.

THORNBER, M.R. (1975): Supergene alteration of sulfides, II. A chemical study of the Kambalda nickel deposits. *Chem. Geol.* 15, 117-144.

_____ (1985): Supergene alteration of sulfides, VII. Distribution of elements during the gossan-forming process. *Chem. Geol.* 53, 279-301.

TORRENT, J. & BARRÓN, V. (1993): Laboratory measurement of soil color: Theory and practice. *In* Soil Color (J.M. Bigham & E.J. Ciolkosz, eds.). Soil Sci. Soc. Am., Madison, Wisconsin, 21-37.

_____ & GUZMAN, R. (1982): Crystallization of Fe(III)-oxides from ferrihydrite in salt solutions: osmotic and specific ion effects *Clays Clay Minerals* 17, 463-469.

_____ SCHWERTMANN, U. & BARRON, V. (1992): Fast and slow phosphate sorption by goethite-rich natural materials. *Clays Clay Minerals* 40, 14-21.

TOWE, K.M. & BRADLEY, W.F. (1967): Mineralogical constitution of colloidal "hydrous ferric oxides". *J. Colloid Interface Sci.* 24, 384-392.

TOWILL, L., DRURY, J., WHITEFIELD, B., LEWIS, E., GALYAN, E. & HAMMONS, A. (1978): Reviews of the environmental effects of pollutants: V. Cyanides. *U.S. Environmental Protection Agency Report* EPA-600/1-78-027.

TSANG, C.F. (1991): The modelling process and model validation. *Ground Water* 29, 825-831.

TSEZOS, M. (1983): The role of chitin in uranium adsorption by R. arrhizus. *Biotechnol. Bioeng.* 25, 225-24.

_____ & MATTAR, S. (1986): A further insight into the mechanism of biosorption of metals, by examining chitin EPR spectra. *Talanta* 33, 225-232.

_____ & VOLESKY, B. (1982): The mechanism of uranium biosorption by Rhizopus arrhizus. *Biotechnol. Bioeng.* 24, 385-41.

_____, McCREADY, R.G.L. & BELL, J.P. (1989): The continuous recovery of uranium from biologically leached solutions using immobilized biomass. *Biotechnol. Bioeng.* 34, 1-17.

_____, NOH, S.H. & BAIRD, M.H.I. (1988): A batch reactor mass transfer kinetic model for immobilized biomass biosorption *Biotechnol. Bioeng.* 32, 545-553.

TUNNELL, G. (1930): *The Oxidation of Disseminated Copper Ores in Altered Porphyry.* Ph.D. thesis, Harvard Univ., Cambridge, Mass.

TUOVINEN, O.H. & KELLY, D.P. (1972): Biology of Thiobacillus ferrooxidans in relation to the microbiological leaching of sulphide ores. *Zeits. Allg. Mikrobiol.* 12, 311-346.

TURNER, L.J. & KRAMER, J.R. (1991): Sulfate ion binding on goethite and hematite. *Soil Sci.* 152, 226-230.

TUTTLE, J.H., DUGAN, P.R., MacMILLAN, C.B. & RANDLES, C.I. (1969a): Microbial dissimilatory sulfur cycle in acid mine water. *J. Bacteriol.* 97, 594-62.

_____, _____ & Randles, C.I. (1969b): Microbial sulfate reduction and its potential utility as an acid mine water pollution abatement procedure. *Appl. Microbiol.* 17, 297-32.

U.S. ENVIRONMENTAL PROTECTION AGENCY (EPA) (1992): Public comment feasibility study, Boulder Creek operable unit, Iron Mountain mine, Redding, California. Vol. 1-2. *EPA Report* WA No. 31-01-9N17.

USEPA (1986): Test methods for evaluating solid waste. *U.S. Environmental Protection Agency Report* SW-846, Third Ed., Vol. IC, Chapter 7, Section 7.3.

VALLÉE, M., DAVID, M., DAGBERT, M. & DESROCHERS, C. (1992): Guide to the evaluation of gold deposits. *CIM Spec. Vol. 45*, 299 pp.

Van BREEMEN, N. (1985): Redox processes of iron and sulfur involved in the formation of acid sulfate soils. *In* Iron in Soils and Clay Minerals (J.W. Stucki, B.A. Goodman & U. Schwertmann, eds.). D. Reidel Publ. Co., Boston, Mass. NATO Advanced Study Institute Series C, 217, 825-841.

VAUGHN, D.J. & CRAIG, J.R. (1978): *Mineral Chemistry of Metal Sulfides.* Cambridge Univ. Press, Cambridge, U.K.

VELBEL, M.A. (1984): Weathering processes of rock-forming minerals. *Mineral. Assoc. Can. Short Course* Vol. 10, 67-111.

_____ (1993): Formation of protective surface layers during silicate-mineral weathering under well-leached, oxidizing conditions. *Am. Mineral.* 78, 405-414.

VENKOBACHAR, C. (1990): Metal removal by waste biomass to upgrade wastewater treatment plants. *Water Sci. Technol.* 22, 319-32.

VLEK, P.L.G., BLOM, T.J.M., BEEK, J. & LINDSAY, W.L. (1974): Determination of the solubility product of various iron hydroxides and jarosite by the chelation method. *Soil Sci. Soc. Am. Proc.* 38, 429-432.

VOGELS, G.D. KELTJENS, J.T. & van der DRIFT, C. (1988): Biochemistry of methane production. *In* Biology of Anaerobic Microorganisms (A.J.B. Zehnder, ed.). John Wiley & Sons, New York, 707-770.

WAGNER, D.P., FANNING, D.S., FOSS, J.E., PATTERSON, M.S. & SNOW, P.A. (1982): Morphological and mineralogical features related to sulfide oxidation under natural and disturbed land surfaces in Maryland. *In* Acid Sulfate Weathering. Soil Science Soc. Am., Madison, Wisconsin, 109-125.

WAJON, J.E., HO, G.E. & MURPHY, P.J. (1985): Rate of precipitation of ferrous iron and formation of mixed iron-calcium carbonates by naturally occurring carbonate materials. *Water Research* 19, 831-837.

WAKAO, N., TAKASHI, T., SAKURAI, Y. & SHIOTA, H. (1979): A treatment of acid mine water using sulphate-reducing bacteria. *J. Ferment. Technol.*

57, 445-452.

WALKER, G.W. & MANNARD, G.W. (1974): Geology of the Kidd Creek mine, a progress report. *CIM Bull.* 67, No. 752, 41-57.

WALSH, F. & MITCHELL, R. (1972): A pH dependent succession of iron bacteria. *Environ. Sci. Technol.* 6, 809-812.

WALTER, A.L., FRIND, E.O., BLOWES, D.W., PTACEK, C.J. & MOLSON, J.W. (1994a): Modelling of multicomponent reactive transport in groundwater. 1. Model development and testing. *Water Resources Research* (accepted).

_____, _____, _____, _____ & _____ (1994b): Modelling of multicomponent reactive transport in groundwater. 2. Metal mobility in aquifers impacted by acidic mine tailings discharge. *Water Resources Research* (accepted).

WAYCHUNAS, G.A. (1991): Crystal chemistry of oxides and oxyhydroxides. *Reviews in Mineralogy* 25, 11-68.

_____, REA, B.A., FULLER, C.C. & DAVIS, J.A. (1993): Surface chemistry of ferrihydrite: Part I. EXAFS studies of the geometry of coprecipitated and adsorbed arsenate. *Geochim. Cosmochim. Acta* 57, 2251-2270.

WEAST, R.C., editor (1969): Handbook of Chemistry and Physics. 50th ed. Chemical Rubber Publ. Co., Cleveland, Ohio.

WEBSTER, J.G., NORSTROM, D.K. & SMITH, K.S. (1994): Transport and natural attenuation of Cu, Zn, As, and Fe in the acid mine drainage of Leviathan and Bryant creeks. *In* Environmental Geochemistry of Sulfide Oxidation (C.N. Alpers & D. W. Blowes, eds.). Am. Chem. Soc. Symp. Series 550, 244-260.

WEIDER, R.K. & LANG, G.E. (1984): Influence of wetlands and coal mining on stream water chemistry. *Water Air Soil Pollut.* 23, 381-396.

WESTALL, J.C. (1986): Reactions at the oxide_solution interface: chemical and electrostatic models. *In* Geochemical Processes at Mineral Surfaces (J.A. Davis & K.F. Hayes, eds.). *Am. Chem. Soc. Symposium Series* 323, 54-78.

_____ & HOHL, H. (1980): A comparison of models for the oxide/solution interface. *Advances Colloid Interface Sci.* 12, 265-294.

WHITLOCK, J., SHARP, C. & MUDDER, T. (1981a): Interferences in Cyanide Analysis: Reflux Methods. Homestake Mining Co., Lead, South Dakota.

_____, _____, & _____ (1981b) *Summary of the Toxicological Significance and Analytical Methodology for Free and Complexed Cyanide.* Homestake Mining Company, Lead, South Dakota.

WIDDEL, F. (1988): Microbiology and ecology of sulfate- and sulfur- reducing bacteria. *In* Biology of Anaerobic Microorganisms (A.J.B. Zehnder, ed.). John Wiley & Sons, New York, 469-585.

WIESE, R.G., Jr., POWELL, M.A. & FYFE, W.S. (1987): Spontaneous formation of hydrated iron sulfates on laboratory samples of pyrite- and marcasite-bearing coals. *Chem. Geol.* 63, 29-38.

WIGGERING, H. (1987): Weathering of clay minerals in the waste dumps of Upper Carboniferous coal-bearing strata, the Ruhr area, West Germany. *Applied Clay Sci.* 2, 353-361.

WILKINSON, L. (1990): *SYSTAT: The System for Statistics*. Systat Inc. Evanston, Illinois, 676 pp.

WILLIAMS, H.E. (1915): Cyanide Compounds. Edward Arnold, London, UK.

WILLIAMS, P.A. (1990): *Oxide Zone Geochemistry*. Ellis Horwood, New York, 286 pp.

WILLIAMSON, M. (1992): *Thermodynamic and Kinetic Studies of Sulfur Geochemistry*. Ph.D. thesis, Virginia Polytechnic Institute and State University, Blacksburg, Virginia.

_____ & RIMSTIDT, J.D. (1992): The kinetics of aqueous pyrite oxidation by ferric iron and dissolved oxygen. Poster, Am. Chem. Soc. 204th National Meeting, Washington, D.C., August 23-28.

WINLAND, R.L., TRAINA, S.J. & BIGHAM, J.M. (1991): Chemical composition of ochreous precipitates from Ohio coal mine drainage. *J. Environ. Qual.* 20, 452-460.

WOLSKA, E. & SCHWERTMANN, U. (1993): The mechanism of solid solution formation between goethite and diaspore. *Neues Jahrb. Mineral. Monatsh.*, 213-223.

WOODS, T.L. & GARRELS, R.M. (1992): Calculated aqueous-solution—solid-solution relations in the low-temperature system CaO-MgO-FeO-CO_2-H_2O. *Geochim. Cosmochim. Acta* 56, 3031-3043.

WOYSHNER, M.R. & ST-ARNAUD, L. (1994): Hydrogeological evaluation and water balance of a thickened tailings deposit near Timmins, ON, Canada. *In* Internat. Land Reclamation Mine Drainage Conf. & Third Internat. Conf. Abatement Acidic Drainage 2, 198-207. U.S. Dept. Interior, Bureau of Mines Special Publication SP 06A-94

YANFUL, E.K. & ST-ARNAUD, L.C. (1991): Design, instrumentation, and construction of engineered soil covers for reactive tailings management. *In* Proceedings Second Internat. Conf. Abatement Acidic Drainage 1,

487-504. MEND Secretariat, Ottawa, Ontario.

_____, AUBE, B.C., WOYSHNER, M. & ST-ARNAUD, L.C. (1994): Field and laboratory performance of engineered covers on the Waite Amulet tailings. *In* Internat. Land Reclamation Mine Drainage Conf. & Third Internat. Conf. Abatement Acidic Drainage 2, 138-147, U.S. Dept. Interior, Bureau of Mines Special Publication SP 06A-94

_____, RILEY, M.D., WOYSHNER, M.R. & DUNCAN, J. (1993): Construction and monitoring of a composite soil cover on an experimental waste rock pile near Newcastle, New Brunswick, Canada. *Can. Geotech. J.* 30, 588-599.

YAPP, C. (1983): Effects of AlOOH—FeOOH solid solution on goethite-hematite equilibrium. *Clays Clay Minerals* 31, 239-240.

YEH, G.T. & TRIPATHI, V.S. (1991): A model for simulating transport of reactive multispecies components: Model development and demonstration. *Water Resources Research* 27, 3075-3094.

YOSHIDA, T., TAMAMURA, Y. & KATSURA, T. (1983): Practical method for determination of total cyanide in metal-containing wastewaters. *Envir. Sci. Technol.* 43, 17, 439-441.

ZAIDI, A., SCHMIDT, J.W., SIMOVIC, L. & SCOTT, J. (1987): The art and science of treating wastewaters from gold mines. Presented at 19th Annual Operators' Conference of the Canadian Mineral Processors. Ottawa, Ontario, Jan. 20-22, 1987.

ZODROW, E.L. & McCANDLISH, K. (1978): Hydrated sulfates in the Sydney coalfield, Cape Breton, Nova Scotia. *Can. Mineral.* 16, 17-22.

_____, WILTSHIRE, J. & McCANDLISH, K. (1979): Hydrated sulfates in the Sydney coalfield, Cape Breton, Nova Scotia, II. Pyrite and its altertion products. *Can. Mineral.* 17, 63-70.